

**THÈSE DE DOCTORAT  
DE SORBONNE UNIVERSITÉ**

**Spécialité : Physique Théorique**  
École doctorale : Physique en Île-de-France

réalisée au

**Laboratoire de Physique Théorique et Hautes Énergies**

présentée par

**Johannes BRAATHEN**

pour obtenir le grade de

**DOCTEUR DE SORBONNE UNIVERSITÉ**

Sujet de la thèse :

**Automating Higgs precision calculations**

**Soutenue le 05/06/2018**

devant le jury composé de :

M.	Eli BEN-HAIM	Examineur
M.	Fawzi BOUDJEMA	Rapporteur
M.	José Ramon ESPINOSA	Rapporteur
M.	Mark GOODSSELL	Directeur de thèse
Mme	Margarete MÜHLLEITNER	Examineur
M.	Pietro SLAVICH	Directeur de thèse



*Til minne om  
min Onkel,  
Terje Nygaard*



# Acknowledgements

The path to complete the work presented here has been long and at times difficult, and there are many people that I would now like to thank for their invaluable help, support, and contributions throughout past years up until today.

First and foremost, I must thank my Ph.D. supervisors, Mark Goodsell and Pietro Slavich. They have always been patient and helpful in answering my numerous questions and correcting my many mistakes, and have guided me towards becoming a true scientist. I thank Mark for being, ever since I was his Master 2 intern, a positive force driving me forward in tackling new notions and calculations, and for encouraging and supporting me in all the projects I undertook during my thesis. I thank Pietro for his door always being open, for the time he took to answer in great detail all my questions – both about Physics and administrative issues – and for all his input and advice on my work. I have learned enormously from them, and under their guidance I have found avenues of research that I would like to pursue further in the future. They both helped me greatly in finding my post-doctoral position, and I am also deeply grateful to them for that. It has been an extraordinary opportunity as well as a true honour to be their student.

I am very grateful to the reviewers of my thesis, Fawzi Boudjema and José Ramon Espinosa, for the time they spent reading my manuscript in great detail and their very helpful comments on how to improve it. I would also like to thank members of the jury, Eli Ben-Haim and Margarete Mühlleitner, for participating in my thesis defense.

I am deeply thankful towards Adam Falkowski who took the time to be my scientific tutor and helped me in my search for a post-doctoral position, and Sofian Teber for his great kindness both as a teacher when I was a Master student and as my “godfather” in LPTHE.

It has been a great pleasure to collaborate during my thesis with Manuel Krauss, Toby Opferkuch, and Florian Staub, and I would like to thank them in particular for the time they took to answer my questions, and for the fruitful results of our work together. I would also like to thank Shinya Kanemura and Kodai Sakurai for our ongoing collaboration, which I very much look forward to continuing and developing in coming years.

I have had the pleasure and chance to meet many researchers in the course of my Ph.D. studies and I would like to thank especially Tomohiro Abe, Ben Allanach, Peter Athron, Emanuele Bagnaschi, Henning Bahl, Ulrich Ellwanger, Martin Gabelman, Thomas Hahn, Katsuya Hashino, Sven Heinemeyer, Yann Mambrini, Kentarou Mawatari, Kin-ya Oda, Werner Porod, Dominik Stöckinger, Alexander Voigt, and Georg Weiglein for many interesting and enriching discussions. I am also very grateful to Professors Hamaguchi, Hikasa, Hisano, Kanemura, Kobayashi, Murayama, and Shindou for the time they gave me when I toured Japan and visited their respective Universities and Institutes to give seminars in early summer 2017.

## Acknowledgements

I must thank members of LPTHE, and in particular of the Particle Physics and Cosmology group, for the nice environment in which I could do my research. I am especially grateful to Benoît Doucot, for his welcoming role as director of LPTHE; to Bruno Machet, for his great heart and his concern about everyone's well-being; and to the secretaries, Francoise Got and Isabelle Nicolai, for all their help in dealing with administrative procedures at various stages of my thesis. I also thank Karim Benakli and Claude Viallet for many discussions at lunch time, and for their helpful advice. I would moreover like to thank the post-docs of the Particle Physics and Cosmology group, and especially Andreas Goudelis, Julia Harz, and Sebastian Pafehr for their kindness and all the advice and support they provided, chiefly during post-doc applications and the writing of my thesis.

My fellow students from LPTHE have been an incredible company for more than three years, through both moments of confidence and of doubt. Thank you Luc Darmé, Frédéric Dreyer, Georgy Feher, Hugo Ricateau, Matthieu Sarkis, Oscar de Felice, Charles Cosnier-Horeau, Thomas Dupic, Chrysoula Markou, Alessandro Tartaglia, Constantin Babenko, Yifan Chen, Sophie Williamson, Kang Yang, Ruben Oncala Mesa, Yoan Gautier, Gaetan Lafforgue, Enrico Russo and Giovanni Stagnitto for numerous lunches, coffee breaks, PhD seminars, PhDrinks, and most of all for the friendships. I would like to thank especially Luc for being so nice and helpful when I was a young student; as well as Matthieu, Hugo, Constantin, Thomas, Yoan, and Sophie for all the time they spent answering my (often stupid) questions about both IT and Physics, and above all for the warm and friendly exchanges and interactions at and after work; and finally Luc, Yifan, Sophie, and Ruben for good memories from travelling to conferences.

I very gratefully acknowledge financial support from Fondation CFM pour la Recherche and Institut Lagrange de Paris, which allowed me to carry out my research in excellent conditions and enabled me to participate in numerous conferences and workshops. I would also like to thank Nathalie Bilimoff for all the help she provided during my thesis, and in particular to establish my work contract.

It has been a great pleasure for me to teach for three years in the course *2P021: Électromagnétisme et électrocinétique*, and I would like to thank Philippe Thomen, Laurent Coolen, and Michel Fioc who were in charge of the course during that time, as well as Laurent Teixeira for all his help with lab classes, and my friends Cédric Enesa and Andrea Mogini for our close collaboration on tutorials, initiated and organised at our many “apéro” evenings. I also thank my colleagues from the course *3P024: Projet en autonomie* in which I have taught this last year.

Studying at Université Pierre et Marie Curie, now Sorbonne Université, for almost eight years – more than one third of my life – has been an extraordinary opportunity, and I have had the chance to meet many exceptionally talented and inspiring professors there. I would like to express all my gratitude to Eli Ben-Haim, Philippe Depondt, Thierry Hocquet, Édouard Kierlik, Émilie Lamour, Vincent Minerbe, Jean-Michel Raymond, A. Marco Saitta, Jean-Paul Tavernet, Sofian Teber, Jérôme Tignion, Philippe Thomen, Matthieu Tissier, Maxime Wolfe, and Jean-Bernard Zuber.

I must also say how indebted I am to Danièle Guiron, Marie Levard, and Alexandre Guesnon for all they did for me during my earlier studies, and to Nicole Boret who first taught me scientific rigor and gave me the love of Physics. Merci infiniment, je vous serais toujours profondément reconnaissant.

I have had the chance of having many wonderful friends, who have supported through all my high-school and University studies. Most sincere thanks go to all my friends,

in particular Pierre-Louis, Nicolas, Manon, Louis, Pauline, Rémy, Loic, Biljana, Hugo A., Cédric, Andrea, Stanley, and Anastasis for our friendship, since Le Bon Sauveur or since undergraduate or Master studies at UPMC. Thank you for listening to me ramble about (Theoretical) Physics on countless occasions and for always believing in me. Un très grand merci à Bernard et Janine Gallet pour leur gentillesse et tous les bons moments passés ensembles. I would also like to thank Mrs. and Mr. Shimizu for their very kind hospitality in receiving me while I was touring Japan for work in June and July 2017, as well as Mrs. and Pr. Nomachi and their family, for all their affection, generosity, and support during the last three years.

No words can express all I owe to my family, first of all to my parents, who moved mountains to help me, never stopped encouraging and comforting me, and drove me to become who I am now. I would never have achieved any of this without them. My most heartfelt thanks also go to Mamaie, to my aunt Aneeta, to my aunt Elisabeth and my uncle Terje (who did not see me finish this work but to whom I wish to dedicate this thesis), to Mona, and to my cousins Martin H., Janvi and Sunena, and Henrik, Martin N., and Maria. They have all believed in me from the beginning, more than I ever believed in myself. Tusen hjertelig takk for all deres kjærighet og støtte.

My last words are for my dear Luna. Thank you so much for your patience, your never-ending support and understanding, and your loving presence by my side throughout the last three years.





# Automating Higgs precision calculations

## Abstract

The Standard Model-like Higgs boson, discovered at the CERN Large Hadron Collider, provides an excellent setting for the indirect search of New Physics, through the study of its properties. In particular the Higgs boson mass is now measured with an astonishing precision – of the order of 0.1% – while being predicted in some models of Beyond the Standard Model Physics, such as supersymmetric (SUSY) models. The main purpose of this thesis is to push further the calculation of radiative corrections to Higgs boson masses in models beyond the Standard Model, as well as the automation of these calculations, in order to set or improve constraints on New Physics coupling to the Higgs boson.

A first chapter is devoted to the computation of the leading two-loop  $\mathcal{O}(\alpha_s\alpha_t)$  corrections to neutral scalar masses in supersymmetric models with Dirac gauginos. We allow both Majorana and Dirac mass terms for the gauginos (more precisely the gluinos), and we derive results for top/stop parameters both in  $\overline{\text{DR}}'$  and in on-shell renormalisation schemes. The analytic results we obtain are implemented in publicly available numerical routines, and constitute the first explicit calculation of Higgs masses at two-loop order in SUSY models beyond the NMSSM.

The core of this thesis is the investigation of the Goldstone Boson Catastrophe – a case of infra-red (IR) divergences due to massless Goldstone bosons that plague the calculation of effective potentials, tadpole equations, and self-energies – and of how to address it. We begin by extending the resummation procedure, recently developed for the Standard Model and applied to the MSSM, to obtain infra-red finite tadpole equations in general renormalisable field theories. We then demonstrate that adopting an on-shell renormalisation scheme for the Goldstone masses would have made the derivation of these results for the tadpoles simpler, and further allows the elimination of all IR divergences in generic neutral scalar mass computations as well. We devise a generalised effective potential approximation to find IR-safe closed-form expressions for all loop functions involved in mass corrections, and we also present a perturbative expansion of parameters that allows for a direct – instead of iterative – solution of the tadpole equations.

Afterwards, we illustrate the numerical implementation of our solution to the Goldstone Boson Catastrophe in the public tool **SARAH**. We compare the results we obtain in the Standard Model to existing calculations, finding remarkable agreement, and we also study new corrections in Split SUSY, the NMSSM, Two-Higgs-Doublet Models

(2HDMs) and the Georgi-Machacek model. In particular, we investigate the dangers involved with the common habit of trading Lagrangian parameters for masses using tree-level relations in non-supersymmetric models, and we show that loop corrections grow out of control well before the naive perturbativity bounds on couplings are reached.

Finally, in a last chapter, we consider the high-scale behaviour of (non-supersymmetric) models with extended Higgs sectors. More specifically, we point out that the order at which couplings are extracted from the physical spectrum before being run with renormalisation group equations has strong effects on the values found at high energy scales, and thus on the high energy properties of the models. We illustrate this statement with both analytical and numerical results where the impact of the matching order is sizeable, in the context of three minimal extensions of the Standard Model: a singlet extension, a model with vector-like quarks, and finally a 2HDM.

# Automating Higgs precision calculations

## Résumé

L'étude des propriétés du boson de Higgs, découvert au Grand Collisionneur de Hadrons du CERN, représente une excellente opportunité pour la recherche de Nouvelle Physique. En particulier, la masse de ce boson est maintenant mesurée expérimentalement avec une précision impressionnante, de l'ordre de 0.1%, tandis qu'elle est également prédite par certains modèles au-delà du Modèle Standard, notamment les modèles supersymétriques. L'objectif de cette thèse est de faire avancer le calcul des corrections radiatives aux masses des bosons de Higgs dans les modèles au-delà du Modèle Standard, ainsi que l'automatisation de ces calculs, afin d'établir ou d'améliorer les limites sur les couplages entre la Nouvelle Physique et le boson de Higgs.

Un premier chapitre est consacré au calcul des corrections dominantes à deux boucles, de la forme  $\mathcal{O}(\alpha_s\alpha_t)$ , aux masses des scalaires neutres dans les modèles supersymétriques à jauginos de Dirac. Nous considérons à la fois des termes de masses de Dirac et de Majorana pour les jauginos (plus précisément les gluinos), et nous établissons des résultats pour des paramètres du secteur des tops/stops à la fois dans les schémas de renormalisations  $\overline{\text{DR}}'$  et “on-shell” (sur couche de masse). Les résultats analytiques que nous obtenons sont inclus dans des routines numériques disponibles publiquement, et constituent les premiers calculs explicites de corrections aux masses des bosons de Higgs à deux boucles dans des modèles supersymétriques au-delà du NMSSM.

Le sujet principal de cette thèse est l'étude de la Catastrophe des Bosons de Goldstone, un cas de divergences infrarouges dues aux bosons de Goldstones de masses nulles qui affecte les calculs de potentiels effectifs, d'équations de minimisation du potentiel (dites équations “tadpoles”) et d'énergies propres, ainsi que de comment surmonter ce problème. Nous étendons tout d'abord la procédure de resommation, développée récemment pour le Modèle Standard et appliquée au MSSM, pour obtenir des équations “tadpoles” finies pour des théories de champs renormalisables générales. Nous démontrons ensuite qu'en adoptant un schéma de renormalisation sur couche de masse pour les masses des bosons de Goldstone, l'obtention de ces résultats aurait été facilitée, et qu'il est aussi possible d'éliminer toutes les divergences infrarouges dans les calculs de masses de scalaires. Nous présentons une approximation du potentiel effectif généralisée permettant de trouver des expressions de corrections de masses libres de toute divergence infrarouge, ainsi qu'un développement perturbatif des paramètres de masses permettant de résoudre directement (plutôt qu'itérativement) les équations “tadpoles”.

Ensuite, nous illustrons la mise en œuvre numérique de notre solution à la Catastrophe

des Bosons de Goldstone dans le programme **SARAH**. Nous comparons les résultats que nous obtenons pour le Modèle Standard aux résultats existants, et trouvons un excellent accord. Nous étudions aussi de nouvelles corrections aux masses des bosons de Higgs en Split SUSY, dans le NMSSM, dans des modèles à deux doublets de Higgs, et dans le modèle de Georgi-Machacek. Nous nous intéressons notamment aux dangers encourus du fait du choix, habituel pour des modèles non-supersymétriques, d'échanger les paramètres du Lagrangien contre des masses en utilisant des relations à l'ordre des arbres, et nous montrons comment les corrections quantiques croissent hors de tout contrôle bien avant que les limites perturbatives habituelles (naïves) ne soit atteintes.

Finalement, nous considérons dans un dernier chapitre le comportement aux hautes énergies de modèles non-supersymétriques avec des secteurs scalaires étendus. Plus spécifiquement, nous montrons que l'ordre (en théorie des perturbations) auquel les couplages sont extraits du spectre de masse physique, avant d'être évolués avec les équations du groupe de renormalisation, a des effets importants sur les valeurs des couplages obtenues aux hautes énergies et par conséquent sur le comportement à ces énergies des modèles considérés. Nous illustrons cette position avec à la fois des résultats analytiques et numériques, dans le cadre d'extensions minimales du Modèle Standard : une extension avec un singlet, un modèle avec des quarks vectoriels, et finalement un modèle à deux doublets de Higgs.

# Abbreviations

<b>1PI</b>	One-Particle-Irreducible
<b>2HDM</b>	Two-Higgs-Doublet Model
<b>2PI</b>	Two-Particle-Irreducible
<b>BSM</b>	Beyond the Standard Model
$\overline{\text{DR}}'$	Modified Dimensional Reduction (Renormalisation Scheme)
<b>DRED</b>	Dimensional Reduction
<b>DREG</b>	Dimensional Regularisation
<b>EW</b>	Electroweak
<b>EWSB</b>	Electroweak Symmetry Breaking
<b>FCNC</b>	Flavour-Changing Neutral Current
<b>GUT</b>	Grand Unified Theory
<b>IR</b>	Infra-red
<b>LHC</b>	Large Hadron Collider
<b>LO</b>	Leading Order
<b>LSP</b>	Lightest Supersymmetric Particle
<b>MDGSSM</b>	Minimal Dirac Gaugino Supersymmetric Standard Model
<b>MRSSM</b>	Minimal R-symmetric Supersymmetric Standard Model
$\overline{\text{MS}}$	Modified Minimal Subtraction (Renormalisation Scheme)
<b>MSSM</b>	Minimal Supersymmetric Standard Model
<b>NMSSM</b>	Next-to-Minimal Supersymmetric Standard Model
<b>N(N)LO</b>	Next-to-(Next-to)-Leading Order
<b>OS</b>	On(-Mass)-Shell
<b>QCD</b>	Quantum Chromodynamics
<b>QED</b>	Quantum Electrodynamics
<b>QFT</b>	Quantum Field Theory

## *Abbreviations*

**RGE** Renormalisation Group Equation

**SLHA** Supersymmetry Les Houches Accord

**SM** Standard Model of Particle Physics

**SSB** Spontaneous Symmetry Breaking

**SSM** Singlet-extended Standard Model

**SUSY** Supersymmetry (or Supersymmetric)

**VEV** Vacuum Expectation Value

**VL** Vector-Like

# Contents

<b>Introduction</b>	<b>1</b>
<b>1 The Higgs boson and Physics beyond the Standard Model</b>	<b>5</b>
1.1 The Standard Model and the Higgs sector . . . . .	5
1.1.1 Mass terms of gauge bosons and fermions . . . . .	5
1.1.2 Electroweak Symmetry Breaking and the Brout-Englert-Higgs mechanism . . . . .	6
1.1.3 Electroweak gauge fixing . . . . .	9
1.1.4 The Higgs sector at tree-level and beyond . . . . .	11
1.1.5 The Goldstone Boson Catastrophe in the Standard Model . . . . .	15
1.2 Going beyond the Standard Model . . . . .	20
1.2.1 The hierarchy problem . . . . .	20
1.2.2 The stability of the electroweak vacuum . . . . .	22
1.2.3 Building models beyond the Standard Model . . . . .	23
1.3 Supersymmetry . . . . .	23
1.3.1 Some basics of SUSY . . . . .	24
1.3.1.1 Fermions in two-component notation	24
1.3.1.2 Supersymmetry, the SUSY algebra and its representations	25
1.3.1.3 Superspace formalism and superfields	26
1.3.1.4 Superpotential and supersymmetric Lagrangians	28
1.3.1.5 $R$ -symmetry	30
1.3.2 SUSY breaking . . . . .	31
1.3.3 The hierarchy problem and Supersymmetry . . . . .	34
1.3.4 Minimal models . . . . .	36
1.3.4.1 The Minimal Supersymmetric Standard Model	36
1.3.4.2 The Higgs sector of the MSSM	38
1.3.4.3 Gauginos in the MSSM	44
1.3.4.4 Shortcomings of the MSSM	44
1.3.4.5 The Next-to-Minimal Supersymmetric Standard Model	46
1.3.4.6 The Higgs sector of the NMSSM	48
1.3.5 Dirac gaugino models . . . . .	48

1.3.5.1	Extended Supersymmetry and supersoft SUSY breaking	50
1.3.5.2	A brief overview of Dirac gaugino models	51
1.3.5.3	Some aspects of the phenomenology of Dirac gaugino models	53
1.3.5.4	Properties of the adjoint scalars	54
1.3.5.5	Gluino masses and couplings	56
1.3.5.6	The MDGSSM and the MRSSM	57
1.4	Non-supersymmetric extensions of the Standard Model . . . . .	58
1.4.1	Singlet extensions of the Standard Model . . . . .	58
1.4.2	Two-Higgs-Doublet Models . . . . .	60
1.4.3	The Georgi-Machacek model . . . . .	62
<b>2</b>	<b>Precision calculations of the Higgs boson mass</b>	<b>65</b>
2.1	Measurements of the Higgs mass . . . . .	65
2.2	Scalar mass calculations . . . . .	65
2.2.1	Regularisation and renormalisation schemes . . . . .	66
2.2.2	Calculations beyond leading order and choice of inputs . . . . .	71
2.2.3	Different types of mass calculations . . . . .	72
2.2.3.1	Fixed-order calculations	72
2.2.3.2	The effective field theory approach	74
2.3	State-of-the-art of Higgs mass calculations . . . . .	75
2.3.1	Real and complex MSSMs . . . . .	76
2.3.1.1	Fixed-order results	76
2.3.1.2	EFT and hybrid results	79
2.3.2	Supersymmetric models beyond the MSSM . . . . .	81
2.3.3	Non-supersymmetric models . . . . .	82
2.4	Calculations in generic theories . . . . .	83
2.4.1	Notations for general field theories . . . . .	83
2.4.2	Two-loop neutral scalar masses in generic theories . . . . .	86
2.4.3	The SARAH/SPheno framework . . . . .	87
2.4.3.1	Analytic calculations with SARAH	87
2.4.3.2	Interfaces with SPheno and other HEP codes	88
2.4.3.3	Numerical set-up of the spectrum calculation	89
<b>3</b>	<b>Leading two-loop corrections to the Higgs boson masses in SUSY models with Dirac gauginos</b>	<b>93</b>
3.1	Two-loop corrections in the effective potential approach . . . . .	94
3.1.1	General results . . . . .	94
3.1.2	Two-loop top/stop contributions to the effective potential . . . . .	97
3.1.3	Mass corrections in the MDGSSM . . . . .	98
3.1.4	Mass corrections in the MRSSM . . . . .	100



3.1.5	On-shell parameters in the top/stop sector . . . . .	101
3.1.6	Obtaining the $\mathcal{O}(\alpha_b\alpha_s)$ corrections . . . . .	102
3.1.7	Simplified formulae . . . . .	103
3.1.7.1	Common SUSY-breaking scale . . . . .	103
3.1.7.2	MRSSM with heavy Dirac gluino . . . . .	104
3.2	Numerical examples . . . . .	107
3.2.1	An example in the MDGSSM . . . . .	108
3.2.2	An example in the MRSSM . . . . .	110
3.3	Conclusions . . . . .	113
<b>4</b>	<b>Avoiding the Goldstone Boson Catastrophe in general renormalisable field theories at two loops</b>	<b>115</b>
4.1	The Goldstone Boson Catastrophe and resummation . . . . .	117
4.1.1	Abelian Goldstone model . . . . .	117
4.1.2	Goldstone bosons in general field theories . . . . .	120
4.1.3	Small $m_G^2$ expansion of the effective potential for general theories	122
4.2	Removing infra-red divergences in the minimum condition . . . . .	124
4.2.1	All-scalar diagrams . . . . .	125
4.2.1.1	Elimination of the divergences by method (i) . . . . .	125
4.2.1.2	Elimination of the divergences by method (ii) . . . . .	126
4.2.1.3	Elimination of the divergences by setting the Goldstone boson on-shell	128
4.2.2	Diagrams with scalars and fermions . . . . .	130
4.2.3	Diagrams with scalars and gauge bosons . . . . .	130
4.2.4	Total tadpole . . . . .	131
4.3	Mass diagrams in the gaugeless limit . . . . .	133
4.3.1	All-scalar terms . . . . .	134
4.3.1.1	Goldstone shifts . . . . .	136
4.3.1.2	Momentum-regulated diagrams . . . . .	137
4.3.2	Fermion-scalar diagrams . . . . .	138
4.4	Self-consistent solution of the tadpole equations . . . . .	139
4.5	Conclusions . . . . .	142
<b>5</b>	<b>Supersymmetric and non-supersymmetric models without catastrophic Goldstone bosons</b>	<b>143</b>
5.1	The Goldstone Boson Catastrophe and its solutions . . . . .	144
5.1.1	Previous approaches in SARAH . . . . .	145
5.1.2	On-shell Goldstone bosons, consistent tadpole solutions, and the implementation in SARAH . . . . .	146
5.2	Standard Model . . . . .	148

5.2.1	A first comparison of our results with existing calculations . . . . .	148
5.2.2	A detailed comparative study of <b>SPheno</b> and <b>SMH</b> results . . . . .	150
5.2.3	Momentum dependence . . . . .	154
5.3	The NMSSM . . . . .	155
5.4	Split SUSY . . . . .	157
5.5	Two-Higgs-Doublet Model . . . . .	160
5.5.1	The alignment in Two-Higgs-Doublet Models . . . . .	160
5.5.2	Renormalisation scale dependence of the Higgs mass computed with <b>SPheno</b> . . . . .	161
5.5.3	Quantum corrections to the alignment limit . . . . .	163
5.5.4	Perturbativity constraints . . . . .	165
5.6	Georgi-Machacek Model . . . . .	166
5.7	Conclusions . . . . .	168
<b>6</b>	<b>Matching and running</b>	<b>171</b>
6.1	Matching and Running . . . . .	172
6.1.1	Renormalisation Group Equations . . . . .	172
6.1.2	Matching . . . . .	173
6.2	Models and results . . . . .	174
6.2.1	Singlet Extension . . . . .	174
6.2.2	Singlet Extension with an additional $\mathbb{Z}_2$ symmetry . . . . .	178
6.2.2.1	Analytical approximation	178
6.2.2.2	Numerical study	180
6.2.3	Vector-like quarks and stability of the SM . . . . .	183
6.2.4	Two-Higgs Doublet model . . . . .	186
6.3	Conclusions . . . . .	191
	<b>Conclusion</b>	<b>193</b>
<b>A</b>	<b>Derivatives of the two-loop effective potential in models with Dirac gauginos</b>	<b>197</b>
<b>B</b>	<b>Definitions and expansions of loop functions</b>	<b>199</b>
B.1	Loop functions . . . . .	199
B.1.1	Definition of loop functions . . . . .	199
B.1.1.1	One-loop functions	199
B.1.1.2	Two-loop functions	201
B.1.2	Small $m_G^2$ expansion . . . . .	203
B.2	Diagrams regulated by momentum . . . . .	204

B.2.1 Limits of the $Z$ and $U$ functions . . . . .	205
B.2.2 Limits of the $M$ function . . . . .	206
B.3 Additional expressions for $\tilde{V}(x, 0, z, u)$ . . . . .	207
B.3.1 Integral representation . . . . .	210
<b>C Consistent solution of the tadpole equations with shifts to fermion masses</b>	<b>211</b>
<b>Bibliography</b>	<b>213</b>
<b>List of Figures</b>	<b>237</b>



# Introduction

The discovery of a 125-GeV Higgs-boson-like particle at the Large Hadron Collider at CERN in 2012 has been a ground-breaking event for Particle Physics. Not only did it complete the field content of the Standard Model (SM), but it confirmed the role of Electroweak Symmetry Breaking (EWSB) as the origin of the masses of fermions and gauge bosons. However, the quest to understand the microscopic behaviour of Nature does not end here; indeed the Standard Model does not provide a quantum description of gravity, so at best it can only be valid up to the Planck scale  $M_{\text{Pl}} \sim 10^{19}$  GeV (at which effects from quantum gravity must be taken into account). Furthermore, a number of signs seem to point towards the existence of yet-unknown phenomena that would also be at play in electroweak (and strong) interactions. These include theoretical arguments such as the hierarchy problem, the question of the stability of the SM electroweak vacuum, the strong-CP problem, the possibility of gauge coupling unification, and the hierarchy between the Yukawa couplings. Additionally there also exist experimental results that are incompatible or conflicting with SM predictions: for example the existence of neutrino masses; the cosmological observations indicating the need for inflation, for dark energy, and for some mechanism to explain baryogenesis; the astrophysical evidence for dark matter; and tensions (some of them long-standing) coming from the measurement of precision observables, such as the muon anomalous moment, or more recently anomalies in  $B$ -physics. It is therefore very likely that the SM is only the manifestation at currently accessible energy scales of a more fundamental underlying theory – or in other words that the SM is an effective theory valid until some intermediate scale (*i.e.* between the Planck and electroweak scales) characterising the New Physics.

A tremendous number of Beyond-the-Standard-Model (BSM) theories have been devised to address some (or even all) of the deficiencies of the SM and must now be confronted with experimental results. Indeed, the search for BSM Physics has become one of the major endeavours of modern High-Energy Physics and, among the different possible avenues, one can distinguish between direct searches – *i.e.* trying to detect new particles or phenomena directly at experiments – or indirect searches, in other words investigating possible effects of unknown Physics at higher scales on the properties (often masses or couplings) of presently observed particles. So far, potential new particles have eluded observation. However, the finding of the Higgs boson has opened a new area for indirect searches through the study – both experimental and theoretical – of its properties. In particular, the Higgs boson mass  $m_h$  is now already measured to an exceptional level of precision – of the order of one per mille – while it is also predicted in certain BSM models.

A special class of BSM theories that exhibit a new type of symmetry relating bosonic and fermionic degrees of freedom – called *Supersymmetry* (SUSY) – stands out because of several theoretical and phenomenological advantages they offer: indeed, at the price of greatly extending the field content of the theory (of which the enriched

Higgs sector is then of particular interest), they can solve the hierarchy problem, allow gauge unification, provide candidates for dark matter particles, etc – to cite only a few of the positive features. Another feature of supersymmetric models, of central importance here, is the fact that because of the relations between parameters of the theory imposed by Supersymmetry, the quartic coupling of the Higgs boson, which controls its tree-level mass, is actually determined in terms of the other couplings of the theory (including the electroweak gauge couplings), unlike what is the case for instance in the SM. The physical mass of the Higgs boson can then be evaluated by adding, to the known tree-level value, quantum (or *radiative*) corrections that are computed in the regime of perturbation theory, and it is therefore a *prediction* of these models. As the radiative corrections to the Higgs mass involve, in principle, all particles that couple to the Higgs, the comparison between the experimentally measured value and the theoretical prediction for  $m_h$  can constrain a large part of (if not the whole of) the physical spectrum of the theory. This situation, combined with the realisation in the early 1990's that the predicted Higgs mass could be compatible with early experimental bounds, has triggered an active and long-lasting interest in the calculation of corrections to the mass of the Higgs boson, in the context of minimal supersymmetric extensions of the SM – *i.e.* the Minimal Supersymmetric Standard Model (MSSM), and the Next-to-Minimal Supersymmetric Standard Model (NMSSM). Similar computations have also been performed in the SM itself, especially in recent years, because they allow a precise extraction of the Higgs quartic coupling from its measured mass in order to investigate the fate of the electroweak vacuum.

However, the field of Higgs mass calculations in BSM (SUSY) models is currently confronted with a number of challenges. Among them, one can first mention the fact that the accuracy to which the lightest Higgs mass is computed is quite far from the precision with which it is measured experimentally: the theoretical uncertainty is at best of the order of a few GeV in the MSSM, which has been studied extensively, but is much larger for other models where fewer corrections are known. Another issue is that the minimal SUSY models that have been studied most (especially the MSSM) are becoming increasingly unnatural and therefore less attractive, thus increasing the need to improve predictions in numerous other extensions of the SM. The aim of this thesis is to participate in addressing these problems, and to increase the number of models in which precise results for Higgs masses are available. We have done so in two different but complementary approaches, working both on explicit calculations of new corrections in particular (non-minimal supersymmetric) models and on computations for general renormalisable theories.

We begin this thesis with two introductory chapters that aim to provide a (pedagogical) overview of the physical and technical setting in which the work presented here has been carried out. In the first of these two chapters, we start by recalling basic notions of the Standard Model and its Higgs sector, before turning to the effect of quantum corrections on the SM Higgs sector. This allows us to introduce the Goldstone Boson Catastrophe, which will be one of the central topics in the thesis, as well as to illustrate the need for some BSM Physics that would couple to the Higgs. Afterwards, we present the different BSM models relevant for this thesis: on the one hand, the framework of Supersymmetry and phenomenological SUSY models; and on the other hand, minimal extensions of the SM with enlarged Higgs sectors. The second introduction chapter is dedicated to a review of precision calculations of Higgs boson masses. After discussing technical points, such as renormalisation schemes and the different possible approaches to computing mass corrections, we review existing results in BSM models – in particular in supersymmetric ones – and we end the chapter by presenting the formalism and the

tools that we will employ for generic calculations.

The third chapter is devoted to a particular class of supersymmetric theories, namely models with Dirac gauginos. These models have been receiving growing interest in recent years because of their rich phenomenology, of which some of the most favourable features are: *(i)* the possibility to evade both current limits on the detection of squarks (via the suppression of the production rates of coloured particles) and constraints from flavour physics; and *(ii)* the increased naturalness of these models – due to an enhancement of the lightest Higgs mass at tree level and to the milder dependence of corrections to scalar masses on gaugino masses. We perform the first explicit calculation of two-loop corrections to Higgs masses in theories beyond the NMSSM by deriving the leading  $\mathcal{O}(\alpha_t\alpha_s)$  contributions in general Dirac gaugino models, using the effective potential technique. We then apply our results to the special cases of the MDGSSM and the MRSSM, two of the most popular Dirac gaugino models, and we also provide approximate expressions in several phenomenologically relevant limits. Moreover, we obtain corrections in terms of top/stop sector parameters renormalised either in an on-shell (OS) scheme and in the  $\overline{\text{DR}}'$  scheme, and we observe how the OS scheme avoids the appearance of large logarithmic contributions leading to a loss of accuracy, or even of perturbativity, when gluinos become much heavier than stops. Finally, by varying the scheme of the top/stop sector inputs, and by changing the determination of the strong gauge coupling, we are able to estimate the theoretical uncertainty of our results.

In the following chapters, we turn to generic calculations – *i.e.* for general renormalisable models – and investigate more specifically the Goldstone Boson Catastrophe and its solution. This catastrophe is a case of infra-red divergence that plagues calculations of effective potentials, tadpole equations, and even self-energies in the SM and most BSM models. It arises because of the masses of the Goldstone bosons, which may run across zero under renormalisation group flow. This problem is especially severe and visible in the Landau gauge, where Goldstones have a vanishing tree-level mass, but this is also the gauge in which many two-loop results for generic theories have been derived (in  $\overline{\text{MS}}/\overline{\text{DR}}'$  renormalisation scheme), as it allows simpler calculations. Therefore, we wish to address the problem in the Landau gauge so as to obtain infra-red-safe versions of these existing expressions. This is the subject of the fourth chapter, where at first we generalise a resummation procedure that had been recently devised and employed for the SM and the MSSM, before finding a new solution by using an OS renormalisation for the Goldstone boson masses – in practice, we find modified expressions for some of the loop functions that appear in tadpoles. Furthermore, for the self-energy diagrams, we combine our “on-shell Goldstone” prescription with a generalised effective potential approximation (which we also devise) to obtain easily calculable divergence-free expressions for the relevant loop functions. Lastly, we also provide a way to solve loop-corrected tadpole equations directly instead of iteratively.

In the fifth chapter, we implement our modified loop functions in the public code **SARAH**, opening the way for two-loop evaluations of neutral scalar (Higgs) masses in non-supersymmetric models – including the SM – with **SARAH** generated **SPheno** spectrum generators. These were previously impossible because of the Goldstone Boson Catastrophe, and of the absence of any work-around in **SARAH** that could be applied outside supersymmetric models. We first compare the Higgs mass found by **SARAH/SPheno** in the SM to the state-of-the-art results (complete two-loop calculations), and find a remarkable agreement. Then, we turn to the NMSSM and illustrate how our solution to the Goldstone Boson Catastrophe indeed eliminates the numerical instabilities

in existing calculations in SUSY. Afterwards, we consider more BSM models – both supersymmetric (Split SUSY), and non-supersymmetric (Two-Higgs-Doublet Models and the Georgi-Machacek model) – and investigate previously unknown two-loop corrections to scalar masses. In particular, we point out the dangers associated with the common habit of using only tree-level relations to extract Lagrangian couplings from the mass spectrum in non-SUSY BSM models.

Finally, in the last chapter, we continue to study the behaviour of non-supersymmetric models, focusing more precisely on how the order in perturbation theory at which the scalar quartic couplings are extracted at a low scale from the mass spectrum affects the high-scale behaviour of the models – *i.e.* the possibility of an instability of the electroweak vacuum, or of a loss of perturbativity or unitarity. We consider three different non-SUSY extensions of the SM – namely a singlet extension, an extension with vector-like quarks and a Two-Higgs-Doublet Model. We show that the threshold corrections to the quartic couplings at low scales can be significant, and moreover can have important effects after running the couplings to high scales. We therefore advocate employing a loop-corrected matching together with two-loop RGEs, which is possible using the corrections available in SARAH/SPheno.

*For the reader's convenience, a list of abbreviations is provided on page xi in the preface, and the definitions of all the loop functions that are used can be found in appendix B.1.1. Let us mention here also that we shall, throughout this thesis, follow the Einstein convention on summation of repeated indices (unless otherwise mentioned), and that we will sometimes refer to mass-squared parameters simply as masses (thereby committing a slight, but common, abuse) when there is no risk of ambiguity.*

This thesis is based on the following publications:

- [1] Johannes BRAATHEN, Mark GOODSSELL and Pietro SLAVICH, *Leading two-loop corrections to the Higgs boson masses in SUSY models with Dirac gauginos*. JHEP **09** (2016) 045, [arXiv:1606.09213 \[hep-ph\]](#),

that corresponds in most part to chapter 3;

- [2] Johannes BRAATHEN and Mark GOODSSELL, *Avoiding the Goldstone Boson Catastrophe in general renormalisable field theories at two loops*. JHEP **12** (2016) 056, [arXiv:1609.06977 \[hep-ph\]](#),

and

- [3] Johannes BRAATHEN, Mark GOODSSELL and Florian STAUB, *Supersymmetric and non-supersymmetric models without catastrophic Goldstone bosons*. Eur. Phys. J. C **11** (2017) 77: 757, [arXiv:1706.05372 \[hep-ph\]](#),

that constitute chapters 4 and 5; and finally

- [4] Johannes BRAATHEN, Mark GOODSSELL, Manuel KRAUSS, Toby OPFERKUCH and Florian STAUB, *N-loop running should be combined with N-loop matching*. Phys. Rev. D **97**, 015011, [arXiv:1711.08460 \[hep-ph\]](#),

corresponding to chapter 6.



# Chapter 1

## The Higgs boson and Physics beyond the Standard Model

This chapter aims at providing a brief overview of Physics in the Higgs sector, in the Standard Model as well as in the models of new Physics that will be studied in the course of this thesis.

### 1.1 The Standard Model and the Higgs sector

The Standard Model (SM) of Particle Physics is currently the most successful theory of the fundamental interactions of Nature, unifying the descriptions of the strong, electromagnetic, and weak forces and of matter, as an  $SU(3)_C \times SU(2)_L \times U(1)_Y$  gauge theory. Matter fields are divided between quarks, which are charged under colour *i.e.* under  $SU(3)_C$ , and leptons, which are not. The study of the dynamics of quarks and gluons, the gauge bosons of  $SU(3)_C$ , is an immensely rich field by itself – Quantum Chromodynamics (QCD) – that will not be considered in this thesis. Note, however, that coloured particles – in particular top quarks (and in supersymmetric models their superpartners, the stops) – will still have effects on Higgs Physics. The remaining  $SU(2)_L \times U(1)_Y$  part constitutes the electroweak (EW) sector of the Standard Model, also referred to as the Glashow-Weinberg-Salam (GWS) model.

#### 1.1.1 Mass terms of gauge bosons and fermions

The first step in the theoretical construction of the Standard Model is to find a way to accommodate in the framework of a gauge – and therefore renormalisable – theory the weak interaction, observed from the 1930's and described first by the non-renormalisable Fermi theory. Some weak interaction processes, such as the muon decay to an electron

$$\mu^- \rightarrow e^- \nu_\mu \bar{\nu}_e$$

involve flavour changing charged currents and must therefore be mediated by charged gauge bosons  $W^\pm$ . A natural choice of gauge group from which charged gauge bosons could be obtained is  $SU(2)$ , but it cannot be considered by itself because it can be shown that the neutral gauge boson associated with the third generator of  $SU(2)$  is not the photon. An additional  $U(1)$  group, with the weak hypercharge  $Y$  as its associated quantum number, thus needs to be introduced so that one can recover the photon among the gauge bosons, to ensure that QED is contained within the SM. However,

an important problem then arises from the requirement that all but one of the gauge bosons associated with the  $SU(2) \times U(1)_Y$  gauge group be massive. Indeed, the weak interactions only have a very short range, meaning that their mediators must be very massive, but the gauge symmetry forbids mass terms, as we can illustrate in the simple case of the gauge boson  $B_\mu$  of  $U(1)_Y$ :

- (i) under a  $U(1)_Y$  gauge transformation  $\beta(x)$ ,  $B_\mu$  transforms as

$$B_\mu(x) \xrightarrow{\beta(x)} B_\mu(x) - \frac{1}{q} \partial_\mu \beta(x) \quad (1.1.1)$$

Skipping a little ahead, one could easily show that requiring the gauge covariance of eq. (1.1.9) gives  $q = Y_\Phi g'$ .

- (ii) if then we had a mass term for  $B_\mu$ , it would transform as

$$\frac{1}{2} m_B^2 B_\mu B^\mu \xrightarrow{\beta(x)} \frac{1}{2} m_B^2 B_\mu B^\mu - \frac{m_B^2}{q} B^\mu \partial_\mu \beta + \frac{m_B^2}{2q^2} \partial_\mu \beta \partial^\mu \beta \neq \frac{1}{2} m_B^2 B_\mu B^\mu \quad (1.1.2)$$

which clearly shows that gauge invariance would be broken by a mass term for  $B$ . Similarly, the same applies to the gauge bosons of  $SU(2)_L$  that cannot have mass terms either.

Furthermore, the violation of parity in weak interactions (discovered in the 1950's) means that only fermions of left-handed helicities couple to the  $SU(2)$  gauge bosons – and for this reason the  $SU(2)$  gauge group is denoted with a lower index  $L$ . In turn, this means fermions are *chiral*, *i.e.* transform differently under  $SU(2)_L \times U(1)_Y$  gauge transformations depending on their left- or right-handed helicity. However then, any mass term of a fermion  $\psi$  (lepton or quark), that could be written

$$-m_\psi \bar{\psi} \psi = -m_\psi (\bar{\psi}_L \psi_R + \bar{\psi}_R \psi_L) \quad (1.1.3)$$

would also be forbidden because it would break gauge invariance. It is also sometimes said that *chiral symmetry* protects fermion masses as it is the different behaviour of left- and right-handed helicities that makes mass terms non-gauge-invariant.

### 1.1.2 Electroweak Symmetry Breaking and the Brout-Englert-Higgs mechanism

The solution to these two problems relies on the mechanism invented in 1964 by Brout and Englert [5] and by Higgs [6, 7], for which a complex scalar  $\Phi$ , transforming in the  $(\mathbf{1}, \mathbf{2}, \frac{1}{2})$  representation of the SM gauge group, is added to the theory together with a potential that allows the spontaneous breaking of electroweak gauge group

$$SU(2)_L \times U(1)_Y \xrightarrow{SSB} U(1)_{\text{QED}}.$$

Let us now illustrate how spontaneous symmetry breaking occurs in the electroweak sector and how this yields masses for gauge bosons and fermions. First, the Higgs doublet  $\Phi$  can be written

$$\Phi = \begin{pmatrix} G^+ \\ \frac{1}{\sqrt{2}}(v + h + iG^0) \end{pmatrix} \quad (1.1.4)$$

with  $v$  the Higgs vacuum expectation value (VEV),  $h$  the physical Higgs state, and  $G^\pm$  and  $G^0$  respectively the charged and neutral would-be Goldstone bosons.<sup>1</sup> For convenience, we use some of the freedom that we are given by the gauge symmetry to rotate away any phase of the Higgs VEV, thereby ensuring that  $v$  is real and non-negative. The Higgs potential  $V^{(0)}$  is taken<sup>2</sup> to be

$$V^{(0)}(\Phi) = \mu^2 |\Phi|^2 + \lambda |\Phi|^4, \quad (1.1.5)$$

where  $\mu^2$  is the *Higgs mass term* and  $\lambda$  the *Higgs quartic coupling*. As the potential need to be bounded from below, the Higgs quartic coupling must be non-negative (actually, it must even be positive if  $\mu^2$  is negative). One can then easily find the minimisation condition of the scalar potential, also called the *tadpole equation*,

$$\left. \frac{\partial V^{(0)}}{\partial h} \right|_{\phi=0} = 0 = (\mu^2 + \lambda v^2)v. \quad (1.1.6)$$

where we use  $\phi = 0$  as a shorthand notation for  $\{h = 0, G^0 = 0, G^\pm = 0\}$ . If  $\mu^2$  (and  $\lambda$ ) are positive, this equation admits only one solution

$$v = 0,$$

and the electroweak gauge symmetry is not broken (this is the unbroken, or symmetric, phase of the SM). However, if  $\mu^2$  is negative, eq. (1.1.6) also admits the solution

$$\mu^2 + \lambda v^2 = 0 \quad \Rightarrow \quad v = \sqrt{\frac{-\mu^2}{\lambda}} > 0. \quad (1.1.7)$$

Furthermore, it is then straightforward to verify that the solution with  $v > 0$  is then the true minimum of the potential, while the solution  $v = 0$  corresponds to an unstable local maximum of the potential. The non-zero value of the Higgs VEV breaks the  $SU(2)_L \times U(1)_Y$ : this is the broken phase of the SM. Because the VEV does not carry electric charge, a residual  $U(1)$  symmetry is preserved in the minimum of the potential, corresponding to the gauge symmetry of QED. The spontaneous breaking of the EW gauge symmetry  $SU(2)_L \times U(1)_Y$  down to the gauge symmetry of QED  $U(1)_{\text{QED}}$ , realised by the Higgs VEV, is called the *electroweak symmetry breaking* (EWSB). Finally, the Higgs VEV can be related to the measured Fermi constant by matching the electroweak sector of the SM onto the Fermi theory at low energies, and one finds

$$v = \frac{1}{\sqrt{\sqrt{2}G_F}} \simeq 246.22 \text{ GeV}. \quad (1.1.8)$$

When considering the gauge bosons  $W_\mu^a$  and  $B_\mu$ , respectively of the groups  $SU(2)_L$  and  $U(1)_Y$ , we obtain for the covariant derivative of  $\Phi$

$$(D_\mu \Phi)_i = \partial_\mu \Phi_i - ig W_\mu^a \frac{\sigma_{ij}^a}{2} \Phi_j - iY_\Phi g' B_\mu \Phi_i, \quad (1.1.9)$$

---

<sup>1</sup>As we will see in what follows, Goldstones do not remain part of the physical spectrum after the electroweak symmetry breaking, therefore they should in principle always be referred to as would-be Goldstone bosons. However, there is almost never any confusion possible with real Goldstone bosons from a spontaneously broken global symmetry, so we will very often to them as Goldstone bosons, in a slightly abusive way.

<sup>2</sup>The “(0)” upper index denotes a tree-level quantity – this will become clearer in section 1.1.4.

where  $g'$  ( $g$ ) is the gauge coupling for  $U(1)_Y$  ( $SU(2)_L$ ),  $Y_\Phi = \frac{1}{2}$  is the Higgs doublet hypercharge,  $i, j$  are  $SU(2)_L$  indices and  $\sigma^a$  are the Pauli matrices

$$\sigma^1 = \begin{pmatrix} 0 & 1 \\ 1 & 0 \end{pmatrix}, \quad \sigma^2 = \begin{pmatrix} 0 & -i \\ i & 0 \end{pmatrix}, \quad \sigma^3 = \begin{pmatrix} 1 & 0 \\ 0 & -1 \end{pmatrix}. \quad (1.1.10)$$

If we now expand the gauge-invariant kinematic term for the Higgs doublet

$$\begin{aligned} |D_\mu \Phi|^2 &\supset \partial_\mu G^+ \partial^\mu G^- + \frac{1}{2}(\partial_\mu h)^2 + \frac{1}{2}(\partial_\mu G^0)^2 \\ &+ \frac{1}{4}g^2 v^2 \left( \frac{W_\mu^1 - iW_\mu^2}{\sqrt{2}} \right) \left( \frac{W_\mu^1 + iW_\mu^2}{\sqrt{2}} \right) + \frac{1}{8}(g'^2 + g^2)v^2 \left( \frac{gW_\mu^3 - g'B_\mu}{\sqrt{g'^2 + g^2}} \right)^2 \\ &+ \mathcal{L}_{\phi\phi V} + \mathcal{L}_{\phi V V} + \mathcal{L}_{\phi\phi V V} + \dots \end{aligned} \quad (1.1.11)$$

$\mathcal{L}_{\phi\phi V}$ ,  $\mathcal{L}_{\phi V V}$ , and  $\mathcal{L}_{\phi\phi V V}$  contain interaction terms between the scalars and the gauge bosons that we will not expand here. With the simple field redefinition

$$W_\mu^\pm \equiv \frac{W_\mu^1 \mp iW_\mu^2}{\sqrt{2}}, \quad Z_\mu \equiv \frac{gW_\mu^3 - g'B_\mu}{\sqrt{g'^2 + g^2}}, \quad (1.1.12)$$

we can rewrite the second line of equation (1.1.11) as

$$|D_\mu \Phi|^2 \supset \frac{1}{4}g^2 v^2 W_\mu^+ W_\mu^- + \frac{1}{8}(g'^2 + g^2)v^2 Z_\mu Z^\mu. \quad (1.1.13)$$

Through the EWSB the would-be Goldstone bosons  $G^\pm$  and  $G^0$  become longitudinal components of the gauge bosons  $W^\pm$  and  $Z$ , which then acquire masses  $m_W = \frac{1}{2}gv$  and  $m_Z = \frac{1}{2}\sqrt{g^2 + g'^2}v$  respectively.<sup>3</sup> This is the *Brout-Englert-Higgs mechanism* [5–7]. One last vector boson state, orthogonal to  $Z_\mu$  in field space

$$A_\mu \equiv \frac{g'W_\mu^3 + gB_\mu}{\sqrt{g^2 + g'^2}}, \quad (1.1.14)$$

remains massless, and is the photon – *i.e.* the gauge boson of  $U(1)_{\text{QED}}$ . The transformation from  $\{W_\mu^3, B_\mu\}$  to  $\{Z_\mu, A_\mu\}$  can be seen as a rotation of angle  $\theta_W$ , the Weinberg (or weak mixing) angle, defined by

$$\tan \theta_W = \frac{g'}{g}. \quad (1.1.15)$$

The Weinberg angle also relates the couplings  $g'$ ,  $g$  to the electric charge  $e$  of the electron

$$e = g' \cos \theta_W = g \sin \theta_W = \frac{gg'}{\sqrt{g^2 + g'^2}}. \quad (1.1.16)$$

Fermions also obtain masses from the scalar sector, via Yukawa interactions that are added by hand in the SM. Quarks and leptons come in both left-handed and right-handed helicities, and it is known from experiments that  $W$  bosons only couple to left-handed fermions. Therefore, fermions of different helicities come in different representations of  $SU(2)_L$  – singlet for right-handed fermions and doublet for left-handed ones – as shown in table 1.1.

---

<sup>3</sup>This would be especially clear in the unitary gauge, in which the Goldstone bosons would not appear any more after the EWSB. However, the unitary gauge is a very inconvenient choice for calculations, and we will use instead  $R_\xi$  gauges, as will be discussed in what follows.

Quarks	$Q_{fL} = (u_{fL}, d_{fL})$	$(\mathbf{3}, \mathbf{2}, \frac{1}{6})$
	$u_{fR}$	$(\mathbf{3}, \mathbf{1}, \frac{2}{3})$
	$d_{fR}$	$(\mathbf{3}, \mathbf{1}, -\frac{1}{3})$
Leptons	$L_{fL} = (\nu_{fL}, e_{fL})$	$(\mathbf{1}, \mathbf{2}, -\frac{1}{2})$
	$e_{fR}$	$(\mathbf{1}, \mathbf{1}, -1)$

Table 1.1 – Fermions and their representations under the SM gauge group  $SU(3)_C \times SU(2)_L \times U(1)_Y$ .  $f = 1, 2, 3$  is the family index. Indices  $L$  and  $R$  denote respectively left- and right-handed states.

With these assignments, gauge-invariant Yukawa terms can be written for the fermions as

$$\mathcal{L} \supset -Y_e^{fg}(\bar{L}_{fL})_i \Phi_i e_{gR} - Y_d^{fg}(\bar{Q}_{fL})_i \Phi_i d_{gR} - Y_u^{fg} \epsilon^{ij}(\bar{Q}_{fL})_i \Phi_j^\dagger u_{gR} + \text{h.c.}, \quad (1.1.17)$$

where  $\epsilon^{ij}$  is the antisymmetric tensor. Note that, by construction, the SM does not accommodate neutrino masses and that there is no right-handed neutrino. The observation of neutrino oscillations by the Super-Kamiokande collaboration is a clear experimental evidence that neutrinos (at least from two of the three families) are massive and therefore that there must exist some Physics beyond the SM in the EW sector. However, it is possible to extend the SM in relatively minimal ways to generate small neutrino masses (via *e.g.* the seesaw mechanism), but this lies beyond the scope both of this introduction and of this thesis, and will not be discussed more here.

### 1.1.3 Electroweak gauge fixing

Something we have not considered yet is how to quantise the  $SU(2)_L \times U(1)_Y$  theory. At this point, the choice of gauge needs to be taken into consideration because the functional integration of the path integral must be done while still obeying the gauge-fixing condition. This is possible when following the quantisation procedure of Faddeev and Popov [8], which will introduce gauge-dependent terms in the Lagrangian.

As mentioned above, a first possible choice of gauge – the *unitary gauge* – has the advantage of eliminating the Goldstones altogether from the Lagrangian. However, it causes at the same time great complications to calculations in perturbation theory, therefore we will use instead  $R_\xi$  gauges, which will prove to be significantly more convenient. Following the Faddeev-Popov procedure [8], the gauge-fixing terms for  $SU(2)_L$  and  $U(1)_Y$  are found to be

$$\begin{aligned} \mathcal{G}_{SU(2)_L}^\pm &= \frac{1}{\sqrt{\xi}} \left( \partial^\mu W_\mu^\pm \mp i\xi \frac{g}{2} v G^\pm \right) \\ \mathcal{G}_{SU(2)_L}^3 &= \frac{1}{\sqrt{\xi}} \left( \partial^\mu W_\mu^3 - \xi \frac{g}{2} v G^0 \right) \\ \mathcal{G}_{U(1)_Y} &= \frac{1}{\sqrt{\xi}} \left( \partial^\mu B_\mu + \xi \frac{g'}{2} v G^0 \right) \end{aligned} \quad (1.1.18)$$

and then we add to the Lagrangian additional terms

$$\begin{aligned}
\mathcal{L} \supset & -\mathcal{G}_{SU(2)_L}^+ \mathcal{G}_{SU(2)_L}^- - \frac{1}{2} \left( (\mathcal{G}_{SU(2)_L}^3)^2 + (\mathcal{G}_{U(1)_Y})^2 \right) \\
& = -\frac{1}{\xi} \left( \partial^\mu W_\mu^+ \partial^\nu W_\nu^- + \frac{1}{2} (\partial^\mu W_\mu^3)^2 + \frac{1}{2} (\partial^\mu B_\mu)^2 \right) \\
& \quad - \frac{i}{2} g v (\partial^\mu W_\mu^+ G^- - \partial^\mu W_\mu^- G^+) + \frac{1}{2} v G^0 (g \partial^\mu W_\mu^3 - g' \partial^\mu B_\mu) \\
& \quad - \xi \frac{g^2}{4} v^2 G^+ G^- - \xi \frac{g'^2 + g^2}{8} v^2 (G^0)^2
\end{aligned} \tag{1.1.19}$$

The gauge fixing (1.1.18) was actually chosen in such a way that the resulting terms in the third line of eq. (1.1.19) would exactly cancel terms like  $v \partial^\mu G^+ W_\mu^-$  or  $v \partial^\mu G^0 Z_\mu$  that appear in the expansion of  $|D_\mu \Phi|^2$ . The terms in the fourth line of eq. (1.1.19) give gauge-dependent contributions to the Goldstone masses, and will be considered as part of the scalar potential.

The Faddeev-Popov procedure also requires the introduction of *ghosts*  $\omega^a, \bar{\omega}^b$  and one can show that they obtain a Lagrangian

$$\mathcal{L}_{\text{ghosts}} = \bar{\omega}^a \left[ -(\partial_\mu D^\mu)^{ab} - \xi \frac{g^2}{4} \sigma_{ij}^a \langle \Phi_j \rangle \sigma_{ik}^b \Phi_k - i \xi \frac{g'^2}{8} v G^0 \delta^{ab} \right] \omega^b \tag{1.1.20}$$

We see from the second and third terms in the above equation that the ghosts couple to the scalar sector. It is then convenient to fix  $\xi = 0$  to avoid couplings between scalars and ghosts: this is the *Landau gauge*. Note that this does not prevent purely gauge couplings between ghosts and gauge bosons, coming from the  $(\partial_\mu D^\mu)^{ab}$  operator in the ghost Lagrangian. In the Landau gauge, the gauge boson propagator becomes [9]

$$\begin{aligned}
\left( \Delta_\xi^{\mu\nu} \right)^{ab} &= \left( \frac{-i}{k^2 - m^2} \left[ g^{\mu\nu} - \frac{k^\mu k^\nu}{k^2 - \xi m^2} (1 - \xi) \right] \right)^{ab} \\
&\rightarrow \left( \Delta_{\xi=0}^{\mu\nu} \right)^{ab} = \left( \frac{-i}{k^2 - m^2} \right)^{ab} \left[ g^{\mu\nu} - \frac{k^\mu k^\nu}{k^2} \right].
\end{aligned} \tag{1.1.21}$$

Another popular gauge choice is the *Feynman gauge*  $\xi = 1$ , which makes the gauge boson propagator even simpler

$$\left( \Delta_{\xi=1}^{\mu\nu} \right)^{ab} = \left( \frac{-i g^{\mu\nu}}{k^2 - m^2} \right)^{ab}. \tag{1.1.22}$$

The Landau and Feynman gauges are probably the two most common choices in the context of perturbative calculations and throughout this thesis we will use these gauges exclusively. Unless otherwise specified, analytic expressions will be given in the Landau gauge although, on the other hand, numerical calculations in the **SARAH/SPHeno** framework – that we will present in chapter 2 – are performed in Feynman gauge.

Finally, note that in the limit  $\xi \rightarrow \infty$ , the Goldstone bosons decouple entirely from the theory and can be eliminated from the Lagrangian: this is the quantised realisation of the unitary gauge [9].

### 1.1.4 The Higgs sector at tree-level and beyond

The tree-level scalar masses are defined as the second derivatives of the potential with respect to the scalar fields:

$$\begin{aligned} (m_h^2)^{\text{tree}} &= \left. \frac{\partial^2 V^{(0)}}{\partial h^2} \right|_{\phi=0} = \mu^2 + 3\lambda v^2 \\ (m_G^2)^{\text{tree}} &= \left. \frac{\partial^2 V^{(0)}}{\partial (G^0)^2} \right|_{\phi=0} = \mu^2 + \lambda v^2 + \xi m_Z^2 = \mu^2 + \lambda v^2 \\ (m_{G^\pm}^2)^{\text{tree}} &= \left. \frac{\partial^2 V^{(0)}}{\partial G^+ \partial G^-} \right|_{\phi=0} = \mu^2 + \lambda v^2 + \xi m_W^2 = \mu^2 + \lambda v^2 \end{aligned} \quad (1.1.23)$$

where the  $\xi$ -dependent terms come from the part of the gauge-fixing terms – equation (1.1.19) – that we have absorbed in the scalar potential  $V^{(0)}$  (see the discussion below eq. (1.1.19)). The last equalities for  $(m_G^2)^{\text{tree}}$  and  $(m_{G^\pm}^2)^{\text{tree}}$  follow from our choice to work in the Landau gauge  $\xi = 0$ .<sup>4</sup> One can notice that the Goldstone boson masses are gauge dependent, however, this is not a problem because the Goldstones are not physical degrees of freedom, having been absorbed by the gauge bosons. Moreover, one can obtain the tree-level masses in the minimum of the potential by imposing the minimum condition (1.1.7) and these read

$$(m_h^2)^{\text{tree}} = 2\lambda v^2, \quad \text{and} \quad (m_G^2)^{\text{tree}} = (m_{G^\pm}^2)^{\text{tree}} = 0. \quad (1.1.24)$$

Until now our discussion has remained only at tree-level, *i.e.* we have not been taking into account *quantum corrections*. Now that we have quantised the theory, we do not expect physical observables to be equal to results of tree-level calculations, but of loop-corrected ones. The works presented in this thesis are done in the regime of perturbation theory, *i.e.* when there is a small parameter (a coupling) with which one can perform a series expansion of the quantum corrections, and physical quantities or observables can then be written as

$$\Theta_{\text{obs}} = \Theta^{(0)} + \frac{1}{16\pi^2} \Theta^{(1)} + \frac{1}{(16\pi^2)^2} \Theta^{(2)} + \dots = \sum_{n=0}^{\infty} \frac{1}{(16\pi^2)^n} \Theta^{(n)} \quad (1.1.25)$$

where  $\Theta^{(n)}$  denotes the  $n$ -loop correction to  $\Theta$ .

First, we can consider the quantum corrections to the scalar potential, which are contained in the *effective potential*, defined as follows (see *e.g.* [11]):

- (i) for a theory with scalars  $\{\phi_i\}$ , one starts with the generating functional of the theory (analogous to a partition function), with a set of external sources  $J_i$

$$Z(\{J_i(x)\}) = \int \prod_i \mathcal{D}\phi_i(x) \exp \left[ i \int d^4x \left( \mathcal{L}(\{\phi_i(x)\}) + J_i(x) \phi_i(x) \right) \right] \quad (1.1.26)$$

- (ii) from  $Z$ , one can then define the generating functional of connected graphs  $W$

$$W(\{J_i(x)\}) = -i \log Z(\{J_i(x)\}) \quad (1.1.27)$$

---

<sup>4</sup>Note also that when we introduce quantum corrections, the value of the gauge parameter  $\xi$  in the Landau gauge is not renormalised and remains 0 – see *e.g.* [10].

- (iii) The next step is to perform a Legendre transform in order to obtain the *effective action*  $\Gamma$ , *i.e.* the generating functional of one-particle-irreducible (1PI) graphs

$$\Gamma(\{\bar{\phi}_i(x)\}) \equiv W(\{J_i(x)\}) - \int d^4x \bar{\phi}_i(x) J_i(x), \text{ where } \bar{\phi}_i(x) \equiv \frac{\delta W(\{J_i\})}{\delta J_i(x)}. \quad (1.1.28)$$

- (iv) It is common to further impose translational invariance of the  $\bar{\phi}_i$ , and then one finds

$$\Gamma(\{\bar{\phi}_i\}) = -V_{\text{eff}}(\{\bar{\phi}_i\}) \int d^4x. \quad (1.1.29)$$

This last new object  $V_{\text{eff}}$  is the *effective potential*. Note that because the fields  $\bar{\phi}_i$  have been required to be invariant under space-time translations, they are often referred to as *background fields*.

One can show, following for example [11], that the one-loop contribution to  $V_{\text{eff}}$  is given by the *supertrace formula*

$$V^{(1)} = \frac{1}{4} \text{STr}[M^4(\overline{\log} M^2 - \delta)], \quad (1.1.30)$$

with the supertrace defined as

$$\text{STr}[M^2] \equiv \sum_s (-1)^{2s} (2s+1) \text{Tr}[M_s^2], \quad (1.1.31)$$

where  $s = 0, \frac{1}{2}, 1$  are the possible values of the spin of the particle – scalar, fermion or gauge boson – that gives a contribution to  $V_{\text{eff}}$ , and with  $M_s^2$  the mass-squared matrix of the corresponding particle. The function  $\overline{\log} x$  denotes (see also eq. (B.1.2))

$$\overline{\log} x \equiv \log \frac{x}{Q^2}, \quad (1.1.32)$$

where  $Q$  is the *renormalisation scale*. Both the regularisation and the renormalisation of loop integrals will be discussed in section 2.2.1, and we will also show there how the renormalisation scale is introduced. Finally,  $\delta$  is defined as

$$\delta_0 = \delta_{\frac{1}{2}} = \frac{3}{2}, \quad \text{and} \quad \delta_1 = \begin{cases} \frac{3}{2} & \text{in } \overline{\text{DR}}' \text{ scheme,} \\ \frac{5}{6} & \text{in } \overline{\text{MS}} \text{ scheme.} \end{cases} \quad (1.1.33)$$

The difference between renormalisation schemes for  $\delta_1$  arises from the fact that gauge bosons have  $d = 4 - 2\epsilon$  component when using dimensional regularisation together with the modified minimal subtraction ( $\overline{\text{MS}}$ ) scheme, while they still have 4 components in the modified dimensional reduction ( $\overline{\text{DR}}'$ ) scheme. The  $\overline{\text{DR}}'$  renormalisation scheme is devised to avoid breaking Supersymmetry as is the case in  $\overline{\text{MS}}$ , by working in  $d = 4 - 2\epsilon$  for momenta and momentum integration, while keeping 4 components for the vector fields. Renormalisation schemes will also be presented in more detail in section 2.2.1.

It was observed already in [11] that the effective potential is not gauge-invariant, however, it can serve to derive physically meaningful – *i.e.* gauge invariant – quantities, a very simple example of which is the value of the potential at its minimum. In particular, it was shown in [12] that the existence of a minimum of the effective potential spontaneously breaking the gauge symmetry does not depend on the gauge – in other



words, for the SM, the occurrence of the EWSB is gauge independent. The gauge (in)dependence of observables computed from the effective potential has been investigated extensively in the literature, but we will not discuss it further here – the reader may refer *e.g.* to [13–15] for recent developments, as well as to references therein.

In the case of the SM, one finds for the one-loop effective potential in the Landau gauge and  $\overline{\text{MS}}$  scheme [16]

$$\begin{aligned} V^{(1)}(h) = & \frac{1}{4}m_h^4(h)\left(\overline{\log} m_h^2(h) - \frac{3}{2}\right) + \frac{3}{4}m_G^4(h)\left(\overline{\log} m_G^2(h) - \frac{3}{2}\right) \\ & - 3 \sum_{q=u,d,c,s,t,b} m_q^4(h)\left(\overline{\log} m_q^2(h) - \frac{3}{2}\right) \\ & + \frac{3}{2}m_W^4(h)\left(\overline{\log} m_W^2(h) - \frac{5}{6}\right) + \frac{3}{4}m_Z^4(h)\left(\overline{\log} m_Z^2(h) - \frac{5}{6}\right) \end{aligned} \quad (1.1.34)$$

where

$$\begin{aligned} m_h^2(h) &= \mu^2 + 3\lambda(v+h)^2, & m_G^2(h) &= \mu^2 + \lambda(v+h)^2, & m_q(h) &= \frac{y_q}{\sqrt{2}}(v+h), \\ m_W^2(h) &= \frac{1}{4}g^2(v+h)^2, & m_Z^2(h) &= \frac{1}{4}(g^2 + g'^2)(v+h)^2, \end{aligned} \quad (1.1.35)$$

are the (Higgs-)field-dependent tree-level masses of the Higgs, Goldstones, quarks, and  $W$  and  $Z$  bosons respectively (and the  $y_q$  are the diagonal Yukawa couplings of each quark). Generally, in the literature as well as in the remainder of this thesis, the field dependence is not kept explicit, but is rather assumed implicitly. Moreover, in most cases, only the top quark contribution is kept because the top Yukawa coupling  $y_t$  is much larger than those of the other quarks. Finally, it is common to express the one-loop contributions to the potential with the loop function  $f(x) = x^2/4(\overline{\log} x - 3/2)$  (also defined in eq. (B.1.3)), which will often be used throughout this thesis.

Higher-order contributions – of two-loop order and more – to  $V_{\text{eff}}$  are found by computing 1PI vacuum bubble diagrams. The two-loop results for the Standard Model were first computed by Ford, Jack, and Jones, in [16], and are written out in equations (5.2)-(5.6) therein. More recently, leading results beyond two loops were calculated by Stephen Martin, with the three-loop leading contributions involving the strong and Yukawa couplings obtained in [17], and the four-loop part at leading order in QCD in [18].

One important point to consider is that when working with the effective potential, the minimum condition is modified by the radiative corrections and becomes

$$\begin{aligned} \left. \frac{\partial V_{\text{eff}}}{\partial h} \right|_{\phi=0} &= \left. \frac{\partial V^{(0)}}{\partial h} \right|_{\phi=0} + \frac{1}{16\pi^2} \left. \frac{\partial V^{(1)}}{\partial h} \right|_{\phi=0} + \frac{1}{(16\pi^2)^2} \left. \frac{\partial V^{(2)}}{\partial h} \right|_{\phi=0} + \dots \\ &= (\mu^2 + \lambda v^2)v + \frac{1}{16\pi^2} \left. \frac{\partial V^{(1)}}{\partial h} \right|_{\phi=0} + \frac{1}{(16\pi^2)^2} \left. \frac{\partial V^{(2)}}{\partial h} \right|_{\phi=0} + \dots, \end{aligned} \quad (1.1.36)$$

which, in turn, means the solution of the tadpole equation is changed. Actually, there are different possible choices of the parameter(s) for which to solve the tadpole equation(s): the typical choices are either some mass parameter(s) of the Lagrangian (the Higgs mass term  $\mu^2$  in the SM), or some VEV(s) ( $v$  in the SM). Throughout this thesis, we will choose the former option and we will consider the values of the VEV, obtained by an independent calculation, as an input for Higgs mass computations. In

the case of the SM, we find for example

$$\mu^2 = -\lambda v^2 - \frac{1}{v} \frac{\partial \Delta V}{\partial h} \Big|_{\phi=0} \quad (1.1.37)$$

with  $\Delta V = V_{\text{eff}} - V^{(0)}$ . Moreover, the tree-level masses in the minimum of the loop-corrected potential are also affected and are now

$$\begin{aligned} (m_h^2)^{\text{tree}} &= \mu^2 + 3\lambda v^2 = 2\lambda v^2 - \frac{1}{v} \frac{\partial \Delta V}{\partial h} \Big|_{\phi=0} \\ (m_G^2)^{\text{tree}} &= \mu^2 + \lambda v^2 = -\frac{1}{v} \frac{\partial \Delta V}{\partial h} \Big|_{\phi=0} \end{aligned} \quad (1.1.38)$$

In later chapters, we will be interested in calculations for generic models (both analytical and in relation to **SARAH**) and we will want to make use of existing results by Martin – in particular [19,20] – and by Goodsell, Nickel, and Staub [21]. In refs. [19–21], the masses that are used in the expressions of the potential at its minimum, as well as in the tadpole equation(s) and in the mass calculations, are the *tree-level masses in the minimum of the (loop-corrected) effective potential*, and we will follow the same choice throughout large parts of this thesis.

Finally, the scalar masses themselves receive radiative corrections that must be taken into account. Indeed the physical mass of a particle is defined by the pole of its full – *i.e.* loop-corrected – propagator (it is therefore also called the *pole mass* or *on-shell* (OS) mass) and differs from its tree-level mass. The radiative corrections to the masses are given by the self-energy diagrams, and the physical Higgs and Goldstone masses are found by solving the equations

$$\begin{aligned} (m_h^2)^{\text{OS}} &= (m_h^2)^{\text{tree}} + \Pi_{hh}(p^2 = (m_h^2)^{\text{OS}}), \\ (m_{G^0}^2)^{\text{OS}} &= (m_G^2)^{\text{tree}} + \Pi_{G^0 G^0}(p^2 = (m_G^2)^{\text{OS}}), \\ (m_{G^\pm}^2)^{\text{OS}} &= (m_G^2)^{\text{tree}} + \Pi_{G^+ G^-}(p^2 = (m_G^2)^{\text{OS}}), \end{aligned} \quad (1.1.39)$$

which is typically done by numerical iterations.

In the Standard Model, the Higgs mass cannot be predicted theoretically as it depends on the Higgs quartic coupling  $\lambda$ , which has not yet been measured experimentally. But, the discovery of the Higgs boson in 2012 and the precise measurement of its mass around 125 GeV means now that the value of the Higgs quartic can be extracted from the knowledge of  $m_h$ , at a given order in perturbation theory. In turn, the value of the Higgs quartic extracted from  $m_h$  – at the scale at which  $m_h$  is computed, typically  $m_t$  – can be run to high scales in order to study the stability of the SM electroweak vacuum (we will come back to this in a short moment).

The expression of the one-loop Higgs self-energy is fairly short and simple to write, and reads in the Landau gauge (see *e.g.* [22])

$$\begin{aligned} \Pi_{hh}^{(1)}(p^2) &= 3y_t^2(4m_t^2 - p^2)B(m_t^2, m_t^2) - 18\lambda^2 v^2 B(m_h^2, m_h^2) + 3\lambda \frac{p^4 - m_h^4}{m_h^2} B(m_G^2, m_G^2) \\ &\quad + \frac{1}{2}(g^2 + g'^2) \left[ \left( p^2 - 3m_Z^2 - \frac{p^4}{4m_Z^2} B(m_Z^2, m_Z^2) - p^2 \frac{A(m_Z^2)}{2m_Z^2} + 2m_Z^2 \right) \right] \\ &\quad + g^2 \left[ \left( p^2 - 3m_W^2 - \frac{p^4}{4m_W^2} B(m_W^2, m_W^2) - p^2 \frac{A(m_W^2)}{2m_W^2} + 2m_W^2 \right) \right] \end{aligned} \quad (1.1.40)$$

where the (one-)loop functions  $A(x)$  and  $B(x, y) = B(p^2, x, y)$  are defined in eqs. (B.1.6) and (B.1.7) (these functions are sometimes called Passarino-Veltman functions [23]). An equivalent equation in the Feynman gauge and gaugeless limit (*i.e.*  $g = g' = 0$ ) is also given in eq. (6.2.5).

The three most complete calculations of Higgs mass corrections available currently are by Buttazzo et al.<sup>5</sup> [25], by Martin and Roberston for the public code **SMH** [22], and by Kniehl, Pikelner, and Veretin [26, 27].

1. The first [25] is a full two-loop computation in a mixed  $\overline{\text{MS}}$ -OS scheme and in the Feynman gauge, that serves as the first step of a study of the (meta)stability of the electroweak vacuum. More precisely, the input parameters are  $G_F$ ,  $m_W$ ,  $m_Z$ ,  $m_H$ ,  $m_t$ , taken as OS inputs, and the strong coupling constant  $\alpha_s$  that is taken in the  $\overline{\text{MS}}$  scheme and at renormalisation scale equal to  $m_Z$  (*i.e.*  $\alpha_s(m_Z)$ ). These are used to compute the  $\overline{\text{MS}}$  values of  $\lambda$ ,  $\mu^2$ ,  $y_t$ ,  $g$ ,  $g'$  and  $g_s$  at scale  $Q = m_t$ , which are then run up to the Planck scale. The result for the Higgs quartic is given as an interpolating function of  $\lambda^{\overline{\text{MS}}}(Q = m_t)$  as a function of the Higgs and top quark masses.
2. The second [22] contains all two-loop order together with leading three-loop corrections to the Higgs mass, in pure  $\overline{\text{MS}}$  scheme and Landau gauge. The analytical results are implemented in the numerical code **SMH**, which computes to the desired order in perturbation theory the Higgs mass as a function of the Higgs quartic  $\lambda$  (and of the renormalisation scale  $Q$ , the gauge couplings  $g, g', g_3$ , the Higgs VEV and the top Yukawa) or inversely the Higgs quartic as a function of the Higgs mass.
3. The last [26] provides a complete two-loop extraction of the  $\overline{\text{MS}}$  running parameters of the SM (in particular of the running mass of the Higgs) from the OS inputs of  $G_F$ ,  $m_W$ ,  $m_Z$ ,  $m_H$ ,  $m_t$ ,  $m_b$  and the  $\overline{\text{MS}}$  input  $\alpha_s(M_Z)$ , and in a general  $R_\xi$  gauge. These analytical results are available numerically in the public code **mr** [27].

The first and second of the computations described above are discussed in more detail in section 5.2, where they are also compared to the result obtained with the latest version of **SARAH**. We will also review the state-of-the-art of Higgs mass calculations in BSM models in the next chapter.

### 1.1.5 The Goldstone Boson Catastrophe in the Standard Model

Before ending our review of Higgs physics in the Standard Model, we take the opportunity of discussing the Goldstone Boson Catastrophe – in the context of the SM – and the first solutions that were found to address it in [28, 29] (see also [13–15] for recent related work). First observed<sup>6</sup> (and named) for the Standard Model in [17], the Goldstone Boson Catastrophe is a case of infra-red divergence in the effective potential and its derivatives, as well as in scalar self-energies, due to the Goldstone bosons. More precisely, if we look back at eq. (1.1.38), we see that the mass  $m_G^2$  that appears

<sup>5</sup>Actually, this paper continues the work started in [24].

<sup>6</sup>For the sake of completeness, let us mention that similar infra-red divergences had been encountered from other states than Goldstones in [30, 31], and from Goldstones in a two-loop calculation of the Higgs masses in the MSSM in the effective potential approximation [32].

for the Goldstones in calculations – the tree-level mass in the minimum of the loop-corrected potential – is not zero and depends on the renormalisation scale  $Q$ . This comes from the renormalisation scale dependence of the corrections to the potential  $\Delta V$  and means that under renormalisation group flow the Goldstone mass  $m_G^2$  can vanish or run to negative values. The origin of the problem lies in the fact that the  $\ell$ -loop contributions to the SM effective potential contain terms that can be expanded in the limit  $m_G^2 \rightarrow 0$  in the form  $(m_G^2)^n \overline{\log}^m m_G^2$  (where  $n \geq 3 - \ell$  and  $m \leq \ell$ ) and are thus infra-red divergent. Let us consider the severity of such terms depending on the order of  $n$ :

- first, terms of the form  $\overline{\log}^m m_G^2$  or  $\overline{\log}^m m_G^2 / (m_G^2)^p$  that appear from three-loop and four-loop orders respectively diverge in the limit  $m_G^2 \rightarrow 0$ , causing in turn an unphysical divergence of the potential itself;
- then, terms like  $m_G^2 \overline{\log}^m m_G^2$  present at two-loop and higher orders are not divergent – *i.e.* are IR safe – but if  $m_G^2$  becomes negative, the logarithms will acquire unphysical imaginary parts (these imaginary parts are deemed unphysical because they are not associated to any instability of the potential). Furthermore, the derivatives of such terms appear in the tadpole equations, and are divergent because

$$\begin{aligned} \frac{\partial}{\partial h} (m_G^2 \overline{\log}^m m_G^2) \Big|_{\min.} &= \left( \frac{\partial m_G^2}{\partial h} \right) \frac{d}{dm_G^2} (m_G^2 \overline{\log}^m m_G^2) \Big|_{\min.} \\ &= 2\lambda v \left[ \overline{\log}^m m_G^2 + m \overline{\log}^{m-1} m_G^2 \right], \end{aligned} \quad (1.1.41)$$

where we have used the derivative of the field-dependent Goldstone mass from eq. (1.1.35).

- finally,  $m_G^4 \overline{\log}^m m_G^2$  terms, present already from the one-loop order, are also IR safe even if they can have imaginary parts, and it is only their second derivatives that will have divergences. Second derivatives of the effective potential are used to compute approximate scalar masses – sometimes called *effective potential masses* – corresponding to the vanishing external momentum limit of the full calculation with self-energies. To illustrate this, one can consider *e.g.* the one-loop Higgs self-energy given above in eq. (1.1.40) and take  $p^2 = 0$  in that expression. The Goldstone term in  $\Pi_{hh}^{(1)}(p^2 = 0)$  is then

$$-3\lambda m_h^2 B(0, m_G^2, m_G^2) = +3\lambda m_h^2 \overline{\log} m_G^2 \quad (1.1.42)$$

which indeed corresponds to a second derivative of  $m_G^4 \overline{\log}^m m_G^2$  and diverges in the limit  $m_G^2 \rightarrow 0$ . The fact that such terms diverge from one-loop order and beyond was not deemed a serious problem because, until recently [2], it was believed that the inclusion of external momentum in the mass calculations would cure all IR problems [32]. As will be shown in chapter 4 (section 4.3), this statement holds at one-loop level (*e.g.* with the  $B(0, m_G^2, m_G^2)$  term), but at two loops the inclusion of momentum is actually not by itself sufficient to cure the IR divergences because some two-loop self-energy diagrams still diverge in the limit  $m_G^2 \rightarrow 0$  even with non-zero external momentum.

It is important to further remark that a simple change of gauge is not sufficient to avoid the Goldstone Boson Catastrophe. Indeed, the tree-level masses of the neutral

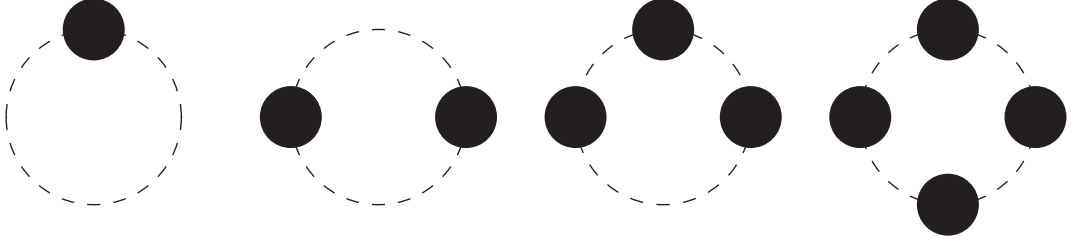


Figure 1.1 – Examples of the most severely divergent contributions of the Goldstone bosons to the effective potential at two, three, four and five loops. The black blobs represent the insertions of the 1PI subdiagrams  $\Gamma(p^2)$ .

or charged Goldstones in the minimum of the loop-corrected potential are in a general  $R_\xi$  gauge

$$m_{G^{0,\pm}}^2 = \xi m_{Z,W}^2 - \frac{1}{v} \frac{\partial \Delta V}{\partial h} \Big|_{\phi=0}, \quad (1.1.43)$$

and can therefore still run to negative values under renormalisation group flow (or if the corrections in the derivative term are large). It is only the scale at which the catastrophe appears that depends on the ( $R_\xi$ ) gauge, not its appearance. One could also think of the unitary gauge, in which the Goldstones would disappear, but as was mentioned earlier loop calculations in this gauge are complicated to such a level that it is preferable to find a solution to avoid the IR divergences in the Landau (or general  $R_\xi$ ) gauge rather than to attempt two-loop calculations in the unitary gauge.

It should also be emphasised that the Goldstone Boson Catastrophe does not arise from a genuine physical problem, but is rather a technical issue of the perturbative calculation with (unphysical) Goldstones. Indeed, Goldstone bosons are not part of the physical spectrum of the SM (or of any spontaneously broken gauge theory) and therefore they cannot cause a physical divergence in calculations. Furthermore, the fact that the appearance of the divergences depends on the choice of gauge is also an indication of their lack of physical meaning. But at the same time, it also means that solutions must exist to cure the IR divergences in the calculations.

Initial methods to cure the Goldstone Boson Catastrophe in the effective potential and its first derivative for the case of the Standard Model were found in references [28, 29] (and later applied to the MSSM in [33]). In both [28] and [29] the infra-red divergences are eliminated through a resummation of contributions from the Goldstone bosons to the effective potential, although the two methods differ slightly in the precise way the resummation is defined. The starting point of both methods is to observe that the most divergent Goldstone contribution in  $V_{\text{eff}}$  at given order  $\ell$  in the perturbative series is the bubble diagram formed of a ring of  $\ell - 1$  Goldstone propagators with  $\ell - 1$  insertions of 1PI subdiagrams  $\Gamma(p^2)$  involving mass scales much larger than the Goldstone masses, as shown in figure 1.1. Moreover, to find the leading divergence in the limit of vanishing  $m_G^2$ , it is sufficient to consider the zero-momentum limit of  $\Gamma(p^2)$  and then we can write the (divergent)  $\ell$ -loop Goldstone contribution to the effective potential as

$$\begin{aligned} V_G^{(\ell)} &= -\frac{3i}{2} C \int d^d k (i\Gamma(0))^{\ell-1} \left( \frac{i}{k^2 - m_G^2} \right)^{\ell-1} \\ &= -\frac{3i}{2} \frac{(\Gamma(0))^{\ell-1}}{(\ell-1)!} \left( \frac{d}{dm_G^2} \right)^{\ell-1} C \int d^d k \log(k^2 - m_G^2) \end{aligned}$$

$$= \frac{(\Gamma(0))^{\ell-1}}{(\ell-1)!} \left( \frac{d}{dm_G^2} \right)^{\ell-1} \left[ \frac{3m_G^4}{4} \left( \overline{\log} m_G^2 - \frac{3}{2} \right) \right], \quad (1.1.44)$$

where the factor 3 comes from the Goldstone multiplicity and the factor  $C$  is defined in eq. (B.1.1). We find that we can sum these terms to all orders and obtain a corrected Goldstone contribution in eq. (1.1.34)

$$V_G^{(1)} = \frac{3}{4} (m_G^2 + \Gamma(0))^2 \left[ \overline{\log} (m_G^2 + \Gamma(0)) - \frac{3}{2} \right], \quad (1.1.45)$$

and a resummed effective potential  $\hat{V}_{\text{eff}}$  at  $\ell$ -loop order

$$\begin{aligned} \hat{V}_{\text{eff}} = V_{\text{eff}} + \frac{3}{16\pi^2} \left\{ \frac{1}{4} (m_G^2 + \Gamma(0))^2 \left[ \overline{\log} (m_G^2 + \Gamma(0)) - \frac{3}{2} \right] \right. \\ \left. - \sum_{n=0}^{\ell-1} \frac{(\Gamma(0))^n}{n!} \left( \frac{d}{dm_G^2} \right)^n \left[ \frac{m_G^4}{4} \left( \overline{\log} m_G^2 - \frac{3}{2} \right) \right] \right\}. \end{aligned} \quad (1.1.46)$$

The term in the second line of eq. (1.1.46) avoids double counting of the Goldstone diagrams and ensure that the original and resummed effective potentials are equal up to terms of order higher than  $\ell$  loops. With a well-chosen  $\Gamma(0)$  the above resummed potential and its first derivative are both free of unphysical IR divergences and imaginary parts (mass calculations were not studied in [28, 29, 33]), and it is then the definition of  $\Gamma(0)$  that constitutes the difference between the procedures in [28] and [29], as we will see now.

On the one hand, in the approach of [29, 33] the insertion  $\Gamma \equiv \Delta$  is obtained by an expansion of the effective potential for small  $m_G^2$ . In particular, if we loop-expand the insertion as

$$\Delta = \frac{1}{16\pi^2} \Delta_1 + \frac{1}{(16\pi^2)^2} \Delta_2 + \dots, \quad (1.1.47)$$

the leading term  $\Delta_1$  can be found (together with another term denoted  $\Omega$ ) when expanding the two-loop potential for small  $m_G^2$  in the following way

$$V^{(2)}(m_G^2) = V^{(2)}(m_G^2 = 0) + \frac{3}{2} \Delta_1 A(G) + \frac{3}{2} \Omega m_G^2 + \mathcal{O}(m_G^4), \quad (1.1.48)$$

where  $A(x)$  is defined in eq. (B.1.6) and the factor 3 comes from the Goldstone multiplicity. Considering only  $\Delta_1$  is actually sufficient because the three-loop terms in the Standard Model potential that would correspond to  $\Delta_2$  were not computed in [17]. In the end, the resummed potential at two-loop order can be written in a simple expression

$$\begin{aligned} \hat{V}_{\text{eff}} = V^{(0)} + \frac{1}{16\pi^2} \left[ V^{(1)}(m_G^2 = 0) + 3f \left( m_G^2 + \frac{1}{16\pi^2} \Delta_1 \right) \right] \\ + \frac{1}{(16\pi^2)^2} \left[ V^{(2)}(m_G^2 = 0) + \frac{3}{2} \Omega m_G^2 \right] \end{aligned} \quad (1.1.49)$$

up to two-loop terms of order  $m_G^4$  that cause no divergence in the two-loop tadpole equation, and where  $f(x)$  is defined in eq. (B.1.3).

On the other hand, [28] shows that the resummation of the Goldstone diagrams contributing to the effective potential can be seen as similar to the construction of an Effective Field Theory describing soft Goldstones only, by integrating out heavy fields

and hard modes of the Goldstone bosons.<sup>7</sup> Note that by *soft* and *hard* Goldstones we mean Goldstones of small momentum  $k^2 \sim m_G^2$  or large momentum  $k^2 \gg m_G^2$  respectively. The divergent diagrams involving Goldstones then correspond in the theory of soft Goldstones to a limited number of diagrams with soft Goldstones, and where masses and couplings have received threshold corrections. In particular, the masses of the soft Goldstones receive a threshold correction denoted  $\Pi_g$ , from the integration of the other (heavy) fields, that is equal to the Goldstone self-energy evaluated at vanishing external momentum, minus the soft Goldstones part. The contributions of the Goldstone bosons to the effective potential of the SM can then be found in terms of diagrams in the low-energy theory of soft Goldstones, and notably, to the two-loop level the only such diagram is the one-loop vacuum bubble that reads

$$\begin{aligned} V_G^{(1)} &= -\frac{3i}{2}C \int d^d k \log(k^2 - m_G^2 - \Pi_g) \\ &= \frac{3}{4}(m_G^2 + \Pi_g)^2 \left[ \overline{\log}(m_G^2 + \Pi_g) - \frac{3}{2} \right], \end{aligned} \quad (1.1.50)$$

which corresponds to eq. (1.1.45) with  $\Pi_g$  playing the role of  $\Gamma(0)$ . The separation between soft and hard modes of the Goldstone bosons may, at first, seem non-trivial and somewhat ambiguous, however, it was suggested in [28] that the splitting of the momentum integrals of Goldstone propagators can be performed consistently with the method of regions [34, 35]. More recently, it was demonstrated in [36] that the separation with the method of regions works to all orders in perturbation theory, thus (formally) extending this resummation prescription to any desired order. For more details on how the method of regions works and how to split momentum integrals with it, the reader may refer to the appendices of [36].

To solve the Goldstone Boson Catastrophe in the SM to two-loop order, only the one-loop expressions of  $\Delta$  and  $\Pi_g$  are needed, and both approaches to the resummation method yield the same results, with

$$\begin{aligned} \Delta_1 = \Pi_g^{(1)} &= -6y_t^2 A(m_t^2) + 3\lambda A(m_h^2) + \frac{3}{2}g^2 \left( A(m_W^2) + \frac{2}{3}m_W^2 \right) \\ &\quad + \frac{3}{4}(g^2 + g'^2) \left( A(m_Z^2) + \frac{2}{3}m_Z^2 \right). \end{aligned} \quad (1.1.51)$$

While providing accurate results for the two-loop effective potential and tadpole equation in the SM, these two methods are difficult to extend to other models and to automate, to a large part because of mixing among the Goldstones. Furthermore, a resummation of the effective potential does not by itself suffice to cure IR divergences appearing in the calculation of mass corrections, because some diagrams diverge in the  $p^2 \rightarrow 0$  limit. This provides motivation to search for a solution to the Goldstone Boson Catastrophe for general models and that can be applied to mass diagrams, which will be the subject of chapter 4.

It is also worth mentioning that for the case of the SM an alternative solution to the Goldstone Boson Catastrophe was found, relying on the use of symmetry-improved two-particle-irreducible (2PI) effective action developed by Pilaftsis and Teresi [37–39]. The 2PI effective action was first introduced in [40], essentially by a generalisation of the derivation of the 1PI effective action in the previous section by introducing bi-local sources in the standard and connected generating functionals  $Z$  and  $W$  (*c.f.*

---

<sup>7</sup> Gluons and photons are also included in the low-energy part of this construction.

eqs. (1.1.26) and (1.1.27)) and then by performing a double Legendre transform of the connected generating functional (*i.e.* modifying eq. (1.1.28)). It is found to be expressed in terms of background fields and dressed (*i.e.* renormalised) propagators, and is therefore free of IR divergences caused by massless particles in the loops by construction. A further refinement was introduced in [37] with the symmetry-improved 2PI effective action that is built so as to respect (global) symmetries at any order in perturbation theory to which it is computed, by imposing on the dressed propagators the Ward identities associated with the symmetries. In [38,39], the use of this improved effective action for the SM was shown to avoid the IR divergences from the Goldstone bosons and the numerical results agree with those of [28,29]. Conceptually, the 2PI effective action approach relates to the method we devise in chapter 4 because it amounts to a resummation of the propagators of all particles, while our method corresponds to a resummation of Goldstone propagators only. However, as this approach does not allow simple analytical calculations (instead the action and derived quantities must be computed numerically) and is difficult to apply to generic models beyond the SM and thus to automate, we will not discuss it further here.

## 1.2 Going beyond the Standard Model

The Standard Model suffers from a number of issues: on the one hand, theoretical deficiencies (some of which have been apparent since its conception) and, on the other hand, experimental observations that are conflicting with the SM or that cannot be accommodated by it. Among these problems, one could mention, for example, on the theoretical side: the lack of explanations of inflation, or of the mechanism of baryogenesis; the strong CP problem; or the absence of a description of quantum gravity. On the experimental side, signs that the SM is not a complete theory of Nature include the observational signs of the existence of dark matter for which the SM provides no candidate particle; the discovery of neutrino masses; or tensions that have appeared between SM predictions and experimental results *e.g.* for the muon anomalous moment or, more recently, in *B* Physics.

Complete lists of the problems of the SM can be found in the literature (see *e.g.* [41,42]), and therefore it makes little sense to attempt to provide an exhaustive presentation here. Instead, we will focus here on the two points that relate the most to the Higgs sector: the hierarchy problem and the fate of the electroweak vacuum.

### 1.2.1 The hierarchy problem

The hierarchy problem has several formulations, of which the first and most straightforward one is to ask why the energy scales appearing in quantum theories of gravitational and electroweak interactions, respectively, are so different. More precisely, the typical scale at which quantum gravity effects appear, the Planck scale  $M_{\text{Pl}}$  found as

$$M_{\text{Pl}} \equiv \sqrt{\frac{\hbar c}{G}} \simeq 1.22 \times 10^{19} \text{ GeV} \quad (1.2.1)$$

is seventeen orders of magnitude larger than the scale of electroweak interactions, usually taken to be the Higgs VEV  $v = 246 \text{ GeV}$ . As a matter of comparison, the typical energy scale of strong interactions (the QCD scale) is only two to three orders of magnitude smaller than the electroweak scale. This may seem as a simple matter of aesthetics, but it comes with other more clearly worrisome consequences.



One of them relates directly to the Higgs boson and to electroweak symmetry breaking: to find a value of the Higgs VEV  $v$  compatible with the  $W$  and  $Z$  bosons masses (or equivalently with the value derived from the measurement of the Fermi constant  $G_F$ ) the Higgs mass term  $\mu^2$  must be of order  $\sim -(100 \text{ GeV})^2$ . However, scalar masses are not protected by either chiral or gauge symmetries as are fermion and gauge boson masses respectively (see section 1.1.1) and therefore the corrections to the Higgs mass term  $\mu^2$  can be huge – actually they are proportional to the mass of the heaviest particle coupling to the Higgs. Obtaining the required value of the loop-corrected  $\mu^2$  would imply that some exceptionally precise cancellation occurs between its tree-level value and the radiative corrections, which seems very strange.

To illustrate this, let us consider a toy model in which a heavy Dirac fermion  $\psi$ , with a mass around the Planck scale  $M_\psi \simeq M_{\text{Pl}}$ , couples to a (light) real scalar  $S$  – corresponding to the SM Higgs – with a Lagrangian

$$\mathcal{L} = \bar{\psi}(i\not{\partial} - M_\psi)\psi + \frac{1}{2}(\partial_\mu S)^2 - \frac{1}{2}m_S^2 S^2 - y_\psi \bar{\psi}\psi S \quad (1.2.2)$$

Such a fermion can be thought of as a heavy particle appearing in a quantum theory of gravity, of which the SM is (supposed to be) an Effective Field Theory below  $M_{\text{Pl}}$ . The one-loop threshold correction to  $m_S^2$  when integrating out  $\psi$  can be found in dimensional regularisation to be

$$\begin{aligned} \delta^{(1)}m_S^2(p^2) &= -(-iy_\psi)^2 C \int d^d k \text{tr} \left[ \frac{i(\not{k} + M_\psi)}{k^2 - M_\psi^2} \frac{i((\not{k} - \not{p}) + M_\psi)}{(p - k)^2 - M_\psi^2} \right] \\ &= \frac{y_\psi^2}{4\pi^2} \left[ A(M_\psi^2) - \left( 2M_\psi^2 - \frac{p^2}{2} \right) B(p^2, M_\psi^2, M_\psi^2) \right]. \end{aligned} \quad (1.2.3)$$

after performing an  $\overline{\text{MS}}$  renormalisation, and with the loop factor  $C$  defined in eq. (B.1.1). The natural value of the momentum flowing in the loop is  $m_S$ , *i.e.* a mass scale much smaller than the fermion mass  $M_\psi$ , and furthermore, it is also common to perform the matching at scale equal to (or of the same order as)  $M_\psi$ . Therefore, we can set  $p^2 \approx m_S^2 \ll M_\psi^2$  and  $Q = M_\psi$ , which greatly simplifies the above expression, and we find

$$\delta^{(1)}m_S^2(0) = -\frac{y_\psi^2}{4\pi^2} M_\psi^2. \quad (1.2.4)$$

When considering heavy fermions interacting with the SM scalar sector, corrections of the above form – referred to as *quadratic divergences*<sup>8</sup> – also occur for the Higgs mass parameter  $\mu^2$ , and can be much larger than the required value of  $\sim -(100 \text{ GeV})^2$  for  $\mu^2$ . The consequent problem of the necessary fine-tuning of  $(\mu^2)^{\text{tree}}$  – the *technical hierarchy problem* – has, for a long time, been a strong motivation for the search of mechanisms beyond the SM to protect scalar mass terms from (divergent) radiative corrections. Among the models that have been shown to solve this problem (a large number of which have been devised especially for the task) one can mention models with new symmetries, such as Supersymmetry [43] or composite Higgs models [44, 45]; models with extended space-time [46, 47]; or as was suggested more recently, new mechanisms like cosmological relaxation [48].

An alternative point of view is not to regard the (technical) hierarchy problem as a problem of the theory, and require for example some anthropic principle to explain the value of  $\mu^2$ .

---

<sup>8</sup> Original corrections to scalar masses from fermions were computed using regularisation with a cut-off scale  $\Lambda_{\text{UV}}$  and were shown to behave like  $\propto y^2 \Lambda_{\text{UV}}^2$  (both for SM and new heavy fermions). The scalar masses then diverge quadratically when  $\Lambda_{\text{UV}} \rightarrow \infty$ , hence the name of quadratic divergences.

### 1.2.2 The stability of the electroweak vacuum

Another puzzle of the Standard Model that relates to the Higgs sector is the question of the stability of the electroweak vacuum. In the previous section, we have discussed the existence of minima of the Higgs potential that break the electroweak gauge symmetry, at tree-level (see eqs. (1.1.5) and (1.1.7)) or once quantum corrections have been taken into account (see eq. (1.1.36)). Nevertheless, one could also ask if other minima may exist, in particular for large Higgs field values, and whether such minima could be more stable than the minimum associated with  $v \simeq 246$  GeV. For large field values – *i.e.*  $h \gg v$  – it is necessary to use a renormalisation-group-improved effective potential, which can be approximated to be

$$V_{\text{eff}}(h) \underset{h \gg v}{\simeq} \frac{\lambda_{\text{eff}}(h)}{4} h^4, \quad (1.2.5)$$

where the effective Higgs quartic  $\lambda_{\text{eff}}$  is related to the tree-level quartic  $\lambda$  by the inclusion of (Higgs-)field-strength renormalisation effects and of higher-order corrections to the potential [24, 25]. However, the difference between  $\lambda_{\text{eff}}$  and  $\lambda$  becomes negligible for large field values [24] and consequently the study of the behaviour of the potential for large Higgs fields amounts to studying the running of the Higgs (tree-level) quartic  $\lambda$  at high scales. To be more specific, one must remember that  $\lambda$  is not predicted in the SM but can, however, be extracted from the measurement of the Higgs mass  $m_h$  [49–52] using the known threshold corrections at the scale at which  $m_h$  is measured – typically taken to be  $Q = m_t$ . Once  $\lambda(Q)$  has been extracted at some low scale, its value at any large scale can be found through renormalisation group running, and the renormalisation group equation (RGE) of  $\lambda$  is presently known to full three-loop order [53, 54].

One of the points of interest in a study of the running of  $\lambda$  is its sign<sup>9</sup> at high scales. In particular, for the Higgs quartic to become negative is a worrisome sign for the theory, because it at least signals the existence of states of energy lower than that of the EW vacuum, and moreover, if  $\lambda$  remains negative at high scales, the scalar potential is not bounded from below. The EW vacuum in which we live is then not absolutely stable: it will be *metastable* or *unstable* depending on whether its lifetime (*i.e.* the typical time until the Higgs tunnels to the lower minimum of the potential) is larger or smaller than the age of the Universe.

An in-depth study of the stability of the electroweak vacuum using the above-mentioned state-of-the-art results was begun in [24] and continued in [25], and showed that if one extrapolates the SM up to the Planck scale, the measured values of the Higgs and top quark masses favour the vacuum being only metastable, as can be seen in figure 3 of [25]. Interestingly, the Higgs quartic becomes negative at a scale  $Q \sim 10^{10}$  GeV and remains negative at higher scales, with a value at the Planck scale very close to 0 –  $\lambda(M_{\text{Pl}}) \simeq -0.014$ , *c.f.* equation (61e) of [25].

There are several possible interpretations of this result of metastability: at first, one may argue that a metastable vacuum is not sufficient to require the presence of some BSM Physics below the Planck scale, and that we may well live in a vacuum that is not the absolute minimum of the Higgs potential, because the characteristic tunnelling time to the absolute minimum is much larger than the age of the Universe. In turn,

---

<sup>9</sup>As was noted in [25],  $\lambda$  is the only SM coupling whose  $\beta$ -function is not proportional to the coupling itself and therefore only  $\lambda$  can change sign. In terms of symmetries, this comes from the fact that the case  $\lambda = 0$  does not have an enhanced symmetry with respect to  $\lambda \neq 0$ .

different options are available to explain the value of  $\lambda(M_{\text{Pl}})$  found close to zero, and in particular one of them is that the small negative  $\lambda(M_{\text{Pl}})$  only arises from threshold corrections to a matching condition between a high energy model and the SM, at some high scale, possibly as high as the Planck scale. For other possibilities, and further discussion of interpretations of the metastability of the electroweak vacuum for Particle Physics and Cosmology, the reader may consult [24,25] and references therein.

Another possibility is to consider the metastability of the electroweak vacuum as an indicator of the existence of New Physics, at some scale below or around where  $\lambda$  becomes negative, that is able somehow stabilise the potential and prevent  $\lambda$  from vanishing. In this context, the SM is viewed as an effective theory below the New Physics scale, or in other words, the scale at which  $\lambda$  runs to negative values (in the SM) can be seen as a cut-off scale up to which the SM can be considered valid.

### 1.2.3 Building models beyond the Standard Model

Before turning to the presentation of some BSM models, let us first make a short comment on the two possible approaches to model building.

On the one hand, one can try to devise a complete theory – valid up to high energies, possibly even up to the Planck scale – that would solve some (or all) of the deficiencies of the SM, and then study the consequences of such a model at energies around the electroweak scale. One of the best known examples of this approach – called the *top-down* approach – is the class of supersymmetric theories, in which fermionic and bosonic states are related by a new symmetry valid at high scales, but spontaneously broken at lower energies. In coming section 1.3 we will consider different Supersymmetry models studied in the course of this thesis, namely the MSSM, the NMSSM, and Dirac gaugino models.

On the other hand, another approach to the construction of models of New Physics is also possible: the *bottom-up* approach. The idea is to extend the Standard Model by new fields and/or new terms in the Lagrangian, at energy scales around or slightly above the electroweak scale, in order to address some of the issues of the Standard Model, or sometimes simply to study the phenomenological consequences of such an extension. We will be more specifically interested in models with extended Higgs sectors, which we will review in section 1.4 (extensions of the SM by a singlet, by a doublet, or by two triplets).

## 1.3 Supersymmetry

This section aims at introducing, from a phenomenological point of view, some key notions about Supersymmetry and some supersymmetric models – in particular Dirac gaugino models – that will appear throughout this thesis. The reader may refer *e.g.* to [41,42,55,56] for reviews of SUSY.

Supersymmetry (SUSY) extends the Poincaré group of space-time invariance by a new symmetry that relates fermions and bosons. We will now recall elements of the SUSY formalism that will be required in this thesis, before showing how in principle SUSY helps solve the hierarchy problem – one great success of Supersymmetry – and finally discussing the supersymmetric extensions of the SM that will be studied in this thesis.

Note that in what follows we will only consider Supersymmetry to be a global symmetry,<sup>10</sup> and we will not be considering gravity.

### 1.3.1 Some basics of SUSY

#### 1.3.1.1 Fermions in two-component notation

In the context of SUSY, the use of two-component Weyl spinors will prove greatly useful, instead of four-component Dirac spinors. Any Dirac spinor  $\psi$  can be written as

$$\psi = \begin{pmatrix} \xi_\alpha \\ \bar{\chi}^{\dot{\alpha}} \end{pmatrix} \quad (1.3.1)$$

where  $\xi_\alpha$  and  $\bar{\chi}^{\dot{\alpha}}$  are the complex and anti-commuting (Grassmanian) components of Weyl spinors  $\xi$  and  $\bar{\chi}$  of left- and right-handed helicities respectively. Dotted and undotted indices correspond to the two possible helicities of the spinors and take values 1 and 2. Non-barred and barred Weyl spinors correspond to two different representations of the Lorentz group  $SO(3,1) \cong SU(2)_L \oplus SU(2)_R$ , more precisely to the  $(\frac{1}{2}, 0)$  and  $(0, \frac{1}{2})$  representations. These two representations can be related by complex conjugation, *i.e.*

$$\bar{\chi}^{\dot{\alpha}} \equiv (\chi^\alpha)^\dagger, \quad (1.3.2)$$

hence the bar on right-handed spinors.

One can change from upper to lower indices using the two-dimensional antisymmetric tensors  $\epsilon^{\alpha\beta}$  or  $\epsilon^{\dot{\alpha}\dot{\beta}}$  with the relations

$$\begin{aligned} \xi^\alpha &= \epsilon^{\alpha\beta} \xi_\beta, & \xi_\alpha &= \epsilon_{\alpha\beta} \xi^\beta, \\ \bar{\xi}^{\dot{\alpha}} &= \epsilon^{\dot{\alpha}\dot{\beta}} \bar{\xi}_{\dot{\beta}}, & \bar{\xi}_{\dot{\alpha}} &= \epsilon_{\dot{\alpha}\dot{\beta}} \bar{\xi}^{\dot{\beta}}, \end{aligned} \quad (1.3.3)$$

having chosen to take  $\epsilon^{12} = -\epsilon_{12} = 1$ . Spinor indices will also often be contracted, with the following conventions

$$\begin{aligned} \xi\chi &= \xi^\alpha \chi_\alpha = -\xi_\alpha \chi^\alpha, \\ \bar{\xi}\bar{\chi} &= \bar{\xi}_{\dot{\alpha}} \bar{\chi}^{\dot{\alpha}} = -\bar{\xi}^{\dot{\alpha}} \bar{\chi}_{\dot{\alpha}}. \end{aligned} \quad (1.3.4)$$

The Dirac conjugate of the four-component spinor  $\psi$  can be written

$$\bar{\psi} \equiv \psi^\dagger \gamma^0 = (\chi^\alpha, \bar{\xi}_{\dot{\alpha}}) \quad (1.3.5)$$

and with this, one can easily introduce the left- and right-handed projectors, using the identity  $\mathbf{1}_4 = \mathcal{P}_L + \mathcal{P}_R = \mathcal{P}_L^2 + \mathcal{P}_R^2$ , in order to rewrite a Dirac mass term as

$$m_\psi \bar{\psi} \psi = m_\psi (\xi\chi + \bar{\xi}\bar{\chi}). \quad (1.3.6)$$

Furthermore the charge conjugate of the Dirac spinor  $\psi$  is

$$\psi^C \equiv i\gamma^0 \gamma^2 \bar{\psi}^T = \begin{pmatrix} \epsilon_{\alpha\beta} & 0 \\ 0 & \epsilon^{\dot{\alpha}\dot{\beta}} \end{pmatrix} \begin{pmatrix} \chi^\alpha \\ \bar{\xi}_{\dot{\alpha}} \end{pmatrix} = \begin{pmatrix} \chi_\alpha \\ \bar{\xi}^{\dot{\alpha}} \end{pmatrix} \quad (1.3.7)$$

so one finds that the Majorana condition

$$\psi_M^C = \psi_M \quad (1.3.8)$$

---

<sup>10</sup>Local Supersymmetry is subject of research on its own, namely Supergravity.

implies for the Weyl spinor components that  $\xi = \chi$ . Then one can write a Majorana spinor and a Majorana mass term in two-component language as

$$\psi_M = \begin{pmatrix} \xi_\alpha \\ \bar{\xi}^{\dot{\alpha}} \end{pmatrix}, \quad \text{and} \quad \frac{1}{2} M_\psi \bar{\psi}_M \psi_M = \frac{1}{2} m_\psi (\xi \xi + \bar{\xi} \bar{\xi}). \quad (1.3.9)$$

### 1.3.1.2 Supersymmetry, the SUSY algebra and its representations

Symmetries play an important role in the study of Quantum Field Theories, and no-go theorems – most famously the Coleman-Mandula theorem [57] – were established, greatly limiting the possible space-time symmetries of physical theories. Actually, Coleman and Mandula showed in [57] that if one considers a physical theory in four dimensions, with only local interactions, and further supposes the states are in finite number and that some of these are massive, then the largest possible symmetry group – when allowing only bosonic symmetry generators – is the Poincaré group. However, Haag, Łopuszański, and Sohnius [58] showed that it is possible to extend Poincaré symmetry by additional *fermionic* symmetry generators, *i.e.* generators that carry spin- $\frac{1}{2}$ , and therefore transform as spinors under transformations of the rest of the Poincaré group and have spinor indices (undotted or dotted). These generators will be denoted  $Q_\alpha^A$  – where index  $A$  labels the possible multiple generators – and the *Supersymmetry* transformations they generate turn bosons into fermions and vice versa. Furthermore, because the fermions are complex states, the complex conjugates of the generators –  $\bar{Q}_{\dot{\alpha}}^A$  – will also be generators of different supersymmetric transformations.

From the above considerations, and with the additional requirement of having a closed algebra, one can derive the SUSY algebra – see *e.g.* section 3.1 of [55] for a derivation in the  $\mathcal{N} = 1$  case. In the presence of  $\mathcal{N}$  supercharges labelled  $A, B, \dots \in [1, \dots, \mathcal{N}]$ , the complete SUSY algebra is

$$\begin{aligned} \{Q_\alpha^A, \bar{Q}_{\dot{\alpha}}^B\} &= 2\sigma_{\alpha\dot{\alpha}}^\mu P_\mu \delta^{AB} \\ \{Q_\alpha^A, Q_\beta^B\} &= \epsilon_{\alpha\beta} Z^{AB} \\ \{\bar{Q}_{\dot{\alpha}}^A, \bar{Q}_{\dot{\beta}}^B\} &= \epsilon_{\dot{\alpha}\dot{\beta}} (Z^{AB})^* \\ [P_\mu, Q_\alpha^A] &= [P_\mu, \bar{Q}_{\dot{\alpha}}^A] = 0 \end{aligned} \quad (1.3.10)$$

where  $\sigma^\mu = (\mathbf{1}_2, \sigma^i)$ ,  $P_\mu$  is the generator of translations, and  $Z^{AB}$  are anti-symmetric tensors called the *central charges*. Note that we will also use  $\bar{\sigma}^\mu = (\mathbf{1}_2, -\sigma^i)$ .

While theories with several supersymmetries are studied, *e.g.* in the context of String Theory, most phenomenologically interesting SUSY models only have a single Supersymmetry ( $\mathcal{N} = 1$  SUSY). One important exception is the case of Dirac gaugino models – which we will consider in depth in section 1.3.5 and in chapter 3 – in which Supersymmetry in the gauge sector is extended to  $\mathcal{N} = 2$ . However, even these models can be studied in the language of  $\mathcal{N} = 1$  SUSY,<sup>11</sup> and for this reason we will now only discuss representations of the SUSY algebra in the  $\mathcal{N} = 1$  case.

---

<sup>11</sup>The states in the gauge sector that would live in a hypermultiplet in  $\mathcal{N} = 2$  SUSY – namely the gauge boson, the gauginos and the (complex) adjoint gauge scalar – can also be seen as one gauge supermultiplet, containing the gauge boson and one gaugino, plus a chiral supermultiplet in the adjoint representation of the gauge group, that will contain the other gaugino and the adjoint scalar.

One-particle states in a SUSY theory live in irreducible representations of the SUSY algebra, called *supermultiplets*, containing both fermionic and bosonic states that will be referred to as *superpartners*. Because gauge symmetries are internal and not space-time symmetries, their generators must commute with SUSY generators and hence all particles of a given supermultiplet belong to the same representation of the gauge group. Moreover, it can be shown [41, 55, 56] that the numbers of fermionic and bosonic states in a given supermultiplet must be the same, which will fix the structure of representations. Indeed there will be two possible ways to construct supermultiplets, as summarised in table 1.2: either a Weyl spinor (two fermionic degrees of freedom when on-shell) together with a complex scalar (two bosonic degrees of freedom) forming a *chiral supermultiplet*; or a massless gauge boson (with two helicities hence two bosonic degrees of freedom when on-shell) together with a Weyl spinor forming a *gauge (or vector) supermultiplet*.

Supermultiplet	Spin-0	Spin- $\frac{1}{2}$	Spin-1
Chiral supermultiplet	Complex scalar	Weyl fermion	-
Gauge supermultiplet	-	Weyl fermion (gaugino)	Massless gauge boson

Table 1.2 – Possible representations of the SUSY algebra (not including gravity).

An important remark should be made here about the above counting of bosonic and fermionic degrees of freedom. The number of degrees of freedom that we considered both for fermions and gauge bosons is only valid on mass-shell, *i.e.* when the equations of motion of the given field applies. Off-shell this counting has to be modified, with four degrees of freedom for fermions and three for gauge bosons, which appears to contradict the requirement of having the same number of fermion and boson states in each supermultiplet. We can solve this problem by introducing new bosonic *auxiliary* fields to match the number of fermionic degrees of freedom in both chiral and gauge supermultiplets. For the chiral supermultiplet, we add a complex scalar  $F$  that vanishes on-shell and therefore has a non-propagating Lagrangian

$$\mathcal{L}_{\text{aux.}} = F^* F. \quad (1.3.11)$$

Similarly, for the gauge supermultiplet we add a real scalar  $D^a$  –  $a$  being the gauge group index – with a Lagrangian

$$\mathcal{L}_{\text{aux.}} = \frac{1}{2} D^a D^a. \quad (1.3.12)$$

Another argument requiring the introduction of these fields is that the SUSY algebra would not close off-shell without them. The auxiliary fields are then introduced with SUSY transformation rules ensuring that the complete Lagrangian remains invariant under SUSY transformations.

### 1.3.1.3 Superspace formalism and superfields

The *superspace* formalism is a powerful tool that simplifies the construction of supermultiplets and of Lagrangians in a SUSY-invariant way. Superspace is an eight-dimensional manifold formed of normal space-time with its four bosonic coordinates  $x^\mu$  to which are added four fermionic coordinates as two two-component anticommuting spinors  $\theta^\alpha$  and  $\bar{\theta}_{\dot{\alpha}}$  (having mass dimension  $-1/2$ ).

We can then build new fields on the superspace, *superfields*, that will contain all the components of supermultiplets, and to obtain their explicit expressions we can perform a power series expansion in terms of  $\theta, \bar{\theta}$ , which must end at a finite order since the components of  $\theta, \bar{\theta}$  are Grassmanian variables. A general superfield can be written [55]

$$S(x, \theta, \bar{\theta}) = a + \theta\xi + \bar{\theta}\bar{\chi} + \theta\theta b + \bar{\theta}\bar{\theta}c + \bar{\theta}\bar{\sigma}^\mu\theta v_\mu + \bar{\theta}\bar{\theta}\theta\eta + \theta\theta\bar{\theta}\bar{\zeta} + \theta\theta\bar{\theta}\bar{\theta}d. \quad (1.3.13)$$

In this expansion,  $a, b, c, d$  are scalar components,  $\xi, \eta$  ( $\bar{\chi}, \bar{\zeta}$ ) are left-handed (right-handed) fermionic components and  $v_\mu$  is a vector component. This number of components is obviously much larger than the number of degrees of freedom in a supermultiplet so there must exist criteria to constrain or relate the components.

Before considering the different types of superfields, let us however first mention briefly the formulation of SUSY transformations in the superspace formalism. The SUSY generators can be written as differential operators acting on superfields

$$\begin{aligned} \hat{Q}_\alpha &= i\frac{\partial}{\partial\theta^\alpha} - (\sigma^\mu\bar{\theta})_\alpha\partial_\mu, & \hat{Q}^\alpha &= -i\frac{\partial}{\partial\theta_\alpha} + (\bar{\theta}\bar{\sigma}^\mu)^\alpha\partial_\mu, \\ \hat{\bar{Q}}^{\dot{\alpha}} &= i\frac{\partial}{\partial\bar{\theta}_{\dot{\alpha}}} - (\bar{\sigma}^\mu\theta)^{\dot{\alpha}}\partial_\mu, & \hat{\bar{Q}}_{\dot{\alpha}} &= -i\frac{\partial}{\partial\bar{\theta}^{\dot{\alpha}}} + (\theta\sigma^\mu)_{\dot{\alpha}}\partial_\mu. \end{aligned} \quad (1.3.14)$$

Then the transformation of a superfield  $S$  under a SUSY transformation of parameters  $\epsilon$  and  $\bar{\epsilon}$  is

$$\begin{aligned} \sqrt{2}\delta_\epsilon S &= S(x^\mu + i\epsilon\sigma^\mu\bar{\theta} + i\bar{\epsilon}\bar{\sigma}^\mu\theta, \theta + \epsilon, \bar{\theta} + \bar{\epsilon}) - S(x^\mu, \theta, \bar{\theta}) \\ &= -i(\epsilon\hat{Q} + \bar{\epsilon}\hat{\bar{Q}})S(x^\mu, \theta, \bar{\theta}) \\ &= \left( \epsilon^\alpha\frac{\partial}{\partial\theta^\alpha} + \bar{\epsilon}_{\dot{\alpha}}\frac{\partial}{\partial\bar{\theta}_{\dot{\alpha}}} + i(\epsilon\sigma^\mu\bar{\theta} + \bar{\epsilon}\bar{\sigma}^\mu\theta)\partial_\mu \right) S(x^\mu, \theta, \bar{\theta}). \end{aligned} \quad (1.3.15)$$

With the above equation, it is possible to derive the transformations of the component fields, either for a generic superfield or for a particular type of superfield – chiral or real as we will see now.

To define superfields for chiral supermultiplets, we need to introduce a last type of object: chiral (SUSY-)covariant derivatives. These are necessary to constrain chiral superfields and are defined as

$$\begin{aligned} D_\alpha &= \frac{\partial}{\partial\theta^\alpha} - i(\sigma^\mu\bar{\theta})_\alpha\partial_\mu, & D^\alpha &= -\frac{\partial}{\partial\theta_\alpha} + i(\bar{\theta}\bar{\sigma}^\mu)^\alpha\partial_\mu, \\ \bar{D}^{\dot{\alpha}} &= \frac{\partial}{\partial\bar{\theta}_{\dot{\alpha}}} - i(\bar{\sigma}^\mu\theta)^{\dot{\alpha}}\partial_\mu, & \bar{D}_{\dot{\alpha}} &= -\frac{\partial}{\partial\bar{\theta}^{\dot{\alpha}}} + i(\theta\sigma^\mu)_{\dot{\alpha}}\partial_\mu, \end{aligned} \quad (1.3.16)$$

where the derivatives with respect to an anti-commuting variable are themselves defined by

$$\frac{\partial\theta^\beta}{\partial\theta^\alpha} = \delta_\alpha^\beta, \quad \frac{\partial\bar{\theta}_{\dot{\beta}}}{\partial\theta^\alpha} = 0, \quad \frac{\partial\bar{\theta}_{\dot{\beta}}}{\partial\bar{\theta}^{\dot{\alpha}}} = \delta_{\dot{\beta}}^{\dot{\alpha}}, \quad \frac{\partial\theta^\beta}{\partial\bar{\theta}^{\dot{\alpha}}} = 0. \quad (1.3.17)$$

A chiral superfield  $\Phi$  is then defined by the condition

$$\bar{D}_{\dot{\alpha}}\Phi = 0, \quad (1.3.18)$$

that strongly constraints the components of  $\Phi$ . One can show that this gives

$$\Phi = \phi + \sqrt{2}\theta\psi + \theta\theta F + i\bar{\theta}\bar{\sigma}^\mu\theta\partial_\mu\phi - \frac{i}{\sqrt{2}}\theta\theta\bar{\theta}\bar{\sigma}^\mu\partial_\mu\psi + \frac{1}{4}\theta\theta\bar{\theta}\bar{\theta}\partial_\mu\partial^\mu\phi, \quad (1.3.19)$$

with  $\psi$  a left-handed fermion,  $\phi$  its complex scalar superpartner, and  $F$  the auxiliary field. Taking the complex conjugate of  $\Phi$  we can also obtain an antichiral superfield.

In turn, gauge supermultiplets are described by *real* superfields, *i.e.* superfields  $V$  that verify the condition

$$V = V^*. \quad (1.3.20)$$

Applying this in eq. (1.3.13), we find<sup>12</sup> for a general gauge group of index  $a$

$$V^a = \bar{\theta}\bar{\sigma}^\mu\theta A_\mu^a + \bar{\theta}\bar{\theta}\theta\lambda^a + \theta\theta\bar{\theta}\bar{\lambda}^a + \frac{1}{2}\theta\theta\bar{\theta}\bar{\theta}D^a, \quad (1.3.21)$$

where  $A_\mu^a$  is a gauge boson,  $\lambda^a$  its associated gaugino, and  $D^a$  is the auxiliary superfield.

#### 1.3.1.4 Superpotential and supersymmetric Lagrangians

With the superspace formalism, one can easily form a SUSY-invariant Lagrangian for a given theory. For chiral supermultiplets  $\Phi_i$  alone, the Lagrangian is

$$\mathcal{L}_{\text{chiral}} = \int d^2\theta d^2\bar{\theta} \Phi_i^* \Phi_i + \left( \int d^2\theta W(\{\Phi_i\}) \Big|_{\bar{\theta}=0} + \text{h.c.} \right), \quad (1.3.22)$$

where  $W(\{\Phi_i\})$  is a holomorphic function of the chiral superfields  $\Phi_i$  called the *superpotential*. This object contains supersymmetric mass terms and self-interactions of the scalars as well as the interactions of fermions with scalars. The most general renormalisable superpotential that can be written for a generic theory is

$$W(\{\Phi_i\}) = L_i \Phi_i + \frac{1}{2} M_{ij} \Phi_i \Phi_j + \frac{1}{6} y^{ijk} \Phi_i \Phi_j \Phi_k. \quad (1.3.23)$$

The requirement of gauge invariance means that  $L_i$  terms are only allowed when  $\Phi_i$  is a gauge singlet (we will see that this is possible in the NMSSM and in Dirac gaugino models, but not in the MSSM).

If one introduces vector superfields  $V^a$  associated with some general gauge group (which we will again index with  $a$ ), the first term in eq. (1.3.22) must be modified to remain supergauge invariant. Furthermore, another purely gauge term must be added containing kinetic terms of gauge bosons and gauginos. For this we need to introduce a *field-strength* chiral superfield, defined as

$$\mathcal{W}_\alpha \equiv -\frac{1}{4} \bar{D} \bar{D} (e^{-V} D_\alpha e^V), \quad (1.3.24)$$

and its components in the adjoint representation of the gauge group (and Wess-Zumino gauge)  $\mathcal{W}_\alpha^a$

$$\mathcal{W}_\alpha \equiv 2g_a T^a \mathcal{W}_\alpha^a \quad (1.3.25)$$

$$\mathcal{W}_\alpha^a = \lambda_\alpha^a + \theta_\alpha D^a - \frac{i}{2} (\sigma^\mu \bar{\sigma}^\nu \theta)_\alpha F_{\mu\nu}^a + i\theta\theta (\sigma^\mu D_\mu \bar{\lambda}^a)_\alpha. \quad (1.3.26)$$

---

<sup>12</sup>In eq. (1.3.21), we have adopted the Wess-Zumino (super)gauge which enables us to eliminate additional bosonic and fermionic auxiliary fields that would be present in the expression of  $V^a$  in a general gauge. This choice being for the supergauge, the ordinary gauge is not fixed. The reader can refer to *e.g.* section 4.5 of [55] for more details.



Here  $T^a$  are the generators of the gauge group in the adjoint representation,  $F_{\mu\nu}^a$  the usual field-strength tensor and  $D_\mu$  the (gauge-)covariant derivative. In the end, one finds that, in all generality, the renormalisable terms that one can write are [42, 55]

$$\begin{aligned} \mathcal{L}_{\text{chiral+gauge}} = & \int d^2\theta d^2\bar{\theta} \left[ \Phi_i^* (\exp(2g_a T^a V^a))_{ij} \Phi_j \right] + \left( \int d^2\theta W(\{\Phi_i\}) \Big|_{\bar{\theta}=0} + \text{h.c.} \right) \\ & + \left( \int d^2\theta [\mathcal{W}^{a\alpha} \mathcal{W}_\alpha^a] \Big|_{\bar{\theta}=0} + \text{h.c.} \right). \end{aligned} \quad (1.3.27)$$

Note that for an Abelian gauge group, an additional type of term – a *Fayet-Iliopoulos* term – of the form

$$\mathcal{L}_{\text{FI}} = -2\kappa \int d^2\theta d^2\bar{\theta} V \quad (1.3.28)$$

is also allowed.

Recalling that integration over a Grassmannian variable amounts to taking a derivative, we can find

$$\begin{aligned} \int d^2\theta d^2\bar{\theta} \left[ \Phi_i^* (\exp(2g_a T^a V^a))_{ij} \Phi_j \right] = & F_i^* F_i + |D_\mu \phi_i|^2 + i\bar{\psi}_i \bar{\sigma}^\mu D_\mu \psi_i \\ & - \sqrt{2} g_a \phi_i^* T_{ij}^a \psi_j^\alpha \lambda_\alpha^a - \sqrt{2} g_a \bar{\lambda}_\alpha^a \bar{\psi}_i^{\dot{\alpha}} T_{ij}^a \phi_j \\ & + g_a \phi_i^* T_{ij}^a \phi_j D^a \end{aligned} \quad (1.3.29)$$

$$\begin{aligned} \int d^2\theta W(\{\Phi_i\}) \Big|_{\bar{\theta}=0} + \text{h.c.} = & - \frac{1}{2} \frac{\partial^2 W}{\partial \Phi_i \partial \Phi_j} \Big|_{\Phi_i=\phi_i} \psi_i \psi_j + \frac{\partial W}{\partial \Phi_i} \Big|_{\Phi_i=\phi_i} F_i + \text{h.c.} \\ = & - \frac{1}{2} (M_{ij} \psi_i \psi_j + \text{h.c.}) - \frac{1}{2} (y^{ijk} \psi_i \psi_j \phi_k + \text{h.c.}) \\ & + \frac{\partial W}{\partial \Phi_i} \Big|_{\Phi_i=\phi_i} F_i + \text{h.c.} \end{aligned} \quad (1.3.30)$$

$$\int d^2\theta [\mathcal{W}^{a\alpha} \mathcal{W}_\alpha^a] \Big|_{\bar{\theta}=0} + \text{h.c.} = \frac{1}{2} D^a D^a + i\bar{\lambda}^a \bar{\sigma}^\mu D_\mu \lambda^a - \frac{1}{4} F^{a\mu\nu} F_{\mu\nu}^a \quad (1.3.31)$$

$$\int d^2\theta d^2\bar{\theta} V = \frac{1}{2} D \quad (1.3.32)$$

We can immediately recognise the usual kinetic terms for scalars, Weyl fermions (including gauginos) and gauge bosons, as well as SUSY masses for fermions and Yukawa interactions between scalars and fermions. New SUSY interactions also appear in the second line of eq. (1.3.29) between scalar and fermions. The auxiliary fields can then be eliminated using their equations of motion that read in the non-Abelian case

$$\begin{aligned} F_i^* &= - \frac{\partial W}{\partial \Phi_i} \Big|_{\Phi_i \rightarrow \phi_i}, \\ D^a &= -g_a \phi_i^* T_{ij}^a \phi_j. \end{aligned} \quad (1.3.33)$$

Using the above equations of motion, terms in the Lagrangian containing the auxiliary fields can be rewritten, and one finds the (tree-level) scalar potential to be

$$V^{(0)}(\{\phi_i, \phi_i^*\}) = \left| \frac{\partial W}{\partial \Phi_i} \Big|_{\Phi_i \rightarrow \phi_i} \right|^2 + \frac{1}{2} \sum_a g_a^2 (\phi_i^* T_{ij}^a \phi_j)^2, \quad (1.3.34)$$

where the two terms will be referred to as the “ $F$ -term(s)” and the “ $D$ -term(s)” respectively. It is interesting to note that, both terms being squares, this potential is

automatically semi-positive definite (however, once SUSY breaking terms are added, it is necessary to verify that they do not destabilise the potential). In the Abelian case, the equation of motion contains an additional term coming from the Fayet-Iliopoulos term

$$D = -gQ_{\phi_i}\phi_i^*\phi_i + \kappa, \quad (1.3.35)$$

$Q_{\phi_i}$  being the charges of the fields  $\phi_i$  under the  $U(1)$  group. With respect to the non-Abelian case, this yields an additional contribution to the scalar masses due to a term

$$\mathcal{L}_{\text{FI}} \supset g\kappa Q_{\phi_i}\phi_i^*\phi_i, \quad (1.3.36)$$

plus some constant terms. In the models considered in this thesis however there will be no Fayet-Iliopoulos terms in the low-energy part of the spectrum.<sup>13</sup>

If we furthermore compute explicitly the  $F$ -terms for a general theory, with the superpotential as defined in eq. (1.3.23), we find

$$\begin{aligned} V_{F\text{-terms}}^{(0)} = & |L_i|^2 + M_{ij}^* M_{ik} \phi_j^* \phi_k + \frac{1}{4} (y^{ijk})^* y^{ilm} \phi_j^* \phi_k^* \phi_l \phi_m \\ & + \left( L_i^* M_{ij} \phi_j + \frac{1}{2} L_i^* y^{ijk} \phi_j \phi_k + \frac{1}{2} M_{ij}^* y^{ikl} \phi_j^* \phi_k^* \phi_l + \text{h.c.} \right). \end{aligned} \quad (1.3.37)$$

Once we have defined the gauge group we are considering and the representations in which the scalars (or equivalently the chiral supermultiplets) are, we can compute the  $D$ -terms explicitly as well (see sections 1.3.4 and 1.3.5). It is worth noticing that from the structure of terms in 1.3.34 and the requirement of gauge invariance of  $W$  and  $\mathcal{L}$  we know that the two scalars in the term  $(\phi_i^* T_{ij}^a \phi_j)^2$  must be in the same representation, while  $\phi_j$  and  $\phi_k$  in the  $(y^{ijk})^* y^{ilm} \phi_j^* \phi_k^* \phi_l \phi_m$  term can live in different representations of the gauge group.

In the end, we see that for a theory in which SUSY is unbroken it is sufficient to give the (super)field content (and the gauge group) together with the superpotential to fix entirely the Lagrangian. However, as we will now see, Supersymmetry cannot be an exact symmetry of Nature and new *SUSY-breaking* terms will appear in the Lagrangian.

### 1.3.1.5 $R$ -symmetry

The above description of supersymmetric Lagrangians can still, in some cases, accommodate an additional global  $U(1)_R$  symmetry – called  $R$ -symmetry – under which the (chiral) superfields can be charged and the superspace coordinates  $\theta, \bar{\theta}$  transform as

$$\theta \xrightarrow{R} e^{i\alpha} \theta, \quad \bar{\theta} \xrightarrow{R} e^{-i\alpha} \bar{\theta}, \quad (1.3.38)$$

where  $\alpha$  is the parameter of the transformation (in other words  $\theta$  and  $\bar{\theta}$  respectively carry  $R$ -charges  $+1$  and  $-1$ ). From this it can be shown (*e.g.* using their representation as differential operators acting on superspace) that the SUSY generators have respective charges  $-1$  and  $+1$  under  $R$  transformations, and hence

$$[R, Q] = -Q, \quad [R, \bar{Q}] = \bar{Q}. \quad (1.3.39)$$

---

<sup>13</sup>Fayet-Iliopoulos terms may appear in some mechanisms of spontaneous SUSY breaking at high-scales as we will briefly discuss later.

Superfields can be assigned additive charges under the  $R$ -symmetry – called  $R$ -charges – and then transform as

$$S(x, \theta, \bar{\theta}) \xrightarrow{R} e^{ir_S\alpha} S(x, e^{-i\alpha}\theta, e^{i\alpha}\bar{\theta}). \quad (1.3.40)$$

The superfield  $S^*$  has  $R$ -charge  $-r_S$ , and therefore real (*i.e.* gauge) superfields can not carry an  $R$ -charge. In the case of chiral superfields, as both the superfield itself and the superspace coordinates can carry an  $R$ -charge, the different components of the superfield will not have the same charge assignments: if the chiral superfield has an  $R$ -charge  $r_\Phi$ , then the scalar, fermion and auxiliary components have charges  $r_\Phi$ ,  $r_\Phi - 1$ , and  $r_\Phi - 2$  respectively. Moreover, one can find from the charge assignments of  $\theta$  and  $\bar{\theta}$  and the definitions in eq. (1.3.16) that the SUSY-covariant derivatives  $D_\alpha$  and  $\bar{D}^{\dot{\alpha}}$  have  $R$ -charges  $-1$  and  $+1$  and in turn one can deduce from this that field-strength superfields have  $r_W = 1$ .

As for any symmetry, the Lagrangian cannot carry any  $R$ -charge, which constrains the allowed terms and couplings in an  $R$ -symmetric SUSY model (depending on the charge assignments of the superfields in the model). The first and third terms in the Lagrangian of a general SUSY model – eq. (1.3.27) – (as well as the Fayet-Iliopoulos term in eq. (1.3.28)) are always  $R$ -symmetric however, the second term will only be so provided that the superpotential  $W$  has an  $R$ -charge equal to 2.

We will encounter  $R$ -symmetry in the MRSSM – a Dirac gaugino model devised to preserve a continuous  $R$ -symmetry – as well as the particular subgroup  $\mathbb{Z}_2$  of  $U(1)_R$  under which the MSSM and the NMSSM are built to be invariant. In both cases ( $U(1)_R$   $R$ -symmetry or  $R$ -parity), we will see that the new symmetry strongly constrains the superpotential and soft SUSY-breaking Lagrangian of the models.

### 1.3.2 SUSY breaking

An important observation one can make from the last equation in (1.3.10) is that as the momentum operator  $P^\mu$  commutes with the SUSY generators, the squared-mass operator  $P^2$  will commute as well and therefore particles in a same supermultiplet must have the same mass. This would mean that if Supersymmetry was not broken, a Standard Model particle and its superpartner would have the identical masses; but this would imply for example selectrons (scalar superpartners of electrons) with a mass of 511 keV! As these would necessarily have been observed a long time ago, Supersymmetry has to be broken, at least at low energies.

The study of SUSY breaking and of the possible mechanisms at work is a vast subject, which partly lies beyond the scope of the phenomenological approach to Supersymmetry. It is well accepted that Supersymmetry is broken spontaneously, or in other words that the complete Lagrangian of the theory is SUSY invariant but that the vacuum of the theory is not. In fact, it can be shown that SUSY is spontaneously broken if any of the (scalar) auxiliary fields  $F_i$  or  $D^a$  have non-zero VEVs. The proof of this statement is simple and is as follows [55]

- first if one takes the first line of eq. (1.3.10) for  $(\alpha, \dot{\alpha}) = (1, \dot{1})$  or  $(2, \dot{2})$  one can recover the Hamiltonian in terms of SUSY generators

$$\{Q_1, \bar{Q}_{\dot{1}}\} + \{Q_2, \bar{Q}_{\dot{2}}\} = 2\sigma_{11}^\mu P_\mu + 2\sigma_{22}^\mu P_\mu = 2\text{tr}(\sigma^\mu)P_\mu = 4P_0 = 4\mathcal{H} \quad (1.3.41)$$

where the trace is in spinor space, and  $\mathcal{H} \equiv P^0$  is the Hamiltonian.

- from the above equation, it follows that if a vacuum state  $|\text{vac}\rangle$  is not invariant under some SUSY transformation, *i.e.* if there exists an  $\alpha$  or  $\dot{\alpha}$  such that  $Q_\alpha|\text{vac}\rangle \neq 0$  and/or  $\bar{Q}_{\dot{\alpha}}|\text{vac}\rangle \neq 0$  then the energy of the vacuum state is non-zero

$$\langle \text{vac} | \mathcal{H} | \text{vac} \rangle > 0 \quad (1.3.42)$$

- if we further consider that there are no space-time dependent effects (and no fermion condensates) then

$$\mathcal{H} = \left( \int d^3x \right) V^{(0)} = \left( \int d^3x \right) [F_i^* F_i + \frac{1}{2} (D^a)^2] \quad (1.3.43)$$

and therefore

$$\langle \text{vac} | \mathcal{H} | \text{vac} \rangle = \left( \int d^3x \right) [\langle F_i^* \rangle \langle F_i \rangle + \frac{1}{2} \langle D^a \rangle^2] \quad (1.3.44)$$

which indeed shows that if SUSY is broken, at least one of the  $F_i$  or  $D^a$  fields must have a non-zero VEV.

The requirement of not breaking gauge symmetries further constrains which auxiliary fields may acquire VEVs, as the supermultiplets that contain them must be gauge singlets. Different scenarios of SUSY breaking exist taking this into account, the two main one being

- $D$ -term (or Fayet-Iliopoulos) breaking, in which an auxiliary field  $D$  of a  $U(1)$  gauge supermultiplet obtains a VEV from a Fayet-Iliopoulos term in the Lagrangian; or,
- $F$ -term (or O’Raifeartaigh) breaking, in which it is the auxiliary field  $F$  of a gauge singlet chiral superfield that acquires a VEV.

In neither case is it possible to accommodate the superfields required for SUSY breaking with the low-energy spectrum of a physically realistic SUSY theory. The SUSY breaking must then occur in some hidden sector and later be propagated to the observed sector by some new mechanism, such as for example<sup>14</sup> gauge mediation or Planck-scale suppressed mediation, typically at a very high-scale.

To study SUSY theories at phenomenologically accessible scales (MSSM, NMSSM, etc.), it is more convenient to work in an effective field theory approach and consider an effective low-energy Lagrangian for the model in which all the hidden and mediation sectors are integrated out. The information about the precise mechanism of SUSY breaking is then contained in new non-renormalisable operators that arise from the matching with the complete SUSY theory and break Supersymmetry explicitly. A subset of these terms have the additional property of not spoiling the solution that SUSY provides to the technical hierarchy problem by reintroducing quadratic divergences in scalar masses [59], and are hence called *soft* terms (because they only reintroduce soft, *i.e.* logarithmic, divergences). More precisely, soft terms can be Majorana mass terms for gauginos, mass terms for scalars, bilinear and trilinear couplings between scalars, and tadpole terms, *i.e.*

$$\mathcal{L}^{\text{soft}} = -\frac{1}{2} M_a \lambda^a \lambda^a + \text{h.c.} - m_{ij}^2 \phi_i^* \phi_j - \left[ \frac{1}{6} a_{ijk} \phi_i \phi_j \phi_k + \frac{1}{2} b_{ij} \phi_i \phi_j + t_i \phi_i + \text{h.c.} \right]. \quad (1.3.45)$$

---

<sup>14</sup>One could also mention mediation through anomalies or extra-dimension. See *e.g.* section 7 of [55] for further discussion of how SUSY breaking can be mediated.

A further type of terms, of the form

$$\mathcal{L}^{\text{soft}} \supset -\frac{1}{2}c_{ijk}\phi_i^*\phi^j\phi_k, \quad (1.3.46)$$

can be soft provided that there is no gauge singlet in the theory (the reason for this condition is that the above terms may generate divergences in singlet tadpoles). The possible soft terms in a given model are of course restricted because of gauge invariance, but it is interesting to note that Majorana masses for gauginos, as well as diagonal scalar masses (*i.e.* taking  $i = j$  in the second term of eq. (1.3.45)) are always allowed. Soft terms are yet further constrained in models that also respect an  $R$ -symmetry (as discussed in the previous section), however without specifying the  $R$ -charge assignments of the superfields, one can only observe that on the one hand, any diagonal soft scalar mass term is  $R$ -symmetric while, on the other hand, a Majorana mass term always breaks the  $R$ -symmetry (because the field-strength superfields, and thus the gauginos, have  $R$ -charge +1).

As soft mass terms and couplings are all produced through the same SUSY breaking process, they are expected to lie around a common mass (or mass-squared) scale, usually called the (soft) SUSY breaking scale, which is also the energy scale around which SUSY particles should be found if they exist. As we will see in more detail in the next chapter when reviewing Higgs mass calculations, the SUSY scale was first believed to be around, or a little above, the electroweak scale, however, as there is not yet any evidence of SUSY in experiments, it is currently expected to be of the order of a few TeV, or possibly much higher.

As a very brief example, let us now examine the case of an operator coupling a field-strength superfield  $\mathcal{W}^a$  of the observed sector to a chiral superfield  $X$  of the hidden sector

$$\mathcal{L} \supset - \int d^2\theta c_a \left[ \frac{X}{M} \mathcal{W}^{a\alpha} \mathcal{W}_\alpha^a \right] \Big|_{\bar{\theta}=0} \quad (1.3.47)$$

with  $c_a$  some coupling and  $M$  a (heavy) mass scale, required to keep the coupling dimensionless – this scale can be for example the Planck scale  $M_{\text{Pl}}$  in models with Planck-scale-mediated SUSY breaking. If we now suppose that the scalar and fermion components of  $X$  vanish and that only the auxiliary field  $F_X$  remains and obtains a VEV  $\langle F_X \rangle$ , then the above operator gives a contribution to the Lagrangian

$$\mathcal{L} \supset - \int d^2\theta c_a \left[ \frac{\theta\theta\langle F_X \rangle}{M} \mathcal{W}^{a\alpha} \mathcal{W}_\alpha^a \right] \Big|_{\bar{\theta}=0} + \text{h.c.} = -\frac{1}{2}M_a\lambda^{a\alpha}\lambda_\alpha^a + \text{h.c.} \quad (1.3.48)$$

Hence, through this toy model of  $F$ -term breaking, we have generated in the low energy theory a Majorana mass term  $M_a \equiv 2c_a\langle F_X \rangle/M$  for the gauginos.

Similarly, we can obtain a soft mass term for the scalar component of a chiral superfield  $\Phi$  through an operator

$$\mathcal{L} \supset - \int d^2\theta d^2\bar{\theta} f \frac{X^*X}{M^2} \Phi^*\Phi = -m_\phi^2\phi^*\phi \quad (1.3.49)$$

where  $m_\phi^2 = f\langle F_X \rangle^*\langle F_X \rangle/M^2$ . Such soft masses will appear for squarks, sleptons and Higgses (see *e.g.* eq. (1.3.61) in the case of the MSSM).

Finally, other types of SUSY breaking terms can exist in models of extended Supersymmetry, for example *supersoft* terms in Dirac gaugino models, which we will study in section 1.3.5.

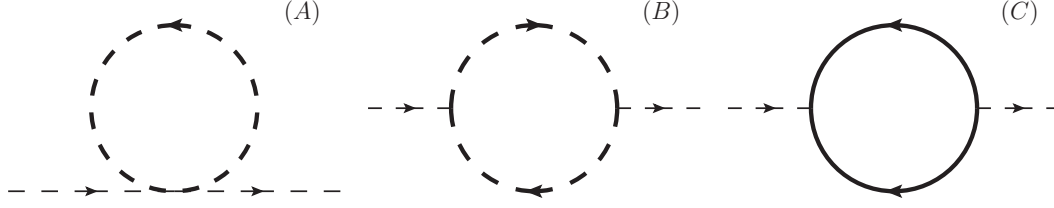


Figure 1.2 – One-loop diagrams contributing to the light scalar self-energy. Thick lines represent heavy states (scalars and fermions) while thin lines are for light states.

### 1.3.3 The hierarchy problem and Supersymmetry

In this section, we will show how Supersymmetry solves the hierarchy problem, presented in section 1.2.1. It is important to note, however, that Supersymmetry was not invented for the purpose of solving the hierarchy problem and that the fact that it does is only a fortuitous by-product of the extended symmetry. More precisely it is a consequence of one of the non-renormalisation theorems that have been proven for SUSY. In particular it has been shown that the superpotential is not renormalised [60, 61].

Let us investigate the cancellation of scalar mass corrections a bit more explicitly by considering a very simple toy model of a massless chiral superfield  $\mathbf{L}$  interacting with another heavy chiral superfield  $\mathbf{H}$ . In order to avoid mixing among the two superfields, we require the model, and hence the superpotential, to be invariant under the  $\mathbb{Z}_2$  transformation  $\mathbf{H} \rightarrow -\mathbf{H}$ . The superpotential is then

$$W(\Phi) = \frac{1}{2}M\mathbf{H}^2 + \frac{1}{2}Y\mathbf{L}\mathbf{H}^2. \quad (1.3.50)$$

Using the results of the previous sections, and assuming  $M$  and  $Y$  to be real, we find the Lagrangian of this model to be

$$\begin{aligned} \mathcal{L} = & |\partial_\mu L|^2 + |\partial_\mu H|^2 + i\bar{\psi}_L \bar{\sigma}^\mu \partial_\mu \psi_L + i\bar{\psi}_H \bar{\sigma}^\mu \partial_\mu \psi_H \\ & - M^2 |H|^2 - \frac{1}{2}M(\psi_H \psi_H + \text{h.c.}) - \frac{1}{2}Y(\psi_H \psi_H L + 2\psi_L \psi_H H + \text{h.c.}) \\ & - YM(L|H|^2 + \text{h.c.}) - Y^2 |L|^2 |H|^2 - \frac{1}{4}Y^2 |H|^4 \end{aligned} \quad (1.3.51)$$

There are three diagrams that will contribute to the radiative corrections to the light scalar mass, as shown in figure 1.2. We can compute each contribution and we find<sup>15</sup>

$$\begin{aligned} \Pi_{LL^*}^{(A)}(p^2) &= -(-iY^2) \int \frac{d^d k}{i(2\pi)^d} \frac{i}{k^2 - M^2} \\ &= \frac{Y^2}{16\pi^2} A(M^2), \end{aligned} \quad (1.3.52)$$

$$\begin{aligned} \Pi_{LL^*}^{(B)}(p^2) &= -(-iYM)^2 \int \frac{d^d k}{i(2\pi)^d} \frac{i}{k^2 - M^2} \frac{i}{(p+k)^2 - M^2} \\ &= -\frac{Y^2 M^2}{16\pi^2} B(p^2, M^2, M^2), \end{aligned} \quad (1.3.53)$$

<sup>15</sup>Note that the coefficient of the  $M^2 \times B$  term in  $\Pi_{LL^*}^{(C)}$  differs from the result in section 1.2.1 because a loop of Weyl fermions with mass insertions is not allowed here, as there is no  $\bar{\psi}_H \bar{\psi}_H L$  term.

$$\begin{aligned}
 \Pi_{LL^*}^{(C)}(p^2) &= + \frac{(-iY)^2}{2} \int \frac{d^d k}{i(2\pi)^d} \frac{i\sigma_{\alpha\dot{\alpha}}^\mu k_\mu}{k^2 - M^2} \frac{i(\bar{\sigma}^\nu)^{\dot{\alpha}\alpha}(k_\nu + p_\nu)}{(p+k)^2 - M^2} \\
 &= Y^2 \int \frac{d^d k}{i(2\pi)^d} \frac{k \cdot (k+p)}{(k^2 - M^2)((p+k)^2 - M^2)} \\
 &= - \frac{Y^2}{16\pi^2} \left[ A(M^2) - \left( M^2 - \frac{p^2}{2} \right) B(p^2, M^2, M^2) \right]
 \end{aligned} \tag{1.3.54}$$

where we used  $\sigma_{\alpha\dot{\alpha}}^\mu (\bar{\sigma}^\nu)^{\dot{\alpha}\alpha} = \text{tr}[\sigma^\mu \bar{\sigma}^\nu] = 2\eta^{\mu\nu}$  (the reader may refer to [62] for details on calculations with two-component spinors). The typical momentum at which these diagrams are is the tree-level light scalar mass, or in other words  $p^2 = 0$ , and we have then

$$\Pi_{LL^*}^{(A)}(0) + \Pi_{LL^*}^{(B)}(0) + \Pi_{LL^*}^{(C)}(0) = 0 \tag{1.3.55}$$

showing that the light scalar mass does not receive any correction, neither a quadratically divergent correction like existed in the SM, nor actually any finite correction.

The above discussion was in the case of unbroken Supersymmetry, but we will now show that the cancellation of quadratic divergences in scalar masses is not spoilt by soft SUSY breaking. For this purpose, let us suppose that the scalar component  $H$  of the superfield  $\mathbf{H}$  in our toy model receives a soft mass, that we denote  $m_{\text{soft}}^2$ .  $H$  then has mass  $m^2 = M^2 + m_{\text{soft}}^2$  and consequently the expressions of the (A) and (B) parts of the  $L$  self-energy must be modified with the replacement of the masses in the loop functions  $M^2 \rightarrow m^2$  (note that the factor  $M^2$  in front of the  $B$  function in eq. (1.3.53) is not changed because it comes from the  $L|H|^2$  coupling in the Lagrangian). In turn, the neat cancellation of the quadratic divergences of each term in eq. (1.3.55) is also modified, however, because we are interested in the behaviour of the light scalar mass corrections for large  $M$  and because we expect the soft SUSY-breaking scale  $m_{\text{soft}}$  to be much lower, we can obtain

$$\begin{aligned}
 A(m^2) - A(M^2) &= m^2 \overline{\log} m^2 - m^2 - M^2 \overline{\log} M^2 + M^2 \\
 &= (M^2 + m_{\text{soft}}^2) \left[ \overline{\log} M^2 + \log \left( 1 + \frac{m_{\text{soft}}^2}{M^2} \right) \right] - M^2 \overline{\log} M^2 - m_{\text{soft}}^2 \\
 &= m_{\text{soft}}^2 \overline{\log} M^2,
 \end{aligned} \tag{1.3.56}$$

to leading order in  $m_{\text{soft}}^2/M^2$ . Similarly, we have in the limit  $p^2 = 0$

$$M^2 (B_0(M^2, M^2) - B_0(m^2, m^2)) = -m_{\text{soft}}^2 + \dots \tag{1.3.57}$$

The one-loop corrections to the light scalar masses are in the end

$$\Pi_{LL^*}^{(A)}(0) + \Pi_{LL^*}^{(B)}(0) + \Pi_{LL^*}^{(C)}(0) = \frac{Y^2}{16\pi^2} (m_{\text{soft}}^2 \overline{\log} M^2 - m_{\text{soft}}^2). \tag{1.3.58}$$

This equation does indeed show new terms with respect to the unbroken-SUSY case of equation (1.3.55), however, the dependence on the heavy mass  $M$  is logarithmic, and not quadratic as we might have feared and as is the case in the SM. Such a logarithmic divergence in the scalar mass is far less severe than a quadratic one, and it is therefore referred to as a *soft* divergence (which also explain the name of soft SUSY breaking terms). A complete discussion, for a realistic model and taking into account the different types of soft terms that are allowed, was done in [59], showing that quadratic divergences are not reintroduced because of soft SUSY breaking.

We have here shown that Supersymmetry is able to solve the technical hierarchy problem, and for this it was not necessary to suppose that the SUSY breaking scale is

around the electroweak scale. We did assume  $m_{\text{soft}} \ll M$ , which served in particular to simplify the term  $M^2 \log(1 + m_{\text{soft}}^2/M^2)$ , but if we imagine once more that  $M \sim M_{\text{Pl}}$ , there is ample space for  $m_{\text{soft}}$  to be small with respect to  $M$  but large with respect to the EW scale  $v$ . However, as the SUSY scale is being driven higher up by experiments comes the problem of explaining the hierarchy between the electroweak and SUSY scales: currently the ratio of these scales is expected to be of the order of or larger than 10. This is called the *little hierarchy problem* and currently poses a challenge to Supersymmetry, at least in its minimal versions (as the MSSM).

### 1.3.4 Minimal models

There are numerous ways of extending the Standard Model into Supersymmetric theories, and SUSY model building is an extremely active domain nowadays. In this section, we will start the discussion of the Supersymmetric models considered in this thesis by minimal extensions of the SM, the MSSM and the NMSSM.

#### 1.3.4.1 The Minimal Supersymmetric Standard Model

The first and most natural way to extend the SM in the context of a (low-energy) SUSY model is to find the simplest way to assign SM fields in chiral and gauge supermultiplets, while adding only the smallest possible number of additional states to ensure the theoretical consistency of the model. This can actually be done quite simply: first, the SM fermions – quarks and leptons – are part of chiral supermultiplets and their superpartners – called squarks and sleptons – belong to the same representations of the SM gauge group (*c.f.* table 1.1). Then the gauge bosons are put in gauge supermultiplets and have fermionic superpartners – respectively gluinos, Winos and the Bino – that transform in the adjoint representation of the corresponding component of the gauge group. Finally, the Higgs boson is also part of a chiral supermultiplet but here the situation requires a little more care, because if there were only one fermionic partner of the Higgs – a higgsino – the electroweak gauge symmetry would be anomalous. Furthermore, with only one Higgs chiral superfield, there would be no way to write a holomorphic superpotential leading to Yukawa interactions for both up- and down-type quarks, nor any possibility to obtain a (supersymmetric) mass term for the higgsino. To avoid these three problems, two Higgs doublet superfields – with opposite weak hypercharges – are needed and we will call them  $\mathbf{H}_u$  and  $\mathbf{H}_d$ , the subscripts  $u$  and  $d$  indicating which type of quarks (up-type or down-type) that each doublet couples to. Moreover, to forbid interactions that violate<sup>16</sup>  $B - L$ , the model can be required to be invariant under a discrete symmetry, called  $R$ -parity, defined by a new quantum number

$$R_P \equiv (-1)^{3(B-L)+2s}, \quad (1.3.59)$$

that takes values  $+1$  for SM particles – including the Higgs bosons – and  $-1$  for all the new superpartners. A very interesting consequence of this  $R$ -parity is that the lightest particle with  $R_P = -1$ , *i.e.* the lightest superpartner (LSP), must be stable, which can obviously have strong phenomenological implications such as the LSP being a possible candidate of dark matter particle.

The model one finally obtains is the *Minimal Supersymmetric Standard Model* (MSSM), and its complete (super)field content is summarised in table 1.3 (on page 49) together

---

<sup>16</sup> $B$  and  $L$  are respectively the baryon and lepton numbers.



with the assignments of each superfield in representations of the  $SU(3)_C \times SU(2)_L \times U(1)_Y$  SM gauge group.

The superpotential of the MSSM is

$$W_{\text{MSSM}} = \mu \mathbf{H}_u \cdot \mathbf{H}_d + y_u^{fg} \mathbf{Q}_f \cdot \mathbf{H}_u \mathbf{u}_g^c - y_d^{fg} \mathbf{Q}_f \cdot \mathbf{H}_d \mathbf{d}_g^c - y_e^{fg} \mathbf{L}_f \cdot \mathbf{H}_d \mathbf{e}_g^c \quad (1.3.60)$$

where we denote all superfields in bold to avoid confusion with their component fields, and we use a dot “ $\cdot$ ” to indicate contracted  $SU(2)_L$  indices as  $\mathbf{H}_u \cdot \mathbf{H}_d = \epsilon^{ij} \mathbf{H}_{ui} \mathbf{H}_{dj}$ , and wrote family indices as in section 1.1. The MSSM Lagrangian also contains several soft SUSY breaking terms, that can be written in all generality as

$$\begin{aligned} \mathcal{L}_{\text{MSSM}}^{\text{soft}} = & -m_{H_u}^2 H_u^* H_u - m_{H_d}^2 H_d^* H_d - (B_\mu H_u \cdot H_d + \text{h.c.}) \\ & - (m_Q^2)_{fg} \tilde{Q}_{fL}^* \tilde{Q}_{gL} - (m_{\tilde{u}}^2)_{fg} \tilde{u}_{fR}^c (\tilde{u}_{gR}^c)^* - (m_{\tilde{d}}^2)_{fg} \tilde{d}_{fR}^c (\tilde{d}_{gR}^c)^* \\ & - (m_{\tilde{L}}^2)_{fg} \tilde{L}_{fL}^* \tilde{L}_{gL} - (m_{\tilde{e}}^2)_{fg} \tilde{e}_{fR}^c (\tilde{e}_{gR}^c)^* \\ & - \left( \frac{1}{2} M_3 \tilde{g}^a \tilde{g}^a + \frac{1}{2} M_2 \tilde{W}^a \tilde{W}^a + \frac{1}{2} M_1 \tilde{B} \tilde{B} + \text{h.c.} \right) \\ & - \left( (a_u)_{fg} \tilde{u}_{fR}^c \tilde{Q}_{gL} \cdot H_u + (a_d)_{fg} \tilde{d}_{fR}^c \tilde{Q}_{gL} \cdot H_d + (a_e)_{fg} \tilde{e}_{fR}^c \tilde{L}_{gL} \cdot H_d + \text{h.c.} \right). \end{aligned} \quad (1.3.61)$$

In the above soft Lagrangian,  $a_u$ ,  $a_d$ , and  $a_e$  are  $3 \times 3$  complex matrices in family space, while  $m_Q^2$ ,  $m_{\tilde{u}}^2$ ,  $m_{\tilde{d}}^2$ ,  $m_{\tilde{L}}^2$ , and  $m_{\tilde{e}}^2$  are  $3 \times 3$  Hermitian matrices in family space. We will follow the commonly choice of expressing soft trilinear couplings as the corresponding (dimensionless) superpotential coupling times a (mass-dimensional) term, which means here that the trilinears  $a_u$ ,  $a_d$ ,  $a_e$  are related to the Yukawas by matrices  $A_u$ ,  $A_d$ ,  $A_e$  such that  $a_u = y_u A_u$ , etc. Moreover, the bilinear coupling  $B_\mu$  can always be chosen to be real and positive, through a redefinition of the phase of one of the Higgs doublets. Mostly because of the SUSY breaking terms, the number of additional free parameters (masses, mixing angles, and phases) in the MSSM with respect to the SM is huge – it found in [63] to be larger than a hundred. Fortunately, many of these parameters are severely constrained, especially by experimental data from flavour physics (one could mention bounds on the  $\mu \rightarrow e \gamma$  process or on mixing between neutral kaons for example). Also, simplifying assumptions are often made from a theoretical point of view: for example when studying radiative corrections, it is common (as in chapter 3) to neglect<sup>17</sup> the effects of all leptons and of lighter quarks (*i.e.* quarks other than the top), and therefore assume that

$$y_u = \begin{pmatrix} 0 & 0 & 0 \\ 0 & 0 & 0 \\ 0 & 0 & y_t \end{pmatrix}, \quad a_u = \begin{pmatrix} 0 & 0 & 0 \\ 0 & 0 & 0 \\ 0 & 0 & y_t A_t \end{pmatrix}, \quad y_d = 0, \quad y_e = 0, \quad a_d = 0, \quad a_e = 0. \quad (1.3.62)$$

In some cases, such as phenomenological studies of models where parameters are scanned over to determine the regions of parameter space that are still allowed by experimental results, stronger assumptions are made to reduce the number of free parameters to one that allows numerical scans. One strategy is to impose unification conditions on parameters at some Grand Unified Theory (GUT) scale ( $M_{\text{GUT}}$ ), together with some particular mechanism of SUSY breaking at high scales. One example of a variant of the MSSM in this setting is the *Constrained MSSM*, or CMSSM

<sup>17</sup>However, as we will see at the end of the next subsection, neglecting the bottom and tau Yukawa couplings is only possible when the ratio of Higgs VEVs –  $\tan \beta$  – is not too large, because of the  $\tan \beta$  enhancement both Yukawas receive (see eq. (1.3.84))

(often called *mSUGRA* because the SUSY breaking is Planck-scale mediated in this model) in which there are only five free parameters: common masses of all sfermions  $m_0(Q = M_{\text{GUT}})$  and of gauginos  $m_{1/2}(Q = M_{\text{GUT}})$ ; a common soft trilinear coupling for all sfermions  $A_0(Q = M_{\text{GUT}})$  (*i.e.*  $A_u = A_d = A_e = \text{diag}(A_0, A_0, A_0)$ ); the ratio of the Higgs doublet VEVs  $\tan\beta$  (we will define this ratio properly in what follows) and finally the sign of the SUSY Higgs mass  $\mu$ . Similar models also exist assuming anomaly-mediated or gauge-mediated SUSY breaking, respectively the mAMSB and the mGMSB. Another possible strategy is to use phenomenological assumptions to limit the possible terms in the low-energy Lagrangian, an example of this being the *phenomenological MSSM* (or pMSSM) relying on three assumptions: that there are no new sources of CP-violation with respect to the SM, that there are no flavour changing neutral currents and that there is first and second generation universality. With these assumptions (motivated by experimental data), the pMSSM has 19 free parameters (see *e.g.* [64] for more details). Additional constraints can be considered, limiting the number of parameters and to distinguish the variants of the pMSSM it is common to refer to the variant with the number of parameters (*e.g.* pMSSM11, pMSSM17, etc.). Such versions of the MSSM, with constraints from the GUT scale or from phenomenological assumptions, are under intense scrutiny from theorists and experimentalists and several studies with likelihood analyses and global fits have been performed in recent years, mostly by the **GAMBIT** [65,66] and **MasterCode** [67–69] groups.

#### 1.3.4.2 The Higgs sector of the MSSM

Let us now investigate further the Higgs sector and how the electroweak symmetry is broken in the MSSM. First, each of the scalar components of the two doublet chiral superfields can be decomposed into their charged and neutral components

$$H_u = (H_u^+, H_u^0), \quad H_d = (H_d^0, H_d^-). \quad (1.3.63)$$

Using eq. (1.3.34) one can compute the tree-level scalar potential in the MSSM. In principle it would contain not only terms involving the Higgs bosons but also terms with squarks and sleptons, however, points in parameter space associated with sfermion VEVs – *e.g.* with negative soft squared masses or very large values of trilinear couplings – will not be considered because they lead to phenomenological problems. More specifically, VEVs for squarks would break  $SU(3)_C$  and  $U(1)_{\text{QED}}$  gauge invariances, and selectron, smuon, or stau VEVs also break  $U(1)_{\text{QED}}$ . Only sneutrino VEVs would in principle be allowed on grounds of preserving gauge invariance, but these would violate both lepton number and  $R$ -parity,<sup>18</sup> and have phenomenological effects on EWSB. We therefore do not consider squark and slepton terms in the scalar potential and find

$$\begin{aligned} V^{(0)} = & \left| \frac{\partial W}{\partial \mathbf{H}_u} \Big|_{\mathbf{H}_u \rightarrow H_u} \right|^2 + \left| \frac{\partial W}{\partial \mathbf{H}_d} \Big|_{\mathbf{H}_d \rightarrow H_d} \right|^2 \\ & + \frac{1}{2} g'^2 [Y_{H_u} H_u^* H_u + Y_{H_d} H_d^* H_d]^2 \\ & + \frac{1}{8} g^2 \left[ (H_u^- (H_u^0)^*) \begin{pmatrix} 1 & 1-i \\ 1+i & -1 \end{pmatrix} \begin{pmatrix} H_u^+ \\ H_u^0 \end{pmatrix} + ((H_d^0)^* H_d^+) \begin{pmatrix} 1 & 1-i \\ 1+i & -1 \end{pmatrix} \begin{pmatrix} H_d^0 \\ H_d^- \end{pmatrix} \right]^2 \\ & - \mathcal{L}_{\text{MSSM}}^{\text{soft}} \Big|_{H_u, H_d} \end{aligned} \quad (1.3.64)$$

---

<sup>18</sup>Note that spontaneous  $R$ -parity violation is actually excluded by experiments for the standard version of the MSSM [70].

$$\begin{aligned}
 &= |\mu|^2 (|H_u^0|^2 + |H_u^+|^2 + |H_d^0|^2 + |H_d^-|^2) \\
 &\quad + m_{H_u}^2 (|H_u^0|^2 + |H_u^+|^2) + m_{H_d}^2 (|H_d^0|^2 + |H_d^-|^2) + B_\mu [(H_u^+ H_d^- - H_u^0 H_d^0) + \text{h.c.}] \\
 &\quad + \frac{1}{8} (g^2 + g'^2) (|H_u^0|^2 + |H_u^+|^2 - |H_d^0|^2 - |H_d^-|^2)^2 + \frac{1}{2} g^2 |H_u^+ (H_d^0)^* + H_u^0 H_d^+|^2.
 \end{aligned}$$

In principle, we need to verify that we can break the electroweak gauge symmetry without also breaking  $U(1)_{\text{QED}}$  with this potential. Actually this is quite straightforward [55]: first with an  $SU(2)_L$  gauge transformation it is possible to rotate away the VEV from one of the components of one of the doublets, say  $\langle H_u^+ \rangle$ . Once that is done, one can take the derivative

$$\left. \frac{\partial V^{(0)}}{\partial H_u^+} \right|_{\text{min.}, \text{ with } \langle H_u^+ \rangle = 0} = B_\mu \langle H_d^- \rangle + g^2 \langle H_d^0 \rangle^* \langle H_u^0 \rangle^* \langle H_d^- \rangle = 0 \quad (1.3.65)$$

If we suppose for a moment that  $\langle H_d^- \rangle \neq 0$ , then the above equation implies that

$$\langle H_d^0 \rangle^* \langle H_u^0 \rangle^* = -B_\mu / g^2 \in \mathbb{R}, \quad (1.3.66)$$

and this means that  $H_u^0$  and  $H_d^0$  must have opposite phases. At this point we can use the remaining  $U(1)_Y$  gauge freedom we have to ensure – without loss of generality – that  $\langle H_d^0 \rangle$  and  $\langle H_u^0 \rangle$  are both real and positive (because  $H_u^0$  and  $H_d^0$  have opposite weak hypercharges), but this contradicts the result of eq. (1.3.66).

Finally this shows that  $\langle H_d^- \rangle = 0$  and that  $U(1)_{\text{QED}}$  indeed remains unbroken in the minimum of the MSSM tree-level potential. Only  $H_u^0$  and  $H_d^0$  can obtain VEVs, denoted  $v_u/\sqrt{2}$  and  $v_d/\sqrt{2}$  respectively from now on, which are related to the SM Higgs VEV  $v$  through the  $Z$  boson mass

$$v_u^2 + v_d^2 = v^2 = \frac{4m_Z^2}{g^2 + g'^2}. \quad (1.3.67)$$

Another very useful quantity is the ratio of the Higgs VEVs

$$\tan \beta \equiv \frac{v_u}{v_d}, \quad (1.3.68)$$

which will appear on many occasions.

In order to study the electroweak symmetry breaking, it is then sufficient to consider only the terms in the potential involving  $H_u^0$  and  $H_d^0$ , *i.e.* use the potential

$$\begin{aligned}
 V^{(0)} = & (|\mu|^2 + m_{H_u}^2) |H_u^0|^2 + (|\mu|^2 + m_{H_d}^2) |H_d^0|^2 - B_\mu [H_u^0 H_d^0 + \text{h.c.}] \\
 & + \frac{1}{8} (g^2 + g'^2) (|H_u^0|^2 - |H_d^0|^2)^2.
 \end{aligned} \quad (1.3.69)$$

We notice at first that along the direction  $H_u^0 = H_d^0$  (called the  $D$ -flat direction) the potential may not be bounded from below, unless [55]

$$2B_\mu < 2|\mu|^2 + m_{H_u}^2 + m_{H_d}^2. \quad (1.3.70)$$

Furthermore, as there are two states that can acquire VEVs, there remains two (non-trivial) minimum conditions for the potential given by its derivatives with respect to  $H_u^0$  and  $H_d^0$ . One can then ensure that  $v_u = v_d = 0$  is an unstable maximum of  $V^{(0)}$  by requiring that the Hessian matrix of  $V^{(0)}$  at  $v_u = v_d = 0$  must have at least one negative eigenvalue, which gives the additional condition on  $B_\mu$  [55]

$$B_\mu^2 > (|\mu|^2 + m_{H_u}^2)(|\mu|^2 + m_{H_d}^2) \quad (1.3.71)$$

Under these assumptions, the tadpole equations at tree-level read

$$\begin{aligned}
 \left. \frac{\sqrt{2}}{v_u} \frac{\partial V^{(0)}}{\partial H_u^0} \right|_{\min.} &= m_{H_u}^2 + |\mu|^2 - B_\mu \frac{v_d}{v_u} - \frac{1}{8}(g^2 + g'^2)(v_u^2 - v_d^2) = 0 \\
 &= m_{H_u}^2 + |\mu|^2 - B_\mu \cot \beta - \frac{m_Z^2}{2} \cos 2\beta = 0, \\
 \left. \frac{\sqrt{2}}{v_d} \frac{\partial V^{(0)}}{\partial H_d^0} \right|_{\min.} &= m_{H_d}^2 + |\mu|^2 - B_\mu \frac{v_u}{v_d} + \frac{1}{8}(g^2 + g'^2)(v_u^2 - v_d^2) = 0 \\
 &= m_{H_d}^2 + |\mu|^2 - B_\mu \tan \beta + \frac{m_Z^2}{2} \cos 2\beta = 0.
 \end{aligned} \tag{1.3.72}$$

The two most common choices for these tadpole equations are to solve for the soft Higgs doublet masses  $m_{H_u}^2$  and  $m_{H_d}^2$ , or to solve for  $|\mu|^2$  and  $B_\mu$ .

Now that we know what the vacuum expectation values of the doublets are, we can consider how to relate the gauge eigenstates  $H_u^+$ ,  $H_u^0$ ,  $H_d^-$ , and  $H_d^0$  to the mass eigenstates. First of all, as the electroweak symmetry breaking is still  $SU(2)_L \times U(1)_Y \rightarrow U(1)_{\text{QED}}$  the number of Goldstone bosons is the same as in the SM, *i.e.* two charged Goldstones  $G^\pm$  and a neutral (pseudoscalar) one  $G^0$ .  $G^+$  must then be expressed in terms of  $H_u^+$  and  $(H_d^-)^*$ , together with another charged state  $H^+$ , a charged Higgs boson

$$\begin{pmatrix} H_u^+ \\ H_d^+ \end{pmatrix} = \begin{pmatrix} s_{\beta\pm} & c_{\beta\pm} \\ -c_{\beta\pm} & s_{\beta\pm} \end{pmatrix} \begin{pmatrix} G^+ \\ H^+ \end{pmatrix} \tag{1.3.73}$$

where we use the short-hand notations  $c_x \equiv \cos x$  and  $s_x \equiv \sin x$ . Turning now to  $H_u^0$  and  $H_d^0$ , we know that they must contain the neutral Goldstone  $G^0$  as well as another CP-odd (pseudoscalar) Higgs  $A$  and two CP-even Higgses  $h$  and  $H$ . Conventionally, the mass eigenstates are defined by

$$\begin{pmatrix} H_u^0 \\ H_d^0 \end{pmatrix} = \frac{1}{\sqrt{2}} \begin{pmatrix} v \sin \beta \\ v \cos \beta \end{pmatrix} + \frac{1}{\sqrt{2}} \begin{pmatrix} c_\alpha & s_\alpha \\ -s_\alpha & c_\alpha \end{pmatrix} \begin{pmatrix} h \\ H \end{pmatrix} + \frac{1}{\sqrt{2}} \begin{pmatrix} s_{\beta_0} & c_{\beta_0} \\ -c_{\beta_0} & s_{\beta_0} \end{pmatrix} \begin{pmatrix} G^0 \\ A \end{pmatrix}. \tag{1.3.74}$$

In general the lightest CP-even Higgs  $h$  is assumed to correspond to the Higgs boson found at the LHC, although scenarios exist in which it is the heavy Higgs  $H$  that corresponds to the observed state, and the lighter  $h$  escapes detection in a very narrow range of masses not probed by the LEP or the LHC (such scenarios are becoming increasingly restricted as experiments further probe the possible parameter space).

At tree-level, a straightforward calculation shows that  $\beta_0 = \beta_\pm = \beta$  and that  $\alpha$  – conventionally taken in the interval  $[-\frac{\pi}{2}, 0]$  (for  $m_A^2 > m_Z^2$ ) – is related to  $\beta$  by the relation

$$\frac{\sin 2\alpha}{\sin 2\beta} = -\frac{m_H^2 + m_h^2}{m_H^2 - m_h^2}, \tag{1.3.75}$$

or equivalently

$$\frac{\tan 2\alpha}{\tan 2\beta} = \frac{m_A^2 + m_Z^2}{m_A^2 - m_Z^2}. \tag{1.3.76}$$

The tree-level scalar masses are (at the minimum of the tree-level potential)

$$\begin{aligned}
 m_A^2 &= \frac{2B_\mu}{\sin 2\beta}, \\
 m_{h,H}^2 &= \frac{1}{2} \left[ m_A^2 + m_Z^2 \mp ((m_A^2 - m_Z^2)^2 + 4m_Z^2 m_A^2 \sin^2 2\beta)^{1/2} \right], \\
 m_{H^\pm}^2 &= m_A^2 + m_W^2,
 \end{aligned} \tag{1.3.77}$$

while the Goldstone masses are zero as expected. The  $m_Z^2$  terms in the CP-even Higgs masses arise from the fact that, as opposed to the SM (and many of its non-SUSY extensions) the Higgs quartic couplings are not free parameters in Supersymmetry, but are related to the electroweak gauge couplings by the  $D$ -terms. A major consequence of this is that there is an upper limit in the MSSM on the lightest Higgs mass at tree-level [71, 72], namely

$$m_h^2 \leq m_Z^2 \cos^2 2\beta, \quad (1.3.78)$$

while the masses of the other Higgs bosons can grow in principle to arbitrarily large values with  $B_\mu$ . Note that this bound can be derived easily by taking the derivative of  $m_h^2$  from eq. (1.3.77) with respect to  $m_A^2$  and observing that it is always positive and only tends to zero in the limit  $m_A^2 \gg m_Z^2$ . At first sight, equation (1.3.78) seems to be incompatible with the observed Higgs mass of 125 GeV, but it was shown in the early 1990's [73–75] that radiative corrections – from top and stop loops – can be huge and pull the lightest Higgs mass up by a significant amount (we will discuss this in more detail in the next chapter). The bound (1.3.78) on  $m_h^2$  is saturated in the so-called *decoupling limit* in which  $m_A^2 \gg m_Z^2$  so that the states  $H$ ,  $A$ ,  $H^\pm$  become very heavy and decouple from the model. At lower energies, only the light state  $h$  is then left, and it becomes Standard Model-like – *i.e.* its interaction to SM particles become the same as in the SM. Such a situation, where one of the CP-even Higgs mass eigenstates is aligned in field-space with the (complete) Higgs VEV  $v$  – therefore becoming SM-like – is called *alignment*. In terms of the above defined mixing angles, alignment implies that

$$\beta = \frac{\pi}{2} - \alpha, \quad (1.3.79)$$

and this can occur even without decoupling (*e.g.* because of some symmetry) – one then talks of *alignment without decoupling*. Alignment, whether through decoupling or without it, is a powerful tool to relax experimental constraints, as signs of new Physics in the Higgs sector are hidden. If furthermore there is decoupling, then an extended Higgs sector cannot be distinguished from the SM one at currently accessible energy scales.

As was the case in the SM, the previous discussion of the Higgs sector is modified when one takes into account radiative corrections to the potential. First of all the tadpole equations (1.3.72) are modified by the inclusion of the derivatives of the radiative corrections to the potential  $\Delta V = V_{\text{eff}} - V^{(0)}$  with respect to  $H_u^0$  and  $H_d^0$  respectively. This in turn changes the parameters for which the tadpole equations are solved (either  $m_{H_u}^2$ ,  $m_{H_d}^2$  or  $|\mu|^2$ ,  $B_\mu$ ) and therefore the Goldstone tree-level masses as well. Unlike the SM, however, the tree-level masses in the minimum of the loop-corrected potential are not the same for the neutral and charged Goldstone bosons. These were shown in [33] to be (up to a different choice of convention for the VEVs)

$$\begin{aligned} m_{G^0}^2 &= -\delta_u s_\beta^2 - \delta_d c_\beta^2 - \frac{(\delta_u - \delta_d)^2}{8B_\mu} s_{2\beta}^3 + \dots \\ m_{G^\pm}^2 &= -\delta_u s_\beta^2 - \delta_d c_\beta^2 - \frac{(\delta_u - \delta_d)^2}{8(B_\mu + g^2 v_u v_d / 4)} s_{2\beta}^3 + \dots \end{aligned} \quad (1.3.80)$$

with the shorthand notations

$$\delta_u \equiv \frac{1}{\sqrt{2}v_u} \frac{\partial \Delta V}{\partial H_u^0} \Big|_{\text{min.}}, \quad \delta_d \equiv \frac{1}{\sqrt{2}v_d} \frac{\partial \Delta V}{\partial H_d^0} \Big|_{\text{min.}}. \quad (1.3.81)$$

In section 4.1.2, we will see how to extend the procedure for deriving the Goldstone tree-level masses in the minimum of the full potential in a general theory and we will

give explicitly the expressions of the leading (*i.e.* one-loop) terms – see eq. (4.1.26). As we had found for the SM in eq. (1.1.38), the Goldstone masses are formally of one-loop order, but can vanish or become negative leading to a Goldstone Boson Catastrophe in the MSSM as well. This was first addressed in Ref. [33] where the resummation method of [29] was applied to the MSSM to obtain an effective potential and tadpole diagrams free of infrared divergences. It is worth mentioning here that many calculations of Higgs masses in the MSSM have been performed in a so-called *gaugeless limit*, in which the electroweak gauge couplings  $g, g'$  are set to zero, and where the Goldstone Boson Catastrophe does not appear. The reason for this is that, as we saw earlier, the Higgs quartic coupling in the MSSM is related to the electroweak gauge couplings, therefore in the gaugeless limit the Higgs quartic coupling also vanishes and the Goldstones decouple from the Higgs bosons.

Finally, let us consider the interactions of the Higgs bosons with fermions and sfermions, and in particular the generation of fermion and sfermion masses. We saw in eq. (1.3.30) that the Yukawa interactions, between fermions and the Higgs doublets, are found via the second derivatives of the superpotential, which in this case gives

$$\begin{aligned} \mathcal{L} \supset & -y_u^{fg}(u_{fL}u_{gR}^c H_u^0 - d_{fL}u_{gR}^c H_u^+) + y_d^{fg}(u_{fL}d_{gR}^c H_d^- - d_{fL}d_{gR}^c H_d^0) \\ & + y_e^{fg}(\nu_{fL}e_{gR}^c H_d^- - e_{fL}e_{gR}^c H_d^0). \end{aligned} \quad (1.3.82)$$

If we only consider the third generation fermions, we find their tree-level masses to be

$$m_t = \frac{y_t}{\sqrt{2}}v_u = \frac{y_t}{\sqrt{2}}v \sin \beta, \quad m_b = \frac{y_b}{\sqrt{2}}v_d = \frac{y_b}{\sqrt{2}}v \cos \beta, \quad m_\tau = \frac{y_\tau}{\sqrt{2}}v_d = \frac{y_\tau}{\sqrt{2}}v \cos \beta, \quad (1.3.83)$$

where  $y_t, y_b$ , and  $y_\tau$  – the top, bottom and tau Yukawas – are the largest eigenvalues of the three Yukawa coupling matrices respectively. With respect to the SM case, the top (or bottom and tau) Yukawa coupling is modified by a new factor  $\sin \beta$  ( $\cos \beta$ ). This is especially noticeable when  $\tan \beta \gg 1$  where (at tree-level)

$$\frac{y_b^{\text{MSSM}}}{y_t^{\text{MSSM}}} = \frac{m_b}{m_t} \tan \beta = \frac{y_b^{\text{SM}}}{y_t^{\text{SM}}} \tan \beta \quad (1.3.84)$$

while  $y_t^{\text{MSSM}} = y_t^{\text{SM}}/\sin \beta \approx y_t^{\text{SM}}$ . This means that in the large  $\tan \beta$  limit of the MSSM, the bottom Yukawa (and similarly the tau one) can be much larger than their SM counterparts, so that even if it is still possible to neglect  $m_b, m_\tau \ll m_t$  it is not possible to neglect consistently  $y_b$  (and  $y_\tau$ ) before  $y_t$ .

If we then turn to couplings between the Higgses and the sfermions, these can arise from different sources. The first one is via the squared first derivatives of the same Yukawa terms in the superpotential, giving quartic interactions of the form  $|\text{sfermion-Higgs}|^2$ . To this are also added cross terms between the derivatives of the Yukawa and SUSY Higgs mass terms of  $W_{\text{MSSM}}$  and soft trilinear couplings, both giving sfermion-sfermion-Higgs interactions. Finally, a last type of terms come from the  $D$ -term part of the scalar Lagrangian yielding terms of the form  $|\text{sfermion}|^2|\text{Higgs}|^2$ . To study the masses of sfermions it actually suffices to compute couplings between sfermions and the neutral Higgses only. Furthermore, in order to simplify the discussion, we will not consider first and second generation sfermions that have very small (and hence usually

neglected) couplings to the Higgs sector. We obtain in this case

$$\begin{aligned}
 \mathcal{L} \supset & -y_t^2(\tilde{t}_L\tilde{t}_L^* + \tilde{t}_R\tilde{t}_R^*)|H_u^0|^2 - y_b^2(\tilde{b}_L\tilde{b}_L^* + \tilde{b}_R\tilde{b}_R^*)|H_d^0|^2 - y_\tau^2(\tilde{\tau}_L\tilde{\tau}_L^* + \tilde{\tau}_R\tilde{\tau}_R^*)|H_d^0|^2 \\
 & + \mu^* \left( y_t\tilde{t}_L\tilde{t}_R^*(H_d^0)^* + y_b\tilde{b}_L\tilde{b}_R^*(H_u^0)^* + y_\tau\tilde{\tau}_L\tilde{\tau}_R^*(H_u^0)^* \right) + \text{h.c.} \\
 & - \left( y_t A_t \tilde{t}_L\tilde{t}_R^* H_u^0 + y_b A_b \tilde{b}_L\tilde{b}_R^* H_d^0 + y_\tau A_\tau \tilde{\tau}_L\tilde{\tau}_R^* H_d^0 + \text{h.c.} \right) \\
 & + \frac{1}{2}(|H_u^0|^2 - |H_d^0|^2) \left[ \left( \frac{1}{2}g^2 - \frac{1}{6}g'^2 \right) \tilde{t}_L\tilde{t}_L^* + \frac{2}{3}g'^2\tilde{t}_R\tilde{t}_R^* \right. \\
 & \quad + \left( -\frac{1}{2}g^2 - \frac{1}{6}g'^2 \right) \tilde{b}_L\tilde{b}_L^* - \frac{1}{3}g'^2\tilde{b}_R\tilde{b}_R^* \\
 & \quad \left. + \left( -\frac{1}{2}g^2 + \frac{1}{2}g'^2 \right) \tilde{\tau}_L\tilde{\tau}_L^* - g'^2\tilde{\tau}_R\tilde{\tau}_R^* \right], \tag{1.3.85}
 \end{aligned}$$

where we use  $(a_u)_{33} = y_t A_t$ ,  $(a_d)_{33} = y_b A_b$ ,  $(a_e)_{33} = y_\tau A_\tau$ . Here we included the contribution from the  $D$ -terms for completeness, however these are sometimes neglected as will be the case in chapter 3 (moreover they vanish in the gaugeless limit).

The field-dependent stop mass matrix  $\mathcal{M}_{\text{stops}}^2$  is defined as

$$\mathcal{L} \supset -(\tilde{t}_L^* \ \tilde{t}_R^*) \mathcal{M}_{\text{stops}}^2 \begin{pmatrix} \tilde{t}_L \\ \tilde{t}_R \end{pmatrix}. \tag{1.3.86}$$

In the notations of chapter 3 (themselves taken from [76, 77]), and neglecting the  $D$ -term contributions, the stop mass matrix in the MSSM are found to be

$$\mathcal{M}_{\text{stops}}^2 = \begin{pmatrix} m_Q^2 + |X|^2 & \tilde{X}^* \\ \tilde{X} & m_U^2 + |X|^2 \end{pmatrix}, \tag{1.3.87}$$

where  $m_Q^2 = (m_Q^2)_{33}$  and  $m_U^2 = (m_U^2)_{33}$  – see eq. (1.3.61) – and

$$|X|^2 = y_t^2 |H_u^0|^2, \tag{1.3.88}$$

$$\tilde{X} = y_t (A_t H_u^0 - \mu^* (H_d^0)^*). \tag{1.3.89}$$

This matrix can be diagonalised to give two field-dependent mass eigenvalues

$$m_{\tilde{t}_{1,2}}^2 = \frac{1}{2} \left[ (m_Q^2 + m_U^2 + 2|X|^2) \pm \sqrt{(m_Q^2 - m_U^2)^2 + 4|\tilde{X}|^2} \right], \tag{1.3.90}$$

and similarly mass eigenvalues can be derived for sbottoms or staus. We will return to and refine the discussion of the stop masses in chapter 3 in the context of Dirac gaugino models. Before we end this section there is a last quantity that we need to define, for the discussion of radiative corrections to Higgs masses, namely the stop mixing, that we define at the minimum of the potential as

$$X_t = \frac{\langle \tilde{X} \rangle}{m_t} = A_t - \mu^* \cot \beta. \tag{1.3.91}$$

Finally, note that in many cases (*e.g.* the real MSSM, or in our study of Dirac gaugino models in chapter 3) the supersymmetric Higgs mass parameter  $\mu$  is taken to be real, which also has consequences for  $\tilde{X}$  and  $X_t$ . For a squark in general, the mixing parameter can be defined as

$$X_q = A_q - \mu^* \mathcal{F}(\beta), \tag{1.3.92}$$

where  $\mathcal{F}(\beta) = \cot \beta$  for  $q = u, c, t$ , and  $\mathcal{F}(\beta) = \tan \beta$  for  $q = d, s, b$ .

### 1.3.4.3 Gauginos in the MSSM

As we will shortly turn our focus to models with Dirac masses for gauginos, it is useful to first shortly review gauginos and their masses in the context of the MSSM. Every gaugino in the MSSM comes as a Weyl spinor – *i.e.* two complex degrees of freedom – in the adjoint representation of the different components of the SM gauge group as the gauge bosons. Unlike SM fermions, fermionic superpartners of SM gauge bosons obtain masses from soft SUSY breaking terms – such terms being allowed because gauge superfields, and hence the gauginos, are not chiral. More specifically, these are Majorana mass terms – see the fourth line of eq. (1.3.61) – that can be generated by high-scale operators such as those shown in eqs. (1.3.47) and (1.3.48).

After the electroweak symmetry breaking, the neutral electroweak gauginos  $\tilde{B}$ ,  $\tilde{W}^3$  mix with the neutral higgsinos  $\tilde{h}_u^0$ ,  $\tilde{h}_d^0$  to form four *neutralino* mass eigenstates, while the charged electroweak gauginos  $\tilde{W}^\pm = (\tilde{W}^1 \mp i\tilde{W}^2)/\sqrt{2}$  form, together with the charged higgsinos  $\tilde{h}_u^\pm$ ,  $\tilde{h}_d^\pm$ , two *chargino* mass eigenstates. The neutralino and chargino sector can have a rich phenomenology: most importantly, the lightest neutralino is often the LSP and consequently a possible candidate of Dark Matter – however its couplings to the Higgs scalars are always related to the electroweak gauge couplings and are hence small and negligible for our concern.

Therefore, we will in what follows not consider the electroweak gauginos, but only the gluinos  $\tilde{g}^a$ , that do not mix with fermions from the Higgs sector (because they are the only fermions to transform as octets under  $SU(3)_C$ ). They couple to squarks with the strong gauge coupling, and for this reason their contributions to the neutral scalar masses from two-loop and beyond can be large and must be taken into account.

### 1.3.4.4 Shortcomings of the MSSM

One serious theoretical issue of the MSSM is the so-called  $\mu$ -problem, *i.e.* the problem of generating the supersymmetric Higgs mass term  $\mu$  that must be of the order of the SUSY breaking scale  $M_{\text{SUSY}}$  (the scale of the SUSY breaking terms). The reason why  $\mu$  must be of the order of  $M_{\text{SUSY}}$  can be explained as follows [78]: on the one hand,  $\mu$  cannot be zero, because (among other reasons) there is a lower bound on the possible value of  $|\mu|$  coming from the experimental lower bound on chargino masses. On the other hand, if  $\mu$  is too large then the extremum of the potential at  $H_u = H_d = 0$  becomes a stable minimum and EWSB cannot take place (*e.g.* relation (1.3.71) cannot be verified). Therefore, the only scale that  $\mu$  can be related to is the SUSY breaking scale  $M_{\text{SUSY}}$ , which is also apparent from eq. (1.3.71) but is contradictory for a SUSY preserving parameter. As we will see in what follows, this problem can be solved in both the NMSSM and Dirac gaugino models [79], by generating the  $\mu$  term through the VEV of a dynamical field having the same quantum numbers as  $\mu$ , *i.e.* a singlet.

Another issue of the MSSM is to find a way to have sufficiently large radiative corrections to the Higgs mass to obtain a Higgs mass of 125 GeV even if the tree-level mass has a low upper-bound (1.3.78). As will be shown in the next chapter where we will discuss Higgs mass calculations, for the radiative corrections to be sufficiently large in the MSSM either of the following conditions needs to be fulfilled: large stop masses, or large stop mixing. Again the NMSSM and Dirac gaugino models improve the situation on this matter, by relaxing the upper-bound on  $m_h$  (more precisely, the equivalents of eq. (1.3.78) contain additional terms, due to the singlet or the adjoint superfields respectively).



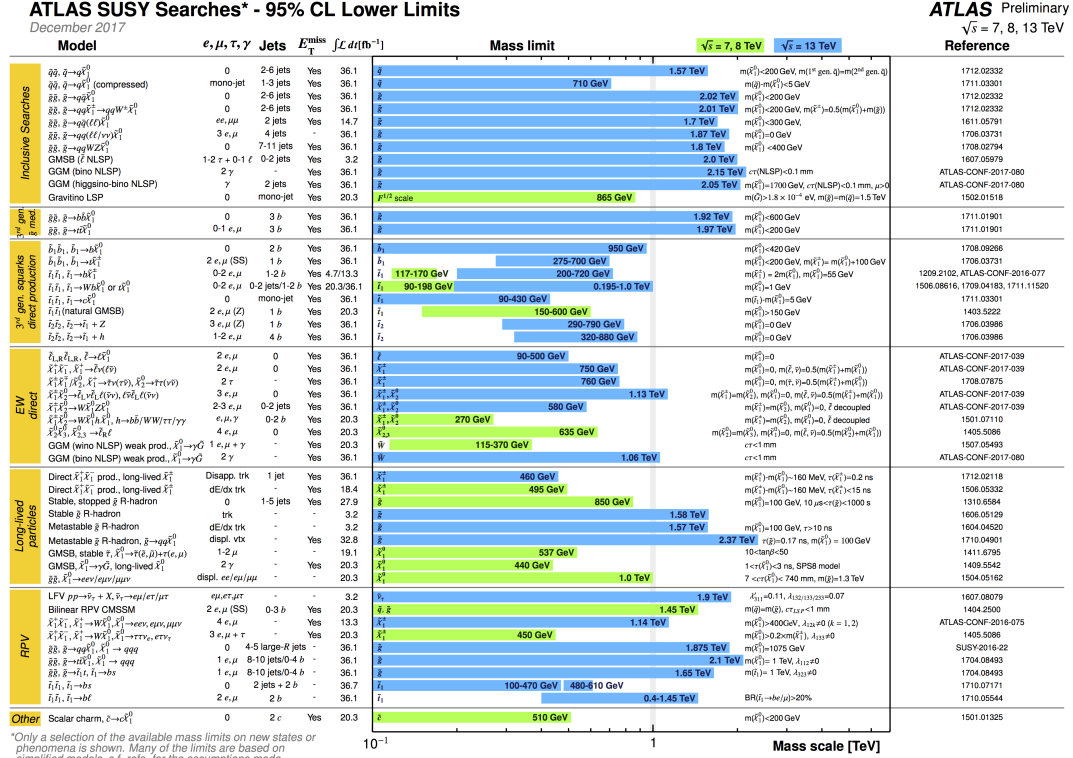


Figure 1.3 – Summary of lower limits on masses of SUSY particles, obtained by the different SUSY searches of the ATLAS collaboration by December 2017. This plot, along with other summary from ATLAS can be found on the web page: <https://atlas.web.cern.ch/Atlas/GROUPS/PHYSICS/CombinedSummaryPlots/SUSY/>. A similar plot for CMS, updated for the Moriond 2017 conference, can be found at [https://twiki.cern.ch/twiki/pub/CMSPublic/PhysicsResultsSUS/Moriond2017\\_BarPlot.pdf](https://twiki.cern.ch/twiki/pub/CMSPublic/PhysicsResultsSUS/Moriond2017_BarPlot.pdf).

Experimental searches have so far not yielded any sign of supersymmetric particles and thus raise the exclusion limits on possible masses for the superpartners – *e.g.* figure 1.3 shows for a summary of SUSY searches from the ATLAS collaboration. In particular, the stops were thought to be among the first superpartners to be observed at the LHC – being coloured particles, with strong couplings to other particles due to the large  $g_S$  and  $y_t$ , and being lighter than first and second family squarks in some models of SUSY breaking<sup>19</sup> – but Runs 1 and 2 have only been able to set a lower limit on their mass. Figure 1.4 provides an example of the limits on  $m_{\tilde{t}_1}$  obtained in the case of stop pair production. More generally, the latest public results for lower bounds on stop masses are – at 95% confidence level – 1150 GeV from ATLAS [80], and 1000 GeV from CMS [81] – in the case of compressed spectra the bounds are weaker, namely 430 GeV for ATLAS [82] and 510 GeV for CMS [83].

As mentioned earlier, this then poses questions as to whether Supersymmetry, if it exists, provides a satisfactory answer to the hierarchy problem, because even if it can protect scalar masses from quadratic divergences, it appears to be reintroducing a little hierarchy problem between the electroweak and the SUSY breaking scales.

<sup>19</sup>In the CMSSM, for example, the soft squark masses unify at the GUT scale, and under RGEs running the soft mass of the stop decreases slower than for the other squarks because the contribution from  $y_t$ .

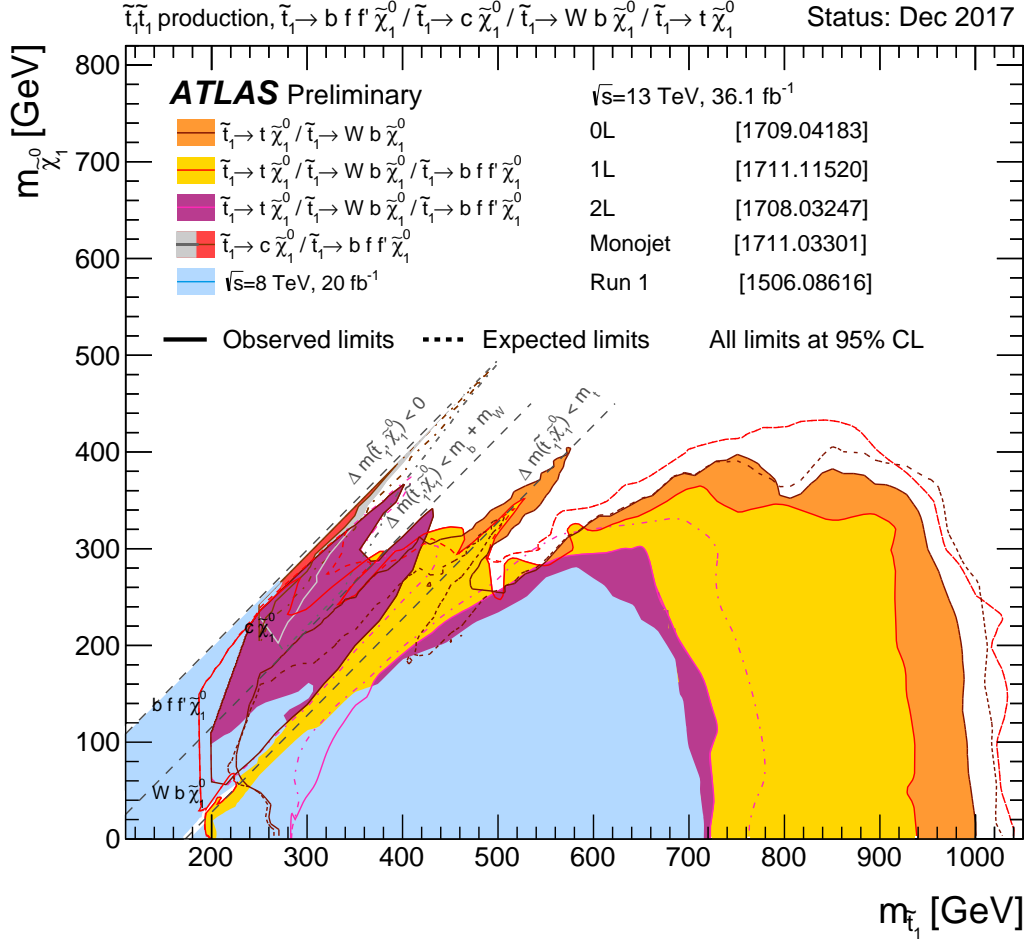


Figure 1.4 – Exclusion limits, at 95% confidence level, on stop and neutralino masses, resulting from the stop pair production search of the ATLAS collaboration. Different decay channels of the stops are considered, with quantities of data comprised between 3.2 and 36 fb<sup>-1</sup> from Run 2 of the LHC at  $\sqrt{s} = 13$  TeV. A comparison with results from Run 1 (light blue) is also provided. This plot can be found on the web page: <https://atlas.web.cern.ch/Atlas/GROUPS/PHYSICS/CombinedSummaryPlots/SUSY/>.

In this pessimistic context, one of the very interesting phenomenological features of models with Dirac gauginos is that stop production is suppressed (as we will discuss in section 1.3.5.3) therefore allowing such models to evade some of the current collider bounds.

#### 1.3.4.5 The Next-to-Minimal Supersymmetric Standard Model

As we have just seen, the MSSM, while solving some of the issues of the SM, still has a number of shortcomings. To address some of these and also because nothing prevents the Higgs sector from being extended, it is common to study extensions of the MSSM, and the simplest and most popular among them is the Next-to-Minimal Supersymmetric Standard Model or NMSSM, which provides a solution to the  $\mu$ -problem of the MSSM and enhances the tree-level mass of the lightest Higgs boson with respect to the MSSM (therefore reducing the size of the radiative corrections

required to have a 125 GeV Higgs). The NMSSM extends the MSSM by a gauge-singlet chiral superfield  $\mathbf{S}$ , and comes with a superpotential that reads in all generality

$$W_{\text{NMSSM}} = (\mu + \lambda_S \mathbf{S}) \mathbf{H}_u \cdot \mathbf{H}_d + T_S \mathbf{S} + \frac{1}{2} \mu_S \mathbf{S}^2 + \frac{1}{3} \kappa \mathbf{S}^3 \\ + y_u^{fg} \mathbf{Q}_f \cdot \mathbf{H}_u \mathbf{u}_g^c - y_d^{fg} \mathbf{Q}_f \cdot \mathbf{H}_d \mathbf{d}_g^c - y_e^{fg} \mathbf{L}_f \cdot \mathbf{H}_d \mathbf{e}_g^c, \quad (1.3.93)$$

while for the soft terms

$$\mathcal{L}_{\text{NMSSM}}^{\text{soft}} = \mathcal{L}_{\text{MSSM}}^{\text{soft}} + \left( a_{\lambda_S} S H_u \cdot H_d + \frac{1}{3} a_\kappa S^3 + \frac{1}{2} B_S S^2 + t_S S + \text{h.c.} \right) - m_S^2 |S|^2. \quad (1.3.94)$$

We choose to denote the superpotential coupling between the new singlet and the two Higgs doublets as  $\lambda_S$  instead of  $\lambda$  (as is often written in the literature) to avoid risks of confusion with the SM Higgs quartic coupling  $\lambda$ . Note also that linear (tadpole) terms, both in the superpotential and in the soft SUSY-breaking Lagrangian are allowed for the new state because it is a gauge singlet. The new trilinear couplings are defined such that  $a_{\lambda_S} = \lambda_S A_{\lambda_S}$  and  $a_\kappa = \kappa A_\kappa$ . While the above equations describe the general NMSSM, one often prefers to consider a restricted version of the NMSSM with a scale-invariant superpotential (*i.e.* without any mass-dimensionful parameters) obtained by imposing an additional, global,  $\mathbb{Z}_3$  symmetry to the theory under which all chiral superfields transform with a phase  $e^{i\frac{2\pi}{3}}$ . This significantly reduces the number of allowed parameters of the theory and the superpotential and soft Lagrangian are then

$$W_{\text{NMSSM}} = \lambda_S \mathbf{S} \mathbf{H}_u \cdot \mathbf{H}_d + \frac{1}{3} \kappa \mathbf{S}^3 \\ + y_u^{fg} \mathbf{Q}_f \cdot \mathbf{H}_u \mathbf{u}_g^c - y_d^{fg} \mathbf{Q}_f \cdot \mathbf{H}_d \mathbf{d}_g^c - y_e^{fg} \mathbf{L}_f \cdot \mathbf{H}_d \mathbf{e}_g^c, \\ \mathcal{L}_{\text{NMSSM}}^{\text{soft}} = - (m_Q^2)_{fg} \tilde{Q}_{fL}^* \tilde{Q}_{gL} - (m_{\tilde{u}}^2)_{fg} \tilde{u}_{fR}^c (\tilde{u}_{gR}^c)^* - (m_{\tilde{d}}^2)_{fg} \tilde{d}_{fR}^c (\tilde{d}_{gR}^c)^* \\ - (m_{\tilde{L}}^2)_{fg} \tilde{L}_{fL}^* \tilde{L}_{gL} - (m_{\tilde{e}}^2)_{fg} \tilde{e}_{fR}^c (\tilde{e}_{gR}^c)^* - m_{H_u}^2 H_u^* H_u - m_{H_d}^2 H_d^* H_d \quad (1.3.95) \\ - \left( \frac{1}{2} M_3 \tilde{g}^a \tilde{g}^a + \frac{1}{2} M_2 \tilde{W}^a \tilde{W}^a + \frac{1}{2} M_1 \tilde{B} \tilde{B} + \text{h.c.} \right) \\ - \left( (a_u)_{fg} \tilde{u}_{fR}^c \tilde{Q}_{gL} \cdot H_u + (a_d)_{fg} \tilde{d}_{fR}^c \tilde{Q}_{gL} \cdot H_d + (a_e)_{fg} \tilde{e}_{fR}^c \tilde{L}_{gL} \cdot H_d + \text{h.c.} \right) \\ + \left( a_{\lambda_S} S H_u \cdot H_d + \frac{1}{3} a_\kappa S^3 + \text{h.c.} \right) - m_S^2 |S|^2. \quad (1.3.96)$$

The absence of any term in  $W_{\text{NMSSM}}$  with a non-zero mass dimension means that there will be no situation analogous to the  $\mu$ -problem of the MSSM, and moreover we see that, if the singlet scalar acquires a VEV  $\langle S \rangle = v_S / \sqrt{2}$ , effective  $\mu$  and  $B_\mu$  terms can be generated as

$$\mu_{\text{eff}} = \frac{1}{\sqrt{2}} \lambda_S v_S, \quad (1.3.97)$$

$$B_\mu^{\text{eff}} = \frac{1}{\sqrt{2}} \lambda_S A_{\lambda_S} v_S + \frac{1}{2} \kappa^* \lambda_S v_S^2 = \mu_{\text{eff}} \left( A_{\lambda_S} + \kappa^* \frac{v_S}{\sqrt{2}} \right). \quad (1.3.98)$$

As in this scenario the only parameters in the scalar potential with a mass dimension are soft SUSY-breaking terms, the singlet VEV and in turn the effective  $\mu_{\text{eff}}$  and  $B_\mu^{\text{eff}}$  must also be of the order of the soft terms, therefore eliminating the possibility of an MSSM-like  $\mu$ -problem.

### 1.3.4.6 The Higgs sector of the NMSSM

The NMSSM has a vast and rich phenomenology, which we will not try to describe here, but instead we will now discuss some aspects of the Higgs sector of the NMSSM that will be useful for later chapters. First, the Higgs potential in the ( $\mathbb{Z}_3$ -invariant) NMSSM is

$$\begin{aligned}
 V^{(0)} = & |\mu + \lambda_S S|^2 (|H_u^0|^2 + |H_u^+|^2 + |H_d^0|^2 + |H_d^-|^2) + m_S^2 |S|^2 \\
 & + m_{H_u}^2 (|H_u^0|^2 + |H_u^+|^2) + m_{H_d}^2 (|H_d^0|^2 + |H_d^-|^2) + |\lambda_S (H_u^+ H_d^- - H_u^0 H_d^0) + \kappa S^2|^2 \\
 & + \frac{1}{8} (g^2 + g'^2) (|H_u^0|^2 + |H_u^+|^2 - |H_d^0|^2 - |H_d^-|^2)^2 + \frac{1}{2} g^2 |H_u^+ (H_d^0)^* + H_u^0 H_d^+|^2 \\
 & + \left[ \lambda_S A_{\lambda_S} S (H_u^+ H_d^- - H_u^0 H_d^0) + \frac{1}{3} \kappa A_\kappa S^3 + \text{h.c.} \right], \tag{1.3.99}
 \end{aligned}$$

having used the same decomposition of the Higgs doublets as in the MSSM. The precise determination of the vacuum state of the NMSSM is a long and difficult task – which we will not consider here (the reader may refer to [78, 84] for more details) – but it can be shown that vacua can exist with non-zero VEVs for both doublets and the singlet.<sup>20</sup> There are then three non-trivial tadpole equations that are typically used to eliminate  $m_{H_u}^2$ ,  $m_{H_d}^2$ , and  $m_S^2$ . The free parameters left to describe the Higgs sector of the NMSSM at tree-level are then

$$\lambda_S, \kappa, A_{\lambda_S}, A_\kappa, \tan \beta, v_S \text{ (or equivalently } \mu_{\text{eff}} \text{)}. \tag{1.3.100}$$

It is worth mentioning finally that the condition  $A_\kappa^2 \gtrsim 8m_S^2(9m_S^2)$  ensures the existence of an (absolute) minimum with  $v_S \neq 0$ .

The three complex neutral scalars appearing in the above potential can be decomposed into mass eigenstates as three real scalars (CP-even) and three pseudoscalars (CP-odd) – one of them being the neutral Goldstone – while the two charged components of the Higgs doublets give a charged Higgs and a charged Goldstone boson. The upper bound on the lightest Higgs mass becomes in the NMSSM

$$m_h^2 \leq m_Z^2 \cos^2 2\beta + \frac{1}{2} \lambda_S^2 v^2 \sin^2 2\beta, \tag{1.3.101}$$

where the second term shows an enhancement with respect to the MSSM, thanks to the presence of the additional singlet.

Another important consequence of the additional singlet and of its coupling  $\lambda_S$  is that the NMSSM is the simplest SUSY models in which the Goldstone Boson Catastrophe is apparent even in the gaugeless limit. Indeed, as can be seen in eq. (1.3.99),  $\lambda_S$  contributes to the Higgs triple and quartic couplings which then do not depend solely on  $g, g'$ . The NMSSM hence provides an excellent setting to compare the numerical workarounds first developed to circumvent the Goldstone Boson Catastrophe in SARAH/SPHeno with the general solution presented in chapter 4.

### 1.3.5 Dirac gaugino models

Many options are available to go beyond the minimal supersymmetric extensions of the Standard Model – MSSM and NMSSM – and among them one of the most promising

---

<sup>20</sup>Actually, depending on the parameters, the  $\mathbb{Z}_3$ -invariant NMSSM can allow several stable vacua which leads to a problem of domain walls in Cosmology, but once more this is far beyond the scope of this short review.

Supermultiplet		Spin-0 state	Spin- $\frac{1}{2}$ state	Spin-1 state	SM gauge group representation
<b>Matter sector</b>					
MSSM CHIRAL SUPERFIELDS					
(S)quarks	$\mathbf{Q}_f$	$\tilde{Q}_{fL} = (\tilde{u}_{fL}, \tilde{d}_{fL})$	$Q_{fL} = (u_{fL}, d_{fL})$	-	$(\mathbf{3}, \mathbf{2}, \frac{1}{6})$
	$\mathbf{u}^c_f$	$\tilde{u}^c_{fR}$	$u^c_{fR}$	-	$(\bar{\mathbf{3}}, \mathbf{1}, -\frac{2}{3})$
	$\mathbf{d}^c_f$	$\tilde{d}^c_{fR}$	$d^c_{fR}$	-	$(\bar{\mathbf{3}}, \mathbf{1}, \frac{1}{3})$
(S)leptons	$\mathbf{L}_f$	$\tilde{L}_{fL} = (\tilde{\nu}_{fL}, \tilde{e}_{fL})$	$L_{fL} = (\nu_{fL}, e_{fL})$	-	$(\mathbf{1}, \mathbf{2}, -\frac{1}{2})$
	$\mathbf{e}^c_f$	$\tilde{e}^c_{fR}$	$e^c_{fR}$	-	$(\mathbf{1}, \mathbf{1}, 1)$
Higgs/ Higgsinos	$\mathbf{H}_u$	$H_u = (H_u^+, H_u^0)$	$(\tilde{h}_u^+, \tilde{h}_u^0)$	-	$(\mathbf{1}, \mathbf{2}, \frac{1}{2})$
	$\mathbf{H}_d$	$H_d = (H_d^0, H_d^-)$	$(\tilde{h}_d^0, \tilde{h}_d^-)$	-	$(\mathbf{1}, \mathbf{2}, -\frac{1}{2})$
NMSSM SINGLET SUPERFIELD					
Singlet/singlino	$\mathbf{S}$	$S$	$\tilde{s}$	-	$(\mathbf{1}, \mathbf{1}, 0)$
MRSSM HIGGS-LIKE SUPERFIELDS					
Higgs-like states	$\mathbf{R}_u$	$(R_u^+, R_u^0)$	$(\tilde{r}_u^+, \tilde{r}_u^0)$	-	$(\mathbf{1}, \mathbf{2}, -\frac{1}{2})$
	$\mathbf{R}_d$	$(R_d^0, R_d^-)$	$(\tilde{r}_d^0, \tilde{r}_d^-)$	-	$(\mathbf{1}, \mathbf{2}, \frac{1}{2})$
<b>Gauge sector</b>					
MSSM GAUGE SUPERFIELDS					
Gluons/Gluinos	$\mathbf{G}$	-	$\tilde{g}^a$	$g^a$	$(\mathbf{8}, \mathbf{1}, 0)$
$W$ /Winos	$\mathbf{W}$	-	$\tilde{W}^a$	$W^a$	$(\mathbf{1}, \mathbf{3}, 0)$
$B$ /Bino	$\mathbf{B}$	-	$\tilde{B}$	$B$	$(\mathbf{1}, \mathbf{1}, 0)$
MDGSSM/MRSSM ADJOINT CHIRAL SUPERFIELDS					
Adjoint octet	$\mathbf{O}$	$O^a$	$\chi^a_O$	-	$(\mathbf{8}, \mathbf{1}, 0)$
Adjoint triplet	$\mathbf{T}$	$T^a$	$\chi^a_T$	-	$(\mathbf{1}, \mathbf{3}, 0)$
Adjoint singlet	$\mathbf{S}$	$S$	$\chi_S$	-	$(\mathbf{1}, \mathbf{1}, 0)$

Table 1.3 – Field contents and representation assignments of the MSSM, the NMSSM, the MDGSSM and the MRSSM. For the models beyond the MSSM, the field content is that of the MSSM plus the relevant additional states. In the MDGSSM, additional Higgs-like lepton and fake electron superfields are sometimes added to ensure the unification of gauge couplings (see *e.g.* [85]), but we will not consider these states in the context of the calculation of leading corrections to neutral scalar masses – in chapter 3 – so we do not mention them in this table. Finally,  $R$ -charges of the different states in the MRSSM are given separately in table 1.4.

is the class of models that allow Dirac masses for the gauginos [86–91], in particular instead of – but possibly in addition to – Majorana ones. Such models have drawn attention from the community in recent years because of various advantages that they provide with respect to the MSSM or NMSSM, from both theoretical and phenomenological points of view. On the theory side, Dirac gaugino models have the attractive feature that they increase the naturalness of the model, because Supersymmetry is broken by *supersoft* operators [89] and the SM-like Higgs boson mass is enhanced at tree level [79, 92]. Moreover, from a phenomenological perspective, Dirac gaugino masses are also interesting as they relax constraints on squark masses (through suppressing

production) [93–95] and flavour constraints [96–98].

Dirac gaugino masses require the addition of two fermionic degrees of freedom (*i.e.*, an extra Weyl spinor) for each gaugino. We can then write a mass term that respects a global chiral symmetry, which in SUSY models is promoted to a global  $U(1)$   $R$ -symmetry. In turn, Supersymmetry requires the same number of extra scalar degrees of freedom as fermionic ones; this implies that after electroweak symmetry breaking (EWSB) we have four new neutral scalar degrees of freedom compared to the MSSM, which may mix with the neutral scalars of the Higgs sector. The new states are packaged in an adjoint chiral multiplet for each gauge group, which should also have couplings to the Higgs scalars, possibly enhancing the SM-like Higgs boson mass at both tree and loop level.

We devote this section to an overview of Dirac gaugino models, for the needs of the study of two-loop corrections to neutral scalar masses in this context in chapter 3.

### 1.3.5.1 Extended Supersymmetry and supersoft SUSY breaking

The starting point for the construction of models with Dirac gauginos is to ask how much Supersymmetry (*i.e.* how many supercharges) can be allowed without encountering a theoretical inconsistency. First of all, the chiral nature of the SM fermions is a strong indication that, if it exists, Supersymmetry in the matter sector must have  $\mathcal{N} = 1$  – because in  $\mathcal{N} = 2$  SUSY, hypermultiplets cannot be chiral. Furthermore, the number of matter states in a theory with  $\mathcal{N} = 2$  SUSY is so large that it would lead to Landau poles at low energies (well before the GUT or Planck scales), for example for the strong gauge coupling. However, in the gauge sector the situation is different and  $\mathcal{N} = 2$  Supersymmetry can be considered without encountering problematic Landau poles [89] (although they would occur for  $\mathcal{N} = 4$ ). The extension of Supersymmetry for gauge states can be realised in an  $\mathcal{N} = 1$  language by adding chiral superfields  $\Sigma^a$  transforming in the adjoint representation of the gauge group (called more shortly *adjoint chiral superfields*).

The enriched structure of the gauge sector allows for new SUSY breaking terms, from which the eponymous Dirac masses of the gauginos result. More precisely, in the context of soft SUSY breaking<sup>21</sup>, the new  $D$ -term breaking operators can appear with the form [89]

$$\mathcal{L}_{\text{supersoft}} = \int d^2\theta \sqrt{2} \frac{\mathbf{W}'^\alpha \mathbf{W}_\alpha^a \Sigma^a}{M} + \text{h.c.} \quad (1.3.102)$$

where  $\mathbf{W}' = \lambda' + \theta D' + \dots$  is the field-strength superfield associated with some spurious vector superfield of the hidden sector, whose auxiliary  $D'$  component acquires a VEV  $\langle D' \rangle$ , and  $\mathbf{W}^a = \lambda^a + \theta D^a + \dots$  is the regular field-strength superfield of the gauge group. Upon spontaneous breaking of Supersymmetry, the above operator can be rewritten in terms of the auxiliary field VEV as

$$\begin{aligned} \mathcal{L}_{\text{supersoft}} &= \int d^2\theta \sqrt{2} \frac{\langle D' \rangle \theta^\alpha \mathbf{W}_\alpha^a \Sigma^a}{M} + \text{h.c.} \\ &= \int d^2\theta \sqrt{2} m_D \theta^\alpha \mathbf{W}_\alpha^a \Sigma^a + \text{h.c.} \\ &\supset -m_D \lambda^a \chi_\Sigma^a + \sqrt{2} m_D \Sigma^a D^a + \text{h.c.}, \end{aligned} \quad (1.3.103)$$

---

<sup>21</sup>It has also been suggested, *e.g.* in ref. [99], that Dirac masses could arise through other operators, but we do not consider them as they potentially correspond to a hard breaking of SUSY.

where we defined  $m_D = \langle D' \rangle / M$  and expanded the adjoint chiral superfield as  $\Sigma^a = \Sigma^a + \sqrt{2}\theta\chi_\Sigma^a + \dots$ . We recall that to derive the last line in the above equation, we made use of the following spinor algebra relation [55]

$$(\theta\xi)(\theta\chi) = -\frac{1}{2}(\theta\theta)(\xi\chi). \quad (1.3.104)$$

The first term in the above equation (1.3.103) is a Dirac mass term for  $\lambda^a$  and  $\chi_\Sigma^a$  – having the same form as equation (1.3.6) for a Dirac spinor made of  $\lambda^a$  and  $\bar{\chi}_\Sigma^a$  – while the second term will generate, for the scalar components of the adjoint chiral superfields (the adjoint scalars), mass terms as well as trilinear interactions with Higgses and sfermions, which we collectively denote as  $\phi$ . Indeed, integrating out the auxiliary field  $D^a$  gives for the adjoint scalars

$$\mathcal{L} \supset -(m_D \Sigma^a + m_D^* \Sigma^{a*})^2 - \sqrt{2}g(m_D \Sigma^a + m_D^* \Sigma^{a*})\phi^* t^a \phi, \quad (1.3.105)$$

where  $t^a$  are the generators of the gauge group in the representation appropriate to  $\phi$ , and a sum over the gauge indices of  $\phi$  is understood.

The reason why these new SUSY-breaking operators are called *supersoft* is actually one of the major features of models with Dirac gaugino, which is that these new operators do not reintroduce any logarithmic (*i.e.* soft) divergence in scalar masses. The only possible corrections are then finite ones, hence the name *supersoft*. A simple argument to prove this statement is provided in [89]: suppose first that the gaugino, having acquired a mass below the scale  $M$ , gives a logarithmically divergent contribution to the mass of a given scalar  $\phi$ . If we use a cut-off regularisation (see footnote 8) this correction takes the form  $m_D^2 \log \Lambda^2$  and the natural cut-off scale is  $\Lambda \sim M$ . Then there must exist a counter-term operator that regulates this divergence in cut-off regularisation, and it can be shown that the only possible supersymmetric and gauge-invariant operator associated with  $D$ -term SUSY breaking is of the form [89]

$$\begin{aligned} \int d^2\theta d^2\bar{\theta} \frac{(\mathbf{W}'^\alpha \mathbf{W}'_\alpha)^* \mathbf{W}'^\beta \mathbf{W}'_\beta}{M^6} \Phi^* \Phi \\ \xrightarrow{\mathbf{W}' \rightarrow \theta \langle D' \rangle} \int d^2\theta d^2\bar{\theta} \frac{\theta^2 \bar{\theta}^2 m_D^4}{M^2} \Phi^* \Phi \underset{M \sim \Lambda}{=} \frac{m_D^4}{\Lambda^2} \phi^* \phi, \end{aligned} \quad (1.3.106)$$

where  $\Phi$  is the chiral superfield containing the scalar  $\phi$ . There is however no way that this operator can cancel a logarithmic  $-\log \Lambda^2$  – divergence, and moreover it vanishes in the limit  $\Lambda \rightarrow \infty$ . Therefore, we can conclude that our original assumption must have been wrong and that corrections to scalar masses from a Dirac gaugino must be finite. In terms of diagrams contributing to the mass of the scalar  $\phi$ , this corresponds to a cancellation of the divergence of the fermion loop involving the fermionic partner of the scalar and a gaugino (left side of figure 1.5) against that of the new scalar diagram involving the scalar itself and the adjoint scalar (right side figure 1.5).

### 1.3.5.2 A brief overview of Dirac gaugino models

There is more than one way to construct a Dirac-gaugino extension of the MSSM. The minimal choice, which we will denote as the Minimal Dirac Gaugino Supersymmetric Standard Model (MDGSSM), consists in simply adding to the field content of the MSSM chiral multiplets that transform in the adjoint representations of each component of the SM gauge group, and allowing for all gauge-invariant terms in the superpotential and in the soft SUSY-breaking Lagrangian. The reader should note that

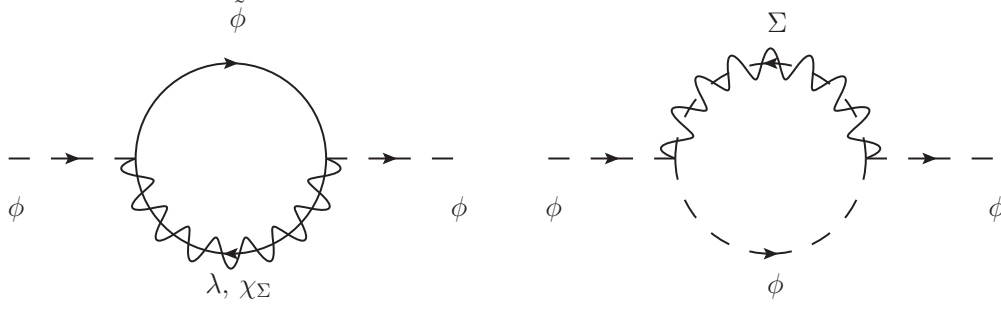


Figure 1.5 – Diagrams contributing to the mass of a scalar  $\phi$ : on the left hand side with  $\tilde{\phi}$ , *i.e.* the fermionic superpartner of  $\phi$ , and a Dirac gaugino ( $\lambda$  and  $\chi\Sigma$  in terms of Weyl spinors); and on the right hand side with the scalar  $\phi$  and the adjoint scalar  $\Sigma$ . The logarithmic divergences from both diagrams cancel out when the gauginos only have Dirac masses.

in recent works [85, 100, 101] the term MDGSSM has also been used to describe a unified scenario where extra lepton-like states are added to ensure natural gauge-coupling unification, but the distinction will be irrelevant for the discussion in chapter 3.

Models with Dirac gauginos also provide a possible setting for building low-energy supersymmetric models that preserve a  $U(1)_R$  symmetry – or  $R$ -symmetry – and not only an  $R$ -parity. First, one can realise that in an  $R$ -symmetry preserving extension of the MSSM, the usual Higgs doublets must have  $R$ -charge 0 – otherwise their VEVs would break the  $R$ -symmetry – and in turn from the structure of the Yukawa terms in the superpotential the quark and lepton superfields can be found to have  $R$ -charges +1 (because all terms in the superpotential must have total charge +2, see section 1.3.1.5).

If we then wish to construct a theory without large Majorana masses for the gauginos – and to be able to benefit from simpler SUSY-breaking scenarios [102] – we should avoid  $R$ -symmetry breaking in the soft terms, which also means removing the MSSM-like  $A$ -terms. Indeed, both Majorana mass terms for gauginos and  $A$ -terms are forbidden by  $R$ -symmetry because they correspond to Lagrangian terms with total  $R$ -charge +2, but it is important to note that the supersoft operator in eq. (1.3.102) is  $R$ -symmetric. Such a low-energy effective SUSY model with  $R$ -symmetry then naturally comes with Dirac gaugino masses and furthermore embeds into gauge-mediated scenarios [91, 103–108]. Moreover, the supersymmetric mass term  $\mu$  is also forbidden by  $R$ -symmetry, but we may retain a  $B_\mu$  term (allowed by the symmetry) since it is required for EWSB and will not generate Majorana masses through renormalisation group evolution.

An early variant of an  $R$ -symmetric SUSY model, with an approximate  $R$ -symmetry, is the  $\mu$ SSM or  $\mu$ -less MSSM [90], however, it should be noted that, as studied in ref. [109], the  $\mu$ SSM is currently challenged by electroweak precision measurements. On the other hand, if we choose to retain the  $R$ -symmetry as exact (possibly broken only by gravitational effects) then one popular construction is the Minimal  $R$ -symmetric Supersymmetric Standard Model, or MRSSM [96]: two additional Higgs-like superfields are included, which have  $R$ -charge +2 and couple in the superpotential to the regular Higgs doublets but obtain no expectation value. They allow the Higgs fields  $H_u$  and  $H_d$  to both have non-zero supersymmetric mass terms (see *e.g.* eq. (1.3.124) in the following) and contribute to the EWSB without violating the  $R$ -symmetry [96] (the  $R$ -charge assignments of all superfields of the MRSSM are given in table 1.4). An even more minimal realisation is the MMRSSM [110, 111], where the down-type Higgs



$H_d$  and its  $R$ -partner are missing, a sneutrino then playing the role of  $H_d$ . Another option to preserve  $R$ -symmetry is the supersymmetric one-Higgs-doublet model [112]: starting from the field content of the MDGSSM, the singlet adjoint superfield is missing and the down-type Higgs does not develop an expectation value, therefore the bino is massless up to anomaly-mediation contributions.

### 1.3.5.3 Some aspects of the phenomenology of Dirac gaugino models

Dirac gaugino models also have several phenomenological properties that are especially attractive with respect to the MSSM (and NMSSM). The first one can mention is that these models can naturally accommodate a relatively large hierarchy between gaugino (in particular gluino) and squark masses. The rationale for this is that, as we saw at the end of section 1.3.5.1, gaugino contributions to scalar mass parameters are smaller in models with Dirac gauginos than with Majorana gauginos (like in the MSSM) [94]. Therefore the Dirac masses for gauginos can be taken to much larger values than in the case of Majorana masses without spoiling the naturalness of the model – *i.e.* without increasing the necessary tuning, between tree-level values and radiative corrections, for scalar and in particular Higgs masses.

A second advantage is the suppression of the production rates of coloured SUSY particles [93–95, 113], which helps evade bounds from experimental searches. On the one hand, as Dirac gluinos can be heavy, both the gluino pair and the associated gluino-squark productions at colliders (*e.g.* the LHC) are typically suppressed by kinematics. On the other hand, the total production of squark pairs – either a squark plus an anti-squark or two squarks – is also suppressed because *(i)* processes with two squarks of the same handedness are absent when the gluino has a Dirac mass (these processes require a chirality flip,<sup>22</sup> which is only possible with a Majorana fermion), and furthermore *(ii)* several other channels involving the exchange of a gluino in a  $t$ -channel – such as for example  $pp \rightarrow \tilde{q}_L \tilde{q}_R, \tilde{q}_L^* \tilde{q}_R^*$  – are more suppressed than in the MSSM (because the gluino is a Dirac instead of a Majorana fermion). The remaining contributions then give a much lower squark pair production cross-section compared to the MSSM, and therefore the constraints obtained for squark masses in the MSSM are relaxed.

Finally, Dirac gaugino models also have favourable properties with respect to flavour constraints [96, 97, 114, 115], in particular when  $R$ -symmetry is preserved. More precisely, supersymmetric models are strongly constrained by experimental results on flavour violating observables, among which the most constraining is kaon-antikaon ( $K - \bar{K}$ ) oscillations. This is sometimes referred to as the *supersymmetric flavour problem* and in general SUSY models it is assumed to imply that the mechanism that mediates SUSY breaking between the hidden and observed sectors is flavour-blind. However, the possibility of constructing  $R$ -symmetric models of SUSY at low energies [96] lifts this requirement, and allows parameter points with large flavour violation to avoid current experimental results. A first reason for this is that all left-right mixing terms (*i.e.*  $A$ -type trilinear couplings), and therefore in particular left-right flavour violating terms, are forbidden by the  $R$ -symmetry. Moreover, if we take the example of kaon oscillations, it is known that new Physics contributions must be very

---

<sup>22</sup>If one considers the expansion of the supersoft operator in eq. (1.3.103) and integrates out the auxiliary fields, one can find that the fermion component of the adjoint superfield  $\chi_\Sigma^a$  does not couple to Higgses and sfermions, while the “MSSM-like” gaugino state  $\lambda^a$  does. For a (purely) Dirac gaugino this means that only one of its helicity states couples to Higgses and sfermions and hence chirality flip diagrams cannot exist. On the other hand, if the gaugino is a Majorana fermion, the two helicity states are equal – see eq. (1.3.9) – and the chirality flip is possible.

small, but in minimal SUSY models (*e.g.* the MSSM) with Majorana gauginos, potentially large and dangerous contributions arise from box diagrams involving effective operators between quarks and squarks like [96]

$$\frac{1}{m_{\tilde{g}}} \tilde{d}_R^* \tilde{s}_L^* \bar{\tilde{d}}_R s_L \quad (1.3.107)$$

Such a dimension-5 operator comes from integrating out the Majorana gauginos, but is forbidden in  $R$ -symmetry preserving models where the gaugino must be purely Dirac fermions. The leading operator obtained from integrating out a Dirac gaugino is a dimension-6 operator of the form

$$\frac{1}{m_{\tilde{g}}^2} \tilde{d}_L \partial_\mu \tilde{s}_L^* \bar{\tilde{d}}_L \gamma^\mu s_L \quad (1.3.108)$$

which is clearly more suppressed than the dimension-5 operator. Furthermore, as Dirac gauginos can naturally be significantly heavier than Majorana ones, the potential SUSY contributions to kaon mixing become strongly suppressed, and much larger amounts of flavour violation become acceptable. Other contributions to flavour violation observables are also suppressed in models with Dirac gauginos: *e.g.* the  $\mu \rightarrow e\gamma$  process requires a chirality flip [96,97] either in a gaugino or in a lepton line and, as we have discussed already, chirality flips are not possible with Dirac gauginos. Similarly, bounds on CP violation (for example from electric dipole moments) are weakened as well with Dirac gauginos [96,114]. We must emphasise however that these attractive results rely heavily on the gauginos being purely Dirac, and it was shown in [98] that if gauginos have both Majorana and Dirac masses (as is the case in the MDGSSM for example) the suppression of dangerous contributions to flavour or CP violating processes is reduced in most of the parameter space.

Let us now consider more closely the setting of our calculation in chapter 3, by discussing the properties of the adjoint scalars and of the gluinos in general Dirac gaugino models, before turning to the two models that will be studied, namely the MDGSSM and the MRSSM, and their respective Higgs sectors.

Supermultiplet		$R$ -charge
(S)quark multiplets	$\mathbf{Q}_f, \mathbf{u}_f^c, \mathbf{d}_f^c$	1
(S)lepton multiplets	$\mathbf{L}_f, \mathbf{e}_f^c$	1
Gauge multiplets	$\mathbf{G}, \mathbf{W}, \mathbf{B}$	0
Adjoint chiral multiplets	$\mathbf{O}, \mathbf{T}, \mathbf{S}$	0
MSSM-like Higgs multiplets	$\mathbf{H}_u, \mathbf{H}_d$	0
Extra Higgs multiplets	$\mathbf{R}_u, \mathbf{R}_d$	2

Table 1.4 – Supermultiplets of the MRSSM and their charges under the  $U(1)_R$  symmetry.

#### 1.3.5.4 Properties of the adjoint scalars

We have already seen that Dirac masses for gauginos as well as masses and couplings for the adjoint scalars are generated by the supersoft operator – see eqs. (1.3.103)

and (1.3.105). Considering now all sources of mass terms for the adjoint scalars  $\Sigma^a$ , we obtain

$$\mathcal{L} \supset -(m_\Sigma^2 + 2|m_D|^2) \Sigma^{a*} \Sigma^a - \frac{1}{2} (B_\Sigma + 2m_D^2) \Sigma^a \Sigma^a - \frac{1}{2} (B_\Sigma^* + 2m_D^{*2}) \Sigma^{a*} \Sigma^{a*} , \quad (1.3.109)$$

where  $m_\Sigma^2$  includes in general contributions from both the superpotential and the soft SUSY-breaking Lagrangian, and  $B_\Sigma$  is a soft SUSY-breaking bilinear term. In addition, mixing with the MSSM-like Higgs scalars may be induced, upon EWSB, by the  $D$ -term interactions in eq. (1.3.105), as well as by superpotential interactions.

We shall denote the adjoint multiplet for  $U(1)_Y$  as a singlet  $\mathbf{S} = S + \sqrt{2}\theta\chi_S + \dots$ , the one for  $SU(2)_L$  as a triplet  $\mathbf{T}^a = T^a + \sqrt{2}\theta\chi_T^a + \dots$ , and the one for  $SU(3)$  as an octet  $\mathbf{O}^a = O^a + \sqrt{2}\theta\chi_O^a + \dots$ . In chapter 3 we shall be interested only in the two-loop corrections to the Higgs masses involving the strong gauge coupling  $g_s$ , thus the relevant trilinear couplings in eq. (1.3.105) will be the ones involving the octet scalar (also called *sgluon*) and the squarks.

We shall make the additional restriction that the octet scalar only interacts via the strong gauge coupling and the above trilinear terms, equivalent to the assumption that it has no superpotential couplings or soft trilinear couplings other than with itself. This shall simplify the computations, and it is true for *almost* all variants of Dirac gaugino models studied so far. To have renormalisable Yukawa couplings between the octet and the MSSM fields we would need to add new coloured states (such as a vector-like top). However, in the most general version of the MDGSSM there could also be terms that violate the above assumption – which have only recently attracted attention [85, 116] – namely couplings between the singlet and the octet of the form

$$W \supset \frac{1}{2} \lambda_{SO} \mathbf{S} \mathbf{O}^a \mathbf{O}^a, \quad \mathcal{L} \supset -\frac{1}{2} T_{SO} S O^a O^a + \text{h.c.} . \quad (1.3.110)$$

The coupling  $\lambda_{SO}$  is typically neglected because it violates  $R$ -symmetry and leads to Majorana gaugino masses: for example, in the restricted version of the MDGSSM or the  $\mu$ SSM the  $R$ -symmetry violation is assumed to only occur in the Higgs sector and possibly only via gravitational effects. On the other hand, there is no symmetry preventing the generation of  $T_{SO}$ , but it is typically difficult for it to obtain a phenomenologically significant magnitude, hence it has been neglected – see [85] for a full discussion (and for cases when it could be large). Furthermore,  $T_{SO}$  is irrelevant in the decoupling limit (when the singlet  $S$  is heavy) that we shall employ later in our simplified formulae.

With the above assumptions, we can make a rotation of the superfield  $\mathbf{O}^a$  such that we can take  $m_D$  to be real without loss of generality, but we cannot simultaneously require that the soft SUSY-breaking bilinear  $B_O$  be real without additionally imposing CP invariance. The octet mass terms are then

$$\mathcal{L} \supset -m_O^2 O^{a*} O^a - \frac{1}{2} B_O O^a O^a - \frac{1}{2} B_O^* O^{a*} O^{a*} - m_D^2 (O^a + O^{a*})^2 . \quad (1.3.111)$$

If  $B_O$  is not real, the real and imaginary parts of the octet scalar mix with each other. Their mass matrix can be diagonalised with a rotation by an angle  $\phi_O$ ,

$$O^a = \frac{e^{i\phi_O}}{\sqrt{2}} (O_1^a + i O_2^a) , \quad \phi_O = -\frac{1}{2} \text{Arg}(B_O + 2m_D^2) , \quad (1.3.112)$$

to obtain the two mass eigenvalues

$$m_{O_{1,2}}^2 = m_O^2 + 2m_D^2 \pm |2m_D^2 + B_O| . \quad (1.3.113)$$

Then the trilinear couplings of the octet mass eigenstates  $O_{1,2}^a$  to squarks  $\tilde{q}_L$  and  $\tilde{q}_R$  read

$$\mathcal{L} \supset -2g_s m_D (\cos \phi_O O_1^a - \sin \phi_O O_2^a) (\tilde{q}_L^* t^a \tilde{q}_L - \tilde{q}_R^* t^a \tilde{q}_R) , \quad (1.3.114)$$

where  $t^a$  are the generators of the fundamental representation of  $SU(3)$ . These couplings lead to new (compared to MSSM and NMSSM) contributions to the two-loop effective potential involving the octet scalars which will affect the Higgs masses. We remark that, since in eq. (1.3.111) the superpotential mass term  $m_D^2$  affects only the real part of the octet scalar, the mixing angle  $\phi_O$  is suppressed by  $m_D^2$  in the limit where the latter is much larger than the soft SUSY-breaking mass terms. In particular,

$$\cos \phi_O \approx 1 + \mathcal{O}(m_D^{-4}) , \quad \sin \phi_O \approx -\frac{\text{Im}(B_O)}{4m_D^2} + \mathcal{O}(m_D^{-4}) . \quad (1.3.115)$$

For the remainder of this thesis, we shall restrict our attention to the CP-conserving case. This is motivated by clarity and simplicity in the calculations, and also physically in that there are strong constraints upon CP violation, even in the Higgs sector [117–120]. However, we shall make an exception in allowing a non-zero angle  $\phi_O$ , because it is particularly simple to do so, and its effects are only felt at an order beyond that considered here: it generates CP-violating phases in the stop mass matrix at two loops, and in the Higgs mass at three. This is because the couplings in eq. (1.3.114) are real, and phases only appear in the octet scalar-gluino-gluino vertex.

### 1.3.5.5 Gluino masses and couplings

In the case of Dirac gauginos, there is mixing between the Weyl fermion of the gauge multiplet  $\lambda^a$  and its Dirac partner  $\chi_\Sigma^a$ . We shall allow in general both Majorana and Dirac masses which, in two-component notation, we write as

$$\mathcal{L} \supset -\frac{1}{2} M_\lambda \lambda^a \lambda^a - \frac{1}{2} M_\Sigma \chi_\Sigma^a \chi_\Sigma^a - m_D \lambda^a \chi_\Sigma^a + \text{h.c.} . \quad (1.3.116)$$

As mentioned in the previous section, we can define  $m_D$  to be real. In general we cannot remove the phases from both  $M_\lambda$  and  $M_\Sigma$ ; however, as also mentioned above, we shall not consider CP violation in the gluino sector, and thus take all three masses to be real. We then rotate  $\lambda^a$  and  $\chi_\Sigma^a$  to mass eigenstates  $\lambda_1^a$  and  $\lambda_2^a$  via a mixing matrix  $R_{ij}$ , so that

$$\lambda^a = R_{11} \lambda_1^a + R_{12} \lambda_2^a , \quad \chi_\Sigma^a = R_{21} \lambda_1^a + R_{22} \lambda_2^a . \quad (1.3.117)$$

In four-component notation, this leads in general to two Majorana gauginos with different masses. In the case of a pure Dirac mass, however, we obtain two Majorana gauginos with degenerate masses  $|m_{\lambda_1}| = |m_{\lambda_2}| = |m_D|$ , which can also be combined in a single Dirac gaugino, written in terms of Weyl spinors as

$$\Psi_D^a = \begin{pmatrix} \lambda^a \\ \bar{\chi}_\Sigma^a \end{pmatrix} . \quad (1.3.118)$$

We recall that in the models of interest here there are no Yukawa couplings of the additional octet superfield, therefore the two gluino mass-eigenstates only couple to quarks and squarks via their gaugino component  $\lambda^a$ . In particular, the couplings

of each (four-component) gluino  $\tilde{g}_i^a$  are simply related to the couplings of the usual (N)MSSM gluino by an insertion of the mixing matrix:

$$\mathcal{L} \supset -\sqrt{2} g_s R_{1i} [\tilde{q}_L^* t^a (\tilde{g}_i^a P_L q) - (\bar{q} P_L \tilde{g}_i^a) t^a \tilde{q}_R] + \text{h.c.}, \quad (1.3.119)$$

where a sum over the  $SU(3)$  indices of quarks and squarks is again understood. Consequently, as we shall see below, the gluino contribution to the two-loop effective potential in Dirac-gaugino models can be trivially recovered from the known results valid in the MSSM and in the NMSSM.

### 1.3.5.6 The MDGSSM and the MRSSM

We now consider the Higgs sector of the theory. Dirac gaugino models extend the (N)MSSM, so we shall assume that we have at least the usual two Higgs doublets  $H_u$  and  $H_d$ . To these we must add the adjoint scalars  $S$  and  $T^a$  mentioned above, which mix with the Higgs fields. The couplings of the adjoint scalars, as well as the presence of any additional fields in the Higgs sector, will, however, depend on the model under consideration. In the following we shall focus on the minimal Dirac-gaugino extension of the MSSM, the MDGSSM, and on the minimal  $R$ -symmetric extension, the MRSSM.

In the MDGSSM there are no additional superfields apart from the adjoint ones, and the superpotential reads

$$W = W_{\text{Yukawa}} + W_{\text{MDGSSM}}, \quad (1.3.120)$$

$$W_{\text{Yukawa}} = Y_u^{fg} \mathbf{u}_f^c \mathbf{Q}_g \cdot \mathbf{H}_u - Y_d^{fg} \mathbf{d}_f^c \mathbf{Q}_g \cdot \mathbf{H}_d - Y_e^{fg} \mathbf{e}_f^c \mathbf{L}_g \cdot \mathbf{H}_d, \quad (1.3.121)$$

$$W_{\text{MDGSSM}} = (\mu + \lambda_S \mathbf{S}) \mathbf{H}_u \cdot \mathbf{H}_d + \lambda_T \mathbf{H}_d \cdot \mathbf{T}^a \sigma^a \mathbf{H}_u + W_\Sigma, \quad (1.3.122)$$

where  $\sigma^a$  are Pauli matrices, and the dot-product denotes the antisymmetric contraction of the  $SU(2)_L$  indices. In addition to the terms explicitly shown in eqs. (1.3.121) and (1.3.122), the most general renormalisable superpotential contains terms involving only the adjoint superfields – namely, mass terms for each of them, all trilinear terms allowed by the gauge symmetries, and a linear term for the singlet – which we denote collectively as  $W_\Sigma$ . The most general soft SUSY-breaking Lagrangian for the MDGSSM contains non-holomorphic mass terms for all of the scalars, as well as Majorana mass terms for the gauginos, plus  $A$ -type (*i.e.*, trilinear),  $B$ -type (*i.e.*, bilinear) and tadpole (*i.e.*, linear) holomorphic terms for the scalars with the same structure as the terms in the superpotential. With the assumption, discussed in section 1.3.5.4, that we neglect the couplings  $\lambda_{SO}$  and  $T_{SO}$  defined in eq. (1.3.110), the superpotential  $W_\Sigma$  and the soft SUSY-breaking terms that involve only the adjoint fields are not relevant to the calculation of the two-loop  $\mathcal{O}(\alpha_t \alpha_s)$  corrections to the Higgs masses presented in chapter 3, apart from contributing to the masses and mixing of the adjoint fields as discussed in sections 1.3.5.4 and 1.3.5.5 above.

In the case of the MRSSM, we must add two superfields  $\mathbf{R}_u$  and  $\mathbf{R}_d$  with the same gauge quantum numbers as  $\mathbf{H}_d$  and  $\mathbf{H}_u$ , respectively, but with different charges under a conserved  $R$ -symmetry. The superpotential reads

$$W = W_{\text{Yukawa}} + W_{\text{MRSSM}}, \quad (1.3.123)$$

$$W_{\text{MRSSM}} = (\mu_d + \lambda_{S_d} \mathbf{S}) \mathbf{R}_d \cdot \mathbf{H}_d + \lambda_{T_d} \mathbf{H}_d \cdot \mathbf{T}^a \sigma^a \mathbf{R}_d \\ + (\mu_u + \lambda_{S_u} \mathbf{S}) \mathbf{H}_u \cdot \mathbf{R}_u + \lambda_{T_u} \mathbf{R}_u \cdot \mathbf{T}^a \sigma^a \mathbf{H}_u, \quad (1.3.124)$$

while all terms involving only the MSSM-like Higgs superfields and/or the adjoint superfields, such as those in eq. (1.3.122), are forbidden by the  $R$ -symmetry. The most general soft SUSY-breaking Lagrangian for the MRSSM contains non-holomorphic mass terms for all of the scalars, plus all of the holomorphic terms involving only the MSSM-like Higgs scalars and/or the adjoint scalars (which, as mentioned above, have no equivalent in the superpotential). In contrast, the  $R$ -symmetry forbids Majorana mass terms for the gauginos, and holomorphic terms for the scalars with the same structure as the terms in the MRSSM superpotential. The requirement that the  $R$ -symmetry is conserved also means that the scalar doublets  $R_u$  and  $R_d$  do not develop a vacuum expectation value (VEV), and do not mix with either the MSSM-like Higgs scalars or the adjoint scalars.

Due to the larger number of additional neutral scalar states, both in the MDGSSM and in the MRSSM, a presentation of the Higgs sector would become quite lengthy, and we refer instead the reader to [79, 85, 92, 109] for discussions of the Higgs sector in the MDGSSM, and for calculations of the Higgs potential at tree and loop level. We however recall here one important result, namely the modified upper bound on the lightest Higgs mass, which reads in the MDGSSM

$$m_h^2 \leq m_Z^2 \cos^2 2\beta + \frac{1}{2}(\lambda_S^2 + \lambda_T^2)v^2 \sin^2 2\beta. \quad (1.3.125)$$

This shows a possible enhancement of the tree-level Higgs mass with respect to the MSSM and NMSSM, once more demonstrating the increase naturalness of models with Dirac gauginos.

## 1.4 Non-supersymmetric extensions of the Standard Model

We will now devote the last section of this chapter to a brief presentation of the non-supersymmetric models that will be considered in this thesis. More specifically, we will only consider here theories with extended Higgs sectors – respectively extensions with a singlet scalar, with a second Higgs doublet, and with two triplets (one real and one complex). Such minimal extensions of the Standard Model (SM) are invaluable tools in the pursuit of physics beyond the SM (BSM). They offer the possibility of studying different effects at energy scales testable by the Large Hadron Collider (LHC) in a comparably clean environment – *i.e.* the models typically contain the minimal numbers of new fields to exhibit novel phenomenology.

### 1.4.1 Singlet extensions of the Standard Model

The simplest and most straightforward way to extend the SM is to add a gauge singlet scalar, which can be either complex or real. Phenomenological motivations for the study of models with singlets include the fact that they can provide candidates for dark matter [121–124], that they can also accommodate a strong first order phase transition [125] (one of the necessary conditions for electroweak baryogenesis), or that they could help stabilise the EW vacuum [126–128]. It is worth noting finally that models with gauge singlet scalars could arise also as low energy limits of theories at higher energies, such as *e.g.* the NMSSM from which all superpartners (sfermions, gauginos, higgsinos) and one Higgs doublet would have been integrated out.

In chapter 6, we will consider a real singlet extension, which we will refer to as the Singlet-extended SM (SSM), with the following scalar potential

$$V^{(0)} = \mu^2 |\Phi|^2 + \frac{1}{2} M_S^2 S^2 + \kappa_1 |\Phi|^2 S + \frac{1}{3} \kappa_2 S^3 + \frac{1}{2} \lambda |\Phi|^4 + \frac{1}{2} \lambda_{SH} S^2 |\Phi|^2 + \frac{1}{2} \lambda_S S^4. \quad (1.4.1)$$

A linear (tadpole) term for the singlet should in principle be present, however, we have the freedom to redefine the parameters of the potential by shifting the singlet by a constant (see *e.g.* Ref. [125]) and we use this to remove the linear term. Furthermore, one should also note that the conventions for the SM-like Higgs quartic  $\lambda$ , and the other quartics  $\lambda_S$ ,  $\lambda_{SH}$ , are chosen so as to match with the model file used in SARAH (having in mind the study of the SSM in chapter 6). In particular,  $\lambda$  is defined with a factor 2 with respect to the SM (eq. (1.1.5)). The Higgs doublet can be decomposed in the same way as in the SM – see eq. (1.1.4) – as a real CP-even Higgs scalar that here we denote  $\phi$ , together with neutral and charged Goldstones  $G^0, G^\pm$ , while the real scalar could in principle also be split into a VEV  $v_S$  plus a real CP-even scalar  $s$  – in practice, however, we will almost never be required to use such a decomposition, so we will mostly work with  $S$ . There are then two tadpole equations in the SSM, reading at tree-level

$$\left. \frac{\partial V^{(0)}}{\partial \phi} \right|_{\min.} = 0 = \mu^2 v + \kappa_1 v v_S + \frac{1}{2} \lambda v^3 + \frac{1}{2} \lambda_{SH} v v_S^2 \quad (1.4.2)$$

$$\left. \frac{\partial V^{(0)}}{\partial s} \right|_{\min.} = 0 = M_S^2 v_S + \frac{1}{2} \kappa_1 v^2 + \kappa_2 v_S^2 + \frac{1}{2} \lambda_{SH} v^2 v_S + 2 \lambda_S v_S^3 \quad (1.4.3)$$

One immediate change with respect to the SM is that in order for the neutral component of the Higgs doublet to obtain a non-zero VEV, it does not suffice any more that  $\mu^2 < 0$ , but instead the condition for EWSB is that

$$\mu^2 + \kappa_1 v_S + \frac{1}{2} \lambda_{SH} v_S^2 < 0 \quad (1.4.4)$$

The singlet also obtains a VEV from the above potential – interestingly eq. (1.4.3) does not even admit  $v_S = 0$  as a solution when  $\kappa_1 \neq 0$ . The usual choice, which will be followed here, is then to solve the tadpole equations for  $\mu^2$  and  $M_S^2$ , which leaves as free parameters of the SSM

$$\lambda, \lambda_{SH}, \lambda_S, \kappa_1, \kappa_2, v_S. \quad (1.4.5)$$

The neutral CP-even component  $\phi$  of the Higgs doublet mixes together with the singlet  $s$  to form two mass eigenstates, which we denote  $h$  and  $H$ . The scalar mixing angle  $\alpha$  is defined by the relation

$$\begin{pmatrix} \phi \\ s \end{pmatrix} = \begin{pmatrix} c_\alpha & -s_\alpha \\ s_\alpha & c_\alpha \end{pmatrix} \begin{pmatrix} h \\ H \end{pmatrix} \quad (1.4.6)$$

and can be found with the relation

$$\cot 2\alpha = \frac{m_{\phi\phi}^2 - m_{ss}^2}{2m_{s\phi}^2} = \frac{\kappa_1 v^2 + 2\lambda v^2 v_S - 2\kappa_2 v_S^2 - 8\lambda_S v_S^3}{4\kappa_1 v v_S + 4\lambda_{SH} v v_S^2} \quad (1.4.7)$$

When studying the SSM (as is also the case for other non-SUSY BSM models), it is common to take the two mass eigenvalues  $m_h^2$ ,  $m_H^2$  and the mixing angle  $\alpha$  as inputs,

and use them to compute the quartic couplings  $\lambda$ ,  $\lambda_{SH}$ ,  $\lambda_S$ . At tree-level, one can find the quartic couplings to be

$$\lambda = \frac{m_h^2 + m_H^2 t_\alpha^2}{v^2(1 + t_\alpha^2)}, \quad (1.4.8)$$

$$\lambda_S = \frac{\kappa_1 v^2}{8v_S^3} - \frac{\kappa_2}{4v_S} + \frac{(m_H^2 + m_h^2 t_\alpha^2)}{4(1 + t_\alpha^2)v_S^2}, \quad (1.4.9)$$

$$\lambda_{SH} = - \frac{m_H^2 t_\alpha - m_h^2 t_\alpha + \kappa_1 v + \kappa_1 t_\alpha^2 v}{vv_S(1 + t_\alpha^2)}. \quad (1.4.10)$$

Moreover, in chapter 6, we will show how to extract – at one- or two-loop order –  $\lambda$ ,  $\lambda_S$ , and  $\lambda_{SH}$  from an on-shell scalar spectrum, and the impact on the high-scale behaviour of the model of the order at which this matching is performed.

It is also possible to restrict the allowed couplings of the model by imposing a  $\mathbb{Z}_2$  symmetry under which the singlet is charged, or in other words transforms as  $S \rightarrow -S$ . This new symmetry then forbids the dimensionful couplings  $\kappa_1$  and  $\kappa_2$ , reducing the scalar potential to

$$V^{(0)} = \mu^2 |\Phi|^2 + \frac{1}{2} M_S^2 S^2 + \frac{1}{2} \lambda |\Phi|^4 + \frac{1}{2} \lambda_{SH} S^2 |\Phi|^2 + \frac{1}{2} \lambda_S S^4 \quad (1.4.11)$$

When  $M_S^2 > 0$  (as we will ensure), the  $\mathbb{Z}_2$  symmetry cannot be broken spontaneously and the singlet does not acquire a VEV (as can be seen from eq. (1.4.3)). We will use the acronym  $\mathbb{Z}_2$ SSM for this restricted version of the SSM (in reference to the additional  $\mathbb{Z}_2$  symmetry and to distinguish it from the general SSM). The fact that  $v_S$  and  $\kappa_1$  vanish means that there is only one useful tadpole equation, eq. (1.4.3) becoming trivial, and furthermore that there is no longer any mixing among the scalars – which greatly simplifies the derivation of an analytical formula for the two-loop extraction of the Higgs quartic  $\lambda$  (*c.f.* section 6.2.2.1).

### 1.4.2 Two-Higgs-Doublet Models

Another popular way of extending the SM Higgs sector is to add a second Higgs doublet, once again without modifying the remainder of the SM field content. The resulting models are called Two-Higgs-Doublet Models (2HDMs, or sometimes THDMs), and come in different variants (or *types*) depending on how the two Higgs doublets couple to fermions, as will be discussed below. The reader may refer to [129] or [130] for complete reviews of 2HDMs.

The most general renormalisable scalar potential that one can write for a model with two doublets – defined with equal hypercharges – takes the form

$$\begin{aligned} V^{(0)} = & m_{11}^2 \Phi_1^\dagger \Phi_1 + m_{22}^2 \Phi_2^\dagger \Phi_2 + m_{12}^2 [\Phi_1^\dagger \Phi_2 + \Phi_2^\dagger \Phi_1] \\ & + \lambda_1 (\Phi_1^\dagger \Phi_1)^2 + \lambda_2 (\Phi_2^\dagger \Phi_2)^2 + \lambda_3 (\Phi_1^\dagger \Phi_1) (\Phi_2^\dagger \Phi_2) \\ & + \lambda_4 (\Phi_1^\dagger \Phi_2) (\Phi_2^\dagger \Phi_1) + \frac{1}{2} \lambda_5 [(\Phi_1^\dagger \Phi_2)^2 + (\Phi_2^\dagger \Phi_1)^2] \\ & + \lambda_6 \Phi_1^\dagger \Phi_1 [\Phi_1^\dagger \Phi_2 + \Phi_2^\dagger \Phi_1] + \lambda_7 \Phi_2^\dagger \Phi_2 [\Phi_1^\dagger \Phi_2 + \Phi_2^\dagger \Phi_1]. \end{aligned} \quad (1.4.12)$$

Note that our sign convention for  $m_{12}^2$  differs from most definitions in the literature. When including fermions and their Yukawa interactions with the Higgs sector, we want



to avoid tree-level Higgs-mediated flavour-changing neutral currents (FCNCs), which would be conflicting with experimental results. These arise because if a certain type of fermions (leptons, or up- or down-type quarks) couples to both Higgs doublets the flavour eigenstates do not in general correspond to the interaction eigenstates. We therefore choose to impose a  $\mathbb{Z}_2$  symmetry under which the scalar doublets transform as

$$\Phi_1 \rightarrow +\Phi_1, \quad \Phi_2 \rightarrow -\Phi_2. \quad (1.4.13)$$

This forbids the couplings  $\lambda_6$  and  $\lambda_7$ , and in principle  $m_{12}^2$  as well. The mass coupling  $m_{12}^2$  is however left in the potential as a soft  $\mathbb{Z}_2$ -symmetry breaking term – in the sense that a non-zero value of  $m_{12}^2$  does not by itself reintroduce phenomenologically dangerous FCNCs.

This  $\{\Phi_1, \Phi_2\}$  basis is sometimes called the  $\mathbb{Z}_2$  basis and the scalar potential then reads

$$\begin{aligned} V^{(0)} = & m_{11}^2 \Phi_1^\dagger \Phi_1 + m_{22}^2 \Phi_2^\dagger \Phi_2 + m_{12}^2 [\Phi_1^\dagger \Phi_2 + \Phi_2^\dagger \Phi_1] \\ & + \lambda_1 (\Phi_1^\dagger \Phi_1)^2 + \lambda_2 (\Phi_2^\dagger \Phi_2)^2 + \lambda_3 (\Phi_1^\dagger \Phi_1) (\Phi_2^\dagger \Phi_2) \\ & + \lambda_4 (\Phi_1^\dagger \Phi_2) (\Phi_2^\dagger \Phi_1) + \frac{1}{2} \lambda_5 [(\Phi_1^\dagger \Phi_2)^2 + (\Phi_2^\dagger \Phi_1)^2]. \end{aligned} \quad (1.4.14)$$

One or both doublet(s)  $\Phi_1$  and  $\Phi_2$  may acquire VEVs if  $m_{ij}^2$  has one or two negative eigenvalues, and we write the doublets and their VEVs as

$$\Phi_i = \begin{pmatrix} \Phi_i^+ \\ \Phi_i^0 \end{pmatrix} \text{ and } \langle \Phi_i \rangle = \frac{1}{\sqrt{2}} \begin{pmatrix} 0 \\ v_i \end{pmatrix}, \text{ for } i = 1, 2. \quad (1.4.15)$$

Through a field redefinition, it is always possible to make  $m_{12}^2$  and  $\lambda_5$  real, but then the doublet VEVs may have complex phases which would lead to CP violation (see *e.g.* [131]). However, in the following we will consider only scenarios in which CP is not violated in the Higgs sector – *i.e.* CP-conserving 2HDMs – and therefore we assume  $v_i \in \mathbb{R}$ , for  $i = 1, 2$ , here. We then define the angle  $\beta$  through the usual relation

$$\tan \beta = \frac{v_2}{v_1} \Leftrightarrow \begin{cases} v_1 = v \cos \beta \\ v_2 = v \sin \beta \end{cases} \quad (1.4.16)$$

where  $v$  is defined by  $v^2 = v_1^2 + v_2^2$ . The mass parameters  $m_{11}^2$  and  $m_{22}^2$  can be determined using the tadpole equations, which read at tree-level

$$\begin{aligned} \left. \frac{\sqrt{2}}{v_1} \frac{\partial V^{(0)}}{\partial \Phi_1^0} \right|_{\min} = 0 &= m_{11}^2 + m_{12}^2 \tan \beta + \left( \lambda_1 \cos^2 \beta + \frac{1}{2} (\lambda_3 + \lambda_4 + \lambda_5) \sin^2 \beta \right) v^2, \\ \left. \frac{\sqrt{2}}{v_2} \frac{\partial V^{(0)}}{\partial \Phi_2^0} \right|_{\min} = 0 &= m_{22}^2 + m_{12}^2 \cot \beta + \left( \lambda_2 \sin^2 \beta + \frac{1}{2} (\lambda_3 + \lambda_4 + \lambda_5) \cos^2 \beta \right) v^2, \end{aligned} \quad (1.4.17)$$

and the 2HDM scalar sector is thus left with seven free parameters which are

$$\lambda_i \text{ (for } i \in \{1, 2, 3, 4, 5\}); \quad m_{12}^2; \quad \tan \beta. \quad (1.4.18)$$

As in the case of the (real) MSSM, the two Higgs doublets of the (CP-conserving) 2HDM can be decomposed in terms of mass eigenstates, namely two CP-even Higgses,  $h$  and  $H$ , a CP-odd pseudoscalar Higgs  $A$ , and a charged Higgs  $H^\pm$ . A common practice, similar to what we saw in the previ is then to take as inputs the four masses

$m_h, m_H, m_A, m_{H^\pm}$  as well as the mixing angle of the CP-even mass matrix  $\alpha$  (or  $t_\alpha \equiv \tan \alpha$ ), instead of the quartic couplings  $\lambda_i$  ( $i \in \{1, 2, 3, 4, 5\}$ ). The latter can in turn be computed at tree-level using the following relations

$$\lambda_1 = \frac{1 + t_\beta^2}{2(1 + t_\alpha^2)v^2} (m_h^2 t_\alpha^2 + m_H^2 + m_{12}^2 t_\beta (1 + t_\alpha^2)), \quad (1.4.19)$$

$$\lambda_2 = \frac{m_{12}^2 (1 + t_\beta^2)}{2t_\beta^3 v^2} + \frac{(1 + t_\beta^2)(m_h^2 + m_H^2 t_\alpha^2)}{2t_\beta^2 (1 + t_\alpha^2)v^2}, \quad (1.4.20)$$

$$\lambda_3 = \frac{1}{(1 + t_\alpha^2)t_\beta v^2} \left[ (m_H^2 - m_h^2)t_\alpha (1 + t_\beta^2) + 2m_{H^\pm}^2 (1 + t_\alpha^2)t_\beta + m_{12}^2 (1 + t_\alpha^2)(1 + t_\beta^2) \right], \quad (1.4.21)$$

$$\lambda_4 = \frac{1}{t_\beta v^2} (-m_{12}^2 (1 + t_\beta^2) + m_A^2 t_\beta - 2m_{H^\pm}^2 t_\beta), \quad (1.4.22)$$

$$\lambda_5 = \frac{1}{t_\beta v^2} (-m_{12}^2 (1 + t_\beta^2) - m_A^2 t_\beta), \quad (1.4.23)$$

using the shorthand notation  $t_\beta = \tan \beta$ .

Finally, assuming that one still wants to avoid tree-level FCNCs, there are several possible ways to assign transformation rules of the fermion under the  $\mathbb{Z}_2$  symmetry (see *e.g.* table 1 in [132]), and these correspond to different ways of coupling the Higgs doublets to fermions, *i.e.* to different types of 2HDMs. The two main types of 2HDMs that one then finds – and that will be considered in chapter 5 – are

- *type I*, in which only one of the doublets – taken to be  $\Phi_2$  – couples to the fermions, with a similar structure of couplings as the SM doublet;
- *type II*, in which the top quarks acquire masses from the doublet  $\Phi_2$  while the down quarks and leptons obtain theirs from the other doublet  $\Phi_1$ . This actually corresponds exactly to the Higgs-fermion couplings of the MSSM, and therefore one of the many motivation for the study of such 2HDMs is that they may appear as low energy limits of SUSY models, once all superpartners have been integrated out.

Other variants of 2HDMs exist with different  $\mathbb{Z}_2$  charge assignments for the fermions (one can mention lepton-specific or flipped 2HDMs for example) and, furthermore, if one abandons the requirement of suppressing FCNCs at tree-level then one obtains a 2HDM where all (gauge invariant) Yukawa interactions between fermions and the two Higgs doublets are allowed, called *type III* – but we will not consider any of these possibilities further in this thesis.

Before concluding this section, let us mention that it has been shown that a low energy Two-Higgs Doublet model with alignment in the Higgs sector can originate naturally from Dirac gaugino models at higher energies – this, and the fact that including loop corrections does not spoil the alignment, was discussed recently in [133]. As mentioned earlier in the context of the MSSM, alignment can further help avoid the experimental detection of an extended Higgs sector, by making one of the CP-even Higgses Standard Model-like – and we will return to alignment in the Higgs sector of 2HDMs in chapter 5.

### 1.4.3 The Georgi-Machacek model

The Georgi-Machacek Model [134] extends the SM by one real scalar  $SU(2)_L$ -triplet  $\eta$  with  $Y = 0$  and one complex scalar  $SU(2)_L$ -triplet  $\chi$  with  $Y = 1$ , in a way that

preserves *custodial symmetry*. Custodial symmetry is an accidental symmetry that appears in the SM, noticed because the Veltman  $\rho$  parameter, defined as

$$\rho \equiv \frac{m_W^2}{m_Z^2 \cos^2 \theta_W} \quad (1.4.24)$$

is exactly equal to 1 at tree-level. Although this equality does not hold when radiative corrections are included, the  $\rho$  parameter has been measured to be extremely close to 1, indeed

$$\rho_{\text{exp.}} = 1.0048 \pm 0.0022. \quad (1.4.25)$$

While the above result provides a strong constraint for BSM models, it also tends to indicate that some additional (approximate) symmetry exists to protect  $\rho$  from receiving large quantum corrections. In fact, it turns out that the SM Higgs kinetic term (1.1.11) and potential (1.1.5) exhibit an approximate symmetry under  $SU(2)_L \times SU(2)_R$  transformations – which becomes exact in the limit  $g' \rightarrow 0$ . Upon electroweak symmetry breaking, it is broken down to an approximate  $SU(2)$  symmetry, called the *custodial symmetry*. The Georgi-Machacek model is built to maintain this symmetry in presence of an extended Higgs sector – and in particular of doubly charged Higgs bosons that may have rich phenomenological properties.

The two additional triplet scalars  $\eta$  and  $\chi$  can be written as

$$\eta = \frac{1}{\sqrt{2}} \begin{pmatrix} \eta^0 & -\sqrt{2}(\eta^-)^* \\ -\sqrt{2}\eta^- & -\eta^0 \end{pmatrix}, \quad \chi = \frac{1}{\sqrt{2}} \begin{pmatrix} \chi^- & \sqrt{2}(\chi^0)^* \\ -\sqrt{2}\chi^{--} & -\chi^- \end{pmatrix}, \quad (1.4.26)$$

however, a very compact form to write the Lagrangian in a  $SU(2)_L \times SU(2)_R$  invariant form is instead to express the SM doublet and the triplets as a bidoublet  $\Phi$  and a bitriplet  $\Delta$

$$\Phi = \begin{pmatrix} \phi^{0*} & \phi^+ \\ \phi^- & \phi^0 \end{pmatrix}, \quad \Delta = \begin{pmatrix} \chi^{0*} & \eta^+ & \chi^{++} \\ \chi^- & \eta^0 & \chi^+ \\ \chi^{--} & \eta^- & \chi^0 \end{pmatrix}. \quad (1.4.27)$$

Here,  $\phi^+$  and  $\phi^0$  are the charged and neutral components of the SM doublet (defined in eq. (1.1.4)) and  $\phi^- = \phi^{+*}$ . Using this notation, the scalar potential of the Georgi-Machacek model reads

$$\begin{aligned} V^{(0)}(\Phi, \Delta) = & \frac{\mu_2^2}{2} \text{Tr} \Phi^\dagger \Phi + \frac{\mu_3^2}{2} \text{Tr} \Delta^\dagger \Delta + \lambda_1 [\text{Tr} \Phi^\dagger \Phi]^2 + \lambda_2 \text{Tr} \Phi^\dagger \Phi \text{Tr} \Delta^\dagger \Delta \\ & + \lambda_3 \text{Tr} \Delta^\dagger \Delta \Delta^\dagger \Delta + \lambda_4 [\text{Tr} \Delta^\dagger \Delta]^2 - \lambda_5 \text{Tr} (\Phi^\dagger \sigma^a \Phi \sigma^b) \text{Tr} (\Delta^\dagger t^a \Delta t^b) \\ & - M_1 \text{Tr} (\Phi^\dagger \tau^a \Phi \tau^b) (U \Delta U^\dagger)_{ab} - M_2 \text{Tr} (\Delta^\dagger t^a \Delta t^b) (U \Delta U^\dagger)_{ab}, \end{aligned}$$

$\tau^a$  and  $t^a$  are the  $SU(2)$  generators for the doublet and triplet representations respectively, while  $U$  is given for instance in [135] as

$$U = \begin{pmatrix} -\frac{1}{\sqrt{2}} & 0 & \frac{1}{\sqrt{2}} \\ -\frac{i}{\sqrt{2}} & 0 & \frac{i}{\sqrt{2}} \\ 0 & 1 & 0 \end{pmatrix}. \quad (1.4.28)$$

The doublet and the triplets obtain VEVs as

$$\langle \Phi \rangle = \frac{1}{\sqrt{2}} \begin{pmatrix} v_\phi & 0 \\ 0 & v_\phi \end{pmatrix}, \quad \langle \eta \rangle = \frac{1}{\sqrt{2}} \begin{pmatrix} v_\eta & 0 \\ 0 & -v_\eta \end{pmatrix}, \quad \langle \chi \rangle = \begin{pmatrix} 0 & v_\chi \\ 0 & 0 \end{pmatrix}, \quad (1.4.29)$$

where the custodial symmetry enforces  $v_\eta = v_\chi \equiv v_T$ , and there are no tree-level contributions to the  $\rho$  parameter. They further fulfil  $v_\phi^2 + 8v_T^2 = v^2$ , which allows us to define

$$s_H = \sin \Theta_H = \frac{2\sqrt{2}v_T}{v}, \quad c_H = \cos \Theta_H = \frac{v_\phi}{v}. \quad (1.4.30)$$

The free parameters of the model are then

$$\lambda_1 \dots \lambda_5, \quad M_1, \quad M_2, \quad s_H \quad (1.4.31)$$

since  $\mu_2^2, \mu_3^2$  can be eliminated by the tadpole equations. The physical eigenstates can be organised into representations of the custodial symmetry as

- a fiveplet consisting of a doubly charged, a singly charged, and a neutral CP-even scalar;
- a triplet consisting of a singly charged and a CP-odd neutral scalar; and,
- two CP-even singlets – typically denoted  $h$  and  $H$  – where the Standard Model Higgs-like boson is the lighter of the two.

Tree-level expressions for the triplet mass  $m_3$ , fiveplet mass  $m_5$  and singlet masses are given, for example, in [136] and read

$$\begin{aligned} m_5^2 &= \frac{M_1 v_\phi^2}{4v_T} + 12M_2 v_T + \frac{3}{2}\lambda_5 v_\phi^2 + 8\lambda_3 v_T^2, \\ m_3^2 &= \left( \frac{M_1}{4v_T} + \frac{1}{2}\lambda_5 \right) v^2, \\ m_{h,H}^2 &= \frac{1}{2} \left[ m_{11}^2 + m_{22}^2 \mp \sqrt{(m_{11}^2 - m_{22}^2)^2 + 4m_{12}^4} \right], \end{aligned} \quad (1.4.32)$$

with

$$\begin{aligned} m_{11}^2 &= 8\lambda_1 v_\phi^2, \\ m_{12}^2 &= -\frac{\sqrt{3}}{2} v_\phi [M_1 - 4(2\lambda_2 - \lambda_5)v_T], \\ m_{22}^2 &= \frac{M_1 v_\phi^2}{4v_T} - 6M_2 v_T + 8(\lambda_3 + 3\lambda_4)v_T^2. \end{aligned} \quad (1.4.33)$$

## Chapter 2

# Precision calculations of the Higgs boson mass

The Higgs boson and its properties provide an excellent setting for indirect searches of Physics beyond the Standard Model. Indeed, as we have seen in the previous chapter, many BSM models exhibit an extended Higgs sector, or contain additional states that have noticeable effects on it (*e.g.* stops in SUSY).

In particular, the mass of the observed (SM-like) Higgs boson is sensitive to radiative corrections from heavy particles and is actually a prediction in numerous extensions of the SM, such as Supersymmetry, while it is now measured to an impressive precision – of the order of 0.1% – making it the ideal tool for BSM searches.

After recalling the available measurements of the Higgs mass, we will in this chapter review some of the main results from the past three decades of activity on Higgs mass calculations in BSM models.

### 2.1 Measurements of the Higgs mass

The SM-like Higgs boson was discovered by the ATLAS and CMS collaborations at the CERN Large Hadron Collider (LHC) [49, 50] as an excess in the distribution of reconstructed Higgs decay products – for the  $h \rightarrow \gamma\gamma$  and  $h \rightarrow ZZ^* \rightarrow 4\ell$  channels – as a function of their invariant mass. Already from the moment of its first discovery the Higgs boson mass was known to a precision of the order of one GeV, which have since been improved to the remarkable level of about 0.2 GeV. At the time of writing, the most accurate experimental determination of  $m_h$  comes from the combined result of ATLAS and CMS using 5 fb<sup>-1</sup> of data at  $\sqrt{s} = 7$  TeV and 20 fb<sup>-1</sup> at  $\sqrt{s} = 8$  TeV, obtained during Run 1 of the LHC and reads [51]

$$m_h^{\text{exp.}} = 125.09 \pm 0.21 \text{ (stat.)} \pm 0.11 \text{ (syst.)} . \quad (2.1.1)$$

A more recent measurement was obtained by the ATLAS collaboration with 36.1 fb<sup>-1</sup> of Run 2 data at  $\sqrt{s} = 13$  TeV [52], see figure 2.1.

### 2.2 Scalar mass calculations

In the Standard Model, the Higgs quartic coupling  $\lambda$  is a yet-unmeasured free parameter, and thus the tree-level Higgs mass cannot be predicted from a theoretical

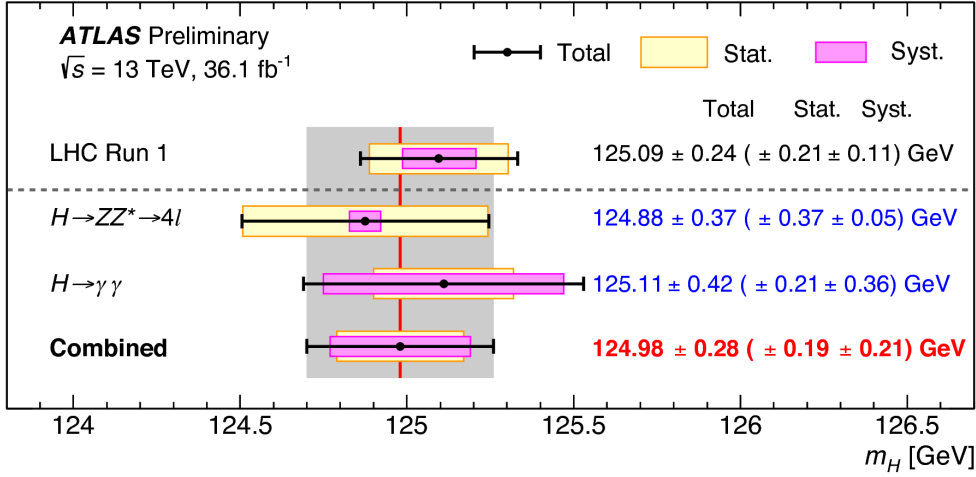


Figure 2.1 – ATLAS results for the SM-like Higgs boson mass, obtained from LHC Run2 data with an integrated luminosity of  $36.1 \text{ fb}^{-1}$  at  $\sqrt{s} = 13 \text{ TeV}$ , in the  $h \rightarrow \gamma\gamma$  and  $h \rightarrow ZZ^* \rightarrow 4\ell$  channels, as well as the combined result and comparison with the combined ATLAS and CMS measurement from Run 1. This plot is taken from [52].

calculation. The computation of quantum corrections to the Higgs mass in the SM then serves to improve the precision of the extraction of the Higgs quartic from the measured value of the Higgs mass – as discussed in section 1.2.2. However, some BSM models do constrain a (tree-level) value for  $\lambda$  and allow a theoretical determination of the Higgs mass. Among them are supersymmetric theories and, although the tree-level Higgs mass typically has a low upper bound in SUSY – see equations (1.3.78), (1.3.101) and (1.3.125) for the bounds in the MSSM, NMSSM and Dirac gaugino models respectively – it was shown already in the early 1990’s that the one-loop corrections from stops could be large enough to raise the Higgs mass to an experimentally acceptable value [73–75]. This result sparked a strong effort, still ongoing today, for the calculation of corrections to scalar masses in SUSY, mostly for the MSSM, but also more recently for the NMSSM and models beyond.

### 2.2.1 Regularisation and renormalisation schemes

Calculations in Quantum Field Theory are notoriously associated with ultra-violet (UV) divergences and before we discuss loop corrections, we should clarify how we regularise these UV divergences (*i.e.* how we separate the divergent and regular parts) and how we renormalise the theory. Numerous methods exist to regulate UV divergent loop integrals, such as fixing a UV cut-off, dimensional regularisation (and its variants), Pauli-Villars regularisation, etc. The first and simplest solution is to impose a UV cut-off  $\Lambda$  on the loop integrals, or in other words subtract the part of the integral for high momentum which causes the divergence. Let us illustrate this with the example of the one-loop integral  $\mathbf{A}$ , which appears in tadpole equations and self-energies: in terms of Euclidean momentum it reads

$$\begin{aligned} \mathbf{A}(x) &= (16\pi^2) \int \frac{d^4k}{(2\pi)^4} \frac{1}{k^2 + x} = 2 \int_{k=0}^{\infty} \frac{k^3}{k^2 + x} dk \\ &\xrightarrow{\text{Cut-off } \Lambda} 2 \int_{k=0}^{\Lambda} \frac{k^3}{k^2 + x} dk = \Lambda^2 + x \log\left(\frac{x}{\Lambda^2 + x}\right). \end{aligned} \quad (2.2.1)$$

However, this type of regularisation has several disadvantages, chief among which the fact that it explicitly breaks Lorentz invariance. It is therefore preferable to employ dimension regularisation (DREG) [137], because it preserves both Lorentz and gauge invariance as well as unitarity, and is of simple use.<sup>1</sup> The idea is to consider the dimension of spacetime as a complex variable  $d$  that is expanded in the form  $d = 4 - 2\epsilon$ . The momentum integration is then not performed in 4 but in  $d$  dimensions, with the replacement (for Euclidean momentum)

$$(16\pi^2) \int \frac{d^4 k}{(2\pi)^4} \xrightarrow{\text{DREG}} (16\pi^2) \mu^{2\epsilon} \int \frac{d^d k}{(2\pi)^d}. \quad (2.2.2)$$

The new parameter  $\mu$  is an arbitrary (and unphysical) mass scale, sometimes called the *regularisation scale*, introduced to preserve the mass dimension of the integral and to be able to keep the usual dimensions of couplings. The UV divergence of a loop integral (coming from the large  $k$  region of the integration) is made apparent in DREG as poles of the form  $1/\epsilon^n$  – with  $1 \leq n \leq \ell$ ,  $\ell$  being the loop order. If we return to our example of the  $\mathbf{A}$  function, its expression becomes in DREG

$$\begin{aligned} \mathbf{A}(x) &= (16\pi^2) \mu^{2\epsilon} \int \frac{d^d k}{(2\pi)^d} \frac{1}{k^2 + x} = (16\pi^2) \frac{\pi^{d/2} \mu^{2\epsilon} \Gamma(1 - \frac{d}{2})}{(2\pi)^d} x^{d/2-1} \\ &= x \left[ -\frac{1}{\epsilon} + \gamma_E - \log 4\pi - \log \mu^2 + \log x - 1 \right] \end{aligned} \quad (2.2.3)$$

where the  $1/\epsilon$  pole is the translation of the UV divergence in 4 dimensions (as it divergences when  $\epsilon \rightarrow 0$ , *i.e.*  $d \rightarrow 4$ ), and  $\gamma_E$  is the Euler-Mascheroni constant.

Still, new problems will appear when considering supersymmetric theories because in DREG the number of components of a vector boson is also changed to  $d$  and thus SUSY is broken explicitly by the regularisation, as a gauge superfield would not contain the same number of bosonic and fermionic components ( $4 - 2\epsilon$  and 4 respectively). A solution was found in [138, 139] with regularisation through dimensional *reduction* (DRED), of which the principle is to reduce the number of spacetime dimensions to  $d = 4 - 2\epsilon$ , similarly to DREG, but at the same time to maintain the number of components of vectors (and of tensors in general) to 4. This ensures that SUSY is preserved, in particular meaning that supersymmetric relations between couplings and SUSY Ward identities still hold, and a difference between DREG and DRED only appears in diagrams involving vector bosons. In the language of DREG, DRED corresponds to the splitting of 4-component vectors into  $d$ -component vectors plus new (unphysical)  $\epsilon$ -scalars that correspond to the remaining  $2\epsilon$  components, and the mass and couplings of the  $\epsilon$ -scalars are related to those of the vector bosons by Supersymmetry.

Once the divergent integral has been regularised, a choice remains on what condition to impose to eliminate the divergence – or in other words on the choice of *renormalisation scheme* – in order to derive the required counter-term(s). As an illustration, let us consider that the parameter that we compute is a mass, with the example<sup>2</sup> of a scalar  $X$  whose tree-level mass is equal to its Lagrangian mass parameter. For this calculation, we will only need wave function and mass renormalisations and it therefore suffices for us to write here the kinetic and mass terms of the Lagrangian describing the

<sup>1</sup>It does however lead to complications when considering the fully antisymmetric tensor  $\epsilon^{\mu\nu\rho\sigma}$ , in particular when defining the matrix  $\gamma_5$ , but we will not encounter this problem in what follows and therefore we will not say more about it.

<sup>2</sup>A more detailed discussion of renormalisation (and in particular on-shell renormalisation), taking into account mixing between several scalars can be found *e.g.* in [140].

behaviour of the scalar  $X$ . We start by writing this Lagrangian in terms of *bare* – *i.e.* non-renormalised – quantities, as

$$\mathcal{L}^{\text{bare}} \supset \frac{1}{2}(\partial_\mu X^0)^2 - \frac{1}{2}m_{0,X}^2(X^0)^2. \quad (2.2.4)$$

Then, field-strength renormalisation is introduced by relating the bare field  $X^0$  to the renormalised field  $X$  with the rescaling

$$X^0 = Z_X^{1/2} X, \quad (2.2.5)$$

after which the bare Lagrangian terms in equation (2.2.4) can be expressed as

$$\mathcal{L}^{\text{bare}} \supset \frac{1}{2}Z_X(\partial_\mu X)^2 - \frac{1}{2}m_{0,X}^2 Z_X X^2. \quad (2.2.6)$$

The field-strength renormalisation counter-term  $\delta^{\text{CT}} Z_X$  can now be defined as

$$\delta^{\text{CT}} Z_X = Z_X - 1. \quad (2.2.7)$$

In turn, we can introduce mass renormalisation, replacing the bare mass parameter  $m_{0,X}^2$  by the renormalised mass parameter  $m_X^2$  and the mass renormalisation counter-term  $\delta^{\text{CT}} m_X^2$ , as

$$m_{0,X}^2 = m_X^2 + \delta^{\text{CT}} m_X^2. \quad (2.2.8)$$

While we only present here field-strength and mass renormalisations, the same can be done for other couplings, and in the end it is possible to rewrite the bare Lagrangian as a renormalised Lagrangian  $\mathcal{L}$  plus a counter-term Lagrangian  $\delta^{\text{CT}} \mathcal{L}$

$$\mathcal{L}^{\text{bare}} = \mathcal{L} + \delta^{\text{CT}} \mathcal{L}, \quad (2.2.9)$$

with here,

$$\mathcal{L} \supset \frac{1}{2}(\partial_\mu X)^2 - \frac{1}{2}m_X^2 X^2, \quad (2.2.10)$$

$$\delta^{\text{CT}} \mathcal{L} \supset \frac{1}{2}\delta^{\text{CT}} Z_X(\partial_\mu X)^2 - \frac{1}{2}\delta^{\text{CT}} m_X^2 X^2 - \frac{1}{2}\delta^{\text{CT}} Z_X m_X^2 X^2. \quad (2.2.11)$$

Two comments should be made here about the above equation for  $\delta^{\text{CT}} \mathcal{L}$ . First, it should be noted that the above expression is the one-loop result of the counter-term Lagrangian (as we neglected a term  $\delta^{\text{CT}} Z_X \delta^{\text{CT}} m_X^2$  that appears from two-loop order), but for the discussion in this section a one-loop discussion is sufficient. Moreover, it would in principle have been possible to reabsorb the third term of  $\delta^{\text{CT}} \mathcal{L}$  into a redefinition of  $\delta^{\text{CT}} m_X^2$ .

The experimentally measurable pole mass  $M_X^2$  of  $X$  is then found in terms of the renormalised mass parameter  $m_X^2$  and of the renormalised self-energy  $\Pi_X$  as

$$M_X^2 = m_X^2 + \Pi_X(p^2 = M_X^2), \quad (2.2.12)$$

with,

$$\Pi_X(p^2) = \mathbf{\Pi}_X(p^2) + \delta^{\text{CT}} m_X^2 - (p^2 - m_X^2)\delta^{\text{CT}} Z_X, \quad (2.2.13)$$

and where  $\mathbf{\Pi}_X$  is the non-renormalised self-energy. It is important to note that, in the above equations, both  $m_X^2$  and  $\Pi_X$  are scheme-dependent.



A first natural choice of scheme is to find the counter-term by relating the quantity (mass, coupling, mixing angle, etc.) that is being computed to a physically meaningful observable. This is usually referred to as an *on-shell* (OS) renormalisation scheme, as it often corresponds to computing  $n$ -point functions or vertex functions with external legs set on-shell. Note however that for a generic quantity (*e.g.* a mixing angle) there may be more than one way to define OS renormalisation conditions. The on-shell renormalisation scheme is defined here by the two following conditions

$$\Pi_X^{\text{OS}}(p^2 = M_X^2) = 0, \quad (2.2.14)$$

$$\lim_{p^2 \rightarrow m_X^2} \frac{\Pi_X^{\text{OS}}(p^2)}{p^2 - m_X^2} = 0. \quad (2.2.15)$$

This fixes the two counter-terms to be

$$\delta_{\text{OS}}^{\text{CT}} m_X^2 = -\mathbf{\Pi}_X(p^2 = M_X^2), \quad (2.2.16)$$

$$\delta_{\text{OS}}^{\text{CT}} Z_X = \left. \frac{d}{dp^2} \mathbf{\Pi}_X(p^2) \right|_{p^2 = M_X^2}. \quad (2.2.17)$$

and the Lagrangian mass parameter is in this OS scheme simply equal to the pole mass

$$(m_X^2)_{\text{OS}} = M_X^2. \quad (2.2.18)$$

Another option is *minimal subtraction*, where one only demands that the counter-terms cancel the divergences while leaving the finite part unchanged. In other words, the equations (2.2.14) and (2.2.15) are replaced in minimal subtraction by the sole condition that

$$\Pi_X^{\text{min.sub.}}(p^2) = \mathbf{\Pi}_X^{\text{reg}}(p^2). \quad (2.2.19)$$

where  $\mathbf{\Pi}_X^{\text{reg}}$  is the finite part of the self-energy. This condition must hold for all  $p^2$ , and renormalisation schemes based on minimal subtraction are said to be mass-independent schemes. One can find of the counter-terms in these schemes to be

$$\delta_{\text{min.sub.}}^{\text{CT}} m_X^2 = -\mathbf{\Pi}_X^{\text{div}}(p^2 = m_X^2), \quad (2.2.20)$$

$$\delta_{\text{min.sub.}}^{\text{CT}} Z_X = \left. \frac{d}{dp^2} \mathbf{\Pi}_X^{\text{div}}(p^2) \right|_{p^2 = m_X^2}. \quad (2.2.21)$$

Finally, equation (2.2.12) becomes in minimal subtraction schemes

$$M_X^2 = (m_X^2)_{\text{min.sub.}} + \mathbf{\Pi}_X^{\text{reg}}(p^2 = M_X^2), \quad (2.2.22)$$

and furthermore, by comparing eqs. (2.2.18) and (2.2.22), we can relate the values of the mass parameter  $m_X^2$  in OS and minimal subtraction as

$$(m_X^2)_{\text{min.sub.}} = (m_X^2)_{\text{OS}} - \mathbf{\Pi}_X^{\text{reg}}(p^2 = (m_X^2)_{\text{OS}}). \quad (2.2.23)$$

Both the results for the renormalised self-energy and the mass parameter retain a dependence on an unphysical scale  $Q$ , the *renormalisation scale*. We choose to define it differently from the regularisation scale  $\mu$  in order to eliminate the constant piece  $-\gamma_E + \log 4\pi$  always associated with a term  $1/\epsilon$ . In this *modified minimal subtraction*,  $Q$  is found – following [141, 142] – as

$$Q^2 = 4\pi e^{-\gamma_E} \mu^2. \quad (2.2.24)$$

Depending on whether DREG or DRED is used, the renormalisation schemes obtained with modified minimal subtraction are referred to as  $\overline{\text{MS}}$  and  $\overline{\text{DR}}$  respectively – the bar differentiating them from the MS and DR schemes obtained with the normal minimal subtraction.

A comment on the distinction between minimal subtraction and modified minimal subtraction is at hand here. In many QFT textbooks, the  $\overline{\text{MS}}$  ( $\overline{\text{DR}}$ ) scheme is defined by starting from MS (DR) and requiring that the counter-term that cures the  $1/\epsilon$  pole also cancel the constant  $-\gamma_E + \log 4\pi$  – see *e.g.* equation (11.77) of [9] – while the renormalisation scale  $Q$  is always equal to the regularisation scale  $\mu$ . However the prescription that we use, coming from the original paper on modified minimal subtraction [141] (see in particular eq. (5.4) therein), is slightly different in that the counter-term is not modified (it only cancels the pole), but instead the distinction between MS (DR) and  $\overline{\text{MS}}$  ( $\overline{\text{DR}}$ ) comes from the definition of  $Q$ , that is equal to  $\mu$  for minimal subtraction but given by eq. (2.2.24) for modified minimal subtraction, *i.e.*

$$Q_{\text{MS (DR)}}^2 = \mu^2 \quad \text{and} \quad Q_{\overline{\text{MS}} (\overline{\text{DR}})}^2 = 4\pi e^{-\gamma_E} \mu^2 \quad (2.2.25)$$

Note that, while they may seem different, these two definitions of modified minimal subtraction are actually equivalent and do not lead to any difference in the results that one obtains.

The parameters computed in either one of these schemes are said to be *running* because of their renormalisation scale dependence, and the relations between parameters in  $\overline{\text{MS}}$  or  $\overline{\text{DR}}$  schemes, which differ already from one-loop order, can be found in [143] – these are obtained by relating parameters in both schemes to their physically meaningful OS counterpart, as we did with our toy example in eq. (2.2.23). Although running parameters are not directly measurable quantities, minimal subtraction schemes are widely employed because they significantly simplify calculations with respect to the OS scheme.

A last subtlety pertaining to the  $\overline{\text{DR}}$  scheme needs to be pointed out before we end this discussion. As mentioned already, DRED implies the addition of  $\epsilon$ -scalars to ensure the equality of the numbers of fermionic and bosonic degrees of freedom in a gauge supermultiplet while working in  $d$  dimensions, and these will appear in calculations. When Supersymmetry is unbroken, it relates their properties to those of the physical gauge bosons and no artefacts are left in the final result of the computation, but once one considers soft SUSY breaking terms, the situation is altered and independent  $\epsilon$ -scalar soft mass terms  $\tilde{m}^2$  arise. In particular, the two-loop  $\beta$ -function of soft scalar masses and the one-loop correction to scalar masses exhibit an unwanted dependence on the unphysical  $\tilde{m}^2$  parameters [144–147]. Fortunately, it has been shown that a simple redefinition of the renormalisation scheme, more precisely a one-loop shift to the soft scalar masses as defined in equation (9) of [147], is sufficient to eliminate all dependence on the  $\epsilon$ -scalar masses. The resulting renormalisation scheme is denoted  $\overline{\text{DR}}'$  so as to distinguish it from the regular  $\overline{\text{DR}}$  scheme [147].

Throughout this thesis, we will employ dimensional regularisation or reduction for calculations in non-supersymmetric or supersymmetric theories respectively, and we will provide results for both when considering generic theories. As for renormalisation schemes, we will employ OS,  $\overline{\text{MS}}$  and  $\overline{\text{DR}}'$  schemes.

### 2.2.2 Calculations beyond leading order and choice of inputs

In the previous section, we have discussed how we regularise and renormalise a given calculation, but without considering its type or its context, and without discussing complications that arise when computing higher-order corrections (*i.e.* beyond one loop). Indeed, when considering a two-loop diagram we actually encounter two types of UV divergences:

- genuine two-loop divergences, which are cancelled by purely two-loop counter-terms (*e.g.* by the two-loop contributions to  $\delta^{\text{CT}} m_X^2$  and  $\delta^{\text{CT}} Z_X$  in our example of the previous section); and,
- divergences that come from subdiagrams, and that must be cancelled by a one-loop diagram with insertion of a one-loop counter-term. This can be interpreted as the need to renormalise the parameters that enter the one-loop corrections when performing a two-loop calculation.

The situation is similar, although even more complicated, when going to yet higher orders. In this thesis, we are interested in Higgs mass calculations, in the sense that we want to relate the Higgs mass(es) to the fundamental parameters of the theory we work in. When calculating corrections at two loops, we will obtain the genuine two-loop counter-terms using minimal subtraction, however, we remain free to choose different ways of renormalising the parameters in the contributions at lower orders, or in other words we have the liberty to choose the renormalisation scheme in which these parameters are derived, either an OS scheme or minimal subtraction ( $\overline{\text{MS}}/\overline{\text{DR}}'$ ).

If one for example computes (as we do in chapter 3) the two-loop  $\mathcal{O}(\alpha_t \alpha_s)$  SUSY-QCD corrections<sup>3</sup> to Higgs masses, then one must specify in what scheme the parameters that appear in the corresponding lower-order corrections, here the one-loop  $\mathcal{O}(\alpha_t)$  terms, are computed. For SUSY-QCD corrections, these involve only the quark/squark sector and, for the more particular case of the  $\mathcal{O}(\alpha_t \alpha_s)$  corrections, these are the top and stop masses  $m_t, m_{\tilde{t}_{1,2}}$ , the stop mixing angle  $\theta_t$  and the stop trilinear coupling  $A_t$ . As an on-shell renormalisation relates fundamental parameters to experimentally measured quantities, it is a natural choice for the mass parameters of observed particles, such as the top quark mass  $m_t$ . However, for properties of particles that have not (yet) been detected, the choice is more open: on the one hand, one can relate them to quantities that could in principle be obtained in an experiment; or, on the other hand, they can be left as  $\overline{\text{DR}}'$  parameters, which simplifies the expressions of counter-terms and is furthermore more convenient if said parameters are obtained through RGE running from a high-scale boundary condition.

The most convenient strategy (which we also follow) is to first perform the two-loop calculation in the  $\overline{\text{DR}}'$  scheme, by which we mean that we compute (modified-)minimal-subtraction renormalised one- and two-loop corrections in terms of  $\overline{\text{DR}}'$  fundamental parameters. Then, once a  $\overline{\text{DR}}'$  result has been obtained, it can be converted to an OS scheme – *i.e.* expressed in terms of input parameters that are renormalised on-shell – by adding to the parameters entering at lower orders a shift obtained by the difference of the counter-terms in OS and  $\overline{\text{DR}}'$  schemes – see *e.g.* eq. (2.2.23) for the conversion of a generic mass parameter, and section 3.1.5 for details on the conversion of top/stop sector parameters. Note that for parameters that only appear in the last order of a given calculation, the choice of renormalisation scheme is irrelevant, as the conversion

---

<sup>3</sup>We recall that  $\alpha_t \equiv y_t^2/4\pi$  and  $\alpha_s \equiv g_s^2/4\pi$ .

between schemes would correspond to a correction of higher order than the order that is considered – for example in the case of the two-loop SUSY-QCD corrections to Higgs masses, one does not need to specify the scheme in which the gluino masses<sup>4</sup>  $m_{\tilde{g}_i}$  are computed because they only enter the calculation at two-loop order, and therefore shifting  $m_{\tilde{g}_i}$  between schemes would only give a correction at three-loop order.

### 2.2.3 Different types of mass calculations

After our discussion of renormalisation and of input choices in the previous two sections, we can now consider scalar (or in particular Higgs) mass calculations. We will first introduce the different possible approaches to these calculations – fixed order (diagrammatic or with the effective potential) or EFT – in a simple setting before turning, in the following section, to some of the results obtained for SUSY theories.

#### 2.2.3.1 Fixed-order calculations

The standard procedure to derive the radiative corrections to masses of particles is to rely on the definition of the physical (or pole) masses as the poles of the renormalised propagator matrix – or equivalently as the zeroes of the renormalised two-point function matrix. In the *diagrammatic approach*, the corrections to the two-point functions can be computed order by order in perturbation theory (hence the name of *fixed-order* calculations) as one-particle-irreducible self-energy diagrams (*i.e.* two-point function diagrams).

Together with the self-energies, one must also take into account the tadpole diagrams. Two different, although equivalent, points of view exist as to how tadpoles appear in mass calculations, and can be explained as follows:

- Calculations must be performed at the minimum of the loop-corrected scalar potential, as that is where (in field space) masses are defined. In turn, this imposes relations between Lagrangian parameters – *i.e.* for each tadpole equation, one parameter can be eliminated;
- In the process of renormalising the scalar sector of a given theory, tadpole counter-terms appear, and the best way to fix these is to impose that the total loop-corrected tadpoles (*i.e.* the renormalised one-point function) vanish.

Throughout this thesis, we take the first of these points of view, and we choose to perform calculations at the minimum of the scalar potential  $V_{\text{eff}}$ , computed to the same order as we work to for the mass calculations.

In the situation where one considers a scalar  $\phi$  that does not mix with any other state, neither at tree level nor when including loop corrections, the pole mass of  $\phi$  is found as the solution of the equation

$$M_\phi^2 = m_\phi^2 + \Pi_\phi(p^2 = M_\phi^2), \quad (2.2.26)$$

where  $m_\phi^2$  is the Lagrangian mass parameter of  $\phi$ ,  $\Pi_\phi$  its renormalised self-energy.

---

<sup>4</sup>We use here the plural form, having in mind Dirac gaugino models where there are two gluinos with masses that can a priori be different. In the (N)MSSM there is only one gluino and the sentence should then be changed to singular form.

However, in the presence of mixing among scalar states  $\phi_i$ , the situation becomes technically more involved and one needs to use a loop-corrected scalar mass matrix, which is obtained at  $n$ -loop order as

$$(\mathcal{M}^2)_{ij}^{\text{loop}}(p^2) = (\mathcal{M}^2)_{ij}^{\text{tree}} + (\Delta\mathcal{M}^2)_{ij}(p^2) = m_{0,ij}^2 + \Pi_{ij}(p^2), \quad (2.2.27)$$

where  $m_{0,ij}^2$  are tree-level mass parameters,  $\Pi_{ij}$  are renormalised self-energies. The pole masses of the scalars are then found by solving for  $p^2$  in the equation

$$\det[p^2\delta_{ij} - (\mathcal{M})_{ij}^{\text{loop}}(p^2)] = 0, \quad (2.2.28)$$

which is the generalisation of equation (2.2.26).

We show, as an example, in figures 2.2 and 2.3 the topologies allowed respectively for one- and two-loop self-energy diagrams, that contribute to mass corrections. Different loop functions are obtained depending on the type of particle (scalar, fermion, vector boson, or ghost) that runs in each internal line of every topology, nevertheless it is possible, using tensor reduction (and tools such as **TARCER** [148]), to express all the functions corresponding to scalar self-energy diagrams in terms of scalar integrals – *i.e* integrals that involve only scalar propagators – which can be computed in DRED or DREG. There are two scalar functions at one loop,  $A$  and  $B$  defined respectively in eqs. (B.1.6) and (B.1.7), and analytic expressions for both have been known for a long time (see *e.g.* [23]). At two-loop order, there are three scalar functions  $S$ ,  $U$ , and  $M$  (defined in eqs. (B.1.18) to (B.1.20)) that appear, together with  $A$  and  $B$ , in the expressions of all self-energy diagrams. However, their expressions are in general not known analytically for non-zero external momentum and for different masses of particles in the loops, but can be computed either by numerical integration (for example with the program **SecDec** [149]), or by solving systems of differential equations that relate the loop functions – such differential equations were derived in [142] and are implemented in the C++ program **TSIL** [150].

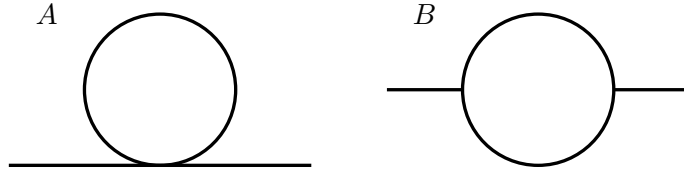


Figure 2.2 – Possible topologies of one-loop self-energy diagrams.

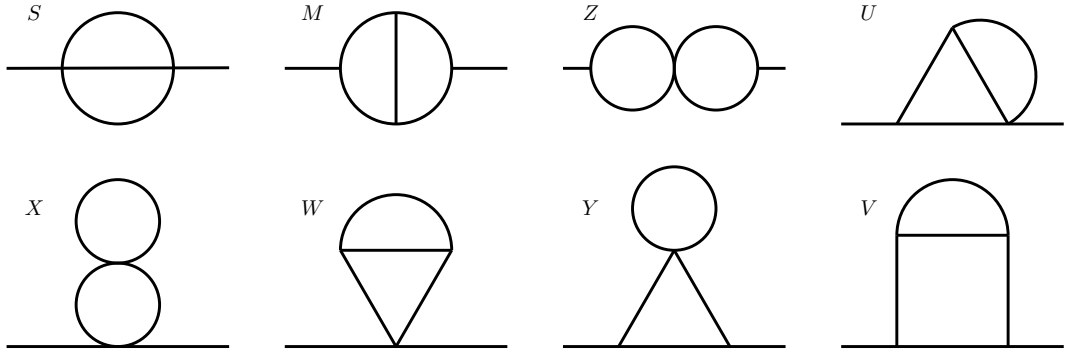


Figure 2.3 – Possible topologies of two-loop self-energy diagrams.

However, numerical evaluations of loop integrals with tools like **SecDec** or **TSIL** are costly (in terms of time, or equivalently computing power) and the effect of momentum at two-loop order is generally expected to be small. Therefore, a simpler approach is often taken by working in the limit of vanishing external momentum, which is actually equivalent to a calculation using second derivatives of the effective potential. This last statement can be proven as follows: we start from the effective action  $\Gamma$  defined in eq. (1.1.28), and that we can expand as

$$\Gamma\{\phi_i(x)\} = \int d^4x \left( -V_{\text{eff}} + \frac{1}{2} Z_{ij} \partial_\mu \phi_i \partial^\mu \phi_j + \dots \right). \quad (2.2.29)$$

We furthermore know that by construction,  $\Gamma$  is the generating functional of 1PI graphs: therefore the second derivative of  $\Gamma$  with respect to two fields  $\phi_i(x)$ ,  $\phi_j(y)$  corresponds to the inverse propagator in position space  $\Delta^{-1}(x-y)$ , and its Fourier transform is then the inverse propagator in momentum space *i.e.*  $i\Delta^{-1}(p^2) \equiv p^2 \delta_{ij} - m_{0,ij}^2 - \Pi_{ij}(p^2)$ . But from eq. (2.2.29) it follows that

$$\left. \frac{\partial^2 V_{\text{eff}}}{\partial \phi_i \partial \phi_j} \right|_{\min} = -i\Delta^{-1}(0) = m_{0,ij}^2 + \Pi_{ij}(0), \quad (2.2.30)$$

or equivalently (with  $V_{\text{eff}} = V^{(0)} + \Delta V$ )

$$\left. \frac{\partial^2 \Delta V}{\partial \phi_i \partial \phi_j} \right|_{\min} = \Pi_{ij}(0). \quad (2.2.31)$$

The *effective potential approach*, or in other words using the second derivatives of the effective potential, greatly simplifies the computation of mass corrections, and in particular, solving eq. (2.2.28) then amounts to finding the eigenvalues of the matrix

$$(\mathcal{M}^2)_{ij}^{\text{eff}} = m_{0,ij}^2 + \left. \frac{\partial^2 \Delta V}{\partial \phi_i \partial \phi_j} \right|_{\min}. \quad (2.2.32)$$

### 2.2.3.2 The effective field theory approach

The Higgs mass computed at renormalisation scale  $Q$  from the fixed-order methods described above can schematically be written as

$$m_h^2 = \sum_{\ell} \frac{1}{(16\pi^2)^\ell} \sum_{n=0}^{\ell} \left[ \sum_{\substack{\{n(i)\} \\ \sum_i n(i)=n}} c_n^{\ell}(\{n(i)\}) \prod_i \log^{n(i)} \frac{m_i^2}{Q^2} \right], \quad (2.2.33)$$

where  $\ell$  is the loop order, the index  $i$  labels the different particles that contribute to the Higgs mass ( $m_i^2$  are then the corresponding masses, etc.), and the factors  $c_n^{\ell}(\{n(i)\})$  can in general be found numerically.

When the hierarchies between (some of) the mass scales in the loop corrections become important, large logarithmic contributions may appear, causing the perturbative expansion done for fixed-order calculations to become inadequate. Indeed, it is natural to compute the Higgs mass at a relatively low scale  $Q = m$  (most usually one takes the top mass,  $m = m_t$ ) and if one or several particles have large masses, denoted  $M$ , then the  $\ell$ -loop corrections will contain terms of the form  $\log^\ell M/m$ , which are greatly enhanced when  $M \gg m$ .

The solution to this problem is to use an effective field theory (EFT) approach to the calculation, which allows a resummation of the large  $\log^\ell M/m$  logarithms. The heavy particles, *i.e.* those of mass higher than, or of the order of,  $M$ , are integrated out at a high scale  $Q$  – typically one takes  $Q = M$  – and below the scale  $Q$  one works with an effective field theory, *i.e.* a low-energy theory containing only light states. The usual way to integrate out heavy states is to perform a matching of  $n$ -point functions, computed (diagrammatically) respectively in the EFT and in the full theory at the scale  $Q$  and at the desired loop order (say  $\ell$ -loop order), which reads

$$\tilde{\Gamma}_{(n)}^{\ell\text{-loop}}(Q) = \Gamma_{(n)}^{\ell\text{-loop}}(Q), \quad (2.2.34)$$

where  $\tilde{\Gamma}_{(n)}^{\ell\text{-loop}}$  and  $\Gamma_{(n)}^{\ell\text{-loop}}$  are functions of the parameters respectively in the low-energy and complete theories. Note that one could equivalently have performed a matching of the effective actions of the EFT and the complete theory to obtain the relations for the couplings. The matching then defines the masses and couplings that will appear in the EFT and the effects of heavy states at low energies come from two sources:

- via the matching conditions for the couplings that already existed in the full theory and receive threshold corrections in the EFT;
- via new operators that arise in the EFT from the matching, and in particular higher-dimensional (in other words non-renormalisable) operators, which are suppressed by powers of  $M$  (also obtained by the matching of  $n$ -point functions between high- and low-energy theories).

Properties of the light particles are then computed using the parameters and field content of the low-energy theory, and with the additional higher-dimensional operators – the impact of the latter however decreases as the ratio  $m/M$  tends to zero (as these operators are suppressed by powers of  $M$ ). For example, one finds that the (running) mass  $\tilde{m}_\phi^2$  of a scalar  $\phi$  (not considering any mixing here) in the EFT is related at the matching scale  $Q$  to the mass parameter in the full theory by threshold corrections  $\Delta m_\phi^2$  as

$$\tilde{m}_\phi^2(Q) = m_\phi^2(Q) + \Delta m_\phi^2(Q). \quad (2.2.35)$$

The running parameter  $\tilde{m}_\phi^2(Q)$  can then be run to the scale at which one wants to compute the pole mass of  $\phi$ , and then, following equation (2.2.26), one finds

$$M_\phi^2 = m_\phi^2 + \tilde{\Pi}_\phi(p^2 = M_\phi^2), \quad (2.2.36)$$

where  $\tilde{\Pi}_\phi$  is calculated in the low energy theory.

In this EFT approach, radiative corrections are resummed to  $N^\ell\text{LL}$  (*i.e.* (next-to-) $^\ell$  leading logarithmic) order when performing the matching of couplings and the calculation of corrections at  $\ell$ -loop order, together with  $\ell + 1$ -loop running of the renormalisation group equations.<sup>5</sup>

## 2.3 State-of-the-art of Higgs mass calculations

In this section, we will attempt to give a brief review of Higgs mass calculations in SUSY models. Providing an exhaustive description of all results in this field during

---

<sup>5</sup>Note that this does not however capture non-logarithmic corrections – as we will return to in chapter 6.

the past three decades would be a near-impossible task, and would go well beyond the scope of this thesis; hence we will instead only mention some of the main contributions, relevant for the lightest Higgs boson mass.

### 2.3.1 Real and complex MSSMs

As we discussed in the previous chapter, in the MSSM the Higgs quartic couplings are related to the electroweak gauge couplings and the tree-level mass of the lightest CP-even Higgs boson is

$$\begin{aligned} (m_h^2)^{\text{tree}} &= \frac{1}{2} \left[ m_A^2 + m_Z^2 - ((m_A^2 - m_Z^2)^2 + 4m_Z^2 m_A^2 \sin^2 2\beta)^{1/2} \right] \\ (m_h^2)^{\text{tree}} &\leq m_Z^2 \cos^2 2\beta. \end{aligned} \quad (2.3.1)$$

The existence of an upper bound on  $(m_h^2)^{\text{tree}}$  is by itself a very important feature of SUSY models. However, from the above equation it may seem that the MSSM is excluded in view of the observation of a 125 GeV Higgs boson (and that it would have been already from the early experimental bounds from LEP). Fortunately, the tree-level Higgs mass is dramatically altered by radiative corrections.

The initial spark of Higgs mass calculations in SUSY was the study in refs. [73–75] of the impact of the one-loop corrections from tops and stops on  $m_h$  and its theoretical upper bound, in the CP-conserving (*i.e.* real) MSSM. In these three references, the dominant  $\mathcal{O}(\alpha_t)$  (with  $\alpha_t \equiv y_t^2/4\pi$ ) corrections<sup>6</sup> to the CP-even Higgs masses are computed – in the effective potential approximation for [73, 74], and a diagrammatic approach for [75] – and it is shown that for a large top mass<sup>7</sup> (and thus a large top Yukawa) the mass of lightest Higgs can become significantly larger than  $m_Z$  (the tree-level bound) due to the radiative corrections. The reason for this is that, while the top quark contributes negatively to scalar masses (because of the minus sign of the fermion loop), the contributions from the heavier stops are positive and larger in absolute value than those from the top. In fact, the one-loop corrections to the lightest Higgs mass from stops and tops can be as large as the tree-level value. While this may seem to contradict perturbativity, such huge corrections are actually not a problem here as they are driven by the large top Yukawa  $y_t$  that only enters the computation at one-loop order. A major consequence of these papers is that not only does Supersymmetry predict a value for the Higgs mass, but that this value can be modified by large radiative corrections, which should therefore be computed to higher accuracy. This led to intensive work on the MSSM with real parameters in the 1990's, and later on its complex counterpart, with numerous fixed-order and EFT calculations. Chronologically, both approaches were considered from an early point, but for clarity we will discuss them separately here.

#### 2.3.1.1 Fixed-order results

In the early 1990's, numerous papers studied Higgs masses in the fixed-order approach, either in the effective potential approximation [73, 74, 151–154], or with diagrammatic

---

<sup>6</sup>Let us specify here that the corrections we are referring to are actually of the form  $m_t^4/v^2 \propto \alpha_t m_t^2$ . We also note that some other notational conventions for radiative corrections may be slightly abused in the following – *e.g.*  $\mathcal{O}(\alpha_t \alpha_s)$  – as is commonly done in the literature.

<sup>7</sup>One must remember that when these three papers were written, the top quark had not yet been detected and its mass was therefore not known. The value of the top mass that has been obtained from Tevatron and LHC measurements around 173 GeV is indeed large for the discussion here.



computations [75, 155–163]. Once radiative corrections are introduced in the real MSSM, mixing appears between the two CP-even Higgses  $h$  and  $H$  (defined in section 1.3.4.2). The easiest way to proceed, for a diagrammatic calculation, is then to compute a loop-corrected scalar mass matrix in the gauge-eigenstate basis  $\{S_1, S_2\}$  – *i.e.* the basis formed by the two real components of  $H_d^0$  and  $H_u^0$ , decomposed respectively as

$$H_d^0 = \frac{1}{\sqrt{2}}(v_d + S_1 + iP_1), \quad \text{and} \quad H_u^0 = \frac{1}{\sqrt{2}}(v_u + S_2 + iP_2). \quad (2.3.2)$$

In the notations of section 1.3.4.2 we find

$$\det[p^2 \cdot \mathbf{1}_2 - (\mathcal{M}_S^2)^{\text{loop}}(p^2)] = 0, \quad (2.3.3)$$

with

$$\begin{aligned} (\mathcal{M}_S^2)_{11}^{\text{loop}}(p^2) &= m_Z^2 c_\beta^2 + m_A^2 s_\beta^2 - \frac{1}{v_d} \frac{\partial \Delta V}{\partial S_1} \Big|_{\text{min.}} + \Pi_{S_1 S_1}(p^2), \\ (\mathcal{M}_S^2)_{12}^{\text{loop}}(p^2) &= -\frac{1}{2}(m_Z^2 + m_A^2) s_{2\beta} + \Pi_{S_1 S_2}(p^2), \\ (\mathcal{M}_S^2)_{22}^{\text{loop}}(p^2) &= m_Z^2 s_\beta^2 + m_A^2 c_\beta^2 - \frac{1}{v_u} \frac{\partial \Delta V}{\partial S_2} \Big|_{\text{min.}} + \Pi_{S_2 S_2}(p^2), \end{aligned} \quad (2.3.4)$$

and where  $m_Z^2$ ,  $m_A^2$ , and  $\tan \beta$  are running parameters. Note that in the above expression, the minimum conditions have already been used to eliminate the soft mass parameters of the two Higgs doublets  $m_{H_u}^2$  and  $m_{H_d}^2$ . We recall that these are of the form

$$\begin{aligned} \frac{1}{v_d} \frac{\partial V_{\text{eff}}}{\partial S_1} \Big|_{\text{min.}} &= \frac{1}{v_d} \frac{\partial V^{(0)}}{\partial S_1} \Big|_{\text{min.}} + \frac{1}{v_d} \frac{\partial \Delta V}{\partial S_1} \Big|_{\text{min.}} = 0, \\ \frac{1}{v_u} \frac{\partial V_{\text{eff}}}{\partial S_2} \Big|_{\text{min.}} &= \frac{1}{v_u} \frac{\partial V^{(0)}}{\partial S_2} \Big|_{\text{min.}} + \frac{1}{v_u} \frac{\partial \Delta V}{\partial S_2} \Big|_{\text{min.}} = 0. \end{aligned} \quad (2.3.5)$$

Furthermore, as  $S_1$  and  $S_2$  are the real components of  $H_u^0$  and  $H_d^0$ , it is clear that

$$\begin{aligned} \frac{1}{v_d} \frac{\partial V^{(0)}}{\partial S_1} \Big|_{\text{min.}} &= \frac{\sqrt{2}}{v_d} \frac{\partial V^{(0)}}{\partial H_d^0} \Big|_{\text{min.}}, \\ \frac{1}{v_u} \frac{\partial V^{(0)}}{\partial S_2} \Big|_{\text{min.}} &= \frac{\sqrt{2}}{v_u} \frac{\partial V^{(0)}}{\partial H_u^0} \Big|_{\text{min.}}, \end{aligned} \quad (2.3.6)$$

and the right-hand sides of these two relations are given in eq. (1.3.72). When applying the minimum conditions to the diagonal terms in eq. (2.3.4), we have split them between tree- and loop-level terms, as shown in (2.3.5), and we have simplified the expressions of the tree-level masses using the corresponding tree-level tadpole terms, *i.e.* equation (2.3.6).

One advantage of this approach is that the expressions (2.3.4) can be used for any desired order in perturbation theory, and that it also allows the definition of an effective mixing angle  $\alpha$  at any order with the relation (see section 1.3.4.2 for its tree-level value)

$$\cot(2\alpha^{\text{loop}}) \equiv \frac{(\mathcal{M}_S^2)_{11}^{\text{loop}} - (\mathcal{M}_S^2)_{22}^{\text{loop}}}{2(\mathcal{M}_S^2)_{12}^{\text{loop}}}. \quad (2.3.7)$$

When defining a loop-corrected mixing angle as in the above equation, it is necessary to specify which mass matrix  $(\mathcal{M}_S^2)^{\text{loop}}(p^2)$  the angle diagonalises – *i.e.* to what value of  $p^2$  it corresponds. We will compute it for  $p^2 = m_h^2$ ,  $m_h^2$  being the lightest loop-corrected mass eigenvalue (corresponding to the lightest loop-corrected mass eigenstate that we denote  $h$ ).

Similarly, one can compute the corrections to the CP-odd states of the Higgs sector – the pseudoscalar Higgs and the neutral Goldstone boson. As for the CP-even Higgses, we can obtain a loop-corrected pseudoscalar mass matrix  $(\mathcal{M}_P^2)^{\text{loop}}(p^2)$  in the gauge eigenstate basis  $\{P_1, P_2\}$ , formed of the two imaginary components of  $H_u^0$  and  $H_d^0$ , as

$$\begin{aligned} (\mathcal{M}_P^2)^{\text{loop}}(p^2)_{11} &= m_A^2 s_\beta^2 - \frac{1}{v_d} \frac{\partial \Delta V}{\partial S_1} \Big|_{\text{min.}} + \Pi_{P_1 P_1}(p^2), \\ (\mathcal{M}_P^2)^{\text{loop}}(p^2)_{12} &= \frac{1}{2} m_A^2 s_{2\beta} + \Pi_{P_1 P_2}(p^2), \\ (\mathcal{M}_P^2)^{\text{loop}}(p^2)_{22} &= m_A^2 c_\beta^2 - \frac{1}{v_u} \frac{\partial \Delta V}{\partial S_2} \Big|_{\text{min.}} + \Pi_{P_2 P_2}(p^2), \end{aligned} \quad (2.3.8)$$

where  $m_A^2$  is again the running pseudoscalar mass.

The leading corrections to  $m_h^2$  at one-loop order are the  $\mathcal{O}(\alpha_t)$  and  $\mathcal{O}(\alpha_b)$  contributions – where  $\alpha_b \equiv y_b^2/4\pi$ . In the decoupling limit  $m_A^2 \gg m_Z^2$  and for large degenerate soft masses for the two stops  $m_Q^2 = m_U^2 = M_S^2 \gg m_t^2$ , the one-loop corrections to  $m_h^2$  can be written in the very simple form

$$\Delta^{(1)} m_h^2 = \frac{3m_t^4}{2\pi^2 v^2} \left( \log \frac{M_S^2}{m_t^2} + \hat{X}_t^2 - \frac{\hat{X}_t^4}{12} \right) - \frac{y_b^4 \mu^4 \tan^4 \beta v^2}{32\pi^2 M_S^4} + \dots, \quad (2.3.9)$$

where we recall that  $X_t$  is the stop mixing  $X_t = A_t - \mu \cot \beta$  (here for the real MSSM in which  $\mu \in \mathbb{R}$ ) and  $\hat{X}_t = X_t/M_S$ . Complete results for the one-loop Higgs masses were obtained in [159, 162, 163].

However, even with a full one-loop calculation, theoretical uncertainties remain large, and higher-order corrections are needed to obtain precise predictions. The first two-loop results were derived for the approximation of zero external momentum [32, 76, 164–175]. While the earliest of these papers have studied the  $\mathcal{O}(\alpha_s \alpha_t)$  and  $\mathcal{O}(\alpha_t^2)$  contributions, ref. [32] gave the complete two-loop corrections to the lightest Higgs mass in the effective potential approach, but encountered for the first time the Goldstone Boson Catastrophe (because computations were performed beyond the gaugeless limit). More recently, the dominant momentum-dependent two-loop [176–178] and the leading three-loop corrections [179, 180] have also been calculated.

When considering the complex MSSM, the distinction between CP-even and CP-odd Higgses cannot be made anymore, and one must therefore work with a  $4 \times 4$  mass matrix – for all neutral states in the Higgs sector – of the form

$$(\mathcal{M}_n^2)^{\text{loop}}(p^2) = \begin{pmatrix} (\mathcal{M}_S^2)^{\text{loop}}(p^2) & (\mathcal{M}_{SP}^2)^{\text{loop}}(p^2) \\ [(\mathcal{M}_{SP}^2)^{\text{loop}}(p^2)]^* & (\mathcal{M}_P^2)^{\text{loop}}(p^2) \end{pmatrix}, \quad (2.3.10)$$

where  $(\mathcal{M}_{S,P}^2)^{\text{loop}}$  are the  $2 \times 2$  scalar and pseudoscalar mass matrices, obtained as in the case of the real MSSM, while  $(\mathcal{M}_{SP}^2)^{\text{loop}}$  are new, CP-violating, corrections. Results for calculations of neutral scalar masses in the complex MSSM were obtained at one loop in [181–184], then the leading contributions at two loops with vanishing

external momentum were found in [185–188], and more recently the complete two-loop SUSY-QCD corrections were given with full momentum dependence in [189].

Since the late 1990’s and early 2000’s, results for fixed-order Higgs mass calculations in the MSSM have been implemented in a number of public *spectrum generators*, *i.e.* codes which determine the complete loop-corrected mass spectrum of the theory (and often use these masses to derive other physical observables). Currently, several such programs provide full one-loop and leading two-loop corrections to Higgs masses, and among the most widely-used of them, one can mention **FeynHiggs** [190], **SoftSUSY** [191, 192], **SuSpect** [193], and **SPheno** [194, 195]. **FeynHiggs** differs from the three other mentioned codes because of the corrections it implements and of the choice of renormalisation scheme it employs for the two-loop corrections: indeed it uses results in the on-shell scheme from [76, 171, 172, 174, 177, 184–187], while **SoftSUSY**, **SuSpect**, and **SPheno** use results in the  $\overline{\text{DR}}'$  scheme from [76, 163, 171, 172, 174, 196]. We will return in more detail to **SPheno**, and especially to its extension to SUSY models beyond the MSSM and to non-SUSY models, in section 2.4.3.2.

A brief remark on the evaluation of the theoretical uncertainties on the determination of  $m_h$  should be made here: in order to compare the result of a given calculation with the measured value of  $m_h$  in a meaningful way, it is necessary to provide an estimate of the uncertainty in the theoretical computation. While crude estimates can be found for example by varying the renormalisation scale at which a computation is done, or by changing how parameters that enter the two-loop corrections are determined (these two methods help give an idea of the size of missing three-loop terms), obtaining a precise number is a difficult task, and furthermore depends on the parameter point for which the masses are computed. We will therefore only keep in mind the estimate of about 3 GeV, obtained in [197, 198] for regions of the MSSM parameters favoured by naturalness.

The observed value of the Higgs mass, at 125 GeV, and the tree-level bound on the lightest Higgs mass  $m_h$  in the MSSM, imply that the radiative corrections  $\Delta m_h^2$  must be of the same order as the tree-level mass-squared  $(m_h^2)^{\text{tree}}$ . If we assume that we are in the most favourable case in which the tree-level bound is saturated (this happens when  $\tan\beta$  and  $m_A$  are both large), the observed Higgs boson mass requires the stop masses to be of the order of 1 TeV in a scenario with maximal stop mixing – *i.e.*  $X_t/M_S \sim 2$ , although the precise number is somewhat dependent on the renormalisation scheme in which  $X_t$  is computed – or stop masses larger than 10 TeV in the absence of mixing ( $X_t = 0$ ). In this regime, logarithms of the form  $\log^\ell M_S/m_t$  become large and cause a (significant) loss of accuracy in fixed-order calculations, which has led to a renewal of the interest for the EFT approach.

### 2.3.1.2 EFT and hybrid results

Effective Field Theory techniques have also been applied to Higgs mass calculations, since the beginning of the 1990’s, by matching the MSSM onto the SM or a (variant of) 2HDM – early examples of these two options include *e.g.* [199–201] and [202, 203] respectively. When integrating out SUSY partners, higher-dimensional operators are generated, which are suppressed by powers of  $v^2/M_S^2$  – where the Higgs VEV  $v$  characterises the EW scale and  $M_S$  denotes the mass scale of the SUSY particles. However, SUSY particles were at first expected to be found at scales not much higher than the electroweak scale, and in that case, fixed-order calculations would not be suffering from the presence of large logarithms while EFT calculations would require

taking into account a large number of higher-dimensional operators to give a precise prediction for  $m_h$ . For this reason, the EFT approach was until recently seldom used to compute complete radiative corrections to Higgs masses – let us mention however ref. [204] where an EFT served to study of the leading two-loop contributions to the Higgs mass in a scenario with a large hierarchy between the stops (the heavy stop being integrated out), and where the effect of higher-dimensional (dimension-6) operators is taken into account. Nevertheless, EFT techniques have been employed to extract the logarithmic contributions to  $m_h^2$ , with results obtained at one loop [199, 200, 202, 203], two loops [201, 205–209], and also three loops [197, 210].

In later years, the discovery of the Higgs boson with a relatively heavy mass and the absence of signs of SUSY partners at the LHC have led the interest for EFTs to rise again – in part because, for larger SUSY-breaking scale, fixed-order calculations exhibit a loss of accuracy and at the same time the effects of higher-dimensional operators become smaller. A first possible, purely EFT, strategy is to match the MSSM with the SM, and take advantage of the current knowledge of three-loop RGEs and full two-loop Higgs mass calculations in the SM – see [25, 53, 54]. More precisely, the idea is to match at a scale  $Q$  the SM Higgs quartic coupling  $\lambda$  to its MSSM value (related to the EW gauge couplings), with threshold corrections that can be expanded in perturbation theory as

$$\lambda(Q) = \frac{1}{4}(g^2(Q) + g'^2(Q)) \cos^2 2\beta + \sum_{n=1}^{\ell} \frac{1}{(16\pi^2)^n} \delta^{(n)} \lambda, \quad (2.3.11)$$

where  $\ell$  is the loop order to which the matching is performed. The threshold corrections have been obtained to full one-loop order in [211–213], and leading two-loop (as well as higher-order) contributions have been studied [170, 213–216]. Combined with the above cited RGEs and corrections for the SM, this makes possible a full next-to-leading and partial next-to-next-to-leading logarithmic order resummation of the corrections to  $m_h$ . Some of these results are implemented in public codes, such as **SusyHD** [215], **MhEFT** (based on [214, 217], and able to accomodate a 2HDM instead of the SM as low energy model), or **HSSUSY** [218] (itself a module of **FlexibleSUSY** [219, 220]).

Different approaches, which we will refer to as *hybrid approaches*, have also been developed recently in order to benefit simultaneously from the advantages of fixed-order and EFT calculations. One of these methods, devised in **FlexibleEFTHiggs** [218, 220], constitutes a variation of the purely-EFT calculation described above in which the matching condition of the quartic constant – as in equation (2.3.11) – is replaced by a matching of Higgs pole masses between the SM and the MSSM, or any general BSM model. Indeed, it should be noted that with the framework of **FlexibleSUSY**/**FlexibleEFTHiggs** computations can be performed for a wide range of BSM models – as is the case with the **SARAH**/**SPheno** framework, to which we will return in section 2.4.3. As in the SM the tree-level mass of the Higgs boson – and in turn its pole mass, see eqs. (1.1.38) and (1.1.39) – depends on the quartic coupling  $\lambda$ , we can extract it at a scale  $Q$  from the pole mass matching and we find

$$\lambda(Q) = \frac{1}{2v^2} \left[ (M_h^2)^{\text{MSSM}} + \frac{1}{v} \frac{\partial(\Delta V)^{\text{SM}}}{\partial h} \Big|_{\text{min.}} - \Pi_{hh}^{\text{SM}}(p^2 = (m_h^2)^{\text{MSSM}}) \right]. \quad (2.3.12)$$

where, quantities on the right-hand side of this equation are also computed at the matching scale  $Q$ . More specifically,  $(M_h^2)^{\text{MSSM}}$  is the pole mass of the Higgs computed in the MSSM (or another BSM model),  $(\Delta V)^{\text{SM}}$  denotes the loop corrections to the SM effective potential and  $\Pi_{hh}^{\text{SM}}$  is the Higgs self-energy computed in the SM. The

**FlexibleEFTHiggs** procedure now allows the combination of a full one-loop calculation of  $m_h$ , together with the resummation of large logarithms up to next-to-leading logarithmic order [220]. A similar calculation has also been made available (for generic models as well) in **SARAH/SPHeno** in [221].

For completeness, we should also mention that another hybrid approach has been taken in [222–224]. The idea is to add to the Higgs mass computed in the Feynman-diagrammatic way an additional term equal to the corrections to  $m_h^2$  in the EFT approach, but from which two types of terms have been subtracted to avoid double-counting of corrections: (i) the one- and two-loop logarithmic terms in the fixed-order calculation (*i.e.* the terms in eq. (2.2.33) for  $\ell = 1, 2$ ); and (ii) the non-logarithmic parts of the EFT corrections. This approach then incorporates both the corrections obtained in the fixed-order approach (and in particular takes into account terms of proportional to powers of  $v^2/M_S^2$ ) and the higher-order logarithms resummed to leading and next-to-leading logarithmic orders in the EFT calculation – this method proves especially useful for intermediate SUSY scales (where the theoretical uncertainties in the two standard approaches, fixed-order and EFT, are large).

Recently, efforts on the determination of Higgs masses in the MSSM have been concentrated on three main areas: (i) completing the computation of the full two-loop momentum dependence in the diagrammatic approach (in the complex MSSM); (ii) improving EFT and hybrid calculations (extend pole mass matching to two loops; integrate out SUSY states gradually, with a tower of EFTs between the MSSM and the SM, etc.); (iii) obtaining the three-loop corrections to the scalar masses and making these new results available in the existing automated tools.

### 2.3.2 Supersymmetric models beyond the MSSM

Efforts to derive corrections to neutral scalar masses in the NMSSM have, until recent years, been somewhat more moderate and therefore the available results in these models are less advanced than in the MSSM. However, one-loop corrections have been studied in the CP-conserving NMSSM already since the 1990’s, with corrections from tops and stops as well as from bottoms and sbottoms obtained, at zero external momentum, in [225–228], while leading logarithmic contributions from charginos, neutralinos and scalars were given in [229]. Complete one-loop diagrammatic calculations – with full momentum dependence – were carried out in [77, 230] (in a pure  $\overline{\text{DR}}'$  scheme), in [231] (both in a mixed  $\overline{\text{DR}}'$ -OS scheme and a pure OS scheme) and in [232] (in a mixed  $\overline{\text{DR}}'$ -OS scheme as well) for the CP-conserving NMSSM. In the presence of CP violation, first investigations of scalar masses at one loop were also performed in the effective potential limit [233–237] and complete results were found in [238] with a diagrammatic approach (previously one-loop and leading two-loop results had been obtained with EFT techniques in [239]). Ref. [77] provided the first explicit two-loop results, by deriving the  $\mathcal{O}(\alpha_t\alpha_s + \alpha_b\alpha_s)$  corrections to Higgs masses in the CP-conserving NMSSM using the effective potential (and a pure  $\overline{\text{DR}}'$  renormalisation scheme). These results were extended in [240] to the case with CP violation, and with a mixed  $\overline{\text{DR}}'$ -OS scheme.

As for the MSSM, the analytic expressions that we have cited here have been implemented in a number of public spectrum generators written specifically for the NMSSM, namely **SoftSUSY** [191, 241], **NMSSMTools** [242–244], and **NMSSMCALC** [245, 246] (for detailed discussions and comparisons of these codes, the reader may also refer to [247, 248]). It should be noted that **SoftSUSY** and **NMSSMTools** also include some

partial contributions that depend only on the third family Yukawa couplings, adapted from the MSSM calculations *i.e.* adding corrections only to the  $2 \times 2$  part of the NMSSM CP-even mass matrix<sup>8</sup> that corresponds to the states present in the MSSM. Moreover, **NMSSMCALC** takes into account terms that arise from the extraction of the  $\overline{\text{DR}}'$  running VEV at two-loop order, and give effects on the scalar masses formally of the form  $\mathcal{O}(\alpha_t \alpha_s)$  (these contributions are not available in the other codes). New corrections to Higgs masses in the NMSSM have also been obtained by employing results for generic theories implemented in **SARAH/SPHeno** and **FlexibleSUSY/FlexibleEFTHiggs** – instead of performing explicit calculations. In particular, ref. [249] investigated contributions beyond  $\mathcal{O}(\alpha_t \alpha_s + \alpha_b \alpha_s)$ , more precisely the effects of the complete corrections of the form  $\mathcal{O}(\alpha_t^2 + \alpha_b^2 + \alpha_\tau^2)$  (and not only the corresponding MSSM contributions), and of terms involving the superpotential singlet coupling  $\lambda_S$ .

For supersymmetric models beyond the NMSSM, no explicit expressions for contributions to Higgs masses at more than one-loop order had been obtained until the calculation of the leading two-loop  $\mathcal{O}(\alpha_t \alpha_s)$  corrections in models with Dirac gauginos that we will present in chapter 3. It should be noted, however, that **SARAH/SPHeno** has allowed studies of Higgs masses at two loops since version 4.4.0 (see ref. [250]), and has indeed been used *e.g.* for the MDGSSM [101] or the MRSSM [251, 252].

### 2.3.3 Non-supersymmetric models

In most non-supersymmetric models, the scalar quartics are free parameters – this is for example the case in BSM models, such as 2HDMs or the Georgi-Machacek model, but also in the Standard Model. The tree-level Higgs masses are then also free parameters, and it is often assumed that radiative corrections to scalar masses and mixing angles can be reabsorbed into a shift of the Lagrangian parameters (in particular of the quartics). There have therefore been very few studies of corrections to Higgs masses in non-SUSY extensions of the SM, and instead efforts have been concentrated on the calculation of corrections to Higgs couplings or observables (decay widths, cross sections, etc.), in terms of scalar (pole) masses – see for example [253–257].

There are nevertheless instances where it is useful to compute masses in such models. On the one hand, in the context of EFT calculations it has become common to integrate out part of the spectrum of a SUSY model, and consider at low energies an extension of the SM with additional fields, and in particular with extended Higgs sectors – *e.g.* consider a 2HDM as a low energy limit of the MSSM. The quartic couplings in the low energy model are then no longer free but are instead fixed by the matching condition with the SUSY model (in which the quartics are related to the EW gauge couplings), and this allows predictive results. On the other hand, one is sometimes interested in deriving the values of the Lagrangian parameters of the scalar sector of a given model from the input of the mass spectrum, and as we will discuss in chapter 6, it is in general crucial to include the effects of quantum corrections in this extraction. The simplest way to proceed is then to determine (typically by numerical iterations) the Lagrangian parameters that correspond to the desired loop-corrected spectrum through a calculation of the Higgs masses (see *e.g.* ref. [128] for an early example in the case of a singlet extension of the SM, and chapter 6 for a more general discussion).

---

<sup>8</sup>We recall that in the CP-conserving NMSSM, there are three CP-even states: the real components  $S_1$ ,  $S_2$  of  $H_u^0$  and  $H_d^0$  as in the MSSM, plus the real component  $S_3$  of the singlet scalar. Their masses are described by a  $3 \times 3$  (loop-corrected) mass matrix. What **SoftSUSY** and **NMSSMTools** are doing is to include the additional corrections only for the upper-left  $2 \times 2$  part of that matrix.

## 2.4 Calculations in generic theories

In the previous sections, we have briefly reviewed some of the results obtained since the early 1990's on the calculation of Higgs boson masses in the minimal supersymmetric extensions of the SM – mostly the MSSM but also to a smaller extent the NMSSM. While considerable efforts have been devoted to this task, achieving a remarkable level of accuracy, there is no guarantee that the MSSM or the NMSSM are realised by Nature, and a tremendous number of other phenomenologically viable models exist and receive interest, such as non-minimal supersymmetric models (Dirac gaugino models would for instance belong to this category) or non-supersymmetric theories. One may wish to study scalar masses in a large variety of such models with a similar level of precision as what has been obtained in the MSSM and NMSSM, and one then arrives to the question of how to proceed to avoid long and painful calculations for each model under consideration. The answer is *automation*, *i.e.* to perform the difficult computation of radiative corrections to an observable – *e.g.* masses – once for a general model, and afterwards apply these results to any number of particular models as desired. The second step in this scheme involves translating the properties (field content, Lagrangian parameters, etc.) of the given model(s) into the general setting in which one has performed the calculation of the radiative corrections. This is actually not a difficult task, provided that suitable conventions are employed for the generic models, and it can even be automated with computer programs – *e.g.* with the **Mathematica** package **SARAH**, see section 2.4.3.

This section will serve to introduce first the necessary notations and the existing results for calculations of Higgs – or more generally neutral scalar – masses in general renormalisable field theories, before presenting the framework provided by the public tools **SARAH** and **SPheno** for the automated and precise study of a wide range of BSM models. While we have already mentioned the fact that these two programs have made possible studies of non-minimal supersymmetric models (more specifically Dirac gaugino models), it is important to note that they have also allowed the study of new two-loop contributions to Higgs masses in the MSSM and NMSSM – not derived in explicit calculations. Such new corrections include the effects at two loops of non-minimal flavour violation [258] or of trilinear  $R$ -parity-violating operators [259] in the MSSM, as well as the additional results in the NMSSM [249] that we mentioned previously.

### 2.4.1 Notations for general field theories

We begin by presenting our notations for the purely scalar sector of a generic theory, following the procedure in [21] (itself in the setting established in [19,20]). We introduce first the scalar Lagrangian and potential in terms of real scalar fields  $\varphi_i^0$ , for which the Lagrangian mass parameters are not necessarily diagonal<sup>9</sup>

$$\mathcal{L}_S = \frac{1}{2}(\partial_\mu \varphi_i^0)^2 - V^{(0)}(\{\varphi_i^0\}),$$

$$V^{(0)}(\{\varphi_i^0\}) = \bar{t}^i \varphi_i^0 + \frac{1}{2} \bar{m}_{0,ij}^2 \varphi_i^0 \varphi_j^0 + \frac{1}{6} \bar{\lambda}_0^{ijk} \varphi_i^0 \varphi_j^0 \varphi_k^0 + \frac{1}{24} \bar{\lambda}_0^{ijkl} \varphi_i^0 \varphi_j^0 \varphi_k^0 \varphi_l^0. \quad (2.4.1)$$

---

<sup>9</sup>This is not uncommon when considering some particular theory: the Lagrangian is typically not written in terms of states with well-defined (*i.e.* diagonal) masses but in terms of interaction eigenstates (*i.e.* gauge and/or flavour eigenstates). One then computes a mass matrix for the interaction eigenstates that can be diagonalised to obtain the mass eigenstates and eigenvalues – see *e.g.* our discussion for stops in the MSSM and equations (1.3.86) to (1.3.90).

Note that the generic scalar index  $i$  can correspond in a given model to a collection of flavour (or family) indices, gauge indices, etc., and that we will also imply a summation on repeated indices. Also, unless otherwise specified, we will in the following assume all scalar couplings to be fully symmetric under the exchange of scalar indices. Furthermore, we have expanded the covariant derivatives in the kinetic terms and we will give the terms other than  $(\partial_\mu \phi_i^0)^2$  separately as scalar–gauge–boson couplings in the following (we will proceed similarly for the fermion and gauge–boson kinetic terms).

We can then expand the scalars as fluctuations  $\phi_i^0$  around vacuum expectation values  $v_i$  such that  $\phi_i^0 \equiv v_i + \phi_i^0$  and rewrite the above potential as

$$V^{(0)}(\{\phi_i^0\}) = V^{(0)}(v_i) + \hat{t}_0^i \phi_i^0 + \frac{1}{2} \hat{m}_{0,ij}^2 \phi_i^0 \phi_j^0 + \frac{1}{6} \hat{\lambda}_0^{ijk} \phi_i^0 \phi_j^0 \phi_k^0 + \frac{1}{24} \hat{\lambda}_0^{ijkl} \phi_i^0 \phi_j^0 \phi_k^0 \phi_l^0. \quad (2.4.2)$$

with the redefinitions

$$\begin{aligned} \hat{t}_0^i &= \bar{t}^i + \bar{m}_{0,ij}^2 v_j + \frac{1}{2} \bar{\lambda}_0^{ijk} v_j v_k + \frac{1}{6} \hat{\lambda}_0^{ijkl} v_j v_k v_l, \\ \hat{m}_{0,ij}^2 &= \bar{m}_{0,ij}^2 + \bar{\lambda}_0^{ijk} v_k + \frac{1}{2} \hat{\lambda}_0^{ijkl} v_k v_l, \\ \hat{\lambda}_0^{ijk} &= \bar{\lambda}_0^{ijk} + \bar{\lambda}_0^{ijkl} v_l, \\ \hat{\lambda}_0^{ijkl} &= \bar{\lambda}_0^{ijkl}. \end{aligned} \quad (2.4.3)$$

The tree-level tadpole equations here simply read  $\hat{t}_0^i = 0$ , and with the first equation in (2.4.3) we find that these impose relations among the parameters in the original basis – *e.g.* one can eliminate one mass parameter  $\bar{m}_{0,ij}^2$  per tadpole equation – and we use these relations to simplify the expression of  $\hat{m}_{0,ij}^2$ . From this we can define the field-dependent masses and couplings,

$$\hat{m}_{ij}^2(\phi^0) \equiv \frac{\partial^2 V^{(0)}}{\partial \phi_i^0 \partial \phi_j^0} = \hat{m}_{0,ij}^2 + \hat{\lambda}_0^{ijk} \phi_k^0 + \frac{1}{2} \hat{\lambda}_0^{ijkl} \phi_k^0 \phi_l^0, \quad (2.4.4)$$

$$\hat{\lambda}^{ijk}(\phi^0) \equiv \frac{\partial^3 V^{(0)}}{\partial \phi_i^0 \partial \phi_j^0 \partial \phi_k^0} = \hat{\lambda}_0^{ijk} + \hat{\lambda}_0^{ijkl} \phi_l^0, \quad (2.4.5)$$

$$\hat{\lambda}^{ijkl}(\phi^0) \equiv \frac{\partial^4 V^{(0)}}{\partial \phi_i^0 \partial \phi_j^0 \partial \phi_k^0 \partial \phi_l^0} = \hat{\lambda}_0^{ijkl}. \quad (2.4.6)$$

We then introduce a new basis  $\{\tilde{\phi}_i\}$  and an orthogonal matrix  $\tilde{R}$  to diagonalise the tree-level mass matrix as

$$\phi_i^0 = \tilde{R}_{ij} \tilde{\phi}_j, \quad (2.4.7)$$

and obtain the new masses and couplings

$$\tilde{m}_i^2 \delta_{ij} = \hat{m}_{kl}^2 \tilde{R}_{ki} \tilde{R}_{lj} \quad (2.4.8)$$

$$\tilde{\lambda}^{ijk} = \hat{\lambda}^{lmn} \tilde{R}_{li} \tilde{R}_{mj} \tilde{R}_{nk} \quad (2.4.9)$$

$$\tilde{\lambda}^{ijkl} = \hat{\lambda}^{mnpq} \tilde{R}_{mi} \tilde{R}_{nj} \tilde{R}_{pk} \tilde{R}_{ql}. \quad (2.4.10)$$

Next we need to define what happens when we introduce the loop corrections to the effective potential  $\Delta V$ . Instead of  $\hat{t}_0^i = 0$ , the loop-corrected tadpole equations are then

$$\hat{t}_0^i + \left. \frac{\partial \Delta V}{\partial \phi_i^0} \right|_{\phi_i^0=0} = 0. \quad (2.4.11)$$



As we mentioned in the case of the SM in the previous chapter, we shall take the expectation values  $v_i$  to be fixed inputs for the scalar mass calculations (*i.e.* we consider that they are computed at the required order in perturbation theory through a separate calculation), and instead we solve the tadpole equations for the mass-squared parameters in the Lagrangian. This means correcting the mass parameters, passing from  $\hat{m}_{0,ij}^2$  (which satisfy the tree-level tadpole equations) to new quantities  $m_{ij}^2$  (which obey the loop-corrected tadpole equations). Using the minimisation conditions, the relationship between them is

$$m_{ij}^2 v_j = \hat{m}_{0,ij}^2 v_j - \frac{\partial \Delta V(\{m_{ij}^2\})}{\partial \phi_i^0} \Big|_{\phi_i^0=0}. \quad (2.4.12)$$

In order to be able to use the results for two-loop radiative corrections of [19–21], we follow the choice of these papers and employ the parameters  $m_{ij}^2$  as masses of scalars in all loop calculations. Diagonalising these requires the introduction of a new basis via  $\phi_i^0 = R_{ij} \phi_j$ , having squared masses  $m_i^2$  and couplings  $\lambda^{ijk}, \lambda^{ijkl}$ .

To illustrate what we mean by the above definitions, let us relate these to the case of the Higgs boson in the SM, which we had discussed in section 1.1.4. First, the mass term in the original Lagrangian is  $\bar{m}_{0,hh}^2 = \mu^2$ , and then if we expand the SM Lagrangian around the Higgs VEV (or equivalently if we compute the second derivative of  $V^{(0)}$  with respect to  $h$ ) we obtain  $\hat{m}_{0,hh}^2 = \mu^2 + 3\lambda v^2$ . Now, as we explained above, the expressions of the  $\hat{m}_{0,ij}^2$  are modified because of the relations among parameters imposed by the tree-level tadpole equations. Solving the tadpole equation  $\hat{t}_0^h = \mu^2 v + \lambda v^3 = 0$  for  $\mu^2$  (*i.e.*  $\bar{m}_{0,hh}^2$ ), we have

$$\hat{m}_{0,hh}^2 = 2\lambda v^2. \quad (2.4.13)$$

When introducing loop corrections to the scalar potential in the SM, the tadpole equation is modified and becomes

$$\hat{t}_0^h + \frac{\partial \Delta V}{\partial h} \Big|_{\min.} = 0, \quad \Rightarrow \quad \mu^2 = -\lambda v^2 - \frac{1}{v} \frac{\partial \Delta V}{\partial h} \Big|_{\min.}. \quad (2.4.14)$$

With this relation, the mass parameter  $m_{ij}^2$  for the Higgs boson (*i.e.*  $m_{hh}^2$ ) is finally

$$m_{hh}^2 = \mu^2 + 3\lambda v^2 = 2\lambda v^2 - \frac{1}{v} \frac{\partial \Delta V}{\partial h} \Big|_{\min.} = \hat{m}_{0,hh}^2 - \frac{1}{v} \frac{\partial \Delta V}{\partial h} \Big|_{\min.}. \quad (2.4.15)$$

This is the equivalent of equation (2.4.12) for the SM (which we already found in eq. (1.1.38)).

We can then consider fermions and gauge bosons, using the notation for a general renormalisable field theory used in [19, 20]. The fermions  $\psi_I$  are taken in Weyl notation and their kinetic and mass Lagrangian terms are written as

$$\mathcal{L}_F = i\bar{\psi}^I \bar{\sigma}^\mu \partial_\mu \psi_I - \frac{1}{2} (M^{IJ} \psi_I \psi_J + M_{IJ}^* \bar{\psi}^I \bar{\psi}^J). \quad (2.4.16)$$

Here we should point out that we have followed the choice of [21] to denote the complex conjugation explicitly on  $M_{IJ}^*$  – while in [19, 20] complex conjugation is implied solely by the lowering and raising of fermion indices. We assume the fermions to be defined in a basis where all their squared masses are diagonal, *i.e.*

$$M^{IJ} M_{JK}^* = m_I^2 \delta_K^I. \quad (2.4.17)$$

The Yukawa couplings are denoted collectively  $y^{IJk}$  and are symmetric under the exchange  $I \leftrightarrow J$ , and thus the scalar-fermion interaction terms read

$$\mathcal{L}_{SF} = -\frac{1}{2}y^{IJk}\psi_I\psi_J\phi_k + \text{h.c.} \quad (2.4.18)$$

Finally, massive vector (gauge) bosons  $A_\mu^a$  can be introduced with kinetic and (diagonal) mass terms

$$\mathcal{L}_V = -\frac{1}{4}\bar{F}^{\mu\nu a}\bar{F}_{\mu\nu}^a - \frac{1}{2}m_a^2 A_\mu^a A^{\mu a}, \quad (2.4.19)$$

where we have expanded the standard (non-Abelian) field-strength tensor as

$$\begin{aligned} F_{\mu\nu}^a &= \bar{F}_{\mu\nu}^a - g^{abc}A_\mu^b A_\nu^c, \\ \bar{F}_{\mu\nu}^a &= \partial_\mu A_\nu^a - \partial_\nu A_\mu^a. \end{aligned} \quad (2.4.20)$$

We have expanded all kinetic terms and we can now give the interaction terms of gauge bosons with scalars, with fermions, or with themselves (and ghosts), as found in [19]

$$\begin{aligned} \mathcal{L}_{SV} &= -\frac{1}{2}g^{abi}A_\mu^a A^{\mu b}\phi_i - \frac{1}{4}g^{abij}A_\mu^a A^{\mu b}\phi_i\phi_j - g^{aij}A_\mu^a\phi_i\partial^\mu\phi_j, \\ \mathcal{L}_{FV} &= g_I^{aJ}\bar{\psi}^I\bar{\sigma}^\mu\psi_J A_\mu^a, \\ \mathcal{L}_{\text{gauge}} &= g^{abc}A_\mu^a A_\nu^b\partial^\mu A^{\nu c} - g^{abe}g^{cde}A^{\mu a}A^{\nu b}A_\mu^c A_\nu^d + g^{abc}A_\mu^a\omega^b\partial^\mu\bar{\omega}^c \end{aligned} \quad (2.4.21)$$

In the above interaction terms, the couplings  $g^{abi}$  and  $g^{abij}$  are symmetric under the interchange either of two vector indices or of two scalar indices. Moreover,  $g^{aij}$  is antisymmetric under the exchange  $i \leftrightarrow j$  and  $g^{abc}$  is fully antisymmetric. Details on how to diagonalise the fermion and gauge-boson squared masses and how to relate the couplings involving gauge bosons to the structure constants and generators of the gauge group can be found in [19].

## 2.4.2 Two-loop neutral scalar masses in generic theories

To calculate the Higgs boson masses in general field theories we require the tadpole diagrams and self-energies. Two-loop order expressions for the former were given in [21], which were derived from the general expression for the effective potential at two loops in the Landau gauge, given in [19]. Hence we must also use the self-energies in the Landau gauge; these were given in [20], in terms of a basis of two-loop functions defined in [142], up to order  $g^2$  in the gauge couplings. Afterwards, in [260], these expressions were extended to order  $g^4$  for unbroken gauge groups (*i.e.* when the gauge bosons remain massless). We therefore restrict ourselves to the “gaugeless limit”, where we ignore the contributions of broken gauge groups for two-loop corrections—for the SM gauge group this means setting  $g = g' = 0$ . As the electroweak gauge couplings  $g$  and  $g'$  are smaller than the strong gauge coupling  $g_s$  and the top Yukawa coupling (and in some models and scenarios<sup>10</sup>, also the remaining third generation Yukawa couplings), we expect the electroweak contributions that we neglect in this limit to be subdominant. The gaugeless limit has a number of advantages, chiefly simplicity and speed of the calculation; but also the fact that we can compute the one-loop corrections in any gauge desired. Once we have dropped the electroweak contributions, it is also tempting to disregard the momentum-dependence of the loop

<sup>10</sup>For example, in models with two Higgs doublets (2HDM, MSSM, etc.) when  $\tan\beta$  is large.

functions, which is typically estimated to contribute at the same order (and indeed is so for the MSSM [177,178]) – hence the popularity of calculations in the effective potential approach.

Note, however, that when addressing the Goldstone Boson Catastrophe in the context of mass calculations for generic models in chapter 4, we will find it necessary to go beyond the (standard) effective potential approximation because the inclusion of external momentum is necessary to regulate the divergences of some of the two-loop self-energy diagrams when  $m_G^2 \rightarrow 0$ . We will therefore devise a *generalised* effective potential approximation to cure the divergent behaviour of the diagrams, while still benefiting from the simplicity of calculations without the full momentum dependence – see section 4.3.

### 2.4.3 The SARAH/SPheno framework

As discussed earlier, once expressions for the contributions to the effective potential, tadpole equations and self-energies have been obtained for a generic model, there remains to translate them for the model one is interested in. This is usually a simple, although tedious, task and can be automatised with programs that handle formal calculations. One – and actually the first – such program is the **Mathematica** package **SARAH** [261–266], and in this section we will give a brief presentation of the framework it provides, and in particular of how its interfacing with the **Fortran** spectrum generator **SPheno** [194,195] allows the study of a wide range of BSM theories taking into account higher-order corrections to physical quantities, including two-loop corrections to neutral scalar masses. We refer the reader to standard references such as [266,267] for more detailed explanations of how to use **SARAH**, and to [194,195] for **SPheno**. For completeness, we should also mention the existence of other codes that can compute the vertices (*i.e.* the Feynman rules) of a given model, namely **FeynRules** [268] and **LanHEP** [269]. It should be noted that **FeynRules** accomodates non-renormalisable operators which is currently not the case in **SARAH**, but at the same time it does not link to a spectrum generator code – a major advantage of **SARAH**. Also, a spectrum generator for a generic BSM model can also be obtained alternatively by using **FlexibleSUSY** [219,220] (based in part on **SARAH** to create a **C++** spectrum generator). However we will not consider these options any further in this thesis.

#### 2.4.3.1 Analytic calculations with SARAH

**SARAH** was written originally for supersymmetric models to derive the tree-level mass matrices and vertices from the input of the superpotential (and soft SUSY-breaking Lagrangian if necessary) of the model and to provide these results as inputs for other codes calculating amplitudes (*e.g.* **CalcHEP**). However, it is now able to handle a wide range of models, both supersymmetric (and not only defined at high scales) and non-supersymmetric. Also, calculations of radiative corrections to physical observables have been gradually included, and the current version of the code (4.12.3) provides:

- full two-loop RGEs, using results derived for general QFTs in [270–273];
- one- and two-loop corrections to the effective potential, implementing results from [19];
- one-loop tadpole equations, and one-loop self-energies for all particles;

- two-loop tadpoles and neutral scalar self-energies. These were first found by taking numerical derivatives of the two-loop effective potential [250] (after interfacing **SARAH** with **SPheno**), but, since version 4.5.0, analytic expressions are computed directly in **SARAH** with results obtained for the tadpoles in [21], and implemented from refs. [20, 142, 260] for the self-energies. Furthermore, since version 4.12.0, the solution to the Goldstone Boson Catastrophe that we present in chapter 4 is also implemented in **SARAH**, as will be discussed in chapter 5;
- one-loop corrections to two-body decays, using the analytic results from [274].

The procedure to investigate a given BSM model is illustrated in figure 2.4 and can be explained as follows. First, the model to study is defined : *i.e.* the user specifies in a **Mathematica** package file (.m) the global and gauge symmetries of the model, the field content (or superfield content for a SUSY model), the Lagrangian (and superpotential if relevant), as well as the VEVs of the states after spontaneous symmetry breaking (EWSB usually) and the way in which states mix after SSB. Then, the **SARAH** package can be called from a **Mathematica** notebook to compute and write out expressions for tree-level properties of the model (mass matrices, vertices, potential, etc.) as well as for the above-listed radiative corrections. All these expressions can be manipulated directly as formal objects by **Mathematica**, which allows for example to check the theoretical consistency of the model or to evolve with its RGE any Lagrangian parameter.

#### 2.4.3.2 Interfaces with SPheno and other HEP codes

Furthermore, since [195, 275], **SARAH** can be interfaced with the **Fortran** code **SPheno** to create a complete spectrum generator for the model under consideration. The program **SPheno** is a spectrum generator written for the MSSM, first for variants defined at a high scale (*e.g.* mSUGRA) [194], and later extended to various other scenarios. It computes the loop-corrected masses and mixings of particles in the spectrum, and in turn uses those to calculate other properties of the particles, such as their decay widths (for two- and three-body decays), as well as low energy precision observables, such as lepton anomalous moments or lepton dipole moments. To extend this program to more general BSM models (including non-SUSY ones), **SARAH** writes new **Fortran** modules that are then compiled together with the **SPheno** routines – in particular routines to compute loop integrals. In the following, we will refer to the resulting program as a **SARAH/SPheno**, or simply **SPheno**, spectrum generator. A further extension in **SARAH**, called **FlavorKit** [276], makes possible calculations of numerous flavour observables in the spectrum generator, for a wide range of models.

However, the computation of particle spectra and physical observables is not the final step in the study of BSM theories, and there are numerous further avenues to investigate, both from the point of view of theoretical consistency and of phenomenology. For this reason the numerical framework of **SARAH/SPheno** can be linked to more High-Energy Physics codes: on the one hand, **Mathematica** routines in **SARAH** can write input files for a range of codes; on the other hand, **SARAH/SPheno** based spectrum generators employ the standard convention of the Supersymmetry Les Houches Accord (SLHA) [277, 278] for their input and output formats. A first possible direction is to determine whether the considered model can accommodate a vacuum state compatible with electroweak symmetry breaking, and moreover to verify the stability of this vacuum if it exists. Finding the global minimum of the scalar potential for a model with an extended Higgs sector is a priori a very complicated task, but it can be performed

to one-loop order by the program **Vevacious** [279], which uses as inputs a model file created by **SARAH**, and spectrum files from **SPheno**.

Moreover, comparing the theoretical predictions of a BSM model to experimental result provides additional criteria to rule in or out parameter points of the model. A great wealth of experimental results is available from a wide range of contexts such as, for example, collider phenomenology – in particular measurements related to Higgs physics or flavour physics – or dark matter. To exploit these results for general models, **SARAH** can be linked to a number of other codes made either: (i) to compute amplitudes or cross-sections; (ii) to generate simulated collider events; or (iii) to verify whether the properties of a model are compatible with data. Among programs that belong to the first and/or second of these categories, **SARAH** can create input files for **CalcHEP** [280], **FeynCalc** [281, 282] or **WHIZARD/O’Mega** [283, 284], as well as create models files in the standardised UFO (for Universal FeynRules Output) format [285], used by **MadGraph5\_aMC@NLO** [286], **GoSam** [287], **Herwig++** [288], or **Sherpa** [289]. Furthermore, **SARAH/SPheno** spectrum generators can provide the Higgs sector predictions (*e.g.* masses, decays, cross-sections, etc.) required as inputs for the programs **HiggsBounds** [290–292] and **HiggsSignals** [293, 294]. These two codes examine whether a given parameter point is allowed by current data or whether it is excluded at 95% confidence level: the former by verifying whether the parameter point is excluded by searches of additional Higgs bosons; and the latter by determining if the Higgs properties obtained for the considered parameter point are compatible with currently available measurements for the observed Higgs. Lastly, the theoretical prediction for the dark matter properties for a generic model (*i.e.* relic density, direct and indirect detection rates, etc.) can be computed by using **micrOMEGAs** [295–298] together with **SARAH/SPheno**. Indeed, implementing a new model in **micrOMEGAs** requires a **CalcHEP** model file, which can be generated automatically by **SARAH** together with a main file for **micrOMEGAs**. Once the executable **micrOMEGAs** program has been compiled, the dark matter calculations can be performed, using as inputs spectrum files from **SARAH/SPheno**.

Finally, we must also mention the **Mathematica** package **SSP** [275] – SSP stands for **SARAH** Scan and Plot – that makes possible parameter scans with **SARAH/SPheno** and linked programs – some of the figures in chapter 5 have been made with **SSP**.

### 2.4.3.3 Numerical set-up of the spectrum calculation

We end our presentation of the framework of **SARAH** and **SPheno** for Higgs mass calculations by describing how to calculate, in a fixed-order approach,<sup>11</sup> the mass spectrum with a **SARAH/SPheno** spectrum generator. First, it is necessary to distinguish two types of inputs that will appear in the computations, namely SM parameters and additional parameters of the BSM model, which are treated differently. The former are given in a particular block of the SLHA input file, called **SMINPUTS**, and consist of the Fermi constant  $G_F$  and the pole masses of the  $Z$  boson, the top quark and tau lepton; together with three  $\overline{\text{MS}}$  values:  $\alpha_s^{\overline{\text{MS}}}(m_Z)$ ,  $\alpha^{\overline{\text{MS}}}(m_Z)$  and  $m_b^{\overline{\text{MS}}}(m_b)$ . From these inputs, the Higgs VEV as well as the gauge and third family Yukawa couplings, *i.e.*

$$v, g_s, g, g', y_t, y_b, y_\tau, \quad (2.4.22)$$

are extracted as  $\overline{\text{MS}}/\overline{\text{DR}}'$  parameters and run to the scale at which the calculation of radiative corrections are performed. There are, in principle, two ways to do this

---

<sup>11</sup>Since [221], **SARAH/SPheno** also accomodates an EFT calculation, but we will not discuss it here.

in **SPheno**, which can be explained as follows (see also appendix A of [221] for more details):

- the first option follows the method from [163] and is referred to as *one-scale matching*. The idea is to extract at the scale  $m_Z$  the values of the couplings and Higgs VEV in the BSM model under consideration, and in an  $\overline{\text{MS}}$  or  $\overline{\text{DR}}'$  scheme (depending on whether the model is supersymmetric or not). These parameters can then be evolved using two-loop RGEs in the BSM model. However, this method encounters problems if some of the new states are heavy, because large logarithmic contributions appear in the threshold corrections that are applied at  $m_Z$ ;
- another strategy, more suited for BSM models involving heavy particles, is the so-called *two-scale matching*. The parameters in (2.4.22) are extracted at  $m_Z$  but this time as Standard Model parameters in the  $\overline{\text{MS}}$  scheme. Afterwards, these are evolved with the known three-loop SM RGEs to the scale at which computations are performed, and are then converted to the BSM model (and appropriate scheme) by applying one-loop threshold corrections.

In the numerical studies that follow, we shall employ the latter approach.

The new parameters of the BSM theories are given in one or several different block(s) in the SLHA input, often exclusively the **MINPAR** block, and are taken as  $\overline{\text{MS}}$  or  $\overline{\text{DR}}'$  parameters at some input scale, which can be varied freely – *e.g.* it can be a high input scale for constrained SUSY models like mSUGRA, or simply be taken equal to the renormalisation scale employed in the rest of the code (we will often choose this when studying non-supersymmetric models). In the following we will call these extra parameters  $\Theta(Q)$  for a generic model.

The different steps performed to compute the spectrum are then:

- (i) The running couplings  $\Theta(Q)$  are (if necessary) run the scale at which the masses and tadpoles are computed – using two-loop RGEs generated by **SARAH** – while the SM parameters are evolved to this same scale including all known SM corrections, *i.e.* three-loop running and two-loop matching for strong coupling  $g_s$  and top Yukawa  $y_t$  (following the second of the two methods discussed above).
- (ii) The tree-level tadpoles  $T_i$  are solved to fix the remaining free parameters, which in what follows are typically the mass parameters  $\mu_i^2 |\phi|^2$ .
- (iii) The tree-level mass are calculated by diagonalising the tree-level mass matrices
- (iv) The  $n$ -loop corrections to the tadpoles  $\delta^{(n)} t_i$  are calculated. The imposed minimisation conditions are:

$$T_i + \sum_j^n \delta^{(j)} t_i = 0, \quad (2.4.23)$$

which cause shifts in  $\mu_i^2$ :

$$\mu_i^2 \rightarrow \mu_i^2 + \sum_j^n \delta^{(j)} \mu_i^2. \quad (2.4.24)$$

- (v) The one- and two-loop self-energies for real scalars are calculated for external gauge eigenstates. The pole masses are the eigenvalues of the loop-corrected mass matrix calculated as

$$M_\phi^{(n)}(p^2) = \tilde{M}_\phi^{(2L)} + \sum_{j=1}^n \Pi_\phi^{(j)}(p^2). \quad (2.4.25)$$

Here,  $\tilde{M}_\phi^{(2L)}$  is the tree-level mass matrix including the shifts eq. (2.4.24) computed to two-loop order.

The calculation of the one-loop self-energies is done iteratively for each eigenvalue  $i$  until the on-shell condition

$$\left[ \text{eig} M_\phi^{(n)}(p^2 = m_{\phi_i}^2) \right]_i \equiv m_{\phi_i}^2 \quad (2.4.26)$$

is fulfilled. The renormalised rotation matrix is taken to be the one calculated for  $p^2 = m_{\phi_1}^2$ .

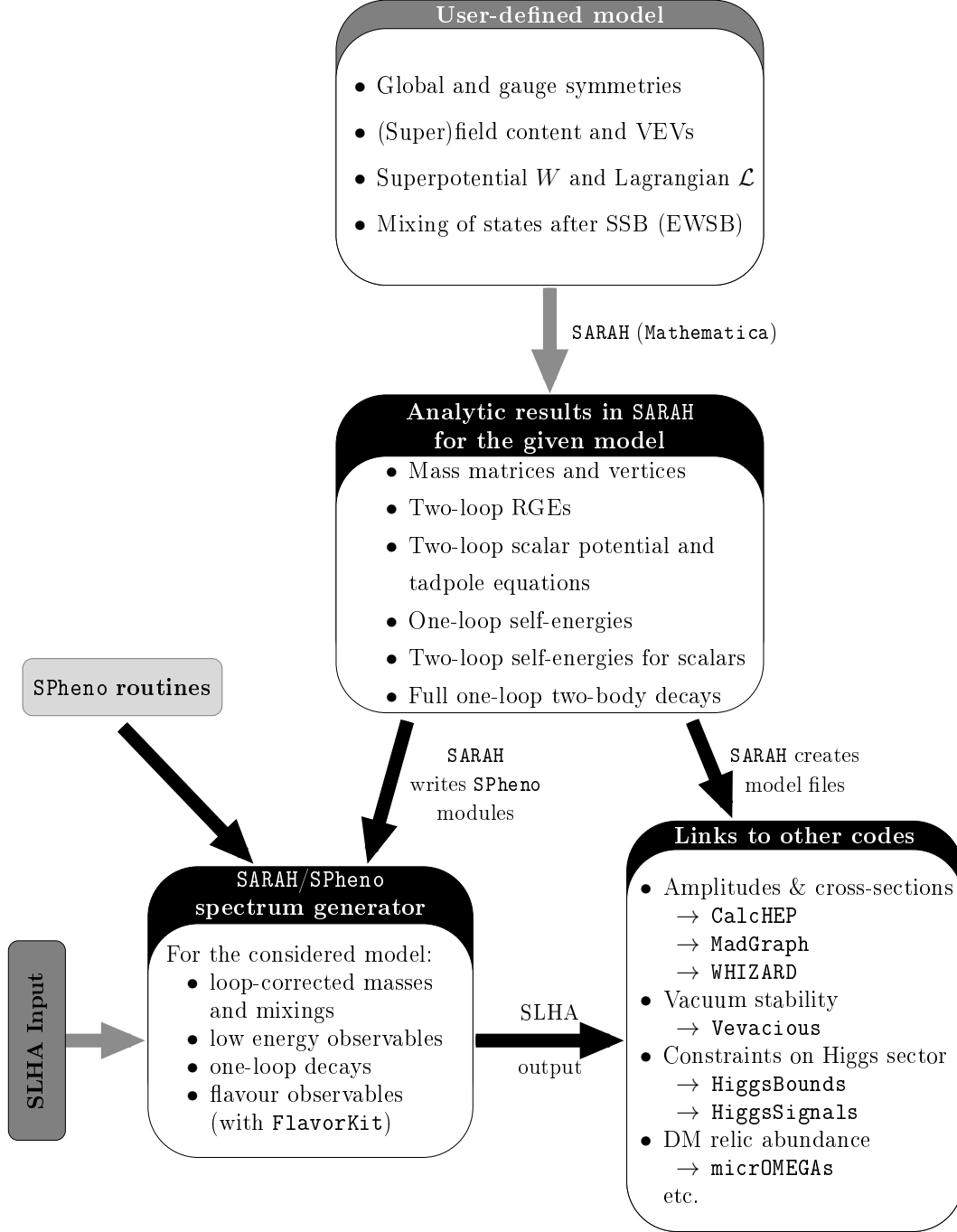


Figure 2.4 – Illustration of the study of a BSM model using SARAH and SPheno, and links to other High-Energy Physics codes.



## Chapter 3

# Leading two-loop corrections to the Higgs boson masses in SUSY models with Dirac gauginos

In this chapter we compute the leading corrections to neutral scalar masses in models with Dirac gauginos (introduced in section 1.3.5). As we have seen in the previous chapter, significant efforts have been devoted to Higgs-mass calculations in the MSSM – and to a lesser extent in the NMSSM – but in contrast, in other supersymmetric extensions of the SM, such as Dirac gaugino models, there have been no *explicit* calculations of the Higgs masses beyond one-loop results.

Dirac gaugino models exhibit extended Higgs sectors with an interesting and varied phenomenology, and from past experience in the study of the Higgs sector of the MSSM and of the NMSSM, we expect the radiative corrections to the Higgs boson masses in these theories to be crucial to obtain a reasonable precision and rule in/out scenarios, or assess their naturalness.

Recently, **SARAH** has made it possible to analyse at the two-loop level the Higgs sector of several non-minimal extensions of the MSSM, see [249,258,259,299,300]. Of particular relevance for this work, it has allowed for Dirac-gaugino masses since version 3.2 [264], incorporating also the results of ref. [301]. Indeed, **SARAH** has been used for detailed phenomenological analyses of the MDGSSM at one loop in ref. [109] and at two loops in refs. [100,101]; and also for the MRSSM at one loop in ref. [302] and two loops in refs. [251,252]. However, while such a numerical tool for generic models fulfils a significant need of the community, it is also important to have explicit results for specific models, and not just as a cross-check.

Here, we shall compute the leading  $\mathcal{O}(\alpha_t\alpha_s)$  corrections to the neutral Higgs boson masses in both the MDGSSM and MRSSM, relying on the effective-potential techniques developed in ref. [76] for the MSSM and in ref. [77] for the NMSSM. This has the following advantages:

- We compute the  $\mathcal{O}(\alpha_t\alpha_s)$  corrections in both the  $\overline{\text{DR}}'$  and on-shell (OS) renormalisation schemes. The latter turns out to be particularly useful in scenarios with heavy gluinos – a feature of many Dirac-gaugino models in the literature (as was also discussed in section 1.3.5.3) – where the use of  $\overline{\text{DR}}'$  formulae for the two-loop Higgs-mass corrections can lead to large theoretical uncertainties.

- We have written a simple and fast stand-alone code implementing our results, which we make available upon request (indeed, a version of the code is already included in **SARAH**).
- We use our results to derive simple approximate expressions for the most important two-loop corrections, applicable in any Dirac gaugino model.

The outline of this chapter is as follows. We first present in section 3.1 our results for the case of a general Dirac-gaugino model, and for the particular cases of the MDGSSM and the MRSSM, then show how we compute the shift to the OS scheme, and give simplified formulae for the SM-like Higgs boson mass either for a common SUSY-breaking scale or for a heavy Dirac gluino. In section 3.2 we give numerical examples of our results, illustrating the advantages of our approach and also discussing the inherent theoretical uncertainties. We conclude in section 3.3. Explicit expressions for the derivatives of the effective potential are given in appendix A.

### 3.1 Two-loop corrections in the effective potential approach

In this section we adapt to the calculation of two-loop corrections to the neutral Higgs masses in Dirac-gaugino models the effective-potential techniques developed in ref. [76] for the MSSM and in ref. [77] for the NMSSM. We start by deriving general results valid for all variants of Dirac-gaugino extensions of the MSSM, then we provide explicit formulae for the MDGSSM and MRSSM models discussed in section 1.3.5.6.

#### 3.1.1 General results

The effective potential for the neutral Higgs sector can be decomposed as  $V_{\text{eff}} = V^{(0)} + \Delta V$ , where  $\Delta V$  incorporates the radiative corrections. We denote collectively as  $\Phi_i^0$  the complex neutral scalars whose masses we want to calculate, and split them into vacuum expectation values  $v_i$ , real scalars  $S_i$  and pseudoscalars  $P_i$  as

$$\Phi_i^0 \equiv v_i + \frac{1}{\sqrt{2}}(S_i + i P_i) . \quad (3.1.1)$$

Then the mass matrices for the scalar and pseudoscalar fields can be decomposed as

$$(\mathcal{M}_S^2)_{ij}^{\text{eff}} = (\mathcal{M}_S^2)_{ij}^{\text{tree}} + (\Delta\mathcal{M}_S^2)_{ij} , \quad (\mathcal{M}_P^2)_{ij}^{\text{eff}} = (\mathcal{M}_P^2)_{ij}^{\text{tree}} + (\Delta\mathcal{M}_P^2)_{ij} , \quad (3.1.2)$$

and the radiative corrections to the mass matrices are

$$(\Delta\mathcal{M}_S^2)_{ij} = -\frac{1}{\sqrt{2}} \frac{\delta_{ij}}{v_i} \frac{\partial \Delta V}{\partial S_i} \Big|_{\min} + \frac{\partial^2 \Delta V}{\partial S_i \partial S_j} \Big|_{\min} , \quad (3.1.3)$$

$$(\Delta\mathcal{M}_P^2)_{ij} = -\frac{1}{\sqrt{2}} \frac{\delta_{ij}}{v_i} \frac{\partial \Delta V}{\partial S_i} \Big|_{\min} + \frac{\partial^2 \Delta V}{\partial P_i \partial P_j} \Big|_{\min} , \quad (3.1.4)$$

where  $v_i$ , which we assume to be real, denote the VEVs of the full radiatively-corrected potential  $V_{\text{eff}}$ , and the derivatives are in turn evaluated at the minimum of the potential. The single-derivative terms in eqs. (3.1.3) and (3.1.4) arise when the minimum conditions of the potential,

$$\frac{\partial V_{\text{eff}}}{\partial S_i} \Big|_{\min} = 0 , \quad (3.1.5)$$

are used to remove the soft SUSY-breaking mass for a given field  $\Phi_i^0$  from the tree-level parts of the mass matrices. It is understood that those terms should be omitted for fields that do not develop a VEV (such as, *e.g.*, the fields  $R_{u,d}$  in the MRSSM). Note that when using the minimum conditions in eqs. (3.1.2), (3.1.3) and (3.1.4), we have proceeded as for the MSSM in section 2.3.1, *i.e.* we have split the tadpole terms between tree- and loop-level, and the tree-level part has already been used to simplify the tree-level mass matrices.

With a straightforward application of the chain rule for the derivatives of the effective potential, the mass-matrix corrections in eqs. (3.1.3) and (3.1.4) and the minimum conditions in eq. (3.1.5) can be computed by exploiting the Higgs-field dependence of the parameters appearing in  $\Delta V$ . We restrict for simplicity our calculation to the so-called “gaugeless limit”, *i.e.* we neglect all corrections controlled by the electroweak gauge couplings  $g$  and  $g'$ . At the two-loop level, we focus on the contributions to  $\Delta V$  from top/stop loops that involve the strong interactions. In Dirac-gaugino models, this results in corrections to mass matrices and minimum conditions that are proportional to  $\alpha_s$  times various combinations of the top Yukawa coupling  $y_t$  with the superpotential couplings of the singlet and triplet fields. It is therefore with a slight abuse of notation that we maintain the MSSM-inspired habit of denoting collectively those corrections as  $\mathcal{O}(\alpha_t \alpha_s)$ .

As detailed in refs. [76, 77], if we neglect the electroweak contributions to the stop mass matrix the parameters in the top/stop sector depend on the neutral Higgs fields only through two combinations, which we denote as  $X \equiv |X| e^{i\varphi}$  and  $\tilde{X} \equiv |\tilde{X}| e^{i\tilde{\varphi}}$ . They enter the stop mass matrix as

$$\mathcal{M}_{\text{stop}}^2 = \begin{pmatrix} m_Q^2 + |X|^2 & \tilde{X}^* \\ \tilde{X} & m_U^2 + |X|^2 \end{pmatrix}, \quad (3.1.6)$$

where  $m_Q^2$  and  $m_U^2$  are the soft SUSY-breaking mass terms for the stops. While  $X = y_t H_u^0$  both in the (N)MSSM and in Dirac-gaugino models, the precise form of  $\tilde{X}$  depends on the model under consideration and will be discussed later. For the time being, we only assume that  $\tilde{X}$  is real at the minimum of the potential, to prevent CP-violating contributions to the Higgs mass matrices. The top/stop  $\mathcal{O}(\alpha_s)$  contribution to  $\Delta V$  can then be expressed in terms of five field-dependent parameters, which can be chosen as follows. The squared top and stop masses

$$m_t^2 = |X|^2, \quad m_{\tilde{t}_{1,2}}^2 = \frac{1}{2} \left[ (m_Q^2 + m_U^2 + 2|X|^2) \pm \sqrt{(m_Q^2 - m_U^2)^2 + 4|\tilde{X}|^2} \right], \quad (3.1.7)$$

a mixing angle  $\bar{\theta}_{\tilde{t}}$ , with  $0 \leq \bar{\theta}_{\tilde{t}} \leq \pi/2$ , which diagonalises the stop mass matrix after the stop fields have been redefined to make it real and symmetric

$$\sin 2\bar{\theta}_{\tilde{t}} = \frac{2|\tilde{X}|}{m_{\tilde{t}_1}^2 - m_{\tilde{t}_2}^2}, \quad (3.1.8)$$

and a combination of the phases of  $X$  and  $\tilde{X}$  that we can choose as

$$\cos(\varphi - \tilde{\varphi}) = \frac{\text{Re}(\tilde{X}) \text{Re}(X) + \text{Im}(\tilde{X}) \text{Im}(X)}{|\tilde{X}| |X|}. \quad (3.1.9)$$

Finally, the gluino masses  $m_{\tilde{g}_i}$  and the octet masses  $m_{O_i}^2$  do not depend on the Higgs background, since we neglect the singlet-octet couplings  $\lambda_{SO}$  and  $T_{SO}$ . In the following

we will also refer to  $\theta_t$ , with  $-\pi/2 < \theta_t < \pi/2$ , *i.e.* the usual field-independent mixing angle that diagonalises the stop mass matrix at the minimum of the scalar potential.

We find general expressions for the top/stop contributions to the minimum conditions of the effective potential and to the corrections to the scalar and pseudoscalar mass matrices:

$$\left. \frac{\partial \Delta V}{\partial S_i} \right|_{\min} = s_{2\theta_t} \frac{\partial \tilde{X}}{\partial S_i} F + \sqrt{2} y_t m_t \delta_{i2} G, \quad (3.1.10)$$

$$\begin{aligned} (\Delta \mathcal{M}_S^2)_{ij} = & \left( s_{2\theta_t} \frac{\partial^2 \tilde{X}}{\partial S_i \partial S_j} + \frac{2}{m_{\tilde{t}_1}^2 - m_{\tilde{t}_2}^2} \frac{\partial \tilde{X}}{\partial S_i} \frac{\partial \tilde{X}}{\partial S_j} - \frac{s_{2\theta_t}}{\sqrt{2}} \frac{\delta_{ij}}{v_i} \frac{\partial \tilde{X}}{\partial S_j} \right) F \\ & + 2 y_t^2 m_t^2 \delta_{i2} \delta_{j2} F_1 + \sqrt{2} m_t y_t s_{2\theta_t} \left( \delta_{i2} \frac{\partial \tilde{X}}{\partial S_j} + \delta_{j2} \frac{\partial \tilde{X}}{\partial S_i} \right) F_2 \\ & + s_{2\theta_t}^2 \frac{\partial \tilde{X}}{\partial S_i} \frac{\partial \tilde{X}}{\partial S_j} F_3, \end{aligned} \quad (3.1.11)$$

$$\begin{aligned} (\Delta \mathcal{M}_P^2)_{ij} = & \left( \frac{1}{m_{\tilde{t}_1}^2 - m_{\tilde{t}_2}^2} \frac{\partial^2 |\tilde{X}|^2}{\partial P_i \partial P_j} - \frac{s_{2\theta_t}}{\sqrt{2}} \frac{\delta_{ij}}{v_i} \frac{\partial \tilde{X}}{\partial S_j} \right) F \\ & + \left( \frac{\delta_{i2}}{v_2} \tilde{X} + \sqrt{2} i \frac{\partial \tilde{X}}{\partial P_i} \right) \left( \frac{\delta_{j2}}{v_2} \tilde{X} + \sqrt{2} i \frac{\partial \tilde{X}}{\partial P_j} \right) \tan \beta F_\varphi, \end{aligned} \quad (3.1.12)$$

where all quantities are understood as evaluated at the minimum of the potential, no summation is implied over repeated indices, the fields are ordered as  $(\Phi_1^0, \Phi_2^0, \dots) = (H_d^0, H_u^0, \dots)$ , and again the terms involving  $\delta_{ij}/v_i$  should be omitted if  $\Phi_i^0$  does not develop a VEV. The angle  $\beta$  is defined as in the MSSM by  $\tan \beta = v_2/v_1$ . Here and thereafter we also adopt the shortcuts  $c_\phi \equiv \cos \phi$  and  $s_\phi \equiv \sin \phi$  for a generic angle  $\phi$ . The functions  $F, G, F_1, F_2, F_3$  and  $F_\varphi$  entering eqs. (3.1.10)–(3.1.12) are combinations of the derivatives of  $\Delta V$ . Explicit expressions for most of those functions can be found *e.g.* in ref. [77], but we display all of them here for completeness:

$$F = \frac{\partial \Delta V}{\partial m_{\tilde{t}_1}^2} - \frac{\partial \Delta V}{\partial m_{\tilde{t}_2}^2} - \frac{4 c_{2\theta_t}^2}{m_{\tilde{t}_1}^2 - m_{\tilde{t}_2}^2} \frac{\partial \Delta V}{\partial c_{2\theta_t}^2}, \quad (3.1.13)$$

$$G = \frac{\partial \Delta V}{\partial m_t^2} + \frac{\partial \Delta V}{\partial m_{\tilde{t}_1}^2} + \frac{\partial \Delta V}{\partial m_{\tilde{t}_2}^2}, \quad (3.1.14)$$

$$F_1 = \frac{\partial^2 \Delta V}{(\partial m_{\tilde{t}_1}^2)^2} + \frac{\partial^2 \Delta V}{(\partial m_{\tilde{t}_2}^2)^2} + \frac{\partial^2 \Delta V}{(\partial m_{\tilde{t}_1}^2 \partial m_{\tilde{t}_2}^2)} + 2 \frac{\partial^2 \Delta V}{\partial m_{\tilde{t}_1}^2 \partial m_{\tilde{t}_2}^2} + 2 \frac{\partial^2 \Delta V}{\partial m_{\tilde{t}_1}^2 \partial m_{\tilde{t}_2}^2} + 2 \frac{\partial^2 \Delta V}{\partial m_{\tilde{t}_1}^2 \partial m_{\tilde{t}_2}^2}, \quad (3.1.15)$$

$$\begin{aligned} F_2 = & \frac{\partial^2 \Delta V}{(\partial m_{\tilde{t}_1}^2)^2} - \frac{\partial^2 \Delta V}{(\partial m_{\tilde{t}_2}^2)^2} + \frac{\partial^2 \Delta V}{\partial m_{\tilde{t}_1}^2 \partial m_{\tilde{t}_2}^2} - \frac{\partial^2 \Delta V}{\partial m_{\tilde{t}_1}^2 \partial m_{\tilde{t}_2}^2} \\ & - \frac{4 c_{2\theta_t}^2}{m_{\tilde{t}_1}^2 - m_{\tilde{t}_2}^2} \left( \frac{\partial^2 \Delta V}{\partial c_{2\theta_t}^2 \partial m_{\tilde{t}_1}^2} + \frac{\partial^2 \Delta V}{\partial c_{2\theta_t}^2 \partial m_{\tilde{t}_2}^2} + \frac{\partial^2 \Delta V}{\partial c_{2\theta_t}^2 \partial m_{\tilde{t}_2}^2} \right), \end{aligned} \quad (3.1.16)$$

$$\begin{aligned} F_3 = & \frac{\partial^2 \Delta V}{(\partial m_{\tilde{t}_1}^2)^2} + \frac{\partial^2 \Delta V}{(\partial m_{\tilde{t}_2}^2)^2} - 2 \frac{\partial^2 \Delta V}{\partial m_{\tilde{t}_1}^2 \partial m_{\tilde{t}_2}^2} - \frac{2}{m_{\tilde{t}_1}^2 - m_{\tilde{t}_2}^2} \left( \frac{\partial \Delta V}{\partial m_{\tilde{t}_1}^2} - \frac{\partial \Delta V}{\partial m_{\tilde{t}_2}^2} \right) \\ & + \frac{16 c_{2\theta_t}^2}{(m_{\tilde{t}_1}^2 - m_{\tilde{t}_2}^2)^2} \left( c_{2\theta_t}^2 \frac{\partial^2 \Delta V}{(\partial c_{2\theta_t}^2)^2} + 2 \frac{\partial \Delta V}{\partial c_{2\theta_t}^2} \right) \end{aligned}$$

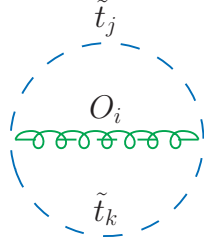


Figure 3.1 – Novel two-loop contribution to the effective potential involving stops and octet scalars.

$$-\frac{8c_{2\theta_t}^2}{m_{\tilde{t}_1}^2 - m_{\tilde{t}_2}^2} \left( \frac{\partial^2 \Delta V}{\partial c_{2\theta_t}^2 \partial m_{\tilde{t}_1}^2} - \frac{\partial^2 \Delta V}{\partial c_{2\theta_t}^2 \partial m_{\tilde{t}_2}^2} \right), \quad (3.1.17)$$

$$F_\varphi = -\frac{2z_t \cot \beta}{s_{2\theta_t}^2 (m_{\tilde{t}_1}^2 - m_{\tilde{t}_2}^2)^2} \frac{\partial \Delta V}{\partial c_{\varphi_t - \tilde{\varphi}_t}}, \quad (3.1.18)$$

where we defined  $z_t \equiv \text{sign}(\tilde{X}|_{\min})$ .

### 3.1.2 Two-loop top/stop contributions to the effective potential

For the computation of the two-loop  $\mathcal{O}(\alpha_t \alpha_s)$  corrections to the Higgs mass matrices in models with Dirac gauginos we need the explicit expression for the top/stop  $\mathcal{O}(\alpha_s)$  contribution to  $\Delta V$ , expressed in terms of the field-dependent parameters defined in the previous section. In addition to the contributions of diagrams involving gluons, gluinos or the D-term-induced quartic stop couplings, which are in common with the (N)MSSM and can be found in ref. [76],  $\Delta V$  receives a contribution from the diagram shown in figure 3.1, involving stops and octet scalars.

We assume that the gaugino masses are real so that the diagonalising matrix  $R_{ij}$  is real and  $R_{1i}^2$  is positive, but allow  $m_{\tilde{g}_i}$  to be negative. Since  $R_{11}^2 + R_{12}^2 = 1$ , we can simply write the top/stop  $\mathcal{O}(\alpha_s)$  contribution to the two-loop effective potential (in units of  $\alpha_s C_F N_c / (4\pi)^3$ , where  $C_F = 4/3$  and  $N_c = 3$  are colour factors) as

$$\Delta V^{\alpha_s} = \sum_{i=1}^2 R_{1i}^2 \Delta V_{\text{MSSM}}^{\alpha_s} + \Delta V_{\text{octet}}^{\alpha_s}, \quad (3.1.19)$$

where  $\Delta V_{\text{MSSM}}^{\alpha_s}$  is the analogous contribution in the (N)MSSM,

$$\begin{aligned} \Delta V_{\text{MSSM}}^{\alpha_s} = & 2J(m_t^2, m_t^2) - 4m_t^2 I(m_t^2, m_t^2, 0) \\ & + \left\{ 2m_{\tilde{t}_1}^2 I(m_{\tilde{t}_1}^2, m_{\tilde{t}_1}^2, 0) + 2L(m_{\tilde{t}_1}^2, m_{\tilde{g}_i}^2, m_t^2) \right. \\ & - 4m_t m_{\tilde{g}_i} s_{2\bar{\theta}} c_{\varphi - \tilde{\varphi}} I(m_{\tilde{t}_1}^2, m_{\tilde{g}_i}^2, m_t^2) + \frac{1}{2}(1 + c_{2\bar{\theta}}^2) J(m_{\tilde{t}_1}^2, m_{\tilde{t}_1}^2) \\ & \left. + \frac{s_{2\bar{\theta}}^2}{2} J(m_{\tilde{t}_1}^2, m_{\tilde{t}_2}^2) + [m_{\tilde{t}_1} \leftrightarrow m_{\tilde{t}_2}, s_{2\bar{\theta}} \rightarrow -s_{2\bar{\theta}}] \right\}, \end{aligned} \quad (3.1.20)$$

while  $\Delta V_{\text{octet}}^{\alpha_s}$  is the additional  $\mathcal{O}(\alpha_s)$  contribution of the two-loop diagram shown in figure 3.1, involving stops and octet scalars. The latter can be decomposed as

$$\Delta V_{\text{octet}}^{\alpha_s} \equiv m_D^2 (c_{\phi O}^2 \Delta V_{O_1} + s_{\phi O}^2 \Delta V_{O_2}), \quad (3.1.21)$$

with

$$\Delta V_{O_i} = -2c_{2\theta_t}^2 \left[ I(m_{t_1}^2, m_{t_1}^2, m_{O_i}^2) + I(m_{t_2}^2, m_{t_2}^2, m_{O_i}^2) \right] - 4s_{2\theta_t}^2 I(m_{t_1}^2, m_{t_2}^2, m_{O_i}^2) . \quad (3.1.22)$$

The two-loop integrals  $J(x, y)$ ,  $I(x, y, z)$  and  $L(x, y, z)$  entering eqs. (3.1.20) and (3.1.22) are defined, *e.g.*, in eqs. (D1)–(D3) of ref. [77], and were first introduced in ref. [16]. Explicit expressions for the derivatives of  $\Delta V^{\alpha_s}$ , valid for all Dirac-gaugino models considered in this chapter, are provided in appendix A.

We remark that, by using the “minimally subtracted” two-loop integrals of ref. [16], we are implicitly assuming a  $\overline{\text{DR}}'$  renormalisation for the parameters entering the tree-level and one-loop parts of the effective potential. Consequently, our results for the two-loop top/stop contributions to mass matrices and minimum conditions also assume that the corresponding tree-level and one-loop parts are expressed in terms of  $\overline{\text{DR}}'$ -renormalised parameters. We will describe in section 3.1.5 how our two-loop formulae should be modified if the top/stop parameters entering the one-loop part of the corrections are expressed in a different renormalisation scheme. For what concerns the parameters entering the tree-level mass matrices for scalars and pseudoscalars – whose specific form depends on the Dirac-gaugino model under consideration – they can be taken directly as  $\overline{\text{DR}}'$ -renormalised inputs at some reference scale  $Q$ , at least in the absence of any experimental information on an extended Higgs sector. Exceptions are given by the electroweak gauge couplings and by the combination of doublet VEVs  $v \equiv (v_1^2 + v_2^2)^{1/2}$ , which in general should be extracted from experimentally known observables such as, *e.g.*, the muon decay constant and the gauge-boson masses. As was pointed out for the NMSSM in ref. [240], the extraction of the  $\overline{\text{DR}}'$  parameter  $v(Q)$  involves two-loop corrections whose effects on the scalar and pseudoscalar mass matrices are formally of the same order as some of the  $\mathcal{O}(\alpha_t \alpha_s)$  corrections computed here.<sup>1</sup> However, a two-loop determination of  $v(Q)$  goes beyond the scope of our calculation, as it requires two-loop contributions to the gauge-boson self-energies which cannot be obtained with effective-potential methods. Besides, ref. [240] showed that, at least in the NMSSM scenarios considered in that paper, the  $\mathcal{O}(\alpha_t \alpha_s)$  effects on the scalar masses arising from the two-loop corrections to  $v$  are quite small, typically of the order of a hundred MeV.

### 3.1.3 Mass corrections in the MDGSSM

The MDGSSM contains a singlet  $S$  and an  $SU(2)$  triplet  $T^a$  which mix with the usual Higgs fields  $H_d$  and  $H_u$ . In this model, the stop mixing term  $\tilde{X}$  defined in eq. (3.1.6) reads

$$\tilde{X} = y_t \left( A_t H_u^0 - \mu H_d^{0*} - \lambda_S S^* H_d^{0*} - \lambda_T T^{0*} H_d^{0*} \right) , \quad (3.1.23)$$

where  $A_t$  is the soft SUSY-breaking trilinear interaction term for Higgs and stops. We order the neutral components of the fields as  $\Phi_i^0 = (H_d^0, H_u^0, S, T^0)$  and expand them as in eq. (3.1.1). For the minimum conditions of the effective potential, eq. (3.1.10) gives

$$\left. \frac{\partial \Delta V}{\partial S_1} \right|_{\min} = -y_t \frac{\tilde{\mu}}{\sqrt{2}} s_{2\theta_t} F , \quad (3.1.24)$$

---

<sup>1</sup>These additional  $\mathcal{O}(\alpha_t \alpha_s)$  effects arise from terms in the tree-level mass matrices in which  $v$  appears in combination with the singlet or triplet superpotential couplings. In contrast, in the MSSM all occurrences of  $v$  in the tree-level mass matrices are multiplied by the electroweak gauge couplings, thus they are not relevant in the gaugeless limit.

$$\left. \frac{\partial \Delta V}{\partial S_2} \right|_{\min} = \sqrt{2} y_t m_t G + y_t \frac{A_t}{\sqrt{2}} s_{2\theta_t} F, \quad (3.1.25)$$

$$\left. \frac{\partial \Delta V}{\partial S_3} \right|_{\min} = -y_t \frac{\lambda_S v_1}{\sqrt{2}} s_{2\theta_t} F, \quad (3.1.26)$$

$$\left. \frac{\partial \Delta V}{\partial S_4} \right|_{\min} = -y_t \frac{\lambda_T v_1}{\sqrt{2}} s_{2\theta_t} F, \quad (3.1.27)$$

where we defined  $\tilde{\mu} \equiv \mu + \lambda_S v_3 + \lambda_T v_4$ . For the corrections to the mass matrices of scalars and pseudoscalars, eqs. (3.1.11) and (3.1.12) give

$$\left( \Delta \mathcal{M}_S^2 \right)_{11} = \frac{1}{2} y_t^2 \tilde{\mu}^2 s_{2\theta_t}^2 F_3 + \frac{y_t^2 A_t \tilde{\mu} \tan \beta}{m_{\tilde{t}_1}^2 - m_{\tilde{t}_2}^2} F, \quad (3.1.28)$$

$$\left( \Delta \mathcal{M}_S^2 \right)_{12} = -y_t^2 m_t \tilde{\mu} s_{2\theta_t} F_2 - \frac{1}{2} y_t^2 A_t \tilde{\mu} s_{2\theta_t}^2 F_3 - \frac{y_t^2 A_t \tilde{\mu}}{m_{\tilde{t}_1}^2 - m_{\tilde{t}_2}^2} F, \quad (3.1.29)$$

$$\left( \Delta \mathcal{M}_S^2 \right)_{22} = 2 y_t^2 m_t^2 F_1 + 2 y_t^2 m_t A_t s_{2\theta_t} F_2 + \frac{1}{2} y_t^2 A_t^2 s_{2\theta_t}^2 F_3 + \frac{y_t^2 A_t \tilde{\mu} \cot \beta}{m_{\tilde{t}_1}^2 - m_{\tilde{t}_2}^2} F, \quad (3.1.30)$$

$$\left( \Delta \mathcal{M}_S^2 \right)_{13} = \frac{1}{2} y_t \lambda_S m_t \tilde{\mu} \cot \beta s_{2\theta_t}^2 F_3 - \frac{y_t \lambda_S m_t (A_t - 2 \tilde{\mu} \cot \beta)}{m_{\tilde{t}_1}^2 - m_{\tilde{t}_2}^2} F, \quad (3.1.31)$$

$$\begin{aligned} \left( \Delta \mathcal{M}_S^2 \right)_{23} = & -y_t \lambda_S m_t^2 \cot \beta s_{2\theta_t} F_2 - \frac{1}{2} y_t \lambda_S A_t m_t \cot \beta s_{2\theta_t}^2 F_3 \\ & - \frac{y_t \lambda_S m_t A_t \cot \beta}{m_{\tilde{t}_1}^2 - m_{\tilde{t}_2}^2} F, \end{aligned} \quad (3.1.32)$$

$$\left( \Delta \mathcal{M}_S^2 \right)_{33} = \frac{1}{2} \lambda_S^2 m_t^2 \cot^2 \beta s_{2\theta_t}^2 F_3 + \frac{\lambda_S m_t^2 \cot \beta (A_t + (\lambda_S v_3 - \tilde{\mu}) \cot \beta)}{v_3 (m_{\tilde{t}_1}^2 - m_{\tilde{t}_2}^2)} F, \quad (3.1.33)$$

$$\left( \Delta \mathcal{M}_S^2 \right)_{14} = \frac{1}{2} y_t \lambda_T m_t \tilde{\mu} \cot \beta s_{2\theta_t}^2 F_3 - \frac{y_t \lambda_T m_t (A_t - 2 \tilde{\mu} \cot \beta)}{m_{\tilde{t}_1}^2 - m_{\tilde{t}_2}^2} F, \quad (3.1.34)$$

$$\begin{aligned} \left( \Delta \mathcal{M}_S^2 \right)_{24} = & -y_t \lambda_T m_t^2 \cot \beta s_{2\theta_t} F_2 - \frac{1}{2} y_t \lambda_T A_t m_t \cot \beta s_{2\theta_t}^2 F_3 \\ & - \frac{y_t \lambda_T m_t A_t \cot \beta}{m_{\tilde{t}_1}^2 - m_{\tilde{t}_2}^2} F, \end{aligned} \quad (3.1.35)$$

$$\left( \Delta \mathcal{M}_S^2 \right)_{34} = \frac{1}{2} \lambda_S \lambda_T m_t^2 \cot^2 \beta s_{2\theta_t}^2 F_3 + \frac{\lambda_S \lambda_T m_t^2 \cot^2 \beta}{m_{\tilde{t}_1}^2 - m_{\tilde{t}_2}^2} F, \quad (3.1.36)$$

$$\left( \Delta \mathcal{M}_S^2 \right)_{44} = \frac{1}{2} \lambda_T^2 m_t^2 \cot^2 \beta s_{2\theta_t}^2 F_3 + \frac{\lambda_T m_t^2 \cot \beta (A_t + (\lambda_T v_4 - \tilde{\mu}) \cot \beta)}{v_4 (m_{\tilde{t}_1}^2 - m_{\tilde{t}_2}^2)} F, \quad (3.1.37)$$

$$\left( \Delta \mathcal{M}_P^2 \right)_{11} = \frac{y_t^2 A_t \tilde{\mu} \tan \beta}{m_{\tilde{t}_1}^2 - m_{\tilde{t}_2}^2} F + y_t^2 \tilde{\mu}^2 \tan \beta F_\varphi, \quad (3.1.38)$$

$$\left( \Delta \mathcal{M}_P^2 \right)_{12} = \frac{y_t^2 A_t \tilde{\mu}}{m_{\tilde{t}_1}^2 - m_{\tilde{t}_2}^2} F + y_t^2 \tilde{\mu}^2 F_\varphi, \quad (3.1.39)$$

$$\left(\Delta\mathcal{M}_P^2\right)_{22} = \frac{y_t^2 A_t \tilde{\mu} \cot \beta}{m_{\tilde{t}_1}^2 - m_{\tilde{t}_2}^2} F + y_t^2 \tilde{\mu}^2 \cot \beta F_\varphi, \quad (3.1.40)$$

$$\left(\Delta\mathcal{M}_P^2\right)_{13} = \frac{y_t \lambda_S m_t A_t}{m_{\tilde{t}_1}^2 - m_{\tilde{t}_2}^2} F + y_t \lambda_S m_t \tilde{\mu} F_\varphi, \quad (3.1.41)$$

$$\left(\Delta\mathcal{M}_P^2\right)_{23} = \frac{y_t \lambda_S m_t A_t \cot \beta}{m_{\tilde{t}_1}^2 - m_{\tilde{t}_2}^2} F + y_t \lambda_S m_t \tilde{\mu} \cot \beta F_\varphi, \quad (3.1.42)$$

$$\left(\Delta\mathcal{M}_P^2\right)_{33} = \frac{\lambda_S m_t^2 \cot \beta \left(A_t + (\lambda_S v_3 - \tilde{\mu}) \cot \beta\right)}{v_3 (m_{\tilde{t}_1}^2 - m_{\tilde{t}_2}^2)} F + \lambda_S^2 m_t^2 \cot \beta F_\varphi, \quad (3.1.43)$$

$$\left(\Delta\mathcal{M}_P^2\right)_{14} = \frac{y_t \lambda_T m_t A_t}{m_{\tilde{t}_1}^2 - m_{\tilde{t}_2}^2} F + y_t \lambda_T m_t \tilde{\mu} F_\varphi, \quad (3.1.44)$$

$$\left(\Delta\mathcal{M}_P^2\right)_{24} = \frac{y_t \lambda_T m_t A_t \cot \beta}{m_{\tilde{t}_1}^2 - m_{\tilde{t}_2}^2} F + y_t \lambda_T m_t \tilde{\mu} \cot \beta F_\varphi, \quad (3.1.45)$$

$$\left(\Delta\mathcal{M}_P^2\right)_{34} = \frac{\lambda_S \lambda_T m_t^2 \cot^2 \beta}{m_{\tilde{t}_1}^2 - m_{\tilde{t}_2}^2} F + \lambda_S \lambda_T m_t^2 \cot \beta F_\varphi, \quad (3.1.46)$$

$$\left(\Delta\mathcal{M}_P^2\right)_{44} = \frac{\lambda_T m_t^2 \cot \beta \left(A_t + (\lambda_T v_4 - \tilde{\mu}) \cot \beta\right)}{v_4 (m_{\tilde{t}_1}^2 - m_{\tilde{t}_2}^2)} F + \lambda_T^2 m_t^2 \cot \beta F_\varphi. \quad (3.1.47)$$

### 3.1.4 Mass corrections in the MRSSM

The MRSSM is defined to be  $R$ -symmetric, and has fields  $R_u, R_d$  which pair with the Higgs fields without themselves developing VEVs. In this model the gluino mass terms are purely Dirac, therefore, in our conventions,  $R_{11}^2 = R_{12}^2 = 1/2$  and  $m_{\tilde{g}_1} = -m_{\tilde{g}_2} = m_D$ . The trilinear Higgs-stop coupling  $A_t$  is forbidden, and the term  $\tilde{X}$  defined in eq. (3.1.6) reads

$$\tilde{X} = -y_t \left( \mu_u + \lambda_{S_u} S^* + \lambda_{T_u} T^{0*} \right) R_u^{0*}, \quad (3.1.48)$$

and vanishes at the minimum of the scalar potential, hence the stops do not mix. Moreover, the term proportional to  $c_{\varphi-\tilde{\varphi}}$  in the second line of eq. (3.1.20) cancels out in the sum over the gluino masses. As a consequence, the radiative corrections induced by top/stop loops are remarkably simple. Ordering the neutral components of the fields as  $\Phi_i^0 = (H_d^0, H_u^0, S, T^0, R_d^0, R_u^0)$ , we find that the only non-vanishing contributions to the minimum conditions of the potential and to the Higgs mass matrices are

$$\left. \frac{\partial \Delta V}{\partial S_2} \right|_{\min} = \sqrt{2} y_t m_t G, \quad (3.1.49)$$

$$\left(\Delta\mathcal{M}_S^2\right)_{22} = 2 y_t^2 m_t^2 F_1, \quad (3.1.50)$$

$$\left(\Delta\mathcal{M}_S^2\right)_{66} = \left(\Delta\mathcal{M}_P^2\right)_{66} = \frac{y_t^2 \tilde{\mu}_u^2}{m_{\tilde{t}_1}^2 - m_{\tilde{t}_2}^2} F, \quad (3.1.51)$$

where we defined  $\tilde{\mu}_u \equiv \mu_u + \lambda_{S_u} v_3 + \lambda_{T_u} v_4$ .



### 3.1.5 On-shell parameters in the top/stop sector

The results presented so far for the two-loop corrections to the neutral Higgs masses in models with Dirac gauginos were obtained under the assumption that the parameters entering the tree-level and one-loop parts of the mass matrices are renormalised in the  $\overline{\text{DR}}'$  scheme. While this choice allows for a straightforward implementation of our results in automated calculations such as the one of **SARAH**, it is well known that, in the  $\overline{\text{DR}}'$  scheme, the Higgs-mass calculation can be plagued by unphysically large contributions if there is a hierarchy between the masses of the particles running in the loops [76]. In particular, the contributions of two-loop diagrams involving stops and gluinos include terms proportional to  $m_{\tilde{g}_i}^2/m_{\tilde{t}_j}^2$ , which can become very large in scenarios with gluinos much heavier than the stops. Since this kind of hierarchy can occur naturally (*i.e.*, without excessive fine tuning in the squark masses) in scenarios with Dirac gluino masses [89], it is useful to re-express the one-loop part of the corrections to the Higgs masses in terms of OS-renormalised top/stop parameters. In that case, the terms proportional to  $m_{\tilde{g}_i}^2$  in the two-loop part of the corrections cancel out against analogous contributions induced by the OS counterterms, leaving only a milder logarithmic dependence of the Higgs masses on the gluino masses.

Since we are focusing on the  $\mathcal{O}(\alpha_t \alpha_s)$  corrections to the Higgs masses, we need to provide an OS prescription only for parameters in the top/stop sector that are subject to  $\mathcal{O}(\alpha_s)$  corrections, *i.e.*  $m_t$ ,  $m_{\tilde{t}_1}^2$ ,  $m_{\tilde{t}_2}^2$  and  $\theta_t$ . In models that allow for a trilinear Higgs-stop coupling  $A_t$  – such as the MDGSSM, see eq. (3.1.23) – its counterterm can be derived from those of the other four parameters via the relation  $(m_{\tilde{t}_1}^2 - m_{\tilde{t}_2}^2) \sin 2\theta_t = 2 \tilde{X}|_{\min}$  (in general, the stop mixing  $\tilde{X}|_{\min}$  contains other terms in addition to  $m_t A_t$ , but they are exempt from  $\mathcal{O}(\alpha_s)$  corrections). Finally, since the VEVs  $v_i$  are not renormalised at  $\mathcal{O}(\alpha_s)$ , the top Yukawa coupling  $y_t$  receives the same relative correction as the top mass. Defining  $x_k^{\overline{\text{DR}}} = x_k^{\text{OS}} + \delta x_k$  for each parameter  $x_k \equiv (m_t, m_{\tilde{t}_1}^2, m_{\tilde{t}_2}^2, \theta_t, A_t)$ , the  $\overline{\text{DR}}'$ –OS shifts of top and stop masses and mixing are given in terms of the finite parts (here denoted by a hat) of the top and stop self-energies

$$\delta m_t = \hat{\Sigma}_t(m_t), \quad \delta m_{\tilde{t}_i}^2 = \hat{\Pi}_{ii}(m_{\tilde{t}_i}^2) \quad (i = 1, 2), \quad \delta \theta_t = \frac{1}{2} \frac{\hat{\Pi}_{12}(m_{\tilde{t}_1}^2) + \hat{\Pi}_{12}(m_{\tilde{t}_2}^2)}{m_{\tilde{t}_1}^2 - m_{\tilde{t}_2}^2}, \quad (3.1.52)$$

and the shift for the trilinear coupling reads

$$\delta A_t = \left( \frac{\delta m_{\tilde{t}_1}^2 - \delta m_{\tilde{t}_2}^2}{m_{\tilde{t}_1}^2 - m_{\tilde{t}_2}^2} - \frac{\delta m_t}{m_t} + 2 \cot 2\theta_t \delta \theta_t \right) \tilde{X}|_{\min}. \quad (3.1.53)$$

As in the case of the two-loop effective potential in eq. (3.1.19), the  $\overline{\text{DR}}'$ –OS shifts  $\delta x_k$  can be cast as

$$\delta x_k = \sum_{i=1}^2 R_{1i}^2 (\delta x_k^{\text{MSSM}})_i + \delta x_k^{\text{octet}}, \quad (3.1.54)$$

where  $(\delta x_k^{\text{MSSM}})_i$  are obtained, with the trivial replacement  $m_{\tilde{g}} \rightarrow m_{\tilde{g}_i}$ , from the MSSM shifts given in appendix B of ref. [76], whereas  $\delta x_k^{\text{octet}}$  are novel contributions involving the octet scalar. In particular,  $\delta m_t^{\text{octet}} = 0$ , and the remaining shifts can be obtained by combining as in eqs. (3.1.52) and (3.1.53) the octet contributions to the finite parts of the stop self-energies:

$$\hat{\Pi}_{11}(m_{\tilde{t}_1}^2)^{\text{octet}} = \frac{g_s^2 m_D^2}{4\pi^2} C_F c_{\phi_O}^2 \left[ c_{2\theta_t}^2 \hat{B}_0(m_{\tilde{t}_1}^2, m_{\tilde{t}_1}^2, m_{O_1}^2) + s_{2\theta_t}^2 \hat{B}_0(m_{\tilde{t}_1}^2, m_{\tilde{t}_2}^2, m_{O_1}^2) \right]$$

$$+ (c_{\phi_O} \rightarrow s_{\phi_O}, m_{O_1} \rightarrow m_{O_2}), \quad (3.1.55)$$

$$\begin{aligned} \hat{\Pi}_{22}(m_{\tilde{t}_2}^2)^{\text{octet}} &= \frac{g_s^2 m_D^2}{4\pi^2} C_F c_{\phi_O}^2 \left[ c_{2\theta_t}^2 \hat{B}_0(m_{\tilde{t}_2}^2, m_{\tilde{t}_2}^2, m_{O_1}^2) + s_{2\theta_t}^2 \hat{B}_0(m_{\tilde{t}_2}^2, m_{\tilde{t}_1}^2, m_{O_1}^2) \right] \\ &+ (c_{\phi_O} \rightarrow s_{\phi_O}, m_{O_1} \rightarrow m_{O_2}), \end{aligned} \quad (3.1.56)$$

$$\begin{aligned} \hat{\Pi}_{12}(p^2)^{\text{octet}} &= -\frac{g_s^2 m_D^2}{4\pi^2} C_F c_{\phi_O}^2 c_{2\theta_t} s_{2\theta_t} \left[ \hat{B}_0(p^2, m_{\tilde{t}_1}^2, m_{O_1}^2) - \hat{B}_0(p^2, m_{\tilde{t}_2}^2, m_{O_1}^2) \right] \\ &+ (c_{\phi_O} \rightarrow s_{\phi_O}, m_{O_1} \rightarrow m_{O_2}), \end{aligned} \quad (3.1.57)$$

where  $\hat{B}_0(p^2, m_1^2, m_2^2)$  is the finite part of the Passarino-Veltman function.

The change in renormalisation scheme for the top/stop parameters entering the one-loop (1 $\ell$ ) part of the corrections to the Higgs mass matrices induces a shift in the two-loop (2 $\ell$ ) part of the corrections:

$$\delta(\Delta\mathcal{M}_{S,P}^2)_{ij}^{2\ell} = \sum_k \delta x_k \frac{\partial}{\partial x_k} (\Delta\mathcal{M}_{S,P}^2)_{ij}^{1\ell}. \quad (3.1.58)$$

Analogous expressions hold for the shifts in the two-loop part of the minimum conditions of the effective potential. The one-loop corrections entering the equation above can be obtained by inserting in eqs. (3.1.10)–(3.1.12) the one-loop expressions for the functions  $F$ ,  $G$ ,  $F_{1,2,3}$  and  $F_\varphi$ . In units of  $N_c/(16\pi^2)$ , these read:

$$\begin{aligned} F^{1\ell} &= m_{\tilde{t}_1}^2 \left( \ln \frac{m_{\tilde{t}_1}^2}{Q^2} - 1 \right) - m_{\tilde{t}_2}^2 \left( \ln \frac{m_{\tilde{t}_2}^2}{Q^2} - 1 \right), \\ G^{1\ell} &= m_{\tilde{t}_1}^2 \left( \ln \frac{m_{\tilde{t}_1}^2}{Q^2} - 1 \right) + m_{\tilde{t}_2}^2 \left( \ln \frac{m_{\tilde{t}_2}^2}{Q^2} - 1 \right) - 2m_t^2 \left( \ln \frac{m_t^2}{Q^2} - 1 \right), \\ F_1^{1\ell} &= \ln \frac{m_{\tilde{t}_1}^2 m_{\tilde{t}_2}^2}{m_t^4}, \quad F_2^{1\ell} = \ln \frac{m_{\tilde{t}_1}^2}{m_{\tilde{t}_2}^2}, \quad F_3^{1\ell} = \left( 2 - \frac{m_{\tilde{t}_1}^2 + m_{\tilde{t}_2}^2}{m_{\tilde{t}_1}^2 - m_{\tilde{t}_2}^2} \ln \frac{m_{\tilde{t}_1}^2}{m_{\tilde{t}_2}^2} \right), \quad F_\varphi^{1\ell} = 0, \end{aligned} \quad (3.1.59)$$

where  $Q$  is the renormalisation scale at which the parameters entering the tree-level and one-loop parts of the mass matrices are expressed. As mentioned above, the  $\overline{\text{DR}}'$ –OS shifts derived in eq. (3.1.58) cancel the power-like dependence of the two-loop corrections on the gluino masses.

### 3.1.6 Obtaining the $\mathcal{O}(\alpha_b \alpha_s)$ corrections

Our  $\overline{\text{DR}}'$  computation of the  $\mathcal{O}(\alpha_t \alpha_s)$  corrections allows us to obtain also the two-loop  $\mathcal{O}(\alpha_b \alpha_s)$  corrections induced by the bottom/sbottom sector, which can be relevant for large values of  $\tan \beta$ . To this purpose, the substitutions  $t \rightarrow b$ ,  $u \rightarrow d$ ,  $\partial \Delta V / \partial S_1 \leftrightarrow \partial \Delta V / \partial S_2$ ,  $(\Delta\mathcal{M}_{S,P}^2)_{11} \leftrightarrow (\Delta\mathcal{M}_{S,P}^2)_{22}$ ,  $(\Delta\mathcal{M}_{S,P}^2)_{1k} \leftrightarrow (\Delta\mathcal{M}_{S,P}^2)_{2k}$  (with  $k > 2$ ) and  $\tan \beta \leftrightarrow \cot \beta$  must be performed in the formulae of sections 3.1.3 and 3.1.4. In the case of the bottom/sbottom corrections, however, passing from the  $\overline{\text{DR}}'$  scheme to the OS scheme would involve additional complications, as explained in ref. [172].

### 3.1.7 Simplified formulae

Having computed the general expressions for the two-loop corrections to the neutral Higgs masses in models with Dirac gauginos, it is now interesting to provide some approximate results for the dominant corrections to the mass of a SM-like Higgs. We focus on the case of a purely-Dirac mass term for the gluinos, which – as mentioned earlier – implies that we can set  $R_{11}^2 = R_{12}^2 = 1/2$  and  $m_{\tilde{g}_1} = -m_{\tilde{g}_2} = m_{\tilde{g}}$ , with  $m_{\tilde{g}} \equiv m_D$ . We also restrict ourselves to the decoupling limit in which all neutral states except a combination of  $H_d^0$  and  $H_u^0$  are heavy, so that

$$H_d^0 \approx \left(v + \frac{h}{\sqrt{2}}\right) \cos \beta + \dots, \quad H_u^0 \approx \left(v + \frac{h}{\sqrt{2}}\right) \sin \beta + \dots, \quad (3.1.60)$$

where  $v \approx 174$  GeV, and all other fields have negligible mixing with the lightest scalar  $h$ , which is SM-like. We can then approximate the correction to the squared mass  $m_h^2$  as

$$\Delta m_h^2 \approx \cos^2 \beta (\Delta \mathcal{M}_S^2)_{11} + \sin^2 \beta (\Delta \mathcal{M}_S^2)_{22} + \sin 2\beta (\Delta \mathcal{M}_S^2)_{12}. \quad (3.1.61)$$

Finally, we assume that the superpotential couplings of the adjoint fields (*e.g.*, the couplings  $\lambda_S$  and  $\lambda_T$  in the MDGSSM) are subdominant with respect to the top Yukawa coupling, so that we can focus on the two-loop corrections proportional to  $\alpha_s m_t^4/v^2$ .

With these restrictions, we shall give useful formulae valid for a phenomenologically interesting subspace of *all* extant Dirac gaugino models; while in the following we refer to simplified MDGSSM and MRSSM scenarios, this merely reflects whether stop mixing is allowed.

#### 3.1.7.1 Common SUSY-breaking scale

We first consider a simplified MDGSSM scenario in which the soft SUSY-breaking masses for the two stops and the Dirac mass of the gluinos are large and degenerate, *i.e.*  $m_Q = m_U = m_{\tilde{g}} = M_S$  with  $M_S \gg m_t$ . Expanding our result<sup>2</sup> for the top/stop contributions to  $\Delta m_h^2$  at the leading order in  $m_t/M_S$ , we can decompose it as

$$\Delta m_h^2 \approx \frac{3m_t^4}{4\pi^2 v^2} \left[ \ln \frac{M_S^2}{m_t^2} + \hat{X}_t^2 - \frac{\hat{X}_t^4}{12} \right] + (\Delta m_h^2)_{2\ell}^{\text{“MSSM”}} + c_{\phi O}^2 (\Delta m_h^2)_{2\ell}^{O_1} + s_{\phi O}^2 (\Delta m_h^2)_{2\ell}^{O_2}, \quad (3.1.62)$$

where  $\hat{X}_t \equiv X_t/M_S$ , in which  $X_t = A_t - \tilde{\mu} \cot \beta$  is the left-right mixing term in the stop mass matrix with  $\tilde{\mu}$  defined as in section 3.1.3. The first term in  $\Delta m_h^2$  is the dominant 1-loop contribution from diagrams with top quarks or stop squarks, which is the same as in the MSSM. The second term is the  $\mathcal{O}(\alpha_t \alpha_s)$  contribution from two-loop, MSSM-like diagrams involving gluons, gluinos or a four-stop interaction. Under the assumption that the parameters  $m_t$ ,  $M_S$  and  $A_t$  entering the one-loop part of the correction are renormalised in the  $\overline{\text{DR}}'$  scheme at the scale  $Q$ , it reads

$$(\Delta m_h^2)_{2\ell}^{\text{“MSSM”}} = \frac{\alpha_s m_t^4}{2\pi^3 v^2} \left\{ \ln^2 \frac{M_S^2}{m_t^2} - 2 \ln^2 \frac{M_S^2}{Q^2} + 2 \ln^2 \frac{m_t^2}{Q^2} + \ln \frac{M_S^2}{m_t^2} - 1 \right\}$$

<sup>2</sup>We have verified that, for  $M_S = 1$  TeV and for  $|\hat{X}_t|$  up to the “maximal mixing” value of  $\sqrt{6}$ , the predictions for  $m_h$  obtained with the simplified formulae of this section agree at the per-mil level with the unexpanded result. For larger  $M_S$  the accuracy of our approximation improves, and for  $|\hat{X}_t| > \sqrt{6}$  it degrades.

$$+ \hat{X}_t^2 \left[ 1 - 2 \ln \frac{M_S^2}{Q^2} \right] - \frac{\hat{X}_t^4}{12} \Big\}. \quad (3.1.63)$$

We remark that this correction differs from the usual one in the MSSM, see *e.g.* eq. (21) of ref. [169], due to the absence of terms involving odd powers of  $\hat{X}_t$ . Indeed, those terms are actually proportional to the gluino masses, and in the considered scenario they cancel out of the sum over the gluino mass eigenstates, because  $m_{\tilde{g}_1} = -m_{\tilde{g}_2}$ . If the parameters  $m_t$ ,  $M_S$  and  $A_t$  are renormalised in the OS scheme as described in section 3.1.5, the correction reads instead

$$(\Delta m_h^2)_{2\ell}^{\text{“MSSM”}} = -\frac{3\alpha_s m_t^4}{2\pi^3 v^2} \left\{ \ln^2 \frac{M_S^2}{m_t^2} + \left[ 2 + \hat{X}_t^2 \right] \ln \frac{M_S^2}{m_t^2} + \frac{\hat{X}_t^4}{4} \right\}. \quad (3.1.64)$$

Note that the explicit dependence on the renormalisation scale  $Q$  drops out. Again, this correction differs from the usual one in the MSSM, see *e.g.* the first line in eq. (20) of ref. [170], due to the absence of a term linear in  $\hat{X}_t$ .

Finally, the last two terms on the right-hand side of eq. (3.1.62) represent the  $\mathcal{O}(\alpha_t \alpha_s)$  contributions of two-loop diagrams with stops and octet scalars, which are specific to models with Dirac gluinos. In the  $\overline{\text{DR}}'$  scheme they read

$$(\Delta m_h^2)_{2\ell}^{O_i} = -\frac{\alpha_s m_t^4}{\pi^3 v^2} \left\{ 1 - \ln \frac{M_S^2}{Q^2} + f(x_i) - \hat{X}_t^2 \left[ 1 - \ln \frac{m_{O_i}^2}{Q^2} + 2x_i f(x_i) \right] + \frac{\hat{X}_t^4}{6} \left[ 1 + 3x_i(1 + \ln x_i) - \ln \frac{m_{O_i}^2}{Q^2} + 6x_i^2 f(x_i) \right] \right\}, \quad (3.1.65)$$

where  $x_i \equiv M_S^2/m_{O_i}^2$ , and the function  $f(x)$  is defined as

$$f(x) = \frac{1}{1-4x} \left[ \ln x + x \phi\left(\frac{1}{4x}\right) \right], \quad (3.1.66)$$

$\phi(z)$  being the function defined in eq. (45) of ref. [171]. Special limits of the function in eq. (3.1.66) above are  $f(1/4) = -2(1 + \ln 4)/3$  and  $f(1) \approx -0.781302$ . In the OS scheme the octet-scalar contributions receive – at the leading order in  $m_t/M_S$  – the shift

$$\delta(\Delta m_h^2)_{2\ell}^{O_i} = \frac{\alpha_s m_t^4}{\pi^3 v^2} \left\{ \mathcal{B}_i - \left( \hat{X}_t^2 - \frac{\hat{X}_t^4}{6} \right) \left[ 3\mathcal{B}_i + 2 \ln \frac{m_{O_i}^2}{Q^2} - 2 \right] \right\}, \quad (3.1.67)$$

where  $\mathcal{B}_i \equiv \hat{B}_0(M_S^2, M_S^2, m_{O_i}^2) = -\ln(m_{O_i}^2/Q^2) + g(M_S^2/m_{O_i}^2)$ , with the function  $g(x)$  defined as

$$g(x) = \begin{cases} 2 - \left(1 - \frac{1}{2x}\right) \ln x - \frac{1}{x} \sqrt{4x-1} \arctan \sqrt{4x-1} & (x > 1/4) \\ 2 - \left(1 - \frac{1}{2x}\right) \ln x + \frac{1}{x} \sqrt{1-4x} \operatorname{arctanh} \sqrt{1-4x} & (x < 1/4) \end{cases}. \quad (3.1.68)$$

Again, it can be easily checked that the explicit dependence on  $Q$  cancels out in the sum of eqs. (3.1.65) and (3.1.67).

### 3.1.7.2 MRSSM with heavy Dirac gluino

The second simplified scenario we consider is the  $R$ -symmetric model of section 3.1.4, in the limit of heavy Dirac gluino, *i.e.*  $m_{\tilde{g}} \gg m_{\tilde{t}_i}$ . This is a phenomenologically interesting limit because Dirac gaugino masses are “supersoft”, *i.e.* they can be substantially larger than the squark masses without spoiling the naturalness of the model [89].

In the MRSSM the left and right stops do not mix, hence we set  $\theta_t = 0$  in our formulae, but we allow for the possibility of different stop masses  $m_{\tilde{t}_1}$  and  $m_{\tilde{t}_2}$ . In the decoupling limit of the Higgs sector, where we neglect the mixing with the heavy neutral states, the correction to the SM-like Higgs mass reduces to  $\Delta m_h^2 \approx \sin^2 \beta (\Delta \mathcal{M}_S^2)_{22}$ . In analogy to eq. (3.1.62), the correction can in turn be decomposed in a dominant one-loop part, a two-loop, MSSM-like  $\mathcal{O}(\alpha_t \alpha_s)$  contribution and two-loop octet-scalar contributions:

$$\Delta m_h^2 \approx \frac{3 m_t^4}{8 \pi^2 v^2} \ln \frac{m_{\tilde{t}_1}^2 m_{\tilde{t}_2}^2}{m_t^4} + (\Delta m_h^2)_{2\ell}^{\text{“MSSM”}} + c_{\phi_O}^2 (\Delta m_h^2)_{2\ell}^{O_1} + s_{\phi_O}^2 (\Delta m_h^2)_{2\ell}^{O_2}. \quad (3.1.69)$$

Assuming that the top and stop masses in the one-loop part of the correction are  $\overline{\text{DR}}'$ -renormalised parameters at the scale  $Q$ , and expanding our results in inverse powers of  $m_{\tilde{g}}^2$ , the contribution of two-loop, MSSM-like diagrams involving gluons, gluinos or a four-stop coupling reads

$$\begin{aligned} (\Delta m_h^2)_{2\ell}^{\text{“MSSM”}} = & \frac{\alpha_s m_t^4}{4 \pi^3 v^2} \left\{ \frac{2 m_{\tilde{g}}^2}{m_{\tilde{t}_1}^2} \left( 1 - \ln \frac{m_{\tilde{g}}^2}{Q^2} \right) + \frac{2\pi^2}{3} - 2 - 6 \ln \frac{m_{\tilde{g}}^2}{m_{\tilde{t}_1}^2} + 2 \ln \frac{m_t^2}{Q^2} \right. \\ & + \frac{2 m_t^2}{m_{\tilde{t}_1}^2} \left( 1 - \ln \frac{m_{\tilde{g}}^2}{Q^2} \right) + \ln^2 \frac{m_{\tilde{g}}^2}{m_t^2} + \ln^2 \frac{m_{\tilde{g}}^2}{m_{\tilde{t}_1}^2} + 2 \ln^2 \frac{m_t^2}{Q^2} - 2 \ln^2 \frac{m_{\tilde{t}_1}^2}{Q^2} \\ & + \frac{2 m_t^2}{m_{\tilde{g}}^2} \left[ \frac{2\pi^2}{3} \left( 2 + \frac{m_{\tilde{t}_1}^2}{m_t^2} \right) - 2 - \left( 8 + \frac{m_t^2}{m_{\tilde{t}_1}^2} \right) \ln \frac{m_{\tilde{g}}^2}{m_t^2} - 4 \ln \frac{m_{\tilde{g}}^2}{m_{\tilde{t}_1}^2} \right. \\ & \quad \left. - \frac{m_{\tilde{t}_1}^2}{m_t^2} \left( 2 + 6 \ln \frac{m_{\tilde{g}}^2}{m_{\tilde{t}_1}^2} + \ln \frac{m_{\tilde{g}}^2}{m_t^2} \right) \right. \\ & \quad \left. + 2 \left( 2 + \frac{m_{\tilde{t}_1}^2}{m_t^2} \right) \ln \frac{m_{\tilde{g}}^2}{m_{\tilde{t}_1}^2} \ln \frac{m_{\tilde{g}}^2}{m_t^2} \right] \\ & \left. + \mathcal{O}(m_{\tilde{g}}^{-4}) \right\} + \left[ m_{\tilde{t}_1}^2 \rightarrow m_{\tilde{t}_2}^2 \right], \quad (3.1.70) \end{aligned}$$

where the last term in square brackets represents the addition of terms obtained from the previous ones by replacing  $m_{\tilde{t}_1}^2$  with  $m_{\tilde{t}_2}^2$ . From eq. (3.1.70) above it is clear that, in the  $\overline{\text{DR}}'$  scheme, the two-loop top-stop-gluino contributions to the SM-like Higgs mass can become unphysically large when  $m_{\tilde{g}} \gg m_{\tilde{t}_i}$ , due to the presence of terms enhanced by  $m_{\tilde{g}}^2/m_{\tilde{t}_i}^2$ . This non-decoupling behaviour of the corrections to the Higgs mass in the  $\overline{\text{DR}}'$  scheme has already been discussed in the context of the MSSM in ref. [76]. Indeed, the correction in eq. (3.1.70) corresponds to the one obtained by setting  $\mu = A_t = 0$  in the MSSM result. The terms enhanced by  $m_{\tilde{g}}^2/m_{\tilde{t}_i}^2$  can be removed by expressing the top and stop masses in the one-loop part of the correction as OS parameters. After including the resulting shifts in the two-loop correction, we find

$$\begin{aligned} (\Delta m_h^2)_{2\ell}^{\text{“MSSM”}} = & \frac{\alpha_s m_t^4}{4 \pi^3 v^2} \left\{ \frac{2\pi^2}{3} - 1 - 6 \ln \frac{m_{\tilde{g}}^2}{m_t^2} - 3 \ln^2 \frac{m_{\tilde{t}_1}^2}{m_t^2} + 2 \ln^2 \frac{m_{\tilde{g}}^2}{m_{\tilde{t}_1}^2} \right. \\ & \left. + \frac{m_t^2}{m_{\tilde{g}}^2} \left[ \frac{4\pi^2}{3} \left( 2 + \frac{m_{\tilde{t}_1}^2}{m_t^2} \right) - \frac{20}{3} - \frac{14 m_{\tilde{t}_1}^2}{3 m_t^2} + \frac{28}{3} \ln \frac{m_{\tilde{t}_1}^2}{m_t^2} \right] \right\} \\ & + \left[ m_{\tilde{t}_1}^2 \rightarrow m_{\tilde{t}_2}^2 \right], \end{aligned}$$

$$\begin{aligned}
& + \frac{2m_{\tilde{t}_1}^2}{m_t^2} \left( 6 + \ln \frac{m_{\tilde{t}_1}^2}{m_t^2} + \ln \frac{m_{\tilde{t}_2}^2}{m_t^2} \right) \ln \frac{m_{\tilde{t}_1}^2}{m_t^2} + \frac{m_{\tilde{t}_2}^2}{m_t^2} \ln \frac{m_{\tilde{t}_1}^2}{m_{\tilde{t}_2}^2} \\
& - 2 \left( 12 + \frac{6m_{\tilde{t}_1}^2}{m_t^2} + 4 \ln \frac{m_{\tilde{t}_1}^2}{m_t^2} + \frac{3m_{\tilde{t}_1}^2 + m_{\tilde{t}_2}^2}{m_t^2} \ln \frac{m_{\tilde{t}_1}^2}{m_t^2} \right) \ln \frac{m_g^2}{m_t^2} \\
& + 4 \left( 2 + \frac{m_{\tilde{t}_1}^2}{m_t^2} \right) \ln^2 \frac{m_g^2}{m_t^2} \Big] + \mathcal{O}(m_g^{-4}) \Big\} \\
& + \left[ m_{\tilde{t}_1}^2 \longleftrightarrow m_{\tilde{t}_2}^2 \right], \tag{3.1.71}
\end{aligned}$$

where the last term in square brackets represents the addition of terms obtained from the previous ones by swapping  $m_{\tilde{t}_1}^2$  and  $m_{\tilde{t}_2}^2$ . By taking the limit  $m_{\tilde{t}_1} = m_{\tilde{t}_2} = m_{\tilde{t}}$  in the equation above we recover eq. (42) of ref. [76].

In the MRSSM, the contributions to  $\Delta m_h^2$  arising from two-loop diagrams with stops and octet scalars allow for fairly compact expressions. If the stop masses in the one-loop part of the correction are renormalised in the  $\overline{\text{DR}}'$  scheme, those contributions read

$$(\Delta m_h^2)_{2\ell}^{O_i} = -\frac{\alpha_s m_t^4}{2\pi^3 v^2} \frac{m_g^2}{m_{\tilde{t}_1}^2} \left\{ 1 - \ln \frac{m_{\tilde{t}_1}^2}{Q^2} + f\left(\frac{m_{\tilde{t}_1}^2}{m_{O_i}^2}\right) \right\} + \left[ m_{\tilde{t}_1}^2 \longrightarrow m_{\tilde{t}_2}^2 \right], \tag{3.1.72}$$

where  $f(x)$  is the function defined in eq. (3.1.66). For OS stop masses, the octet-scalar contributions to  $\Delta m_h^2$  read instead

$$(\Delta m_h^2)_{2\ell}^{O_i} = -\frac{\alpha_s m_t^4}{2\pi^3 v^2} \frac{m_g^2}{m_{\tilde{t}_1}^2} \left\{ 1 - \ln \frac{m_{\tilde{t}_1}^2}{m_{O_i}^2} + f\left(\frac{m_{\tilde{t}_1}^2}{m_{O_i}^2}\right) - g\left(\frac{m_{\tilde{t}_1}^2}{m_{O_i}^2}\right) \right\} + \left[ m_{\tilde{t}_1}^2 \longrightarrow m_{\tilde{t}_2}^2 \right], \tag{3.1.73}$$

where  $g(x)$  is the function defined in eq. (3.1.68). It would appear from eqs. (3.1.72) and (3.1.73) above that, independently of the renormalisation scheme adopted for the stop masses, the octet-scalar contributions to  $\Delta m_h^2$  are enhanced by a factor  $m_g^2$ . This is due to the fact that the trilinear squark-octet interaction, see eq. (1.3.114), is proportional to the Dirac mass term  $m_D$  – i.e., to  $m_{\tilde{g}}$ . However, as discussed in section 1.3.5.4, one of the mass eigenvalues for the octet scalars – to fix the notation, let us assume it is  $m_{O_1}^2$  – does in turn grow with the gluino mass, namely  $m_{O_1}^2 \approx 4m_D^2$  when  $m_D^2$  becomes much larger than the soft SUSY-breaking mass terms for the octet scalars. Expanding the corresponding contribution to  $\Delta m_h^2$  in inverse powers of  $m_{O_1}^2$  we find, in the  $\overline{\text{DR}}'$  scheme,

$$\begin{aligned}
(\Delta m_h^2)_{2\ell}^{O_1} = & -\frac{\alpha_s m_t^4}{4\pi^3 v^2} \frac{m_g^2}{m_{O_1}^2} \left\{ 2 \frac{m_{O_1}^2}{m_{\tilde{t}_1}^2} \left( 1 - \ln \frac{m_{O_1}^2}{Q^2} \right) + \frac{2\pi^2}{3} + 8 \ln \frac{m_{\tilde{t}_1}^2}{m_{O_1}^2} + 2 \ln^2 \frac{m_{\tilde{t}_1}^2}{m_{O_1}^2} \right. \\
& \left. + \frac{4m_{\tilde{t}_1}^2}{m_{O_1}^2} \left[ \pi^2 - 2 + 10 \ln \frac{m_{\tilde{t}_1}^2}{m_{O_1}^2} + 3 \ln^2 \frac{m_{\tilde{t}_1}^2}{m_{O_1}^2} \right] + \mathcal{O}(m_{O_1}^{-4}) \right\} \\
& + \left[ m_{\tilde{t}_1}^2 \longrightarrow m_{\tilde{t}_2}^2 \right], \tag{3.1.74}
\end{aligned}$$

which does indeed contain potentially large terms enhanced by the ratio  $m_g^2/m_{\tilde{t}_i}^2$ . Note that those terms cancel only partially the corresponding terms in the MSSM-like

contribution – see the first term in the curly brackets of eq. (3.1.70) – leaving residues proportional to  $m_g^2/m_{\tilde{t}_i}^2 \ln(m_{O_1}^2/m_g^2)$ . On the other hand, in the OS scheme we find

$$\begin{aligned}
(\Delta m_h^2)_{2\ell}^{O_1} = & -\frac{\alpha_s m_t^4}{4\pi^3 v^2} \frac{m_g^2}{m_{O_1}^2} \left\{ \frac{2\pi^2}{3} - 1 + 6 \ln \frac{m_{\tilde{t}_1}^2}{m_{O_1}^2} + 2 \ln^2 \frac{m_{\tilde{t}_1}^2}{m_{O_1}^2} \right. \\
& + \frac{4m_{\tilde{t}_1}^2}{m_{O_1}^2} \left[ \pi^2 - \frac{17}{6} + 9 \ln \frac{m_{\tilde{t}_1}^2}{m_{O_1}^2} + 3 \ln^2 \frac{m_{\tilde{t}_1}^2}{m_{O_1}^2} \right] + \mathcal{O}(m_{O_1}^{-4}) \Big\} \\
& + \left[ m_{\tilde{t}_1}^2 \longrightarrow m_{\tilde{t}_2}^2 \right]. \tag{3.1.75}
\end{aligned}$$

Thus, we see that in the OS scheme the contribution to  $\Delta m_h^2$  from two-loop diagrams involving the heaviest octet scalar  $O_1$  does not grow unphysically large when  $m_g^2$  increases, because the ratio  $m_g^2/m_{O_1}^2$  tends to  $1/4$ . In contrast, for the contribution of the lightest octet scalar  $O_2$ , whose squared mass does not grow with  $m_g^2$ , the unexpanded formulae in eqs. (3.1.72) and (3.1.73) should always be used. However, in the total correction to  $m_h^2$  – see eq. (3.1.69) – the  $m_g^2$  enhancement of  $(\Delta m_h^2)_{2\ell}^{O_2}$  is compensated for by the factor  $s_{\phi_O}^2$ , which, as discussed in section 1.3.5.4, is in fact suppressed by  $m_g^{-4}$  in the heavy-gluino limit. In summary, we find that, in the MRSSM with heavy Dirac gluino, neither of the octet scalars can induce unphysically large contributions to  $\Delta m_h^2$ , as long as the stop masses in the one-loop part of the correction are renormalised in the OS scheme.

## 3.2 Numerical examples

In this section we discuss the numerical impact of the two-loop  $\mathcal{O}(\alpha_t \alpha_s)$  corrections to the Higgs boson masses whose computation was described in the previous section. As we did for the simplified formulae of section 3.1.7, we focus on “decoupling” scenarios in which the lightest neutral scalar is SM-like and the superpotential couplings  $\lambda_{S,T}$  are subdominant with respect to the top Yukawa coupling. Our purpose here is to elucidate the dependence of the corrections to the SM-like Higgs boson mass  $m_h$  on relevant parameters such as the stop masses and mixing and the gluino masses, rather than provide accurate predictions for all Higgs boson masses in realistic scenarios. We therefore approximate the one-loop part of the corrections with the dominant top/stop contributions at vanishing external momentum, obtained by combining the formulae for the Higgs mass matrices given for MDGSSM and MRSSM in sections 3.1.3 and 3.1.4, respectively, with the one-loop functions given in eq. (3.1.59). We recall that a computation of the Higgs boson masses in models with Dirac gauginos could also be obtained in an automated way by means of the package **SARAH** [261–266]. That would include the full one-loop corrections [264] and the two-loop corrections computed in the gaugeless limit at vanishing external momentum [21, 250]. However, the computation implemented in **SARAH** employs the  $\overline{\text{DR}}'$  renormalisation scheme, and does not easily lend itself to an adaptation to the OS scheme which, as discussed in section 3.1.7.2, can be more appropriate in scenarios with heavy gluinos.

The SM parameters entering our computation of the Higgs boson masses, which we take from ref. [303], are the  $Z$  boson mass  $m_Z = 91.1876$  GeV, the Fermi constant  $G_F = 1.16637 \times 10^{-5}$  GeV<sup>-2</sup> (from which we extract  $v = (2\sqrt{2}G_F)^{-1/2} \approx 174$  GeV), the pole top-quark mass  $m_t = 173.21$  GeV and the strong gauge coupling of the

SM in the  $\overline{\text{MS}}$  renormalisation scheme,  $\bar{\alpha}_s(m_Z) = 0.1185$ . Concerning the SUSY parameters entering the scalar mass matrix at tree-level, we set  $\lambda_S = \lambda_T = 0$  and push the parameters that determine the heavy-scalar masses to multi-TeV values, so that  $(m_h^2)^{\text{tree}} \approx m_Z^2 \cos^2 2\beta$ . We also set  $\tan \beta = 10$ , so that the tree-level mass of the SM-like Higgs boson is almost maximal but the corrections from diagrams involving sbottom squarks, which we neglect, are not particularly enhanced. For the parameters in the stop mass matrices we take degenerate soft SUSY-breaking masses  $m_Q = m_U = M_S$ , we neglect D-term-induced electroweak contributions and we treat the whole left-right mixing term  $X_t = A_t - \mu \cot \beta$  as a single input. Finally, for what concerns the parameters that determine the gluino and octet-scalar masses we focus again on the case of purely-Dirac gluinos, with  $m_{\tilde{g}_1} = -m_{\tilde{g}_2} = m_{\tilde{g}}$  and  $R_{11}^2 = R_{12}^2 = 1/2$ . We also take a vanishing soft SUSY-breaking bilinear  $B_O$ , so that  $\phi_O = 0$  and only the CP-even octet scalar  $O_1$ , with mass  $m_{O_1}^2 = m_O^2 + 4m_{\tilde{g}}^2$ , participates in the  $\mathcal{O}(\alpha_t \alpha_s)$  corrections to the Higgs masses.

### 3.2.1 An example in the MDGSSM

In figure 3.2 we illustrate some differences between the  $\mathcal{O}(\alpha_t \alpha_s)$  corrections to the SM-like Higgs boson mass in the MDGSSM and in the MSSM. We plot  $m_h$  as a function of the ratio  $X_t/M_S$ , setting  $M_S = 1.5$  TeV and  $m_{\tilde{g}} = m_O = 2$  TeV and adopting the OS renormalisation scheme for the parameters  $m_t$ ,  $M_S$  and  $X_t$ . We employ the renormalisation-group equations of the SM to evolve the coupling  $\bar{\alpha}_s$  from the input scale  $m_Z$  to the scale  $M_S$ , then we convert it to the  $\overline{\text{DR}}'$ -renormalised coupling of the considered SUSY model, which we denote as  $\hat{\alpha}_s(M_S)$ , by including the appropriate threshold corrections (in this step, we assume that all soft SUSY-breaking squark masses are equal to  $M_S$ ). The solid (black) and dashed (red) curves in figure 3.2 represent the SM-like Higgs boson mass in the MDGSSM and in the MSSM, respectively. The comparison between the two curves highlights the fact that, in contrast with the case of the MSSM, in the MDGSSM with purely-Dirac gluinos the  $\mathcal{O}(\alpha_t \alpha_s)$  corrections to  $m_h$  are symmetric with respect to a change of sign in  $X_t$ . As mentioned in section 3.1.7.1, this stems from cancellations between terms proportional to odd powers of the gluino masses. In the points where  $m_h$  is maximal, which in the OS calculation happens for  $|X_t/M_S| \approx 2$ , the difference between the MDGSSM and MSSM predictions for  $m_h$  is about 1 or 2 GeV, depending on the sign of  $X_t$ . Finally, the dotted (blue) curve in figure 3.2 represents the prediction for  $m_h$  obtained in the MDGSSM by omitting the contributions of two-loop diagrams involving the octet scalars. The comparison between the solid and dotted curves shows that, in the considered point of the parameter space, the effect on  $m_h$  of the octet-scalar contributions is positive but rather small, of the order of a few hundred MeV. Varying the parameters  $M_S$ ,  $m_{\tilde{g}}$  and  $m_O$  by factors of order two around the values used in figure 3.2, we find that this is a typical size for the octet-scalar contributions to  $m_h$  in the OS scheme.

A discussion of the theoretical uncertainty of our calculation is now in order. In our numerical examples we are not implementing the full one-loop corrections to the Higgs boson masses, nor the two-loop corrections beyond  $\mathcal{O}(\alpha_t \alpha_s)$  that are available in SARAH, in order to focus purely on the  $\mathcal{O}(\alpha_t \alpha_s)$  corrections. Therefore the only sources of uncertainty that we can meaningfully estimate are the uncomputed effects of  $\mathcal{O}(\alpha_t \alpha_s^2)$ , *i.e.* those arising from genuine three-loop diagrams with four strong-interaction vertices and from SUSY-QCD renormalisation effects of the parameters entering the one- and two-loop corrections. A common procedure for estimating those effects consists in comparing the results of the  $\mathcal{O}(\alpha_t \alpha_s)$  calculation of  $m_h$  in the OS scheme with the



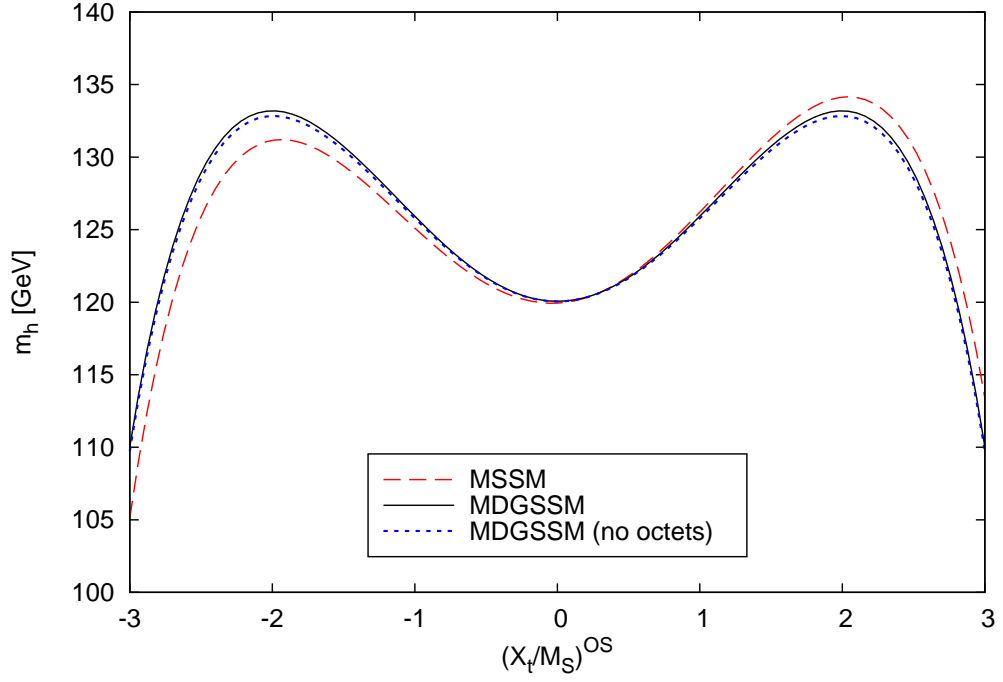


Figure 3.2 – Mass of the SM-like Higgs boson as a function of  $(X_t/M_S)^{\text{OS}}$ , for  $\tan \beta = 10$ ,  $M_S = 1.5$  TeV and  $m_{\tilde{g}} = m_{\tilde{O}} = 2$  TeV. The dashed curve represents the MSSM result, whereas the solid (dotted) curve represents the MDGSSM result with (without) the octet-scalar contributions.

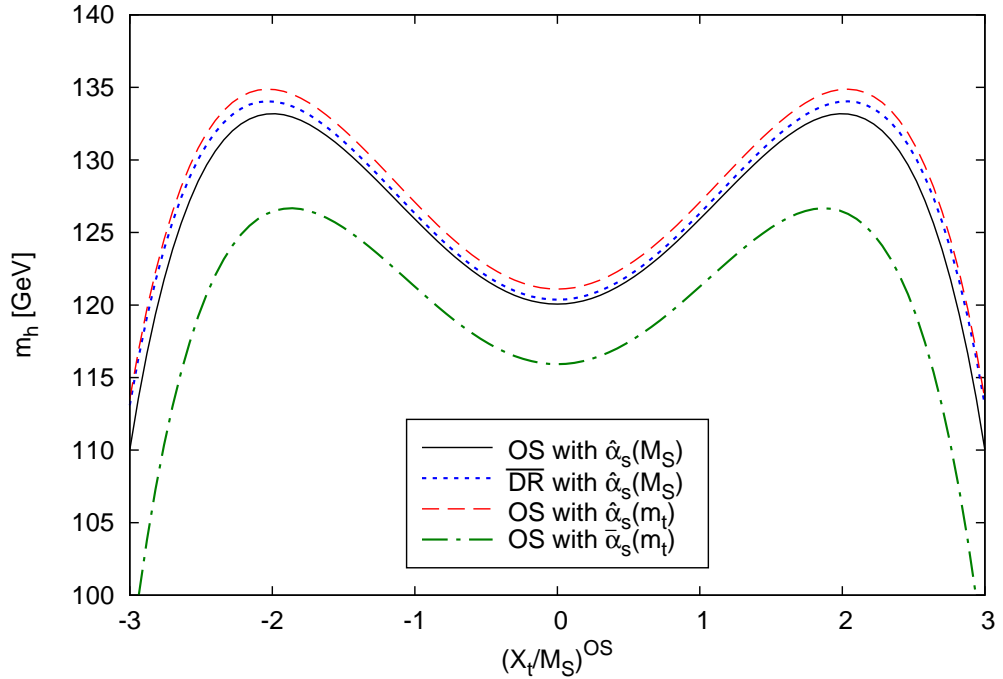


Figure 3.3 – Different determinations of the SM-like Higgs boson mass in the MDGSSM as a function of  $(X_t/M_S)^{\text{OS}}$ , for the same choices of parameters as in figure 3.2. The solid curve represents the original OS calculation; the dotted curve represents the  $\overline{\text{DR}}'$  calculation; the dashed and dot-dashed curves were obtained using  $\hat{\alpha}_s(m_t)$  and  $\bar{\alpha}_s(m_t)$ , respectively, in the OS calculation instead of  $\hat{\alpha}_s(M_S)$ .

results obtained by (i) converting the OS input parameters – *i.e.*, the top mass and the stop masses and mixing – to the  $\overline{\text{DR}}'$  scheme by means of  $\mathcal{O}(\alpha_s)$  shifts, and (ii) computing  $m_h$  using these  $\overline{\text{DR}}'$  parameters in both the one-loop and two-loop corrections, with the appropriate  $\overline{\text{DR}}'$  formulae for the  $\mathcal{O}(\alpha_t\alpha_s)$  corrections. The two sources of  $\mathcal{O}(\alpha_t\alpha_s^2)$  discrepancies in such a comparison are the omission of terms quadratic in  $\delta x_k$  in the expansion of the one-loop part of the corrections, eq. (3.1.58), and the different definition of the top and stop parameters entering the two-loop part of the corrections. In figure 3.3 we illustrate the renormalisation-scheme dependence of the  $\mathcal{O}(\alpha_t\alpha_s)$  determination of  $m_h$ , in the same MDGSSM scenario as in figure 3.2. The solid (black) curve represents the results of the original OS calculation, whereas the dotted (blue) curve represents the results of the  $\overline{\text{DR}}'$  calculation described above (note that both curves are plotted as functions of the ratio of OS parameters  $X_t/M_S$ ). The comparison between the solid and dotted curves would suggest a rather small impact of the uncomputed  $\mathcal{O}(\alpha_t\alpha_s^2)$  corrections, of the order of one GeV or even less (at least for the considered scenario).

Besides the top mass and the stop masses and mixing, there are a few more parameters entering the  $\mathcal{O}(\alpha_t\alpha_s)$  corrections to the Higgs boson masses whose  $\mathcal{O}(\alpha_s)$  definition amounts to a three-loop  $\mathcal{O}(\alpha_t\alpha_s^2)$  effect, namely the gluino and octet-scalar masses and the strong gauge coupling itself. Concerning the masses, in an OS calculation it seems natural to interpret them as pole ones. For  $\alpha_s$ , on the other hand, there is no obvious “on-shell” definition available, and different choices of scheme, scale and even underlying theory – while all formally equivalent at  $\mathcal{O}(\alpha_t\alpha_s)$  for the Higgs-mass calculation – can lead to significant variations in the numerical results. As mentioned earlier, the solid curve in figure 3.3 was obtained with top/stop parameters in the OS scheme, but with  $\alpha_s$  defined as the  $\overline{\text{DR}}'$ -renormalised coupling of the MDGSSM at the stop-mass scale, *i.e.*  $\hat{\alpha}_s(M_S)$ . However, since both stop squarks and top quarks enter the relevant two-loop diagrams, it would not seem unreasonable to evaluate the strong gauge coupling at the top-mass scale either. The dashed (red) and dot-dashed (green) curves in figure 3.3 represent the predictions for  $m_h$  obtained with top/stop parameters still in the OS scheme, but with  $\alpha_s$  defined as the  $\overline{\text{DR}}'$ -renormalised coupling of the MDGSSM at the top-mass scale,  $\hat{\alpha}_s(m_t)$ , and as the  $\overline{\text{MS}}$ -renormalised coupling of the SM at the same scale,  $\bar{\alpha}_s(m_t)$ , respectively. The comparison of these two curves with the solid curve shows that a variation in the definition of the coupling  $\alpha_s$  entering the two-loop corrections provides a less-optimistic estimate of the uncertainty associated to the  $\mathcal{O}(\alpha_t\alpha_s^2)$  corrections compared with the scheme variation of the top/stop parameters. In particular, for the considered scenario the use of  $\bar{\alpha}_s(m_t)$  would induce a negative variation with respect to the results obtained with  $\hat{\alpha}_s(M_S)$  of about 4 GeV for  $X_t \approx 0$  and about 7 GeV for  $|X_t/M_S| \approx 2$ . In contrast, the use of  $\hat{\alpha}_s(m_t)$  would induce a positive variation of about 1 GeV for  $X_t \approx 0$  and about 2 GeV for  $|X_t/M_S| \approx 2$ , *i.e.* more modest than the previous one but still larger than the one induced by a scheme change in the top/stop parameters. While remaining agnostic about the true size (and sign) of the three-loop  $\mathcal{O}(\alpha_t\alpha_s^2)$  corrections, we take this as a cautionary tale against putting too much stock in any single estimate of the theoretical uncertainty of a fixed-order calculation of  $m_h$  in scenarios with TeV-scale superparticles.

### 3.2.2 An example in the MRSSM

In our second numerical example we consider the MRSSM, and illustrate the dependence of the SM-like Higgs boson mass on the gluino mass. In ref. [251] it was pointed out that, for multi-TeV values of  $m_{\tilde{g}}$ , the contribution of two-loop diagrams involving

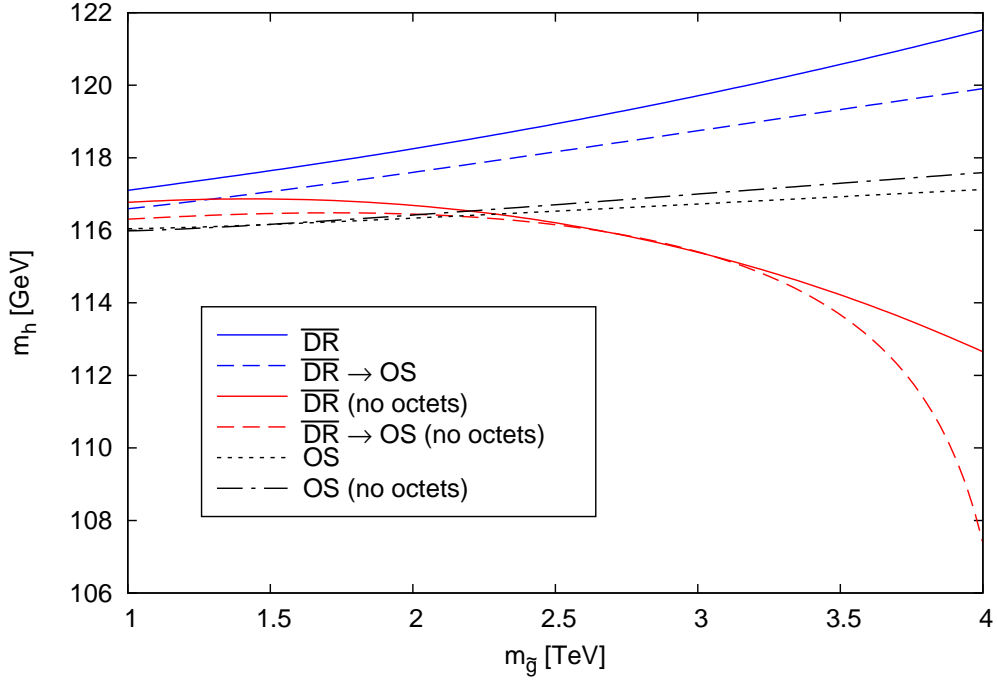


Figure 3.4 – Mass of the SM-like Higgs boson as a function of  $m_{\tilde{g}}$  in the MRSSM, for  $\tan\beta = 10$ ,  $M_S = 1$  TeV and  $m_O = 2$  TeV. The meaning of the different curves is explained in the text.

octet scalars can increase the prediction for  $m_h$  by more than 10 GeV. We will show that such large effects are related to the non-decoupling behaviour of the  $\overline{\text{DR}}'$  calculation of  $m_h$  that we discussed in section 3.1.7.2, and that the octet-scalar contributions are much more modest in an OS calculation.

The upper (blue) and lower (red) solid curves in figure 3.4 represent the SM-like Higgs boson mass obtained from the  $\overline{\text{DR}}'$  calculation as a function of  $m_{\tilde{g}}$ , with and without the octet-scalar contributions, respectively. We set  $m_O = 2$  TeV and  $M_S = 1$  TeV. The latter is interpreted as a  $\overline{\text{DR}}'$ -renormalised soft SUSY-breaking parameter evaluated at a scale equal to  $M_S$  itself, which means that each point in the solid curves corresponds to a different value of the physical stop masses. Both curves show a marked dependence on  $m_{\tilde{g}}$ , and the comparison between them shows that, for the highest value of  $m_{\tilde{g}}$  considered in the plot, the effect on  $m_h$  of the two-loop octet-scalar contributions does indeed grow to about 9 GeV. However, as can be seen in the explicit formulae for the two-loop corrections in the  $\overline{\text{DR}}'$  scheme of eqs. (3.1.70) and (3.1.74), this marked dependence of both the gluino and octet-scalar contributions on  $m_{\tilde{g}}$  is induced by terms enhanced by the ratio  $m_{\tilde{g}}^2/M_S^2$ . When that ratio becomes large, which in Dirac-gaugino models can occur naturally, the size of the two-loop  $\mathcal{O}(\alpha_t\alpha_s)$  corrections to  $m_h$  can grow up to a point where the accuracy of the perturbative expansion is called into question. To visualise this aspect, we perform a change of renormalisation scheme for the top and stop masses that mirrors the one represented by the dotted curve in figure 3.3. The upper (blue) and lower (red) dashed curves in figure 3.4 represent the values of  $m_h$  obtained with and without octet-scalar contributions, respectively, after converting the  $\overline{\text{DR}}'$  stop masses into the physical ones and using the latter, together with the physical top mass, in both the one-loop and two-loop corrections, with the appropriate OS formulae for the  $\mathcal{O}(\alpha_t\alpha_s)$  corrections. For our choice of the  $\overline{\text{DR}}'$  input parameter  $M_S(M_S) = 1$  TeV, we find that the physical stop masses range between

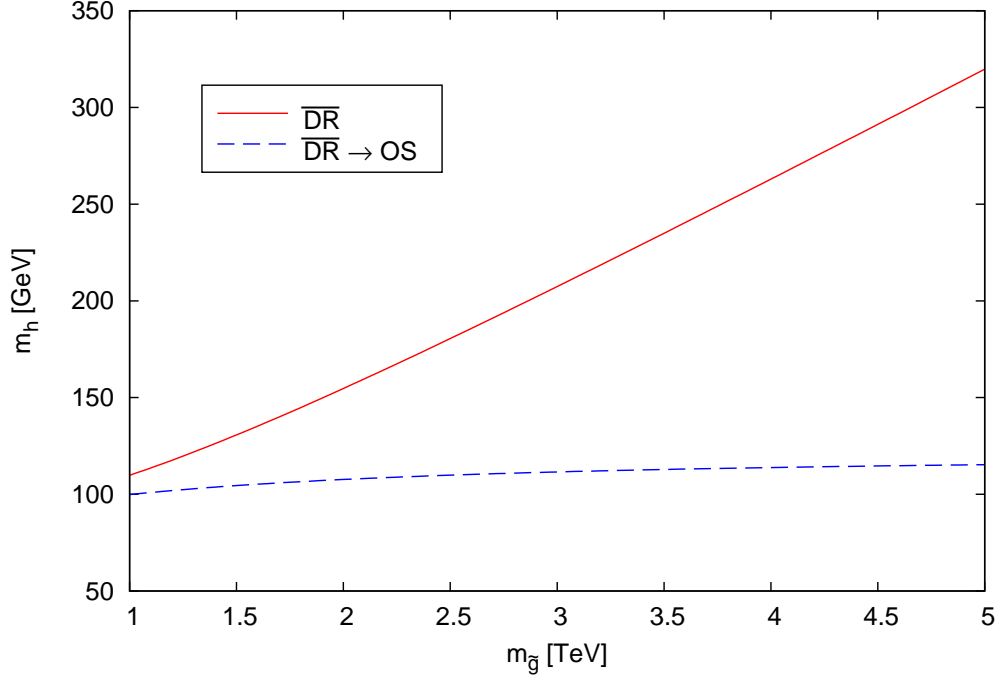


Figure 3.5 – Mass of the SM-like Higgs boson as a function of  $m_{\tilde{g}}$  in the *supersoft* limit of the MRSSM, for  $\tan\beta = 10$ . The solid curve represents the results of the  $\overline{\text{DR}}'$  calculation, in which the two-loop  $\mathcal{O}(\alpha_t\alpha_s)$  corrections become unphysically large. The dashed curve was obtained by converting the top and stop masses to the OS scheme and using the corresponding formulae for the  $\mathcal{O}(\alpha_t\alpha_s)$  corrections.

1072 GeV and 1392 GeV for the values of  $m_{\tilde{g}}$  shown in the plot. If the octet-scalar contributions to the  $\mathcal{O}(\alpha_s)$  stop self-energies are omitted, the stop masses range instead between 1049 GeV and 346 GeV, *i.e.* they become smaller for increasing  $m_{\tilde{g}}$  (indeed, in this case  $m_{\tilde{g}}$  cannot be pushed to values much larger than those shown in the plot without rendering the stop masses tachyonic). The comparison between the solid and dashed curves shows that the scheme dependence of the  $\mathcal{O}(\alpha_t\alpha_s)$  calculation of  $m_h$  becomes increasingly worse at large values of  $m_{\tilde{g}}$ , especially in the lower curves where the octet-scalar contributions are omitted. Finally, the (black) dotted and dot-dashed curves in figure 3.4 represent the predictions for  $m_h$  obtained directly from the OS calculation with and without octet-scalar contributions, respectively. In this case the input  $M_S = 1$  TeV is interpreted as an OS-renormalised parameter, meaning that the physical stop masses correspond to  $(M_S^2 + m_t^2)^{1/2} \approx 1015$  GeV for all points in the curves. We stress that direct comparisons between these two curves and the solid (and dashed) ones would not be appropriate, because they refer to different points of the MRSSM parameter space. However, the dotted and dot-dashed curves show that, when the physical stop masses are taken as input, the prediction for  $m_h$  in the MRSSM depends only mildly on the value of  $m_{\tilde{g}}$ , and the effect of the octet-scalar contributions is below one GeV. This is explained by the fact that, as discussed in section 3.1.7.2, in the OS scheme there are no terms enhanced by  $m_{\tilde{g}}^2/M_S^2$  in either the gluino or the octet-scalar contributions to the  $\mathcal{O}(\alpha_t\alpha_s)$  corrections.

Before concluding, we note that there are extreme situations in which a  $\overline{\text{DR}}'$  calculation of  $m_h$  is not workable at all, and a conversion to the OS scheme such as the one represented by the dashed lines in figure 3.4 is necessary. In the so-called *supersoft* scenario,

all soft SUSY-breaking masses vanish, and sizeable sfermion masses – proportional to the Dirac-gaugino masses – are induced only by radiative corrections. Such a scenario can be realised *e.g.* in the MRSSM by setting  $m_O = 0$  and  $M_S = 0$ , where the latter is interpreted as a  $\overline{\text{DR}}'$ -renormalised parameter. At the scale where this condition is imposed, the  $\overline{\text{DR}}'$  stop masses coincide with the top mass, with the result that, in the  $\overline{\text{DR}}'$  calculation, the one-loop correction in the first term of eq. (3.1.69) vanishes, while the two-loop corrections in eqs. (3.1.70) and (3.1.74) contain terms enhanced by  $m_{\tilde{g}}^2/m_t^2$  (concerning the octet-scalar contributions, we recall that  $m_{O_1} = 2m_{\tilde{g}}$  in this scenario). Since the Dirac-gluino mass needs to be in the multi-TeV range to generate realistic values for the physical stop masses, the non-decoupling terms in the two-loop corrections can become unphysically large. This is illustrated by the solid (red) curve in figure 3.5, which represents the SM-like Higgs boson mass obtained with the  $\overline{\text{DR}}'$  calculation as a function of the gluino mass (here we fix the renormalisation scale as  $Q = m_t$  and use  $\bar{\alpha}_s(m_t)$  in the two-loop corrections). It appears that the  $\overline{\text{DR}}'$  prediction for  $m_h$  becomes essentially proportional to  $m_{\tilde{g}}$ , and quickly grows to nonsensical values as the latter increases. In contrast, the dashed (blue) curve is obtained with the same procedure as the dashed curves in figure 3.4, *i.e.* by computing the physical stop masses at  $\mathcal{O}(\alpha_s)$  as a function of  $m_{\tilde{g}}$  and using them in conjunction with the appropriate OS formulae for the  $\mathcal{O}(\alpha_t\alpha_s)$  corrections to  $m_h$ . In our example the stop masses range between 302 GeV and 1272 GeV, while the SM-like Higgs boson mass shows only a mild dependence on  $m_{\tilde{g}}$  and remains confined to values well below the observed one.

### 3.3 Conclusions

Supersymmetric models with Dirac gaugino masses have attracted considerable attention in the past few years, because they are subject to looser experimental constraints and require less fine-tuning than the MSSM. Besides the extended gaugino sector, such models feature additional colourless scalars which mix with the usual Higgs doublets of the MSSM, as well as additional coloured scalars in the octet representation of  $SU(3)$  which contribute to the Higgs boson masses at the two-loop level. In this chapter we presented a computation of the dominant two-loop corrections to the Higgs boson masses in Dirac-gaugino models, relying on effective-potential techniques that had previously been applied to the MSSM [76] and to the NMSSM [77]. We obtained analytic formulae for the  $\mathcal{O}(\alpha_t\alpha_s)$  corrections to the scalar and pseudoscalar Higgs mass matrices valid for arbitrary choices of parameters in the squark and gaugino sectors, both in the  $\overline{\text{DR}}'$  and in the OS renormalisation schemes, which we make available upon request as a **Fortran** code. We also presented compact approximate formulae for the dominant corrections to the mass of the SM-like Higgs boson, valid under a number of simplifying assumptions for the SUSY parameters. Finally, we studied the numerical impact of the newly-computed corrections on the predictions for the SM-like Higgs boson mass in some representative scenarios. In particular, we elucidated the differences between the predictions for  $m_h$  in the MSSM and those in its Dirac-gaugino extensions; we discussed the theoretical uncertainty of our predictions stemming from uncomputed higher-order corrections; we stressed that a judicious choice of renormalisation scheme is required to obtain reliable predictions in scenarios where the gluinos are much heavier than the squarks, which can occur naturally in Dirac-gaugino models.



## Chapter 4

# Avoiding the Goldstone Boson Catastrophe in general renormalisable field theories at two loops

We now return to the Goldstone Boson Catastrophe, which we already encountered for the SM and the MSSM in sections 1.1.5 and 1.3.4.2 respectively, and in this chapter we will demonstrate how to address it for general renormalisable field theories.

This problem of infra-red divergences appears in generic models as in the SM and MSSM: for reasons of calculational simplicity, the effective potential beyond one loop has been calculated only in the Landau gauge (as this allows to decouple the ghosts), which means that the Goldstone bosons are treated as actual massless Goldstone bosons. Once loop corrections are taken into account, the mass-squared Lagrangian parameters of the Goldstone bosons determined from the tadpole equations<sup>1</sup> are small and can even be negative (as opposed to the pole mass, which is always zero) and this causes the loop integrals for the tadpoles to diverge or be complex. While this problem can in principle be circumvented by dropping the complex parts and changing the renormalisation scale to attempt to find non-negligible positive squared masses, this is not easy to implement consistently in the context of automated calculations.

We presented in section 1.1.5 a solution for the tadpoles that was first proposed in [28,29] for the Standard Model and later applied to the MSSM in [33]: (a subset of) the terms involving the Goldstone boson should be resummed to all orders, roughly speaking replacing its mass-squared parameter (which appears in the loop functions) with the equivalent mass parameter derived from the loop-corrected effective potential (*i.e.* zero, since it is a Goldstone boson). In section 4.2 we show how this can be extended to general renormalisable theories.

In [28,29] it was noted that the Goldstone resummation would not regulate divergences in the second derivatives of the effective potential, and so to have a divergence-free calculation of the neutral scalar (*i.e.* Higgs) masses it would be necessary to include the external momentum in the self energies rather than using an effective potential approximation. This is particularly important because the zero momentum approximation is widely used to calculate the Higgs mass [1, 21, 32, 76, 77, 164–175, 179, 180,

---

<sup>1</sup>Note that we take the expectation values to be fixed and loop-correct the mass-squared terms rather than vice versa – as explained in more detail below eq. (1.1.36).

210,240,247,250–252,258,259,299,300] – indeed there are few publicly available implementations of diagrammatic calculations of the Higgs mass beyond one loop in BSM theories which do not use it (some momentum-dependent diagrammatic calculations are available for the MSSM [176–178, 189]). While the Goldstone Boson Catastrophe can be avoided in the MSSM in the gaugeless limit (where the Goldstone boson does not couple to the Higgs, and so generates no divergences) it is of pressing concern for more general theories. Since the two-loop computation has become publicly available through SARAH [21, 250, 261–266], the Goldstone Boson Catastrophe as it affects that implementation has been discussed in [249, 300], and has recently manifested itself in [85, 101, 218]. Indeed, while the numerical impact of the problem in the Standard Model seems to be small (at least away from the divergent points, simply neglecting the imaginary part of the potential seems to give results close to those of the full solutions), in more complicated theories it can cause divergent contributions to the masses for many regions of the parameter space; for example, in [85, 101] it was necessary to restrict to only the two-loop corrections proportional to the strong gauge coupling for those regions in performing parameter scans.

In section 4.3, we shall show that the inclusion of external momentum in the scalar self-energies does *not* by itself avoid all divergences. In fact, it is necessary to resum the Goldstone boson contributions in the mass diagrams too – to cancel the divergences in a class of diagrams which do not depend on momentum. We will also show that the resummation can be implemented most easily to two-loop order by using an “on-shell” scheme for the Goldstone bosons. With these modifications to cure the remaining divergences, the diagrammatic implementation in [21] could in principle be extended to include the external momentum by changing the loop functions to those implemented in TSIL [142, 150]. However, analytic expressions for general loop functions with momenta are not known: they are in general obtained by solving differential equations, which is numerically expensive. Therefore, in appendix B.2 we give a complete set of analytic expressions for expansions of the necessary functions including all divergent and constant terms in an expansion of the four-momentum-squared  $s$  around zero (neglecting those of  $\mathcal{O}(s)$ ). This allows fast evaluation of a “generalised effective potential approximation” for the neutral scalar masses – although for this part we shall be restricted to the gaugeless limit (setting the couplings of all broken gauge groups to zero) since the mass diagrams are known only up to second order in the gauge couplings.

A comment is at hand also about the gauge dependence of the results obtained in this chapter: our calculations are performed in the Landau gauge, and we could in principle expect results to differ if we used another gauge – in particular the expressions we obtain with the “on-shell” Goldstone method only apply in the Landau gauge where the Goldstone “pole” mass is zero. However it should be noted that we use the gaugeless limit for the mass calculations, which means that there is no longer any gauge, and therefore we will not consider issues of gauge dependence further here.

Once the Goldstone Boson Catastrophe has been solved, using similar techniques it was shown in [28, 29, 33] that it is also possible to improve the solution of the tadpole equations for the other mass-squared parameters (not just the one corresponding to the tree-level Goldstone boson mass). In general, the same mass-squared parameters  $m^2$  appear both as solutions of the tadpole equations, and in the loop functions, in the schematic form

$$m^2 = m_0^2 - \frac{1}{v} \frac{\partial \Delta V(m^2)}{\partial v}$$

where  $m_0^2$  is the tree-level solution of the tadpole equation,  $v$  is some expectation value and  $\Delta V$  are the loop corrections to the effective potential. Although resummation



is not required for them (except perhaps for the Higgs boson, where the quantum corrections are so large that they force its tree-level mass to become negative – we shall not discuss such a case here), these other mass-squared parameters can be expanded perturbatively in the loop functions so that the equations can be solved directly rather than iteratively. In other words, we find only the tree-level values of the parameters on the right-hand side of the equation, and the loop-corrected solution on the left (as opposed to the loop-corrected value on both sides):

$$m^2 = m_0^2 - \frac{1}{v} \frac{\partial \Delta V(m_0^2)}{\partial v} - \delta \left( \frac{1}{v} \frac{\partial \Delta V(m_0^2)}{\partial v} \right);$$

we shall refer to these throughout as “self-consistent equations”. In section 4.4, we will show how to carry out this procedure in general, showing that the formulae can be given in simpler form than in, e.g., [33] for the MSSM case. We shall also go further and show how this shifts the mass diagrams.

Finally, a set of definitions of all the loop functions used throughout this chapter is provided in appendix B.1.

## 4.1 The Goldstone Boson Catastrophe and resummation

### 4.1.1 Abelian Goldstone model

Let us begin by recalling the problem of the Goldstone Boson Catastrophe. For simplicity we shall take the simplest Abelian Goldstone model defined by a complex scalar field  $\Phi$  (and no gauge group) with potential

$$V = \mu^2 |\Phi|^2 + \lambda |\Phi|^4 \quad (4.1.1)$$

and expand around an expectation value  $v$  as  $\Phi = \frac{1}{\sqrt{2}}(v + h + iG)$  to obtain

$$\begin{aligned} V^{(0)} &= \frac{v^2}{4}(\lambda v^2 + 2\mu^2) + hv(v^2\lambda + \mu^2) + \frac{1}{2}(3v^2\lambda + \mu^2)h^2 + \frac{1}{2}(\mu^2 + \lambda v^2)G^2 \\ &\quad + v\lambda(h^3 + hG^2) + \frac{\lambda}{4}(h^4 + 2G^2h^2 + G^4). \end{aligned} \quad (4.1.2)$$

Defining  $m_G^2 \equiv \mu^2 + \lambda v^2$ ,  $M_h^2 \equiv \mu^2 + 3\lambda v^2$ , we can then compute the effective potential up to two loops:

$$\begin{aligned} V_{\text{eff}}(v) &\equiv V^{(0)}|_{h,G=0} + \frac{1}{16\pi^2}V^{(1)} + \frac{1}{(16\pi^2)^2}V^{(2)} + \dots \\ &= V^{(0)}|_{h,G=0} + \frac{1}{16\pi^2}(f(m_G^2) + f(M_h^2)) \\ &\quad + \frac{\lambda}{(16\pi^2)^2} \left[ \frac{3}{4}A(m_G^2)^2 + \frac{1}{2}A(m_G^2)A(M_h^2) + \frac{3}{4}A(M_h^2)^2 \right] \\ &\quad - \frac{\lambda^2 v^2}{(16\pi^2)^2} \left[ 3I(M_h^2, M_h^2, M_h^2) + I(M_h^2, m_G^2, m_G^2) \right] + \dots \end{aligned} \quad (4.1.3)$$

where the one-loop functions  $f(x)$ ,  $A(x)$  and the two-loop function  $I(x, y, z)$  are defined in the appendix, equations (B.1.3), (B.1.6), and (B.1.24). The potential is regular as  $m_G \rightarrow 0$  but does contain terms of order  $m_G^2 \bar{\log} m_G^2$  (where  $\bar{\log} x$  is also defined in the

appendix – eq. (B.1.2)) so that when we derive the tadpole equation and expand the derivative of  $I(M_h^2, m_G^2, m_G^2)$  around  $m_G^2 = 0$  we find<sup>2</sup>

$$\begin{aligned} 0 = \frac{\partial V_{\text{eff}}}{\partial v} &= m_G^2 v + \frac{2\lambda v}{16\pi^2} \left[ \frac{1}{2} A(m_G^2) + \frac{3}{2} A(M_h^2) \right] \\ &+ \frac{2\lambda^2 v}{(16\pi^2)^2} \overline{\log} m_G^2 \left[ \frac{3}{2} A(m_G^2) + \frac{1}{2} A(M_h^2) + \frac{2\lambda v^2}{M_h^2} A(M_h^2) \right] \\ &+ \text{other non – singular terms.} \end{aligned} \quad (4.1.4)$$

The  $\overline{\log} m_G^2$  terms on the second line are the manifestation of the Goldstone Boson Catastrophe: we cannot insert the tree-level solution  $m_G^2 = 0$  into them, and will have a complex potential if we find  $m_G^2 < 0$ . The solution proposed in [28, 29] is to resum the Goldstone boson propagators – in the one-loop effective potential we make the substitution

$$\begin{aligned} V_{\text{eff}}^{(1)} &\supset -\frac{i}{2} C \int d^d k \log(-k^2 + m_G^2) \rightarrow -\frac{i}{2} C \int d^d k \log(-k^2 + m_G^2 + \Pi_{GG}(k^2)) \\ &\rightarrow -\frac{i}{2} C \int d^d k \log(-k^2 + m_G^2 + \Pi_{GG}(0)) + \dots \end{aligned} \quad (4.1.5)$$

where  $C$  is a constant defined in equation (B.1.1), and  $\Pi_{GG}(k^2)$  is the Goldstone boson self energy, given here at one loop by

$$\Pi_{GG}(k^2) = \frac{1}{16\pi^2} \left[ 3\lambda A(m_G^2) + \lambda A(M_h^2) - 4\lambda^2 v^2 B(k^2, m_G^2, M_h^2) \right]. \quad (4.1.6)$$

With zero external momentum, this becomes

$$\Pi_{GG}(0) = \frac{1}{16\pi^2} \left[ \lambda A(m_G^2) + 3\lambda A(M_h^2) \right]. \quad (4.1.7)$$

The term involving only the Goldstone mass-squared will not have a well-defined derivative, and this also leads to divergences when we resum the effective potential at three loops and above. The prescription of [28] is to drop it in favour of  $\Pi_g = \frac{1}{16\pi^2} \Pi_g^{(1)} + \dots$  where

$$\Pi_g^{(1)}(0) = 3\lambda A(M_h^2) = \lambda A(M_h^2) - 4\lambda^2 v^2 B(0, 0, M_h^2). \quad (4.1.8)$$

Note that this does not correspond to dropping one particular class of diagrams (at one loop it is a combination of the one- and two-propagator diagrams) but instead must be defined in terms of dropping contributions from “soft” Goldstone bosons. Defining

$$\Delta \equiv \Pi_g(0) \equiv \frac{1}{16\pi^2} \Delta_1 + \frac{1}{(16\pi^2)^2} \Delta_2 + \dots, \quad (4.1.9)$$

we then should use instead the resummed potential

$$\hat{V}_{\text{eff}} \equiv V_{\text{eff}} + \frac{1}{16\pi^2} \left[ f(m_G^2 + \Delta) - \sum_{n=0}^{l-1} \frac{\Delta^n}{n!} \left( \frac{\partial}{\partial m_G^2} \right)^n f(m_G^2) \right] \quad (4.1.10)$$

---

<sup>2</sup>Let us briefly comment here on the choice of argument with respect to which we compute derivatives. Until now we have been taking derivatives with respect to a real scalar fluctuation (or field) – in this case it would be  $h$  – before setting all fluctuations to zero (here  $h$  and  $G$ ). However, this is exactly equivalent to setting first the fluctuations to zero and then taking a derivative with respect to the VEV (here  $v$ ), because the real part of the fluctuation and the VEV always come with the same prefactor – in the present example,  $v$  and  $h$  always appear together in terms of the form  $(v + h)$ .

where  $l$  is the loop order to which  $V_{\text{eff}}$  has been calculated; the terms in square brackets simply ensure that the potentials are identical up to  $l$  loops and only differ at higher orders. Performing this procedure for the potential above we find

$$\begin{aligned} \hat{V}_{\text{eff}} = & V^{(0)} + \frac{1}{16\pi^2} (f(m_G^2 + \Delta) + f(M_h^2)) + \frac{\lambda}{(16\pi^2)^2} \left[ \frac{3}{4} A(m_G^2)^2 + \frac{3}{4} A(M_h^2)^2 \right] \\ & - \frac{\lambda^2 v^2}{(16\pi^2)^2} \left[ 3I(M_h^2, M_h^2, M_h^2) + I(M_h^2, m_G^2, m_G^2) + \frac{1}{\lambda v^2} A(M_h^2) A(m_G^2) \right]. \end{aligned} \quad (4.1.11)$$

With the above procedure, we have resummed the leading divergences at two loops, *i.e.* the terms of order  $m_G^2 \overline{\log} m_G^2$  for small  $m_G^2$  (we expect  $m_G^2$  it to be of order a one-loop quantity at the minimum). If we are interested in the first derivative of the potential then this is sufficient; to find the minimum to two-loop order we can expand the potential to order  $m_G^2$  with the help of eq. (B.1.54):

$$\begin{aligned} \hat{V}_{\text{eff}} = & V^{(0)} + \frac{1}{16\pi^2} (f(m_G^2 + \Delta) + f(M_h^2)) + \frac{\lambda}{(16\pi^2)^2} \left[ \frac{3}{4} A(M_h^2)^2 \right] \\ & - \frac{\lambda^2 v^2}{(16\pi^2)^2} \left[ 3I(M_h^2, M_h^2, M_h^2) + I(M_h^2, 0, 0) - 2R_{SS}(0, M_h^2) m_G^2 \right] + \mathcal{O}(m_G^4), \end{aligned} \quad (4.1.12)$$

making the regularity apparent, although note that the higher-order terms still contain a  $m_G^4 \overline{\log} m_G^2$  term. The tadpole equation, neglecting terms of three-loop order, is then

$$\begin{aligned} 0 = & v \left( m_G^2 + \frac{1}{16\pi^2} \Delta_1 \right) + \frac{\lambda v + \Delta'/2}{16\pi^2} A(m_G^2 + \Delta) \\ & + \frac{1}{(16\pi^2)^2} \left\{ \lambda \left[ 9\lambda v A(M_h^2) \overline{\log} M_h^2 \right] - 2\lambda^2 v \left[ 3I(M_h^2, M_h^2, M_h^2) + I(M_h^2, 0, 0) \right] \right. \\ & \quad \left. + \lambda^2 v^2 \left[ 6\lambda v \left( 9U_0(M_h^2, M_h^2, M_h^2, M_h^2) + U_0(M_h^2, M_h^2, 0, 0) \right) \right. \right. \\ & \quad \left. \left. + 4\lambda v R_{SS}(0, M_h^2) \right] \right\}. \end{aligned} \quad (4.1.13)$$

Noting that the solution to the one-loop equation is  $m_G^2 + \frac{1}{16\pi^2} \Delta_1 = 0$ , we see that we can neglect the  $A(m_G^2 + \Delta)$  term as it gives a correction of order three loops. We ought then to find that we can identify the term in curly brackets with  $\Delta_2$ : for a Goldstone boson we should find  $m_G^2 + \Pi_{GG}(0) = 0$ , so we expect that we should be able in general to identify  $\frac{1}{v} \frac{\partial V^{(\ell)}}{\partial v} = \Pi_{GG}^{(\ell)}(0)$ , and therefore for our modified potential we should expect

$$\frac{1}{v} \frac{\partial \hat{V}^{(\ell)}}{\partial v} = \Pi_g^{(\ell)}(0). \quad (4.1.14)$$

This leads to the prescription in [29, 33], which is somewhat simpler: we expand the potential  $V_{\text{eff}}$  as a series in  $m_G^2$ :

$$V^{(2)} = V^{(2)}|_{m_G^2=0} + \frac{1}{2} \Delta_1 A(m_G^2) + \frac{1}{2} \Omega m_G^2 + \mathcal{O}(m_G^4). \quad (4.1.15)$$

We can then use this as the *definition* of  $\Delta_1$  instead of equation (4.1.9). We then resum the effective potential as

$$\hat{V}_{\text{eff}} = V^{(0)} + \frac{1}{16\pi^2} \left[ V^{(1)}|_{m_G^2=0} + f(m_G^2 + \Delta) \right] + \frac{1}{(16\pi^2)^2} \left[ V^{(2)}|_{m_G^2=0} + \frac{1}{2} \Omega m_G^2 \right]. \quad (4.1.16)$$

By doing this, we immediately find the expression in (4.1.12), with

$$\Omega \equiv 4\lambda^2 v^2 R_{SS}(0, M_h^2). \quad (4.1.17)$$

When we take the derivative and expand up to two-loop order then the minimum is at  $m_G^2 + \Delta = 0$  with

$$\Delta_2 = \left[ \frac{1}{v} \frac{\partial}{\partial v} \left( V^{(2)}|_{m_G^2=0} \right) + \lambda \Omega \right]. \quad (4.1.18)$$

We shall follow this second procedure to find the minimum condition in general renormalisable field theories at two loop order.

We shall also consider a hybrid approach, which is to adopt an *on-shell* condition for the Goldstone boson: we define

$$(m_G^2)^{\text{dim. reg}} \equiv (m_G^2)^{\text{OS}} - \Pi_{GG}((m_G^2)^{\text{OS}}) = -\Pi_{GG}(0). \quad (4.1.19)$$

This is particularly effective at two loops, where we only need  $\Pi_{GG}^{(1)}$ ; furthermore, since  $(m_G^2)^{\text{OS}} = 0$ , at this loop order there is no difference between  $\Pi_{GG}$  and  $\Pi_g$ . Making the above substitution in the potential we find exactly the same result as our resummed version in equation (4.1.12). However, we also have the advantage that we can make this substitution directly *in the tadpole equation*:

$$\begin{aligned} 0 &= v(m_G^2)^{\text{dim. reg}} + \frac{\lambda v}{16\pi^2} A((m_G^2)^{\text{dim. reg}}) + \frac{3\lambda v}{16\pi^2} A(M_h^2) + \frac{1}{(16\pi^2)^2} \frac{\partial V^{(2)}}{\partial v} \\ &= v(m_G^2)^{\text{dim. reg}} + \frac{3\lambda v}{16\pi^2} A(M_h^2) \\ &\quad + \frac{1}{(16\pi^2)^2} \lim_{(m_G^2)^{\text{OS}} \rightarrow 0} \left[ \frac{\partial V^{(2)}}{\partial v} ((m_G^2)^{\text{OS}}) - 3\lambda^2 v A(M_h^2) \overline{\log}((m_G^2)^{\text{OS}}) \right], \end{aligned} \quad (4.1.20)$$

which gives *exactly* the expression that we found above in (4.1.13). We shall find in the following that this simple approach is also exactly what we need for the *mass* diagrams. However, we must first introduce some notation and formalism to handle the general case when (potentially several) Goldstone bosons and neutral scalars can mix.

#### 4.1.2 Goldstone bosons in general field theories

In the previous subsection we considered the simplest possible model where there were only two real scalars which cannot mix. Once we consider more general theories, there can be more Goldstone bosons and, even when they have been identified at tree level, they can in general mix with other scalars (only pseudoscalars in the case of CP conservation) once loop corrections are included. This problem does not arise in the Standard Model as treated in references [28, 29], because all of the pseudoscalars are would-be Goldstone bosons and the neutral and charged Goldstones cannot mix, so can be treated as two separate sectors. In the MSSM, there are additional scalars and pseudoscalars, but in the CP-conserving case considered in [33] the mixing is at most among *pairs* of fields, and could be written in each case in terms of mixing angles and  $2 \times 2$  matrices.

To deal with Goldstone boson mixing in general theories (using the conventions introduced in section 2.4.1), we will need some notation and simple results. We start

from a theory with a global symmetry such that the scalars transform under a set of infinitesimal shifts as  $\phi_i \rightarrow \phi_i + \epsilon^G \alpha_i^G$ . Then the standard result is to expand  $V(\phi_i + \epsilon^G \alpha_i^G) = V(\phi_i)$  and differentiate the relation once:

$$\epsilon^G \alpha_i^G \frac{\partial V}{\partial \phi_i^0} = 0, \quad \frac{\partial(\epsilon^G \alpha_i^G)}{\partial \phi_j^0} \frac{\partial V}{\partial \phi_i^0} + \epsilon^G \alpha_i^G \frac{\partial^2 V}{\partial \phi_i^0 \partial \phi_j^0} = 0. \quad (4.1.21)$$

When we sit at the minimum of the potential  $\frac{\partial V}{\partial \phi_i^0} = 0$  but for a spontaneously broken symmetry  $\alpha_i^G$  is not zero for all  $i$ , and thus we have a null eigenvector of the scalar mass matrix – *i.e.* the Goldstone boson. For more than one symmetry broken then there will be multiple null eigenvectors and these should be formed into an orthonormal set. Let us write the symmetry shifts as linear coefficients  $\alpha_i^G = a_{ij}^G \phi_j^0$  after this has been performed so that  $\sum_i \alpha_i^G \alpha_i^{G'} = \delta^{GG'}$  and then

$$G_G = \phi_G = R_{jG} \phi_j^0, \text{ where } R_{jG} = \alpha_j^G. \quad (4.1.22)$$

We use the index “ $G$ ” now to refer to the Goldstone boson(s) in the diagonal basis. The first identity that we need arises from taking a further derivative of the above equations to give

$$\begin{aligned} \epsilon^G \alpha_i^G \frac{\partial^3 V}{\partial \phi_i^0 \partial \phi_j^0 \partial \phi_k^0} + \frac{\partial^2(\epsilon^G \alpha_i^G)}{\partial \phi_j^0 \partial \phi_k^0} \frac{\partial V}{\partial \phi_i^0} + \frac{\partial(\epsilon^G \alpha_i^G)}{\partial \phi_j^0} \frac{\partial^2 V}{\partial \phi_i^0 \partial \phi_k^0} + \frac{\partial(\epsilon^G \alpha_i^G)}{\partial \phi_k^0} \frac{\partial^2 V}{\partial \phi_i^0 \partial \phi_j^0} = 0 \\ \rightarrow \alpha_i^G \alpha_j^{G'} \alpha_k^{G''} \frac{\partial^3 V}{\partial \phi_i^0 \partial \phi_j^0 \partial \phi_k^0} \Big| = 0, \end{aligned} \quad (4.1.23)$$

*i.e.* there are no three-Goldstone couplings.

If we were able to work at the true minimum of the potential and with self-consistent values of all the parameters then this would be sufficient. However, we must use the minimum conditions to determine the parameters – a subset of the mass-squared parameters, in our case – and this means that the above equations will be violated by loop corrections. In particular, the mass-squared parameter – in the diagonal basis – for the would-be Goldstone boson is no longer zero. To see this, let us define the loop tadpoles

$$\delta_i \equiv \frac{1}{v_i} \frac{\partial \Delta V}{\partial \phi_i^0} \Big|_{\phi_i^0=0} \quad (4.1.24)$$

so that we can solve (2.4.12) with the commonly-made choice of

$$m_{ij}^2 = -\delta_i \delta_{ij} + \hat{m}_{0,ij}^2. \quad (4.1.25)$$

Note that this is the value at the minimum of the potential – so  $\delta_i$  is *not* regarded as a function of  $\{\phi_i^0\}$  when we take derivatives below. Now

$$m_G^2 = (R^T m^2 R)_{GG} = -\sum_i \tilde{R}_{iG}^2 \delta_i + \mathcal{O}(2 \text{ loops}), \quad (4.1.26)$$

*i.e.* we can use the tree-level rotation matrices to obtain the Goldstone mass from the loop tadpoles up to corrections of two-loop order, which is all we shall require in the following. This generalises, for example, equations (2.26) and (2.27) of [33].

Following equation (4.1.23) above, we then see that

$$\tilde{\lambda}^{GG'G''} = 0, \quad \lambda^{GG'G''} = \mathcal{O}(1 \text{ loop}) \quad (4.1.27)$$

in general. This is a crucial result in the following, even if in theories that preserve CP both couplings are zero to all orders. For theories breaking CP that could generate such a term at one or two loops, when we expand the potential as a series in  $m_G^2$  as in section 4.1.1 (justified by it being a one-loop quantity) we shall *also implicitly expand the Goldstone self-coupling*  $\lambda^{GG'G''}$  for the same reason; implicitly because we shall not need the higher-order terms and this just corresponds to setting  $\lambda^{GG'G''} = 0$  everywhere. Note that this is automatic once we also employ re-expansion of the tadpoles and masses in terms of tree-level parameters to obtain consistent tadpole equations in section 4.4.

In practice when we are considering the broken gauge groups to be  $SU(2) \times U(1)_Y$  the unbroken  $U(1)_{\text{QED}}$  allows the Goldstones to be separated into one neutral and one (complex) charged Goldstone that cannot mix. Hence in the following to simplify the notation we will restrict to a single neutral Goldstone boson and drop the lower index  $G$ , but the treatment of the charged Goldstone is identical. In this case we can also write  $\epsilon^G \alpha_i^G \rightarrow a_{ij} \phi_j^0$  and thus  $R_{jG} = \frac{a_{ij} v_j}{\sqrt{a_{ij} a_{ik} v_j v_k}}$  (where we now allow the normalisation of  $a_{ij} v_j$  to be arbitrary) for the linearly realised symmetries considered here.

### 4.1.3 Small $m_G^2$ expansion of the effective potential for general theories

To close this section we can now apply the notation and machinery from the previous subsections to resum the general effective potential at two loops, generalising the procedure of [28, 29].

The total potential up to two loops expands as

$$V_{\text{eff}} = V^{(0)} + \frac{1}{16\pi^2} V^{(1)} + \frac{1}{(16\pi^2)^2} V^{(2)}. \quad (4.1.28)$$

For use in the elimination of the infrared divergences in the derivatives of the effective potential, we expand  $V_{\text{eff}}$  for small  $m_G^2$ . More precisely, we want to write the two-loop part of  $V_{\text{eff}}$  as

$$V^{(2)} = V^{(2)}|_{m_G=0} + \frac{1}{2} A(m_G^2) \Delta_1 + \frac{1}{2} m_G^2 \Omega + \mathcal{O}(m_G^4), \quad (4.1.29)$$

where the quantities  $\Delta_1$  and  $\Omega$  are to be determined.

The two-loop potential splits into contributions [19]:

$$\begin{aligned} V^{(2)} = & V_{SSS}^{(2)} + V_{SS}^{(2)} + V_{FFS}^{(2)} + V_{\overline{F}FS}^{(2)} + V_{SSV}^{(2)} + V_{SV}^{(2)} + V_{VV}^{(2)} \\ & + \left( V_{FFV}^{(2)} + V_{\overline{F}FV}^{(2)} + V_{\text{gauge}}^{(2)} \right) \end{aligned} \quad (4.1.30)$$

where the subscripts denote the propagators in the loops as scalar, fermion or vector (gauge sector). The terms in the brackets will not be resummed (since they contain no scalars) and so can be taken to be unchanged from the expressions in [19]. The loop functions appearing in the other terms are recalled in the  $\overline{\text{MS}}$  and  $\overline{\text{DR}}'$  schemes and Landau gauge in appendix B.1.1.2.

First, the scalar contributions to the effective potential at two-loop order  $V_S^{(2)} \equiv V_{SSS}^{(2)} + V_{SS}^{(2)}$  read

$$V_{SSS}^{(2)} \equiv \frac{1}{12}(\lambda^{ijk})^2 f_{SSS}(m_i^2, m_j^2, m_k^2), \quad (4.1.31)$$

$$V_{SS}^{(2)} \equiv \frac{1}{8}\lambda^{iijj} f_{SS}(m_i^2, m_j^2), \quad (4.1.32)$$

and these functions can be expanded using formulae (3.7), (3.8) of [33]. Separating terms with one or more Goldstone bosons from the terms without any, and using the fact that  $\lambda^{GGG}$  vanishes at leading order – see the discussion around equation (4.1.27) – we find the expansion of  $V_S^{(2)}$ :

$$\begin{aligned} V_S^{(2)} = & V_S^{(2)}|_{\text{no GB}} + \sum_{j,k \neq G} \frac{1}{4}(\lambda^{Gjk})^2 f_{SSS}(0, m_j^2, m_k^2) + \sum_{k \neq G} \frac{1}{4}(\lambda^{GGk})^2 f_{SSS}(0, 0, m_k^2) \\ & + A(m_G^2) \left( \sum_{j,k \neq G} \frac{1}{4}(\lambda^{Gjk})^2 P_{SS}(m_j^2, m_k^2) + \sum_{j \neq G} \frac{1}{4}\lambda^{GGjj} A(m_j^2) \right. \\ & \quad \left. + \sum_{k \neq G} \frac{1}{2}(\lambda^{GGk})^2 P_{SS}(0, m_k^2) \right) \\ & + m_G^2 \left( \sum_{j,k \neq G} \frac{1}{4}(\lambda^{Gjk})^2 R_{SS}(m_j^2, m_k^2) + \sum_{k \neq G} \frac{1}{2}(\lambda^{GGk})^2 R_{SS}(0, m_k^2) \right) + \mathcal{O}(m_G^4), \end{aligned} \quad (4.1.33)$$

from which we can identify the scalar part of  $\Delta_1$  and  $\Omega$

$$\begin{aligned} (\Delta_1)_S = & \sum_{j,k \neq G} \frac{1}{2}(\lambda^{Gjk})^2 P_{SS}(m_j^2, m_k^2) + \sum_{j \neq G} \frac{1}{2}\lambda^{GGjj} A(m_j^2) + \sum_{k \neq G} (\lambda^{GGk})^2 P_{SS}(0, m_k^2), \\ \Omega_S = & \sum_{j,k \neq G} \frac{1}{2}(\lambda^{Gjk})^2 R_{SS}(m_j^2, m_k^2) + \sum_{k \neq G} (\lambda^{GGk})^2 R_{SS}(0, m_k^2). \end{aligned} \quad (4.1.34)$$

Next, the terms in  $V^{(2)}$  involving fermions and scalars are

$$V_{FFS}^{(2)} \equiv \frac{1}{2}y^{IJk} y_{IJk} f_{FFS}(m_I^2, m_J^2, m_k^2), \quad (4.1.35)$$

$$V_{\overline{FF}S}^{(2)} \equiv \frac{1}{2}\text{Re} \left[ y^{IJk} y^{I'J'k} M_{II'}^* M_{JJ'}^* \right] f_{\overline{FF}S}(m_I^2, m_J^2, m_k^2). \quad (4.1.36)$$

Here, there are only two cases to consider, either  $k \neq G$  or  $k = G$ , and for the latter case, we can use eqs. (3.9) and (3.10) from [33] to expand the loop functions for small  $m_G^2$ . We then obtain for  $(\Delta_1)_{FS}$  and  $\Omega_{FS}$

$$(\Delta_1)_{FS} = y^{IJG} y_{IJG} P_{FF}(m_I^2, m_J^2) + \text{Re} \left[ y^{IJG} y^{I'J'G} M_{II'}^* M_{JJ'}^* \right] P_{\overline{FF}}(m_I^2, m_J^2), \quad (4.1.37)$$

$$\Omega_{FS} = y^{IJG} y_{IJG} R_{FF}(m_I^2, m_J^2) + \text{Re} \left[ y^{IJG} y^{I'J'G} M_{II'}^* M_{JJ'}^* \right] R_{\overline{FF}}(m_I^2, m_J^2). \quad (4.1.38)$$

Finally, the terms with scalars and gauge bosons read

$$V_{SSV}^{(2)} = \frac{1}{4}(g^{aij})^2 f_{SSV}(m_i^2, m_j^2, m_a^2), \quad (4.1.39)$$

$$V_{VS}^{(2)} = \frac{1}{4}g^{aaii} f_{VS}(m_a^2, m_i^2), \quad (4.1.40)$$

$$V_{VVS}^{(2)} = \frac{1}{4}(g^{abi})^2 f_{VVS}(m_a^2, m_b^2, m_i^2). \quad (4.1.41)$$

As previously, we can expand these terms and separate the contributions of the Goldstone boson, and we find

$$(\Delta_1)_{VS} = \frac{3}{2}g^{aaGG}A(m_a^2) + \frac{1}{2}(g^{abG})^2P_{VV}(m_a^2, m_b^2), \quad (4.1.42)$$

$$\Omega_{VS} = (g^{aGj})^2R_{SV}(m_j^2, m_a^2) + (g^{aGG})^2R_{SV}(0, m_a^2) + \frac{1}{2}(g^{abG})^2R_{VV}(m_a^2, m_b^2). \quad (4.1.43)$$

The expansion (4.1.29) of  $V^{(2)}$  enables us to rewrite the two-loop effective potential after resummation of the leading Goldstone boson contributions as

$$\begin{aligned} \hat{V}_{\text{eff}} &= V^{(0)} + \frac{1}{16\pi^2} \left( V^{(1)}|_{m_G^2=0} + f(m_G^2 + \Delta_G) \right) + \frac{1}{(16\pi^2)^2} \left( V^{(2)}|_{m_G^2=0} + \frac{1}{2}\Omega m_G^2 \right), \\ \Omega &= \Omega_S + \Omega_{FS} + \Omega_{VS}, \\ \Delta_G &\equiv \sum_i R_{iG}^2 \frac{1}{v_i} \frac{\partial \hat{V}_{\text{eff}}}{\partial \phi_i^0} = \frac{1}{16\pi^2} \left[ (\Delta_1)_S + (\Delta_1)_{FS} + (\Delta_1)_{VS} \right] + \mathcal{O}(2 \text{ loop}). \end{aligned} \quad (4.1.44)$$

The minimum of this potential will be found at  $m_G^2 + \Delta_G = 0$  (along with the minimisation conditions for the additional scalars) and clearly contains no logarithmic divergences for small  $m_G^2$ .

The above expression could now be used for studies of general theories: the simplest would be for numerical studies where the potential is evaluated as a function of the expectation values and the derivatives taken numerically, as performed for the MSSM in [32,173] and implemented generally in [250]. However, there are potential numerical instabilities when the expectation values of additional scalars are small, and for complicated models many evaluations of the potential are required which can be slow: it is therefore useful to have explicit expressions for the tadpoles, as were derived at two loops in [21]. In the next section we shall compute these for the resummed potential.

## 4.2 Removing infra-red divergences in the minimum condition

In the previous section we derived the resummed two-loop effective potential expanded in  $m_G^2$  that explicitly contains no infra-red divergences in its derivatives. In this section we shall present these derivatives. However, we shall also present a new approach to the problem which allows us to calculate the derivatives simply, and so we shall also give our derivations. For the scalar-only diagrams we do this by three methods:

- (i) The first method is to generalise the approach of [29,33], and simply take the derivatives of the resummed potential (4.1.44). However, this has the disadvantage of requiring us to compute the derivative of the rotation matrix elements  $\left. \frac{\partial R_{ij}}{\partial \phi_r^0} \right|_{\varphi=v}$  and proves to be cumbersome: there are dramatic simplifications in the final result.
- (ii) To avoid the derivatives of rotation matrix elements, we instead take the derivatives of  $\hat{V}_{\text{eff}}$  before diagonalising the mass matrix and singling out the Goldstone boson and expanding the potential in  $m_G^2$ . This leads to a simpler derivation of the results.



- (iii) For our third method, we introduce a new approach: we set the Goldstone boson mass “on-shell” in the (non-resummed) effective potential. We shall show that this gives the same result as the other methods but (much) more simply, and does not suffer from the problem of needing to exclude Goldstone self interactions by hand. Furthermore, in the next section we shall employ this approach to compute the mass digrams, which would be more complicated using the alternative methods.

## 4.2.1 All-scalar diagrams

### 4.2.1.1 Elimination of the divergences by method (i)

Generalising the approach of [33] to extract the tadpoles we take the derivatives of equation (4.1.33). Starting with the one-loop potential, we note that, since  $m_G^2 + \Delta_G = 0$  at the minimum, the derivative of  $f(m_G^2 + \Delta_G)$  will vanish. Hence we only require

$$\frac{\partial \hat{V}_S^{(1)}}{\partial \phi_r^0} = \sum_{i \neq G} \frac{1}{2} A(m_i^2) \lambda^{iik} R_{rk}. \quad (4.2.1)$$

Note that throughout we shall adopt the Einstein convention for summing repeated indices when all indices are to be summed over; when there is an index that is summed over only a subset (*i.e.* excluding the Goldstone boson indices) we shall write an explicit sum symbol.

For the two-loop terms, recall the scalar part

$$\begin{aligned} \hat{V}_S^{(2)} = & V_{SSS}^{(2)}|_{\text{no GB}} + \sum_{j,k \neq G} \frac{1}{4} (\lambda^{Gjk})^2 f_{SSS}(0, m_j^2, m_k^2) + \sum_{k \neq G} \frac{1}{4} (\lambda^{GGk})^2 f_{SSS}(0, 0, m_k^2) \\ & + V_{SS}^{(2)}|_{m_G^2=0} + \frac{1}{2} \Omega_S m_G^2. \end{aligned} \quad (4.2.2)$$

Treating each of these pieces in turn we find:

$$\begin{aligned} \frac{\partial V_{SSS}^{(2)}|_{\text{no GB}}}{\partial \phi_r^0} &= \sum_{i,j,k \neq G} \left[ \frac{1}{4} \lambda^{iil} R_{rl} (\lambda^{ijk})^2 f_{SSS}^{(1,0,0)}(m_i^2, m_i^2; m_j^2, m_k^2) \right. \\ &\quad + \frac{1}{2} \lambda^{ijk} \lambda^{i'jk} (R^T \partial_r R)_{i'i} f_{SSS}(m_i^2, m_j^2, m_k^2) \\ &\quad \left. + \frac{1}{6} \lambda^{ijk} \lambda^{ii'jk} R_{ri'} f_{SSS}(m_i^2, m_j^2, m_k^2) \right] \\ &= R_{rl} \sum_{i,j,k \neq G} \left[ \frac{1}{4} \lambda^{ijk} \lambda^{i'jk} \lambda^{ii'l} U_0(m_i^2, m_{i'}^2; m_j^2, m_k^2) \right. \\ &\quad \left. - \frac{1}{6} \lambda^{ijk} \lambda^{iljk} I(m_i^2, m_j^2, m_k^2) \right] \end{aligned} \quad (4.2.3)$$

and similarly we see

$$\begin{aligned} \frac{\partial}{\partial \phi_r^0} \sum_{j,k \neq G} \frac{1}{4} (\lambda^{Gjk})^2 f_{SSS}(0, m_j^2, m_k^2) &= R_{rl} \sum_{j,k \neq G} \left[ -\frac{1}{2} \lambda^{Gjk} \lambda^{Gljk} I(0, m_j^2, m_k^2) \right. \\ &\quad \left. + \frac{1}{4} \lambda^{Gjk} \lambda^{Gj'k} \lambda^{jj'l} U_0(m_j^2, m_{j'}^2; 0, m_k^2) \right], \end{aligned} \quad (4.2.4)$$

$$\begin{aligned} \frac{\partial}{\partial \phi_r^0} \sum_{k \neq G} \frac{1}{4} (\lambda^{GGk})^2 f_{SSS}(0, 0, m_k^2) &= R_{rl} \sum_{k \neq G} \left[ -\frac{1}{2} \lambda^{GGk} \lambda^{GGlk} I(0, 0, m_k^2) \right. \\ &\quad \left. + \frac{1}{4} \lambda^{GGk} \lambda^{GGk'} \lambda^{kk'l} U_0(m_k^2, m_{k'}^2; 0, 0) \right]. \end{aligned} \quad (4.2.5)$$

Putting this all together we see that they combine to give the compact expression

$$\begin{aligned} \frac{\partial V_{SSS}^{(2)}|_{m_G^2=0}}{\partial \phi_r^0} &= R_{rl} \sum_{i \neq G, j, k} \left[ \sum_{i'} \frac{1}{4} \lambda^{ijk} \lambda^{i'jk} \lambda^{ii'l} U_0(m_i^2, m_{i'}^2; m_j^2, m_k^2) \right. \\ &\quad \left. - \frac{1}{6} \lambda^{ijk} \lambda^{iljk} I(m_i^2, m_j^2, m_k^2) \right] \Big|_{m_G^2 \rightarrow 0}. \end{aligned} \quad (4.2.6)$$

Next we turn to the  $SS$  terms:

$$\begin{aligned} \frac{\partial V_{SS}^{(2)}|_{m_G^2=0}}{\partial \phi_r^0} &= R_{rl} \sum_{i,j \neq G} \left[ -\frac{1}{4} \lambda^{iijj} \lambda^{iil} B(0, m_i^2, m_i^2) A(m_j^2) \right. \\ &\quad \left. + \frac{1}{2} \lambda^{ii'jj} (R^T \partial_r R)_{i'i} A(m_i^2) A(m_j^2) \right] \\ &= \frac{1}{4} R_{rl} \sum_{i,j \neq G} \lambda^{ii'jj} \lambda^{iil} P_{SS}(m_i^2, m_{i'}^2) A(m_j^2) \Big|_{m_G^2=0}, \end{aligned} \quad (4.2.7)$$

where the two terms again combine into a single compact expression. The final piece is

$$\frac{1}{2} \Omega_S \frac{\partial m_G^2}{\partial \phi_r^0} = \lambda^{GGl} R_{Gl} \sum_{(j,k) \neq (G,G)} \frac{1}{4} (\lambda^{Gjk})^2 R_{SS}(m_j^2, m_k^2) \Big|_{m_G^2=0}, \quad (4.2.8)$$

using the expression of  $\Omega_S$  from eq. (4.1.34). The total scalar tadpole is then the sum of equations (4.2.6), (4.2.7) and (4.2.8). Clearly the simplicity of the final result compared to the intermediate expressions implies that there should be a simpler way of deriving it – as indeed we shall show.

#### 4.2.1.2 Elimination of the divergences by method (ii)

From inspection it is clear that the one-loop tadpole is not divergent when we send  $m_G^2 \rightarrow 0$ . However, at two loops we found that the process of isolating the divergences in the potential, expanding it in the Goldstone mass, and then taking the derivatives was rather cumbersome due to the derivatives of the mixing matrix elements  $R_{ij}$ . Instead we could consider taking the derivatives before having cancelled out the divergent parts, and then ensure the cancellations later. Hence we rewrite the resummed effective potential as

$$\hat{V}_{\text{eff}} = V_{\text{eff}} + \frac{1}{16\pi^2} (f(m_G^2 + \Delta_G) - f(m_G^2)) - \frac{1}{16\pi^2} \frac{1}{2} A(m_G^2) \Delta_G, \quad (4.2.9)$$

using formulae (4.1.29) and (4.1.44). We expect the terms from the derivative of  $-\frac{1}{2}A(m_G^2)\Delta_G$  to cancel off the IR divergences in the derivatives of  $V_{\text{eff}}$ . To show this, we use the expression of  $\Delta_G$  derived in eq. (4.1.34). The relevant contribution to the minimum condition at two-loop order is

$$\begin{aligned} 16\pi^2 \frac{\partial}{\partial \phi_r^0} \left( -\frac{1}{2}A(m_G^2)\Delta_G \right) \Big|_{\varphi=v} &\supset -\frac{1}{2} \frac{\partial m_G^2}{\partial \phi_r^0} \Big|_{\varphi=v} \overline{\log} m_G^2 (\Delta_1)_S \\ &= -\frac{1}{2} R_{rp} \lambda^{GGp} \overline{\log} m_G^2 \left( \sum_{(j,k) \neq (G,G)} \frac{1}{2} (\lambda^{Gjk})^2 P_{SS}(m_j^2, m_k^2) + \sum_{j \neq G} \frac{1}{2} \lambda^{GGjj} A(m_j^2) \right). \end{aligned} \quad (4.2.10)$$

The purely scalar contribution to the *non-resummed* tadpoles is, at one-loop order

$$\frac{\partial V_S^{(1)}}{\partial \phi_r^0} \Big|_{\varphi=v} = \frac{1}{2} R_{rk} \lambda^{iik} A(m_i^2) \quad (4.2.11)$$

and at two loops

$$\frac{\partial V_S^{(2)}}{\partial \phi_r^0} \Big|_{\varphi=v} = R_{rp} (T_{SS}^p + T_{SSS}^p + T_{SSSS}^p), \quad (4.2.12)$$

where [21]

$$T_{SS}^p = \frac{1}{4} \lambda^{jkl} \lambda^{jkl} f_{SS}^{(1,0)}(m_j^2, m_k^2; m_l^2) = \frac{1}{4} \lambda^{jkl} \lambda^{jkl} P_{SS}(m_j^2, m_k^2) A(m_l^2), \quad (4.2.13)$$

$$T_{SSS}^p = \frac{1}{6} \lambda^{pjkl} \lambda^{jkl} f_{SSS}(m_j^2, m_k^2, m_l^2) = -\frac{1}{6} \lambda^{pjkl} \lambda^{jkl} I(m_j^2, m_k^2, m_l^2), \quad (4.2.14)$$

$$T_{SSSS}^p = \frac{1}{4} \lambda^{pj j'} \lambda^{jkl} \lambda^{j'kl} f_{SSSS}^{(1,0,0)}(m_j^2, m_{j'}^2; m_k^2, m_l^2) = \frac{1}{4} \lambda^{pj j'} \lambda^{jkl} \lambda^{j'kl} U_0(m_j^2, m_{j'}^2; m_k^2, m_l^2), \quad (4.2.15)$$

with the notation  $f_\alpha^{(1,0,0)}$  defined in eq. (B.1.40).

In these formulae, we can then consider separately the Goldstone contributions and investigate the divergent terms. We find two types of divergent terms in eq. (4.2.12) :

- The first type of divergent term comes from  $T_{SS}$ , for  $j = k = G$ , and<sup>3</sup>  $l \neq G$ , and reads

$$\begin{aligned} \frac{\partial V_S^{(2)}}{\partial \phi_r^0} \Big|_{\varphi=v} &\supset -\frac{1}{4} R_{rp} \sum_{l \neq G} \lambda^{GGl} \lambda^{GGp} B_0(m_G^2, m_G^2) A(m_l^2) \\ &= \frac{1}{4} R_{rp} \sum_{l \neq G} \lambda^{GGl} \lambda^{GGp} \overline{\log} m_G^2 A(m_l^2) \end{aligned} \quad (4.2.16)$$

- The other divergent terms, coming from  $T_{SSSS}^p$  with  $j = j' = G$ , are

$$\frac{\partial V_S^{(2)}}{\partial \phi_r^0} \Big|_{\varphi=v} \supset \frac{1}{4} R_{rp} \lambda^{pGG} \lambda^{Gkl} \lambda^{Gkl} \overline{\log} m_G^2 P_{SS}(m_k^2, m_l^2) \quad (4.2.17)$$

---

<sup>3</sup>The term with  $l = G$  is proportional to  $\overline{\log} m_G^2 A(m_G^2)$ , which tends to zero when  $m_G^2 \rightarrow 0$ .

- A potentially more dangerous element of those terms, for the particular case  $k = l = G$  is not present as  $\lambda^{GGG} = 0$  (at least up to terms of one-loop order).

All the other terms in  $\left. \frac{\partial V_S^{(2)}}{\partial \phi_r^0} \right|_{\varphi=v}$  are regular in the limit  $m_G^2 \rightarrow 0$ .

After relabelling of the indices in the sums, we observe that the  $\overline{\log} m_G^2$  divergences from the terms in eqs. (4.2.16) and (4.2.17) cancel out perfectly with the ones from eq. (4.2.10). We can then take the limit  $m_G^2 \rightarrow 0$  in the one-loop and two-loop parts of the minimum condition: this limit is regular in the one-loop tadpole (4.2.11) so we recover eq. (4.2.1), while we find

$$\begin{aligned} \left. \frac{\partial \hat{V}_S^{(2)}}{\partial \phi_r^0} \right|_{\varphi=v} = & \frac{1}{4} R_{rp} \left\{ \sum_{j,k,l \neq G} \lambda^{jkl} \lambda^{jkl} P_{SS}(m_j^2, m_k^2) A(m_l^2) \right. \\ & \left. + 2 \sum_{k,l \neq G} \lambda^{Gkl} \lambda^{Gkl} P_{SS}(0, m_k^2) A(m_l^2) \right\} \\ & + \frac{1}{6} R_{rp} \lambda^{pjkl} \lambda^{jkl} f_{SSS}(m_j^2, m_k^2, m_l^2) \Big|_{m_G^2 \rightarrow 0} \\ & + \frac{1}{4} R_{rp} \left\{ \sum_{(j,j') \neq (G,G)} \lambda^{pj'j} \lambda^{jkl} \lambda^{j'kl} U_0(m_j^2, m_{j'}^2, m_k^2, m_l^2) \Big|_{m_G^2 \rightarrow 0} \right. \\ & \left. + \sum_{(k,l) \neq (G,G)} \lambda^{pGG} (\lambda^{Gkl})^2 R_{SS}(m_k^2, m_l^2) \Big|_{m_G^2 \rightarrow 0} \right\}, \quad (4.2.18) \end{aligned}$$

at two-loop order. It is important to notice that all three functions  $f_{SSS}$ ,  $U_0$  and  $R_{SS}$  are regular when one of their arguments goes to zero, hence the result we find is indeed free of infrared divergences.

#### 4.2.1.3 Elimination of the divergences by setting the Goldstone boson on-shell

Here we shall introduce a new approach to the Goldstone Boson Catastrophe: we shall treat the Goldstone boson mass as an on-shell parameter and enforce that it is identically zero. This means replacing the dimensionally regularised ( $\overline{\text{DR}}'$  or  $\overline{\text{MS}}$ ) Goldstone mass by the on-shell (or pole) mass in the following way

$$(m_G^2)^{\text{dim. reg}} \equiv (m_G^2)^{\text{OS}} - \Pi_{GG}^{(1)}((m_G^2)^{\text{OS}}) = -\Pi_{GG}^{(1)}(0) \quad (4.2.19)$$

where the pole mass is  $(m_G^2)^{\text{OS}} = 0$ . Note that we only need the one-loop relation here, so any mixing in the mass terms between the Goldstone boson and other (pseudo-)scalars is irrelevant – it would be proportional to  $(\Pi_{iG}^{(1)})^2$  and thus a two-loop effect. When we write the effective potential in terms of the on-shell Goldstone boson mass we should find that it is free of divergences. To do this, we shall start from the dimensionally regularised potential and substitute the Goldstone boson mass in equation (4.2.19), expanding out to the appropriate loop order; this gives the result that we would obtain by performing the calculation using the on-shell mass with the appropriate counterterms. For our case, we only need to use the one-loop self-energy

in the one-loop tadpole; the scalar contribution to the Goldstone boson self-energy at one-loop order is

$$\Pi_{GG}^{(1),S}(p^2) = \frac{1}{2}\lambda^{GGjj}A(m_j^2) - \frac{1}{2}(\lambda^{Gjk})^2B(p^2, m_j^2, m_k^2) \quad (4.2.20)$$

where we again require the result  $\lambda^{GGG} = 0$  to leading order – although in this case we could (if desired) make it an on-shell condition. Applying the above relation to the tadpole in eq. (4.2.11) we obtain the following shift to the two-loop tadpole:

$$\begin{aligned} \frac{1}{2}R_{rp}\lambda^{GGp}A(m_G^2) &= \frac{1}{2}R_{rp}\lambda^{GGp}A((m_G^2)^{\text{OS}}) - \frac{1}{2}R_{rp}\lambda^{GGp}\overline{\log}(m_G^2)^{\text{OS}}\Pi_{GG}^{(1)}((m_G^2)^{\text{OS}}) \\ &\quad + \mathcal{O}(3\text{-loop}) \\ \rightarrow \frac{\partial V_S^{(2)}}{\partial \phi_r^0}((m_G^2)^{\text{OS}}) &= \frac{\partial V_S^{(2)}}{\partial \phi_r^0}\bigg|_{m_G^2 \rightarrow (m_G^2)^{\text{OS}}} \\ &\quad - \frac{1}{4}R_{rp}\lambda^{GGp}\overline{\log}(m_G^2)^{\text{OS}}\left(\lambda^{GGjj}A(m_j^2) - (\lambda^{Gjk})^2B(0, m_j^2, m_k^2)\right). \end{aligned} \quad (4.2.21)$$

Since  $B(0, m_j^2, m_k^2) = -P_{SS}(m_j^2, m_k^2)$ , these shifts correspond exactly to the divergent terms we saw in equations (4.2.16) and (4.2.17) and so when we formally take the limit  $(m_G^2)^{\text{OS}} \rightarrow 0$  we find exactly the same tadpole given explicitly in (4.2.18) that we found by the two other methods. This derivation is certainly much faster than the first method, but note that the principle is different to the previous calculations: there is no ad-hoc resummation, nor are we required to expand the potential as a series in  $m_G^2$ . However, perhaps remarkably, we find exactly the same result for the tadpole that remains, implying that, at least at two loops, the two approaches are equivalent. This new approach will prove to be simpler than both previous methods when we turn our attention to mass diagrams; for now we shall simply complete the set of tadpole equations.

Before moving on to diagrams with fermions, we shall comment on the prescription to follow when there is more than one Goldstone boson. In that case, since the Goldstone bosons are all degenerate the mutual mixing between them becomes a leading-order effect and we must diagonalise the self-energies  $\Pi_{GG'}$  on the subspace of indices  $G, G'$  which run over all Goldstones. However, we can also easily write this in the non-diagonalised basis as a generalisation of (4.2.19):

$$(m_{GG'}^2)^{\text{dim. reg}} \equiv (m_G^2)^{\text{OS}} - \Pi_{GG'}^{(1)}((m_G^2)^{\text{OS}}) = -\Pi_{GG'}^{(1)}(0), \quad (4.2.22)$$

where formally all Goldstone bosons have the same mass  $m_G^2$  which we set to zero. Then we can rewrite the tadpole as

$$\begin{aligned} \frac{1}{2}R_{rp}\lambda^{GG'p}A(m_{GG'}^2) &= \sum_G \frac{1}{2}R_{rp}\lambda^{GGp}A((m_G^2)^{\text{OS}}) \\ &\quad - \sum_{G,G'} \frac{1}{2}R_{rp}\lambda^{GG'p}\overline{\log}(m_G^2)^{\text{OS}}\Pi_{GG'}^{(1)}((m_G^2)^{\text{OS}}) + \mathcal{O}(3\text{-loop}). \end{aligned} \quad (4.2.23)$$

If the gauge group of the model of interest is just that of the Standard Model, then clearly the charged and neutral Goldstone bosons cannot mix, so this becomes trivial – hence in the following we shall restrict for clarity to the one-Goldstone case. However, we shall later write the full result in the general case.

#### 4.2.2 Diagrams with scalars and fermions

The one-loop tadpoles involving fermions are

$$\left. \frac{\partial V_F^{(1)}}{\partial \phi_r^0} \right|_{\varphi=v} = R_{rp} T_F^p = -R_{rp} \text{Re}[y^{KLp} M_{KL}^*] (A(m_K^2) + A(m_L^2)) \quad (4.2.24)$$

and these do not present any divergence in the limit of vanishing Goldstone boson mass. The two-loop contributions are [21],

$$\left. \frac{\partial V_{FS}^{(2)}}{\partial \phi_r^0} \right|_{\varphi=v} = R_{rp} (T_{SSFF}^p + T_{FFFS}^p), \quad (4.2.25)$$

where

$$T_{SSFF}^p = \frac{1}{2} y^{IJk} y_{IJl} \lambda^{klp} f_{FFS}^{(0,0,1)}(m_I^2, m_J^2; m_k^2, m_l^2) - \text{Re} \left[ y^{IJk} y^{I'J'k} M_{II'}^* M_{JJ'}^* \right] \lambda^{klp} U_0(m_k^2, m_l^2, m_I^2, m_J^2), \quad (4.2.26)$$

$$T_{FFFS}^p = 2\text{Re}[y^{IJp} y_{IKn} y^{KLn} M_{JL}^*] T_{F\overline{F}FS}(m_I^2, m_J^2, m_K^2, m_n^2) + 2\text{Re}[y_{IJp} y^{IKn} y^{JLn} M_{KL}^*] T_{FF\overline{F}S}(m_I^2, m_J^2, m_K^2, m_n^2) - 2\text{Re}[y^{IJp} y^{KLn} y^{MPn} M_{IK}^* M_{JM}^* M_{LP}^*] T_{\overline{F}FFS}(m_I^2, m_J^2, m_L^2, m_n^2), \quad (4.2.27)$$

with the loop functions from eq. (II.38) of [21].

The second term  $T_{FFFS}$  is regular when  $m_G^2 \rightarrow 0$ , because the loop functions,  $B_0$ ,  $I$ ,  $U_0$ , that appear in its expression are all regular when only one of their argument goes to zero. However, the  $k = l = G$  terms in  $T_{SSFF}$  are divergent:

$$T_{SSFF}^p \supset \frac{1}{2} y^{IJG} y_{IJG} \lambda^{GGp} \overline{\log m_G^2} P_{FF}(m_I^2, m_J^2) + \frac{1}{2} \text{Re} \left[ y^{IJG} y^{I'J'G} M_{II'}^* M_{JJ'}^* \right] \lambda^{GGp} \overline{\log m_G^2} P_{\overline{F}\overline{F}}(m_I^2, m_J^2). \quad (4.2.28)$$

After either resummation or setting the Goldstone boson on-shell we find the total, finite, two-loop contribution  $T_{SSFF}^p$  in equation (4.2.41) and note that  $T_{FFFS}^p$  is not modified from eq. (4.2.27).

#### 4.2.3 Diagrams with scalars and gauge bosons

The one-loop tadpole involving (massive) gauge bosons is

$$\left. \frac{\partial V_V^{(1)}}{\partial \phi_r^0} \right|_{\varphi=v} = R_{rp} T_V^p = \frac{1}{2} R_{rp} g^{aap} A(m_a^2), \quad (4.2.29)$$

which contains no scalar propagators so has no divergences in the Goldstone boson mass.

However, the gauge boson contribution to the one-loop scalar self-energy in Landau gauge is [20]:

$$\Pi_{ij}^{(1,V)} = g^{aik} g^{ajk} B_{SV}(m_k^2, m_a^2) + \frac{1}{2} g^{aij} A_V(m_a^2) + \frac{1}{2} g^{abi} g^{abj} B_{VV}(m_a^2, m_b^2), \quad (4.2.30)$$

## 4.2 Removing infra-red divergences in the minimum condition

where the loop functions are given in [20, 142] but simplify for zero momentum in Landau gauge to

$$\begin{aligned} B_{SV}(x, y)|_{p^2=0} &= 0, \\ A_V(x)|_{p^2=0} &= 3A(x) + 2x\delta_{\overline{\text{MS}}}, \\ B_{VV}(x, y)|_{p^2=0} &= 3P_{SS}(x, y) + 2\delta_{\overline{\text{MS}}}. \end{aligned} \quad (4.2.31)$$

Recall that there are six scalar-gauge boson contributions to the two-loop tadpole [21]:

$$T_{SSV}^p = \frac{1}{2}g^{aij}g^{akj}\lambda^{ikp}f_{SSV}^{(1,0,0)}(m_i^2, m_k^2, m_j^2, m_a^2) + \frac{1}{4}g^{aij}g^{bij}g^{abp}f_{SSV}^{(0,0,1)}(m_i^2, m_j^2, m_a^2, m_b^2) \quad (4.2.32)$$

$$T_{VS}^p = \frac{1}{4}g^{abii}g^{abp}f_{VS}^{(1,0)}(m_a^2, m_b^2, m_i^2) + \frac{1}{4}g^{aaiik}\lambda^{ikp}f_{VS}^{(0,1)}(m_a^2, m_i^2, m_k^2) \quad (4.2.33)$$

$$T_{VVS}^p = \frac{1}{2}g^{abi}g^{cbi}g^{acp}f_{VVS}^{(1,0,0)}(m_a^2, m_c^2, m_b^2, m_i^2) + \frac{1}{4}g^{abi}g^{abj}\lambda^{ijp}f_{VVS}^{(0,0,1)}(m_a^2, m_b^2, m_i^2, m_j^2). \quad (4.2.34)$$

Of these only three are potentially singular –  $f_{SSV}^{(1,0,0)}$ ,  $f_{VS}^{(0,1)}$  and  $f_{VVS}^{(0,0,1)}$ ; from shifting the tadpoles we obtain

$$\begin{aligned} \Delta T_{SV}^p &= -\frac{1}{2}\lambda^{GGr}\overline{\log}m_G^2\left[g^{aGk}g^{aGk}B_{SV}(m_k^2, m_a^2) \right. \\ &\quad \left. + \frac{1}{2}g^{aaGG}A_V(m_a^2) + \frac{1}{2}g^{abG}g^{abG}B_{VV}(m_a^2, m_b^2)\right] \\ &\equiv \lambda^{GGr}g^{aGk}g^{aGk}\Delta f_{SSV}^{(1,0,0)}(m_G^2, m_G^2, m_k^2, m_a^2) \\ &\quad + \lambda^{GGr}g^{aaGG}\Delta f_{VS}^{(0,1)}(m_a^2, m_G^2, m_G^2) \\ &\quad + \lambda^{GGr}g^{abG}g^{abG}\Delta f_{VVS}^{(0,0,1)}(m_a^2, m_b^2, m_G^2, m_G^2) \end{aligned} \quad (4.2.35)$$

*i.e.* they correspond exactly to the potentially singular terms. However, note that  $B_{SV}$  term is zero – and indeed we find that  $f_{SSV}^{(1,0,0)}(m_G^2, m_G^2, m_k^2, m_a^2)$  is non-singular; we find

$$\begin{aligned} f_{SSV}^{(1,0,0)}(m_G^2, m_G^2, x, y) &= -R_{SV}(x, y) + \mathcal{O}(m_G^2) \\ f_{VS}^{(0,1)}(x, m_G^2, m_G^2) &= (3A(x) + 2x\delta_{\overline{\text{MS}}})\overline{\log}m_G^2 + \mathcal{O}(m_G^2) \\ f_{VVS}^{(0,0,1)}(y, z, m_G^2, m_G^2) &= -(3P_{SS}(y, z) + \delta_{\overline{\text{MS}}})\overline{\log}m_G^2 - R_{VV}(y, z) + \mathcal{O}(m_G^2). \end{aligned} \quad (4.2.36)$$

We give the final finite tadpoles in equation (4.2.44).

### 4.2.4 Total tadpole

Here we gather the results of the previous subsections and rewrite them for the most general case, that of multiple Goldstone bosons. The total tadpole, after curing the Goldstone boson catastrophe and taking  $m_G^2 \rightarrow 0$  everywhere, is

$$\begin{aligned} \frac{\partial \hat{V}^{(2)}}{\partial \phi_r^0} &= R_{rp}\left[\overline{T}_{SS}^p + \overline{T}_{SSS}^p + \overline{T}_{SSSS}^p + \overline{T}_{SSFF}^p + \overline{T}_{FFFS}^p + \overline{T}_{SSV}^p + \overline{T}_{VS}^p + \overline{T}_{VVS}^p \right. \\ &\quad \left. + \overline{T}_{FFV}^p + \overline{T}_{\overline{FFV}}^p + \overline{T}_{\text{gauge}}^p\right]. \end{aligned} \quad (4.2.37)$$

The all-scalar diagrams are

$$\bar{T}_{SS}^p = \frac{1}{4} \sum_{j,k,l \neq G} \lambda^{jkl} \lambda^{jkl} P_{SS}(m_j^2, m_k^2) A(m_l^2) + \frac{1}{2} \sum_{k,l \neq G} \lambda^{Gkl} \lambda^{Gkp} P_{SS}(0, m_k^2) A(m_l^2), \quad (4.2.38)$$

$$\bar{T}_{SSS}^p = \frac{1}{6} \lambda^{pjkl} \lambda^{jkl} f_{SSS}(m_j^2, m_k^2, m_l^2) \Big|_{m_G^2 \rightarrow 0}, \quad (4.2.39)$$

$$\begin{aligned} \bar{T}_{SSSS}^p &= \frac{1}{4} \sum_{(j,j') \neq (G,G')} \lambda^{pj'j'} \lambda^{jkl} \lambda^{j'kl} U_0(m_j^2, m_{j'}^2, m_k^2, m_l^2) \\ &\quad + \frac{1}{4} \sum_{(k,l) \neq (G,G')} \lambda^{pGG'} \lambda^{Gkl} \lambda^{G'kl} R_{SS}(m_k^2, m_l^2), \end{aligned} \quad (4.2.40)$$

where by  $(j, j') \neq (G, G')$  we mean that  $j, j'$  are not both Goldstone indices. The fermion-scalar diagrams are

$$\begin{aligned} \bar{T}_{SSFF}^p &= \sum_{(k,l) \neq (G,G')} \left\{ \frac{1}{2} y^{IJk} y_{IJl} \lambda^{klp} f_{FFS}^{(0,0,1)}(m_I^2, m_J^2; m_k^2, m_l^2) \right. \\ &\quad \left. - \text{Re} \left[ y^{IJk} y^{I'J'k} M_{II'}^* M_{JJ'}^* \right] \lambda^{klp} U_0(m_k^2, m_l^2, m_I^2, m_J^2) \right\} \\ &\quad + \frac{1}{2} \lambda^{GG'p} y^{IJG} y_{IJG'} (-I(m_I^2, m_J^2, 0) - (m_I^2 + m_J^2) R_{SS}(m_I^2, m_J^2)) \\ &\quad - \lambda^{GG'p} \text{Re} \left[ y^{IJG} y^{I'J'G'} M_{II'}^* M_{JJ'}^* \right] R_{SS}(m_I^2, m_J^2), \end{aligned} \quad (4.2.41)$$

$$\bar{T}_{FFFS}^p = T_{FFFS}^p \Big|_{m_G^2 \rightarrow 0}, \quad (4.2.42)$$

while the gauge boson-scalar tadpoles are

$$\begin{aligned} \bar{T}_{SSV}^p &= T_{SSV}^p \Big|_{m_G^2 \rightarrow 0}, \\ \bar{T}_{VS}^p &= \frac{1}{4} g^{abii} g^{abp} f_{VS}^{(1,0)}(m_a^2, m_b^2; m_i^2) \Big|_{m_G^2 \rightarrow 0} + \sum_{(i,k) \neq (G,G')} \frac{1}{4} g^{aai} \lambda^{ikp} f_{VS}^{(0,1)}(m_a^2; m_i^2, m_k^2), \\ \bar{T}_{VVS}^p &= \frac{1}{2} g^{abi} g^{cbi} g^{acp} f_{VVS}^{(1,0,0)}(m_a^2, m_c^2; m_b^2, m_i^2) \Big|_{m_G^2 \rightarrow 0} \\ &\quad + \sum_{(i,j) \neq (G,G')} \frac{1}{4} g^{abi} g^{abj} \lambda^{ijp} f_{VVS}^{(0,0,1)}(m_a^2, m_b^2; m_i^2, m_j^2) \\ &\quad - \frac{1}{4} g^{abG} g^{abG'} \lambda^{GG'p} R_{VV}(m_a^2, m_b^2). \end{aligned} \quad (4.2.43)$$

Finally the gauge boson-fermion and gauge diagrams are not affected by the Goldstone boson catastrophe, as scalar masses do not appear in them, and can be found in the appendix C.2 of [21]

$$\begin{aligned} \bar{T}_{FFV}^p &= 2g_I^{aJ} \bar{g}_{bJ}^K \text{Re}[M_{KI'} y^{I'Ip}] f_{FFV}^{(1,0,0)}(m_I^2, m_K^2; m_J^2, m_a^2) \\ &\quad + \frac{1}{2} g_I^{aJ} \bar{g}_{bJ}^I g^{abp} f_{FFV}^{(0,0,1)}(m_I^2, m_J^2; m_a^2, m_b^2), \end{aligned} \quad (4.2.44)$$

$$\begin{aligned} \bar{T}_{FFV}^p &= g_I^{aJ} g_{I'}^{aJ'} \text{Re}[y^{II'p} M_{JJ'}^*] [f_{FFV}^{(1,0,0)}(m_I^2, m_J^2, m_a^2) + M_I^2 f_{FFV}^{(1,0,0)}(m_I^2, m_{I'}^2; m_J^2, m_a^2)] \\ &\quad + g_I^{aJ} g_{I'}^{aJ'} \text{Re}[M^{IK'} M^{KI'} M_{JJ'}^* y_{KK'p}] f_{FFV}^{(1,0,0)}(m_I^2, m_{I'}^2; m_J^2, m_a^2) \\ &\quad + \frac{1}{2} g_I^{aJ} g_{I'}^{bJ'} g^{abp} M^{II'} M_{JJ'}^* f_{FFV}^{(0,0,1)}(m_I^2, m_J^2; m_a^2, m_b^2), \end{aligned} \quad (4.2.45)$$

$$\bar{T}_{\text{gauge}}^p = \frac{1}{4} g^{abc} g^{dbc} g^{adp} f_{\text{gauge}}^{(1,0,0)}(m_a^2, m_d^2; m_b^2, m_c^2). \quad (4.2.46)$$



### 4.3 Mass diagrams in the gaugeless limit

As discussed in the introduction, the scalar masses are among the most interesting electroweak precision observables, and their calculation also suffers from the Goldstone Boson Catastrophe. Earlier literature pointed out that the calculation in the effective potential approximation contains more severe divergences that cannot be solved by re-summation, and thus the inclusion of the external momentum is necessary. However, we shall find that there are also divergences that are not regulated by external momentum – and thus both setting the Goldstone boson on-shell *and* external momentum are required to obtain finite, accurate results.

On the other hand, the effective potential approximation is still useful and has advantages over a full momentum-dependent result, chief among these being simplicity and speed of calculation. In particular, the evaluation of the loop functions at arbitrary external momentum requires the numerical solution of differential equations [142] which, although implemented in the fast package **TSIL** [150], is still much slower than the zero-momentum functions, and when the functions must be repeatedly called can lead to times orders of magnitude longer for complicated models. Hence we shall consider expanding the two-loop self-energies as a series in  $s \equiv -p^2$  (for metric signature  $(-, +, +, +)$ ) as

$$\begin{aligned} \Pi_{ij}^{(2)}(s) = & \frac{\overline{\log}(-s)}{s} \Pi_{-1l,ij}^{(2)} + \frac{1}{s} \Pi_{-1,ij}^{(2)} + \Pi_{l^2,ij}^{(2)} \overline{\log}^2(-s) + \Pi_{l,ij}^{(2)} \overline{\log}(-s) + \Pi_{0,ij}^{(2)} \\ & + \sum_{k=1}^{\infty} \Pi_{k,ij}^{(2)} \frac{s^k}{k!} \end{aligned} \quad (4.3.1)$$

and we shall neglect terms of  $\mathcal{O}(s)$ , giving a “generalised effective potential” approximation: for loop functions where the singular terms  $\Pi_{-1l,ij}^{(2)}, \Pi_{-1,ij}^{(2)}, \Pi_{l^2,ij}^{(2)}, \Pi_{l,ij}^{(2)}$  vanish the result is identical to the second derivative of the effective potential. This approximation is particularly good when the mass of the scalars considered is smaller than the scale of other particles that they couple to; but even when they are similar we find that typically the difference is only a few percent. This should then be within other uncertainties in the calculation for most purposes.

We shall perform our calculations using our procedure of taking the Goldstone boson mass(es) on-shell as before, working in the general case now of allowing multiple Goldstone bosons throughout. We shall make heavy use of the existing expressions for two-loop scalar self energies from [20]; however, these are only available up to second order in the gauge coupling. Hence we shall be restricted to work in the very popular “gaugeless limit” where we neglect the gauge couplings of broken gauge groups (including electromagnetism, since hypercharge and weak  $SU(2)$  are both broken so their gauge couplings are neglected). The two-loop self-energy in this limit can be decomposed as follows:

$$\Pi_{ij}^{(2)} = \Pi_{ij}^S + \Pi_{ij}^{SF(W)} + \Pi_{ij}^{SF_4(M)} + \Pi_{ij}^{S_2F_3(M)} + \Pi_{ij}^{S_3F_2(V)} + \Pi_{ij}^{SF_4(V)} + \Pi_{ij}^{SV} + \Pi_{ij}^{FV}. \quad (4.3.2)$$

This consists of scalar-only propagators, diagrams with scalar and fermion propagators, diagrams with scalar and vector propagators, and fermions and vectors. We find that  $\Pi_{ij}^{SF_4(M)}$  and  $\Pi_{ij}^{SF_4(V)}$  are nonsingular as  $m_G^2 \rightarrow 0$  and  $s \rightarrow 0$ , so the relevant formulae in that limit are equations (B.15) and (B.28) of [21]. Furthermore, in the gaugeless limit the Goldstone bosons do not couple to the vectors, so  $\Pi_{ij}^{SV}$

and  $\Pi_{ij}^{FV}$  are unchanged from (B.36) and (B.41) of [21]. However, the remaining diagrams require regulation: our new expressions for  $\Pi_{ij}^S$  are presented in section 4.3.1;  $\Pi_{ij}^{SF(W)}$ ,  $\Pi_{ij}^{S_2F_3(M)}$  and  $\Pi_{ij}^{S_3F_2(V)}$  are derived in section 4.3.2.

### 4.3.1 All-scalar terms

The two-loop scalar self-energy contribution with only scalar propagators is given by [20]:

$$\begin{aligned}
\Pi_{ij}^S = & \frac{1}{4} \lambda^{ijkl} \lambda^{kmn} \lambda^{lmn} W_{SSSS}(m_k^2, m_l^2, m_m^2, m_n^2) \\
& + \frac{1}{4} \lambda^{ijkl} \lambda^{klmm} X_{SSS}(m_k^2, m_l^2, m_m^2) \\
& + \frac{1}{2} \lambda^{ikl} \lambda^{jkm} \lambda^{lmnn} Y_{SSSS}(m_k^2, m_l^2, m_m^2, m_n^2) \\
& + \frac{1}{4} \lambda^{ikl} \lambda^{jmn} \lambda^{klmn} Z_{SSSS}(m_k^2, m_l^2, m_m^2, m_n^2) \\
& + \frac{1}{6} \lambda^{iklm} \lambda^{jklm} S_{SSS}(m_k^2, m_l^2, m_m^2) \\
& + \frac{1}{2} \left( \lambda^{ikl} \lambda^{jkmn} + \lambda^{jkl} \lambda^{ikmn} \right) \lambda^{lmn} U_{SSSS}(m_k^2, m_l^2, m_m^2, m_n^2) \\
& + \frac{1}{2} \lambda^{ikl} \lambda^{jkm} \lambda^{lnp} \lambda^{mnp} V_{SSSSS}(m_k^2, m_l^2, m_m^2, m_n^2, m_p^2) \\
& + \frac{1}{2} \lambda^{ikm} \lambda^{jln} \lambda^{klp} \lambda^{mnp} M_{SSSSS}(m_k^2, m_l^2, m_m^2, m_n^2, m_p^2). \tag{4.3.3}
\end{aligned}$$

The loop integral functions are recalled in (B.1.52).

When at most one of the propagators is a Goldstone boson, we can set  $m_G^2 \rightarrow 0, s \rightarrow 0$  and use the simplified expressions below (B.2) of [21]. However, for cases including more Goldstone bosons we must look for singularities since, in general, only the  $S_{SSS}$  term is regular. Furthermore, we can divide the functions into those regulated by the momentum and those that are not. In particular, by inspection we see that for two or more Goldstone bosons  $W, X, Y, V$  can be divergent as  $m_G^2 \rightarrow 0$ , *even for finite momentum*; this means those terms must be regulated by resummation – or, in our case, by shifts from the one-loop self energy by putting the Goldstone bosons on shell. On the other hand, the terms  $U, M$  and  $Z$  must be regulated by including finite momentum.

It should be noted that the divergences that are not regulated by momentum all involve a Goldstone boson self-energy as a subdiagram. It is then logical to consider how they relate to the divergent terms in the tadpole graphs. If we consider the effective potential approximation and take the derivatives of the tadpoles as in [21], then we see that the topologies  $X, Y, Z$  descend from the  $T_{SS}$  graphs;  $S, U$  arise from  $T_{SSS}$ ; and  $M, V, W$  from  $T_{SSSS}$ . Then it is clear that, since the  $T_{SSS}$  graphs contain no divergences, resummation is irrelevant for  $S$  and  $U$ , while  $T_{SS}$  and  $T_{SSSS}$  are both divergent when there is part of a Goldstone boson self-energy as a subdiagram. We also see that  $W$  and  $X$  topologies arise from  $T_{SSSS}$  and  $T_{SS}$  respectively by replacing a three-point vertex with a four-point one, and likewise  $V$  and  $Y$  arise by adding a leg connected directly by a propagator to the other leg; we illustrate this whole discussion in figure 4.1. Hence we expect that these special divergences should follow the same pattern as the tadpoles, and be cured in the same way. However, we shall also find below some subtleties remain in the  $V$  topology.

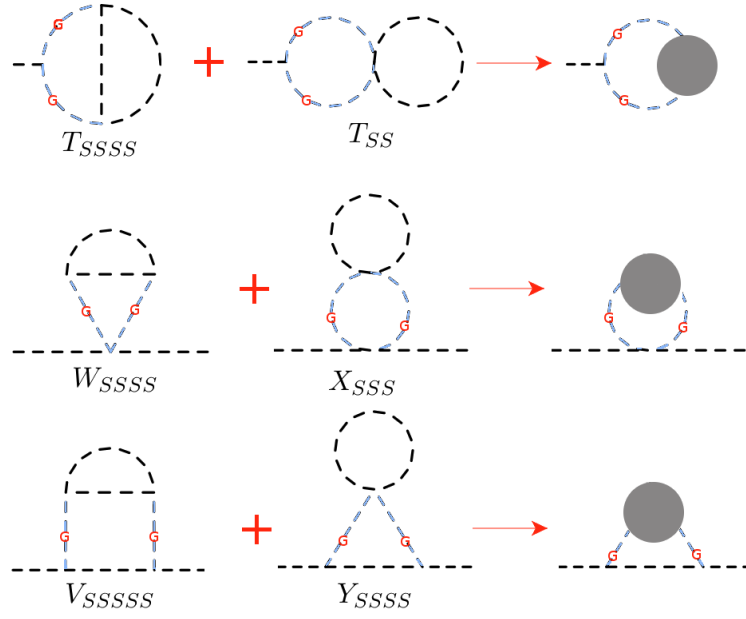


Figure 4.1 – Divergent scalar-only diagrams that require regulation (by resummation or using our on-shell scheme), even in the presence of external momentum. The light blue dashed lines marked with a small red “G” denote Goldstone boson propagators. The dark blobs in the diagrams on the right-hand side represent full one-loop one-particle-irreducible corrections inserted on the line. On the top line we show the tadpoles (with their clear relation to the sunset and figure-eight diagrams in the potential); on the lower two we show the corrections to the self-energies, which clearly follow the same pattern.

#### 4.3.1.1 Goldstone shifts

To determine the effect on the mass diagrams, let us make the shifts using the method of an on-shell Goldstone boson. Recall that the contribution to the one-loop self-energy is

$$\Pi_{ij}^{(1),S}(s) = \frac{1}{2}\lambda^{ijkk}A(m_k^2) - \frac{1}{2}\lambda^{ikl}\lambda^{jkl}B(s, m_k^2, m_l^2) \quad (4.3.4)$$

so we can write  $\Pi_{ij}^S \rightarrow \Pi_{ij}^S + \Delta\Pi_{ij}^S$  where

$$\begin{aligned} \Delta\Pi_{ij}^S &= -\frac{1}{2}\lambda^{ijGG'}\overline{\log m_G^2}\Pi_{GG'}^{(1),S}(0) + \lambda^{iGl}\lambda^{jG'l}B'(s, m_G^2, m_l^2)\Pi_{GG'}^{(1),S}(0) \\ &\equiv \frac{1}{4}\lambda^{ijGG'}\lambda^{GG'kk}\Delta X_{SSS}(m_G^2, m_G^2, m_k^2) \\ &\quad + \frac{1}{4}\lambda^{ijGG'}\lambda^{Gmn}\lambda^{G'mn}\Delta W_{SSSS}(m_G^2, m_G^2, m_m^2, m_n^2) \\ &\quad + \frac{1}{2}\lambda^{iGk}\lambda^{jG'k}\lambda^{GG'nn}\Delta Y_{SSSS}(m_k^2, m_G^2, m_G^2, m_n^2) \\ &\quad + \frac{1}{2}\lambda^{ikG}\lambda^{jkG'}\lambda^{Gnp}\lambda^{G'np}\Delta V_{SSSSS}(m_k^2, m_G^2, m_G^2, m_n^2, m_p^2), \end{aligned} \quad (4.3.5)$$

where  $B'$  is defined in eq. (B.1.13), and

$$\begin{aligned} \Delta X_{SSS}(m_G^2, m_G^2, m_k^2) &\equiv -A(m_k^2)\overline{\log m_G^2} = -X_{SSS}(m_G^2, m_G^2, m_k^2) \\ \Delta W_{SSSS}(m_G^2, m_G^2, m_m^2, m_n^2) &\equiv B(0, m_m^2, m_n^2)\overline{\log m_G^2} \\ \Delta Y_{SSSS}(m_k^2, m_G^2, m_G^2, m_n^2) &\equiv B'(s, m_G^2, m_k^2)A(m_n^2) = -Y_{SSSS}(m_k^2, m_G^2, m_G^2, m_n^2) \\ \Delta V_{SSSSS}(m_k^2, m_G^2, m_G^2, m_n^2, m_p^2) &\equiv -B'(s, m_G^2, m_k^2)B(0, m_n^2, m_p^2) \\ &= B'(s, m_G^2, m_k^2)P_{SS}(m_n^2, m_p^2). \end{aligned} \quad (4.3.6)$$

These *exactly* cancel the divergent parts in the mass diagrams. In the case of the  $X$  and  $Y$  diagrams, they go further and leave no finite parts; for the  $W$  diagrams, what remains is

$$\begin{aligned} W_{SSSS}(m_G^2, m_G^2, m_m^2, m_n^2) + \Delta W_{SSSS}(m_G^2, m_G^2, m_m^2, m_n^2) \\ = U_0(m_G^2, m_G^2, m_m^2, m_n^2) + \Delta W_{SSSS}(m_G^2, m_G^2, m_m^2, m_n^2) \\ = R_{SS}(m_m^2, m_n^2). \end{aligned} \quad (4.3.7)$$

We have no further divergences in  $W$  (in particular,  $U_0(x, y, 0, 0)$  is non-singular).

In the  $V$  diagrams there is also a finite piece that remains, since

$$\begin{aligned} V_{SSSSS}(m_k^2, m_G^2, m_G^2, m_n^2, m_p^2) \\ = -V(m_k^2, m_G^2, m_n^2, m_p^2) \\ = -\overline{V}(m_k^2, m_n^2, m_p^2) + \frac{[P_{SS}(m_n^2, m_p^2)\overline{\log m_G^2} + R_{SS}(m_n^2, m_p^2)]}{s - m_k^2} + \mathcal{O}(m_G^2). \end{aligned} \quad (4.3.8)$$

Now, using

$$\begin{aligned} B'(s, m_G^2, m_k^2) &= -\frac{1}{s - m_k^2}\overline{\log m_G^2} \\ &\quad - \frac{1}{(s - m_k^2)^2}[(m_k^2 + s)(B(s, 0, m_k^2) - 2) + 2m_k^2\overline{\log m_k^2}] + \mathcal{O}(m_G^2), \end{aligned} \quad (4.3.9)$$

we find that

$$\begin{aligned}
 & V_{SSSSS}(m_k^2, m_G^2, m_G^2, m_n^2, m_p^2) + \Delta V_{SSSSS}(m_k^2, m_G^2, m_G^2, m_n^2, m_p^2) \\
 &= -\bar{V}(m_k^2, m_n^2, m_p^2) \\
 &+ \frac{1}{(s - m_k^2)} \left[ R_{SS}(m_n^2, m_p^2) \right. \\
 &\quad \left. + \frac{P_{SS}(m_n^2, m_p^2)}{s - m_k^2} \left( (m_k^2 + s)(B(s, 0, m_k^2) - 2) + 2m_k^2 \overline{\log} m_k^2 \right) \right] \\
 &+ \mathcal{O}(m_G^2).
 \end{aligned} \tag{4.3.10}$$

Now we can look at what divergences might remain and need regulating by the momentum. For future reference let us define

$$V_{SSSSS}(m_k^2, m_G^2, m_G^2, m_n^2, m_p^2) + B'(s, m_G^2, m_k^2) P_{SS}(m_n^2, m_p^2) \equiv \tilde{V}(m_k^2, m_n^2, m_p^2). \tag{4.3.11}$$

Since we take  $\lambda^{GGG} = 0$ , we never have a divergence from  $n = p = G$ . On the other hand, when  $k = G$  we do have a divergence that needs regulating by the momentum; recalling  $B(s, 0, 0) = -\overline{\log}(-s) + 2$  we can write

$$\begin{aligned}
 \tilde{V}(m_G^2, m_n^2, m_p^2) &= V_{SSSSS}(m_G^2, m_G^2, m_G^2, m_n^2, m_p^2) + \Delta V_{SSSSS}(m_G^2, m_G^2, m_G^2, m_n^2, m_p^2) \\
 &= -\bar{V}(0, m_n^2, m_p^2) + \frac{1}{s} \left[ R_{SS}(m_n^2, m_p^2) - P_{SS}(m_n^2, m_p^2) \overline{\log}(-s) \right] \\
 &+ \mathcal{O}(m_G^2).
 \end{aligned} \tag{4.3.12}$$

For the other cases we can set  $s = 0$  and write

$$\begin{aligned}
 \tilde{V}(m_k^2, m_n^2, m_p^2) &= V_{SSSSS}(m_k^2, m_G^2, m_G^2, m_n^2, m_p^2) + \Delta V_{SSSSS}(m_k^2, m_G^2, m_G^2, m_n^2, m_p^2) \\
 &\stackrel{k \neq G}{=} -\bar{V}(m_k^2, m_n^2, m_p^2) + \frac{1}{k} \left[ R_{SS}(m_n^2, m_p^2) - P_{SS}(m_n^2, m_p^2) [\overline{\log} m_k^2 - 1] \right] \\
 &+ \mathcal{O}(m_G^2).
 \end{aligned} \tag{4.3.13}$$

#### 4.3.1.2 Momentum-regulated diagrams

There are other  $V_{SSSSS}$  diagrams that are not regulated by the Goldstone boson shifts. While  $V_{SSSSS}(x, y, z, 0, 0)$ ,  $V_{SSSSS}(0, x, y, 0, z)$ ,  $V_{SSSSS}(0, x, y, 0, 0)$ ,  $V_{SSSSS}(x, 0, y, 0, 0)$  are all regular, the diagrams  $V_{SSSSS}(0, 0, x, y, z)$  and  $V_{SSSSS}(0, 0, x, 0, y)$  are divergent, and their expression may be found simply by using those for  $U(0, 0, x, y)$  and  $U(0, 0, 0, x)$  given in appendix B.2:

$$V_{SSSSS}(0, 0, x, y, z) = \frac{1}{x} [U_0(0, x, y, z) - U(0, 0, y, z)]. \tag{4.3.14}$$

All other  $V_{SSSSS}$  diagrams are either regular or vanish due to the prefactor  $\lambda^{GGG}$ .

The remaining functions  $U_{SSSS}$ ,  $M_{SSSSS}$  and  $Z_{SSSS}$  require regulation by momentum: we give expressions for the expansion of these in appendix B.2.

### 4.3.2 Fermion-scalar diagrams

The potentially singular mass diagrams are  $\Pi_{ij}^{SF(W)}$ ,  $\Pi_{ij}^{S_2 F_3(M)}$  and  $\Pi_{ij}^{S_3, F_2(V)}$ , but among these there are only a subset once more that are regulated by the Goldstone boson shifts; indeed, as in the purely scalar case we find that the topology  $M$  is purely regulated by momentum for which all of the limits of the loop functions are provided in appendix B.2. For the other two, there are exactly four diagrams to regulate, which will match exactly. They have the form [20]:

$$\begin{aligned}\Pi_{ij}^{SF(W)} &= \frac{1}{2} \lambda^{ijkl} \text{Re}[y^{MNk} y^{M'N'l} M_{MM'}^* M_{NN'}^*] W_{SS\overline{FF}}(m_k^2, m_l^2, m_M^2, m_N^2) \\ &\quad + \frac{1}{2} \lambda^{ijkl} y^{MNk} y_{MNI} W_{SSFF}(m_k^2, m_l^2, m_M^2, m_N^2),\end{aligned}\quad (4.3.15)$$

$$\begin{aligned}\Pi_{ij}^{S_3 F_2(V)} &= \lambda^{ikl} \lambda^{jkm} \left( \text{Re}[y^{NPl} y^{N'P'm} M_{NN'}^* M_{PP'}^*] V_{SS\overline{SFF}}(m_k^2, m_l^2, m_m^2, m_N^2, m_P^2) \right. \\ &\quad \left. + \text{Re}[y^{NPl} y_{NPM}] V_{SSSFF}(m_k^2, m_l^2, m_m^2, m_N^2, m_P^2) \right),\end{aligned}\quad (4.3.16)$$

and the loop functions are defined in section B.1.1.2.

As in the scalar case, we look at the shift in the one-loop scalar mass contribution involving Goldstone bosons:

$$\begin{aligned}\Delta\Pi_{ij}^{SF} &= \left[ -\frac{1}{2} \lambda^{ijGG'} \overline{\log} m_G^2 + \lambda^{iGl} \lambda^{jG'l} B'(s, m_G^2, m_l^2) \right] \\ &\quad \times \left[ \text{Re}(y^{KLG} y_{KLG'}) \Pi_{FF}(m_K^2, m_L^2) + 2\text{Re}(y^{KLG} y^{K'L'G'} M_{KK'}^* M_{LL'}^*) \Pi_{\overline{FF}} \right] \\ &\equiv \lambda^{ijGG'} \text{Re}(y^{KLG} y_{KLG'}) \Delta W_{SSFF} \\ &\quad + \lambda^{ijGG'} \text{Re}(y^{KLG} y^{K'L'G'} M_{KK'}^* M_{LL'}^*) \Delta W_{SS\overline{FF}} \\ &\quad + \lambda^{iGl} \lambda^{jG'l} \text{Re}(y^{KLG} y_{KLG'}) \Delta V_{SSSFF} \\ &\quad + \lambda^{iGl} \lambda^{jG'l} \text{Re}(y^{KLG} y^{K'L'G'} M_{KK'}^* M_{LL'}^*) \Delta V_{SS\overline{SFF}}\end{aligned}\quad (4.3.17)$$

where

$$\begin{aligned}\Pi_{FF}(x, y) &\equiv -[(x+y)P_{SS}(x, y) + A(x) + A(y)], \\ \Pi_{\overline{FF}}(x, y) &\equiv -P_{SS}(x, y),\end{aligned}\quad (4.3.18)$$

and compare to the relevant expressions for the loop functions:

$$\begin{aligned}W_{SS\overline{FF}}(m_G^2, m_G^2, x, y) &= -2U_0(m_G^2, m_G^2, x, y), \\ W_{SSFF}(m_G^2, m_G^2, x, y) &= -(x+y-m_G^2)U_0(m_G^2, m_G^2, x, y) - I(0, x, y) \\ &\quad - \overline{\log} m_G^2 (A(x) + A(y)), \\ V_{SSSFF}(k, m_G^2, m_G^2, x, y) &= -2V_{SSSSS}(k, m_G^2, m_G^2, x, y), \\ V_{SS\overline{SFF}}(k, m_G^2, m_G^2, x, y) &= -(x+y-m_G^2)V_{SSSSS}(k, m_G^2, m_G^2, x, y) + U(k, m_G^2, x, y) \\ &\quad + B'(s, m_G^2, k)(A(x) + A(y)).\end{aligned}\quad (4.3.19)$$

We should deal with each of these in turn. Firstly for the  $W$  topology:

$$\begin{aligned}W_{SSFF}(m_G^2, m_G^2, x, y) + \Delta W_{SSFF}(m_G^2, m_G^2, x, y) &\rightarrow -I(0, x, y) - (x+y)R_{SS}(x, y), \\ W_{SS\overline{FF}}(m_G^2, m_G^2, x, y) + \Delta W_{SS\overline{FF}}(m_G^2, m_G^2, x, y) &\rightarrow -2R_{SS}(x, y).\end{aligned}\quad (4.3.20)$$

For topology  $V$ , the first combination is proportional to the scalar case in equations (4.3.12) and (4.3.13):

$$\begin{aligned} V_{SS\overline{S}\overline{F}}(k, m_G^2, m_G^2, x, y) + \Delta V_{SS\overline{S}\overline{F}}(k, m_G^2, m_G^2, x, y) \\ = -2V_{SSSSS}(k, m_G^2, m_G^2, x, y) - 2B'(s, m_G^2, k)P_{SS}(x, y) \\ \rightarrow -2\tilde{V}(k, x, y), \end{aligned} \quad (4.3.21)$$

while the second also contains an additional  $U$  function:

$$\begin{aligned} V_{SS\overline{S}FF}(k, m_G^2, m_G^2, x, y) + \Delta V_{SS\overline{S}FF}(k, m_G^2, m_G^2, x, y) \\ \rightarrow -(x+y)\tilde{V}(k, x, y) + U(k, m_G^2, x, y). \end{aligned} \quad (4.3.22)$$

For this case, when  $k \neq m_G^2$  it is non-singular as in the scalar case, and when  $k = m_G^2$  we require the expansions with finite  $s$  from equation (4.3.12) and for  $U(0, 0, x, y)$  from appendix B.2.

## 4.4 Self-consistent solution of the tadpole equations

We have shown how to avoid the Goldstone Boson Catastrophe in general renormalisable field theories, and how this can be applied to calculating neutral scalar masses in the gaugeless limit in a generalised effective potential approximation. However, we still have two possible ways of calculating both tadpoles and self-energies, which differ in terms of how we solve the tadpole equations. The choice arises because the mass parameters  $m_{ij}^2$  appear on both the left- and right-hand sides of equation (2.4.12) – or equivalently, because when considering equation (4.1.25) the  $m_{ij}^2$  appear in the  $\delta_i$ . Therefore we can:

1. Numerically solve equation (2.4.12) to find the  $m_{ij}^2$  *exactly*.
2. Perturbatively expand the  $m_{ij}^2$  around the  $\hat{m}_{0,ij}^2$  so that

$$m_{ij}^2 = \hat{m}_{0,ij}^2 + \delta^{(1)}m_{ij}^2 + \delta^{(2)}m_{ij}^2 + \dots \quad (4.4.1)$$

and solve for the desired loop order.

Since the effective potential  $\Delta V$  will only be computed to a given loop order, the two approaches are formally equivalent. For the first approach, in practice, this means that we must iteratively solve the tadpole equations: at each iteration we put  $m_i^2 = R_{ki}R_{li}m_{kl}^2$  for the tree-level mass parameters, computing a new  $R$  each time and therefore modifying the couplings, and then set the Goldstone boson mass to zero in the loop functions and compute the tadpole equations from the expressions in section 4.2.

We find in this case that the couplings are no longer guaranteed to satisfy certain relationships imposed by the broken symmetries; only the full on-shell amplitudes will satisfy the appropriate Slavnov-Taylor identities. This is only a problem for the coupling  $\lambda^{GG'G''}$  between three Goldstone bosons, which is zero at tree-level and on-shell; because the parameter in the Lagrangian will in general obtain a small non-zero value (in theories with CP-violation) and yet leads to divergent Goldstone boson self-energies we must impose that this is also on-shell (*i.e.* zero). Since this coupling does not appear at one-loop in the calculation of the Higgs boson mass, taking this coupling

to vanish causes no shift at two loops. On the other hand, if we want to calculate the Goldstone boson self-energy at two loops then we *do* find a set of shifts when we take this coupling “on-shell”: we would need to include the vertex corrections and define a set of shifted loop functions for those contributions (which, of course, only affect the self-energies). We shall return to this in future work.

Instead, we will take the second approach in the list above, and while we cannot do the same as we did for the Goldstone boson and put the other scalars on shell, we can follow [33] and re-expand the masses  $m_{ij}^2$  as a series in the couplings to one-loop order in the one-loop tadpole. We then use the tree-level masses in the loop functions and solve the tadpole equations perturbatively instead of iteratively as we have just described. Let us define a set of masses  $\tilde{m}^2 = \{m_G^2, \tilde{m}_{i \neq G}^2\}$  *i.e.* we use the on-shell mass for the Goldstone, and the tree-level masses for the other scalars. To single out the Goldstone boson we use the tree-level mixing matrix  $\tilde{R}_{kG}$  which in any case should correspond to the all-loop expression, depending as it does only on the symmetries and VEVs. We can first define a perturbation to the non-diagonal tree-level mass matrix as

$$\tilde{\Delta}_{ij} \equiv m_{ij}^2 - \hat{m}_{0,ij}^2, \quad (4.4.2)$$

which can then be rotated to the diagonal basis – using rotation matrices  $\tilde{R}$  – so that we obtain a perturbation  $\Delta_{ij}$  in the basis that diagonalise the tree-level mass matrix. If we use equation (4.1.25), we find that

$$\tilde{\Delta}_{ij} = -\delta_i \delta_{ij}, \quad \Rightarrow \quad \Delta_{ij} \equiv -\tilde{R}_{ki} \tilde{R}_{kj} \delta_k. \quad (4.4.3)$$

However, this equation fails for pseudoscalars, and we will instead allow  $\Delta_{ij}$  to be an implicit function of the tadpole shifts. Indeed, we solve the tadpole equations for some variables  $\{x_i\}$  with

$$x_i = c_{0,i} + c_{ij} \times \frac{\partial \Delta V}{\partial \phi_j^0}, \quad (4.4.4)$$

and then

$$\tilde{\Delta}_{ij} = \sum_{k,l} \frac{\partial m_{ij}^2}{\partial x_k} c_{kl} \frac{\partial \Delta V}{\partial \phi_l^0}. \quad (4.4.5)$$

For example, let us consider again the Abelian Goldstone model of section 4.1.1, with a single complex scalar  $\Phi = \frac{1}{\sqrt{2}}(v + h + iG)$ , and with a potential given in eq. (4.1.1). We solve the tadpole equations for the parameter  $\mu^2$  so that

$$\mu^2 + \lambda v^2 + \frac{1}{v} \frac{\Delta V}{\partial h} = 0. \quad (4.4.6)$$

However, both the mass of the Goldstone boson and the Higgs are controlled by the  $\mu^2$  parameter;

$$M_h^2 = \mu^2 + 3\lambda v^2, \quad m_G^2 = \mu^2 + \lambda v^2. \quad (4.4.7)$$

So in our notation,  $x_h \rightarrow \mu^2$ ,  $c_{0,h} \rightarrow -\lambda v^2$ ,  $c_{hh} \rightarrow -\frac{1}{v}$  and so

$$\Delta_{hh} = -\frac{1}{v} \frac{\Delta V}{\partial h} = \Delta_{GG}. \quad (4.4.8)$$

We can expand  $\Delta_{ij}$  as usual in perturbation theory using  $\Delta_{ij} = \frac{1}{16\pi^2} \Delta_{ij}^{(1)} + \frac{1}{(16\pi^2)^2} \Delta_{ij}^{(2)} + \dots$  to find that we should shift the tadpoles according to

$$\frac{\partial \hat{V}^{(2)}}{\partial \phi_r^0}(m^2) = \frac{\partial \hat{V}^{(2)}}{\partial \phi_r^0}(\tilde{m}^2) + \frac{1}{2} \sum_{(i,i') \neq (G,G')} \tilde{R}_{ri} \tilde{\lambda}^{ii'l} \Delta_{ii'}^{(1)} P_{SS}(\tilde{m}_i^2, \tilde{m}_{i'}^2). \quad (4.4.9)$$



By  $(i, i') \neq (G, G')$  we mean that the sum over  $(i, i')$  excludes the cases where *both*  $i$  and  $i'$  are Goldstone boson indices. This allows us to express the  $\Delta_{ii'}$  entirely in terms of the tree-level  $\tilde{m}^2$  parameters and obtain a perturbative expansion for  $m^2$  – note that we should also replace all of the couplings  $\lambda^{ijk}, \lambda^{ijkl}$  etc and rotation matrices  $R_{ij}$  with their tree-level values  $\tilde{\lambda}^{ijk}, \tilde{\lambda}^{ijkl}, \tilde{R}_{ij}$  (we already implicitly used this to disregard the  $\lambda^{GGG}$  terms). The only subtlety occurs when  $\tilde{m}_i^2 = \tilde{m}_j^2$  for some  $i, j$  which is not ensured by a symmetry so that  $\Delta_{ii} \neq \Delta_{jj}$ ; in that case as usual the  $\tilde{R}$  matrix must be modified to diagonalise  $\Delta_{ij}^{(1)}$  on those indices. However the expression above is still valid in that case. Note that the shift only occurs for scalar propagators in the one-loop diagrams, which is why there is no modification of the fermionic or vector tadpole diagrams.

We can apply the same procedure to use the tree-level masses in the mass diagrams: after some algebra we find (in the gaugeless limit – otherwise we will have some additional shifts from scalar-vector diagrams) that

$$\begin{aligned} \Pi_{ij}^{(2)}(s, m^2) = \Pi_{ij}^{(2)}(s, \bar{m}^2) + \sum_{(k, k') \neq (G, G')} \left( \frac{1}{2} \tilde{\lambda}^{ijkk'} \Delta_{kk'}^{(1)} P_{SS}(\bar{m}_k^2, \bar{m}_{k'}^2) \right. \\ \left. - \tilde{\lambda}^{ikl} \tilde{\lambda}^{jk'l} \Delta_{kk'}^{(1)} C(s, s, 0, \bar{m}_k^2, \bar{m}_l^2, \bar{m}_{k'}^2) \right), \end{aligned} \quad (4.4.10)$$

where we used the usual  $C$  function defined in eq. (B.1.17). These together then allow us to determine the scalar masses to be the values of  $s$  that give solutions to:

$$\begin{aligned} 0 = \text{Det} \left[ s\delta_{ij} - m_{0,ij}^2 + \delta_i(\bar{m}^2)\delta_{ij} - \frac{\Pi_{ij}^{(1)}(s, \bar{m}^2)}{16\pi^2} - \frac{\Pi_{ij}^{(2)}(s, \bar{m}^2)}{(16\pi^2)^2} \right. \\ - \frac{\delta_{ij}}{2} \frac{1}{(16\pi^2)^2} \sum_{(j, j') \neq (G, G')} \tilde{R}_{il} \tilde{\lambda}^{jj'l} \Delta_{jj'}^{(1)} P_{SS}(\bar{m}_j^2, \bar{m}_{j'}^2) \\ - \frac{\tilde{R}_{ii'} \tilde{R}_{jj'}}{(16\pi^2)^2} \sum_{(k, k') \neq (G, G')} \left( \frac{1}{2} \tilde{\lambda}^{i'j'kk'} \Delta_{kk'}^{(1)} P_{SS}(\bar{m}_k^2, \bar{m}_{k'}^2) \right. \\ \left. \left. - \tilde{\lambda}^{i'kl} \tilde{\lambda}^{j'k'l} \Delta_{kk'}^{(1)} C(s, s, 0, \bar{m}_k^2, \bar{m}_l^2, \bar{m}_{k'}^2) \right) \right]. \end{aligned} \quad (4.4.11)$$

Typically in spectrum generators the two-loop corrections are computed at fixed momentum and then the eigenvalues of the above matrix computed iteratively. Since we have given the expansion of all the loop functions relevant for the two-loop corrections up to terms of order  $\mathcal{O}(s)$ , this could be generalised to include our simple momentum dependence for the two-loop part as in equation (4.3.1) without significant loss of speed since the computationally expensive parts of the two-loop functions would only need to be evaluated once. However, since all of the expansions are strictly valid only up to two-loop order, the equation above could be solved perturbatively itself with no significant loss of accuracy.

Now, let us end this discussion by a comment on the relation between the “on-shell” method and the self-consistent solution of the tadpole equations. Since the Goldstone boson is massless at tree-level, this means that we automatically have the Goldstone boson “on-shell.” This means that the “on shell” and “consistent solution” approaches are more closely related than first appears: since the Goldstone boson mass must be zero on-shell and we can identify the Goldstone boson eigenstates using a matrix  $R_{kG}$  derived just from the broken symmetries (see sections 2.4.1 and 4.1.2) then the on-shell

condition becomes

$$\det(p^2 - m_{ij}^2 - \Pi_{ij}(p^2)) = 0 \rightarrow R_{kG} R_{lG} m_{kl}^2 + \Pi_{GG}(0) = 0. \quad (4.4.12)$$

and since  $\hat{m}_{0,GG}^2 = 0$  we have

$$\begin{aligned} \delta m_G^2 &= R_{kG} R_{lG} m_{kl}^2 = -\Pi_{GG}(0) \\ \Delta_{GG} &= \delta m_G^2 + \mathcal{O}(2 - \text{loop}) \rightarrow \Delta_{GG} = -\Pi_{GG}(0) + \mathcal{O}(2 - \text{loop}), \end{aligned} \quad (4.4.13)$$

*i.e.* the approach of adjusting the loop functions (as we do when setting the Goldstone boson on-shell) or defining a set of shifts to the tadpoles and self-energies involving  $\Delta_{ij}$  should give the same result when we just consider the shifts to the Goldstone boson masses, even though the expressions look very different.

## 4.5 Conclusions

We have presented a solution to the Goldstone Boson Catastrophe in general renormalisable theories to two-loop order. We showed that the approach of Goldstone boson resummation is equivalent (at least at two-loop order) to an on-shell scheme for the Goldstone boson(s), the latter being much more convenient calculationally. We then showed how there are a set of self-energy diagrams that also exhibit the Goldstone Boson Catastrophe even when external momentum is included – but that our solution naturally avoids those singularities. We were then able to give expressions for a “generalised effective potential approximation” for neutral scalar masses in the gaugeless limit, that are free of infra-red divergences and give a good approximation to the full momentum-dependent result. This also included the re-expansion of the masses in terms of the values obtained from the tree-level tadpole equations, allowing a self-consistent solution of the tadpole equations (*i.e.* equations where no terms to be solved for appear on both left and right hand sides).

The expressions obtained in this chapter now allow simple infra-red safe calculations in a wide variety of theories. Most practically, it would be simple to implement them in a package such as **SARAH**, to enable automated calculations for *any* model and avoid the problems seen, for example, in [218, 249, 300], with the existing implementation. This should also enable more reliable and accurate explorations of the parameter space of many models with the **SARAH/SPHeno** numerical framework – in particular for non-supersymmetric models (such as 2HDMs), where the existing “solution”<sup>4</sup> to the Goldstone Boson Catastrophe is not particularly successful, relying as it does on there being a gauge-coupling dependent part of the scalar potential (as is the case in supersymmetric theories). This will be the subject of the next chapter.

---

<sup>4</sup>We will review the previous approaches in **SARAH** in section 5.1. See also [250], appendix 2b of [249] and especially section 2 of [300].

## Chapter 5

# Supersymmetric and non-supersymmetric models without catastrophic Goldstone bosons

In the previous chapter, we have presented a general procedure to cure the Goldstone Boson Catastrophe in two-loop Higgs mass calculations for general renormalisable theories. Our method is based on setting the Goldstone boson propagators on-shell, and we have provided a complete set of modified loop functions for the tadpoles and self-energies that were finite. Thus, combining these results with those of [20, 21, 142, 260] which provide fully generic expressions for the two-loop corrections to real scalar masses in supersymmetric and non-supersymmetric models, all ingredients are present to calculate Higgs masses up to two-loop order in *any* renormalisable model.

The generic expressions of [20, 21, 142, 260] are already used by the `Mathematica` package `SARAH` [261–266] to calculate in combination with `SPheno` [194, 195] the Higgs masses in supersymmetric models at the two-loop level [21, 250, 300] – for more details see section 2.4.3. Before version 4.12.0 of `SARAH`, the workaround for the Goldstone boson catastrophe in this setup was to introduce finite masses for the electroweak Goldstones by dropping the  $D$ -terms in the mass matrices. However, there were many regions of parameter space where the divergences reappeared (see *e.g.* [85, 101, 218]) and this does not work at all for non-supersymmetric models, which have no  $D$ -term potential. For this reason, we here implement in `SARAH` the results of chapter 4, and fill some additional technical gaps that we describe in section 5.1; in particular, we complete the basis of required loop functions. New versions of `SARAH` – since 4.12.0 – therefore now offer the possibility to calculate two-loop masses for neutral scalars in non-supersymmetric models, as well as substantially improving the calculation in supersymmetric ones. As the only non-supersymmetric model for which comparable results exist is the Standard Model, in section 5.2 we compare our new calculation against the public code `SMH` [22] and the results of Buttazzo et al. [25], finding excellent agreement (even if our results do not include all of the contributions included in those references). In section 5.3, we show how our new approach improves our previous calculation for supersymmetric models through the example of the NMSSM, for which our results should now be considered state of the art. We then illustrate our new routines by computing some new results in Split SUSY in section 5.4.

Momentum-independent renormalisation schemes are the most convenient choices for applying to a large variety of models, and so all mass calculations in **SARAH** are performed in the  $\overline{\text{MS}}$  or  $\overline{\text{DR}}'$  scheme. In contrast, on-shell schemes might offer some model dependent advantages. This is for instance the case in supersymmetric models with Dirac gauginos, which we studied in chapter 3. In particular, we found that when there is a large mass splitting between the stops and the gluino, an on-shell scheme leads to an improved convergence of the perturbative series. It is also very useful often if a  $\overline{\text{DR}}'$  and on-shell calculation exists for the same supersymmetric model: the difference between the results can be used as estimate of the missing higher-order corrections; this can now be done for the MSSM and certain classes of NMSSM and Dirac gaugino contributions. On the other hand, there has been hardly any discussion in the literature about radiative corrections to Higgs masses in non-supersymmetric BSM models. One reason for this, besides the technical hurdles, is that the additional freedom in non-supersymmetric models introduces a large number of free parameters, *i.e.* in some cases it might be possible to absorb any finite correction in the scalar sector into the counter-terms of these parameters. Thus, it is often implicitly assumed that the masses, but also the mixing angles, in the extended Higgs sector in BSM could be kept at their tree-level values. However, this is fraught with danger: *(i)* not all non-supersymmetric models really have a sufficiently large number of free parameters to absorb all radiative corrections. This is for instance the case in the Georgi-Machacek model; *(ii)* if a low-energy model is combined with an explicit UV completion (such as a GUT theory), the freedom to adjust the couplings is usually lost; *(iii)* using masses instead of couplings as input hides the presence of huge or even non-perturbative quartic couplings; *(iv)* even if parameters are checked with respect to simple limits such as  $\lambda < 4\pi$  or tree-level unitarity bounds, this does not guarantee that the considered parameter point is perturbative or that strongly coupled effects do not appear at energy scales already explored at the LHC. Partly motivated by the growing interest in exploring quantum corrections to non-supersymmetric models, we explore here in sections 5.5 and 5.6 the corrections to the Two-Higgs-Doublet Model (2HDM) and Georgi-Machacek model (GM), drawing attention to the fact that the corrections pass out of control well before the naive perturbativity or unitarity bounds.

Finally, an  $\overline{\text{MS}}$  calculation has the advantage that it can give an estimate of the size of the theoretical uncertainty by varying the renormalisation scale. Moreover, to obtain more reliable results for the vacuum stability by considering the renormalisation group equation (RGE) improved effective potential, a translation of masses into  $\overline{\text{MS}}$  parameters is necessary. We show in this work how these aspects can be analysed in non-supersymmetric models with the new calculation available now in **SARAH**.

## 5.1 The Goldstone Boson Catastrophe and its solutions

The Goldstone Boson Catastrophe appears because the mass-squared parameter(s) of the Goldstone boson(s) in the Lagrangian is(are) zero at tree-level, but non-zero once we take into account the loop corrections to the potential. Then at two loops and higher we must calculate loop corrections with a small and/or negative mass-squared parameter, which leads to large logarithms and/or phases – this can in fact be a complete obstacle to a precise calculation..

This problem was only noticed in the first attempt to go beyond the gaugeless limit in the MSSM at more than one loop [32]. Indeed, in the MSSM, the gaugeless limit turns off the Goldstone boson couplings to the Higgs, and the other (momentum-dependent)

calculations that have been performed beyond this limit only consider the sector of the theory without the Goldstones. However, as soon as one considers non-minimal supersymmetric models in which trilinear interactions of the Higgs superfields occur in the superpotential, the gaugeless limit no longer offers much protection against the problem, since the quartic coupling is not determined by the gauge couplings; and this is also a generic feature of non-supersymmetric models (such as the Standard Model).

In the following we shall describe the previous approaches to the problem and the implementation of our new results in **SARAH**.

### 5.1.1 Previous approaches in **SARAH**

Up until now, in **SARAH** the catastrophe appeared in an even more acute form because all of the one- and two-loop tadpoles and self-energies are computed using the tree-level masses in the loops, so without a solution to the problem, the Goldstone bosons are massless and cause several loop functions to diverge. However, for supersymmetric models the original workaround implemented in [21, 250] and explored in more detail in [300] relies on the fact that the electroweak gauge couplings appear in the D-term potential.<sup>1</sup> We therefore used the tree-level parameters that are solutions of the full tree-level tadpole equations including the electroweak couplings to calculate the tree-level masses (but set the electroweak gauge couplings to zero in the mass matrices) used in the two-loop routines' loop functions. In other words, the masses in the loop functions are not at the minimum of the potential, and are typically tachyonic<sup>2</sup>, with a size of order the electroweak scale. Since we are neglecting two-loop corrections proportional to these couplings, this error is acceptable. On the other hand, for models beyond the MSSM (in particular, the NMSSM) there are typically regions of the parameter space where the Higgs sector masses still pass near to zero and cause the loop functions to diverge; for example such problems were observed in [85, 101, 218].

A more recent approach was to introduce regulator masses. All scalar masses in the two-loop routines which are below a certain threshold are set in terms of the renormalisation scale  $Q$  and a constant  $R$ :

$$m_{S,\min}^2 = RQ^2 \quad (5.1.1)$$

This approach was introduced in **SARAH** to stabilise cases in which the  $D$ -term approach fails. This could either be, as demonstrated in an example in sec. 5.3, if other scalars artificially become very light, or if the supersymmetric scale is much higher than the electroweak scale. However, in contrast to the D-term solution, this approach violates the symmetries of the theory and can lead to non-zero masses for Goldstone bosons. Furthermore, there is no a priori indication for the optimal size of  $R$ ; too large and the Goldstone/Higgs contributions are suppressed (because logarithmic contributions including them are artificially reduced), too small and the results become numerically unstable, and the user must use trial and error. Finally, it implicitly assumes that the corrections coming from the Higgs/Goldstone bosons to the Higgs mass are small (so that modifying them is benign). This is not a good approximation in many non-SUSY models, and for this reason the newly implemented solution described in the next subsection allows non-SUSY models to be studied accurately for the first time.

---

<sup>1</sup>Indeed, the gaugeless limit (turning off the electroweak gauge couplings) completely cures the problem in the MSSM by eliminating all of the Goldstone boson couplings to the Higgs.

<sup>2</sup>Since the mass was tachyonic and generally not small, we then neglected the imaginary part of the self energies/tadpoles.

### 5.1.2 On-shell Goldstone bosons, consistent tadpole solutions, and the implementation in SARAH

In the previous chapter, a genuine solution was presented for *generic* field theories, which we will now implement in SARAH. We should treat the Goldstone boson mass as an on-shell parameter, and a set of modified expressions for tadpoles and self-energies were derived – indeed, it was shown that there were a class of loop diagrams that were not made finite purely by including external momenta. In addition, expressions for the “consistent solution” of the tadpole equations were given.

For the evaluation of tadpoles and self-energies we proposed in section 4.3 a “generalised effective potential limit,” where the self-energies are expanded in  $s = -p^2$  ( $= m^2$  on shell) and all terms of order  $\mathcal{O}(s)$  are neglected (but crucially retaining terms that diverge at  $s = 0$ ). We therefore require the following basis of loop functions, where  $\{x, y, z, u, v\} \neq 0$  are masses squared:

$$\begin{aligned}
 \text{Momentum independent : } & J(x), P_{SS}(x, y), P_{SS}(0, y), \\
 & I(x, y, z), I(0, y, z), I(0, 0, z), \\
 & U_0(x, y, z, u), U_0(0, y, z, u), U_0(x, y, 0, u), \\
 & U_0(0, y, 0, u), U_0(x, y, 0, 0), U_0(0, y, 0, 0), \\
 & M_0(x, y, z, u, v), M_0(0, y, z, u, v), M_0(0, 0, z, u, v), \\
 & M_0(0, 0, 0, u, v), \tilde{V}(x, y, z). \\
 \text{Momentum dependent : } & B(0, 0), \\
 & M(x, 0, 0, 0, 0), M(0, y, 0, u, v), \\
 & M(0, 0, 0, u, v), M(0, 0, 0, 0, v) \\
 & U(0, 0, x, y), U(0, 0, 0, y) \\
 & \tilde{V}(0, y, z), \tilde{V}(0, 0, z). \tag{5.1.2}
 \end{aligned}$$

All of these functions are implicitly dependent on the renormalisation scale  $Q$ , typically containing factors of  $\overline{\log x} \equiv \log(x/Q^2)$ . Expressions for all of these functions expanded up to  $\mathcal{O}(1)$  in the external momenta (or the reference for them) are given in appendices B.2 and B.3. Note in particular that the functions  $\tilde{V}(x, y, z)$  are given in terms of the regularised function  $\bar{V}(u, 0, y, z)$  defined in [20]<sup>3</sup>; in appendix B.3 we derive explicit compact expressions for this function – first with full momentum dependence, and then expanded up to  $\mathcal{O}(1)$  in the external momenta.

In our practical implementation in SARAH we have extended the available routines for calculating two-loop integrals with the missing ingredients to address the Goldstone boson catastrophe. Moreover, there are three loop functions involving fermions and gauge bosons which needed modification for the  $\overline{\text{MS}}$  scheme as used for non-supersymmetric models, as compared to the  $\overline{\text{DR}}'$  for supersymmetric models; the tadpole and self-energies contain

$$\begin{aligned}
 & \frac{\partial \hat{V}^{(2)}}{\partial \phi_r^0} \supset R_{rp} T_{FV}^p, \\
 & T_{FV}^p = g^2 d(I) C(I) \text{Re}(M_{II'} y^{II' r}) \times \left( \frac{1}{2} F'_{FV}(x) \right), \\
 & \Pi_{ij}^{(2)} \supset \Pi_{ij}^{FV} = g^2 d(K) C(K) [\text{Re}(y^{iKL} y_{jKL}) G_{FF}(m_K^2, m_L^2)
 \end{aligned}$$

---

<sup>3</sup>Note that our  $\tilde{V}$  uses one fewer variable than the definition of  $V$  in [20] because in our case it always appears in the form  $\bar{V}(u, 0, y, z)$ .

$$+ \text{Re}(y^{iKL} y^{jK'L'} M_{KK'} M_{LL'}) G_{\overline{FF}}(m_K^2, m_L^2)], \quad (5.1.3)$$

where  $\hat{V}^{(2)}$  is the two-loop contribution to the effective potential,  $d(I), C(I)$  are the dimension and quadratic Casimirs of representation  $I$  of the gauge group having coupling  $g$ , and the loop functions are:

$$\begin{aligned} \left( \frac{1}{2} F'_{FV}(x) \right) &= 4x \left[ 6 - 7 \overline{\log} x + 3 \overline{\log}^2 x + \delta_{\overline{MS}} [2 \overline{\log} x - 1] \right], \\ G_{FF}(x, y) &= G_{\overline{FF}}^{\overline{DR}'}(x, y) + 2\delta_{\overline{MS}} \left[ x + y + 2J(x) + 2J(y) \right. \\ &\quad \left. - (x + y) \left( 2B(x, y) + xB(y, x') + yB(x, y') \right) \right] \\ &\xrightarrow{s \rightarrow 0} \left[ 2(x + y) [3U_0(x, y, x, 0) + 3U_0(x, y, y, 0) + 5P_{SS}(x, y)] \right. \\ &\quad \left. - 6I(x, x, 0) - 6I(y, y, 0) + 10J(x) + 10J(y) - 16(x + y) \right] \\ &\quad + 4\delta_{\overline{MS}} \left[ x + y + J(x) + J(y) + (x + y)P_{SS}(x, y) \right], \\ G_{\overline{FF}}(x, y) &= G_{\overline{FF}}^{\overline{DR}'}(x, y) - 4\delta_{\overline{MS}} \left[ 2B(x, y) + yB(x, y') + xB(y, x') \right] \\ &\xrightarrow{s \rightarrow 0} 4 \left( 3U_0(x, y, x, 0) + 3U_0(x, y, y, 0) + 5P_{SS}(x, y) - 4 \right) \\ &\quad + 4\delta_{\overline{MS}} \left[ 2P_{SS}(x, y) + 1 \right]. \end{aligned} \quad (5.1.4)$$

Here  $\delta_{\overline{MS}}$  is one for  $\overline{MS}$  masses and zero for  $\overline{DR}'$ .

We have also implemented in **SARAH** the consistent tadpole solution of section 4.4, under the assumption that the variables  $\{x_i\}$ , for which the tadpole equations are solved, are dimensionful and there is no *explicit* dependence of the trilinear/quartic couplings on them (only implicitly through the mixing matrices  $R$ ); and also we assume that the *fermion* mass matrices do not depend on these parameters. These assumptions are fulfilled *e.g.* for  $\{m_{H_u}^2, m_{H_d}^2\}$  in the MSSM, but not  $\{\mu, B_\mu\}$  chosen as parameters to solve the tadpole equations. On the other hand, we give expressions for the shifts to the tadpoles and self-energies when fermion masses depend on the  $\{x_i\}$  in appendix C, and plan to implement these in future.

The routines to calculate the consistent tadpole solution are generated during the output of **SPheno** code; this is fully automatised beginning with **SARAH** version 4.12.0 and the user can obtain a **SPheno** version for non-supersymmetric models as before – with the difference that two-loop mass corrections are now included. The only requirements are recent versions of **SARAH** and **SPheno** which are available at [www.hepforge.org](http://www.hepforge.org).

The new features can now be adjusted in the Block **SPHENOINPUT** in the Les Houches input file:

```

1 Block SPhenoInput #
2 ...
3 7 0 # Skip two loop masses: True/False
4 8 3 # Choose two-loop method
5 150 1 # Use consistent tadpole solution: True/False
6 151 1 # Generalised effective potential calculations: ↔
    True/False
    
```

Note that the solution to the Goldstone boson catastrophe exists only for the diagrammatic calculation (flag  $8 \rightarrow 3$ ), but not for the effective potential calculations using numerical derivatives to obtain the tadpoles and self-energies (flag  $8 \rightarrow 1,2$ ). By default, the new calculation is used now, but could be turned off if demanded (flag  $151 \rightarrow 0$ ). In this case, it is usually necessary to include a non-zero regulator mass via flag 410 for non-supersymmetric models. In principle, there should not be any reason to revert to the old calculation with regulator masses except for double-checking the result.

The consistent tadpole solution is turned off by default but can be turned on by setting flag  $150 \rightarrow 1$ . This is because, while strictly it is more accurate to include it, there is also the possibility of numerical instability if the shift in the tree-level mass parameters is large; for example, if the expectation values of some scalars are small (such as *e.g.* the neutral scalar of an electroweak triplet which must have a small expectation value from electroweak precision constraints) then the shift in the mass parameter can be much larger than the tree-level value and the perturbative solution fails. In such cases, it would be better to use a recursive approach which is currently not possible for the reasons given in section 4.4.

## 5.2 Standard Model

### 5.2.1 A first comparison of our results with existing calculations

Now that two-loop corrections to scalar masses are available in **SARAH**, free of the Goldstone boson catastrophe, it is important to compare the results we obtain to other computations available in the literature, as a verification of our results and as a way to estimate the impact of missing corrections. We consider in this section the Higgs mass calculations in the Standard Model, and we will compare the results obtained with **SPheno** with the computations performed at complete two-loop calculation in [25], and the full two-loop (plus leading three-loop) Higgs mass calculation implemented in the public code **SMH** [22]. These works take into account two-loop electroweak corrections, which are not available for generic theories and are not included in our code, hence we will quantify the size of these effects, together with effects from momentum, and investigate the discrepancy in masses coming from the different determination of the top Yukawa coupling.

It is interesting to examine the way that the two calculations avoid the Goldstone Boson Catastrophe. The calculation of Buttazzo et al. [25] was performed in Feynman gauge and using certain parameters on-shell, whereas the results implemented in **SMH** are in a pure  $\overline{\text{MS}}$  scheme and Landau gauge, which is closer to our approach. In the latter paper, some resummation is performed by hand to eliminate the divergence in the mass calculation; it is perhaps surprising that the absence of the function  $\overline{V}(0,0,y,z)$  from the basis in **TSIL** was not problematic, but there the calculation was performed by computing the set of integrals explicitly using **TARCER** [148] rather than starting from a set of generic expressions, so the result was found directly in terms of the other basis functions. In principle this should agree with our equation (B.3.10).

A first approach for the comparison between **SPheno** and [25] is to compute the Higgs mass with the quartic coupling  $\lambda$  ranging in the interval  $[0.125, 0.130]$ , and only setting



the SM inputs to the same values as in [25], which we recall here

$$\begin{aligned}
G_F &= 1.16638 \times 10^{-5} \text{ GeV}^{-2}, \\
\alpha_s(M_Z) &= 0.1184, \\
M_Z &= 91.1876 \text{ GeV}, \\
m_t &= 173.34 \text{ GeV}.
\end{aligned} \tag{5.2.1}$$

They furthermore took the experimentally determined central value of the Higgs mass to be 125.15 GeV, which we shall take as a reference value rather than an input. The use of consistent solutions to the tadpole equations – as derived in section 4.4 – has also been implemented in the **SPheno** code and this comparison in the context of the SM is a good occasion to study the effect of this additional shift to the tadpoles and mass diagrams, thus we compute the Higgs mass in this first method both with and without using the consistent tadpole solutions. A second approach to compute  $m_h$  with **SPheno**, which could potentially improve the comparison, is to use as well the same values for the top-Yukawa  $y_t$  and electroweak gauge couplings  $g_1, g_2$  as those given for each order in table 3 of [25].

We obtain another result for  $m_h$  with **SMH** [22], and although this code is made to perform Higgs mass calculations in the Standard Model to partial three-loop order, we use it here with the three-loop corrections always switched off, for the purpose of our comparison with **SPheno**. We use the routine `calc_Mh` that gives for a given loop order the value of  $m_h$  from the inputs of the renormalisation scale  $Q$ , the quartic coupling  $\lambda$ , the top-Yukawa  $y_t$ , the Higgs VEV  $v$ , and the gauge couplings  $g_3, g, g'$ , all given at scale  $Q$ . In order to improve the comparison, we take the same values for the inputs as used at each order in **SPheno**. We give in table 5.1 the values we find for the Higgs mass when taking the same values of  $\lambda$  as found in [25], with the two methods described above for **SPheno** and with **SMH**.

Loop order	Value of $\lambda$ found in [25]	$m_h$ in 1 <sup>st</sup> approach without consistent tadpole solutions	$m_h$ in 1 <sup>st</sup> approach with consistent tadpole solutions	$m_h$ in 2 <sup>nd</sup> approach	$m_h$ with <b>SMH</b>
Tree level	0.12917	125.79 GeV	125.79 GeV	125.79 GeV	125.79 GeV
One loop	0.12774	125.77 GeV	125.77 GeV	125.66 GeV	126.10 GeV
Two loops	0.12604	125.11 GeV	125.08 GeV	125.10 GeV	125.46 GeV

Table 5.1 – Values of the Higgs mass at scale  $Q = m_t$  for the values of the quartic couplings  $\lambda$  found in [25] at tree level, one loop and two loops, in the two approaches we used for **SPheno**, and with **SMH**. The first approach was to change only the SM parameter inputs while letting **SPheno** determine the top-Yukawa and electroweak gauge couplings, and the Higgs mass is then computed both with and without the consistent tadpole solutions. The second method was to take the same values of  $y_t, g_1, g_2$  in **SPheno** as in [25] (and switch off the consistent tadpole routines). For **SMH**, the values of the input parameters – the top-Yukawa, the electroweak gauge couplings, the Higgs VEV and the strong gauge coupling – were taken from the outputs of the **SPheno** scans. Computations are made with **SARAH-4.12.0**, **SPheno-4.0.3** and **SMH-1.0** [22].

At tree-level, all the values we find with **SPheno** and **SMH** obviously match as the tree-level Higgs mass only depends on  $\lambda$  and  $v$  which have almost the same values here, and the divergence from the value of 125.15 GeV is solely explained by the Higgs VEV which is not the same as in [25] since they take it as an on-shell parameter, while we use the  $\overline{\text{MS}}$  value as described in [221]. More importantly, the loop corrected values in

the different methods also agree quite well, thanks to the improved determination of the top Yukawa coupling  $y_t$  (including leading two-loop effects) recently implemented in **SARAH** [221], and at each order in perturbation theory the Higgs masses we find are less than a GeV away from 125.15 GeV. It is interesting to note that the values of  $m_h$  found using the **SPheno** code generated by **SARAH** version 4.9.3 – in which  $y_t$  is only determined at one-loop order – are approximately 2 – 2.5 GeV below those shown in table 5.1, and hence illustrate the importance of the precise determination of the top Yukawa coupling for calculations of  $m_h$ . The small size of the difference between the values found with the couplings computed by **SPheno** or taken from [25] – a few tens of MeV at two loops – tend to indicate that the precision of the extraction of  $y_t$  in **SPheno** is now comparable to that in [25]. Considering now the effect of the consistent tadpole solutions – that appears only in the two-loop masses – we observe a small shift of about 30 MeV to  $m_h$ , indicating that the perturbative expansion we perform in the tadpole equation is valid for the SM. Finally, the reasons explaining the remaining deviation of our results with respect to 125.15 GeV are the following:

- (i) the difference in the calculation of the Higgs VEV;
- (ii) the two-loop electroweak corrections that are not (yet) implemented in **SARAH**;
- (iii) the momentum dependence currently missing at two loops in **SARAH**.

The different value of the Higgs VEV is also quite certainly the main reason for the discrepancies between the values we obtain using **SMH** and those from [25]. I.e. it is because we use the VEV computed in **SPheno** in **SMH**, which does not correspond to the same accuracy of parameter extraction as used in [25], which would be required for a fair comparison directly between the two prior approaches: here our aim was to compare *our* result separately with [25] and **SMH**.

A further way to compare our results to those of [22] and [25] is to find for each order what value of the quartic Higgs coupling we need to obtain  $m_h = 125.15$  GeV, and our results are given in table 5.2.

Loop order	$\lambda$ found in [25]	$\lambda$ in 1 <sup>st</sup> approach without consistent tadpole solutions	$\lambda$ in 1 <sup>st</sup> approach with consistent tadpole solutions	$\lambda$ in 2 <sup>nd</sup> approach	$\lambda$ with <b>SMH</b>
Tree level	0.12917	0.12786	0.12786	0.12786	0.12786
One loop	0.12774	0.12647	0.12647	0.12669	0.12580
Two loops	0.12604	0.12613	0.12619	0.12614	0.12541

Table 5.2 – Values of the Higgs quartic coupling  $\lambda$  extracted from  $m_h = 125.15$  GeV, at tree level, one loop and two loops. The methods we used are explained in the caption of table 5.1. Values found using **SARAH**-4.12.0 and **SMH**-1.0.

We observe that the change of  $\lambda$  between each order of the perturbation expansion is approximately the same in all four methods. Moreover, the value we extract at two loops with **SPheno** is very close to the value found in [25], only differing by 0.1%.

### 5.2.2 A detailed comparative study of **SPheno** and **SMH** results

After this first comparison, we may now investigate in more depth the effects of the three sources of differences on the Higgs masses listed above, using **SPheno** and **SMH**. To begin with, we should consider the Higgs VEV and its calculation: in **SMH**, calculations are performed in the Landau gauge, while **SPheno** is by default set to use the

Feynman gauge, and while the Higgs mass should in principle be gauge independent, its vacuum expectation value is not, hence there is an inconsistency coming from the use of a Feynman gauge VEV in **SMH**. The easiest way to correct this is to switch the **SPheno** calculation to the Landau gauge – we set in the code the gauge parameter  $\xi$  to a very small finite value to approach the limit of the Landau gauge (the current implementation gives a numerical divergence when  $\xi = 0$ ) – and then to use the new value of the Landau gauge VEV in **SMH**. The values we find for  $m_h^{2\ell}$  with the two codes for the two different choices of gauge parameter and fixed values of  $Q$  and  $\lambda$  are given in table 5.3. The first observation that can be made from these results is that the Higgs mass shows residual dependence on the gauge –  $m_h^{2\ell}$  varies by about 50 MeV between  $\xi = 1$  and  $\xi = 0.01$ . This is explained mainly<sup>4</sup> by the difference in the calculation of the  $\overline{\text{MS}}$  value for the electroweak VEV in **SPheno** between the Feynman gauge and other gauges: in the case of Feynman gauge one-loop corrections from  $\delta_{VB}$  as well as two-loop corrections from  $\delta_r$  are included which are not available in a general  $R_\xi$  gauge (see the appendix A of [221] for details of the matching in Feynman gauge). On the other hand, in an  $R_\xi$  gauge, the VEV is calculated from  $M_Z^{2,\overline{\text{MS}}} = 1/4(g_1^2 + g_2^2)v^2 = M_Z^{2,\text{pole}} - \Pi_{ZZ}^T$  where  $\Pi_{ZZ}^T$  is the transversal self-energy of the Z-boson at one-loop. What is more interesting is that the agreement between the two codes improves greatly once we use the Landau gauge in **SPheno**; indeed the difference in the Higgs mass results is reduced from approximately 0.4 GeV to less than 0.05 GeV.

A second point we can study is the effect of the two-loop momentum dependence and two-loop electroweak corrections. Let us introduce the notation for calculating the pole mass via

$$m_h^2 = 2\lambda v^2 + \Delta^{(1)}M_h^2(m_h^2) + \Delta^{(2)}M_h^2(m_h^2) \quad (5.2.2)$$

where

$$\begin{aligned} \Delta^{(\ell)}M_h^2(s) &\equiv -\frac{1}{v}\frac{\partial\Delta V^{(\ell)}}{\partial h}\bigg|_{h=G=G^+=0} + \Pi_{hh}^{(\ell)}(s) \\ &\equiv \text{div}\left[\Pi_{hh}^{(\ell)}(s)\right] + \overline{\Delta}^{(\ell)}M_h^2(0) + \mathcal{O}(s), \end{aligned} \quad (5.2.3)$$

where  $\text{div}\left[f(s)\right]$  denotes all terms in  $f(s)$  that diverge as  $s \rightarrow 0$ . Our **SPheno** code computes the one-loop corrections in any  $R_\xi$  gauge with full momentum dependence, but the two-loop corrections are performed in a generalised effective potential approach – *i.e.* we keep only the divergent part of the momentum dependence (see section 4.3 for more details). The momentum in the two-loop routines is fixed (for speed of calculation) whereas that in the one-loop routines is adjusted to solve the on-shell condition:

$$\begin{aligned} s &= 2\lambda v^2 + \Delta^{(1)}M_h^2(s) + \Delta^{(2)}M_{h,\text{SPheno}}^2(s), \\ \Delta^{(2)}M_{h,\text{SPheno}}^2(s) &\equiv \text{div}\left[\Pi_{hh,\text{gaugeless}}^{(2)}(s)\right] + \Delta^{(2)}M_{h,\text{gaugeless}}^2(0). \end{aligned} \quad (5.2.4)$$

This begs the question of how to compare our result with **SMH**: ideally, we would like to extract a result from **SMH** which is comparable to ours. However, this is confounded by several factors:

---

<sup>4</sup>In practice, there is always an additional residual gauge dependence as the Higgs mass is computed to finite order in perturbation theory and as not all parameters used for to compute  $m_h$  are determined to the same loop order.

- (i) It is impossible to remove or extract the electroweak contributions in **SMH**, because the individual contributions in the computation diverge as the electroweak gauge couplings become zero; and the total result is not finite at vanishing external momentum.
- (ii) To avoid the Goldstone boson catastrophe and ensure cancellation between Goldstone boson and longitudinal gauge boson diagrams, in the two-loop corrections in **SMH** the external momentum  $s$  has been replaced by  $2\lambda v^2$  wherever it appears in a pre-factor (but not in the arguments of the loop functions).
- (iii) The term

$$\Delta^{(1)} M_h^2 \supset \frac{3\lambda}{16\pi^2} (s^2 - 4\lambda^2 v^4) \frac{B(0,0)}{2\lambda v^2}, \quad (5.2.5)$$

which is part of the one-loop correction coming from Goldstone bosons and longitudinal gauge bosons, is moved into the two-loop corrections, with the justification that on-shell  $s = 2\lambda v^2 + \Delta^{(1)} M_h^2$  so will give a contribution at two-loop order when solving for the on-shell mass.

If it were not for point (2) above, it would perhaps have been possible to extract the result for the generalised effective potential approximation for the electroweak corrections. Instead, we will simply compare the results as we vary the momentum in **SMH**; by modifying slightly the source code, we obtain a version of **SMH** without the momentum dependence at two loops (but retaining the dependence at one loop). Interestingly, the result of **SMH** is finite even when  $s = 0$  meaning that the divergence as  $s \rightarrow 0$  has been removed. It turns out that this is because of the term (5.2.5), which has the effect of cancelling the divergences as  $s \rightarrow 0$  (even though this cancellation is fictitious). If we write  $\delta^{(2)}(s)$  for the missing momentum dependence in **SMH** from setting the coefficients of loop functions equal to  $2\lambda v^2$ , then we have

$$\begin{aligned} \Delta^{(2)} M_{h,\text{SMH}}^2(s) &= \frac{6\lambda}{16\pi^2} \left( \Delta^{(1)} M_h^2(s) \right) B(0,0) + \Delta^{(2)} M_{h,\text{gaugeless}}^2(s) \\ &\quad + \Delta^{(2)} M_{h,\text{electroweak}}^2(s) + \delta^{(2)}(s) \\ &= \frac{6\lambda}{16\pi^2} \left( -\frac{6\lambda^2 v^2}{16\pi^2} B(0,0) + \Delta^{(1)} M_{h,\text{SMH}}^2(0) \right) B(0,0) \\ &\quad + \text{div} \left[ \Pi_{hh,\text{gaugeless}}^{(2)}(s) + \Pi_{hh,\text{electroweak}}^{(2)}(s) + \delta^{(2)}(s) \right] \\ &\quad + \overline{\Delta}^{(2)} M_{h,\text{gaugeless}}^2(0) + \overline{\Delta}^{(2)} M_{h,\text{electroweak}}^2(0) + \bar{\delta}^{(2)}(0) + \mathcal{O}(s), \\ &= \frac{12\lambda}{16\pi^2} \left( \overline{\Delta}^{(1)} M_h^2(0) \right) + \Delta^{(2)} M_{h,\text{gaugeless}}^2(0) + \Delta^{(2)} M_{h,\text{electroweak}}^2(0) \\ &\quad + \bar{\delta}^{(2)}(0) + \mathcal{O}(s). \end{aligned}$$

The cancellations of the divergences imply that

$$\begin{aligned} &\text{div} \left[ \Pi_{hh,\text{gaugeless}}^{(2)}(s) + \Pi_{hh,\text{electroweak}}^{(2)}(s) + \delta^{(2)}(s) \right] \\ &\stackrel{?}{=} \frac{1}{(16\pi^2)^2} \left[ 36\lambda^2 v^2 \overline{\log}^2(-s) - 72\lambda^2 v^2 \overline{\log}(-s) \right] + \frac{6\lambda}{16\pi^2} \left( \overline{\Delta}^{(1)} M_h^2(0) \right) \overline{\log}(-s), \end{aligned} \quad (5.2.6)$$

where

$$\begin{aligned}
(16\pi^2)\overline{\Delta}^{(1)}M_h^2(0) &\equiv (16\pi^2)\Delta^{(1)}M_{h,\text{SMH}}^2(0) - 12\lambda^2v^2 \\
&= -12\lambda^2v^2 + 18\lambda^2v^2\overline{\log}(m_h^2) - 12y_t^2m_t^2\overline{\log}(m_t^2) \\
&\quad + \left(\frac{g_Y^2 + g_2^2}{2}\right)m_Z^2\left[3\overline{\log}m_Z^2 + 2\right] + g_2^2m_W^2\left[3\overline{\log}m_W^2 + 2\right].
\end{aligned} \tag{5.2.7}$$

On the other hand, by evaluating the diagrams for the Standard Model in the gaugeless limit retaining only the top Yukawa coupling and the Higgs quartic  $\lambda$  we find

$$\begin{aligned}
\text{div}\left[\Pi_{hh,\text{gaugeless}}^{(2)}(s)\right] &= \frac{6\lambda v^2}{(16\pi^2)^2}\overline{\log}(-s)\left[\lambda^2\left(-14 + 18\overline{\log}(m_h^2) + 3\overline{\log}(-s)\right)\right. \\
&\quad \left.- 2y_t^2\left(\lambda + (y_t^2 - \lambda)\overline{\log}(m_t^2)\right)\right],
\end{aligned} \tag{5.2.8}$$

so we can see there are several remaining pieces that must be cancelled by

$\text{div}\left[\Pi_{hh,\text{electroweak}}^{(2)}(s) + \delta^{(2)}(s)\right]$ . But if we set  $s_{\text{fixed}}^2 = -Q^2$  in our routines we should cancel the divergent part exactly, and leave us only with  $\Pi_{hh,\text{gaugeless}}^{(2)}(0)$ . We can then determine

$$\begin{aligned}
\overline{\Delta}^{(2)}M_{h,\text{electroweak}}^2(0) + \overline{\delta}^{(2)}(0) &= \Delta^{(2)}M_{h,\text{SMH}}^2(0) - \Delta^{(2)}M_{h,\text{SPheno}}^2(-Q^2) \\
&\quad - \frac{12\lambda}{16\pi^2}\left(\overline{\Delta}^{(1)}M_h^2(0)\right).
\end{aligned} \tag{5.2.9}$$

We find that this residual difference is tiny; at  $Q = m_t = 173.34$  GeV with the Higgs quartic  $\lambda = 0.12604$ , the top Yukawa  $y_t = 0.9345$ , the gauge couplings  $(g_3, g_2, g_Y) = (1.1654, 0.6442, 0.2782)$ , and the VEV  $v = 247.07$  GeV we have:

$$\overline{\Delta}^{(2)}M_{h,\text{electroweak}}^2(0) + \overline{\delta}^{(2)}(0) \simeq -0.03(\text{GeV})^2 = -0.0002\%m_h^2! \tag{5.2.10}$$

This corresponds to a tiny value of the electroweak corrections; a similar observation was made in [25].

Finally, we compare the more physically meaningful differences between the codes when we take  $s = m_h^2|_{\text{tree}}$  in our routines. The values of the Higgs mass computed with **SPheno** after turning off the light SM fermion contributions and with the modified version of **SMH** is given in table 5.3, and strikingly they only differ by 40 MeV when we include the momentum dependence in **SMH** – in other words, for  $Q = 173.34$  GeV, the momentum dependence and electroweak corrections amount to only 0.03% of  $m_h$ . We further examine the importance of both the momentum dependence and EW corrections by varying now the renormalisation scale at which we compute the Higgs mass: for this purpose, figure 5.1 shows the difference of the two-loop masses between the two codes – more precisely  $(m_h^{2\ell})^{\text{SPheno}} - (m_h^{2\ell})^{\text{SMH}}$  – with and without momentum, as a function of the renormalisation scale  $Q$  (where the  $\overline{\text{MS}}$  parameters are extracted by **SPheno** at each value while keeping  $\lambda$  fixed rather than evolving the parameters: the idea is to show the importance of the choice of scale rather than the stability of the computation). While for large scales the two-loop momentum effects may become large (1 GeV or more), the electroweak corrections represent at most 0.2 GeV and even vanish for a scale close to the  $\overline{\text{MS}}$  top mass.

	SPheno			SMH	
$\xi$	1	0.01	0.01	0	
$v$ [GeV]	247.494	246.914			
$y_t$	0.939	0.939	0.940		
$(g_3, g_2, g_Y)$	(1.1654, 0.6452, 0.2780)				
2 $\ell$ momentum dependence	partial $s = m_h^2 ^\text{tree}$	partial $s = m_h^2 ^\text{tree}$	partial $s = m_h^2 ^\text{tree}$	full iterative	none $s = 0$
Light SM fermions	yes	yes	no	no	no
$m_h^{2\ell}$ [GeV]	125.083	125.134	125.133	125.176	125.121

Table 5.3 – Comparison of two-loop Higgs masses calculated with the codes **SPheno** and **SMH**, for different choices of gauge in **SPheno** and switching on and off the two-loop momentum dependence in **SMH**. The renormalisation scale is fixed to  $Q = 173.34$  GeV, and the Higgs quartic coupling is  $\lambda = 0.12604$  and is not varied (the idea being to illustrate the importance of the choice of scale, rather than the stability of the result). All other inputs for **SMH** are taken to the same values as in **SPheno**. In **SPheno** the only two-loop momentum dependence is from pseudo-scalar diagrams and only a generalised effective potential approach (see main text) with  $s = m_h^2|_{\text{tree}}$ , while in **SMH** the full two-loop dependence is implemented and is used to find  $m_h$  iteratively.

### 5.2.3 Momentum dependence

Implementing the solution to the Goldstone boson catastrophe in **SARAH** has required the insertion of external momentum in infra-red divergent loop integrals, and thus we should also investigate the impact of the momentum  $s = -p^2$  on the Higgs mass calculation in **SPheno**. In practise, we have set for the majority of scans the external momentum for the two-loop calculations to be equal to  $m_h^2|_{\text{tree}}$  but we will now vary the momentum to study its impact on  $m_h$ . Table 5.4 shows the shift to the two-loop Higgs mass – with respect to the value computed with  $s = (125 \text{ GeV})^2$  – for external momentum in loops equal to  $s = \alpha \times (125 \text{ GeV})^2$ , where  $\alpha$  ranges from  $10^{-6}$  to  $10^6$  and for  $\lambda = 0.126$  and  $\lambda = 0.130$ . For all values of the external momentum considered here, the variation of the Higgs mass remains small: at most they become of order  $\sim 0.13$  GeV for  $\alpha = 10^{-6}$  (*i.e.*  $\sqrt{s} = 0.125$  GeV), and while this effect is noticeable, it is far from the divergences that could have been feared when approaching the limit of  $s \rightarrow 0$ . All in all, although pole masses – as we compute here – are in principle found as the zero of the inverse propagator, that has to be found iteratively as the self-energy contains momentum dependence, we see from the minute effects of momentum in the range  $\alpha \in [1/2, 100]$ , relevant for scalar masses, that we will not require an iterative solution and that simply taking  $s = (125 \text{ GeV})^2$  in the loop diagrams with pseudo-scalars will be a satisfactory approximation. In particular, changing  $s$  between  $m_h^2|_{\text{tree}}$  and 125 GeV causes a difference in  $m_h^{2\ell}$  of less than an MeV.

We emphasise however that the effect of momentum on Goldstone boson mass diagrams discussed here is only a subset of the general momentum dependence of the two-loop masses, which should in principle be taken into account, as seen in the previous subsections.

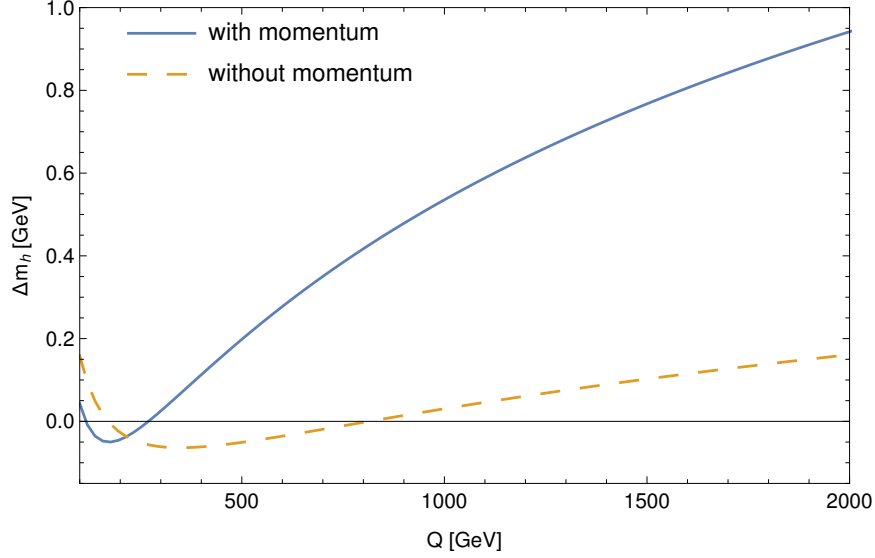


Figure 5.1 – Difference between the two-loop Higgs mass computed by **SMH** and **SPheno** –  $(m_h^{2\ell})^{\text{SPheno}} - (m_h^{2\ell})^{\text{SMH}}$  – as a function of the renormalisation scale  $Q$ , with (*blue curve*) and without (*orange dashed curve*) the momentum dependence at two loops in **SMH**. The Higgs quartic coupling is here  $\lambda = 0.12604$ . In **SPheno** the contributions of the light SM fermions are turned off and the external momentum in the two-loop routines is set to  $s = m_h^2|_{\text{tree}}$ .

$\delta m_h^{2\ell}$ [GeV]					
$\lambda$	$\alpha = 10^{-6}$	$\alpha = 10^{-4}$	$\alpha = 10^{-2}$	$\alpha = 1/2$	$\alpha = 1$
0.126	0.1210	0.0655	0.0252	0.0028	0.0
0.130	0.1302	0.0704	0.0270	0.0030	0.0
$\lambda$	$\alpha = 2$	$\alpha = 100$	$\alpha = 10^4$	$\alpha = 10^6$	
0.126	-0.0025	-0.0100	-0.0048	0.0155	
0.130	-0.0026	-0.0106	-0.0048	0.0560	

Table 5.4 – Shift in GeV of the two-loop Higgs mass in the Standard Model – computed with **SPheno** and with respect to the value obtained for  $p = 125$  GeV – for different values of the quartic coupling  $\lambda$ , and of the incoming momentum  $s = \alpha \times (125 \text{ GeV})^2$  in the two loop routines.

### 5.3 The NMSSM

As a second check of our new solution, and demonstration of its importance, we shall compare the results for the three different options to solve the Goldstone Boson Catastrophe in the example of the Next-to-minimal supersymmetric standard model (NMSSM) – see [78] and references therein for a detailed description of the model, or section 1.3.4.5 for a brief introduction. Indeed, the NMSSM is the first supersymmetric model for which the problems at certain points in the parameter space were found in earlier versions of **SARAH**. Here we shall show that this is avoided, and have a preliminary look at the impact of the “consistent tadpole solutions.”

We start with a test point defined by the following input parameters:

$$\lambda_S = 0.7, \quad \kappa = 0.25, \quad A_{\lambda_S} = 1350 \text{ GeV}, \quad A_{\kappa} = -500 \text{ GeV}, \quad \mu_{\text{eff}} = 600 \text{ GeV}, \\ M_1 = M_2 = 1000 \text{ GeV}, \quad M_3 = 2000 \text{ GeV},$$

	$D$	$R = 10^{-5}$	$R = 10^{-4}$	$R = 10^{-3}$	$R = 10^{-2}$	$R = 10^{-1}$	OS	OS+Tad
$h_1$	129.58	65.27	124.63	129.07	129.82	130.58	129.70	129.97
$h_2$	315.64	312.84	315.39	315.59	315.55	315.67	315.09	315.60
$h_3$	1632.28	1627.55	1631.77	1632.36	1632.63	1632.81	1632.51	1633.39
$A_1$	582.02	582.61	582.31	582.02	581.74	581.63	580.94	581.23
$A_2$	1631.98	1630.38	1631.15	1631.88	1632.43	1632.59	1632.04	1632.60

Table 5.5 – The Higgs masses in the NMSSM (in GeV) for the parameter point defined by eq. (5.3.1) for different choices for the two-loop corrections.

$$(m_Q)_{33} = 1500 \text{ GeV}, \quad (m_{\bar{u}})_{33} = 1000 \text{ GeV}, \quad (5.3.1)$$

and all other soft-masses set to 2 TeV. Table 5.5 gives the results for the Higgs masses obtained with the following calculations:

- (i)  $D$ -terms turned off in mass matrices but retained in tadpole solutions (as in previous versions of **SARAH**), labelled “ $D$ ” in the table.
- (ii) Regulator masses with  $R = 10^{-5}$ – $10^{-1}$ .
- (iii) Goldstones set on shell, with and without consistent tadpole solutions, labelled OS and OS+Tad respectively.

We see from this table that there is an agreement in the light Higgs mass of about 0.4 GeV between all the calculations if  $R$  is chosen to be about  $10^{-2}$ .

While the new “on-shell” solution of the Goldstone boson catastrophe is optimal, between introducing a regulator  $R$  and the previous approach with neglected  $D$ -terms in the scalar mass matrix, the latter is preferred because one does not need to check for a suitable choice of  $R$  to stabilise the results. However, we can now consider parameter points where the old method fails. This is shown for the point defined by

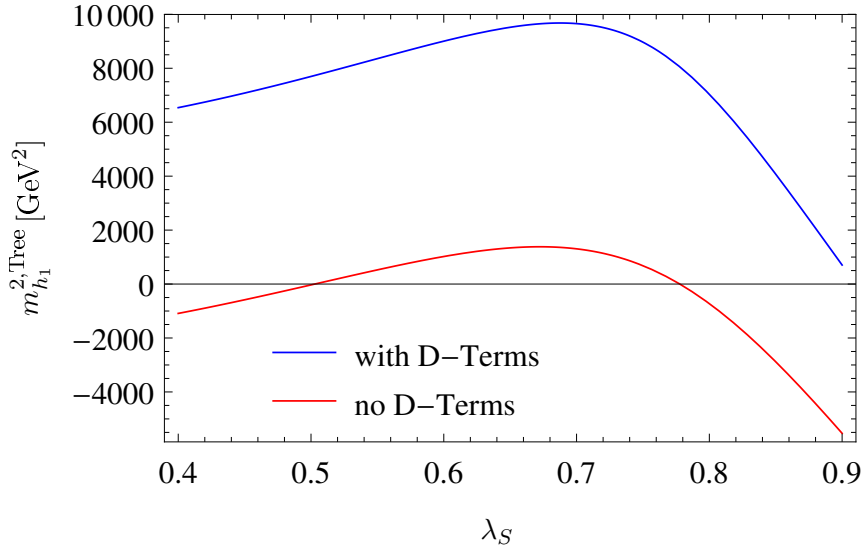


Figure 5.2 – The lightest scalar mass squared for the parameter point defined by eq. (5.3.2) when calculating with and without  $D$ -term contributions.

$$\begin{aligned} \kappa = 0.6, \quad A_{\lambda_S} = 200 \text{ GeV}, \quad A_{\kappa} = -200 \text{ GeV}, \quad \mu_{\text{eff}} = 150 \text{ GeV} \quad (5.3.2) \\ M_1 = M_2 = 1000 \text{ GeV}, \quad M_3 = 2000 \text{ GeV} \end{aligned}$$



and all scalar soft-masses set to 2 TeV. The lightest scalar tree-level mass with and without the  $D$ -terms as function of  $\lambda_S$  is shown in figure 5.2. One can see that for  $\lambda_S \simeq 0.5, 0.8$ , the lightest scalar becomes massless in the limit of vanishing  $D$ -terms. Thus, for these values, divergences in the two-loop corrections can be expected which are this time not associated with the Goldstone but with the lightest CP even state.

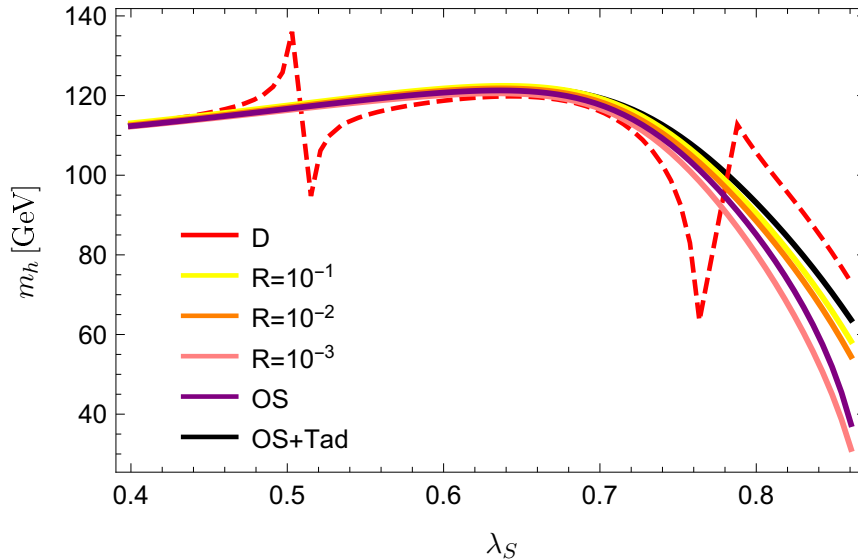


Figure 5.3 – The lightest Higgs mass at the two-loop level for the parameter point defined by eq. (5.3.2) for different methods to regulate the two-loop corrections.

We show the lightest Higgs mass in figure 5.3 as function of  $\lambda_S$  for different methods to regulate the two-loop corrections. Obviously, the approach of neglecting electroweak  $D$ -terms fails for values of  $\lambda_S$  at which the masses entering the loop calculations become very light. However, for very large values of  $\lambda_S$  which are away from the poles, the agreement with the other calculations is also rather poor. In contrast, over the entire range of  $\lambda_S$  we see a good agreement between the methods using regulator masses, if  $R = 10^{-2}$  or  $10^{-3}$  is chosen, and the method of treating the Goldstones on-shell. It is interesting that for these values of  $R$  the minimum mass is  $\sqrt{R} \times M_{\text{SUSY}} \simeq 100$  GeV, *i.e.* logarithmic contributions involving the light scalars are being excised.

We note that the corrections from the consistent tadpole solution are small until  $\lambda_S$  becomes large, at which point we see significant deviations. However, as  $\lambda_S$  approaches 0.9 we see from figure 5.2 that the tree-level lightest Higgs mass approaches zero, so we expect our perturbative calculation of the “consistent tadpole solution” to break down and become unreliable.

## 5.4 Split SUSY

In Split SUSY scenarios [211,212,304–307], the SUSY scalars are much heavier than the gauginos and Higgsinos. Consequently, these models should be studied in an effective approach where all SUSY scalars are integrated out at some matching scale. The

Lagrangian below this scale is given by

$$\mathcal{L} = \mathcal{L}_{\text{SM}} - \left( \frac{1}{2} M_3 \tilde{g}^\alpha \tilde{g}^\alpha + \frac{1}{2} M_2 \tilde{W}^a \tilde{W}^a + \frac{1}{2} M_B \tilde{B} \tilde{B} + \mu \tilde{H}_u^T \epsilon \tilde{H}_d + \text{h.c.} \right) \quad (5.4.1)$$

$$- \left[ \frac{1}{\sqrt{2}} H^\dagger \left( \tilde{g}_{2u} \sigma^a \tilde{W}^a + \tilde{g}_{1u} \tilde{B} \right) \tilde{H}_u + \frac{1}{\sqrt{2}} H^T \epsilon \left( -\tilde{g}_{2d} \sigma^a \tilde{W}^a + \tilde{g}_{1d} \tilde{B} \right) \tilde{H}_d + \text{h.c.} \right] \quad (5.4.2)$$

where  $\mathcal{L}_{\text{SM}}$  is the Standard Model Lagrangian with Higgs potential (1.1.5). Because of the matching between the effective, non-supersymmetric model and the MSSM, the quartic Higgs coupling  $\lambda$  as well as the new Yukawa-like interactions  $\tilde{g}_{(1,2)(u,d)}$  are not free parameters but fixed by the matching conditions at the scale  $M_M$ . At tree-level, the following relations hold

$$\tilde{g}_{2u}(M_M) = g_2(M_M) \sin \beta \quad (5.4.3)$$

$$\tilde{g}_{2d}(M_M) = g_2(M_M) \cos \beta \quad (5.4.4)$$

$$\tilde{g}_{1u}(M_M) = \sqrt{\frac{3}{5}} g_1(M_M) \sin \beta \quad (5.4.5)$$

$$\tilde{g}_{1d}(M_M) = \sqrt{\frac{3}{5}} g_1(M_M) \cos \beta \quad (5.4.6)$$

$$\lambda(M_M) = \frac{1}{8} (g_1^2(M_M) + g_2^2(M_M)) \cos^2 2\beta \quad (5.4.7)$$

Here,  $g_1$  and  $g_2$  are the running gauge couplings of  $U(1)_Y$  and  $SU(2)_L$  and  $\beta$  is defined as the mixing angle of the two Higgs doublets in the MSSM (in contrast to the definition in the MSSM as a ratio of expectation values). There are important higher-order corrections to the matching conditions which are necessary to have a precise prediction for the Higgs mass at the low scale. In particular  $\lambda$  has been calculated including the two-loop SUSY corrections [213, 215, 216]. The numerical value of these corrections depends on the many SUSY parameters at the matching scale; however, a commonly taken useful approximation is to give the scalars a common mass  $M_{\text{mess}}$ , in which case the corrections can be given in terms of just this scale and the squark mixing. Moreover, in strict split SUSY where the fermion masses are protected by an  $R$ -symmetry (or another symmetry in Fake Split SUSY [308, 309]) near the electroweak or TeV scale and well below  $M_{\text{mess}}$ , the squark mixing must be very small. In which case, the leading corrections to the Higgs quartic coupling are purely electroweak at one loop, and at two loops contain no logarithmic terms – meaning that they are very small (in particular since the strong gauge and top Yukawa couplings run to small values at higher scales), so using the tree-level relationship above can be good enough.

Below the scale  $M_{\text{mess}}$ , we must run to the scale of the fermion masses, before also integrating them out, and then running to the electroweak scale in the Standard Model. In some previous approaches, the running was performed all the way down to the electroweak scale, before calculating the Higgs mass in the full Lagrangian (5.4.2); however, it was found in [308] that in this approach it is necessary to include the *three-loop* leading logarithm involving the gluino mass to obtain good agreement between the two results – this is automatically resummed by the renormalisation group running in the former approach. In either case, the full contribution of the gauginos and Higgsinos to the matching conditions is only known in the literature to *one-loop* order [213].

Hence in this section we are interested in the effect of the two-loop corrections to the Higgs mass stemming from the  $\tilde{g}_{(1,2)(u,d)}$  couplings which have not been studied in the

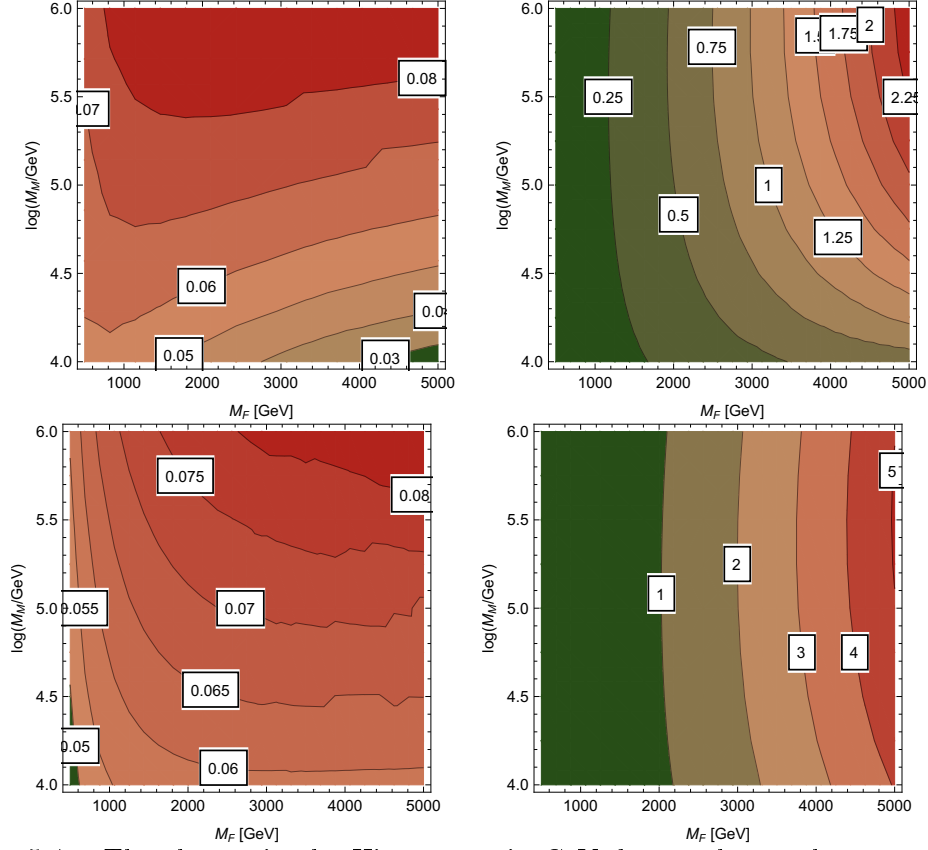


Figure 5.4 – The change in the Higgs mass in GeV due to the two-loop corrections involving the new Yukawa-like interactions  $\tilde{g}_{(1,2)(u,d)}$ . On the top, we used  $\tan \beta = 1$  at  $M_M$  and on the bottom  $\tan \beta = 10$ . The left plots are with the consistent tadpole solutions, the right ones without.

literature before. They are expected to be small since they originate from electroweak interactions at the matching scale (and so, admittedly, one could argue that we should neglect them in the gaugeless limit). We shall not discuss the absolute value of the Higgs mass, for which we would need to include all higher-order corrections to the matching that have been calculated elsewhere, but only on the impact of the new two-loop corrections. The overall size of these corrections is rather insensitive to the exact matching conditions and we will be using the above tree-level relations; but as we noted earlier, these should be a particularly good approximation for larger matching scales.

We make in addition the simplifying assumption that at  $M_M$  the SUSY fermions are degenerate, *i.e.*

$$\mu(M_M) = M_1(M_M) = M_2(M_M) = M_3(M_M) \equiv M_F \quad (5.4.8)$$

and thus we are left with three free parameters:

$$M_F, \quad M_M, \quad \tan \beta.$$

SARAH uses two-loop RGEs for the running between  $M_M$  and the renormalisation scale  $Q$  that we set to  $M_F$ , which as mentioned above is necessary to avoid large logarithmic contributions from the gluino. The size of the two-loop corrections proportional to the  $\tilde{g}_{(1,2)(u,d)}$  couplings in the  $(M_M, M_F)$  plane is shown in figure 5.4 for  $\tan \beta = 1$  and 10 for a calculation with and without the consistent tadpole solutions explained in

section 4.4. We show here results for  $M_F$  up to 5 TeV. In order not to increase the theoretical uncertainty in the presence of new fermions in the multi-TeV range, we made use of the functionality in **SARAH** to perform the Higgs mass calculation in the effective SM [221]. For this purpose, a second matching is performed to extract  $\lambda$  at the renormalisation scale  $Q$ . The imposed matching condition is

$$m_h^{\text{SM}}(M_F) \equiv m_h^{\text{Split}}(M_F) \quad (5.4.9)$$

*i.e.* we perform a matching of the Higgs pole masses as suggested in [218], from which an effective  $\lambda$  is derived.  $\lambda$  is then evolved to  $m_t$  using three-loop RGEs of the SM. At  $m_t$  the Higgs mass is calculated within the SM at the two-loop level. The additional loop-corrections discussed here enter the calculation of  $m_h^{\text{Split}}(M_F)$ , and in turn that of  $\lambda^{\text{SM}}(M_F)$ .

We see that the additional corrections for SUSY fermions are always well below 1 GeV once the consistent solution to the tadpole equations are included. However, if those are not used, the misleading impression of sizeable corrections of a few GeV is given; it would be interesting to investigate this phenomenon further.

## 5.5 Two-Higgs-Doublet Model

In this section we will be interested in the effect of two-loop scalar mass corrections in the CP-conserving 2HDM. For most scans and figures presented below, we worked in the *type-I* 2HDM if not indicated otherwise. However as the difference with *type-II* comes from the couplings of the scalars to the down-type quarks and to the leptons which are light and give much smaller contributions to the lightest Higgs mass than the top quark, we do not expect large effects on our results (even for large  $\tan\beta$ , since the contributions typically involve the quark masses rather than just the couplings).

### 5.5.1 The alignment in Two-Higgs-Doublet Models

Instead of the  $\mathbb{Z}_2$  basis defined in eq. (1.4.14), it is often more convenient to work in another basis – the so-called Higgs basis  $\{H_1, H_2\}$  – where the neutral component of the doublet  $H_1$  is aligned in field space with the total VEV  $v$ , with a rotation of angle  $\beta$

$$\begin{cases} \Phi_1 &= H_1 c_\beta - H_2 s_\beta \\ \Phi_2 &= H_1 s_\beta + H_2 c_\beta \end{cases} \Leftrightarrow \begin{cases} H_1 &= \Phi_1 c_\beta + H_2 s_\beta \\ H_2 &= -\Phi_1 s_\beta + \Phi_2 c_\beta \end{cases} \quad (5.5.1)$$

We choose to write these two new doublets as

$$H_1 = \begin{pmatrix} H_1^+ \\ \frac{1}{\sqrt{2}}(v + H_1^0) \end{pmatrix}, \quad H_2 = \begin{pmatrix} H_2^+ \\ \frac{1}{\sqrt{2}}H_2^0 \end{pmatrix}. \quad (5.5.2)$$

In this new basis, following the notation of [132], the potential can be written as

$$\begin{aligned} V^{(0)} &= Y_1 (H_1^\dagger \cdot H_1) + Y_2 (H_2^\dagger \cdot H_2) + Y_3 (H_1^\dagger \cdot H_2 + H_2^\dagger \cdot H_1) \\ &+ \frac{Z_1}{2} (H_1^\dagger \cdot H_1)^2 + \frac{Z_2}{2} (H_2^\dagger \cdot H_2)^2 + Z_3 (H_1^\dagger \cdot H_1) (H_2^\dagger \cdot H_2) \\ &+ Z_4 (H_1^\dagger \cdot H_2) (H_2^\dagger \cdot H_1) + \frac{1}{2} Z_5 \left[ (H_1^\dagger \cdot H_2)^2 + (H_2^\dagger \cdot H_1)^2 \right] \\ &+ \left[ Z_6 (H_1^\dagger \cdot H_1) + Z_7 (H_2^\dagger \cdot H_2) \right] [H_1^\dagger \cdot H_2 + H_2^\dagger \cdot H_1]. \end{aligned} \quad (5.5.3)$$

The CP-even physical states are eigenstates of the mass matrix

$$\mathcal{M}_H^2 = \begin{pmatrix} Z_1 v^2 & Z_6 v^2 \\ Z_6 v^2 & m_A^2 + Z_5 v^2 \end{pmatrix}, \quad (5.5.4)$$

$$\text{where } m_A^2 = -\frac{2m_{12}^2}{s_{2\beta}} - \lambda_5 v^2 \quad (5.5.5)$$

which is diagonalised with an angle  $\alpha$ , and are given by

$$\begin{cases} h = (\sqrt{2}\Re(\Phi_1^0) - v_1)s_\alpha + (\sqrt{2}\Re(\Phi_2^0) - v_2)c_\alpha = \Re(H_1^0)s_{\beta-\alpha} + \Re(H_2^0)c_{\beta-\alpha} \\ H = (\sqrt{2}\Re(\Phi_1^0) - v_1)c_\alpha - (\sqrt{2}\Re(\Phi_2^0) - v_2)s_\alpha = \Re(H_1^0)c_{\beta-\alpha} - \Re(H_2^0)s_{\beta-\alpha} \end{cases} \quad (5.5.6)$$

The *alignment limit* is defined as the limit in which the neutral components of the Higgs-basis doublets are also mass eigenstates, or in other words, the limit in which one of the CP-even neutral scalar mass eigenstates is aligned with the VEV  $v$ . From eq. (5.5.6) we see that this can be realised in two ways:

- (i)  $s_{\beta-\alpha} = 0$  in which  $H$  carries the VEV and is identified with the SM-like Higgs.
- (ii)  $c_{\beta-\alpha} = 0$  which means that  $h$  is the SM-like Higgs.

We do not make any assumption on the size of the masses of the different scalars *i.e.* we do not suppose that we are in the decoupling limit as well. Consequently, at tree-level we only require  $Z_6 v^2 \rightarrow 0$ , and hence with the expression of  $Z_6$  derived in [132], we have

$$Z_6 \equiv -s_{2\beta} \left[ \lambda_1 c_\beta^2 - \lambda_2 s_\beta^2 - \frac{1}{2} \lambda_{345} c_{2\beta} \right] = 0 \quad (5.5.7)$$

where  $\lambda_{345} \equiv \lambda_3 + \lambda_4 + \lambda_5$ . The simplest, and  $\tan\beta$ -independent, way to fulfil this condition is to have

$$\lambda_1 = \lambda_2 = \frac{1}{2} \lambda_{345}, \quad (5.5.8)$$

which we will use in the following to constrain tree-level alignment. Also, we will require that the SM-like Higgs be the lightest mass eigenstate  $h$  (case (ii) above), by ensuring that

$$Z_1 v^2 < m_A^2 + Z_5 v^2 \quad (5.5.9)$$

This implies that  $c_{\beta-\alpha} = 0$ , and thus, with the conventional choice that  $\beta \in [0, \frac{\pi}{2}]$  and  $|\alpha| \leq \frac{\pi}{2}$ , we have that

$$\beta - \alpha = \frac{\pi}{2} \Rightarrow \alpha \in [-\frac{\pi}{2}, 0]. \quad (5.5.10)$$

The constrain for tree-level alignment given in eq. (5.5.8) reduces the number of free parameters of the model from seven to five, as two of the quartic couplings (eg.  $\lambda_2$  and  $\lambda_3$ ) can be found as a function of the three other ones.

### 5.5.2 Renormalisation scale dependence of the Higgs mass computed with SPheno

The masses computed by **SPheno** are pole masses, which should in principle not depend on the renormalisation scale at which they are computed. Evaluating the variation of the masses with the scale  $Q$  hence provides a consistency check of our results and an estimate of the theoretical uncertainty as the variation of the two-loop masses with  $Q$  corresponds roughly to the three-loop corrections. For this purpose, we have tuned the

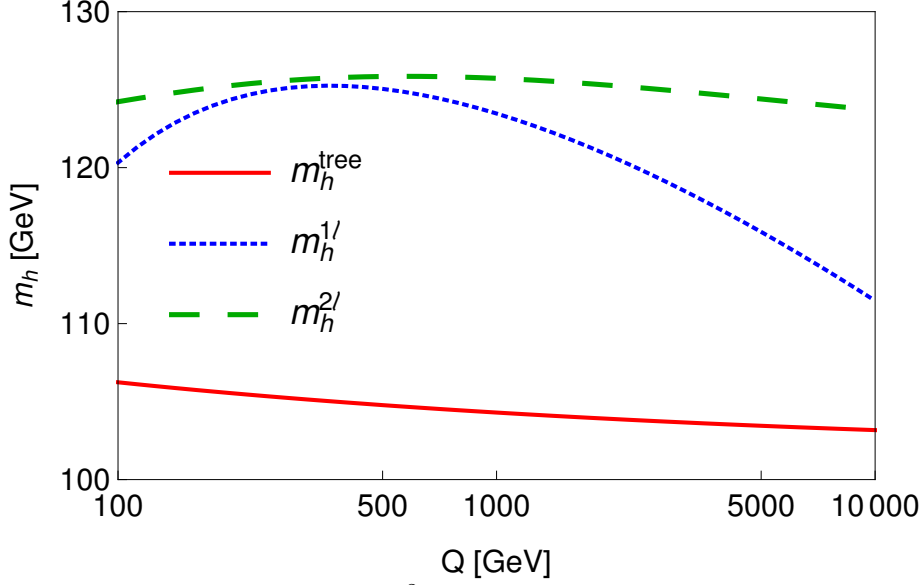


Figure 5.5 – Lightest Higgs mass  $m_h^2$  as a function of the renormalisation scale  $Q$ , considering only the running of SM parameters. In other words, for this figure, the values of the BSM parameters  $\lambda_i$ ,  $m_{12}^2$ , and  $\tan\beta$  given in eq. (5.5.11) are considered to be input values at the scale  $Q$  at which the Higgs mass is computed, instead of being evolved from 160 GeV to  $Q$ . *Red curve*: tree-level; *Blue dot-dashed curve*: one-loop order; *Green dashed curve*: two-loop order.

$\lambda_i$  couplings to ensure a two-loop Higgs mass of 125.09 GeV, at scale  $Q = 160$  GeV, together with tree-level alignment and find the following values

$$\begin{aligned} \lambda_1 = \lambda_2 = 0.0911, \quad \lambda_3 = 0.3322, \quad \lambda_4 = 0.8000, \quad \lambda_5 = -0.9500 \\ m_{12}^2 = -50\,000 \text{ GeV}^2, \quad \tan\beta = 50. \end{aligned} \quad (5.5.11)$$

Using **HiggsBounds** we have verified that this point in parameter space is not excluded by the current experimental constraints.

At first we only take into account the running of SM parameters, and we then consider that the above input parameters (*i.e.* those in eq. (5.5.11)) are given to **SPheno** as the values of the couplings at the scale  $Q$  at which the Higgs mass is computed, which we vary in the range  $[100 \text{ GeV}, 10\,000 \text{ GeV}]$ . We find the results shown in figure 5.5 for the tree-level, one-loop and two-loop Higgs mass  $m_h$ . Since phenomenological analyses typically supply the quartic couplings without reference to a higher-energy theory or the scale where they are determined, this plot shows the importance of the choice of that scale.

We have verified that the renormalisation scale dependence of  $m_h^{\text{tree}}$  (that is computed in terms of the parameters of the 2HDM scalar sector, *i.e.* the parameters in eq. (5.5.11) and  $v$ ) is entirely due to the scale dependence of the Higgs VEV  $v$ ,<sup>5</sup> as the running of the quartic couplings is for the moment not applied. The renormalisation scale  $Q$  is seen to have only a limited effect on the two-loop value of  $m_h$  which varies of about 2 GeV on the range of scales considered here, while the one-loop result varies by about 15 GeV. Since the two-loop curve is so flat, this shows that most of the variation in

<sup>5</sup>We recall that **SARAH/SPheno** employs here a running VEV, extracted from the  $Z$  boson pole mass at one-loop order. The reader may refer to appendix A of [221] for more details.

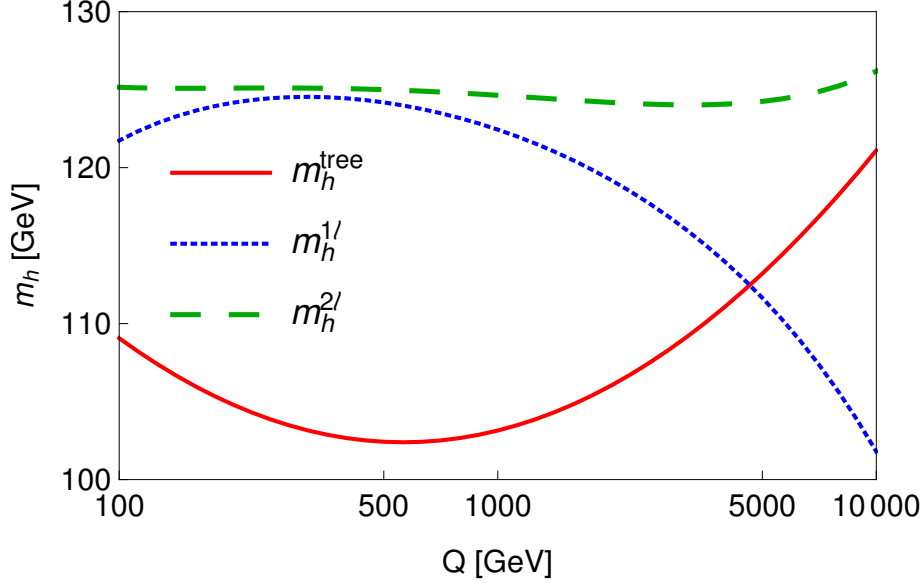


Figure 5.6 – Lightest Higgs mass  $m_h^2$  as a function of the renormalisation scale  $Q$ , taking into account the running of all parameters – both SM and BSM ones – with the RGEs included in **SPheno**. The difference between this figure and figure 5.5 is that here we do not consider the inputs given in equation (5.5.11) to be taken at the scale  $Q$  at which we compute  $m_h$  but at the scale  $m_t$ , and then we evolve them from  $m_t$  to  $Q$ . *Red curve*: tree-level; *Blue dot-dashed curve*: one-loop order; *Green dashed curve*: two-loop order.

the calculation of Higgs mass for the chosen quartics must come from variation of the Standard Model parameters, and that a two-loop calculation (rather than one-loop) is necessary not just for precision but also to ensure scale stability.

Using the two-loop RGEs implemented in **SARAH/SPheno**, we can also include the evolution of the 2HDM parameters to obtain a more complete scale dependence of the masses, as shown in figure 5.6. To be more specific, here we do not consider the inputs in eq. (5.5.11) to be given at the scale  $Q$  at which we compute  $m_h$ , but instead we run these values from  $m_t$  to  $Q$ .

Once more, the two-loop value of Higgs mass depends less on the renormalisation scale than the tree-level or one-loop values. This smaller dependence of the two-loop Higgs mass on  $Q$ , compared with the one-loop mass, even for choices of parameters that give large loop corrections is a first verification of the validity of our new two-loop routines. In the following we will therefore work at a fixed scale  $Q = m_t$ , confident that the results will be for the most part independent of this choice.

### 5.5.3 Quantum corrections to the alignment limit

The relations defining the alignment limit, in section 5.5.1, are only valid at tree level and we expect them to receive corrections at one- and two-loop order, and in this section we will discuss the importance of these effects on the mixing angle of the neutral CP-even scalars  $\alpha$ .

Scanning over the different free couplings of the model –  $m_{12}^2$  and  $\lambda_i$  ( $i \in \{3, 4, 5\}$ ) – we compare the values of the CP-even Higgs mixing angle  $\alpha$  at tree level, one-loop and two-loop order, as shown in figure 5.7, and as expected, loop corrections cause

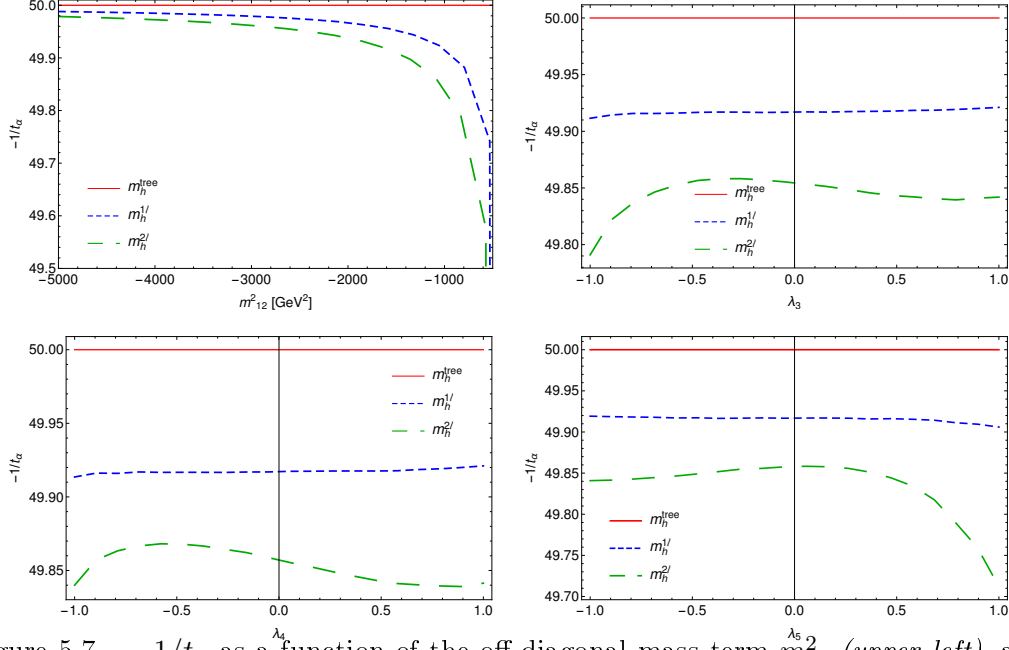


Figure 5.7 –  $-1/t_\alpha$  as a function of the off-diagonal mass term  $m_{12}^2$  (*upper left*), and of quartic couplings  $\lambda_3$  (*upper right*),  $\lambda_4$  (*lower left*) and  $\lambda_5$  (*lower right*) at each order in perturbation theory. For each plot we vary the parameters as follows: we choose one parameter as the abscissa; the tree-level alignment condition  $\lambda_1 = \lambda_2 = 1/2\lambda_{345}$  plus the requirement that the Higgs mass is 125.09 GeV fixes *three* parameters, namely  $\lambda_1, \lambda_2$  and either  $\lambda_4$  for the bottom right plot or  $\lambda_5$  for the other three; the remaining parameters are held fixed at values  $\lambda_3 = 0.5$ ,  $\lambda_4 = 0.5$ ,  $m_{12}^2 = -1000$  GeV<sup>2</sup> (when they are not otherwise varying). All plots are for  $\tan\beta = 50$ . *Red curve*: tree-level; *Blue dot-dashed curve*: one-loop order; *Green dashed curve*: two-loop order.

deviations from the tree-level relation  $t_\alpha = -1/t_\beta \Leftrightarrow c_{\beta-\alpha} = 0$ . The observations we can make from these plots are the following:

- (i) in the ranges of parameters that we considered, the effect of loop corrections on the value of  $\alpha$  is small, at most of the order of 1%;
- (ii) the one-loop corrections to  $\alpha$  show very little dependence on the quartic couplings  $\lambda_{i=3,4,5}$ ;
- (iii) it appears that for most parameter points, the two-loop corrections to  $\alpha$  are of similar magnitude than the one-loop ones – although somewhat smaller when  $|\lambda_i| \lesssim 1$ .
- (iv) for some parameter points however, the two-loop corrections to  $\alpha$  become significantly larger than the one-loop corrections, see the lower right plot in figure 5.7. We have verified that this happens when one of the quartic couplings  $\lambda_i$  becomes large (typically  $|\lambda_i| \gtrsim 1$ ) – in the plot mentioned above of  $-1/t_\alpha$  as a function of  $\lambda_5$  it is  $\lambda_4$  that becomes smaller than  $-1$ . We may suspect the large two-loop effects are due to a loss of perturbativity: this will be discussed in more detail in the next section.



### 5.5.4 Perturbativity constraints

It is common in practice to use the physical scalar masses, the  $\mathbb{Z}_2$  breaking parameter  $m_{12}$  as well as the angles  $\alpha, \beta$  as input for the 2HDM in numerical studies. However, this input often hides that it corresponds to huge quartic couplings which spoil unitarity and the perturbative behaviour of the theory. Therefore, the constraints that all quartic couplings must be smaller than  $4\pi$  as well as the tree-level unitarity constraints [310–312] are applied to sort such points out. However, it was already shown in the SM that the limit of  $\lambda < 4\pi$  might be too weak [313].

We now have all the machinery at hand to impose another constraint on the 2HDM model namely that the radiative corrections to the Higgs mass converge. We show here in one example that this can be a much stronger constraint than tree-level unitarity, while a more detailed analysis of this constraint on the parameter space of 2HDM models is left for future work.

We consider here a point for type-II defined by <sup>6</sup>

$$\begin{aligned} m_H &= 593.6 \text{ GeV}, & m_A &= 535.2 \text{ GeV}, & m_{H^\pm} &= 573.2 \text{ GeV}, \\ m_{12}^2 &= -165675 \text{ GeV}^2, & \tan \alpha &= -0.235, & \tan \beta &= 1.017. \end{aligned} \quad (5.5.12)$$

Since the masses are treated as pole-masses and only tree-level relations are used in the above work, no scale for the  $\overline{\text{MS}}$  parameters is given. On the other side, it is usually checked that the translation of these masses into quartic couplings results in parameters which are allowed by tree-level unitarity. However, this treatment implicitly assumes that one can define at each loop level suitable counter-terms to renormalise the Higgs sector in a way that the masses can be kept constant, and that this renormalisation converges. This is however not the case for the parameter point defined by eq. (5.5.12) as one can see as follows. Using the tree-level relations (1.4.19) to (1.4.23), the input given in eq. (5.5.12) translates into the following<sup>7</sup> set of quartic couplings:

$$\lambda_1 = 2.831, \quad \lambda_2 = -2.134, \quad \lambda_3 = 7.974, \quad \lambda_4 = -0.660, \quad \lambda_5 = 0.753, \quad (5.5.13)$$

which fulfil the tree-level unitarity constraints [310–312].

To check the perturbative behaviour, we show the scale dependence in figure 5.8. Here, we used the values of the quartic couplings in eq. (5.5.13) as inputs – computed from eq. (5.5.12) at scale  $m_t$ , and evolved to the scale  $Q$  at which we compute the Higgs mass – and checked the scale dependence of the Higgs mass at different loop levels.

For the evaluation of couplings at the considered scale, we used the two-loop RGEs calculated by **SARAH**. One sees that the scale dependence increases with increasing loop-level. Of course, one might wonder if this is just an effect from our choice to define the quartic couplings at  $Q = m_t$  as input. Therefore, we show in figure 5.9 the size of the loop corrections for different choices of our input scale  $Q$ . We see that the size of the loop corrections rapidly increases for  $Q > m_t$  and the spread between one- and two-loop becomes even larger. Also choosing  $Q \simeq 160 \text{ GeV}$  where the mass at one- and two-loop level seem to be roughly identical does not solve the problem: this is just a numerical coincidence and the scale dependence at two loops is even larger than at one loop.

<sup>6</sup>We used **HiggsBounds** [290, 292] to check that this point passes all current collider limits.

<sup>7</sup>Note, negative  $\lambda_2$  is usually taken to be forbidden because the potential is unbounded from below. However, this only holds for the tree-level potential. If RGE effects are included,  $\lambda_2$  becomes positive after a few hundred GeV of running [314].

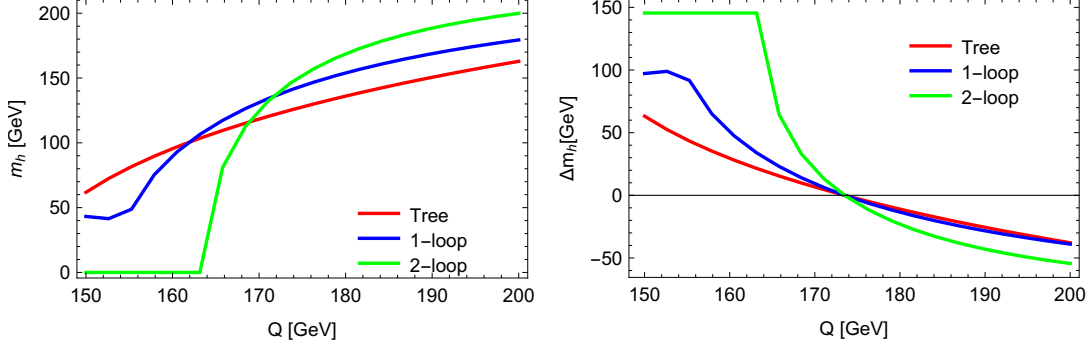


Figure 5.8 – The dependence of the lightest scalar mass on the renormalisation scale  $Q$ , considering that the quartic couplings of eq. (5.5.13) are used as input at the scale  $Q = m_t$ . *Left:*  $m_h(Q)$  at tree-, one-loop, and two-loop levels; *Right:*  $\Delta m_h \equiv m_h(m_t) - m_h(Q)$  at tree-, one-loop, and two-loop levels

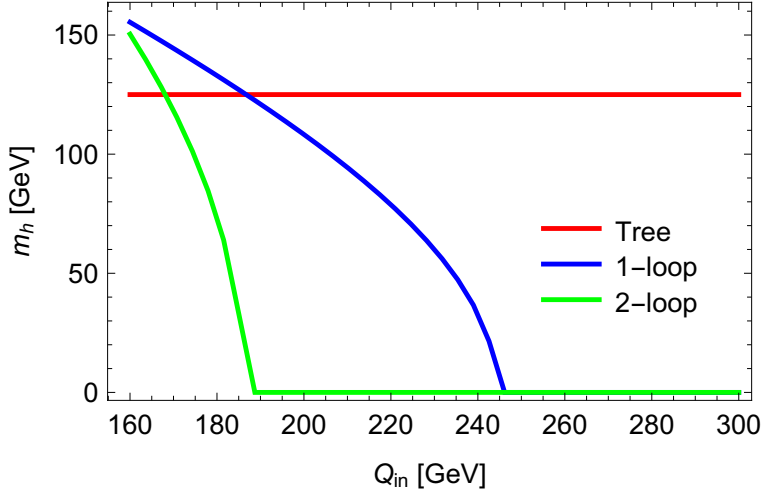


Figure 5.9 – The size of the one- and two-loop corrections of the lightest scalar mass as function of the scale  $Q_{in}$  at which the input masses of eq. (5.5.12) are translated into quartic couplings (or in other words, the scale at which the quartic couplings in eq. (5.5.13) are defined as inputs).

## 5.6 Georgi-Machacek Model

Finally, we turn to the Georgi-Machacek model, described in section 1.4.3, to investigate the impact of the choice of inputs at different orders in perturbation theory. The free Lagrangian parameters in the Higgs sector, left after solving the tadpole equations, are the quartic couplings  $\lambda_i$  ( $i \in \{1, 2, 3, 4, 5\}$ ), the mass parameters  $M_1$ ,  $M_2$  and the ratio of VEVs  $s_H$ , but one can always use different inputs.

In particular,  $m_h$ ,  $s_H$ ,  $m_5$  seem to be a suitable – and popular [136] – choice for the input parameters and can be traded for  $\lambda_1$ ,  $\lambda_5$  and  $v_T$ . In the following we shall do this using tree-level relations derived from those presented in section 1.4.3 (or [136]). However, the choice to use masses instead of couplings as input can have the danger that one enters a non-perturbative regime without recognising it, as we already have pointed out for the 2HDM. We will discuss the importance of higher-order corrections in general in this model in the following: in contrast for instance to the 2HDM, it is not possible to renormalise all mixing angles and masses on-shell in this model. One reason for this is that the masses of the five-plet are only exactly degenerate at tree-

	tree	one-loop	two-loop
$m_{h_1}$ [GeV]	125.00	210.45	$< 0$
$m_{h_2}$ [GeV]	1000.00	950.56	916.96
$m_{h_3}$ [GeV]	1054.67	975.20	954.03
$m_{A_1}$ [GeV]	1049.31	998.41	896.13
$m_{H_1^+}$ [GeV]	1000.00	950.80	-
$m_{H_2^+}$ [GeV]	1049.31	998.21	-
$m_{H^{++}}$ [GeV]	1000.00	951.55	-

Table 5.6 – The scalar masses at tree- and loop-level for the parameter point  $\lambda_2 = \lambda_3 = \lambda_4 = 0$ ,  $m_5 = 1$  TeV and  $s_H = 0.75$ . The renormalisation scale was set to  $m_5$ .

level but the custodial symmetry is not protected against loop effects [315]. Therefore, the number of mass parameters but also of rotation angles is extended at the loop level: one needs three instead of two angles to diagonalise the loop-corrected CP-even mass matrix, and also the CP-odd and charged Higgs mass matrix no longer share the same angle. Therefore, an  $\overline{\text{MS}}$  renormalisation of the scalar sector is the natural option to check the impact of higher order corrections to the masses and angles. We give in Tab. 5.6 the loop corrected masses for all scalars for the parameter point  $\lambda_2 = \lambda_3 = \lambda_4 = 0$ ,  $m_5 = 1$  TeV, and  $s_H = 0.75$ .

We see in these numbers that not only a mass splitting between the components of the fiveplet and triplet is induced at the one-loop level, but also that the loop corrections to the SM-like Higgs scalar can be huge. One can understand these large loop corrections for the chosen parameter point to some extent analytically: the one-loop corrections to the (1,1)-element of the CP even mass matrix are given in the effective potential in the limit  $m_5 \gg v$  by

$$\Delta m_h^2 \sim v^2 \frac{8m_5^4 s_H^4}{9\pi^2 v^4}. \quad (5.6.1)$$

Thus, for large values of  $m_5$  and/or  $s_H$  one can expect huge corrections to the mass. Note, there are additional loop corrections to the off-diagonal elements of the scalar mass matrix which can have a significant impact on the masses. Therefore, one needs a full numerical calculation already at the one-loop level to obtain an accurate number for the SM-like Higgs mass.

Before we further investigate the loop corrections, we want to comment briefly on the choice for the renormalisation scale  $Q$ . In the SM, but also in other models like 2HDMs, it is suitable to set  $Q = m_t$  to give a good convergence and ensure that there are no large logarithmic contributions from top loops. However, in the GM model the dominant loop corrections involve often scalar fields with masses of the order of  $m_5$ . Therefore, the overall size of the loop corrections is usually smaller for  $Q = m_5$  as one can see in figure 5.10.

We check now the Higgs mass in the  $(m_5, s_H)$  plane proposed in [136] always using  $Q = m_5$ . The other parameters are fixed in this plane to

$$m_h^{\text{tree}} = 125 \text{ GeV}, \quad M_1 = \sqrt{2} \frac{s_H}{v} (m_5^2 + v^2), \quad M_2 = \frac{1}{6} M_1 \\ \lambda_3 = -0.1, \quad \lambda_2 = 0.4 \frac{m_5}{1000 \text{ GeV}}, \quad \lambda_4 = 0.2$$

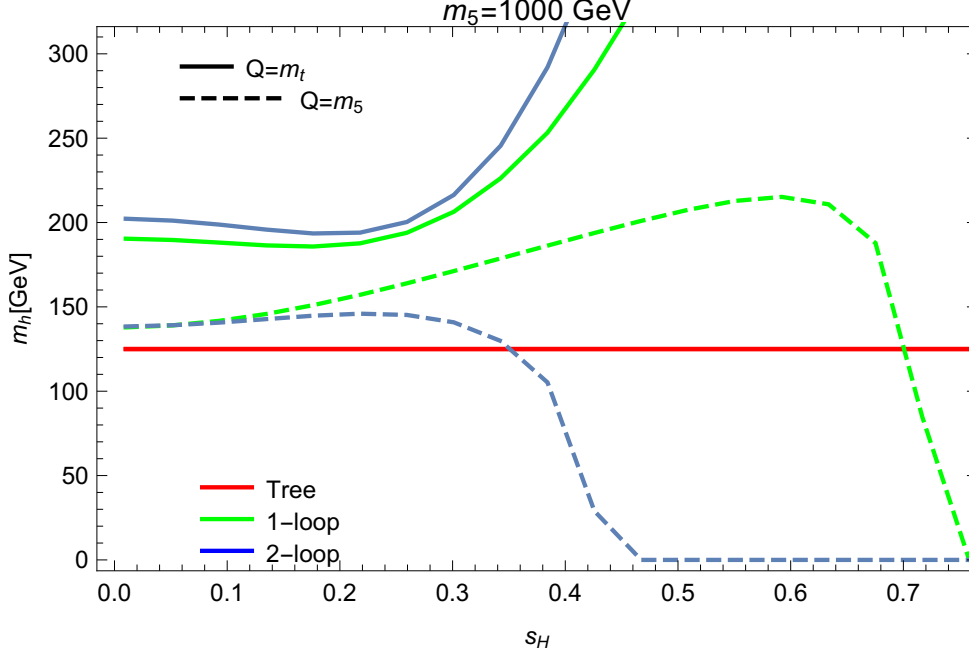


Figure 5.10 – The SM-like Higgs mass at tree-, one- and two-loop level for  $m_5 = 1$  TeV and as a function of  $s_H$ . The results are shown for two different choices for the renormalisation  $Q$  scale, namely  $Q = m_t$  and  $Q = m_5$ .

The light Higgs mass at the one- and two-loop level is shown in figure 5.11. As expected, we see that the two-loop corrections are large for large  $s_H$  and  $m_5$ . In order to further demonstrate this, we show in figure 5.11 also explicitly the size of the one- and two-loop corrections for all three CP-even scalars.

We see that in the upper right corner in the  $(s_H, m_5)$  plane the two-loop corrections are much larger than the one-loop ones and the Higgs can even become tachyonic. For  $m_5 = 1$  TeV, this already happens at  $s_H > 0.5$ , while for  $m_5 = 1.5$  TeV the upper limit of  $s_H$  is as low as 0.25. For large  $m_5$  this limit is much stronger than the one from perturbative unitarity of  $VV \rightarrow VV$  scattering amplitudes which gives  $s_H < \frac{667 \text{ GeV}}{m_5}$  [316]. Thus, even if it might still be possible to obtain the correct Higgs mass at two-loop level by adjusting the other input parameters or by absorbing finite corrections into counter-terms, the results in this parameter region should be taken with a lot of care. Most likely, they are meaningless. However, also for the other parameter regions with a reasonable hierarchy of the one- and two-loop corrections, one would need large adjustments in the input parameters to compensate for these loop corrections. These changes would then reflect in the couplings and some decay widths of the 125-GeV scalar will deviate for large  $s_H$  and/or  $m_5$  clearly from the tree-level expectation. Finally, one can also see in figure 5.12 that the loop corrections to the masses of other scalars are sizeable and can shift the masses easily by tens to hundreds of GeV.

## 5.7 Conclusions

In this chapter we have presented several varied results relating to the calculation of two-loop corrections to the Higgs mass in general models. Chief among these are:

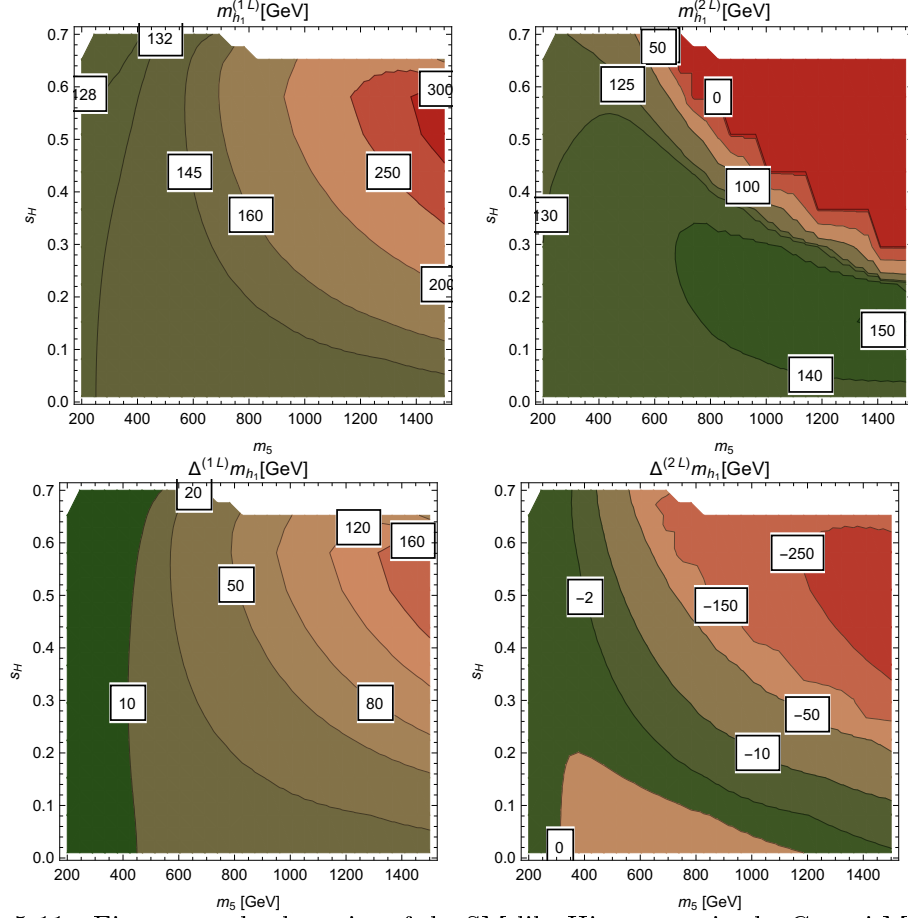


Figure 5.11 – First row: absolute size of the SM-like Higgs mass in the Georgi-Machacek model as a function of  $s_H$  and  $m_5$  and including one- (left) and two-loop (right) corrections. Second row: the size of the one- (left) and two-loop (right) corrections.

- (i) We completed the basis of necessary loop functions for our on-shell solution, with a new expression for  $\tilde{V}(0, x, y)$  given in appendix B.3.
- (ii) We extended the derivation of shifts to the tadpoles and Higgs mass from consistently solving the tadpole equations by allowing fermion masses to be directly dependent on the parameters (such as  $\mu$  in the MSSM), with the expressions given in appendix C.
- (iii) We compared our results with those available for the Standard Model. In particular, this allowed a comparison within the same code of calculations in two different gauges, and we also found that the electroweak corrections are negligible, while those from momentum dependence are very small.
- (iv) We showed that our new computation does indeed remove the instabilities (sharp peaks in the Higgs mass for certain parameter choices) in the previous approach for supersymmetric models; however, the reader should be aware that there are still some limitations when scalar masses in the loops become small compared to the renormalisation scale.
- (v) We explored the corrections to the mixing angle in the alignment limit in the Two Higgs Doublet Model using the  $\overline{\text{MS}}$  *couplings* as inputs, and found that provided the quartic couplings are chosen to be small, the loop corrections are safely under control.

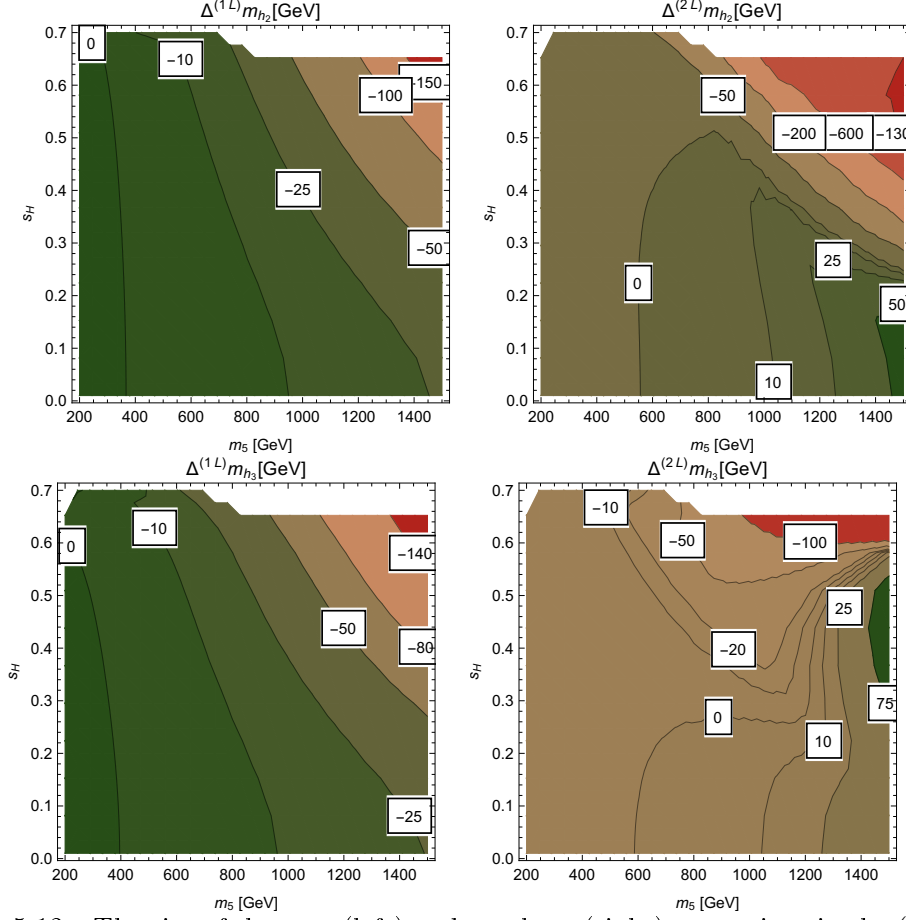


Figure 5.12 – The size of the one- (left) and two-loop (right) corrections in the  $(s_H, m_5)$  plane for the second (first row) and third (second row) CP-even scalar.

- (vi) We explored the 2HDM and Georgi-Machacek models with masses as physical inputs and using tree-level relations to obtain  $\overline{\text{MS}}$  couplings, as commonly done in the literature. We find that in most regions of the parameter space these lead to large quartic couplings, which rapidly lead to loss of control of the loop corrections. Perhaps surprisingly, this often occurs well before the couplings reach naive perturbativity bounds. In the next chapter we will continue investigating the use of masses (and mixing angles) as inputs, but we will go beyond tree-level relations and perform the extraction of the Lagrangian parameters at one- and two-loop orders.

All of the shown results are available to the community with **SARAH** version 4.12.0, and can hopefully contribute to an efficient and more precise study of many extensions of the SM; this should open the avenue to much future work. It would be particularly interesting to explore more carefully the relationship between on-shell and  $\overline{\text{MS}}$  calculations in non-supersymmetric models, to better understand how the divergent behaviour of the masses that we observe for the  $\overline{\text{MS}}$  scheme translates into differences in physical couplings – or even possibly ruling out certain parameter regions of models as unphysical. Note that this programme was continued in [317], where the renormalisation of the Georgi-Machacek model and the possible perturbativity constraints in that model were studied.

## Chapter 6

# Matching and running

In this last chapter, we investigate the high-scale behaviour of Higgs sectors beyond the Standard Model and in particular the importance of performing a proper matching of couplings before applying the renormalisation group equations.

Additional states in models with extended Higgs sectors alter the high-scale behaviour of the theory compared to the SM expectations. For instance, it is known today that the SM becomes metastable if it is extrapolated to very high energies [24,25,318,319]: at a scale of  $10^{9-11}$  GeV the Higgs quartic coupling  $\lambda$  runs negative. The scale at which the potential becomes unstable could be significantly affected by the presence of new states – it could even completely disappear. This would then indicate that the BSM model is valid up to the Planck scale. An opposite effect can occur if large couplings are present. In this case, a Landau pole might be present which points towards the breakdown of the theory. Both effects, the presence of Landau poles or deeper vacua, can also be used to directly constrain the parameters of a new physics model. A parameter point can be discarded if the model becomes strongly interacting at energies already probed by the LHC, or if the life-time of the electroweak breaking vacuum is too short on cosmological time scales.

Many of these effects have already been studied in the literature for plethora of different models such as singlet extensions [124,126–128,320], triplet extensions [321,322], Two-Higgs-Doublet-Models (2HDMs) [323–331] or models with vector-like fermions [332]. These studies utilise the one- and sometimes even two-loop renormalisation group equations (RGEs). However, less care was taken in the determination of the parameters which enter the RGE running. Often, two-loop RGEs were combined with a *tree-level* matching.

A proper determination including higher-order corrections of the quartic coupling, which enters the RGE running, was so far only performed for the SM [25].<sup>1</sup> It was shown that even the two-loop shifts to  $\lambda$  are important for determining the fate of the model. This is remarkable, because it is well known that the loop corrections to the Higgs mass are small if they are calculated at  $Q = m_t$ : the corresponding shifts in  $\lambda$  are only 2.5%. While the corrections from top quarks are of a similar order in many BSM models, other corrections like the ones from Higgs self-interactions can be much larger, as we found for example in the previous chapter for 2HDMs and the Georgi-

---

<sup>1</sup>Loop corrections in the scalar sector were taken into account in [333] for a singlet extension and in [131,334] for a 2HDM. These studies did not however investigate the impact on the high-scale behaviour of the model. In ref. [335] in turn, a one-loop matching has been performed for that purpose in the context of a seesaw-II as well as a left-right symmetric model.

Machacek model where the two-loop corrections to the Higgs masses were calculated for the first time.

We show in this chapter that higher-order corrections can be very important for the study of the UV behaviour of a theory leading to four main conclusions:

- (i) The threshold corrections at low energies can lead to substantial shifts in the running parameters of a model.
- (ii) The change from one-loop to two-loop running can flatten the running at large values of the coupling, preventing the onset of a Landau pole at high energies – leading to a form of asymptotic safety.
- (iii) Alternatively, in the case where the running drives some quartic coupling negative, higher-order corrections can lead to significant changes to the predicted scale of metastability.
- (iv) As a by-product of the above, we find that new *fermionic* fields at low energies can stabilise the SM potential.

We illustrate the above with a detailed examination of three examples: a singlet extension, the SM extended by vector-like quarks and a Two-Higgs-Doublet Model.

This chapter is organised as follows: in section 6.1 we give a step-by-step prescription for the general matching procedure including loop effects, as well as details into the procedure used to obtain higher order-corrections to the quartic couplings in the different models considered. Afterwards, we discuss in section 6.2 the numerical results, providing insights including approximate formulae.

## 6.1 Matching and Running

To extrapolate a theory from the electroweak scale to high energies, we require two ingredients:

- (i) The value of the couplings at the “low scale” where the running starts;
- (ii) The RGE running of all parameters.

### 6.1.1 Renormalisation Group Equations

We shall always work in the  $\overline{\text{MS}}$  scheme. In this scheme, the  $\beta$ -functions, which describe the energy dependence of the parameters  $\Theta$ , are defined as

$$\beta_i = \mu \frac{d\Theta_i}{d\mu}. \quad (6.1.1)$$

Here,  $\mu$  is an arbitrary mass scale.  $\beta_i$  can be expanded in a perturbative series:

$$\beta_i = \sum_n \frac{1}{(16\pi^2)^n} \beta_i^{(n)} \quad (6.1.2)$$

$\beta_i^{(1)}$  and  $\beta_i^{(2)}$  are the one- and two-loop contributions to the running which we are mainly interested in. The expressions for the two-loop running of the parameters appearing in a given model can be obtained from the generic expressions valid for a general quantum field theory, given in Refs. [270–273].



### 6.1.2 Matching

The renormalised coupling constants  $\Theta_i$  in  $d = 4 - 2\epsilon$  dimensions, which enter the running, are related to the corresponding bare couplings  $\Theta_i^0$  by

$$\Theta_i^0 \mu^{-C_i \epsilon} = \Theta_i + \sum_n \frac{a_i^{(n)}}{\epsilon^n}. \quad (6.1.3)$$

Here,  $C_i$  are constant factors depending on the character of  $\Theta_i$ .<sup>2</sup> The coefficients  $a_i$  are the result of a perturbative expansion. In general, two approaches are possible to determine the Lagrangian parameters as function of physical observables such as masses:

- (i) In an on-shell calculation the physical observables are identical at each loop-level, but all finite and infinite corrections are absorbed into the counter-terms of the Lagrangian parameters ( $\delta\Theta_i^{\text{OS}}$ ).
- (ii) In an  $\overline{\text{MS}}$  calculation the counter-terms of the Lagrangian parameters ( $\delta\Theta_i^{\overline{\text{MS}}}$ ) contain only the divergences. Therefore, the calculated masses depend on the loop-level at which the calculation is performed.

The bare Lagrangian parameters are identical in both cases

$$\Theta_i^0 = \Theta_i^{\text{OS}} - \delta\Theta_i^{\text{OS}} = \Theta_i(\mu) - \delta\Theta_i^{\overline{\text{MS}}}. \quad (6.1.4)$$

In an on-shell calculation, however, there is no generic set of renormalisation group equations known, and therefore to explore a theory at high energies it is necessary to use  $\overline{\text{MS}}$  equations – *i.e.* to extract the underlying  $\overline{\text{MS}}$  parameters of the theory, and then run them. On the other hand, in an  $\overline{\text{MS}}$  calculation, the physical parameters are functions of the Lagrangian parameters: so if we are given the physical quantities, we must invert these functions to extract the  $\overline{\text{MS}}$  ones. This is where complications appear, and why many studies in the literature resort to simply using tree-level matching.

For example, suppose that we want to extract the quartic coupling of the SM from the Higgs mass (see eq. (1.1.5) for our definition of the Higgs potential). The Higgs mass  $M_h$  is, however, calculated in terms of the underlying Lagrangian parameters as a loop expansion via the on-shell condition

$$M_h^2 = 2\lambda v^2 + \sum_{n=1}^{\infty} \frac{1}{(16\pi^2)^n} \Delta^{(n)} M_h^2(\lambda). \quad (6.1.5)$$

This is in general a highly non-linear equation in  $\lambda$ , but fortunately since the series is perturbative we can solve it through expanding

$$\lambda = \lambda^{(0)} + \frac{1}{16\pi^2} \delta^{(1)} \lambda + \frac{1}{(16\pi^2)^2} \delta^{(2)} \lambda + \dots, \quad (6.1.6)$$

to find

$$\begin{aligned} \lambda^{(0)} &= \frac{M_h^2}{2v^2}, \\ \delta^{(1)} \lambda &= -\frac{1}{2v^2} \Delta^{(1)} M_h^2|_{\lambda=\lambda^{(0)}}, \\ \delta^{(2)} \lambda &= -\frac{1}{2v^2} \left[ \Delta^{(1)} \lambda \frac{\partial}{\partial \lambda} \Delta^{(1)} M_h^2 + \Delta^{(2)} M_h^2 \right]_{\lambda=\lambda^{(0)}}, \end{aligned} \quad (6.1.7)$$

---

<sup>2</sup>Gauge and Yukawa couplings have  $C_i = 1$ , quartic couplings  $C_i = 2$ .

which is simple enough for the Standard Model and extensions without scalar mixing – so we shall give analytical expressions in sections 6.2.2.1 and 6.2.3. We recall also that the Higgs VEV  $v$  used in the above equations – and throughout this chapter – is the running VEV (extracted from the  $Z$  boson pole mass in a separate calculation).

On the other hand, for more complicated models, we need to solve the equivalent of eq. (6.1.5) through iteration, and we shall adopt this approach in general for the numerical studies. More precisely, we will compute – with the **SARAH/SPHeno** spectrum generator created for the model at hand – the mass spectrum using a set of  $\overline{\text{MS}}$  parameters that we call in general  $\Theta(Q)$  (for details on this, see the description of the **SARAH/SPHeno** setup in section 2.4.3). If a chosen set of input parameters  $\Theta(Q)$  results in the desired physical masses and mixing angles when using a  $N$ -loop calculation, we refer to them as  $N$ -loop couplings. Thus, with tree-level relations we have leading order (LO) parameters, while the one- and two-loop mass corrections result respectively in the NLO and NNLO couplings. Finding the correct set of  $\overline{\text{MS}}$  couplings corresponding to the desired physical parameters at loop-level is non-trivial. In the numerical studies presented in section 6.2, we use a simple fitting algorithm which varies the input parameters until the desired masses and mixing angles are obtained.

## 6.2 Models and results

### 6.2.1 Singlet Extension

We start by studying the singlet-extended SM (SSM), which has been described in section 1.4.1. For clarity, we recall that the scalar potential in the SSM reads

$$V^{(0)} = \mu^2 |\Phi|^2 + \frac{1}{2} M_S^2 S^2 + \kappa_1 |\Phi|^2 S + \frac{1}{3} \kappa_2 S^3 + \frac{1}{2} \lambda |\Phi|^4 + \frac{1}{2} \lambda_{SH} S^2 |\Phi|^2 + \frac{1}{2} \lambda_S S^4. \quad (6.2.1)$$

After electroweak symmetry breaking (EWSB) the CP even scalar components mix to two physical states  $h, H$  via a rotation angle  $\alpha$ , as shown in eqs. (1.4.6) and (1.4.7) (in these equations,  $v$  and  $v_S$  are the VEVs of the Higgs doublet and singlet scalar respectively). At tree-level we can use  $m_h, m_H$  and  $t_\alpha \equiv \tan \alpha$  as inputs to calculate the quartic couplings  $\lambda, \lambda_{SH}, \lambda_S$  with relations (1.4.8)-(1.4.10). Interpreting  $m_h, m_H$  and  $t_\alpha$  as physical on-shell parameters,<sup>3</sup> the quartic couplings calculated via these equations are the LO values.

Asides from the typical requirement that the quartic couplings remain perturbative, the constraints from perturbative unitarity need to be taken into account. For that, we can evaluate the scalar  $2 \rightarrow 2$  scattering amplitude in the limit of high energies and demand that the eigenvalues stay below  $8\pi$ . The conditions for the model under consideration read

$$|\lambda_{SH}| < 8\pi, \quad (6.2.2)$$

$$|\lambda| < 8\pi, \quad (6.2.3)$$

$$\left| -6\lambda_S - 3\lambda \pm \sqrt{4\lambda_{SH}^2 + 9(\lambda - 2\lambda_S)^2} \right| < 16\pi, \quad (6.2.4)$$

---

<sup>3</sup>We recall that we choose to define the loop-corrected value of  $\alpha$  as the angle that diagonalises the loop-corrected  $2 \times 2$  mass matrix evaluated at  $p^2 = m_{\phi_1}^2$  ( $m_{\phi_1}^2$  being the lightest mass eigenvalue) – see eq. (2.3.7), and the text below. The tree-level value of  $\alpha$  is given in eq. (1.4.7).

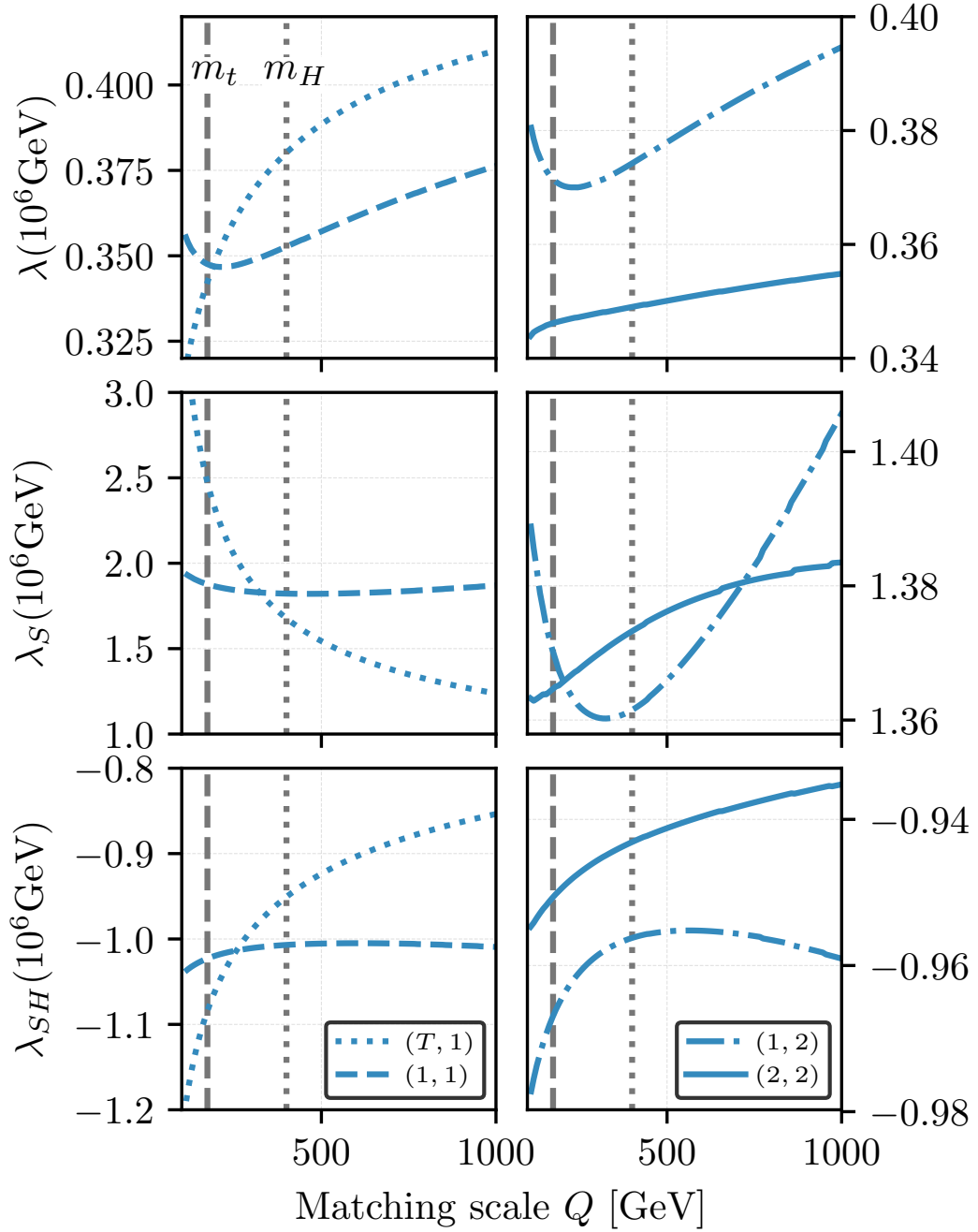


Figure 6.1 – Values of the running quartic couplings at the scale  $Q = 10^6$  GeV using one-loop (left) and two-loop RGEs (right) as function of the matching scale at which the quartic couplings were calculated. The labels  $(n, m)$  refer to  $n$ -loop level matching of the quartics and  $m$ -loop RGEs. We choose the parameters of the singlet extended SM at the matching scale to be  $m_h = 125$  GeV,  $m_H = 400$  GeV,  $\tan \alpha = 0.3$  and  $v_S = 300$  GeV. Cubic terms were set to zero to ensure a scale invariant input. Note that the  $y$ -axes ranges are different on each sub-figure.

which leads to  $\lambda_S < 4\pi/3$  for small  $\lambda$  and  $\lambda_{SH}$ . Although a seemingly weak constraint at first sight, this can become a severe constraint particularly in the case of small  $v_S$ , cf. eq. (1.4.9).

$(n, m)$	$\lambda$	$\lambda_S$	$\lambda_{SH}$	$\Lambda_{4\pi}$ [GeV]	$\Lambda_{4\pi}^{\text{unit.}}$ [GeV]
$(T, 1)$	0.34	1.1	-1.1	$6.4 \cdot 10^3$	$3.2 \cdot 10^3$
$(T, 2)$				$8.0 \cdot 10^6$	$1.3 \cdot 10^4$
$(1, 1)$	0.33	0.24	-0.97	$6.4 \cdot 10^8$	$3.2 \cdot 10^8$
$(1, 2)$				$1.3 \cdot 10^{12}$	$2.5 \cdot 10^9$
$(2, 1)$	0.32	0.18	-0.94	$5.1 \cdot 10^{10}$	$2.5 \cdot 10^{10}$
$(2, 2)$				$1.0 \cdot 10^{14}$	$2.0 \cdot 10^{11}$

Table 6.1 – Values of the quartic couplings and the cut-off for different combinations of parameters,  $\lambda^{(n)}$ , and RGEs,  $\beta^{(m)}$  at the loop-orders  $n$  and  $m$  respectively.  $\Lambda_{4\pi}$  is the scale at which the quartic coupling first exceed  $4\pi$  while  $\Lambda_{4\pi}^{\text{unit.}}$  is the naive  $4\pi$  cut-off augmented by the unitarity constraint of Eq. 6.2.4. The observables are fixed at the  $n$ -loop order to be  $m_h = 125$  GeV,  $m_H = 700$  GeV,  $\tan \alpha = 0.1$  while the remaining input parameters are chosen as  $\kappa_1 = 0$  GeV,  $\kappa_2 = 2000$  GeV,  $v_S = 175$  GeV.

In the following, we compare different approaches for the matching of the quartic couplings. In Fig. 6.1, we show the values of the quartic couplings at the scale  $10^6$  GeV as a function of the scale  $Q$  where the matching is performed. This is done by first running the SM RGEs to the scale  $Q$  where we then match the quartic couplings to the spectrum at tree-level, one-loop as well as two-loop. The final step is the running of the singlet-extended SM RGEs (both at one- or two-loop order) up to  $10^6$  GeV. On the left-hand plots, we use one-loop RGEs for the cases of tree-level matching (dotted) and one-loop matching (dashed). Although there is no dependence of the quartics on the matching scale when using tree-level matching, the scale dependence induced by the RGEs is larger than for the case of one-loop matching and one-loop RGEs. On the right-hand planes, we show the quartics at  $10^6$  GeV, evaluated with two-loop RGEs, when using one-loop (dashed) and two-loop matching (solid lines). Once again, the scale dependence is decreased when the highest available order of matching is employed (in this case, at two loops).

Also visible in Fig. 6.1 are the large differences between the eventual coupling values when using the “traditional” approach of tree-level matching with one-loop RGEs and the approach of including all available corrections to the matching and RGE running (here two loops for both). This also means that large differences are expected when evaluating the cut-off scale of a theory, *i.e.* the scale at which the model becomes non-perturbative or violates unitarity. In Tab. 6.1, we show the cut-off scale of a particular parameter point when using  $n$ -loop matching in conjunction with  $m$ -loop RGEs. We show the scale at which the quartics become non-perturbative ( $\Lambda_{4\pi}$ ) separately from the case where either perturbativity or unitarity is violated ( $\Lambda_{4\pi}^{\text{unit.}}$ ). The corresponding running of the individual couplings is displayed in Fig. 6.2. Note that we only display the cases  $(n, m) = (T, 1), (1, 1), (1, 2)$ , and  $(2, 2)$  in this figure as dotted, dot-dashed, dashed and full lines corresponding to the comparison of  $N$  versus  $N - 1$  matching. The impact of the two-loop RGEs is a moderation of the one-loop RGEs: while the one-loop  $\beta$ -function of  $\lambda_S$  is given by  $\beta_{\lambda_S}^{(1)} = \frac{1}{16\pi^2}(36\lambda_S^2 + \lambda_{SH}^2)$ , so that  $\lambda_S$  tends to grow very rapidly, there is a moderating term from the two-loop RGEs which goes with  $\frac{1}{(16\pi^2)^2}(-816\lambda_S^3 - 20\lambda_S\lambda_{SH}^2)$ . Therefore, using the one-loop RGEs only,  $\lambda_S$  grows large very quickly – whereas the unitarity limit is reached at a much later scale when using two-loop RGEs. Nevertheless, a complete stalling of the evolution is typically only reached at  $\lambda_S$  values which already violate the unitarity limit according to Eq. (6.2.4), see the black dashed (full) line between  $10^9$  and  $10^{13}$  GeV ( $10^{12}$  and  $10^{15}$  GeV). The

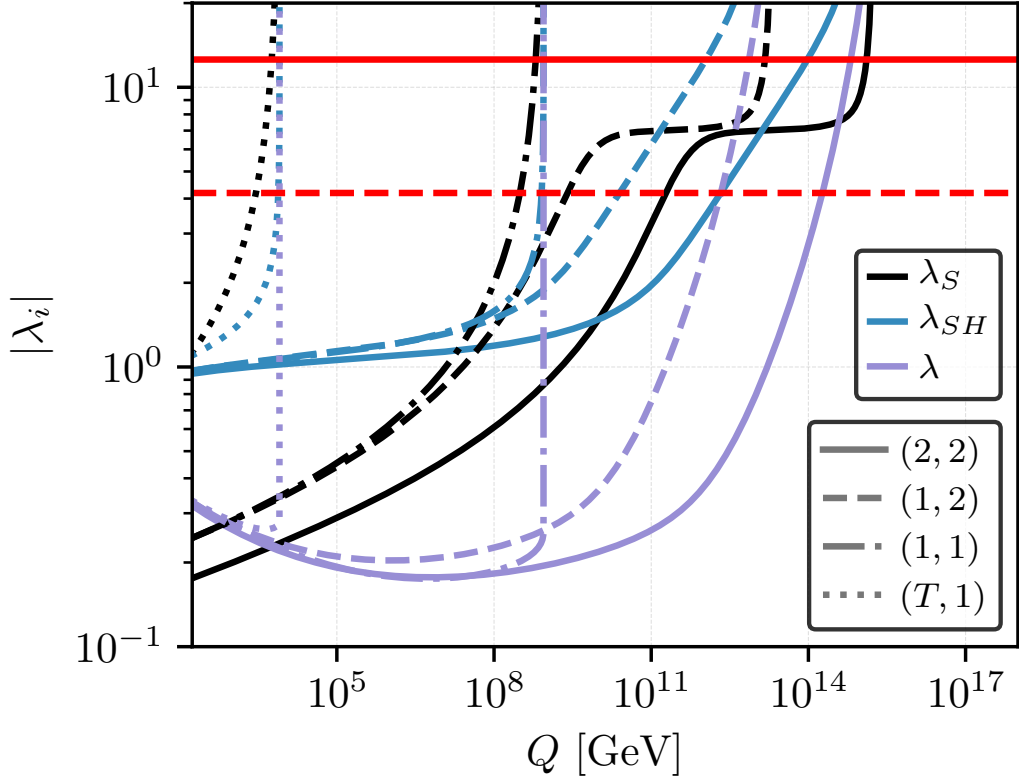


Figure 6.2 – The running of the quartic couplings for the point given in Tab. 6.1. The line-styles refer to the loop order of the matching and RGE running as described in Tab. 6.1, namely  $(n, m)$  refers to the matching at  $n$ -loop order with  $m$ -loop RGEs. The solid red line is the  $4\pi$  perturbativity limit, while the dashed-red line is the unitarity constraint of  $4\pi/3$  obtained from eq. (6.2.4) in the limit  $\lambda_S \gg \lambda_{SH}, \lambda$ .

moderation of the evolution of  $\lambda_{SH}$  and  $\lambda$  is not as pronounced. For  $\lambda_{SH}$ , the corresponding  $\beta$ -function grows with  $\frac{1}{16\pi^2} 12\lambda_S \lambda_{SH}$  with only a small moderating effect from the two-loop RGEs. As a consequence, it becomes larger than  $4\pi$  before  $\lambda_S$  and then drags the latter with it. To summarise, in particular because of the large two-loop contributions to  $\beta_{\lambda_S}$ , there can be several orders of magnitude between the eventual cut-off scales when using one- or two-loop RGEs.

The effect of using a higher-order (two-loop) matching instead of a tree-matching, in turn, is a reduction of the quartic couplings. The reason is the positive mass corrections to  $m_H$ , leading to smaller  $\overline{\text{MS}}$  couplings when doing the proper loop-level matching. As shown here, the impact can be large and we observe positive shifts in the eventual cut-off scale by several orders of magnitude when including the matching.

Finally in Fig. 6.3, we show in the  $m_H$ - $v_S$  plane the differences between using  $N - 1$ -loop and  $N$ -loop matching when applying  $N$ -loop RGE running. The cut-off scale here and in what follows is defined as the scale at which *either* one of the couplings grows larger than  $4\pi$  *or* any of the conditions for perturbative unitarity are violated, each evaluated with the running  $\overline{\text{MS}}$  quartic couplings. The grey contours in the left-hand pane of Fig. 6.3 display the ratio of the evaluated cut-off scales for  $N = 1$ . In particular for small values of  $v_S$ , which lead to large quartic couplings, the effects are quite drastic as loop effects become very important. The differences between one- and

two-loop matching (shown as blue coloured contours) are significantly milder in this region, the maximum difference is just a factor of three. For large  $v_S$ , instead, the quartic couplings are comparably small, leading to large cut-off scales in general. This also means, however, that during the long RGE running, small shifts in couplings can lead to more drastic effects as is seen in the upper region in the plot with  $v_S \gtrsim 350$  GeV. However, the cut-off scale differences stay below an order of magnitude for  $N = 2$ .

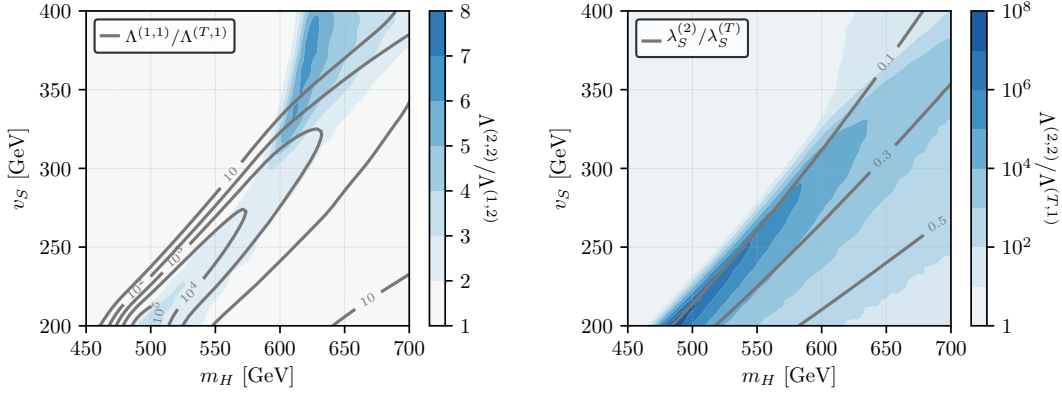


Figure 6.3 – Difference in the predicted cut-off scale depending on the matching performed as a function of the singlet VEV  $v_S$  and the heavy CP-even Higgs mass  $m_H$ . *Left:* We show the ratio of the obtained cut-off given matching at  $N$  versus  $N - 1$  order using the RGEs at  $N$ -loop order. The coloured(grey) contours use the two(one)-loop RGEs, therefore showing the ratio of the matching at two(one)-loop versus one-loop(tree-level), respectively. *Right:* Ratio of the calculation performed using both matching and RGEs at two-loop order versus the leading order (tree-level matching and one-loop RGEs). The grey contours correspond to the ratios of the quartic coupling  $\lambda_S$  for these two scenarios. Here we have fixed the physical parameters such that  $m_h = 125$  GeV,  $\tan \alpha = 0.2$ , while the remaining parameters are chosen as  $\kappa_1 = 0$  GeV and  $\kappa_2 = 1000$  GeV.

On the right-hand side of Fig. 6.3 we present the difference in cut-off scales between the most extreme cases, tree-level matching using one-loop RGEs versus two-loop matching using two-loop RGEs. In particular for small values of the singlet VEV, the eventual cut-off scale can be many orders of magnitude larger than the cut-off scale evaluated with tree-level matching. In grey contours we show the ratios of the singlet quartic couplings at  $Q = m_t$  between the two matching approaches,  $\lambda_S^{(2)}/\lambda_S^{(T)}$ . Already at the matching scale, differences of an order of magnitude between tree and two-loop matching can appear, emphasising the requirement for proper matching and running when analysing the high-scale behaviour of a given model.

## 6.2.2 Singlet Extension with an additional $\mathbb{Z}_2$ symmetry

### 6.2.2.1 Analytical approximation

We may now make a further simplification to the singlet extension studied in Sec. 6.2.1, namely adding an additional  $\mathbb{Z}_2$  symmetry under which the singlet scalar is charged – this is the  $\mathbb{Z}_2$ SSM described in section 1.4.1. This symmetry forbids non-zero values for the couplings  $\kappa_1, \kappa_2$  and for the singlet VEV  $v_S$ , and furthermore eliminates mixing in the Higgs sector. Therefore, the derivation of analytic expressions for the radiative

corrections to the matching of the Higgs quartic coupling  $\lambda$ , and their comparison to numerical studies, are significantly simpler, and follow the procedure outlined in section 6.1.2. Here we will be interested in the part of the corrections that come on top of the purely SM corrections due to the singlet scalar, and shall give expressions including two-loop contributions.

The one- and two-loop corrections to the Higgs mass in the SM are well-known and small; however, in our model there may be large corrections from the singlet scalar. In order to extract the two-loop contributions via eq. (6.2.1) we require the two-loop mass correction, and also the derivatives of the one-loop part. However, our two-loop calculation is performed in the gaugeless limit in Feynman gauge, so we require the full one-loop Higgs mass correction in this limit

$$\begin{aligned}\Delta^{(1)}M_h^2(p^2) &= 3y_t^2(4m_t^2 - p^2)B(m_t^2, m_t^2) - \frac{3}{2}\lambda^2 v^2 B(0, 0) \\ &\quad - \frac{9}{2}\lambda^2 v^2 B(m_h^2, m_h^2) - \frac{1}{2}v^2 \lambda_{SH}^2 B(m_S^2, m_S^2).\end{aligned}\quad (6.2.5)$$

Here we have defined  $m_S^2 \equiv M_S^2 + \frac{1}{2}\lambda_{SH}v^2$ ,  $m_h^2 \equiv \lambda v^2$  which are the tree-level squared masses of the singlet and Higgs respectively, while a complete list of the definitions for our loop functions can be found in appendix B.1 (based upon the basis defined in [20, 142]). This gives us

$$\begin{aligned}\lambda^{(0)} &= \frac{M_h^2}{v^2}, \\ \delta^{(1)}\lambda &= \delta_{\text{SM}}^{(1)}\lambda + \frac{1}{2}\lambda_{SH}^2 B(m_S^2, m_S^2), \\ \delta^{(2)}\lambda &= \delta_{\text{SM}}^{(2)}\lambda - \frac{1}{2v^2} \left[ \Delta_{\mathbb{Z}_2\text{SSM}}^{(2)} M_h^2 \right]_{\lambda=\lambda^{(0)}} \\ &\quad + \frac{3}{2}\lambda_{SH}^2 \lambda B(m_S^2, m_S^2) \left( 3B(m_h^2, m_h^2) + 3m_h^2 B((m_h^2)', m_h^2) + B(0, 0) \right).\end{aligned}\quad (6.2.6)$$

where we use the shorthand notation  $B(x', y) \equiv \frac{\partial}{\partial x} B(x, y)$ . We note that the infrared divergent piece  $B(0, 0)$  will cancel against an equivalent piece from  $\Delta_{\mathbb{Z}_2\text{SSM}}^{(2)} M_h^2$ , similarly to the effect noted in [22].

For the  $\mathbb{Z}_2\text{SSM}$ , we obtain

$$\begin{aligned}\delta^{(2)}\lambda &= \delta_{\text{SM}}^{(2)}\lambda - \frac{1}{2}\lambda_{SH} \left( \lambda_{SH}^3 v^2 M_{SSSSS}(m_S^2, m_S^2, m_S^2, m_S^2, m_h^2) \right. \\ &\quad + 6\lambda\lambda_{SH}^2 v^2 M_{SSSSS}(m_h^2, m_S^2, m_h^2, m_S^2, m_S^2) \\ &\quad - 6\lambda\lambda_{SH} U_{SSSS}(m_h^2, m_h^2, m_S^2, m_S^2) \\ &\quad - 4\lambda_{SH}^2 U_{SSSS}(m_S^2, m_S^2, m_h^2, m_S^2) \\ &\quad + 9\lambda^2 \lambda_{SH} v^2 V_{SSSSS}(m_h^2, m_h^2, m_h^2, m_S^2, m_S^2) \\ &\quad + 2\lambda_{SH}^3 v^2 V_{SSSSS}(m_S^2, m_S^2, m_S^2, m_h^2, m_S^2) \\ &\quad - \lambda_{SH}^2 Y_{SSSS}(m_S^2, m_S^2, m_S^2, m_h^2) \\ &\quad - 9\lambda^2 Y_{SSSS}(m_h^2, m_h^2, m_h^2, m_S^2) \\ &\quad - 12\lambda_{SH} \lambda_S Y_{SSSS}(m_S^2, m_S^2, m_S^2, m_S^2) \\ &\quad - 6\lambda_{SH} \lambda_S Z_{SSSS}(m_S^2, m_S^2, m_S^2, m_S^2) \\ &\quad \left. - 12\lambda\lambda_{SH} Z_{SSSS}(m_h^2, m_h^2, m_S^2, m_S^2) \right)\end{aligned}$$

$M_S$ [GeV]	$\lambda_{SH}$	$\lambda_{\text{tree}}$	$\lambda_{1\ell}$	$\lambda_{2\ell}$
200	0.25	0.2610	0.2627	0.2552
	3	0.2610	0.2166	0.2099
500	0.25	0.2610	0.2623	0.2551
	3	0.2610	0.1885	0.1794
1000	0.25	0.2610	0.2651	0.2546
	3	0.2610	0.1548	0.1385

Table 6.2 – Values of the Higgs quartic  $\lambda$  obtained from matchings at tree-level, one-loop and two-loop orders, for different choices of  $M_S$  and  $\lambda_{SH}$ . The singlet quartic coupling  $\lambda_S$  is set to be 0.1.

$$\begin{aligned}
 & -\frac{1}{2v^2}\lambda_{SH}^2\left(S_{SSS}(m_h^2, m_S^2, m_S^2) - I(m_h^2, m_S^2, m_S^2)\right) \\
 & +\frac{9}{2}\lambda_{SH}^2\lambda m_h^2 B(m_S^2, m_S^2)B((m_h^2)', m_h^2).
 \end{aligned} \tag{6.2.7}$$

This expression is valid for the gaugeless limit but with generic external momentum (so we can take the momentum in the loop integrals on-shell as the procedure demands, if we wish). However, if we take the “generalised effective potential limit” introduced in section 4.3 and employed in **SARAH**, then the penultimate line vanishes and the loop functions simplify considerably. We can then obtain a further simplified version of this expression by replacing  $m_h^2$  by its tree-level value  $\lambda v^2$  and by performing an expansion in powers of  $v^2/m_S^2$  and keeping only the leading and sub-leading terms, giving

$$\begin{aligned}
 \delta^{(2)}\lambda & \simeq \delta_{\text{SM}}^{(2)}\lambda + \frac{9}{4v^2}\lambda_{SH}\lambda A(m_S^2) + \lambda_{SH}^3[1 - 2\overline{\log} m_S^2 + \overline{\log}^2 m_S^2] \\
 & + \frac{1}{4}\lambda_{SH}^2\lambda[-18 - 6\overline{\log}^2 m_S^2 + (36\overline{\log} m_h^2 - 12)\overline{\log} m_S^2] \\
 & + 3\lambda_{SH}^2\lambda_S[-1 + \overline{\log} m_S^2 + \overline{\log}^2 m_S^2].
 \end{aligned} \tag{6.2.8}$$

### 6.2.2.2 Numerical study

Because the  $\mathbb{Z}_2$  symmetry forbids some couplings, the corrections to the matching conditions can be understood in terms of only three parameters added to the SM ones:  $\lambda_{SH}$ ,  $M_S$ , and (to a lesser extent)  $\lambda_S$ . The effects of using loop-corrected matching and RGEs in the  $\mathbb{Z}_2$ SSM are similar to those observed in Sec. 6.2.1 for the SSM, although for most values of  $\lambda_{SH}$  and  $M_S$  the shift to the quartic coupling has only a very small effect on the value of the cut-off scale. We give in Tab. 6.2 our results for  $\lambda$  obtained for the three different orders of matching, for both small and large  $\lambda_{SH}$  and for two choices of  $M_S$ . For small  $\lambda_{SH}$  the one-loop shift to  $\lambda$  is small, because of a cancellation between the purely-SM part – dominated by the effect of the top quark – and the singlet part of  $\delta^{(1)}\lambda$ . If one then considers larger values of  $\lambda_{SH}$ , the term from the singlet becomes dominant over the SM one, and  $\delta^{(1)}\lambda$  is a large negative shift – the evolution of  $\lambda$ , extracted at different orders, as a function of  $\lambda_{SH}$  is also shown in Fig. 6.5, discussed below. At two loops however, there is no cancellation between SM and singlet contributions, and  $\delta^{(2)}\lambda$  is always a negative shift to the Higgs quartic, as was observed previously for the general SSM. On the other hand, it is always small, showing – importantly – that perturbativity of the model is preserved.

Having fewer parameters allows for a more detailed study of the different phases of the theory. Indeed, there are two transitions that occur respectively



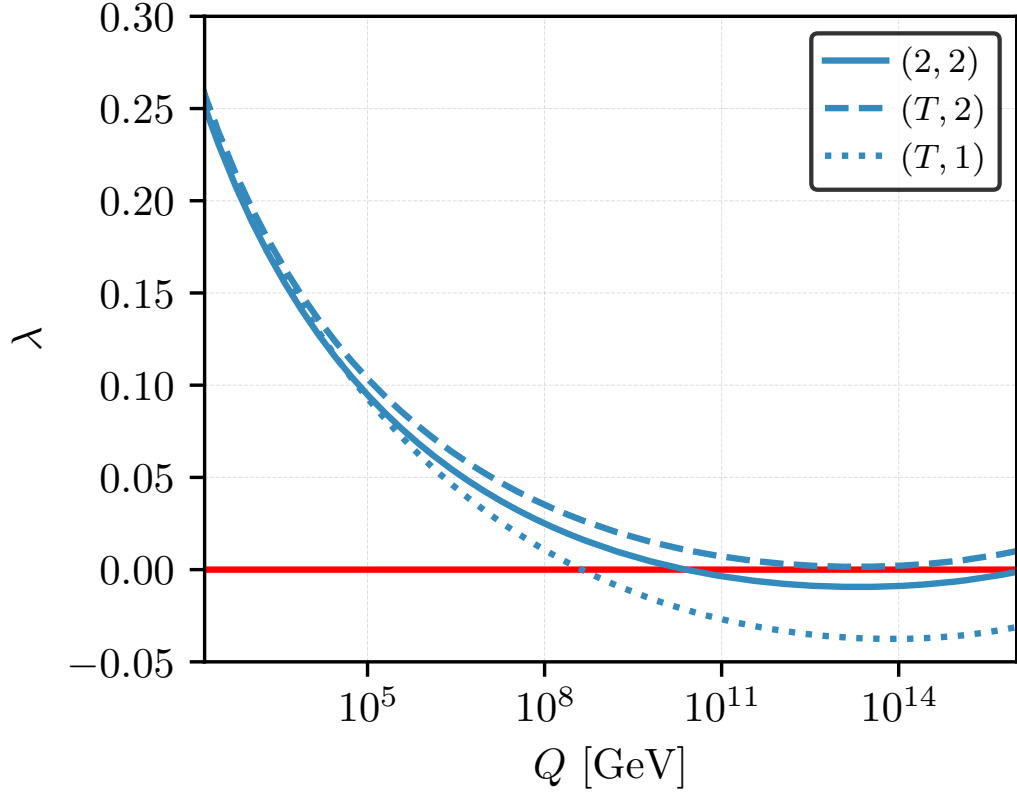


Figure 6.4 – Running of the Higgs quartic coupling as a function of the renormalisation scale  $Q$ , having taken  $\lambda_{SH} = 0.28$ ,  $\lambda_S = 0.1$  and  $m_S = 500$  GeV. The value of  $\lambda(m_t)$  is obtained by requiring  $m_h = 125.15$  GeV, with different orders of matchings depending on the curve. The solid line corresponds to the use of two-loop matching and two-loop RGE running, the dashed line to tree-level matching and two-loop RGEs, and the dotted line to tree-level matching and one-loop RGEs. Note that because of the cancellation that occurs in the one-loop correction for small  $\lambda_{SH}$  (discussed in the main text), the curves we would have obtained using one-loop matching would have been very similar to those with tree-level matching.

- between a metastable and a stable vacuum of the theory; for the physically relevant values of  $\lambda$  around 0.25-0.26, this happens for  $\lambda_{SH} \sim 0.3$  and depends very little on  $M_S$  or  $\lambda_S$ .
- between a UV-complete model to a UV-incomplete one – in other words the cut-off scale of the model becomes smaller than the Planck scale for sufficiently large couplings.

Fig. 6.4 shows an example in which the order of the matching performed to extract  $\lambda$  causes differences in the stability of the vacuum of the theory. Indeed, while the curve with two-loop matching and two-loop RGE running (solid line) crosses to negative values of  $\lambda$  – for  $10^{10}$  GeV  $\lesssim Q \lesssim 10^{16}$  GeV – the curve with tree-level matching (dashed line) does not, because of the negative shift to the initial value of  $\lambda$  at scale  $Q = m_t$  at two-loop order. Two-loop corrections to the matching of  $\lambda$  may exclude some parameter points that appear viable when only using a tree-level matching and are therefore important in the discussion of allowed regions of parameter space. Comparing

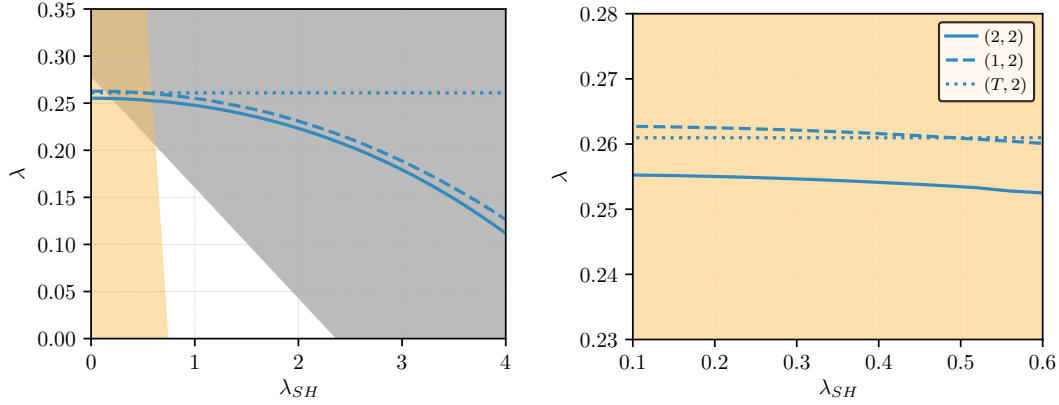


Figure 6.5 – Different phases in the  $\mathbb{Z}_2$ SSM shown in the  $\lambda_{SH} - \lambda$  plane, where the couplings are taken at scale  $Q = m_t$ . The orange shaded region of parameter space corresponds to UV-complete theories, *i.e.* none of the three quartic couplings ( $\lambda$ ,  $\lambda_{SH}$ ,  $\lambda_S$ ) become non-perturbative and the constraints from unitarity are not violated before the Planck scale; the black shaded region corresponds to theories with stable vacua. The thin blue lines give  $\lambda$  as a function of  $\lambda_{SH}$  when imposing  $m_h = 125.15$  GeV with a matching condition at respectively tree-level (dotted curve), one-loop order (dashed curve) and two-loop order (solid line). The other parameters of the scalar sector are  $\lambda_S = 0.1$ , and  $M_S = 500$  GeV.

the dashed and dotted lines, we also observe the stabilising effect of the use of the two-loop RGEs, as discussed in section 6.2.1.

Fig. 6.5 shows how both types of transitions occur in this model. The different domains in this figure were obtained as follows: we start with values of the couplings, at scale  $Q = m_t$ , in the range  $\lambda \in [0, 0.35]$  and  $\lambda_{SH} \in [0, 4]$ , and take  $\lambda_S = 0.1$  and  $M_S = 500$  GeV. We then use two-loop RGEs to run the couplings up to the Planck scale, and we verify whether the Higgs quartic  $\lambda$  becomes negative at any point, and whether perturbativity or unitarity are lost below the Planck scale. The left pane of Fig. 6.5 presents the whole range of couplings that we considered, while the right pane shows an enlargement of the region in which the transition between stable and metastable phases occur.

We observe that the UV-complete phase of the model corresponds to smaller values of the inputs at scale  $Q = m_t$  – which can easily be understood as large values of the couplings at  $m_t$  naturally lead to even larger values at higher scales. Furthermore, we can see that the phase of the model with stable vacua is associated with larger values of  $\lambda_{SH}$ , and that when  $\lambda$  decreases, the value of  $\lambda_{SH}$  needed to ensure a stable vacuum increases. While the SM part of the  $\beta$ -function of  $\lambda$  is negative and tends to drive it to negative values, the additional piece in  $\beta_\lambda$  in the  $\mathbb{Z}_2$ SSM is positive and is of the form  $\beta_\lambda^{(1)} \supset \frac{1}{16\pi^2} \lambda_{SH}^2$ . When lowering  $\lambda(m_t)$  a higher value of  $\lambda_{SH}$  is needed so that the  $\beta$ -function of  $\lambda$  changes sign earlier, and that  $\lambda$  does not run negative at some scale.

The blue lines in Fig. 6.5 give  $\lambda(m_t)$ , obtained from the requirement that  $m_h = 125.1$  GeV, as a function of  $\lambda_{SH}$ . The different curves correspond to the different orders at which the matching can be done: dotted for tree-level matching, dashed for one-loop and solid for two-loop order. The most important point to notice is that, as for the vacuum stability as we saw with Fig. 6.4, there is a value of  $\lambda_{SH}$  – here around 0.65 – for which the UV-completeness – in other words whether perturbativity

or unitarity are broken at some scale below  $M_{Pl}$  – of a given parameter point depends greatly on the order at which  $\lambda(m_t)$  has been extracted from the Higgs mass.

### 6.2.3 Vector-like quarks and stability of the SM

From the SM, it is known that the quartic coupling  $\lambda$  runs negative at a scale  $Q \simeq 10^9 - 10^{11}$  GeV, leading to a metastable but long-lived vacuum [24,25]. While extensions with a heavy singlet similar to the previous subsections can have a stabilising effect on the potential [126,127], fermionic extensions typically have the opposite effect through the negative impact of the vector-like (VL) fermions Yukawa coupling on the running of  $\lambda$ , see e.g. [336,337]. A model where the latter is compensated by the effect of the former is discussed in ref. [332].

Here, we shall extend the SM by one generation of a VL quark doublet  $Q'$  as well as an up-type quark singlet  $t'$  with their corresponding counterparts  $\tilde{Q}'$ ,  $\tilde{t}'$ , with quantum numbers under the SM gauge group of  $t' : (\mathbf{\bar{3}}, \mathbf{1}, -\frac{2}{3})$ ,  $\tilde{t}' : (\mathbf{3}, \mathbf{1}, \frac{2}{3})$ ,  $Q' : (\mathbf{3}, \mathbf{2}, \frac{1}{6})$ ,  $\tilde{Q}' : (\mathbf{\bar{3}}, \mathbf{2}, -\frac{1}{6})$ . The Lagrangian of the model reads (in terms of two-component spinors)

$$\mathcal{L} = \mathcal{L}_{\text{SM}} - (Y'_t Q' \cdot H t' + \tilde{Y}'_t \tilde{Q}' \cdot \bar{H} \tilde{t}' + m_T \tilde{t}' t' + m_Q \tilde{Q}' Q' + \text{h.c.}). \quad (6.2.9)$$

For simplicity we take  $m_Q = m_T \equiv M_Q$ ; we then find that, with the normalisation  $\mathcal{L} \supset -\frac{1}{2}\lambda|H|^4$ , the one-loop matching of the Higgs quartic coupling at scale  $\mu$  gives

$$\begin{aligned} \lambda_{\text{SM}} = \lambda_{\text{VLQ}} - \frac{1}{16\pi^2} & \left[ (Y'_t + \tilde{Y}'_t)^2 (5Y_t'^2 - 2Y'_t \tilde{Y}'_t + 5\tilde{Y}'_t{}^2) + 6(Y_t'^4 + \tilde{Y}'_t{}^4) \log \frac{M_Q^2}{\mu^2} \right] \\ & + \frac{2\lambda_{\text{VLQ}}}{16\pi^2} \left[ (Y'_t - \tilde{Y}'_t)^2 + 3(Y_t'^2 + \tilde{Y}'_t{}^2) \log \frac{M_Q^2}{\mu^2} \right]. \end{aligned} \quad (6.2.10)$$

Let us first consider the impact of the new vector-like states on the running quartic Higgs coupling. For simplicity, we consider here and in the following examples only one extra non-zero Yukawa interaction  $Y'_t$  and consequently set  $\tilde{Y}'_t = 0$  as it does not play a role in the following discussion.<sup>4</sup> Then for matching at  $\mu = m_t$  with  $M_Q < 1$  TeV, the shifts to  $\lambda$  are less than 10% for  $Y'_t \lesssim 0.7$ , but grow rapidly to  $\sim 50\%$  for  $Y'_t \sim 1$ . On the other hand, the direct impact of  $Y'_t$  on the running of  $\lambda$  at one-loop is given by

$$16\pi^2 \beta_\lambda^{(1)} \supset 12Y_t'^2 (\lambda - Y_t'^2), \quad (6.2.11)$$

which contributes significantly to the negative slope of  $\lambda$  for large values but plays a negligible role when  $Y'_t$  is small. In the latter case, the impact of the new fermions on the running of the gauge couplings may outweigh their direct impact on  $\lambda$ . Consider the potential of eq. (6.2.9). Due to the additional coloured fermions, the running of  $g_s$  changes at one-loop to

$$16\pi^2 \beta_{g_s}^{(1)} = \left( -7 + \frac{4}{3}n_T + \frac{2}{3}n_Q \right) g_s^3 \rightarrow -5g_s^3, \quad (6.2.12)$$

*i.e.* it decreases more slowly when increasing the scale compared to the SM. In addition, we also obtain a shift in  $\alpha_S^{\overline{\text{MS}}}(m_t)$  of

$$\alpha_S^{\overline{\text{MS}}} \rightarrow \frac{\alpha_S^{\overline{\text{MS}}}}{1 - \frac{\alpha_S^{\overline{\text{MS}}}}{\pi} \log(M_Q/m_t)} \quad (6.2.13)$$

---

<sup>4</sup>Although this leads to a stable lightest VL quark, there could for instance be couplings to a hidden sector, leading to a relaxation of the direct collider constraints.

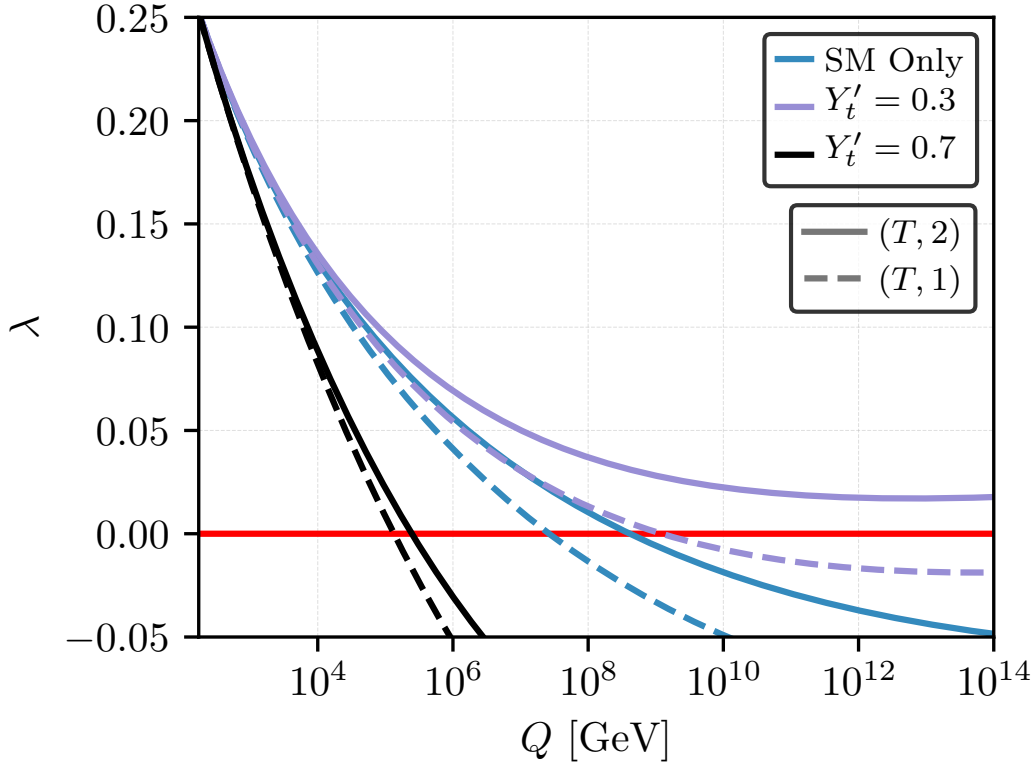


Figure 6.6 – Simplified comparison between the running of  $\lambda$  in the SM with and without vector-like states. Here, we used full one-loop (dashed lines) and two-loop RGEs (full lines) in both models and as starting point the SM best-fit values from ref. [25]. For the purple (black) lines we use  $Y'_t = 0.3$  (0.7).

with respect to the SM. In total, both effects increase the influence of the strong force on the running of  $\lambda$ , adding positively to the slope. The impact on  $\lambda$  is shown in Fig. 6.6 where the running  $\lambda$  is computed using two-loop RGEs when assuming the pure SM (blue) and the VL extension (purple and black). No matching was applied yet here (*i.e.* the shift in  $\alpha_S$  was also neglected) – the changes in the VL case therefore entirely stem from the altered running of the gauge couplings, most importantly eq. (6.2.12). As starting value for  $\lambda$  we used the best-fit value from ref. [25]. The increased  $g_s$  throughout higher energy scales leads to a positive contribution to the slope of  $\lambda$ . One can observe that it can even lead to a stabilisation of the potential at high energies as long as the direct impact of  $Y'_t$  is kept under control by taking it small – this is seen in the purple curve where we have chosen  $Y'_t = 0.3$ . For larger values, the known destabilising effect can overcome the stabilisation from  $g_s$ . As a consequence, the scale of metastability would coincide with the SM for values of  $Y'_t \sim 0.5$  and decreases quickly with larger values. This is also shown in the figure for  $Y'_t = 0.7$  (black line) where  $\lambda$  enters the metastable region already at energies of  $\sim 10^5$  GeV. We remark that the inclusion of the shift in  $\alpha_S$  according to eq. (6.2.13) would lead to an even milder running of  $\lambda$ . In fact, just using the one-loop RGEs for the case  $Y'_t = 0.3$  the quartic coupling stays positive over the entire energy range. We will discuss the effects of the proper matching, including the shifts in  $\lambda$ , in what follows.

Solving equation (6.2.10) for the matched  $\lambda_{\text{VLQ}}$  at  $\mu = m_t$  and keeping  $\tilde{Y}'_t = 0$ , we see that the shifts are slightly negative for small  $Y'_t \lesssim 0.45$  and positive for larger

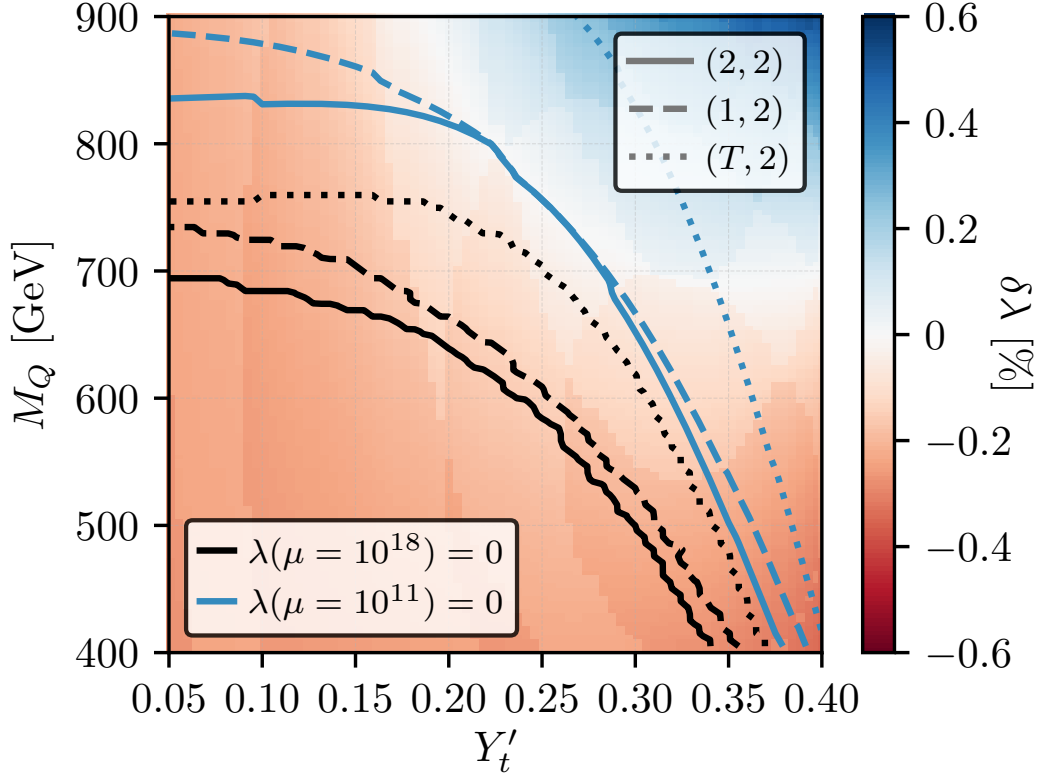


Figure 6.7 – Contours of the scale  $\Lambda_0$  at which  $\lambda$  runs negative with full two-loop RGEs and one-loop (dashed) or two-loop (full lines) matching, and for comparison when using the best-fit value  $\lambda^{\text{SM}} = 0.25208$  at the top mass scale (dotted). Black lines correspond to  $\Lambda_0 = 10^{18}$  GeV, blue lines to  $10^{11}$  GeV. The background shows the two-loop shift in  $\lambda(m_t)$  in percent, defined as  $(\lambda^{(2)} - \lambda^{(1)})/\lambda^{(1)}$ .

Yukawa couplings. This has as a consequence that for low  $Y'_t$  where the VL quarks help increasing the scale of metastability, loop corrections have the opposite effect. However, the size of the shifts stays below 1%. In Fig. 6.7, we present as contour lines the predictions for the scale of metastability as a function of  $Y'_t$  and  $M_Q = m_Q = m_T$  using tree-level (dotted), one-loop (dashed) as well as two-loop matching (full lines) while applying two-loop RGEs. The colour code in the background quantifies the relative two-loop shift in  $\lambda(m_t)$ ,  $(\lambda^{(2)} - \lambda^{(1)})/\lambda^{(1)}$ , which stays below roughly half a percent. Nevertheless, the impact of these small shifts is non-negligible: the corresponding  $Y'_t$  values at which  $\lambda$  crosses zero at a given scale typically change by more than 10% between tree- and two-loop matching. That is, the scale at which metastability occurs is very sensitive on the starting value of  $\lambda$  – meaning that matching is absolutely crucial to make reliable statements. After including the shifts for  $\lambda$  at  $\mu = m_t$ , the picture nevertheless remains the same as that for small  $Y'_t$ ; the impact of the VL quarks on  $\alpha_S$  can be such that the scale of metastability is *increased* with respect to the SM, leading to the possibility of absolute stability all the way up to the Planck scale.

The situation is reversed if  $Y'_t$  is large. In that case, we enter the known scenario in which the additional impact of  $Y'_t$  on the RGEs of  $\lambda$  drives it negative faster when compared to the SM, further destabilising the vacuum. We show this in Fig. 6.8. The background shading indicates the scale  $\Lambda_0$  at which  $\lambda$  crosses zero as a function of

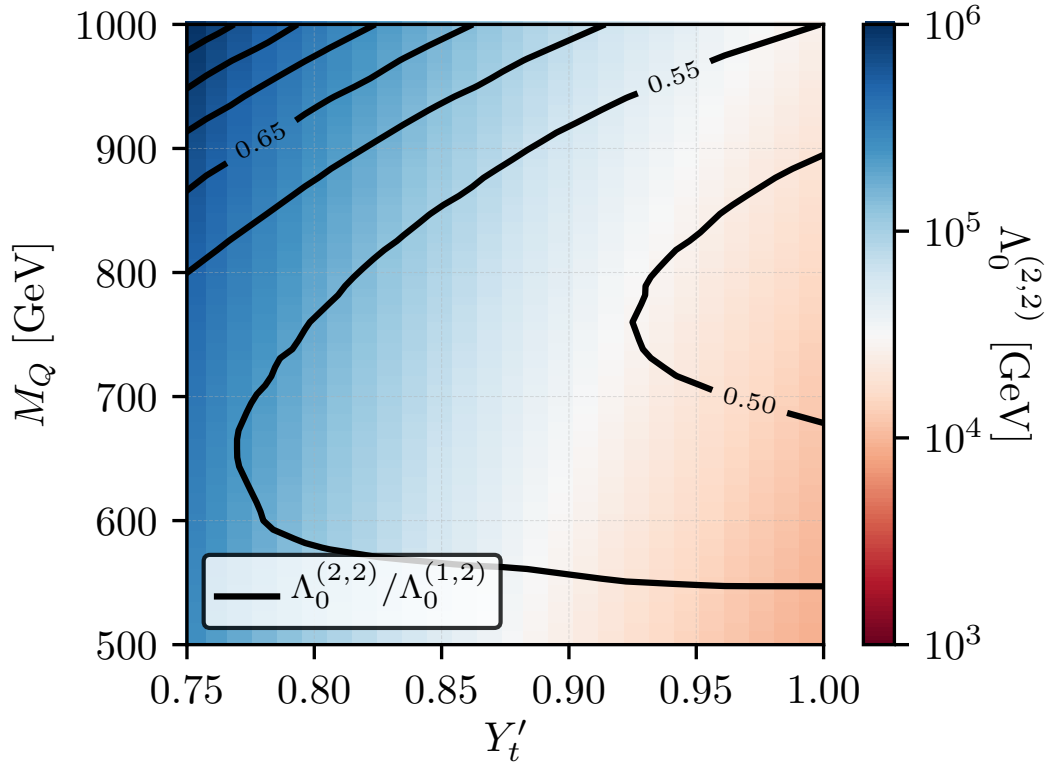


Figure 6.8 – The scale of metastability  $\Lambda_0$  in the case of large  $Y'_t$  using two-loop running with two-loop matching for  $\lambda$ . The black contours show the size of  $\Lambda_0$  with respect to using one-loop matching.

$Y'_t$  and  $M_Q$ , using two-loop matching, whereas the contour lines represent the relative changes with respect to using one-loop matching,  $\Lambda_0^{(2,2)}/\Lambda_0^{(1,2)}$ . As expected,  $\Lambda_0$  is well below the pure SM prediction, and becomes smaller for larger  $Y'_t$  and smaller  $M_Q$ . The differences in  $\Lambda_0$  between one- and two-loop matching are quite mild here – “only”  $\mathcal{O}(100\%)$  – since the two-loop corrections to  $\lambda$  are small. We remark however, that going one order lower and comparing tree-level with one-loop matching using one-loop RGEs, we would see up to an order of magnitude differences in the eventual scale  $\Lambda_0$ .

Summarising, we have shown that vector-like quarks can have both a destabilising but also a stabilising effect on the SM Higgs potential, and that the inclusion of threshold effects are crucial for obtaining precise predictions about the fate of the electroweak vacuum.

### 6.2.4 Two-Higgs Doublet model

Finally, as a last example, we study the impact of loop-level matching on Two-Higgs Doublet models. Here we will restrict ourselves to the CP-conserving version with a softly broken  $\mathbb{Z}_2$  symmetry – as presented in section 1.4.2. The scalar potential we consider is given in eq. (1.4.14), and we recall that, after EWSB, we decompose the scalar fields – see eq. (1.4.15) – according to

$$\Phi_k = \begin{pmatrix} \phi_k^+ \\ \frac{1}{\sqrt{2}}(v_k + \phi_k^0 + i\sigma_k) \end{pmatrix}, \quad i = 1, 2, \quad (6.2.14)$$

where  $v_1^2 + v_2^2 = v^2$  and we define  $t_\beta = \tan \beta = v_2/v_1$ . The charged (neutral CP-odd) fields mix to one physical charged Higgs  $H^\pm$  (pseudoscalar  $A$ ) and the corresponding would-be Goldstone bosons. At LO, the angle  $\beta$  coincides with the mixing angle in the pseudoscalar and charged Higgs sector. In the CP-even sector, there are two fields which mix to one light and one heavy eigenstate, with masses  $m_h$  and  $m_H$ . In the same fashion as for the models considered above, we can relate the scalar masses and mixing angles to the quartic couplings  $\lambda_i$  ( $i \in \{1, 2, 3, 4, 5\}$ ), and corresponding tree-level expressions are given in equations (1.4.19) to (1.4.23).

Analogously to the case of the singlet extension of the SM in section 6.2.1, we define the cut-off scale of a particular scenario as the scale at which either one of the  $\lambda_i$  becomes larger than  $4\pi$  or the unitarity constraints using the running couplings are violated. The latter are too long to show here but can e.g. easily be computed using the **SARAH** implementation of the model in conjunction with appendix D of Ref. [317].

First we are going to look at the matching at the top mass scale. It has already been pointed out in chapter 5 that the loop corrections to the mass spectrum of 2HDMs can be significant. In Fig. 6.9, we show on the left-hand side the size of the individual couplings  $\lambda_i$  for the three matching orders as a function of the charged Higgs mass. The leading order  $\lambda_i$  are simple linear functions of this mass according to eqs. (1.4.19) to (1.4.23), whereas the  $\lambda_i$  evaluated with higher-order matching contain the shifts due to self-energy and tadpole corrections. We see that large differences of  $\mathcal{O}(100\%)$  or even larger can appear between leading and next-to-leading order. The size of the relative shifts is displayed on the right-hand side each. As expected for a converging perturbative series, the differences between one- and two-loop matching are much less pronounced, however they can still range around tens of percent. Obviously these large differences necessarily have a significant effect on the validity of the theory at higher scales. In the following we will therefore investigate the changes in cut-off scales between the different approaches.

As mentioned in the introduction, the two-loop RGEs are well-known but often neglected in the literature – although it is known that large differences can appear, see e.g. ref. [328]. Similar to the singlet-extended SM, the two-loop RGEs tend to moderate the one-loop running. As a result, Landau poles typically appear at much higher scales when including the two-loop effects. For instance, for both  $i = 1$  and  $2$ ,  $16\pi^2\beta_{\lambda_i} \supset 24\lambda_i^2(1 - \frac{13}{16\pi^2}\lambda_i)$ . The two-loop contribution thereby counteracts the large one-loop slope, stalling the evolution for  $\lambda_i$  just below  $4\pi$ . In contrast, the two-loop RGEs to  $\lambda_3$  for instance do have a mitigating effect on the evolution, however a complete stalling only occurs for values much larger than  $4\pi$ . In Fig. 6.10 we show for a particular parameter point the running of the couplings  $\lambda_1$  (black) and  $\lambda_3$  (blue) for  $n$ -loop matching and  $m$ -loop RGEs. The influence of the two-loop RGEs can be best gauged for the cases  $(n, m) = (1, 1)$  versus  $(1, 2)$ , displayed in dot-dashed and dashed lines, respectively. It is clearly seen that, while both quartic couplings run into a Landau pole close to  $Q = 3\text{ TeV}$  when using one-loop RGEs, the inclusion of the two-loop terms leads to a significant flattening and therefore splitting between the two cases.

Let us look at the impact of the threshold corrections next. As shown in the example of Fig. 6.9, the threshold corrections for the  $\lambda_i$  can be significant. This can also be seen in the starting values of the couplings at  $m_t$  in Fig. 6.10: the values for  $\lambda_1$  using tree-level (one-loop) [two-loop] matching are 1.88 (1.45) [1.14] whereas for  $\lambda_3$ , the values are 5.7 (4.5) [4.3]. The decrease in value at higher loop orders comes from the fact that in this particular scenario, the average loop corrections to the scalar masses are

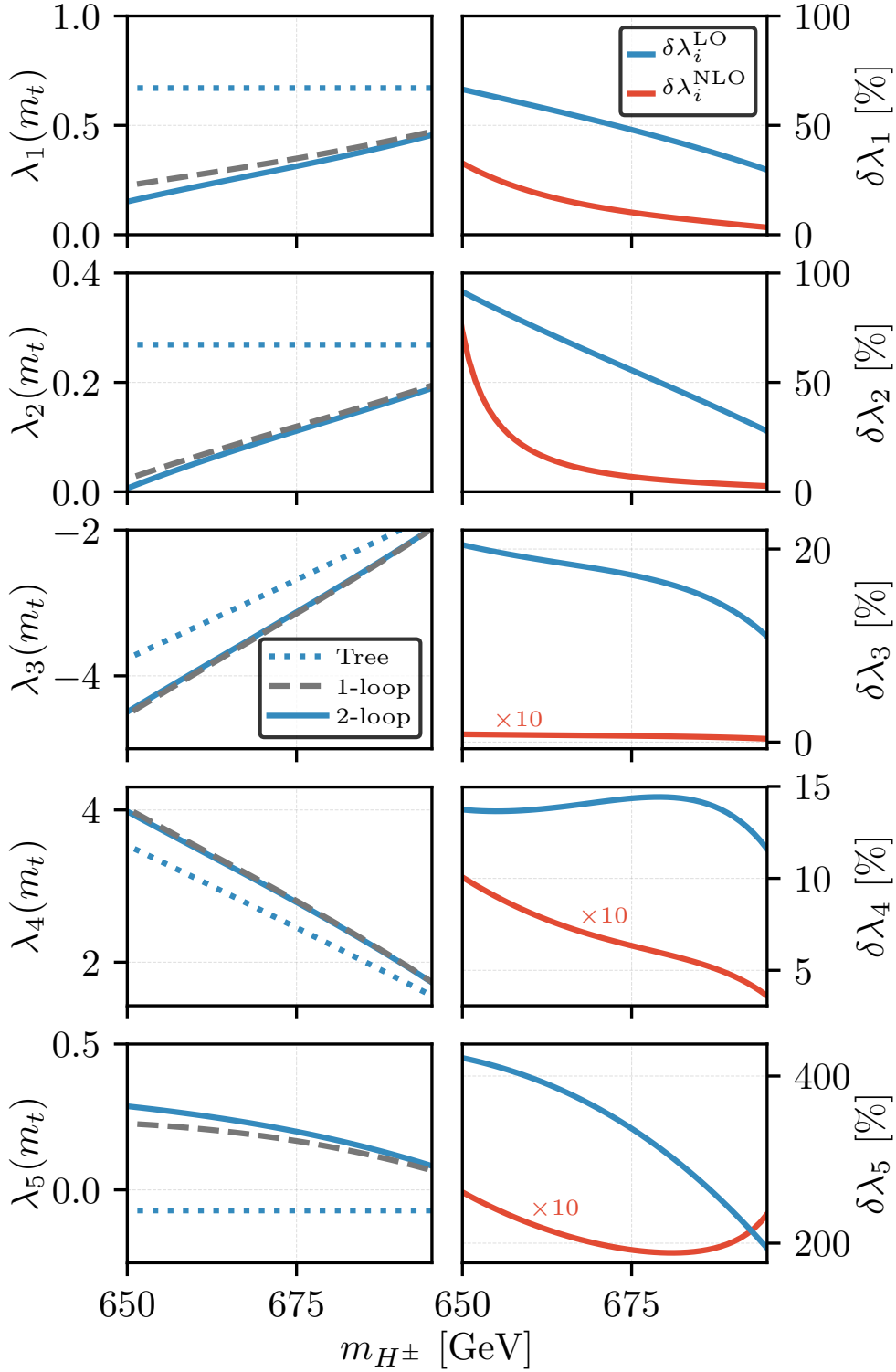


Figure 6.9 – The size of the quartic couplings at  $m_t$  at LO (blue dotted), NLO (grey dashed) and NNLO (blue solid) as a function of  $m_{H^\pm}$ . Here, we set the other physical masses and mixing angle to  $m_h = 125$  GeV,  $m_H = 750$  GeV,  $m_A = 730$  GeV and  $\tan\alpha = -0.71$ . The other model parameters are  $\tan\beta = 1.4$  and  $m_{12}^2 = -500^2$  GeV<sup>2</sup>. On the right, we show the relative differences  $\delta\lambda_i^{\text{LO}} \equiv |(\lambda_i^{(T)} - \lambda_i^{(1)})/\lambda_i^{(T)}|$  and  $\delta\lambda_i^{\text{NLO}} \equiv |(\lambda_i^{(1)} - \lambda_i^{(2)})/\lambda_i^{(1)}|$ . Note that for  $\lambda_i$  where  $i = 3, 4, 5$  the NLO difference have been multiplied by an additional factor of 10 to increase visibility.



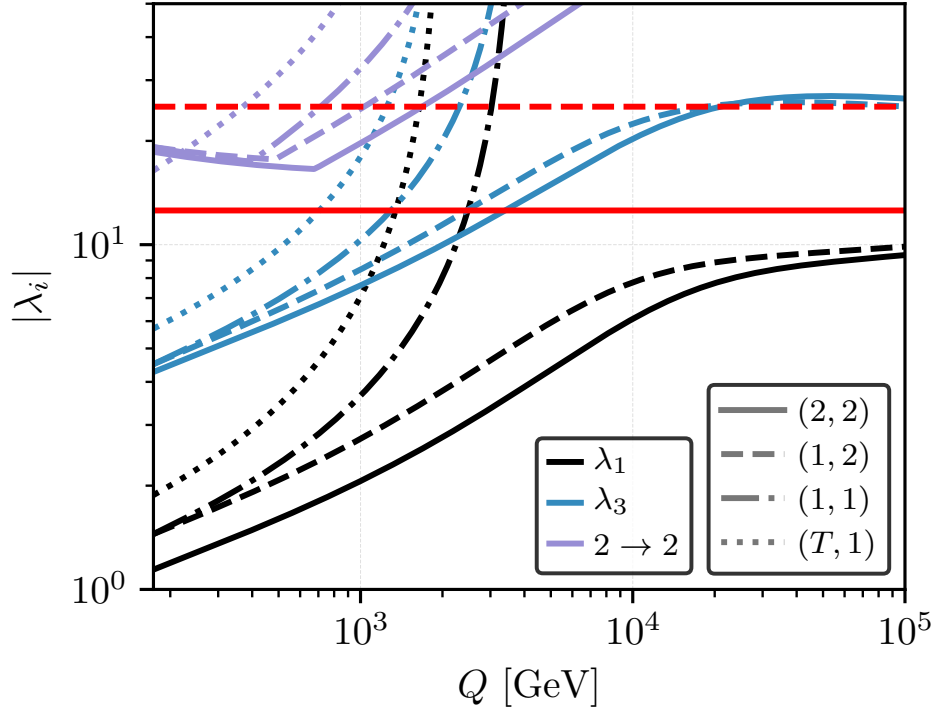


Figure 6.10 – RGE running of the individual quartic couplings  $\lambda_1$  (black) and  $\lambda_3$  (blue) for the parameter point defined by  $m_H = 511$  GeV,  $m_A = 607$  GeV,  $m_{H^\pm} = 605$  GeV,  $t_\beta = 1.45$ ,  $t_\alpha = -0.82$ ,  $m_{12}^2 = -(250 \text{ GeV})^2$ , using  $n$ -loop level matching and  $m$ -loop RGEs. The dotted lines stand for  $(T, 1)$ , dot-dashed for  $(1, 1)$ , dashed for  $(1, 2)$  and full lines for  $(2, 2)$ . Coupling values of  $\pm 4\pi$  are indicated by a red solid line. In addition, we display the largest eigenvalue of the scalar  $2 \rightarrow 2$  scattering amplitude in purple. The upper bound of  $8\pi$  is indicated by a dashed red line. We used the Yukawa scheme of type II.

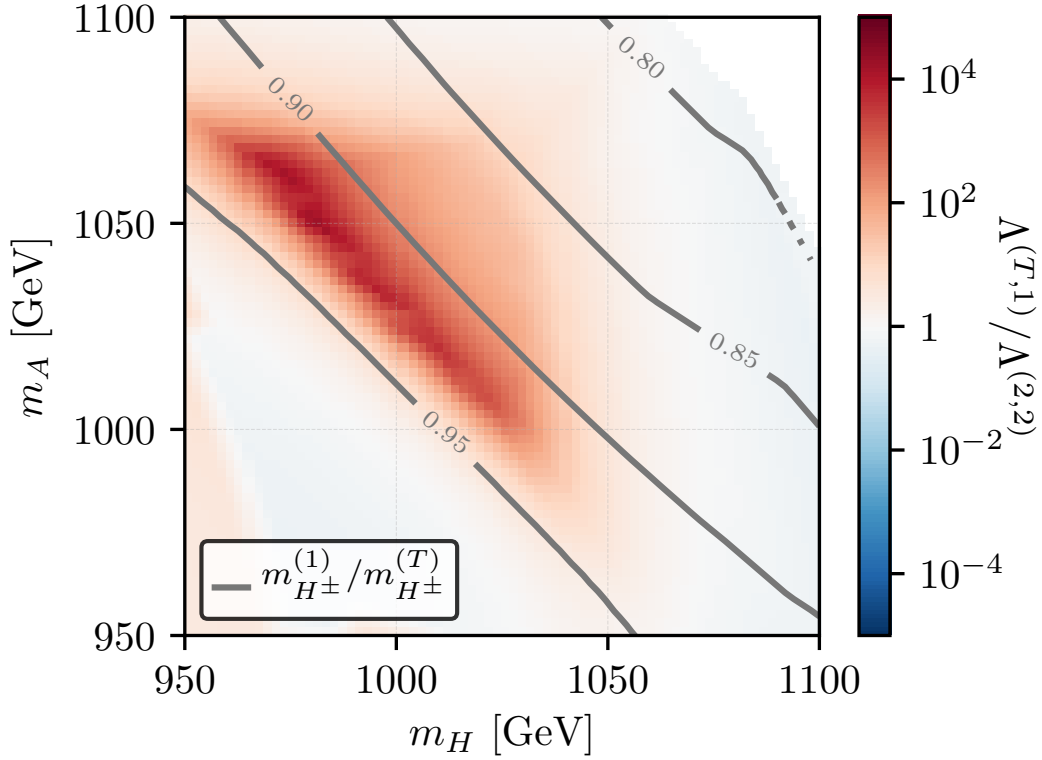


Figure 6.11 – Comparison of the cut-off scales between using tree matching and one-loop RGEs and both two-loop matching and RGEs for a 2HDM region with large  $m_{12}^2 = -(750 \text{ GeV})^2$ . The loop-level spectrum was evaluated taking the tree-level values  $m_{H^\pm} = 1.14 \text{ TeV}$  and  $t_\alpha = -0.95$  as inputs. The ratio of the loop-corrected charged Higgs mass to its tree-level input is shown as grey contour lines. The quartic couplings for the case of tree-matching were obtained using the leading order relations Eqs. (1.4.19) to (1.4.23), taking the spectrum of the two-loop calculation as input. We further fixed  $\tan\beta = 1.14$  and applied the Yukawa scheme of type I.

positive. As a result, one obtains a negative shift in the  $\lambda_i$  at the matching scale when imposing a given physical spectrum.

However, it need not be the case that the cut-off scale is raised by higher loop effects. Indeed, for large values of  $|m_{12}|$  and therefore large heavy scalar masses, the mass corrections can be large and negative – leading to the opposite effects, *i.e.* a decreased cut-off scale due to larger quartic couplings after the inclusion of the proper matching. An example where this happens is presented in Fig. 6.11. For this figure we have evaluated the spectrum at the two-loop level while fixing the tree-level input values of  $t_\alpha$  as well as  $m_{H^\pm}$  which enter the spectrum calculation at the loop level. Therefore, the loop-corrected  $m_{H^\pm}$  varies over this plane. The grey contours show the ratio of the loop-corrected charged Higgs mass over the tree-level input,  $m_{H^\pm}^{(1)}/m_{H^\pm}^{(T)}$ . To obtain the LO couplings, *i.e.* the case of tree-level matching, we take the scalar spectrum and calculate  $\lambda_i$  according to eqs. (1.4.19) to (1.4.23). Finally, we run the couplings up in scale using two-loop RGEs for the two-loop- and one-loop RGEs for the tree-level-matched couplings in order to evaluate the cut-off scale. The coloured contours show the ratio of the cut-off scales,  $\Lambda^{(T,1)}/\Lambda^{(2,2)}$ , obtained with tree-level matching and one-

loop RGEs and with two-loop matching and two-loop RGEs, respectively. In particular in the region where all heavy scalar masses are approximately equal, we observe large differences in cut-off scales. In fact, while the tree-level matching approach suggests a cut-off at  $\mathcal{O}(10^7 \text{ GeV})$ , the full two-loop matching procedure demands new physics restoring unitarity and perturbativity already at the TeV scale.

Concluding, the conventional approach of tree-level matching and one-loop RGEs can both over- but also underestimate the cut-off scale by many orders of magnitude. It is therefore of crucial importance to *(i)* take into account the – known – RGEs beyond one-loop and to *(ii)* perform a loop-corrected matching of the couplings before running.

## 6.3 Conclusions

In this chapter, we have investigated the impact that matching plays in the high-scale validity of minimal extensions of the Standard Model (SM). While for most non-supersymmetric models studies beyond tree-level matching and one-loop RGEs are rare or even absent, we have analysed in different scenarios the impact of both loop-corrected matching as well as using two-loop RGEs, highlighting the differences with respect to previous approaches. For simple models, we provide an analytical computation of the matching conditions. We point out how sensitive the cut-off scale of the real-singlet-extended SM is on the loop order of both matching and RGE running and show that the scale dependence decreases when all available corrections are included in the matching. Imposing an additional  $\mathbb{Z}_2$  symmetry to this model furthermore enables us to study the fate of the electroweak vacuum as well as the UV completion analytically. We highlight regions of parameter space where the model can in principle be valid up to the Planck scale – a statement which crucially depends on the proper matching of the quartic couplings at the low scale.

In a scenario where the SM is extended by vector-like quarks, we show that the impact of the latter can actually increase the Higgs quartic interaction such that it does not become negative at higher scales – an observation that we have not encountered before in the literature. The reason is that, despite the negative impact of the additional Yukawa coupling on the running of  $\lambda$ , the presence of additional coloured states modifies the running strong coupling in such a way that it adds positively to the  $\beta$ -function of  $\lambda$ . Also in this scenario, the matching of  $\lambda$  before the RGE evolution has a significant impact on the predicted high-scale behaviour of the model.

As a final example we show in a Two-Higgs Doublet model that the loop-level matching of the quartic couplings can lead to significant changes in both the  $\overline{\text{MS}}$  values of scalar quartic couplings and subsequently the cut-off scale of the theory.

To conclude, we observe that robust statements about the UV-behaviour of non-supersymmetric, weakly-coupled BSM models can only be made when including, at the very least, loop-level matching. We stress that the required loop corrections, as well as two-loop RGEs, are readily accessible with the computer tool **SARAH** for any generic renormalisable field theory. In light of our results, we strongly encourage its use when accurate high-scale predictions are required.



# Conclusion

The 125-GeV Higgs boson, discovered at the CERN Large Hadron Collider in 2012, represents an invaluable probe of BSM Physics, via the study of its properties. One property that has received considerable interest is the Higgs boson mass  $m_h$ . Indeed,  $m_h$  is now measured to a precision of about 0.1%, while intensive efforts have been spent on its computation, in the Standard Model, and in the BSM models – like Supersymmetry – where a tree-level value of  $m_h$  is predicted by the theory. Adding then radiative corrections (which involve all the particle spectrum) to the tree-level contribution yields a result for the Higgs pole mass and allows to constrain the parameter space of these models. However, corrections to Higgs masses have only been studied (explicitly) beyond one loop in a limited number of BSM models (mostly in the minimal supersymmetric extensions of the SM, namely the MSSM and NMSSM), which means that precise predictions are missing for most models. Furthermore, even in the models that have concentrated most computational efforts, the accuracy of theoretical results is still not comparable to the experimental error on the Higgs mass measurement. The work presented in this thesis has therefore been aimed towards making new radiative corrections to scalar masses available in BSM models. We have done so with two complementary approaches: *(i)* by deriving explicitly new corrections in SUSY models beyond the MSSM and the NMSSM, and *(ii)* by addressing technical hurdles in the calculation of Higgs mass corrections for generic models and in the automation of these computations.

First, we have calculated the leading two-loop  $\mathcal{O}(\alpha_t\alpha_s)$  corrections to neutral scalar and pseudoscalar masses in supersymmetric theories with Dirac gauginos, in the effective potential approximation. These models constitute a very attractive class of non-minimal SUSY extensions of the SM because of their rich phenomenology, and some advantages they offer – in particular their ability to evade experimental constraints and their increased naturalness. Our results have allowed us to compare the predictions for the lightest (CP-even) Higgs mass  $m_h$  between the MSSM and the minimal Dirac gaugino model (the MDGSSM), and in particular we could investigate the effects of the new coloured particles, the octet scalars (or sgluons), on  $m_h$ . We have also considered scenarios with large mass hierarchies between the gluinos and the stops, which remain natural because of the lesser dependence of the scalar masses on the Dirac mass of the gluinos. We could there point out the loss of accuracy associated with the choice of a  $\overline{\text{DR}}'$  renormalisation scheme for the parameters of the top/stop sector, and the fact that an on-shell scheme is more suitable in such scenarios. In particular, the phenomenologically relevant supersoft limit (where all soft SUSY-breaking terms vanish) can only be studied when using an OS scheme, as perturbativity is lost with the  $\overline{\text{DR}}'$  scheme.

In the remainder of the thesis, a particular emphasis has been put on the Goldstone Boson Catastrophe and its solution for general renormalisable theories. By employing

## Conclusion

an on-shell scheme for the Goldstone boson masses, we have obtained infra-red-safe expressions for the loop functions that appear in two-loop tadpole and self-energy diagrams – in the gaugeless limit and a generalised effective potential approach for the self-energies. We have also shown that by an expansion of the mass parameters in the loop functions, we could solve the tadpole equations directly, instead of iteratively. Nevertheless, several questions remain concerning this catastrophe, such as how to extend its solution to higher orders. Recently, ref. [36] proved that the resummation prescription first presented in [28] (see the description in section 1.1.5) can be extended to all orders in perturbation theory. It would then be interesting to find out how in practice to apply this method to general renormalisable theories, and to study further the relation between this resummation and the “on-shell” solution presented in chapter 4 (especially beyond two loops).

Our analytic results now allow investigating scalar masses at two-loop order in both supersymmetric and non-supersymmetric theories (Standard Model or extensions of it), without the numerical instabilities due to the Goldstones. This can be done either by applying the results to the desired model by hand, or by using automated tools like **SARAH/SPHeno**, in which the modified loop functions are implemented. An important result we find is the very good agreement between the value of the Higgs mass in the SM now obtained by **SARAH/SPHeno** and the existing complete two-loop results from dedicated calculations [22,25], indicating that – at least at the scale  $Q = m_t$  at which we performed the comparison – the purely-electroweak corrections and the two-loop momentum effects are both small. We have also considered several BSM models, illustrating in the NMSSM how well our “on-shell” method cures all the numerical instabilities caused by the Goldstone bosons, and investigating previously unknown two-loop corrections in various other models. This has in particular enabled us to make several findings for non-supersymmetric models, among which: *(i)* that loop corrections often grow out of control well before the Lagrangian parameters (couplings) reach the naive perturbativity bounds (in turn this signals the danger of trading Lagrangian parameters for masses using only tree-level masses as is often done for these models); and *(ii)* that the order at which the scalar quartic couplings are extracted from the physical spectrum can affect their high-scale evolution significantly, which can then have consequences on whether the considered parameter point is deemed valid or not.

There are numerous further avenues of research from this point. First of all, our investigations in non-supersymmetric models have shown the need for a more precise determination of perturbativity and unitarity constraints (note that in the continuation of the work presented in chapter 5, ref. [317] studied perturbativity bounds in the Georgi-Machacek model). For Higgs mass calculations, one should of course continue to improve the precision of theoretical predictions. On the one hand, for explicit computations, this is done by considering corrections in new models, as well as by deriving additional corrections in already studied theories. On the other hand, in the context of generic calculations, work is still needed to reach the level of precision currently available for the MSSM. A natural next step (also needed for the MSSM) would be to complete the set of two-loop mass contributions, by obtaining the momentum dependence of the diagrams that are of quartic order in the couplings of broken gauge groups (*e.g.* the electroweak couplings for a model with the same gauge group as the SM), even if we showed in chapter 5 that these must be very small in the case of the Standard Model. Moreover, in the context of numerical calculations in generic theories (for example in **SARAH/SPHeno**), it would be desirable to find an applicable way of going beyond the generalised effective potential approximation that is currently used. Indeed, it would be important to work towards a fast implementation of the two-loop

momentum dependence of general scalar mass corrections, in order for example to allow parameter scans (which cannot be performed currently with full two-loop momentum dependence because of excessively long computing times). It is also worth mentioning that in the last two years results have become available at three loops for the effective potential of generic theories [338,339], which may at some point serve for the calculation of tadpoles and mass corrections at three-loop order. Furthermore, in this work we have only considered fixed-order calculations in generic models. However, as the scale of New Physics seems to be driven to higher values by experimental searches, it appears necessary to make EFT calculations possible in general theories. In particular, obtaining analytic expressions for the matching of scalar quartic couplings between two generic models would be very important.

Finally, one should mention also that we have focussed here on the Higgs mass because it is now extremely well measured, as opposed to other Higgs properties, *e.g.* couplings, that are currently measured with a much worse accuracy or not even measured at all (this is for example the case for the Higgs trilinear coupling). However, it remains important to compute radiative corrections to these other properties, in expectation of future experimental results.

When, hopefully, conclusive experimental signs of some New Physics coupling to the Higgs sector are found, the analytic results and numerical tools developed to perform precision calculations of Higgs properties both in specific and in generic models – to which this thesis has contributed – will play a crucial role in understanding the nature of the newly observed phenomena.





## Appendix A

# Derivatives of the two-loop effective potential in models with Dirac gauginos

We present here the derivatives of the two-loop effective potential used to calculate the Higgs masses in section 3.1. We recall that the effective potential and its derivatives are expressed in units of  $\alpha_s C_F N_c / (4\pi)^3$ . The derivatives of the first term in eq. (3.1.19) can be trivially obtained by multiplying the formulae in appendix C of ref. [77] by  $R_{1i}^2$  and summing over the two gluino masses  $m_{\tilde{g}_i}$ , hence we do not repeat them here. The only exception is the single derivative of  $\Delta V_{\text{MSSM}}^{\alpha_s}$  with respect to  $m_t^2$ , which was not needed in ref. [77]. Adapted to the Dirac-gaugino case, it reads

$$\frac{\partial \Delta V^{\alpha_s}}{\partial m_t^2} = \sum_{i=1}^2 R_{1i}^2 \frac{\partial \Delta V_{\tilde{g}_i}}{\partial m_t^2}, \quad (\text{A.1})$$

with

$$\begin{aligned} \frac{\partial \Delta V_{\tilde{g}_i}}{\partial m_t^2} = & 2 m_t^2 \left( 3 - 4 \ln \frac{m_t^2}{Q^2} + 3 \ln^2 \frac{m_t^2}{Q^2} \right) \\ & + 2 \left[ m_t^2 \ln \frac{m_{\tilde{g}_i}^2}{m_t^2} + m_{\tilde{t}_1}^2 \left( 2 - \ln \frac{m_t^2}{Q^2} - \ln \frac{m_{\tilde{g}_i}^2}{Q^2} \right) \right] \ln \frac{m_{\tilde{t}_1}^2}{Q^2} \\ & + \left[ 2 (m_{\tilde{t}_1}^2 - m_t^2) - \frac{m_{\tilde{g}_i} m_{\tilde{t}_1}^2 s_{2\theta_t}}{m_t} \right] \ln \frac{m_t^2}{Q^2} \ln \frac{m_{\tilde{g}_i}^2}{Q^2} \\ & - 2 m_{\tilde{g}_i}^2 \left( 3 - 2 \ln \frac{m_{\tilde{g}_i}^2}{Q^2} \right) - m_{\tilde{t}_1}^2 \left( 4 - \frac{5 m_{\tilde{g}_i} s_{2\theta_t}}{m_t} \right) \\ & - \frac{m_{\tilde{g}_i} s_{2\theta_t}}{m_t} \left[ (3 m_t^2 - m_{\tilde{g}_i}^2) \ln \frac{m_{\tilde{g}_i}^2}{m_t^2} + m_{\tilde{t}_1}^2 \left( 4 - \ln \frac{m_t^2}{Q^2} - \ln \frac{m_{\tilde{g}_i}^2}{Q^2} \right) \right] \ln \frac{m_{\tilde{t}_1}^2}{Q^2} \\ & + 2 \left[ \frac{m_{\tilde{g}_i}^2}{m_t^2} (m_{\tilde{g}_i}^2 - m_t^2 - m_{\tilde{t}_1}^2) - \frac{\Delta_{\tilde{g}_i}}{m_t^2} \right. \\ & \quad \left. + \frac{m_{\tilde{g}_i} s_{2\theta_t}}{m_t} \left( m_t^2 - m_{\tilde{g}_i}^2 - m_{\tilde{t}_1}^2 + \frac{\Delta_{\tilde{g}_i}}{2 m_t^2} \right) \right] \Phi(m_{\tilde{t}_1}^2, m_{\tilde{g}_i}^2, m_t^2) \\ & + \left[ m_{\tilde{t}_1}^2 \rightarrow m_{\tilde{t}_2}^2, \quad s_{2\theta_t} \rightarrow -s_{2\theta_t} \right], \end{aligned} \quad (\text{A.2})$$

where  $Q$  is the renormalisation scale, the function  $\Phi(x, y, z)$  is defined in appendix D of ref. [77], and we used the shortcut

$$\Delta_{\tilde{g}_i} \equiv (m_{\tilde{g}_i}^2 - m_t^2 - m_{t_1}^2)^2 - 4 m_t^2 m_{t_1}^2. \quad (\text{A.3})$$

The derivatives of the octet-scalar contribution  $\Delta V_{O_i}$ , computed at the minimum of the potential, are

$$\frac{\partial \Delta V_{O_i}}{\partial c_{2\theta_t}^2} = -2 \left[ I(m_{t_1}^2, m_{t_1}^2, m_{O_i}^2) + I(m_{t_2}^2, m_{t_2}^2, m_{O_i}^2) - 2I(m_{t_1}^2, m_{t_2}^2, m_{O_i}^2) \right], \quad (\text{A.4})$$

$$\begin{aligned} \frac{\partial \Delta V_{O_i}}{\partial m_{t_1}^2} = & 2 \left( \ln \frac{m_{t_1}^2}{Q^2} - 1 \right)^2 + 2 s_{2\theta_t}^2 \ln \frac{m_{O_i}^2}{m_{t_1}^2} \ln \frac{m_{t_1}^2}{m_{t_2}^2} \\ & - 2 \left[ c_{2\theta_t}^2 \Phi(m_{t_1}^2, m_{t_1}^2, m_{O_i}^2) + s_{2\theta_t}^2 \frac{m_{O_i}^2 - m_{t_1}^2 + m_{t_2}^2}{m_{O_i}^2} \Phi(m_{t_1}^2, m_{t_2}^2, m_{O_i}^2) \right], \end{aligned} \quad (\text{A.5})$$

$$\begin{aligned} \frac{\partial^2 \Delta V_{O_i}}{(\partial m_{t_1}^2)^2} = & -\frac{4 s_{2\theta_t}^2}{m_{t_1}^2} + \frac{4 c_{2\theta_t}^2}{m_{O_i}^2 - 4 m_{t_1}^2} \left[ \frac{m_{O_i}^2}{m_{t_1}^2} \left( \ln \frac{m_{O_i}^2}{Q^2} - 1 \right) \right. \\ & \left. - 4 \left( \ln \frac{m_{t_1}^2}{Q^2} - 1 \right) - \Phi(m_{t_1}^2, m_{t_1}^2, m_{O_i}^2) \right] \\ & + \frac{4 s_{2\theta_t}^2}{\Delta_{O_i}} \left[ \frac{m_{O_i}^2}{m_{t_1}^2} (m_{O_i}^2 - m_{t_1}^2 - m_{t_2}^2) \ln \frac{m_{O_i}^2}{Q^2} - (m_{O_i}^2 - m_{t_1}^2 + m_{t_2}^2) \ln \frac{m_{t_1}^2}{Q^2} \right. \\ & \left. - \frac{m_{t_2}^2}{m_{t_1}^2} (m_{O_i}^2 + m_{t_1}^2 - m_{t_2}^2) \ln \frac{m_{t_2}^2}{Q^2} - 2 m_{t_2}^2 \Phi(m_{t_1}^2, m_{t_2}^2, m_{O_i}^2) \right], \end{aligned} \quad (\text{A.6})$$

$$\begin{aligned} \frac{\partial^2 \Delta V_{O_i}}{\partial m_{t_1}^2 \partial c_{2\theta_t}^2} = & -2 \left[ \ln \frac{m_{O_i}^2}{m_{t_1}^2} \ln \frac{m_{t_1}^2}{m_{t_2}^2} + \Phi(m_{t_1}^2, m_{t_1}^2, m_{O_i}^2) \right. \\ & \left. - \frac{m_{O_i}^2 - m_{t_1}^2 + m_{t_2}^2}{m_{O_i}^2} \Phi(m_{t_1}^2, m_{t_2}^2, m_{O_i}^2) \right], \end{aligned} \quad (\text{A.7})$$

$$\begin{aligned} \frac{\partial^2 \Delta V_{O_i}}{\partial m_{t_1}^2 \partial m_{t_2}^2} = & \frac{4 s_{2\theta_t}^2}{\Delta_{O_i}} \left[ m_{O_i}^2 \ln \frac{m_{O_i}^4}{m_{t_1}^2 m_{t_2}^2} - (m_{t_1}^2 - m_{t_2}^2) \ln \frac{m_{t_1}^2}{m_{t_2}^2} \right. \\ & \left. - (m_{O_i}^2 - m_{t_1}^2 - m_{t_2}^2) \Phi(m_{t_1}^2, m_{t_2}^2, m_{O_i}^2) \right], \end{aligned} \quad (\text{A.8})$$

where we used the shortcut

$$\Delta_{O_i} \equiv (m_{O_i}^2 - m_{t_1}^2 - m_{t_2}^2)^2 - 4 m_{t_1}^2 m_{t_2}^2. \quad (\text{A.9})$$

The derivatives of  $\Delta V_{O_i}$  that involve  $m_{t_2}^2$  can be trivially obtained from the ones in eqs. (A.5)–(A.7) by means of the replacement  $m_{t_1}^2 \leftrightarrow m_{t_2}^2$ , while the derivatives with respect to all other combinations of field-dependent parameters vanish.

## Appendix B

# Definitions and expansions of loop functions

### B.1 Loop functions

Throughout our work, we have followed closely the notations of [142], however we present in this appendix the loop functions and the notations that were used. These definitions of loop functions use Euclidean momentum integrals in dimensional reduction to  $d = 4 - 2\epsilon$  dimensions, and involve the loop factor

$$C = 16\pi^2 \frac{\mu^{2\epsilon}}{(2\pi)^d}. \quad (\text{B.1.1})$$

We also recall the following shorthand notations

$$\overline{\log} x \equiv \log \frac{x}{Q^2}, \quad (\text{B.1.2})$$

where  $Q^2 = 4\pi e^{-\gamma_E} \mu^2$  is the renormalisation scale squared.

#### B.1.1 Definition of loop functions

##### B.1.1.1 One-loop functions

In the expression of the one-loop effective potential, we make use of the function  $f$  defined as

$$f(x) \equiv \frac{x^2}{4} \left( \overline{\log} x - \frac{3}{2} \right) \quad (\text{B.1.3})$$

Two important one-loop functions that will appear in the expression of the effective potential, of its derivatives and in the self-energies are the finite parts of

$$\mathbf{A}(x) \equiv C \int \frac{d^d k}{k^2 + x} \quad (\text{B.1.4})$$

$$\mathbf{B}(p^2, x, y) \equiv C \int \frac{d^d k}{(k^2 + x)((p - k)^2 + y)}, \quad (\text{B.1.5})$$

namely

$$A(x) \equiv \lim_{\epsilon \rightarrow 0} \left( \mathbf{A}(x) + \frac{x}{\epsilon} \right) = x(\overline{\log} x - 1) = 2 \frac{d}{dx} f(x), \quad (\text{B.1.6})$$

$$B(p^2, x, y) = B(x, y) \equiv \lim_{\epsilon \rightarrow 0} \left( \mathbf{B}(p^2, x, y) - \frac{1}{\epsilon} \right) = -\overline{\log} p^2 - f_B(x_+) - f_B(x_-), \quad (\text{B.1.7})$$

where

$$f_B(x) = \log(1 - x) - x \log \left( 1 - \frac{1}{x} \right) - 1, \quad (\text{B.1.8})$$

and

$$x_{\pm} = \frac{p^2 + x + y \pm \sqrt{(p^2 + x + y)^2 - 4p^2x}}{2p^2}. \quad (\text{B.1.9})$$

In two-loop order expressions, the function  $J$  is sometimes used, although it is equal to  $A$

$$J(x) = A(x). \quad (\text{B.1.10})$$

A limit of particular interest of  $B$  is the limit of vanishing external momentum, that we denote  $B_0$ , and is related to the  $P_{SS}$  function we have used

$$B(p^2, x, y) \xrightarrow{p^2 \rightarrow 0} B_0(x, y) = -P_{SS}(x, y) \equiv -\frac{A(x) - A(y)}{x - y}. \quad (\text{B.1.11})$$

and furthermore, we have that

$$B_0(x, x) = -\overline{\log} x \Leftrightarrow P_{SS}(x, x) = \overline{\log} x \quad (\text{B.1.12})$$

The derivative of the  $B$  function with respect to one of the mass arguments is also used, with the notation

$$B'(p^2, x, y) = \frac{\partial}{\partial x} B(p^2, x, y). \quad (\text{B.1.13})$$

For the fermion and gauge boson contributions to the scalar self-energy we also use the functions  $P_{FF}$ ,  $P_{\overline{FF}}$  and  $P_{VV}$  related to  $A$  and  $P_{SS}$  as

$$P_{FF}(x, y) \equiv -2 \frac{x A(x) - y A(y)}{x - y} = -A(x) - A(y) - (x + y) P_{SS}(x, y), \quad (\text{B.1.14})$$

$$P_{\overline{FF}}(x, y) \equiv -2 P_{SS}(x, y), \quad (\text{B.1.15})$$

$$P_{VV}(x, y) \equiv 3 P_{SS}(x, y). \quad (\text{B.1.16})$$

In the context of the reexpansion of the mass diagrams, we also make use of the one-loop three-point function  $C(p_1^2, p_2^2, (p_1 + p_2)^2, x, y, z)$ , which is the finite part of the following integral

$$\mathbf{C}(p_1^2, p_2^2, (p_1 + p_2)^2, x, y, z) \equiv -C \int \frac{d^d k}{(k^2 + x)((k - p_1)^2 + y)((k - p_1 - p_2)^2 + z)}. \quad (\text{B.1.17})$$

### B.1.1.2 Two-loop functions

We recall the definition of the following two-loop integrals

$$\mathbf{S}(x, y, z) \equiv C^2 \int d^d k \int d^d q \frac{1}{(k^2 + x)(q^2 + y)((k + q - p)^2 + z)}, \quad (\text{B.1.18})$$

$$\mathbf{U}(x, y, z, u) \equiv C^2 \int d^d k \int d^d q \frac{1}{(k^2 + x)((k - p)^2 + y)(q^2 + z)((k + q - p)^2 + u)}, \quad (\text{B.1.19})$$

$$\mathbf{M}(x, y, z, u, v) \equiv C^2 \int d^d k \int d^d q \frac{1}{(k^2 + x)(q^2 + y)((k - p)^2 + z)((q - p)^2 + u)((k - q)^2 + v)}. \quad (\text{B.1.20})$$

of which we take the finite parts

$$S(x, y, z) = \lim_{\epsilon \rightarrow 0} [\mathbf{S}(x, y, z) - (\mathbf{A}(x) + \mathbf{A}(y) + \mathbf{A}(z))/\epsilon - (x + y + z)/2\epsilon^2 - (p^2/2 - x - y - z)/2\epsilon],$$

$$U(x, y, z, u) = \lim_{\epsilon \rightarrow 0} [\mathbf{U}(x, y, z, u) - \mathbf{B}(p^2, x, y)/\epsilon + 1/2\epsilon^2 - 1/2\epsilon], \quad (\text{B.1.21})$$

$$U_0(x, y, z, u) \equiv U(x, y, z, u)|_{p^2=0} = \frac{I(x, z, u) - I(y, z, u)}{y - x}, \quad (\text{B.1.22})$$

$$M(x, y, z, u, v) = \lim_{\epsilon \rightarrow 0} \mathbf{M}(x, y, z, u, v). \quad (\text{B.1.23})$$

We also require the related functions (where  $\bar{V}$  differs slightly from [20])

$$I(x, y, z) \equiv S(x, y, z)|_{p^2=0}, \quad (\text{B.1.24})$$

$$V(x, y, z, u) \equiv -\frac{\partial}{\partial y} U(x, y, z, u), \quad (\text{B.1.25})$$

$$\bar{V}(x, y, z) \equiv \lim_{u \rightarrow 0} \left[ V(x, u, y, z) - \frac{1}{s - x} \frac{\partial}{\partial u} I(u, y, z) \right]. \quad (\text{B.1.26})$$

The integral  $I$  is symmetric on all three indices, and thus  $U_0$  is symmetric on  $x \leftrightarrow y$  and  $z \leftrightarrow u$  separately etc; the  $I$  integral is fundamental for the two-loop effective potential, all other functions being obtained from it and  $A(x)$ . It can be written explicitly although the expression is rather involved; it can be found in equations (D1) to (D3) of [77] although it was first derived in [16]. Here we note the useful limiting cases

$$\begin{aligned} I(x, y, 0) &= \frac{1}{2} \left( -5x - 5y + (-x + y) \overline{\log^2 x} + 4y \overline{\log y} + \overline{\log x} (4x - 2y \overline{\log y}) \right. \\ &\quad \left. - 2(x - y) \text{Li}_2(1 - y/x) \right), \\ I(x, x, x) &= \frac{3}{2} x (-5 + 4 \overline{\log x} - \overline{\log^2 x} + c_{xxx}), \\ I(x, x, 0) &= x (-5 + 4 \overline{\log x} - \overline{\log^2 x}), \\ I(x, 0, 0) &= -x \left( \frac{1}{2} \overline{\log^2 x} + 2 \overline{\log x} - \frac{5}{2} - \frac{\pi^2}{6} \right), \end{aligned} \quad (\text{B.1.27})$$

where  $c_{xxx} \approx 2.3439$  is a constant.

The two-loop functions appearing in the effective potential were defined in [19] and read

$$f_{SSS}(x, y, z) = -I(x, y, z), \quad (\text{B.1.28})$$

$$f_{SS}(x, y) = J(x, y), \quad (\text{B.1.29})$$

$$f_{FFS}(x, y, z) = J(x, y) - J(x, z) - J(y, z) + (x + y - z)I(x, y, z), \quad (\text{B.1.30})$$

$$f_{\overline{FFS}}(x, y, z) = 2I(x, y, z), \quad (\text{B.1.31})$$

$$\begin{aligned} f_{SSV}(x, y, z) = & \frac{1}{z} \left[ (-x^2 - y^2 - z^2 + 2xy + 2xz + 2yz)I(x, y, z) + (x - y)^2 I(0, x, y) \right. \\ & \left. + (y - x - z)J(x, z) + (x - y - z)J(y, z) + zJ(x, y) \right] \\ & + 2 \left( x + y - \frac{z}{3} \right) J(z), \end{aligned} \quad (\text{B.1.32})$$

where

$$J(x, y) \equiv J(x)J(y) = A(x)A(y). \quad (\text{B.1.33})$$

To these functions we must also add the scheme dependent functions  $f_{VS}$ ,  $f_{VVS}$ ,  $f_{FFV}$ ,  $f_{\overline{FFV}}$  and  $f_{\text{gauge}}$  that we give for the  $\overline{\text{DR}}'$  and  $\overline{\text{MS}}$  schemes (slightly modifying the notation of [19])

$$f_{VS}(x, y) = 3J(x, y) + \delta_{\overline{\text{MS}}} 2xJ(y), \quad (\text{B.1.34})$$

$$\begin{aligned} f_{VVS}(x, y, z) = & \frac{1}{4xy} \left[ (-x^2 - y^2 - z^2 - 10xy + 2xz + 2yz)I(x, y, z) \right. \\ & + (x - z)^2 I(0, x, z) + (y - z)^2 I(0, y, z) - z^2 I(0, 0, z) \\ & \left. + (z - x - y)J(x, y) + yJ(x, z) + xJ(y, z) \right] \\ & + \frac{1}{2}J(x) + \frac{1}{2}J(y) + \delta_{\overline{\text{MS}}} (2J(z) - x - y - z), \end{aligned} \quad (\text{B.1.35})$$

$$\begin{aligned} f_{FFV}(x, y, z) = & \frac{1}{z} \left[ (x^2 + y^2 - 2z^2 - 2xy + xz + yz)I(x, y, z) - (x - y)^2 I(0, x, y) \right. \\ & \left. + (x - y - 2z)J(x, z) + (y - x - 2z)J(y, z) + 2zJ(x, y) \right] \\ & + 2 \left( -x - y + \frac{z}{3} \right) J(z) - \delta_{\overline{\text{MS}}} (2xJ(x) + 2yJ(y) - (x + y)^2 + z^2), \end{aligned} \quad (\text{B.1.36})$$

$$f_{\overline{FFV}}(x, y, z) = 6I(x, y, z) + \delta_{\overline{\text{MS}}} (2(x + y + z) - 4J(x) - 4J(y)), \quad (\text{B.1.37})$$

$$\begin{aligned} f_{\text{gauge}}(x, y, z) = & \frac{1}{4xyz} \left[ (-x^4 - 8x^3y - 8x^3z + 32x^2yz + 18y^2z^2)I(x, y, z) \right. \\ & + (y - z)^2 (y^2 + 10yz + z^2)I(0, y, z) + x^2 (2yz - x^2)I(0, 0, x) \\ & + (x^2 - 9y^2 - 9z^2 + 9xy + 9xz + 14yz)xJ(y, z) \\ & + \left( 22y + 22z - \frac{40}{3}x \right) xyzJ(x) \\ & \left. + \delta_{\overline{\text{MS}}} (4x^3yz + 48xy^2z^2 + 8x^2yzJ(x)) \right] \\ & + (x \leftrightarrow y) + (x \leftrightarrow z) \end{aligned} \quad (\text{B.1.38})$$

where

$$\delta_{\overline{\text{MS}}} = \begin{cases} 1 & \text{in the } \overline{\text{MS}} \text{ scheme} \\ 0 & \text{in the } \overline{\text{DR}}' \text{ scheme} \end{cases} \quad (\text{B.1.39})$$

Taking derivatives of these functions with respect to one argument is required for the two-loop tadpoles, and we use the notations

$$\begin{aligned} f_{\alpha}^{(1,0,0)}(x, y; z, u) &= \frac{f_{\alpha}(x, z, u) - f_{\alpha}(y, z, u)}{x - y} \\ f_{\alpha}^{(0,0,1)}(x, y; z, u) &= \frac{f_{\alpha}(x, y, z) - f_{\alpha}(x, y, u)}{z - u} \end{aligned} \quad (\text{B.1.40})$$

For the mass diagrams, we require the following loop integral functions:

$$W_{SSSS}(x, y, z, u) = [I(x, z, u) - I(y, z, u)]/(y - x), \quad (\text{B.1.41})$$

$$X_{SSS}(x, y, z) = J(z)P_{SS}(x, y), \quad (\text{B.1.42})$$

$$Y_{SSSS}(x, y, z, u) = J(u)[B(p^2, x, z) - B(p^2, x, y)]/(y - z), \quad (\text{B.1.43})$$

$$Z_{SSSS}(x, y, z, u) = B(p^2, x, y)B(p^2, z, u), \quad (\text{B.1.44})$$

$$S_{SSS}(x, y, z) = -S(x, y, z), \quad (\text{B.1.45})$$

$$U_{SSSS}(x, y, z, u) = U(x, y, z, u), \quad (\text{B.1.46})$$

$$V_{SSSSS}(x, y, z, u, v) = [U(x, y, u, v) - U(x, z, u, v)]/(y - z), \quad (\text{B.1.47})$$

$$M_{SSSSS}(x, y, z, u, v) = -M(x, y, z, u, v), \quad (\text{B.1.48})$$

$$\begin{aligned} W_{SSFF}(x, y, z, u) &= \frac{1}{x - y}[(z + u - x)I(x, z, u) - A(x)[A(z) + A(u)] \\ &\quad + (x \leftrightarrow y)], \end{aligned} \quad (\text{B.1.49})$$

$$W_{SS\overline{FF}}(x, y, z, u) = -2W_{SSSS}(x, y, z, u), \quad (\text{B.1.50})$$

$$\begin{aligned} V_{SSSFF}(x, y, z, u, v) &= \frac{(y - u - v)U(x, y, u, v) + [A(u) + A(v)]B(s, x, y)}{y - z} \\ &\quad + (y \leftrightarrow z), \end{aligned} \quad (\text{B.1.51})$$

$$V_{SSS\overline{FF}}(x, y, z, u, v) = -2V_{SSSSS}(x, y, z, u, v). \quad (\text{B.1.52})$$

### B.1.2 Small $m_G^2$ expansion

For completeness, we recall equations (3.7)-(3.10) from [33] for the expansion of the loop functions appearing in the two-loop effective potential

$$f_{SSS}(m_G^2, x, y) = f_{SSS}(0, x, y) + P_{SS}(x, y)A(m_G^2) + R_{SS}(x, y)m_G^2 + \mathcal{O}(m_G^4), \quad (\text{B.1.53})$$

$$f_{SSS}(m_G^2, m_G^2, x) = f_{SSS}(0, 0, x) + 2P_{SS}(0, x)A(m_G^2) + 2R_{SS}(0, x)m_G^2 + \mathcal{O}(m_G^4), \quad (\text{B.1.54})$$

$$f_{SS}(m_G^2, x) = A(x)A(m_G^2), \quad (\text{B.1.55})$$

$$f_{FFS}(m_G^2, x, y) = f_{FFS}(0, x, y) + P_{FF}(x, y)A(m_G^2) + R_{FF}(x, y)m_G^2 + \mathcal{O}(m_G^4), \quad (\text{B.1.56})$$

$$f_{\overline{FF}S}(m_G^2, x, y) = f_{\overline{FF}S}(0, x, y) + P_{\overline{FF}}(x, y)A(m_G^2) + R_{\overline{FF}}(x, y)m_G^2 + \mathcal{O}(m_G^4), \quad (\text{B.1.57})$$

$$f_{SSV}(m_G^2, x, y) = f_{SSV}(0, x, y) + R_{SV}(x, y)m_G^2 + \mathcal{O}(m_G^4), \quad (\text{B.1.58})$$

$$f_{SSV}(m_G^2, m_G^2, x) = f_{SSV}(0, 0, x) + 2R_{SV}(0, x)m_G^2 + \mathcal{O}(m_G^4), \quad (\text{B.1.59})$$

$$f_{VS}(m_G^2, x) = 3A(x)A(m_G^2) + 2x\delta_{\overline{\text{MS}}}A(m_G^2), \quad (\text{B.1.60})$$

$$\begin{aligned} f_{VVS}(m_G^2, x, y) &= f_{VVS}(0, x, y) + (P_{VV}(x, y) + 2\delta_{\overline{\text{MS}}})A(m_G^2) \\ &\quad + (R_{VV}(x, y) - \delta_{\overline{\text{MS}}})m_G^2 + \mathcal{O}(m_G^4), \end{aligned} \quad (\text{B.1.61})$$

where the  $R$  functions are defined in [33] as

$$\begin{aligned} R_{SS}(x, y) &= \{(x+y)^2 + 2A(x)A(y) - 2xA(x) - 2yA(y) \\ &\quad + (x+y)I(0, x, y)\}/(x-y)^2, \end{aligned} \quad (\text{B.1.62})$$

$$\begin{aligned} R_{FF}(x, y) &= - \left[ (x+y)\{(x+y)^2 + 2A(x)A(y) - 2xA(x) - 2yA(y) + (x+y)^2\} \right. \\ &\quad \left. + 2(x^2 + y^2)I(0, x, y) \right] / (x-y)^2, \end{aligned} \quad (\text{B.1.63})$$

$$R_{\overline{FF}}(x, y) = -2R_{SS}(x, y), \quad (\text{B.1.64})$$

$$R_{SV}(x, y) = \frac{1}{y} \left( 3(x+y)I(0, x, y) - 3xI(0, 0, x) + 3A(x)A(y) + 2xy + y^2 \right), \quad (\text{B.1.65})$$

$$\begin{aligned} R_{VV}(x, y) &= \frac{1}{4xy(x-y)^2} \left[ 3A(x)A(y)(x^2 + y^2 + 6xy) - 24xy(xA(x) + yA(y)) \right. \\ &\quad \left. + 14xy(x^2 + y^2) + 20x^2y^2 + 3(x+y)^3I(0, x, y) \right. \\ &\quad \left. - 3(x-y)^2(xI(0, 0, x) + yI(0, 0, y)) \right]. \end{aligned} \quad (\text{B.1.66})$$

One can see from the expression (B.1.24) that  $I(= -f_{SSS})$  is regular for any number of its arguments vanishing. Using eq. (B.1.21) and (B.1.53), we can find the expansion of  $U_0(x, y, m_G^2, m_G^2)$

$$\begin{aligned} U_0(x, y, m_G^2, m_G^2) &= - \frac{d}{dm_G^2} I(m_G^2, x, y) = \frac{d}{dm_G^2} f_{SSS}(m_G^2, x, y) \\ &= P_{SS}(x, y) \overline{\log} m_G^2 + R_{SS}(x, y) + \dots \end{aligned} \quad (\text{B.1.67})$$

For the derivatives of the two-loop  $f$  functions, we use the following expansions

$$\begin{aligned} f_{FFS}^{(0,0,1)}(x, y, m_G^2, m_G^2) &= - \overline{\log} m_G^2 [J(x) + J(y)] - I(x, y, 0) - (x+y)U_0(x, y, m_G^2, m_G^2) \\ &= - \overline{\log} m_G^2 \left[ (x+y)P_{SS}(x, y) + A(x) + A(y) \right] - I(x, y, 0) \\ &\quad - (x+y)R_{SS}(x, y) + \mathcal{O}(m_G^2), \end{aligned} \quad (\text{B.1.68})$$

$$f_{SSV}^{(1,0,0)}(m_G^2, m_G^2; x, y) = -R_{SV}(x, y) + \mathcal{O}(m_G^2) \quad (\text{B.1.69})$$

$$f_{VS}^{(0,1)}(x, m_G^2, m_G^2) = (3A(x) + 2x\delta_{\overline{\text{MS}}}) \overline{\log} m_G^2 + \mathcal{O}(m_G^2) \quad (\text{B.1.70})$$

$$f_{VVS}^{(0,0,1)}(y, z; m_G^2, m_G^2) = - (3P_{SS}(y, z) + \delta_{\overline{\text{MS}}}) \overline{\log} m_G^2 - R_{VV}(y, z) + \mathcal{O}(m_G^2). \quad (\text{B.1.71})$$

## B.2 Diagrams regulated by momentum

When studying the mass terms, we encountered some diagrams for which the resummation of the Goldstone contributions provide no shift to regulate an infrared divergence and hence these diagrams must be regulated by momentum. More precisely, this is the case for the functions  $U$ ,  $M$ ,  $Z$  and for some of the  $V$  diagrams. In this section,



we give the expansions for small external momentum  $s \equiv -p^2$  of the diagrams that diverge as  $s \rightarrow 0$ , taken from expanding expressions in [142, 340] or found by newly solving or expanding the integral equations in [142]. Hence we stress that (most of) this section contains new results not found elsewhere.

### B.2.1 Limits of the $Z$ and $U$ functions

First, for  $Z$ , we only need the fact that

$$B(p^2, m_G^2, m_G^2) \xrightarrow{m_G \rightarrow 0} 2 - \overline{\log}(-s). \quad (\text{B.2.1})$$

Then, for the  $U$  function, taking one argument to zero does not cause any divergence, and we find, looking at the integral definition (B.1.19) of  $U$ , that  $U(x, y, 0, 0)$ ,  $U(0, x, y, 0)$ ,  $U(x, 0, y, 0)$ ,  $U(x, 0, 0, 0)$  and  $U(0, y, 0, 0)$  are all regular so we can substitute them for  $U_0 + \mathcal{O}(s)$ . The only divergent function is  $U(0, 0, x, y)$  that has the form

$$U(0, 0, x, y) = A_U(x, y) \overline{\log}(-s) + B_U(x, y) + \mathcal{O}(s) \quad (\text{B.2.2})$$

with

$$A_U(x, y) = -1 + \frac{x \overline{\log} x - y \overline{\log} y}{x - y} = P_{SS}(x, y) \rightarrow A_U(x, x) = \overline{\log} x, \quad (\text{B.2.3})$$

$$\begin{aligned} B_U(x, y) = & \frac{5}{2} + \frac{1}{2(y-x)} \left[ -(x+y) \overline{\log}^2 y + 4x \overline{\log} x - 4y \overline{\log} y \right. \\ & \left. + 2x \overline{\log} x \overline{\log} y - 2(x+y) \text{Li}_2\left(1 - \frac{x}{y}\right) \right] \\ = & \frac{5}{2} + \frac{1}{2(y-x)} \left[ 8(x \overline{\log} x - y \overline{\log} y) + (x+y)(\overline{\log}^2 x - \overline{\log}^2 y) \right. \\ & \left. - 2(y-x) \overline{\log} x \overline{\log} y - (x+y) \left( \text{Li}_2\left(1 - \frac{x}{y}\right) - \text{Li}_2\left(1 - \frac{y}{x}\right) \right) \right], \quad (\text{B.2.4}) \end{aligned}$$

$$B_U(x, x) = -\frac{3}{2} - 3 \overline{\log} x - \frac{1}{2} \overline{\log}^2 x, \quad (\text{B.2.5})$$

where we have written the  $B_U$  coefficient in two ways, one for computational simplicity, and the other to explicitly show the symmetry in  $x \leftrightarrow y$ . The limit as  $x \rightarrow 0$  can be smoothly taken to give

$$U(0, 0, 0, u) = (\overline{\log} u - 1) \overline{\log}(-s) - \frac{\pi^2}{6} + \frac{5}{2} - 2 \overline{\log} u - \frac{1}{2} \overline{\log}^2 u + \mathcal{O}(s). \quad (\text{B.2.6})$$

which matches an expansion of the full momentum-dependence expression in equation (6.24) of [142].

Finally,

$$U(0, 0, 0, 0) = \frac{1}{2} (\overline{\log}(-s) - 3)^2 + 1$$

is not required, as it always appears with  $\lambda^{GGG}$  as a factor, which is zero up to higher order corrections.

### B.2.2 Limits of the $M$ function

Turning now to the  $M$  function, there are more cases to consider. In the case of only one argument vanishing, we see from the integral expression (B.1.20) that the function is regular. From eqs.(6.28) and (6.31) in [142], we also find that  $M(x, y, z, 0, 0)$ ,  $M(x, y, 0, 0, v)$  and  $M(x, y, 0, 0, 0)$  are finite. Then we have

$$M(0, y, 0, u, v) = A_M(y, u, v) \overline{\log}(-s) + B_M(y, u, v) \quad (\text{B.2.7})$$

where

$$A_M(y, u, v) = \frac{u \overline{\log} u}{(y-u)(u-v)} - \frac{y \overline{\log} y}{(y-u)(y-v)} - \frac{v \overline{\log} v}{(y-v)(u-v)}, \quad (\text{B.2.8})$$

$$B_M(y, u, v) = -(2 + \overline{\log} v) A_M(y, u, v) + \frac{u+v}{(y-u)(u-v)} \text{Li}_2(1-u/v) - \frac{v+y}{(y-u)(y-v)} \text{Li}_2(1-y/v). \quad (\text{B.2.9})$$

$A_M$  is symmetric on all three indices, and as  $M(0, 0, 0, u, 0)$  or  $M(0, y, 0, 0, 0)$  have prefactor  $\lambda^{GG}$ , we only need to consider the following cases

$$\begin{aligned} A_M(0, u, v) &= \frac{\overline{\log}(v/u)}{u-v} \\ B_M(0, u, v) &= -(2 + \overline{\log} v) A_M(0, u, v) - \frac{\pi^2}{6u} - \frac{(u+v) \text{Li}_2(1-u/v)}{u(u-v)} \\ B_M(y, u, 0) &= \frac{\log u/y [4 + \overline{\log} u + \overline{\log} y]}{2(u-y)} \\ B_M(y, y, 0) &= \frac{2 + \overline{\log} y}{y} \\ A_M(y, y, v) &= \frac{v \log y/v}{(y-v)^2} - \frac{1}{y-v} \\ A_M(y, y, 0) &= -\frac{1}{y} \\ B_M(y, y, v) &= -(2 + \overline{\log} v) A_M(y, y, v) + \frac{1}{(y-v)^2} \left[ (v+y) \log y/v + 2v \text{Li}_2(1-y/v) \right] \\ A_M(y, y, y) &= -\frac{1}{2y} \\ B_M(y, y, y) &= \frac{1}{2y} (3 + \overline{\log}(y)) = -(2 + \overline{\log} y) A_M(y, y, y) + \frac{1}{2y} \\ B_M(y, u, u) &= -(2 + \overline{\log} u) A_M(y, u, u) + \frac{2}{u-y} - \frac{(u+y) \text{Li}_2(1-y/u)}{(u-y)^2}. \end{aligned} \quad (\text{B.2.10})$$

The only additional case is  $M(0, 0, 0, 0, v)$  that we have to consider separately and that we find to be

$$M(0, 0, 0, 0, v) = \frac{1}{v} \left( \log^2(-s/v) - 2 \log(-s/v) + \frac{\pi^2}{3} \right). \quad (\text{B.2.11})$$

Finally, the expression of  $M(x, 0, 0, 0, 0)$  with full momentum dependence can be found in equation (6.31) of [142], and becomes when expanding to leading order for small  $s$

$$M(x, 0, 0, 0, 0) = \frac{1}{6x} \left( 18 + \pi^2 - 12 \log(-s/x) + 3 \log^2(-s/x) \right). \quad (\text{B.2.12})$$

The approximate formulae for  $U(0, 0, x, y)$ ,  $M(0, y, 0, u, v)$  and  $M(0, 0, 0, 0, v)$  have been checked against the numerical results from TSIL [150] and show excellent agreement until  $s$  becomes of the order of the arguments in the functions – even when  $s$  is of the order of the mass parameters, the difference between the approximate result and the numerical from TSIL is about 10%.

### B.3 Additional expressions for $\tilde{V}(x, 0, z, u)$

One of the key functions of the basis set is  $V(x, y, z, u)$ . This is defined as

$$V(x, y, z, u) \equiv -\frac{\partial}{\partial y} U(x, y, z, u). \quad (\text{B.3.1})$$

It is singular as  $y \rightarrow 0$ , so we define the regularised version (defined with one fewer explicit index to [20]):

$$\bar{V}(x, y, z) \equiv \lim_{u \rightarrow 0} \left[ V(x, u, y, z) - \frac{1}{s-x} \frac{\partial}{\partial u} I(u, y, z) \right]. \quad (\text{B.3.2})$$

On the other hand, we require a slightly *different* regularised function:

$$\tilde{V}(x, y, z) \equiv \lim_{u \rightarrow 0} \left[ -V(x, u, y, z) + P_{SS}(y, z) B(u, x') \right]. \quad (\text{B.3.3})$$

For the case  $x \neq 0$ , we can simply extract the result at vanishing external momentum:

$$\begin{aligned} \lim_{s \rightarrow 0} \bar{V}(x, z, u) &= \lim_{y \rightarrow 0} \left[ -U_0(x, y', z, u) - \frac{1}{x} P_{SS}(z, u) \overline{\log y} \right] \\ &= \frac{I(x, z, u) - I(0, z, u)}{x^2} = -\frac{1}{x} U_0(x, 0, z, u). \end{aligned} \quad (\text{B.3.4})$$

Then constructing  $\tilde{V}$  gives

$$\begin{aligned} \lim_{s \rightarrow 0} \tilde{V}(x, z, u) &= -\lim_{s \rightarrow 0} \bar{V}(x, z, u) - \frac{1}{x} \left[ R_{SS}(z, u) + P_{SS}(z, u) (\overline{\log x} - 1) \right] \\ &= \frac{1}{x} \left[ U_0(x, 0, z, u) + R_{SS}(z, u) + P_{SS}(z, u) (\overline{\log x} - 1) \right]. \end{aligned} \quad (\text{B.3.5})$$

On the other hand, for  $x \rightarrow 0$  we cannot take the above limit. In principle we could start again from the expressions for  $\bar{V}(x, y, z)$  given in the appendix of [20] and take the smooth limit  $x \rightarrow 0$ . Instead, here we provide *two* direct derivations of a compact expression for  $\tilde{V}(0, z, u)$ , with both general external momentum and then for our generalised effective potential limit. The starting point for the first derivation is the set of differential equations given in [142], in this case

$$\begin{aligned} \frac{\partial}{\partial y} U(x, y, z, u) &= k_{UU} U(x, y, z, u) + k_{UT1} T(x, z, u) + k_{UT2} T(u, x, z) + k_{UT2} T(z, x, u) \\ &\quad + k_{US} \left[ S(x, z, u) - \frac{1}{2} (A(x) + A(z) + A(u) + I(y, z, u)) \right] \\ &\quad + k_{UB} B(x, y) + k_U \\ &\equiv k_{UU} U(x, y, z, u) + \Delta, \end{aligned} \quad (\text{B.3.6})$$

where the coefficients of the loop functions are themselves functions of  $s, x, y, z, u$ . However, here we encounter the problem that several of these coefficients are actually

*Definitions and expansions of loop functions*

singular as  $y \rightarrow 0$  – so we cannot simply evaluate the right-hand side of the equation to determine  $V(x, 0, z, u)$ !

However, we can obtain such a closed-form expression by using the ansatz

$$\begin{aligned} U(x, y, z, u) &= f_0(s; x, z, u) + f(s; x, z, u)A(y) + f_1(s; x, z, u)y + \mathcal{O}(y^2) \\ f_0(s; x, z, u) &= U(x, 0, z, u), \\ k_U &= -\frac{1}{y} + k_{UU}^0 + \mathcal{O}(y) \\ \Delta &= \frac{\Delta^{(-1)}}{y} + \Delta_l \overline{\log y} + \Delta^0 + \dots \end{aligned} \quad (\text{B.3.7})$$

and substituting it into the above differential equation, to find  $f$  and  $f_1$ :

$$\begin{aligned} f \overline{\log y} + f_1 + \dots &= \left(-\frac{1}{y} + k_{UU}^0\right) \left(f_0(s; x, z, u) + f(s; x, z, u)A(y) + f_1(s; x, z, u)y\right) + \Delta \\ &= -\frac{f_0}{y} - f \overline{\log y} + (f - f_1 + f_0 k_{UU}^0) + \frac{\Delta^{(-1)}}{y} + \Delta_l \overline{\log y} + \Delta^0 + \dots \\ &\rightarrow \Delta^{(-1)} = f_0, \quad f = \frac{1}{2}\Delta_l, \quad f_1 = \frac{1}{2}\left(f + \Delta^0 + \Delta^{(-1)}k_{UU}^0\right). \end{aligned} \quad (\text{B.3.8})$$

The form of  $f$  must correspond to the singularity; indeed we have

$$f(s; x, z, u) = \frac{1}{s-x} P_{SS}(z, u). \quad (\text{B.3.9})$$

However,  $f_1$  is more work; we eventually obtain in the limit  $x \rightarrow 0$  that we are interested in

$$\begin{aligned} \tilde{V}(0, z, u) &= \left(\frac{uz \log z/u}{(u-z)^3} + \frac{u+z}{2(u-z)^2}\right) B(0, 0) \\ &+ \frac{1}{s} \left[ \frac{2A(u)A(z) + (u+z)^2 + 2(u+z)I(z, u, 0)}{2(u-z)^2} \right] \\ &+ \frac{1}{2} \left[ \mathcal{K}_{UT2}T(u, 0, z) + \mathcal{K}_{UT3}T(z, 0, u) + \mathcal{K}_{US}S(0, z, u) + \mathcal{K}_U \right] \end{aligned} \quad (\text{B.3.10})$$

and

$$\begin{aligned} f_1(s; 0, z, u) &= \tilde{V}(0, z, u) - \frac{P_{SS}(z, u)}{s} \overline{\log(-s)}, \\ \bar{V}(0, z, u) &= -f_1(s; 0, z, u) + \frac{1}{s} R_{SS}(z, u). \end{aligned} \quad (\text{B.3.11})$$

The coefficients defined in the above are

$$\begin{aligned} \mathcal{K}_{UT2} &= -\frac{2uz(s+u-z)}{s(u-z)^3} \\ \mathcal{K}_{UT3} &= \frac{2uz(s-u+z)}{s(u-z)^3} \\ \mathcal{K}_{US} &= -\frac{2(u+z)}{s(u-z)^2} \\ \mathcal{K}_U &= -\frac{(u+z)^2}{(u-z)^2 s} + \frac{5(u+z)}{4(u-z)^2}. \end{aligned} \quad (\text{B.3.12})$$

If we then make our generalised effective potential expansion, we find

$$\begin{aligned}
 f_1(s; 0, z, u) = & -\frac{P_{SS}(z, u) \overline{\log}(-s)}{s} \\
 & -\frac{\overline{\log}(-s)}{2(u-z)^3} \left[ u^2 - z^2 - 2uz \log \frac{u}{z} \right] \\
 & +\frac{1}{4(u-z)^4} \left[ 5(u+z)^3 + 8uzI(u, z, 0) + 2z \overline{\log} z (2u^2 - 11uz + z^2) \right. \\
 & \quad \left. + 2u \overline{\log} u (u^2 - 11uz + 2z^2) + 4uz(u+z) \overline{\log} u \overline{\log} z \right].
 \end{aligned} \tag{B.3.13}$$

We do not need the limit when  $u = z = 0$  because in that case we have couplings  $\lambda^{GGG}$ . However, for  $z = 0$  or  $u = 0$  we do see that there is a smooth limit of the above.

Let us define

$$f_1 = -\frac{P_{SS}(z, u)}{s} \overline{\log}(-s) + f_1^\ell \overline{\log}(-s) + f_1^0. \tag{B.3.14}$$

We can then write

$$\tilde{V}(0, z, u) = f_1^\ell \overline{\log}(-s) + f_1^0. \tag{B.3.15}$$

We have

$$\begin{aligned}
 f_1^\ell(z, u) &= -\frac{1}{2(u-z)^3} \left[ u^2 - z^2 - 2uz \log \frac{u}{z} \right] \\
 f_1^\ell(z, z) &= -\frac{1}{6z}, \quad f_1^\ell(0, u) = -\frac{1}{2u}
 \end{aligned} \tag{B.3.16}$$

If we now substitute in the standard expressions for  $I(z, u, 0)$  then we can simplify the above to

$$\begin{aligned}
 f_1^0(z, u) = & \frac{1}{4(u-z)^3} \left[ 5(u^2 - z^2) + 2z \overline{\log} z (2u - z + u \overline{\log} z) \right. \\
 & + 2u \overline{\log} u (u - 2z - z \overline{\log} u) \\
 & \left. - 4uz \left( \text{Li}_2(1 - z/u) - \text{Li}_2(1 - u/z) \right) \right].
 \end{aligned} \tag{B.3.17}$$

We can also it in a shorter but less symmetric form

$$\begin{aligned}
 f_1^0(z, u) = & \frac{1}{4(u-z)^3} \left[ 5(u^2 - z^2) + 2z \overline{\log} z (2u - z + 2u \overline{\log} u) \right. \\
 & \left. + 2u \overline{\log} u (u - 2z - 2z \overline{\log} u - 8uz \text{Li}_2(1 - z/u)) \right].
 \end{aligned} \tag{B.3.18}$$

We can also take the limits:

$$f_1^0(z, z) = \frac{11 + 3 \overline{\log} z}{18z}, \quad f_1^0(0, u) = \frac{5 + 2 \overline{\log} u}{4u}. \tag{B.3.19}$$

### B.3.1 Integral representation

Our expression for  $\tilde{V}$  actually lends itself to an interesting finite integral representation. We start with the definition

$$\tilde{V}(0, z, u) \equiv \lim_{y \rightarrow 0} \left[ -V(y, y, z, u) + B(s, y, y') P_{SS}(z, u) \right]. \quad (\text{B.3.20})$$

Then, using  $C \equiv 16\pi^2 \frac{\mu^{2\epsilon}}{(2\pi)^{4-2\epsilon}}$  we have

$$\begin{aligned} V(x, y, z, u) &= -\frac{\partial}{\partial y} U(x, y, z, u) \\ &= -\frac{\partial}{\partial y} \lim_{\epsilon \rightarrow 0} \left[ \mathbf{U}(x, y, z, u) + 1/2\epsilon^2 - 1/2\epsilon - \mathbf{B}(x, y)/\epsilon \right] \end{aligned} \quad (\text{B.3.21})$$

$$\begin{aligned} &= \lim_{\epsilon \rightarrow 0} \left[ -\mathbf{U}(x, y', z, u) + \mathbf{B}(x, y')/\epsilon \right] \\ P_{SS}(z, u) &= -B(0; z, u) = -\lim_{\epsilon \rightarrow 0} \left[ \mathbf{B}(0; z, u) - 1/\epsilon \right]. \end{aligned} \quad (\text{B.3.22})$$

So then

$$\begin{aligned} V(x, y, z, u) &= \lim_{\epsilon \rightarrow 0} \left[ C^2 \int \int \frac{1}{k^2 + x} \frac{1}{((k-p)^2 + y)^2} \frac{1}{q^2 + z} \frac{1}{(q+k-p)^2 + u} + \frac{\mathbf{B}(x, y')}{\epsilon} \right] \\ \tilde{V}(x, z, u) &= \lim_{y \rightarrow 0} \lim_{\epsilon \rightarrow 0} \left[ -\mathbf{V}(x, y, z, u) - \mathbf{B}(x, y') \left( \mathbf{P}_{SS}(z, u) + \frac{1}{\epsilon} \right) \right. \\ &\quad \left. + \mathbf{B}(x, y') \mathbf{P}_{SS}(z, u) + B(x, y') P_{SS}(z, u) \right] \\ &= \lim_{y \rightarrow 0} \lim_{\epsilon \rightarrow 0} \left[ -\mathbf{V}(x, y, z, u) + \mathbf{B}(x, y') \mathbf{P}_{SS}(z, u) \right] \quad (\text{B.3.23}) \\ &= \lim_{y \rightarrow 0} \lim_{\epsilon \rightarrow 0} \left[ -C^2 \int \int \frac{1}{k^2 + x} \frac{1}{((k-p)^2 + y)^2} \frac{1}{q^2 + z} \frac{1}{(q+k-p)^2 + u} \right. \\ &\quad \left. + C^2 \int \int \frac{1}{k^2 + x} \frac{1}{((k-p)^2 + y)^2} \frac{1}{q^2 + z} \frac{1}{q^2 + u} \right] \\ &= \lim_{\epsilon \rightarrow 0} \left[ C^2 \int \int \frac{1}{k^2 + x} \frac{1}{((k-p)^2 + y)^2} \frac{1}{q^2 + z} \frac{2q \cdot (k-p) + (k-p)^2}{(q^2 + u)((q+k-p)^2 + u)} \right]. \end{aligned}$$

We can then integrate this expression. For the case  $x \rightarrow 0$  we can simplify a little:

$$\begin{aligned} \tilde{V}(0, z, u) &= \lim_{y \rightarrow 0} \lim_{\epsilon \rightarrow 0} \left[ C^2 \int \int \frac{1}{(k+p)^2} \frac{1}{(k^2 + y)^2} \frac{1}{q^2 + z} \frac{2q \cdot k + k^2}{(q^2 + u)((q+k)^2 + u)} \right] \\ &\equiv \lim_{\epsilon \rightarrow 0} \left( -\frac{1}{z-u} \mathbf{F}(z, u) \right) \\ \mathbf{F}(z, u) &\equiv C^2 \int \int \frac{1}{(k+p)^2} \frac{1}{k^4} \frac{1}{q^2 + z} \frac{2q \cdot k + k^2}{(q+k)^2 + u}. \end{aligned} \quad (\text{B.3.24})$$

This integral is finite; we have checked that explicitly performing the integral using TARCER [148] exactly yields expression (B.3.10).

## Appendix C

# Consistent solution of the tadpole equations with shifts to fermion masses

Here we give the two-loop shifts to the tadpoles and self-energies due to shifts in fermion masses when we solve the tadpole equations consistently.

We denote the undiagonalised fermion mass matrix as  $m^{IJ}$ . The mass-squared matrix is defined [19] as

$$(m^2)_I{}^J = m_{IK}^* m^{KJ}, \quad (\text{C.0.1})$$

and is diagonalised by a unitary matrix  $N$  defined such that

$$\begin{aligned} m_I^2 \delta_I{}^J &= N_I^K N_L^*{}^J (m^2)_K{}^L, & M^{IJ} &\equiv N_K^*{}^I N_L^*{}^J m^{KL} \\ \rightarrow M^{IK} M_{JK}^* &= m_I^2 \delta_I{}^J. \end{aligned} \quad (\text{C.0.2})$$

Then if the tree-level matrices depend on some parameters  $\{x_i\}$  for which we solve the tadpole equations as in equation (4.4.4) we have

$$\delta M^{IJ} = N_K^*{}^I \frac{\partial m^{KL}}{\partial x_k} N_L^*{}^J c_{kl} \frac{\partial \Delta V^{(1)}}{\partial \phi_l^0}. \quad (\text{C.0.3})$$

Then the shift to the fermion contribution to the tadpole is

$$\begin{aligned} \delta^{(2)} \left( \frac{\partial V_F^{(1)}}{\partial \phi_r^0} \right) \Big|_{\varphi=v} &= - R_{rp} \text{Re}[y^{KLp} \delta M_{KL}^*] (A(m_K^2) + A(m_L^2)) \\ &\quad - 2 R_{rp} \text{Re}[Y^{IJp} M_{JK}^*] (\delta M^{KL} M_{IL}^* + \delta M_{IL}^* M^{KL}) P_{SS}(m_I^2, m_K^2), \end{aligned} \quad (\text{C.0.4})$$

while the shift to the scalar self-energy is

$$\begin{aligned}
\delta\Pi_{ij}^{(2),F} = & -2\text{Re}[y^{KLi}y_{K'Lj}](M_{KJ}^*\delta M^{K'J} + \delta M_{KJ}^*\bar{M}^{K'J}) \\
& \times \left[ P_{SS}(m_K^2, m_{K'}^2) - B(m_{K'}^2, m_L^2) \right. \\
& \quad \left. - (m_K^2 + m_{K'}^2 - s) C(s, s, 0, m_K^2, m_L^2, m_{K'}^2) \right] \\
& + 4\text{Re}[y^{KLi}y^{K'L'j}\delta M_{KK'}^*M_{LL'}^*]B(m_K^2, m_L^2) \\
& + 4\text{Re}[y^{KLi}y^{K'L'j}M_{IK'}^*M_{LL'}^*] \\
& \quad (M_{KJ}^*\delta M^{IJ} + \delta M_{KJ}^*M^{IJ})C(s, s, 0, m_K^2, m_L^2, m_I^2). \quad (\text{C.0.5})
\end{aligned}$$

To illustrate this, consider the MSSM, where the tadpole equations read

$$\begin{aligned}
(|\mu|^2 + m_{H_u}^2)v_u - B_\mu v_d + \frac{1}{8}(g_Y^2 + g_2^2)(v_u^2 - v_d^2)v_u &= -\frac{\partial\Delta V}{\partial v_u} \\
(|\mu|^2 + m_{H_d}^2)v_d - B_\mu v_u - \frac{1}{8}(g_Y^2 + g_2^2)(v_u^2 - v_d^2)v_d &= -\frac{\partial\Delta V}{\partial v_d}. \quad (\text{C.0.6})
\end{aligned}$$

Solving for  $|\mu|^2$  we have

$$|\mu|^2 = -\frac{M_Z^2}{2} + \frac{1}{c_{2\beta}} \left[ m_{H_u}^2 s_\beta^2 - m_{H_d}^2 c_\beta^2 + \frac{1}{v} s_\beta \frac{\partial\Delta V}{\partial v_u} - \frac{1}{v} c_\beta \frac{\partial\Delta V}{\partial v_d} \right], \quad (\text{C.0.7})$$

so we have

$$\delta\mu = \frac{1}{2\mu^* v c_{2\beta}} \left[ s_\beta \frac{\partial\Delta V}{\partial v_u} - c_\beta \frac{\partial\Delta V}{\partial v_d} \right]. \quad (\text{C.0.8})$$

This in turn will lead to a shift in the neutralino and chargino masses, which lead to a shift to the two-loop tadpoles.



# Bibliography

- [1] J. Braathen, M. D. Goodsell, and P. Slavich, *Leading two-loop corrections to the Higgs boson masses in SUSY models with Dirac gauginos*. JHEP **09** (2016) 045, [arXiv:1606.09213 \[hep-ph\]](#).
- [2] J. Braathen and M. D. Goodsell, *Avoiding the Goldstone Boson Catastrophe in general renormalisable field theories at two loops*. JHEP **12** (2016) 056, [arXiv:1609.06977 \[hep-ph\]](#).
- [3] J. Braathen, M. D. Goodsell, and F. Staub, *Supersymmetric and non-supersymmetric models without catastrophic Goldstone bosons*. Eur. Phys. J. **C77** (2017) no. 11, 757, [arXiv:1706.05372 \[hep-ph\]](#).
- [4] J. Braathen, M. D. Goodsell, M. E. Krauss, T. Opferkuch, and F. Staub, *N-loop running should be combined with N-loop matching*. Phys. Rev. **D97** (2018) no. 1, 015011, [arXiv:1711.08460 \[hep-ph\]](#).
- [5] F. Englert and R. Brout, *Broken Symmetry and the Mass of Gauge Vector Mesons*. Phys. Rev. Lett. **13** (1964) 321–323.
- [6] P. W. Higgs, *Broken symmetries, massless particles and gauge fields*. Phys. Lett. **12** (1964) 132–133.
- [7] P. W. Higgs, *Broken Symmetries and the Masses of Gauge Bosons*. Phys. Rev. Lett. **13** (1964) 508–509.
- [8] L. D. Faddeev and V. N. Popov, *Feynman Diagrams for the Yang-Mills Field*. Phys. Lett. **25B** (1967) 29–30.
- [9] M. E. Peskin and D. V. Schroeder, *An Introduction to quantum field theory*. Addison-Wesley, Reading, USA, 1995.  
<http://www.slac.stanford.edu/~mpeskin/QFT.html>.
- [10] J. C. Collins, *Renormalization*, vol. 26 of *Cambridge Monographs on Mathematical Physics*. Cambridge University Press, Cambridge, 1986. <http://www-spires.fnal.gov/spires/find/books/www?cl=QC174.17.R46C65::1985>.
- [11] R. Jackiw, *Functional evaluation of the effective potential*. Phys. Rev. **D9** (1974) 1686.
- [12] N. K. Nielsen, *On the Gauge Dependence of Spontaneous Symmetry Breaking in Gauge Theories*. Nucl. Phys. **B101** (1975) 173–188.
- [13] A. Andreassen, W. Frost, and M. D. Schwartz, *Consistent Use of Effective Potentials*. Phys. Rev. **D91** (2015) no. 1, 016009, [arXiv:1408.0287 \[hep-ph\]](#).

- [14] J. R. Espinosa, M. Garny, T. Konstandin, and A. Riotto, *Gauge-Independent Scales Related to the Standard Model Vacuum Instability*. [arXiv:1608.06765](#) [hep-ph].
- [15] J. R. Espinosa, M. Garny, and T. Konstandin, *Interplay of Infrared Divergences and Gauge-Dependence of the Effective Potential*. [arXiv:1607.08432](#) [hep-ph].
- [16] C. Ford, I. Jack, and D. R. T. Jones, *The Standard model effective potential at two loops*. Nucl. Phys. **B387** (1992) 373–390, [arXiv:hep-ph/0111190](#) [hep-ph]. [Erratum: Nucl. Phys. **B504**, 551(1997)].
- [17] S. P. Martin, *Three-loop Standard Model effective potential at leading order in strong and top Yukawa couplings*. Phys. Rev. **D89** (2014) no. 1, 013003, [arXiv:1310.7553](#) [hep-ph].
- [18] S. P. Martin, *Four-loop Standard Model effective potential at leading order in QCD*. Phys. Rev. **D92** (2015) no. 5, 054029, [arXiv:1508.00912](#) [hep-ph].
- [19] S. P. Martin, *Two loop effective potential for a general renormalizable theory and softly broken supersymmetry*. Phys. Rev. **D65** (2002) 116003, [arXiv:hep-ph/0111209](#) [hep-ph].
- [20] S. P. Martin, *Two loop scalar self energies in a general renormalizable theory at leading order in gauge couplings*. Phys. Rev. **D70** (2004) 016005, [arXiv:hep-ph/0312092](#) [hep-ph].
- [21] M. Goodsell, K. Nickel, and F. Staub, *Generic two-loop Higgs mass calculation from a diagrammatic approach*. Eur. Phys. J. **C75** (2015) no. 6, 290, [arXiv:1503.03098](#) [hep-ph].
- [22] S. P. Martin and D. G. Robertson, *Higgs boson mass in the Standard Model at two-loop order and beyond*. Phys. Rev. **D90** (2014) no. 7, 073010, [arXiv:1407.4336](#) [hep-ph].
- [23] G. Passarino and M. J. G. Veltman, *One Loop Corrections for  $e^+ e^-$  Annihilation Into  $\mu^+ \mu^-$  in the Weinberg Model*. Nucl. Phys. **B160** (1979) 151–207.
- [24] G. Degrandi, S. Di Vita, J. Elias-Miro, J. R. Espinosa, G. F. Giudice, G. Isidori, and A. Strumia, *Higgs mass and vacuum stability in the Standard Model at NNLO*. JHEP **08** (2012) 098, [arXiv:1205.6497](#) [hep-ph].
- [25] D. Buttazzo, G. Degrandi, P. P. Giardino, G. F. Giudice, F. Sala, A. Salvio, and A. Strumia, *Investigating the near-criticality of the Higgs boson*. JHEP **12** (2013) 089, [arXiv:1307.3536](#) [hep-ph].
- [26] B. A. Kniehl, A. F. Pikelner, and O. L. Veretin, *Two-loop electroweak threshold corrections in the Standard Model*. Nucl. Phys. **B896** (2015) 19–51, [arXiv:1503.02138](#) [hep-ph].
- [27] B. A. Kniehl, A. F. Pikelner, and O. L. Veretin, *mr: a C++ library for the matching and running of the Standard Model parameters*. Comput. Phys. Commun. **206** (2016) 84–96, [arXiv:1601.08143](#) [hep-ph].

- [28] J. Elias-Miro, J. R. Espinosa, and T. Konstandin, *Taming Infrared Divergences in the Effective Potential*. JHEP **08** (2014) 034, [arXiv:1406.2652 \[hep-ph\]](#).
- [29] S. P. Martin, *Taming the Goldstone contributions to the effective potential*. Phys. Rev. **D90** (2014) no. 1, 016013, [arXiv:1406.2355 \[hep-ph\]](#).
- [30] C. Ford, D. R. T. Jones, P. W. Stephenson, and M. B. Einhorn, *The Effective potential and the renormalization group*. Nucl. Phys. **B395** (1993) 17–34, [arXiv:hep-lat/9210033 \[hep-lat\]](#).
- [31] M. B. Einhorn and D. R. T. Jones, *The Effective potential, the renormalisation group and vacuum stability*. JHEP **04** (2007) 051, [arXiv:hep-ph/0702295 \[HEP-PH\]](#).
- [32] S. P. Martin, *Complete two loop effective potential approximation to the lightest Higgs scalar boson mass in supersymmetry*. Phys. Rev. **D67** (2003) 095012, [arXiv:hep-ph/0211366 \[hep-ph\]](#).
- [33] N. Kumar and S. P. Martin, *Resummation of Goldstone boson contributions to the MSSM effective potential*. Phys. Rev. **D94** (2016) no. 1, 014013, [arXiv:1605.02059 \[hep-ph\]](#).
- [34] M. Beneke and V. A. Smirnov, *Asymptotic expansion of Feynman integrals near threshold*. Nucl. Phys. **B522** (1998) 321–344, [arXiv:hep-ph/9711391 \[hep-ph\]](#).
- [35] B. Jantzen, *Foundation and generalization of the expansion by regions*. JHEP **12** (2011) 076, [arXiv:1111.2589 \[hep-ph\]](#).
- [36] J. R. Espinosa and T. Konstandin, *Resummation of Goldstone Infrared Divergences: A Proof to All Orders*. [arXiv:1712.08068 \[hep-ph\]](#).
- [37] A. Pilaftsis and D. Teresi, *Symmetry Improved CJT Effective Action*. Nucl. Phys. **B874** (2013) no. 2, 594–619, [arXiv:1305.3221 \[hep-ph\]](#).
- [38] A. Pilaftsis and D. Teresi, *Symmetry Improved 2PI Effective Action and the Infrared Divergences of the Standard Model*. J. Phys. Conf. Ser. **631** (2015) no. 1, 012008, [arXiv:1502.07986 \[hep-ph\]](#).
- [39] A. Pilaftsis and D. Teresi, *Symmetry-Improved 2PI Approach to the Goldstone-Boson IR Problem of the SM Effective Potential*. Nucl. Phys. **B906** (2016) 381–407, [arXiv:1511.05347 \[hep-ph\]](#).
- [40] J. M. Cornwall, R. Jackiw, and E. Tomboulis, *Effective Action for Composite Operators*. Phys. Rev. **D10** (1974) 2428–2445.
- [41] F. Quevedo, S. Krippendorff, and O. Schlotterer, *Cambridge Lectures on Supersymmetry and Extra Dimensions*. [arXiv:1011.1491 \[hep-th\]](#).
- [42] M. D. Goodsell, *Lectures on Supersymmetry*, 2016. (*Unpublished*).
- [43] S. Dimopoulos and H. Georgi, *Softly Broken Supersymmetry and SU(5)*. Nucl. Phys. **B193** (1981) 150–162.
- [44] S. Dimopoulos and J. Preskill, *Massless Composites With Massive Constituents*. Nucl. Phys. **B199** (1982) 206–222.

- [45] D. B. Kaplan, H. Georgi, and S. Dimopoulos, *Composite Higgs Scalars*. Phys. Lett. **136B** (1984) 187–190.
- [46] L. Randall and R. Sundrum, *A Large mass hierarchy from a small extra dimension*. Phys. Rev. Lett. **83** (1999) 3370–3373, [arXiv:hep-ph/9905221](#) [hep-ph].
- [47] N. Arkani-Hamed, S. Dimopoulos, and G. R. Dvali, *The Hierarchy problem and new dimensions at a millimeter*. Phys. Lett. **B429** (1998) 263–272, [arXiv:hep-ph/9803315](#) [hep-ph].
- [48] P. W. Graham, D. E. Kaplan, and S. Rajendran, *Cosmological Relaxation of the Electroweak Scale*. Phys. Rev. Lett. **115** (2015) no. 22, 221801, [arXiv:1504.07551](#) [hep-ph].
- [49] **ATLAS** Collaboration, G. Aad *et al.*, *Observation of a new particle in the search for the Standard Model Higgs boson with the ATLAS detector at the LHC*. Phys. Lett. **B716** (2012) 1–29, [arXiv:1207.7214](#) [hep-ex].
- [50] **CMS** Collaboration, S. Chatrchyan *et al.*, *Observation of a new boson at a mass of 125 GeV with the CMS experiment at the LHC*. Phys. Lett. **B716** (2012) 30–61, [arXiv:1207.7235](#) [hep-ex].
- [51] **ATLAS, CMS** Collaboration, G. Aad *et al.*, *Combined Measurement of the Higgs Boson Mass in  $pp$  Collisions at  $\sqrt{s} = 7$  and 8 TeV with the ATLAS and CMS Experiments*. Phys. Rev. Lett. **114** (2015) 191803, [arXiv:1503.07589](#) [hep-ex].
- [52] **ATLAS** Collaboration, T. A. collaboration, *Measurement of the Higgs boson mass in the  $H \rightarrow ZZ^* \rightarrow 4\ell$  and  $H \rightarrow \gamma\gamma$  channels with  $\sqrt{s}=13\text{TeV}$   $pp$  collisions using the ATLAS detector*.
- [53] A. V. Bednyakov, A. F. Pikelner, and V. N. Velizhanin, *Higgs self-coupling beta-function in the Standard Model at three loops*. Nucl. Phys. **B875** (2013) 552–565, [arXiv:1303.4364](#) [hep-ph].
- [54] K. G. Chetyrkin and M. F. Zoller,  *$\beta$ -function for the Higgs self-interaction in the Standard Model at three-loop level*. JHEP **04** (2013) 091, [arXiv:1303.2890](#) [hep-ph]. [Erratum: JHEP09,155(2013)].
- [55] S. P. Martin, *A Supersymmetry primer*. [arXiv:hep-ph/9709356](#) [hep-ph]. [Adv. Ser. Direct. High Energy Phys.18,1(1998)].
- [56] J. Wess and J. Bagger, *Supersymmetry and supergravity*. Princeton, USA: Univ. Pr. (1992) 259 p, 1992.
- [57] S. R. Coleman and J. Mandula, *All Possible Symmetries of the  $S$  Matrix*. Phys. Rev. **159** (1967) 1251–1256.
- [58] R. Haag, J. T. Lopuszanski, and M. Sohnius, *All Possible Generators of Supersymmetries of the  $s$  Matrix*. Nucl. Phys. **B88** (1975) 257.
- [59] L. Girardello and M. T. Grisaru, *Soft Breaking of Supersymmetry*. Nucl. Phys. **B194** (1982) 65.
- [60] M. T. Grisaru, W. Siegel, and M. Rocek, *Improved Methods for Supergraphs*. Nucl. Phys. **B159** (1979) 429.

- [61] N. Seiberg, *Naturalness versus supersymmetric nonrenormalization theorems*. Phys. Lett. **B318** (1993) 469–475, [arXiv:hep-ph/9309335](#) [hep-ph].
- [62] H. K. Dreiner, H. E. Haber, and S. P. Martin, *Two-component spinor techniques and Feynman rules for quantum field theory and supersymmetry*. Phys. Rept. **494** (2010) 1–196, [arXiv:0812.1594](#) [hep-ph].
- [63] S. Dimopoulos and D. W. Sutter, *The Supersymmetric flavor problem*. Nucl. Phys. **B452** (1995) 496–512, [arXiv:hep-ph/9504415](#) [hep-ph].
- [64] **MSSM Working Group** Collaboration, A. Djouadi *et al.*, “The Minimal supersymmetric standard model: Group summary report,” in *GDR (Groupement De Recherche) - Supersymetrie Montpellier, France, April 15-17, 1998*. 1998. [arXiv:hep-ph/9901246](#) [hep-ph]. [https://inspirehep.net/record/481987/files/arXiv:hep-ph\\_9901246.pdf](https://inspirehep.net/record/481987/files/arXiv:hep-ph_9901246.pdf).
- [65] **GAMBIT** Collaboration, P. Athron *et al.*, *Global fits of GUT-scale SUSY models with GAMBIT*. Eur. Phys. J. **C77** (2017) no. 12, 824, [arXiv:1705.07935](#) [hep-ph].
- [66] **GAMBIT** Collaboration, P. Athron *et al.*, *A global fit of the MSSM with GAMBIT*. Eur. Phys. J. **C77** (2017) no. 12, 879, [arXiv:1705.07917](#) [hep-ph].
- [67] E. Bagnaschi *et al.*, *Likelihood Analysis of the Minimal AMSB Model*. Eur. Phys. J. **C77** (2017) no. 4, 268, [arXiv:1612.05210](#) [hep-ph].
- [68] J. C. Costa *et al.*, *Likelihood Analysis of the Sub-GUT MSSM in Light of LHC 13-TeV Data*. Eur. Phys. J. **C78** (2018) no. 2, 158, [arXiv:1711.00458](#) [hep-ph].
- [69] E. Bagnaschi *et al.*, *Likelihood Analysis of the pMSSM11 in Light of LHC 13-TeV Data*. [arXiv:1710.11091](#) [hep-ph].
- [70] R. Barbier *et al.*, *R-parity violating supersymmetry*. Phys. Rept. **420** (2005) 1–202, [arXiv:hep-ph/0406039](#) [hep-ph].
- [71] K. Inoue, A. Kakuto, H. Komatsu, and S. Takeshita, *Low-Energy Parameters and Particle Masses in a Supersymmetric Grand Unified Model*. Prog. Theor. Phys. **67** (1982) 1889.
- [72] R. A. Flores and M. Sher, *Higgs Masses in the Standard, Multi-Higgs and Supersymmetric Models*. Annals Phys. **148** (1983) 95.
- [73] J. R. Ellis, G. Ridolfi, and F. Zwirner, *Radiative corrections to the masses of supersymmetric Higgs bosons*. Phys. Lett. **B257** (1991) 83–91.
- [74] Y. Okada, M. Yamaguchi, and T. Yanagida, *Upper bound of the lightest Higgs boson mass in the minimal supersymmetric standard model*. Prog. Theor. Phys. **85** (1991) 1–6.
- [75] H. E. Haber and R. Hempfling, *Can the mass of the lightest Higgs boson of the minimal supersymmetric model be larger than  $m(Z)$ ?* Phys. Rev. Lett. **66** (1991) 1815–1818.
- [76] G. Degrandi, P. Slavich, and F. Zwirner, *On the neutral Higgs boson masses in the MSSM for arbitrary stop mixing*. Nucl. Phys. **B611** (2001) 403–422, [arXiv:hep-ph/0105096](#) [hep-ph].

- [77] G. Degrandi and P. Slavich, *On the radiative corrections to the neutral Higgs boson masses in the NMSSM*. Nucl. Phys. **B825** (2010) 119–150, [arXiv:0907.4682 \[hep-ph\]](#).
- [78] U. Ellwanger, C. Hugonie, and A. M. Teixeira, *The Next-to-Minimal Supersymmetric Standard Model*. Phys. Rept. **496** (2010) 1–77, [arXiv:0910.1785 \[hep-ph\]](#).
- [79] K. Benakli, M. D. Goodsell, and A.-K. Maier, *Generating  $\mu$  and  $B\mu$  in models with Dirac Gauginos*. Nucl. Phys. **B851** (2011) 445–461, [arXiv:1104.2695 \[hep-ph\]](#).
- [80] **ATLAS** Collaboration, M. Aaboud *et al.*, *Search for squarks and gluinos in final states with jets and missing transverse momentum using  $36\text{ fb}^{-1}$  of  $\sqrt{s}=13\text{ TeV}$   $pp$  collision data with the ATLAS detector*. [arXiv:1712.02332 \[hep-ex\]](#).
- [81] **CMS** Collaboration, A. M. Sirunyan *et al.*, *Search for natural and split supersymmetry in proton-proton collisions at  $\sqrt{s} = 13\text{ TeV}$  in final states with jets and missing transverse momentum*. [arXiv:1802.02110 \[hep-ex\]](#).
- [82] **ATLAS** Collaboration, M. Aaboud *et al.*, *Search for dark matter and other new phenomena in events with an energetic jet and large missing transverse momentum using the ATLAS detector*. JHEP **01** (2018) 126, [arXiv:1711.03301 \[hep-ex\]](#).
- [83] **CMS** Collaboration, A. M. Sirunyan *et al.*, *Search for the pair production of third-generation squarks with two-body decays to a bottom or charm quark and a neutralino in proton-proton collisions at  $\sqrt{s} = 13\text{ TeV}$* . Phys. Lett. **B778** (2018) 263–291, [arXiv:1707.07274 \[hep-ex\]](#).
- [84] U. Ellwanger, M. Rausch de Traubenberg, and C. A. Savoy, *Phenomenology of supersymmetric models with a singlet*. Nucl. Phys. **B492** (1997) 21–50, [arXiv:hep-ph/9611251 \[hep-ph\]](#).
- [85] K. Benakli, L. Darmé, M. D. Goodsell, and J. Harz, *The Di-Photon Excess in a Perturbative SUSY Model*. [arXiv:1605.05313 \[hep-ph\]](#).
- [86] P. Fayet, *Massive Gluinos*. Phys. Lett. **B78** (1978) 417–420.
- [87] J. Polchinski and L. Susskind, *Breaking of Supersymmetry at Intermediate-Energy*. Phys. Rev. **D26** (1982) 3661.
- [88] L. J. Hall and L. Randall,  *$U(1)$ - $R$  symmetric supersymmetry*. Nucl. Phys. **B352** (1991) 289–308.
- [89] P. J. Fox, A. E. Nelson, and N. Weiner, *Dirac gaugino masses and supersoft supersymmetry breaking*. JHEP **08** (2002) 035, [arXiv:hep-ph/0206096 \[hep-ph\]](#).
- [90] A. E. Nelson, N. Rius, V. Sanz, and M. Unsal, *The Minimal supersymmetric model without a  $\mu$  term*. JHEP **08** (2002) 039, [arXiv:hep-ph/0206102 \[hep-ph\]](#).
- [91] I. Antoniadis, K. Benakli, A. Delgado, and M. Quiros, *A New gauge mediation theory*. Adv. Stud. Theor. Phys. **2** (2008) 645–672, [arXiv:hep-ph/0610265 \[hep-ph\]](#).

- [92] G. Belanger, K. Benakli, M. Goodsell, C. Moura, and A. Pukhov, *Dark Matter with Dirac and Majorana Gaugino Masses*. JCAP **0908** (2009) 027, [arXiv:0905.1043 \[hep-ph\]](#).
- [93] M. Heikinheimo, M. Kellerstein, and V. Sanz, *How Many Supersymmetries?* JHEP **04** (2012) 043, [arXiv:1111.4322 \[hep-ph\]](#).
- [94] G. D. Kribs and A. Martin, *Supersoft Supersymmetry is Super-Safe*. Phys. Rev. **D85** (2012) 115014, [arXiv:1203.4821 \[hep-ph\]](#).
- [95] G. D. Kribs and A. Martin, *Dirac Gauginos in Supersymmetry – Suppressed Jets + MET Signals: A Snowmass Whitepaper*. [arXiv:1308.3468 \[hep-ph\]](#).
- [96] G. D. Kribs, E. Poppitz, and N. Weiner, *Flavor in supersymmetry with an extended R-symmetry*. Phys. Rev. **D78** (2008) 055010, [arXiv:0712.2039 \[hep-ph\]](#).
- [97] R. Fok and G. D. Kribs,  *$\mu$  to  $e$  in R-symmetric Supersymmetry*. Phys. Rev. **D82** (2010) 035010, [arXiv:1004.0556 \[hep-ph\]](#).
- [98] E. Dudas, M. Goodsell, L. Heurtier, and P. Tziveloglou, *Flavour models with Dirac and fake gluinos*. Nucl. Phys. **B884** (2014) 632–671, [arXiv:1312.2011 \[hep-ph\]](#).
- [99] S. P. Martin, *Nonstandard supersymmetry breaking and Dirac gaugino masses without supersoftness*. Phys. Rev. **D92** (2015) no. 3, 035004, [arXiv:1506.02105 \[hep-ph\]](#).
- [100] K. Benakli, M. Goodsell, F. Staub, and W. Porod, *Constrained minimal Dirac gaugino supersymmetric standard model*. Phys. Rev. **D90** (2014) no. 4, 045017, [arXiv:1403.5122 \[hep-ph\]](#).
- [101] M. D. Goodsell, M. E. Krauss, T. Müller, W. Porod, and F. Staub, *Dark matter scenarios in a constrained model with Dirac gauginos*. JHEP **10** (2015) 132, [arXiv:1507.01010 \[hep-ph\]](#).
- [102] A. E. Nelson and N. Seiberg, *R symmetry breaking versus supersymmetry breaking*. Nucl. Phys. **B416** (1994) 46–62, [arXiv:hep-ph/9309299 \[hep-ph\]](#).
- [103] S. D. L. Amigo, A. E. Blechman, P. J. Fox, and E. Poppitz, *R-symmetric gauge mediation*. JHEP **01** (2009) 018, [arXiv:0809.1112 \[hep-ph\]](#).
- [104] K. Benakli and M. D. Goodsell, *Dirac Gauginos in General Gauge Mediation*. Nucl. Phys. **B816** (2009) 185–203, [arXiv:0811.4409 \[hep-ph\]](#).
- [105] K. Benakli and M. D. Goodsell, *Dirac Gauginos, Gauge Mediation and Unification*. Nucl. Phys. **B840** (2010) 1–28, [arXiv:1003.4957 \[hep-ph\]](#).
- [106] L. M. Carpenter, *Dirac Gauginos, Negative Supertraces and Gauge Mediation*. JHEP **09** (2012) 102, [arXiv:1007.0017 \[hep-th\]](#).
- [107] S. Abel and M. Goodsell, *Easy Dirac Gauginos*. JHEP **06** (2011) 064, [arXiv:1102.0014 \[hep-th\]](#).
- [108] C. Csaki, J. Goodman, R. Pavesi, and Y. Shirman, *The  $m_D - b_M$  problem of Dirac gauginos and its solutions*. Phys. Rev. **D89** (2014) no. 5, 055005, [arXiv:1310.4504 \[hep-ph\]](#).

- [109] K. Benakli, M. D. Goodsell, and F. Staub, *Dirac Gauginos and the 125 GeV Higgs*. JHEP **06** (2013) 073, [arXiv:1211.0552 \[hep-ph\]](#).
- [110] C. Frugiuele and T. Gregoire, *Making the Sneutrino a Higgs with a  $U(1)_R$  Lepton Number*. Phys. Rev. **D85** (2012) 015016, [arXiv:1107.4634 \[hep-ph\]](#).
- [111] E. Bertuzzo, C. Frugiuele, T. Gregoire, and E. Ponton, *Dirac gauginos,  $R$  symmetry and the 125 GeV Higgs*. JHEP **04** (2015) 089, [arXiv:1402.5432 \[hep-ph\]](#).
- [112] R. Davies, J. March-Russell, and M. McCullough, *A Supersymmetric One Higgs Doublet Model*. JHEP **04** (2011) 108, [arXiv:1103.1647 \[hep-ph\]](#).
- [113] P. Diessner, W. Kotlarski, S. Liebschner, and D. Stöckinger, *Squark production in  $R$ -symmetric SUSY with Dirac gluinos: NLO corrections*. JHEP **10** (2017) 142, [arXiv:1707.04557 \[hep-ph\]](#).
- [114] J. Hisano, M. Nagai, T. Naganawa, and M. Senami, *Electric Dipole Moments in PseudoDirac Gauginos*. Phys. Lett. **B644** (2007) 256–264, [arXiv:hep-ph/0610383 \[hep-ph\]](#).
- [115] A. Kumar, D. Tucker-Smith, and N. Weiner, *Neutrino Mass, Sneutrino Dark Matter and Signals of Lepton Flavor Violation in the MRSSM*. JHEP **09** (2010) 111, [arXiv:0910.2475 \[hep-ph\]](#).
- [116] T. Cohen, G. D. Kribs, A. E. Nelson, and B. Ostdiek, *750 GeV Diphotons from Supersymmetry with Dirac Gauginos*. [arXiv:1605.04308 \[hep-ph\]](#).
- [117] T. Ibrahim and P. Nath, *The Neutron and the electron electric dipole moment in  $N=1$  supergravity unification*. Phys. Rev. **D57** (1998) 478–488, [arXiv:hep-ph/9708456 \[hep-ph\]](#). [Erratum: Phys. Rev.D60,119901(1999)].
- [118] T. Ibrahim and P. Nath, *The Neutron and the lepton EDMs in MSSM, large CP violating phases, and the cancellation mechanism*. Phys. Rev. **D58** (1998) 111301, [arXiv:hep-ph/9807501 \[hep-ph\]](#). [Erratum: Phys. Rev.D60,099902(1999)].
- [119] S. Abel, S. Khalil, and O. Lebedev, *EDM constraints in supersymmetric theories*. Nucl. Phys. **B606** (2001) 151–182, [arXiv:hep-ph/0103320 \[hep-ph\]](#).
- [120] M. Pospelov and A. Ritz, *Electric dipole moments as probes of new physics*. Annals Phys. **318** (2005) 119–169, [arXiv:hep-ph/0504231 \[hep-ph\]](#).
- [121] V. Silveira and A. Zee, *SCALAR PHANTOMS*. Phys. Lett. **161B** (1985) 136–140.
- [122] J. McDonald, *Gauge singlet scalars as cold dark matter*. Phys. Rev. **D50** (1994) 3637–3649, [arXiv:hep-ph/0702143 \[HEP-PH\]](#).
- [123] C. P. Burgess, M. Pospelov, and T. ter Veldhuis, *The Minimal model of nonbaryonic dark matter: A Singlet scalar*. Nucl. Phys. **B619** (2001) 709–728, [arXiv:hep-ph/0011335 \[hep-ph\]](#).
- [124] R. N. Lerner and J. McDonald, *Gauge singlet scalar as inflaton and thermal relic dark matter*. Phys. Rev. **D80** (2009) 123507, [arXiv:0909.0520 \[hep-ph\]](#).



- [125] J. R. Espinosa, T. Konstandin, and F. Riva, *Strong Electroweak Phase Transitions in the Standard Model with a Singlet*. Nucl. Phys. **B854** (2012) 592–630, [arXiv:1107.5441 \[hep-ph\]](#).
- [126] J. Elias-Miro, J. R. Espinosa, G. F. Giudice, H. M. Lee, and A. Strumia, *Stabilization of the Electroweak Vacuum by a Scalar Threshold Effect*. JHEP **06** (2012) 031, [arXiv:1203.0237 \[hep-ph\]](#).
- [127] O. Lebedev, *On Stability of the Electroweak Vacuum and the Higgs Portal*. Eur. Phys. J. **C72** (2012) 2058, [arXiv:1203.0156 \[hep-ph\]](#).
- [128] R. Costa, A. P. Morais, M. O. P. Sampaio, and R. Santos, *Two-loop stability of a complex singlet extended Standard Model*. Phys. Rev. **D92** (2015) 025024, [arXiv:1411.4048 \[hep-ph\]](#).
- [129] J. F. Gunion, H. E. Haber, G. L. Kane, and S. Dawson, *The Higgs Hunter's Guide*. Front. Phys. **80** (2000) 1–404.
- [130] G. C. Branco, P. M. Ferreira, L. Lavoura, M. N. Rebelo, M. Sher, and J. P. Silva, *Theory and phenomenology of two-Higgs-doublet models*. Phys. Rept. **516** (2012) 1–102, [arXiv:1106.0034 \[hep-ph\]](#).
- [131] P. Basler, M. Muhlleitner, and J. Wittbrodt, *The CP-Violating 2HDM in Light of a Strong First Order Electroweak Phase Transition and Implications for Higgs Pair Production*. [arXiv:1711.04097 \[hep-ph\]](#).
- [132] J. Bernon, J. F. Gunion, H. E. Haber, Y. Jiang, and S. Kraml, *Scrutinizing the alignment limit in two-Higgs-doublet models:  $m_h=125$  GeV*. Phys. Rev. **D92** (2015) no. 7, 075004, [arXiv:1507.00933 \[hep-ph\]](#).
- [133] K. Benakli, M. D. Goodsell, and S. L. Williamson, *Higgs alignment from extended supersymmetry*. [arXiv:1801.08849 \[hep-ph\]](#).
- [134] H. Georgi and M. Machacek, *DOUBLY CHARGED HIGGS BOSONS*. Nucl. Phys. **B262** (1985) 463–477.
- [135] K. Hartling, K. Kumar, and H. E. Logan, *The decoupling limit in the Georgi-Machacek model*. Phys. Rev. **D90** (2014) no. 1, 015007, [arXiv:1404.2640 \[hep-ph\]](#).
- [136] **LHC Higgs Cross Section Working Group** Collaboration, D. de Florian *et al.*, *Handbook of LHC Higgs Cross Sections: 4. Deciphering the Nature of the Higgs Sector*. [arXiv:1610.07922 \[hep-ph\]](#).
- [137] G. 't Hooft and M. J. G. Veltman, *Regularization and Renormalization of Gauge Fields*. Nucl. Phys. **B44** (1972) 189–213.
- [138] W. Siegel, *Supersymmetric Dimensional Regularization via Dimensional Reduction*. Phys. Lett. **84B** (1979) 193–196.
- [139] D. M. Capper, D. R. T. Jones, and P. van Nieuwenhuizen, *Regularization by Dimensional Reduction of Supersymmetric and Nonsupersymmetric Gauge Theories*. Nucl. Phys. **B167** (1980) 479–499.
- [140] A. Pilaftsis, *Resonant CP violation induced by particle mixing in transition amplitudes*. Nucl. Phys. **B504** (1997) 61–107, [arXiv:hep-ph/9702393 \[hep-ph\]](#).

- [141] W. A. Bardeen, A. J. Buras, D. W. Duke, and T. Muta, *Deep Inelastic Scattering Beyond the Leading Order in Asymptotically Free Gauge Theories*. Phys. Rev. **D18** (1978) 3998.
- [142] S. P. Martin, *Evaluation of two loop selfenergy basis integrals using differential equations*. Phys. Rev. **D68** (2003) 075002, [arXiv:hep-ph/0307101](#) [hep-ph].
- [143] S. P. Martin and M. T. Vaughn, *Regularization dependence of running couplings in softly broken supersymmetry*. Phys. Lett. **B318** (1993) 331–337, [arXiv:hep-ph/9308222](#) [hep-ph].
- [144] I. Jack and D. R. T. Jones, *Soft supersymmetry breaking and finiteness*. Phys. Lett. **B333** (1994) 372–379, [arXiv:hep-ph/9405233](#) [hep-ph].
- [145] S. P. Martin and M. T. Vaughn, *Two loop renormalization group equations for soft supersymmetry breaking couplings*. Phys. Rev. **D50** (1994) 2282, [arXiv:hep-ph/9311340](#) [hep-ph]. [Erratum: Phys. Rev. **D78**, 039903(2008)].
- [146] Y. Yamada, *Two loop renormalization group equations for soft SUSY breaking scalar interactions: Supergraph method*. Phys. Rev. **D50** (1994) 3537–3545, [arXiv:hep-ph/9401241](#) [hep-ph].
- [147] I. Jack, D. R. T. Jones, S. P. Martin, M. T. Vaughn, and Y. Yamada, *Decoupling of the epsilon scalar mass in softly broken supersymmetry*. Phys. Rev. **D50** (1994) R5481–R5483, [arXiv:hep-ph/9407291](#) [hep-ph].
- [148] R. Mertig and R. Scharf, *TARCEr: A Mathematica program for the reduction of two loop propagator integrals*. Comput. Phys. Commun. **111** (1998) 265–273, [arXiv:hep-ph/9801383](#) [hep-ph].
- [149] S. Borowka, G. Heinrich, S. P. Jones, M. Kerner, J. Schlenk, and T. Zirke, *SecDec-3.0: numerical evaluation of multi-scale integrals beyond one loop*. Comput. Phys. Commun. **196** (2015) 470–491, [arXiv:1502.06595](#) [hep-ph].
- [150] S. P. Martin and D. G. Robertson, *TSIL: A Program for the calculation of two-loop self-energy integrals*. Comput. Phys. Commun. **174** (2006) 133–151, [arXiv:hep-ph/0501132](#) [hep-ph].
- [151] S. P. Li and M. Sher, *Upper Limit to the Lightest Higgs Mass in Supersymmetric Models*. Phys. Lett. **140B** (1984) 339–343.
- [152] D. M. Pierce, A. Papadopoulos, and S. Johnson, *Limits on the CP even Higgs boson masses in the MSSM*. Phys. Rev. Lett. **68** (1992) 3678–3681.
- [153] J. R. Ellis, G. Ridolfi, and F. Zwirner, *On radiative corrections to supersymmetric Higgs boson masses and their implications for LEP searches*. Phys. Lett. **B262** (1991) 477–484.
- [154] M. Drees and M. M. Nojiri, *One loop corrections to the Higgs sector in minimal supergravity models*. Phys. Rev. **D45** (1992) 2482–2492.
- [155] M. S. Berger, *Radiative Corrections to Higgs Boson Mass Sum Rules in the Minimal Supersymmetric Extension to the Standard Model*. Phys. Rev. **D41** (1990) 225.
- [156] M. A. Diaz and H. E. Haber, *One loop radiative corrections to the charged Higgs mass of the minimal supersymmetric model*. Phys. Rev. **D45** (1992) 4246–4260.

- [157] A. Yamada, *Radiative corrections to the Higgs masses in the minimal supersymmetric standard model*. Phys. Lett. **B263** (1991) 233–238.
- [158] P. H. Chankowski, S. Pokorski, and J. Rosiek, *Charged and neutral supersymmetric Higgs boson masses: Complete one loop analysis*. Phys. Lett. **B274** (1992) 191–198.
- [159] P. H. Chankowski, S. Pokorski, and J. Rosiek, *Complete on-shell renormalization scheme for the minimal supersymmetric Higgs sector*. Nucl. Phys. **B423** (1994) 437–496, [arXiv:hep-ph/9303309](#) [hep-ph].
- [160] A. Brignole, *Radiative corrections to the supersymmetric neutral Higgs boson masses*. Phys. Lett. **B281** (1992) 284–294.
- [161] A. Yamada, *The Higgs sector of the minimal supersymmetric standard model including radiative corrections*. Z. Phys. **C61** (1994) 247–263.
- [162] A. Dabelstein, *The One loop renormalization of the MSSM Higgs sector and its application to the neutral scalar Higgs masses*. Z. Phys. **C67** (1995) 495–512, [arXiv:hep-ph/9409375](#) [hep-ph].
- [163] D. M. Pierce, J. A. Bagger, K. T. Matchev, and R.-j. Zhang, *Precision corrections in the minimal supersymmetric standard model*. Nucl. Phys. **B491** (1997) 3–67, [arXiv:hep-ph/9606211](#) [hep-ph].
- [164] R. Hempfling and A. H. Hoang, *Two loop radiative corrections to the upper limit of the lightest Higgs boson mass in the minimal supersymmetric model*. Phys. Lett. **B331** (1994) 99–106, [arXiv:hep-ph/9401219](#) [hep-ph].
- [165] S. Heinemeyer, W. Hollik, and G. Weiglein, *QCD corrections to the masses of the neutral CP - even Higgs bosons in the MSSM*. Phys. Rev. **D58** (1998) 091701, [arXiv:hep-ph/9803277](#) [hep-ph].
- [166] S. Heinemeyer, W. Hollik, and G. Weiglein, *Precise prediction for the mass of the lightest Higgs boson in the MSSM*. Phys. Lett. **B440** (1998) 296–304, [arXiv:hep-ph/9807423](#) [hep-ph].
- [167] R.-J. Zhang, *Two loop effective potential calculation of the lightest CP even Higgs boson mass in the MSSM*. Phys. Lett. **B447** (1999) 89–97, [arXiv:hep-ph/9808299](#) [hep-ph].
- [168] S. Heinemeyer, W. Hollik, and G. Weiglein, *The Masses of the neutral CP - even Higgs bosons in the MSSM: Accurate analysis at the two loop level*. Eur. Phys. J. **C9** (1999) 343–366, [arXiv:hep-ph/9812472](#) [hep-ph].
- [169] J. R. Espinosa and R.-J. Zhang, *MSSM lightest CP even Higgs boson mass to  $O(\alpha(s)\alpha(t))$ : The Effective potential approach*. JHEP **03** (2000) 026, [arXiv:hep-ph/9912236](#) [hep-ph].
- [170] J. R. Espinosa and R.-J. Zhang, *Complete two loop dominant corrections to the mass of the lightest CP even Higgs boson in the minimal supersymmetric standard model*. Nucl. Phys. **B586** (2000) 3–38, [arXiv:hep-ph/0003246](#) [hep-ph].
- [171] A. Brignole, G. Degrandi, P. Slavich, and F. Zwirner, *On the  $O(\alpha(t)^{**2})$  two loop corrections to the neutral Higgs boson masses in the MSSM*. Nucl. Phys. **B631** (2002) 195–218, [arXiv:hep-ph/0112177](#) [hep-ph].

- [172] A. Brignole, G. Degrassi, P. Slavich, and F. Zwirner, *On the two loop sbottom corrections to the neutral Higgs boson masses in the MSSM*. Nucl. Phys. **B643** (2002) 79–92, [arXiv:hep-ph/0206101](#) [hep-ph].
- [173] S. P. Martin, *Two loop effective potential for the minimal supersymmetric standard model*. Phys. Rev. **D66** (2002) 096001, [arXiv:hep-ph/0206136](#) [hep-ph].
- [174] A. Dedes, G. Degrassi, and P. Slavich, *On the two loop Yukawa corrections to the MSSM Higgs boson masses at large tan beta*. Nucl. Phys. **B672** (2003) 144–162, [arXiv:hep-ph/0305127](#) [hep-ph].
- [175] S. Heinemeyer, W. Hollik, H. Rzehak, and G. Weiglein, *High-precision predictions for the MSSM Higgs sector at  $O(\alpha(b) \alpha(s))$* . Eur. Phys. J. **C39** (2005) 465–481, [arXiv:hep-ph/0411114](#) [hep-ph].
- [176] S. P. Martin, *Strong and Yukawa two-loop contributions to Higgs scalar boson self-energies and pole masses in supersymmetry*. Phys. Rev. **D71** (2005) 016012, [arXiv:hep-ph/0405022](#) [hep-ph].
- [177] S. Borowka, T. Hahn, S. Heinemeyer, G. Heinrich, and W. Hollik, *Momentum-dependent two-loop QCD corrections to the neutral Higgs-boson masses in the MSSM*. Eur. Phys. J. **C74** (2014) no. 8, 2994, [arXiv:1404.7074](#) [hep-ph].
- [178] G. Degrassi, S. Di Vita, and P. Slavich, *Two-loop QCD corrections to the MSSM Higgs masses beyond the effective-potential approximation*. Eur. Phys. J. **C75** (2015) no. 2, 61, [arXiv:1410.3432](#) [hep-ph].
- [179] R. V. Harlander, P. Kant, L. Mihaila, and M. Steinhauser, *Higgs boson mass in supersymmetry to three loops*. Phys. Rev. Lett. **100** (2008) 191602, [arXiv:0803.0672](#) [hep-ph]. [Phys. Rev. Lett.101,039901(2008)].
- [180] P. Kant, R. V. Harlander, L. Mihaila, and M. Steinhauser, *Light MSSM Higgs boson mass to three-loop accuracy*. JHEP **08** (2010) 104, [arXiv:1005.5709](#) [hep-ph].
- [181] D. A. Demir, *Effects of the supersymmetric phases on the neutral Higgs sector*. Phys. Rev. **D60** (1999) 055006, [arXiv:hep-ph/9901389](#) [hep-ph].
- [182] A. Pilaftsis and C. E. M. Wagner, *Higgs bosons in the minimal supersymmetric standard model with explicit CP violation*. Nucl. Phys. **B553** (1999) 3–42, [arXiv:hep-ph/9902371](#) [hep-ph].
- [183] S. Heinemeyer, *The Higgs boson sector of the complex MSSM in the Feynman diagrammatic approach*. Eur. Phys. J. **C22** (2001) 521–534, [arXiv:hep-ph/0108059](#) [hep-ph].
- [184] M. Frank, T. Hahn, S. Heinemeyer, W. Hollik, H. Rzehak, and G. Weiglein, *The Higgs Boson Masses and Mixings of the Complex MSSM in the Feynman-Diagrammatic Approach*. JHEP **02** (2007) 047, [arXiv:hep-ph/0611326](#) [hep-ph].
- [185] S. Heinemeyer, W. Hollik, H. Rzehak, and G. Weiglein, *The Higgs sector of the complex MSSM at two-loop order: QCD contributions*. Phys. Lett. **B652** (2007) 300–309, [arXiv:0705.0746](#) [hep-ph].

- [186] W. Hollik and S. Paßehr, *Two-loop top-Yukawa-coupling corrections to the Higgs boson masses in the complex MSSM*. Phys. Lett. **B733** (2014) 144–150, [arXiv:1401.8275 \[hep-ph\]](#).
- [187] W. Hollik and S. Paßehr, *Higgs boson masses and mixings in the complex MSSM with two-loop top-Yukawa-coupling corrections*. JHEP **10** (2014) 171, [arXiv:1409.1687 \[hep-ph\]](#).
- [188] S. Paßehr and G. Weiglein, *Two-loop top and bottom Yukawa corrections to the Higgs-boson masses in the complex MSSM*. [arXiv:1705.07909 \[hep-ph\]](#).
- [189] S. Borowka, S. Paßehr, and G. Weiglein, *Complete two-loop QCD contributions to the lightest Higgs-boson mass in the MSSM with complex parameters*. [arXiv:1802.09886 \[hep-ph\]](#).
- [190] S. Heinemeyer, W. Hollik, and G. Weiglein, *FeynHiggs: A Program for the calculation of the masses of the neutral CP even Higgs bosons in the MSSM*. Comput. Phys. Commun. **124** (2000) 76–89, [arXiv:hep-ph/9812320 \[hep-ph\]](#).
- [191] B. C. Allanach, *SOFTSUSY: a program for calculating supersymmetric spectra*. Comput. Phys. Commun. **143** (2002) 305–331, [arXiv:hep-ph/0104145 \[hep-ph\]](#).
- [192] B. C. Allanach, A. Bednyakov, and R. Ruiz de Austri, *Higher order corrections and unification in the minimal supersymmetric standard model: SOFTSUSY3.5*. Comput. Phys. Commun. **189** (2015) 192–206, [arXiv:1407.6130 \[hep-ph\]](#).
- [193] A. Djouadi, J.-L. Kneur, and G. Moultaka, *SuSpect: A Fortran code for the supersymmetric and Higgs particle spectrum in the MSSM*. Comput. Phys. Commun. **176** (2007) 426–455, [arXiv:hep-ph/0211331 \[hep-ph\]](#).
- [194] W. Porod, *SPheno, a program for calculating supersymmetric spectra, SUSY particle decays and SUSY particle production at  $e^+e^-$  colliders*. Comput. Phys. Commun. **153** (2003) 275–315, [arXiv:hep-ph/0301101 \[hep-ph\]](#).
- [195] W. Porod and F. Staub, *SPheno 3.1: Extensions including flavour, CP-phases and models beyond the MSSM*. Comput. Phys. Commun. **183** (2012) 2458–2469, [arXiv:1104.1573 \[hep-ph\]](#).
- [196] A. Dedes and P. Slavich, *Two loop corrections to radiative electroweak symmetry breaking in the MSSM*. Nucl. Phys. **B657** (2003) 333–354, [arXiv:hep-ph/0212132 \[hep-ph\]](#).
- [197] G. Degrandi, S. Heinemeyer, W. Hollik, P. Slavich, and G. Weiglein, *Towards high precision predictions for the MSSM Higgs sector*. Eur. Phys. J. **C28** (2003) 133–143, [arXiv:hep-ph/0212020 \[hep-ph\]](#).
- [198] B. C. Allanach, A. Djouadi, J. L. Kneur, W. Porod, and P. Slavich, *Precise determination of the neutral Higgs boson masses in the MSSM*. JHEP **09** (2004) 044, [arXiv:hep-ph/0406166 \[hep-ph\]](#).
- [199] R. Barbieri, M. Frigeni, and F. Caravaglios, *The Supersymmetric Higgs for heavy superpartners*. Phys. Lett. **B258** (1991) 167–170.

- [200] Y. Okada, M. Yamaguchi, and T. Yanagida, *Renormalization group analysis on the Higgs mass in the softly broken supersymmetric standard model*. Phys. Lett. **B262** (1991) 54–58.
- [201] J. R. Espinosa and M. Quiros, *Two loop radiative corrections to the mass of the lightest Higgs boson in supersymmetric standard models*. Phys. Lett. **B266** (1991) 389–396.
- [202] K. Sasaki, M. Carena, and C. E. M. Wagner, *Renormalization group analysis of the Higgs sector in the minimal supersymmetric standard model*. Nucl. Phys. **B381** (1992) 66–86.
- [203] H. E. Haber and R. Hempfling, *The Renormalization group improved Higgs sector of the minimal supersymmetric model*. Phys. Rev. **D48** (1993) 4280–4309, [arXiv:hep-ph/9307201 \[hep-ph\]](#).
- [204] J. R. Espinosa and I. Navarro, *Radiative corrections to the Higgs boson mass for a hierarchical stop spectrum*. Nucl. Phys. **B615** (2001) 82–116, [arXiv:hep-ph/0104047 \[hep-ph\]](#).
- [205] J. Kodaira, Y. Yasui, and K. Sasaki, *The Mass of the lightest supersymmetric Higgs boson beyond the leading logarithm approximation*. Phys. Rev. **D50** (1994) 7035–7041, [arXiv:hep-ph/9311366 \[hep-ph\]](#).
- [206] J. A. Casas, J. R. Espinosa, M. Quiros, and A. Riotto, *The Lightest Higgs boson mass in the minimal supersymmetric standard model*. Nucl. Phys. **B436** (1995) 3–29, [arXiv:hep-ph/9407389 \[hep-ph\]](#). [Erratum: Nucl. Phys. **B439**, 466 (1995)].
- [207] M. Carena, J. R. Espinosa, M. Quiros, and C. E. M. Wagner, *Analytical expressions for radiatively corrected Higgs masses and couplings in the MSSM*. Phys. Lett. **B355** (1995) 209–221, [arXiv:hep-ph/9504316 \[hep-ph\]](#).
- [208] M. Carena, M. Quiros, and C. E. M. Wagner, *Effective potential methods and the Higgs mass spectrum in the MSSM*. Nucl. Phys. **B461** (1996) 407–436, [arXiv:hep-ph/9508343 \[hep-ph\]](#).
- [209] H. E. Haber, R. Hempfling, and A. H. Hoang, *Approximating the radiatively corrected Higgs mass in the minimal supersymmetric model*. Z. Phys. **C75** (1997) 539–554, [arXiv:hep-ph/9609331 \[hep-ph\]](#).
- [210] S. P. Martin, *Three-loop corrections to the lightest Higgs scalar boson mass in supersymmetry*. Phys. Rev. **D75** (2007) 055005, [arXiv:hep-ph/0701051 \[hep-ph\]](#).
- [211] N. Bernal, A. Djouadi, and P. Slavich, *The MSSM with heavy scalars*. JHEP **07** (2007) 016, [arXiv:0705.1496 \[hep-ph\]](#).
- [212] G. F. Giudice and A. Strumia, *Probing High-Scale and Split Supersymmetry with Higgs Mass Measurements*. Nucl. Phys. **B858** (2012) 63–83, [arXiv:1108.6077 \[hep-ph\]](#).
- [213] E. Bagnaschi, G. F. Giudice, P. Slavich, and A. Strumia, *Higgs Mass and Unnatural Supersymmetry*. JHEP **09** (2014) 092, [arXiv:1407.4081 \[hep-ph\]](#).

- [214] P. Draper, G. Lee, and C. E. M. Wagner, *Precise estimates of the Higgs mass in heavy supersymmetry*. Phys. Rev. **D89** (2014) no. 5, 055023, [arXiv:1312.5743](#) [hep-ph].
- [215] J. Pardo Vega and G. Villadoro, *SusyHD: Higgs mass Determination in Supersymmetry*. JHEP **07** (2015) 159, [arXiv:1504.05200](#) [hep-ph].
- [216] E. Bagnaschi, J. Pardo Vega, and P. Slavich, *Improved determination of the Higgs mass in the MSSM with heavy superpartners*. Eur. Phys. J. **C77** (2017) no. 5, 334, [arXiv:1703.08166](#) [hep-ph].
- [217] G. Lee and C. E. M. Wagner, *Higgs bosons in heavy supersymmetry with an intermediate  $m_A$* . Phys. Rev. **D92** (2015) no. 7, 075032, [arXiv:1508.00576](#) [hep-ph].
- [218] P. Athron, J.-h. Park, T. Steudtner, D. Stöckinger, and A. Voigt, *Precise Higgs mass calculations in (non-)minimal supersymmetry at both high and low scales*. [arXiv:1609.00371](#) [hep-ph].
- [219] P. Athron, J.-h. Park, D. Stöckinger, and A. Voigt, *FlexibleSUSY—A spectrum generator generator for supersymmetric models*. Comput. Phys. Commun. **190** (2015) 139–172, [arXiv:1406.2319](#) [hep-ph].
- [220] P. Athron, M. Bach, D. Harries, T. Kwasnitza, J.-h. Park, D. Stöckinger, A. Voigt, and J. Ziebell, *FlexibleSUSY 2.0: Extensions to investigate the phenomenology of SUSY and non-SUSY models*. [arXiv:1710.03760](#) [hep-ph].
- [221] F. Staub and W. Porod, *Improved predictions for intermediate and heavy Supersymmetry in the MSSM and beyond*. Eur. Phys. J. **C77** (2017) no. 5, 338, [arXiv:1703.03267](#) [hep-ph].
- [222] T. Hahn, S. Heinemeyer, W. Hollik, H. Rzehak, and G. Weiglein, *High-Precision Predictions for the Light CP -Even Higgs Boson Mass of the Minimal Supersymmetric Standard Model*. Phys. Rev. Lett. **112** (2014) no. 14, 141801, [arXiv:1312.4937](#) [hep-ph].
- [223] H. Bahl and W. Hollik, *Precise prediction for the light MSSM Higgs boson mass combining effective field theory and fixed-order calculations*. Eur. Phys. J. **C76** (2016) no. 9, 499, [arXiv:1608.01880](#) [hep-ph].
- [224] H. Bahl, S. Heinemeyer, W. Hollik, and G. Weiglein, *Reconciling EFT and hybrid calculations of the light MSSM Higgs-boson mass*. Eur. Phys. J. **C78** (2018) no. 1, 57, [arXiv:1706.00346](#) [hep-ph].
- [225] U. Ellwanger, *Radiative corrections to the neutral Higgs spectrum in supersymmetry with a gauge singlet*. Phys. Lett. **B303** (1993) 271–276, [arXiv:hep-ph/9302224](#) [hep-ph].
- [226] T. Elliott, S. F. King, and P. L. White, *Supersymmetric Higgs bosons at the limit*. Phys. Lett. **B305** (1993) 71–77, [arXiv:hep-ph/9302202](#) [hep-ph].
- [227] T. Elliott, S. F. King, and P. L. White, *Radiative corrections to Higgs boson masses in the next-to-minimal supersymmetric Standard Model*. Phys. Rev. **D49** (1994) 2435–2456, [arXiv:hep-ph/9308309](#) [hep-ph].

- [228] T. Elliott, S. F. King, and P. L. White, *Squark contributions to Higgs boson masses in the next-to-minimal supersymmetric standard model*. Phys. Lett. **B314** (1993) 56–63, [arXiv:hep-ph/9305282](#) [hep-ph].
- [229] U. Ellwanger and C. Hugonie, *Yukawa induced radiative corrections to the lightest Higgs boson mass in the NMSSM*. Phys. Lett. **B623** (2005) 93–103, [arXiv:hep-ph/0504269](#) [hep-ph].
- [230] F. Staub, W. Porod, and B. Herrmann, *The Electroweak sector of the NMSSM at the one-loop level*. JHEP **10** (2010) 040, [arXiv:1007.4049](#) [hep-ph].
- [231] K. Ender, T. Graf, M. Muhlleitner, and H. Rzehak, *Analysis of the NMSSM Higgs Boson Masses at One-Loop Level*. Phys. Rev. **D85** (2012) 075024, [arXiv:1111.4952](#) [hep-ph].
- [232] P. Drechsel, L. Galeta, S. Heinemeyer, and G. Weiglein, *Precise Predictions for the Higgs-Boson Masses in the NMSSM*. Eur. Phys. J. **C77** (2017) no. 1, 42, [arXiv:1601.08100](#) [hep-ph].
- [233] S. W. Ham, J. Kim, S. K. Oh, and D. Son, *The Charged Higgs boson in the next-to-minimal supersymmetric standard model with explicit CP violation*. Phys. Rev. **D64** (2001) 035007, [arXiv:hep-ph/0104144](#) [hep-ph].
- [234] S. W. Ham, S. K. Oh, and D. Son, *Neutral Higgs sector of the next-to-minimal supersymmetric standard model with explicit CP violation*. Phys. Rev. **D65** (2002) 075004, [arXiv:hep-ph/0110052](#) [hep-ph].
- [235] S. W. Ham, Y. S. Jeong, and S. K. Oh, *Radiative CP violation in the Higgs sector of the next-to-minimal supersymmetric model*. [arXiv:hep-ph/0308264](#) [hep-ph].
- [236] K. Funakubo and S. Tao, *The Higgs sector in the next-to-MSSM*. Prog. Theor. Phys. **113** (2005) 821–842, [arXiv:hep-ph/0409294](#) [hep-ph].
- [237] S. W. Ham, S. H. Kim, S. K. OH, and D. Son, *Higgs bosons of the NMSSM with explicit CP violation at the ILC*. Phys. Rev. **D76** (2007) 115013, [arXiv:0708.2755](#) [hep-ph].
- [238] T. Graf, R. Grober, M. Muhlleitner, H. Rzehak, and K. Walz, *Higgs Boson Masses in the Complex NMSSM at One-Loop Level*. JHEP **10** (2012) 122, [arXiv:1206.6806](#) [hep-ph].
- [239] K. Cheung, T.-J. Hou, J. S. Lee, and E. Senaha, *The Higgs Boson Sector of the Next-to-MSSM with CP Violation*. Phys. Rev. **D82** (2010) 075007, [arXiv:1006.1458](#) [hep-ph].
- [240] M. Muhlleitner, D. T. Nhung, H. Rzehak, and K. Walz, *Two-loop contributions of the order  $\mathcal{O}(\alpha_t\alpha_s)$  to the masses of the Higgs bosons in the CP-violating NMSSM*. JHEP **05** (2015) 128, [arXiv:1412.0918](#) [hep-ph].
- [241] B. C. Allanach, P. Athron, L. C. Tunstall, A. Voigt, and A. G. Williams, *Next-to-Minimal SOFTSUSY*. Comput. Phys. Commun. **185** (2014) 2322–2339, [arXiv:1311.7659](#) [hep-ph].
- [242] U. Ellwanger, J. F. Gunion, and C. Hugonie, *NMHDECAY: A Fortran code for the Higgs masses, couplings and decay widths in the NMSSM*. JHEP **02** (2005) 066, [arXiv:hep-ph/0406215](#) [hep-ph].



- [243] U. Ellwanger and C. Hugonie, *NMHDECAY 2.0: An Updated program for sparticle masses, Higgs masses, couplings and decay widths in the NMSSM*. Comput. Phys. Commun. **175** (2006) 290–303, [arXiv:hep-ph/0508022 \[hep-ph\]](#).
- [244] U. Ellwanger and C. Hugonie, *NMSPEC: A Fortran code for the sparticle and Higgs masses in the NMSSM with GUT scale boundary conditions*. Comput. Phys. Commun. **177** (2007) 399–407, [arXiv:hep-ph/0612134 \[hep-ph\]](#).
- [245] J. Baglio, R. Gröber, M. Mühlleitner, D. T. Nhung, H. Rzehak, M. Spira, J. Streicher, and K. Walz, *NMSSMCALC: A Program Package for the Calculation of Loop-Corrected Higgs Boson Masses and Decay Widths in the (Complex) NMSSM*. Comput. Phys. Commun. **185** (2014) no. 12, 3372–3391, [arXiv:1312.4788 \[hep-ph\]](#).
- [246] S. F. King, M. Muhlleitner, R. Nevzorov, and K. Walz, *Exploring the CP-violating NMSSM: EDM Constraints and Phenomenology*. Nucl. Phys. **B901** (2015) 526–555, [arXiv:1508.03255 \[hep-ph\]](#).
- [247] F. Staub, P. Athron, U. Ellwanger, R. Gröber, M. Mühlleitner, P. Slavich, and A. Voigt, *Higgs mass predictions of public NMSSM spectrum generators*. Comput. Phys. Commun. **202** (2016) 113–130, [arXiv:1507.05093 \[hep-ph\]](#).
- [248] P. Drechsel, R. Gröber, S. Heinemeyer, M. M. Muhlleitner, H. Rzehak, and G. Weiglein, *Higgs-Boson Masses and Mixing Matrices in the NMSSM: Analysis of On-Shell Calculations*. Eur. Phys. J. **C77** (2017) no. 6, 366, [arXiv:1612.07681 \[hep-ph\]](#).
- [249] M. D. Goodsell, K. Nickel, and F. Staub, *Two-loop corrections to the Higgs masses in the NMSSM*. Phys. Rev. **D91** (2015) 035021, [arXiv:1411.4665 \[hep-ph\]](#).
- [250] M. D. Goodsell, K. Nickel, and F. Staub, *Two-Loop Higgs mass calculations in supersymmetric models beyond the MSSM with SARAH and SPheno*. Eur. Phys. J. **C75** (2015) no. 1, 32, [arXiv:1411.0675 \[hep-ph\]](#).
- [251] P. Diessner, J. Kalinowski, W. Kotlarski, and D. Stöckinger, *Two-loop correction to the Higgs boson mass in the MRSSM*. Adv. High Energy Phys. **2015** (2015) 760729, [arXiv:1504.05386 \[hep-ph\]](#).
- [252] P. Diessner, J. Kalinowski, W. Kotlarski, and D. Stöckinger, *Exploring the Higgs sector of the MRSSM with a light scalar*. JHEP **03** (2016) 007, [arXiv:1511.09334 \[hep-ph\]](#).
- [253] S. Kanemura, Y. Okada, E. Senaha, and C. P. Yuan, *Higgs coupling constants as a probe of new physics*. Phys. Rev. **D70** (2004) 115002, [arXiv:hep-ph/0408364 \[hep-ph\]](#).
- [254] M. Krause, M. Muhlleitner, R. Santos, and H. Ziesche, *Higgs-to-Higgs boson decays in a 2HDM at next-to-leading order*. Phys. Rev. **D95** (2017) no. 7, 075019, [arXiv:1609.04185 \[hep-ph\]](#).
- [255] M. Krause, R. Lorenz, M. Muhlleitner, R. Santos, and H. Ziesche, *Gauge-independent Renormalization of the 2-Higgs-Doublet Model*. JHEP **09** (2016) 143, [arXiv:1605.04853 \[hep-ph\]](#).

- [256] S. Kanemura, M. Kikuchi, K. Sakurai, and K. Yagyu, *Gauge invariant one-loop corrections to Higgs boson couplings in non-minimal Higgs models*. Phys. Rev. **D96** (2017) no. 3, 035014, [arXiv:1705.05399 \[hep-ph\]](#).
- [257] S. Kanemura, M. Kikuchi, K. Sakurai, and K. Yagyu, *H-COUP: a program for one-loop corrected Higgs boson couplings in non-minimal Higgs sectors*. [arXiv:1710.04603 \[hep-ph\]](#).
- [258] M. D. Goodsell, K. Nickel, and F. Staub, *The Higgs Mass in the MSSM at two-loop order beyond minimal flavour violation*. Phys. Lett. **B758** (2016) 18–25, [arXiv:1511.01904 \[hep-ph\]](#).
- [259] H. K. Dreiner, K. Nickel, and F. Staub, *On the two-loop corrections to the Higgs mass in trilinear R-parity violation*. Phys. Lett. **B742** (2015) 261–265, [arXiv:1411.3731 \[hep-ph\]](#).
- [260] S. P. Martin, *Two-loop scalar self-energies and pole masses in a general renormalizable theory with massless gauge bosons*. Phys. Rev. **D71** (2005) 116004, [arXiv:hep-ph/0502168 \[hep-ph\]](#).
- [261] F. Staub, *SARAH*. [arXiv:0806.0538 \[hep-ph\]](#).
- [262] F. Staub, *From Superpotential to Model Files for FeynArts and CalcHep/CompHep*. Comput. Phys. Commun. **181** (2010) 1077–1086, [arXiv:0909.2863 \[hep-ph\]](#).
- [263] F. Staub, *Automatic Calculation of supersymmetric Renormalization Group Equations and Self Energies*. Comput. Phys. Commun. **182** (2011) 808–833, [arXiv:1002.0840 \[hep-ph\]](#).
- [264] F. Staub, *SARAH 3.2: Dirac Gauginos, UFO output, and more*. Comput. Phys. Commun. **184** (2013) 1792–1809, [arXiv:1207.0906 \[hep-ph\]](#).
- [265] F. Staub, *SARAH 4 : A tool for (not only SUSY) model builders*. Comput. Phys. Commun. **185** (2014) 1773–1790, [arXiv:1309.7223 \[hep-ph\]](#).
- [266] F. Staub, *Exploring new models in all detail with SARAH*. Adv. High Energy Phys. **2015** (2015) 840780, [arXiv:1503.04200 \[hep-ph\]](#).
- [267] A. Vicente, *Computer tools in particle physics*. [arXiv:1507.06349 \[hep-ph\]](#).
- [268] N. D. Christensen and C. Duhr, *FeynRules - Feynman rules made easy*. Comput. Phys. Commun. **180** (2009) 1614–1641, [arXiv:0806.4194 \[hep-ph\]](#).
- [269] A. V. Semenov, *LanHEP: A Package for automatic generation of Feynman rules in gauge models*. [arXiv:hep-ph/9608488 \[hep-ph\]](#).
- [270] M. E. Machacek and M. T. Vaughn, *Two Loop Renormalization Group Equations in a General Quantum Field Theory. 1. Wave Function Renormalization*. Nucl. Phys. **B222** (1983) 83–103.
- [271] M. E. Machacek and M. T. Vaughn, *Two Loop Renormalization Group Equations in a General Quantum Field Theory. 2. Yukawa Couplings*. Nucl. Phys. **B236** (1984) 221–232.

- [272] M. E. Machacek and M. T. Vaughn, *Two Loop Renormalization Group Equations in a General Quantum Field Theory. 3. Scalar Quartic Couplings*. Nucl. Phys. **B249** (1985) 70–92.
- [273] M.-x. Luo, H.-w. Wang, and Y. Xiao, *Two loop renormalization group equations in general gauge field theories*. Phys. Rev. **D67** (2003) 065019, [arXiv:hep-ph/0211440](#) [hep-ph].
- [274] M. D. Goodsell, S. Liebler, and F. Staub, *Generic calculation of two-body partial decay widths at the full one-loop level*. Eur. Phys. J. **C77** (2017) no. 11, 758, [arXiv:1703.09237](#) [hep-ph].
- [275] F. Staub, T. Ohl, W. Porod, and C. Speckner, *A Tool Box for Implementing Supersymmetric Models*. Comput. Phys. Commun. **183** (2012) 2165–2206, [arXiv:1109.5147](#) [hep-ph].
- [276] W. Porod, F. Staub, and A. Vicente, *A Flavor Kit for BSM models*. Eur. Phys. J. **C74** (2014) no. 8, 2992, [arXiv:1405.1434](#) [hep-ph].
- [277] P. Z. Skands *et al.*, *SUSY Les Houches accord: Interfacing SUSY spectrum calculators, decay packages, and event generators*. JHEP **07** (2004) 036, [arXiv:hep-ph/0311123](#) [hep-ph].
- [278] B. C. Allanach *et al.*, *SUSY Les Houches Accord 2*. Comput. Phys. Commun. **180** (2009) 8–25, [arXiv:0801.0045](#) [hep-ph].
- [279] J. E. Camargo-Molina, B. O’Leary, W. Porod, and F. Staub, *Vevacious: A Tool For Finding The Global Minima Of One-Loop Effective Potentials With Many Scalars*. Eur. Phys. J. **C73** (2013) no. 10, 2588, [arXiv:1307.1477](#) [hep-ph].
- [280] A. Belyaev, N. D. Christensen, and A. Pukhov, *CalcHEP 3.4 for collider physics within and beyond the Standard Model*. Comput. Phys. Commun. **184** (2013) 1729–1769, [arXiv:1207.6082](#) [hep-ph].
- [281] T. Hahn, *Generating Feynman diagrams and amplitudes with FeynArts 3*. Comput. Phys. Commun. **140** (2001) 418–431, [arXiv:hep-ph/0012260](#) [hep-ph].
- [282] T. Hahn, S. Paßehr, and C. Schappacher, *FormCalc 9 and Extensions*. PoS **LL2016** (2016) 068, [arXiv:1604.04611](#) [hep-ph]. [J. Phys. Conf. Ser.762,no.1,012065(2016)].
- [283] W. Kilian, T. Ohl, and J. Reuter, *WHIZARD: Simulating Multi-Particle Processes at LHC and ILC*. Eur. Phys. J. **C71** (2011) 1742, [arXiv:0708.4233](#) [hep-ph].
- [284] M. Moretti, T. Ohl, and J. Reuter, *O’Mega: An Optimizing matrix element generator*. [arXiv:hep-ph/0102195](#) [hep-ph].
- [285] C. Degrande, C. Duhr, B. Fuks, D. Grellscheid, O. Mattelaer, and T. Reiter, *UFO - The Universal FeynRules Output*. Comput. Phys. Commun. **183** (2012) 1201–1214, [arXiv:1108.2040](#) [hep-ph].

- [286] J. Alwall, R. Frederix, S. Frixione, V. Hirschi, F. Maltoni, O. Mattelaer, H. S. Shao, T. Stelzer, P. Torrielli, and M. Zaro, *The automated computation of tree-level and next-to-leading order differential cross sections, and their matching to parton shower simulations*. JHEP **07** (2014) 079, [arXiv:1405.0301 \[hep-ph\]](#).
- [287] G. Cullen *et al.*, *GOSAM-2.0: a tool for automated one-loop calculations within the Standard Model and beyond*. Eur. Phys. J. **C74** (2014) no. 8, 3001, [arXiv:1404.7096 \[hep-ph\]](#).
- [288] J. Bellm *et al.*, *Herwig++ 2.7 Release Note*. [arXiv:1310.6877 \[hep-ph\]](#).
- [289] S. Höche, S. Kuttimalai, S. Schumann, and F. Siegert, *Beyond Standard Model calculations with Sherpa*. Eur. Phys. J. **C75** (2015) no. 3, 135, [arXiv:1412.6478 \[hep-ph\]](#).
- [290] P. Bechtle, O. Brein, S. Heinemeyer, G. Weiglein, and K. E. Williams, *HiggsBounds: Confronting Arbitrary Higgs Sectors with Exclusion Bounds from LEP and the Tevatron*. Comput. Phys. Commun. **181** (2010) 138–167, [arXiv:0811.4169 \[hep-ph\]](#).
- [291] P. Bechtle, O. Brein, S. Heinemeyer, G. Weiglein, and K. E. Williams, *HiggsBounds 2.0.0: Confronting Neutral and Charged Higgs Sector Predictions with Exclusion Bounds from LEP and the Tevatron*. Comput. Phys. Commun. **182** (2011) 2605–2631, [arXiv:1102.1898 \[hep-ph\]](#).
- [292] P. Bechtle, O. Brein, S. Heinemeyer, O. Stål, T. Stefaniak, G. Weiglein, and K. E. Williams, *HiggsBounds – 4: Improved Tests of Extended Higgs Sectors against Exclusion Bounds from LEP, the Tevatron and the LHC*. Eur. Phys. J. **C74** (2014) no. 3, 2693, [arXiv:1311.0055 \[hep-ph\]](#).
- [293] P. Bechtle, S. Heinemeyer, O. Stål, T. Stefaniak, and G. Weiglein, *HiggsSignals: Confronting arbitrary Higgs sectors with measurements at the Tevatron and the LHC*. Eur. Phys. J. **C74** (2014) no. 2, 2711, [arXiv:1305.1933 \[hep-ph\]](#).
- [294] P. Bechtle, S. Heinemeyer, O. Stål, T. Stefaniak, and G. Weiglein, *Probing the Standard Model with Higgs signal rates from the Tevatron, the LHC and a future ILC*. JHEP **11** (2014) 039, [arXiv:1403.1582 \[hep-ph\]](#).
- [295] G. Belanger, F. Boudjema, A. Pukhov, and A. Semenov, *MicrOMEGAs: A Program for calculating the relic density in the MSSM*. Comput. Phys. Commun. **149** (2002) 103–120, [arXiv:hep-ph/0112278 \[hep-ph\]](#).
- [296] G. Belanger, F. Boudjema, A. Pukhov, and A. Semenov, *MicrOMEGAs 2.0: A Program to calculate the relic density of dark matter in a generic model*. Comput. Phys. Commun. **176** (2007) 367–382, [arXiv:hep-ph/0607059 \[hep-ph\]](#).
- [297] D. Barducci, G. Belanger, J. Bernon, F. Boudjema, J. Da Silva, S. Kraml, U. Laa, and A. Pukhov, *Collider limits on new physics within micrOMEGAs4.3*. Comput. Phys. Commun. **222** (2018) 327–338, [arXiv:1606.03834 \[hep-ph\]](#).
- [298] G. Bélanger, F. Boudjema, A. Goudelis, A. Pukhov, and B. Zaldivar, *micrOMEGAs5.0 : freeze-in*. [arXiv:1801.03509 \[hep-ph\]](#).

- [299] K. Nickel and F. Staub, *Precise determination of the Higgs mass in supersymmetric models with vectorlike tops and the impact on naturalness in minimal GMSB*. JHEP **07** (2015) 139, [arXiv:1505.06077 \[hep-ph\]](#).
- [300] M. D. Goodsell and F. Staub, *The Higgs mass in the CP violating MSSM, NMSSM, and beyond*. [arXiv:1604.05335 \[hep-ph\]](#).
- [301] M. D. Goodsell, *Two-loop RGEs with Dirac gaugino masses*. JHEP **01** (2013) 066, [arXiv:1206.6697 \[hep-ph\]](#).
- [302] P. Dießner, J. Kalinowski, W. Kotlarski, and D. Stöckinger, *Higgs boson mass and electroweak observables in the MRSSM*. JHEP **12** (2014) 124, [arXiv:1410.4791 \[hep-ph\]](#).
- [303] **Particle Data Group** Collaboration, K. A. Olive *et al.*, *Review of Particle Physics*. Chin. Phys. **C38** (2014) 090001.
- [304] N. Arkani-Hamed and S. Dimopoulos, *Supersymmetric unification without low energy supersymmetry and signatures for fine-tuning at the LHC*. JHEP **06** (2005) 073, [arXiv:hep-th/0405159 \[hep-th\]](#).
- [305] G. F. Giudice and A. Romanino, *Split supersymmetry*. Nucl. Phys. **B699** (2004) 65–89, [arXiv:hep-ph/0406088 \[hep-ph\]](#). [Erratum: Nucl. Phys. **B706**, 487(2005)].
- [306] N. Arkani-Hamed, S. Dimopoulos, G. F. Giudice, and A. Romanino, *Aspects of split supersymmetry*. Nucl. Phys. **B709** (2005) 3–46, [arXiv:hep-ph/0409232 \[hep-ph\]](#).
- [307] W. Kilian, T. Plehn, P. Richardson, and E. Schmidt, *Split supersymmetry at colliders*. Eur. Phys. J. **C39** (2005) 229–243, [arXiv:hep-ph/0408088 \[hep-ph\]](#).
- [308] K. Benakli, L. Darmé, M. D. Goodsell, and P. Slavich, *A Fake Split Supersymmetry Model for the 126 GeV Higgs*. JHEP **05** (2014) 113, [arXiv:1312.5220 \[hep-ph\]](#).
- [309] K. Benakli, L. Darmé, and M. D. Goodsell, *(O)Mega Split*. JHEP **11** (2015) 100, [arXiv:1508.02534 \[hep-ph\]](#).
- [310] S. Kanemura, T. Kubota, and E. Takasugi, *Lee-Quigg-Thacker bounds for Higgs boson masses in a two doublet model*. Phys. Lett. **B313** (1993) 155–160, [arXiv:hep-ph/9303263 \[hep-ph\]](#).
- [311] A. G. Akeroyd, A. Arhrib, and E.-M. Naimi, *Note on tree level unitarity in the general two Higgs doublet model*. Phys. Lett. **B490** (2000) 119–124, [arXiv:hep-ph/0006035 \[hep-ph\]](#).
- [312] J. Horejsi and M. Kladiva, *Tree-unitarity bounds for THDM Higgs masses revisited*. Eur. Phys. J. **C46** (2006) 81–91, [arXiv:hep-ph/0510154 \[hep-ph\]](#).
- [313] U. Nierste and K. Riesselmann, *Higgs sector renormalization group in the  $\overline{MS}$  and  $\overline{OMS}$  scheme: The Breakdown of perturbation theory for a heavy Higgs*. Phys. Rev. **D53** (1996) 6638–6652, [arXiv:hep-ph/9511407 \[hep-ph\]](#).
- [314] F. Staub, *Reopen parameter regions in Two-Higgs Doublet Models*. [arXiv:1705.03677 \[hep-ph\]](#).

- [315] S. Blasi, S. De Curtis, and K. Yagyu, *Effects of custodial symmetry breaking in the Georgi-Machacek model at high energies*. [arXiv:1704.08512](#) [hep-ph].
- [316] H. E. Logan and V. Rentala, *All the generalized Georgi-Machacek models*. Phys. Rev. **D92** (2015) no. 7, 075011, [arXiv:1502.01275](#) [hep-ph].
- [317] M. E. Krauss and F. Staub, *Perturbativity Constraints in BSM Models*. [arXiv:1709.03501](#) [hep-ph].
- [318] A. Andreassen, W. Frost, and M. D. Schwartz, *Scale Invariant Instantons and the Complete Lifetime of the Standard Model*. [arXiv:1707.08124](#) [hep-ph].
- [319] A. Spencer-Smith, *Higgs Vacuum Stability in a Mass-Dependent Renormalisation Scheme*. [arXiv:1405.1975](#) [hep-ph].
- [320] G. M. Pruna and T. Robens, *Higgs singlet extension parameter space in the light of the LHC discovery*. Phys. Rev. **D88** (2013) no. 11, 115012, [arXiv:1303.1150](#) [hep-ph].
- [321] Y. Hamada, K. Kawana, and K. Tsumura, *Landau pole in the Standard Model with weakly interacting scalar fields*. Phys. Lett. **B747** (2015) 238–244, [arXiv:1505.01721](#) [hep-ph].
- [322] N. Khan, *Exploring Hyperchargeless Higgs Triplet Model up to the Planck Scale*. [arXiv:1610.03178](#) [hep-ph].
- [323] H. S. Cheon and S. K. Kang, *Constraining parameter space in type-II two-Higgs doublet model in light of a 126 GeV Higgs boson*. JHEP **09** (2013) 085, [arXiv:1207.1083](#) [hep-ph].
- [324] N. Chakrabarty, U. K. Dey, and B. Mukhopadhyaya, *High-scale validity of a two-Higgs doublet scenario: a study including LHC data*. JHEP **12** (2014) 166, [arXiv:1407.2145](#) [hep-ph].
- [325] N. Chakrabarty and B. Mukhopadhyaya, *High-scale validity of a two Higgs doublet scenario: metastability included*. Eur. Phys. J. **C77** (2017) no. 3, 153, [arXiv:1603.05883](#) [hep-ph].
- [326] P. Ferreira, H. E. Haber, and E. Santos, *Preserving the validity of the Two-Higgs Doublet Model up to the Planck scale*. Phys. Rev. **D92** (2015) 033003, [arXiv:1505.04001](#) [hep-ph]. [Erratum: Phys. Rev. D94, no. 5, 059903(2016)].
- [327] N. Chakrabarty and B. Mukhopadhyaya, *High-scale validity of a two Higgs doublet scenario: predicting collider signals*. Phys. Rev. **D96** (2017) no. 3, 035028, [arXiv:1702.08268](#) [hep-ph].
- [328] D. Chowdhury and O. Eberhardt, *Global fits of the two-loop renormalized Two-Higgs-Doublet model with soft  $Z_2$  breaking*. JHEP **11** (2015) 052, [arXiv:1503.08216](#) [hep-ph].
- [329] S. Gori, H. E. Haber, and E. Santos, *High scale flavor alignment in two-Higgs doublet models and its phenomenology*. JHEP **06** (2017) 110, [arXiv:1703.05873](#) [hep-ph].

- [330] P. Basler, P. M. Ferreira, M. Muhlleitner, and R. Santos, *High scale impact in alignment and decoupling in two-Higgs doublet models*. [arXiv:1710.10410](#) [hep-ph].
- [331] P. S. Bhupal Dev and A. Pilaftsis, *Maximally Symmetric Two Higgs Doublet Model with Natural Standard Model Alignment*. JHEP **12** (2014) 024, [arXiv:1408.3405](#) [hep-ph]. [Erratum: JHEP11,147(2015)].
- [332] M.-L. Xiao and J.-H. Yu, *Stabilizing electroweak vacuum in a vectorlike fermion model*. Phys. Rev. **D90** (2014) no. 1, 014007, [arXiv:1404.0681](#) [hep-ph]. [Addendum: Phys. Rev.D90,no.1,019901(2014)].
- [333] S. Kanemura, M. Kikuchi, and K. Yagyu, *Radiative corrections to the Higgs boson couplings in the model with an additional real singlet scalar field*. Nucl. Phys. **B907** (2016) 286–322, [arXiv:1511.06211](#) [hep-ph].
- [334] P. Basler, M. Krause, M. Muhlleitner, J. Wittbrodt, and A. Wlotzka, *Strong First Order Electroweak Phase Transition in the CP-Conserving 2HDM Revisited*. JHEP **02** (2017) 121, [arXiv:1612.04086](#) [hep-ph].
- [335] A. Kobakhidze and A. Spencer-Smith, *Neutrino Masses and Higgs Vacuum Stability*. JHEP **08** (2013) 036, [arXiv:1305.7283](#) [hep-ph].
- [336] J. Elias-Miro, J. R. Espinosa, G. F. Giudice, G. Isidori, A. Riotto, and A. Strumia, *Higgs mass implications on the stability of the electroweak vacuum*. Phys. Lett. **B709** (2012) 222–228, [arXiv:1112.3022](#) [hep-ph].
- [337] G. Bambhaniya, P. Bhupal Dev, S. Goswami, S. Khan, and W. Rodejohann, *Naturalness, Vacuum Stability and Leptogenesis in the Minimal Seesaw Model*. Phys. Rev. **D95** (2017) no. 9, 095016, [arXiv:1611.03827](#) [hep-ph].
- [338] S. P. Martin and D. G. Robertson, *Evaluation of the general 3-loop vacuum Feynman integral*. Phys. Rev. **D95** (2017) no. 1, 016008, [arXiv:1610.07720](#) [hep-ph].
- [339] S. P. Martin, *Effective potential at three loops*. Phys. Rev. **D96** (2017) no. 9, 096005, [arXiv:1709.02397](#) [hep-ph].
- [340] R. Scharf and J. B. Tausk, *Scalar two loop integrals for gauge boson selfenergy diagrams with a massless fermion loop*. Nucl. Phys. **B412** (1994) 523–552.

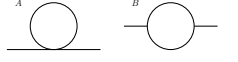
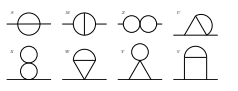
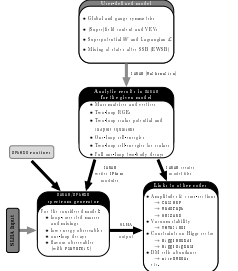


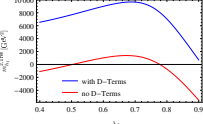
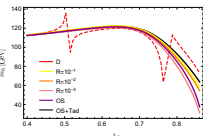


# List of Figures

1.1	Examples of the most severely divergent contributions of the Goldstone bosons to the effective potential at two, three, four and five loops. The black blobs represent the insertions of the 1PI subdiagrams $\Gamma(p^2)$ . . . . .	17
1.2	One-loop diagrams contributing to the light scalar self-energy. Thick lines represent heavy states (scalars and fermions) while thin lines are for light states. . . . .	34
1.3	Summary of lower limits on masses of SUSY particles, obtained by the different SUSY searches of the ATLAS collaboration by December 2017. This plot, along with other summary from ATLAS can be found on the web page: <a href="https://atlas.web.cern.ch/Atlas/GROUPS/PHYSICS/CombinedSummaryPlots/SUSY/">https://atlas.web.cern.ch/Atlas/GROUPS/PHYSICS/CombinedSummaryPlots/SUSY/</a> . A similar plot for CMS, updated for the Moriond 2017 conference, can be found at <a href="https://twiki.cern.ch/twiki/pub/CMSPublic/PhysicsResultsSUS/Moriond2017_BarPlot.pdf">https://twiki.cern.ch/twiki/pub/CMSPublic/PhysicsResultsSUS/Moriond2017_BarPlot.pdf</a> . . . . .	45
1.4	Exclusion limits, at 95% confidence level, on stop and neutralino masses, resulting from the stop pair production search of the ATLAS collaboration. Different decay channels of the stops are considered, with quantities of data comprised between 3.2 and 36 fb <sup>-1</sup> from Run 2 of the LHC at $\sqrt{s} = 13$ TeV. A comparison with results from Run 1 (light blue) is also provided. This plot can be found on the web page: <a href="https://atlas.web.cern.ch/Atlas/GROUPS/PHYSICS/CombinedSummaryPlots/SUSY/">https://atlas.web.cern.ch/Atlas/GROUPS/PHYSICS/CombinedSummaryPlots/SUSY/</a> . . . . .	46
1.5	Diagrams contributing to the mass of a scalar $\phi$ : on the left hand side with $\tilde{\phi}$ , <i>i.e.</i> the fermionic superpartner of $\phi$ , and a Dirac gaugino ( $\lambda$ and $\chi_\Sigma$ in terms of Weyl spinors); and on the right hand side with the scalar $\phi$ and the adjoint scalar $\Sigma$ . The logarithmic divergences from both diagrams cancel out when the gauginos only have Dirac masses. . . . .	52
2.1	ATLAS results for the SM-like Higgs boson mass, obtained from LHC Run2 data with an integrated luminosity of 36.1 fb <sup>-1</sup> at $\sqrt{s} = 13$ TeV, in the $h \rightarrow \gamma\gamma$ and $h \rightarrow ZZ^* \rightarrow 4\ell$ channels, as well as the combined result and comparison with the combined ATLAS and CMS measurement from Run 1. This plot is taken from [52]. . . . .	66

## List of Figures

2.2	Possible topologies of one-loop self-energy diagrams.	73	
2.3	Possible topologies of two-loop self-energy diagrams.	73	
2.4	Illustration of the study of a BSM model using SARAH and SPheno, and links to other High-Energy Physics codes.	92	
3.1	Novel two-loop contribution to the effective potential involving stops and octet scalars.	97	
3.2	Mass of the SM-like Higgs boson as a function of $(X_t/M_S)^{\text{OS}}$ , for $\tan \beta = 10$ , $M_S = 1.5$ TeV and $m_{\tilde{g}} = m_O = 2$ TeV. The dashed curve represents the MSSM result, whereas the solid (dotted) curve represents the MDGSSM result with (without) the octet-scalar contributions.	109	
3.3	Different determinations of the SM-like Higgs boson mass in the MDGSSM as a function of $(X_t/M_S)^{\text{OS}}$ , for the same choices of parameters as in figure 3.2. The solid curve represents the original OS calculation; the dotted curve represents the $\overline{\text{DR}}'$ calculation; the dashed and dot-dashed curves were obtained using $\hat{\alpha}_s(m_t)$ and $\overline{\alpha}_s(m_t)$ , respectively, in the OS calculation instead of $\hat{\alpha}_s(M_S)$ .	109	
3.4	Mass of the SM-like Higgs boson as a function of $m_{\tilde{g}}$ in the MRSSM, for $\tan \beta = 10$ , $M_S = 1$ TeV and $m_O = 2$ TeV. The meaning of the different curves is explained in the text.	111	
3.5	Mass of the SM-like Higgs boson as a function of $m_{\tilde{g}}$ in the <i>supersoft</i> limit of the MRSSM, for $\tan \beta = 10$ . The solid curve represents the results of the $\overline{\text{DR}}'$ calculation, in which the two-loop $\mathcal{O}(\alpha_t \alpha_s)$ corrections become unphysically large. The dashed curve was obtained by converting the top and stop masses to the OS scheme and using the corresponding formulae for the $\mathcal{O}(\alpha_t \alpha_s)$ corrections.	112	

- 4.1 Divergent scalar-only diagrams that require regulation (by resummation or using our on-shell scheme), even in the presence of external momentum. The light blue dashed lines marked with a small red “G” denote Goldstone boson propagators. The dark blobs in the diagrams on the right-hand side represent full one-loop one-particle-irreducible corrections inserted on the line. On the top line we show the tadpoles (with their clear relation to the sunset and figure-eight diagrams in the potential); on the lower two we show the corrections to the self-energies, which clearly follow the same pattern. . . . . 135
- 5.1 Difference between the two-loop Higgs mass computed by **SMH** and **SPheno** –  $(m_h^{2\ell})^{\text{SPheno}} - (m_h^{2\ell})^{\text{SMH}}$  – as a function of the renormalisation scale  $Q$ , with (*blue curve*) and without (*orange dashed curve*) the momentum dependence at two loops in **SMH**. The Higgs quartic coupling is here  $\lambda = 0.12604$ . In **SPheno** the contributions of the light SM fermions are turned off and the external momentum in the two-loop routines is set to  $s = m_h^2|_{\text{tree}}$ . . . . . 155
- 5.2 The lightest scalar mass squared for the parameter point defined by eq. (5.3.2) when calculating with and without  $D$ -term contributions.
- 
- . . . . . 156
- 5.3 The lightest Higgs mass at the two-loop level for the parameter point defined by eq. (5.3.2) for different methods to regulate the two-loop corrections.
- 
- . . . . . 157
- 5.4 The change in the Higgs mass in GeV due to the two-loop corrections involving the new Yukawa-like interactions  $\tilde{g}_{(1,2)(u,d)}$ . On the top, we used  $\tan\beta = 1$  at  $M_M$  and on the bottom  $\tan\beta = 10$ . The left plots are with the consistent tadpole solutions, the right ones without. . . . . 159
- 5.5 Lightest Higgs mass  $m_h^2$  as a function of the renormalisation scale  $Q$ , considering only the running of SM parameters. In other words, for this figure, the values of the BSM parameters  $\lambda_i$ ,  $m_{12}^2$ , and  $\tan\beta$  given in eq. (5.5.11) are considered to be input values at the scale  $Q$  at which the Higgs mass is computed, instead of being evolved from 160 GeV to  $Q$ . *Red curve*: tree-level; *Blue dot-dashed curve*: one-loop order; *Green dashed curve*: two-loop order. . . . . 162
- 5.6 Lightest Higgs mass  $m_h^2$  as a function of the renormalisation scale  $Q$ , taking into account the running of all parameters – both SM and BSM ones – with the RGEs included in **SPheno**. The difference between this figure and figure 5.5 is that here we do not consider the inputs given in equation (5.5.11) to be taken at the scale  $Q$  at which we compute  $m_h$  but at the scale  $m_t$ , and then we evolve them from  $m_t$  to  $Q$ . *Red curve*: tree-level; *Blue dot-dashed curve*: one-loop order; *Green dashed curve*: two-loop order. . . . . 163

- 5.7  $-1/t_\alpha$  as a function of the off-diagonal mass term  $m_{12}^2$  (*upper left*), and of quartic couplings  $\lambda_3$  (*upper right*),  $\lambda_4$  (*lower left*) and  $\lambda_5$  (*lower right*) at each order in perturbation theory. For each plot we vary the parameters as follows: we choose one parameter as the abscissa; the tree-level alignment condition  $\lambda_1 = \lambda_2 = 1/2\lambda_{345}$  plus the requirement that the Higgs mass is 125.09 GeV fixes *three* parameters, namely  $\lambda_1, \lambda_2$  and either  $\lambda_4$  for the bottom right plot or  $\lambda_5$  for the other three; the remaining parameters are held fixed at values  $\lambda_3 = 0.5$ ,  $\lambda_4 = 0.5$ ,  $m_{12}^2 = -1000 \text{ GeV}^2$  (when they are not otherwise varying). All plots are for  $\tan\beta = 50$ . *Red curve*: tree-level; *Blue dot-dashed curve*: one-loop order; *Green dashed curve*: two-loop order. 164
- 5.8 The dependence of the lightest scalar mass on the renormalisation scale  $Q$ , considering that the quartic couplings of eq. (5.5.13) are used as input at the scale  $Q = m_t$ . *Left*:  $m_h(Q)$  at tree-, one-loop, and two-loop levels; *Right*:  $\Delta m_h \equiv m_h(m_t) - m_h(Q)$  at tree-, one-loop, and two-loop levels . . . 166
- 5.9 The size of the one- and two-loop corrections of the lightest scalar mass as function of the scale  $Q_{in}$  at which the input masses of eq. (5.5.12) are translated into quartic couplings (or in other words, the scale at which the quartic couplings in eq. (5.5.13) are defined as inputs). . . . . 166
- 5.10 The SM-like Higgs mass at tree-, one- and two-loop level for  $m_5 = 1 \text{ TeV}$  and as a function of  $s_H$ . The results are shown for two different choices for the renormalisation  $Q$  scale, namely  $Q = m_t$  and  $Q = m_5$ . . . . . 168
- 5.11 First row: absolute size of the SM-like Higgs mass in the Georgi-Machacek model as a function of  $s_H$  and  $m_5$  and including one- (left) and two-loop (right) corrections. Second row: the size of the one- (left) and two-loop (right) corrections. . . . . 169
- 5.12 The size of the one- (left) and two-loop (right) corrections in the  $(s_H, m_5)$  plane for the second (first row) and third (second row) CP-even scalar. . . 170
- 6.1 Values of the running quartic couplings at the scale  $Q = 10^6 \text{ GeV}$  using one-loop (left) and two-loop RGEs (right) as function of the matching scale at which the quartic couplings were calculated. The labels  $(n, m)$  refer to  $n$ -loop level matching of the quartics and  $m$ -loop RGEs. We choose the parameters of the singlet extended SM at the matching scale to be  $m_h = 125 \text{ GeV}$ ,  $m_H = 400 \text{ GeV}$ ,  $\tan\alpha = 0.3$  and  $v_S = 300 \text{ GeV}$ . Cubic terms were set to zero to ensure a scale invariant input. Note that the  $y$ -axes ranges are different on each sub-figure. . . . . 175
- 6.2 The running of the quartic couplings for the point given in Tab. 6.1. The line-styles refer to the loop order of the matching and RGE running as described in Tab. 6.1, namely  $(n, m)$  refers to the matching at  $n$ -loop order with  $m$ -loop RGEs. The solid red line is the  $4\pi$  perturbativity limit, while the dashed-red line is the unitarity constraint of  $4\pi/3$  obtained from eq. (6.2.4) in the limit  $\lambda_S \gg \lambda_{SH}, \lambda$ . . . . . 177

- 6.3 Difference in the predicted cut-off scale depending on the matching performed as a function of the singlet VEV  $v_S$  and the heavy CP-even Higgs mass  $m_H$ . *Left:* We show the ratio of the obtained cut-off given matching at  $N$  versus  $N - 1$  order using the RGEs at  $N$ -loop order. The coloured(grey) contours use the two(one)-loop RGEs, therefore showing the ratio of the matching at two(one)-loop versus one-loop(tree-level), respectively. *Right:* Ratio of the calculation performed using both matching and RGEs at two-loop order versus the leading order (tree-level matching and one-loop RGEs). The grey contours correspond to the ratios of the quartic coupling  $\lambda_S$  for these two scenarios. Here we have fixed the physical parameters such that  $m_h = 125$  GeV,  $\tan \alpha = 0.2$ , while the remaining parameters are chosen as  $\kappa_1 = 0$  GeV and  $\kappa_2 = 1000$  GeV. . . . . 178
- 6.4 Running of the Higgs quartic coupling as a function of the renormalisation scale  $Q$ , having taken  $\lambda_{SH} = 0.28$ ,  $\lambda_S = 0.1$  and  $m_S = 500$  GeV. The value of  $\lambda(m_t)$  is obtained by requiring  $m_h = 125.15$  GeV, with different orders of matchings depending on the curve. The solid line corresponds to the use of two-loop matching and two-loop RGE running, the dashed line to tree-level matching and two-loop RGEs, and the dotted line to tree-level matching and one-loop RGEs. Note that because of the cancellation that occurs in the one-loop correction for small  $\lambda_{SH}$  (discussed in the main text), the curves we would have obtained using one-loop matching would have been very similar to those with tree-level matching. . . . . 181
- 6.5 Different phases in the  $\mathbb{Z}_2$ SSM shown in the  $\lambda_{SH} - \lambda$  plane, where the couplings are taken at scale  $Q = m_t$ . The orange shaded region of parameter space corresponds to UV-complete theories, *i.e.* none of the three quartic couplings ( $\lambda$ ,  $\lambda_{SH}$ ,  $\lambda_S$ ) become non-perturbative and the constraints from unitarity are not violated before the Planck scale; the black shaded region corresponds to theories with stable vacua. The thin blue lines give  $\lambda$  as a function of  $\lambda_{SH}$  when imposing  $m_h = 125.15$  GeV with a matching condition at respectively tree-level (dotted curve), one-loop order (dashed curve) and two-loop order (solid line). The other parameters of the scalar sector are  $\lambda_S = 0.1$ , and  $M_S = 500$  GeV. . . . . 182
- 6.6 Simplified comparison between the running of  $\lambda$  in the SM with and without vector-like states. Here, we used full one-loop (dashed lines) and two-loop RGEs (full lines) in both models and as starting point the SM best-fit values from ref. [25]. For the purple (black) lines we use  $Y'_t = 0.3$  (0.7). . . . . 184
- 6.7 Contours of the scale  $\Lambda_0$  at which  $\lambda$  runs negative with full two-loop RGEs and one-loop (dashed) or two-loop (full lines) matching, and for comparison when using the best-fit value  $\lambda^{\text{SM}} = 0.25208$  at the top mass scale (dotted). Black lines correspond to  $\Lambda_0 = 10^{18}$  GeV, blue lines to  $10^{11}$  GeV. The background shows the two-loop shift in  $\lambda(m_t)$  in percent, defined as  $(\lambda^{(2)} - \lambda^{(1)})/\lambda^{(1)}$ . . . . . 185
- 6.8 The state of metastability  $\Lambda_0$  in the case of large  $Y'_t$  using two-loop running with two-loop matching for  $\lambda$ . The black contours show the size of  $\Lambda_0$  with respect to using one-loop matching. . . . . 186

- 6.9 The size of the quartic couplings at  $m_t$  at LO (blue dotted), NLO (grey dashed) and NNLO (blue solid) as a function of  $m_{H^\pm}$ . Here, we set the other physical masses and mixing angle to  $m_h = 125$  GeV,  $m_H = 750$  GeV,  $m_A = 730$  GeV and  $\tan \alpha = -0.71$ . The other model parameters are  $\tan \beta = 1.4$  and  $m_{12}^2 = -500^2$  GeV<sup>2</sup>. On the right, we show the relative differences  $\delta\lambda_i^{\text{LO}} \equiv |(\lambda_i^{(T)} - \lambda_i^{(1)})/\lambda_i^{(T)}|$  and  $\delta\lambda_i^{\text{NLO}} \equiv |(\lambda_i^{(1)} - \lambda_i^{(2)})/\lambda_i^{(1)}|$ . Note that for  $\lambda_i$  where  $i = 3, 4, 5$  the NLO difference have been multiplied by an additional factor of 10 to increase visibility. . . . . 188
- 6.10 RGE running of the individual quartic couplings  $\lambda_1$  (black) and  $\lambda_3$  (blue) for the parameter point defined by  $m_H = 511$  GeV,  $m_A = 607$  GeV,  $m_{H^\pm} = 605$  GeV,  $t_\beta = 1.45$ ,  $t_\alpha = -0.82$ ,  $m_{12}^2 = -(250 \text{ GeV})^2$ , using  $n$ -loop level matching and  $m$ -loop RGEs. The dotted lines stand for  $(T, 1)$ , dot-dashed for  $(1, 1)$ , dashed for  $(1, 2)$  and full lines for  $(2, 2)$ . Coupling values of  $\pm 4\pi$  are indicated by a red solid line. In addition, we display the largest eigenvalue of the scalar  $2 \rightarrow 2$  scattering amplitude in purple. The upper bound of  $8\pi$  is indicated by a dashed red line. We used the Yukawa scheme of type II. . . . . 189
- 6.11 Comparison of the cut-off scales between using tree matching and one-loop RGEs and both two-loop matching and RGEs for a 2HDM region with large  $m_{12}^2 = -(750 \text{ GeV})^2$ . The loop-level spectrum was evaluated taking the tree-level values  $m_{H^\pm} = 1.14$  TeV and  $t_\alpha = -0.95$  as inputs. The ratio of the loop-corrected charged Higgs mass to its tree-level input is shown as grey contour lines. The quartic couplings for the case of tree-matching were obtained using the leading order relations Eqs. (1.4.19) to (1.4.23), taking the spectrum of the two-loop calculation as input. We further fixed  $\tan \beta = 1.14$  and applied the Yukawa scheme of type I. . . . . 190